

Combustion Research Gas Phase Chemical Physics Program

DOE Principal Investigators'
Abstracts

May, 2015

Chemical Sciences, Geosciences, and Biosciences Division
Office of Basic Energy Sciences
Office of Science
U.S. Department of Energy

The research grants and contracts described in this document are supported by the U.S. DOE Office of Science, Office of Basic Energy Sciences, Chemical Sciences, Geosciences and Biosciences Division.

Foreword

This collection of active research abstracts illustrates the breadth and depth of basic research supported by the Department of Energy's Office of Basic Energy Sciences (BES) and, in large measure, by the chemical physics program that contributes to the development of a predictive capability for combustion processes. The long-term objective of this effort is the provision of theories, data, and procedures to enable the development of reliable computational models of combustion processes, systems, and devices.

We appreciate the privilege of serving in the management of this research program. In carrying out these tasks, we learn from the achievements and share the excitement of the research of the many sponsored scientists and students whose work is summarized in the abstracts published on the following pages. This year we have included a discussion on critical issues in the gas phase chemical physics energy mission, which will play an important role in strategic planning. Ten critical issues slides were received following a request from the 28 principal investigators scheduled to speak. These 10 slides are included at the end of this abstract.

We thank all of the researchers whose dedication and innovation have advanced DOE BES research. We look forward to our assembly in 2016 for our 36th annual meeting.

Jeff Krause
Mark Pederson
Wade Sisk

Table of Contents

Table of Contents

Foreword	iii
Table of Contents	v
Abstracts	1
<u>Keynote Speaker Abstract</u>	
James Gord Air Force Research Laboratory Aerospace Systems Directorate - Optical Optical Combustion Diagnostics: New Developments and Continuing Challenges.....	1
<u>Principal Investigators' Abstracts</u>	
Musahid Ahmed, Kevin Wilson & Oleg Kostko – The Chemical Dynamics Beamline.....	5
Wesley Allen and Henry F. Schaefer III - Theoretical Studies of Elementary Hydrocarbon Species and Their Reactions.....	9
Robert S. Barlow - Turbulence-Chemistry Interactions in Reacting Flows.....	13
Josette Bellan - Predictive Large-Eddy Simulation of Supercritical-Pressure Reactive Flows in the Cold Ignition Regime	17
Guillaume Blanquart - Towards predictive simulations of soot formation: from surrogate to turbulence.....	21
Joel M. Bowman - Theoretical Studies of Combustion Dynamics.....	25
Laurie J. Butler - Dynamics of Product Branching in Elementary Combustion Reactions: OH + Alkenes and Nitrogen Chemistry.....	29
David W. Chandler - Chemical Dynamics and Spectroscopy of Gas Phase Species Utilizing Velocity Mapped Ion Imaging.....	33
Jacqueline H. Chen - Petascale Direct Numerical Simulation and Modeling of Turbulent Combustion.....	37
Robert E. Continetti - Dynamics and Energetics of Elementary Combustion Reactions and Transient Species.....	41
F.F. Crim - Vibrational Dynamics and Dissociation of Ground- and Excited-State Cluster.....	45
Paul J. Dagdigian and Millard Alexander - Theoretical Investigation of Kinetic Processes in Small Radicals	49
Rainer N. Dahms - Theory and Modeling of Multiphase Reacting Flow Dynamics in Simulations and Experiments.....	53
H. Floyd Davis - Bimolecular Dynamics of Combustion Reactions.....	57
Michael J. Davis - Exploration and validation of chemical-kinetic mechanisms.....	59
Richard Dawes - Multiple Coupled Potential Energy Surfaces with Application to Combustion.....	63
Theodore S. Dibble - Dynamics of Peroxy and Alkenyl Radicals Undergoing Competing Rearrangements in Biodiesel Combustion.....	67

Gary Douberly - Vibrational Spectroscopy of Transient Combustion Intermediates Trapped in Helium Nanodroplets.....	71
Robert W. Field - Spectroscopic and Dynamical Studies of Highly Energized Small Polyatomic Molecules.....	75
Jonathan H. Frank - Quantitative Imaging Diagnostics for Reacting Flows.....	79
William H. Green - Computer-Aided Construction of Chemical Kinetic Models.....	83
Hua Guo - Quantum Dynamics of Elementary Combustion Reactions.....	87
Gregory E. Hall - Gas-Phase Molecular Dynamics: High Resolution Spectroscopy and Collision Dynamics of Transient Species.....	91
Nils Hansen - Flame Chemistry and Diagnostics.....	95
Ronald K. Hanson and Craig T. Bowman – Kinetics and Spectroscopy of Combustion Gases at High Temperatures.....	99
Lawrence B. Harding - Theoretical Studies of Potential Energy Surfaces.....	103
Martin Head-Gordon, William A. Lester Jr., and William H. Miller - Chemical Accuracy from Ab-Initio Molecular Orbital Calculations.....	107
John F. Hershberger - Laser Studies of Combustion Chemistry.....	111
So Hirata - Breakthrough Design and Implementation of Electronic and Vibrational Many-Body Theories.....	115
Mark R. Hoffmann - Generalized Van Vleck Variant of Multireference Perturbation Theory.....	119
Ahren W. Jasper - Theoretical Methods for Pressure Dependent Kinetics and Electronically Nonadiabatic Chemistry.....	123
Ralf I. Kaiser - Probing the Reaction Dynamics of Hydrogen-Deficient Hydrocarbon Molecules and Radical Intermediates via Crossed Molecular Beams.....	127
Michael E. Kellman - Dynamical Analysis of Highly Excited Molecular Spectra.....	131
Christopher J. Kliewer - Time-Resolved Diagnostics.....	135
Stephen J. Klippenstein - Theoretical Chemical Kinetics.....	139
Stephen J. Klippenstein and Craig A. Taatjes et. al - Argonne-Sandia Consortium on High- Pressure Combustion Chemistry.....	143
Anna I. Krylov - Theoretical Modeling of Spin-Forbidden Channels in Combustion Reactions.....	147
Marsha I. Lester – Spectroscopy and Dynamics of Reactive Intermediates in Combustion Chemistry.....	151
Tianfeng Lu - Computational Flame Diagnostics for Direct Numerical Simulations with Detailed Chemistry of Transportation Fuels.....	155
Robert P. Lucht - Advanced Nonlinear Optical Methods for Quantitative Measurements in Flames.....	159
Alexander M. Mebel - Theoretical Studies of Chemical Reactions Related to the Formation and Growth of PAHs and Molecular Properties of Their Key Intermediates.....	163
Joe V. Michael - Flash Photolysis-Shock Tube Studies.....	167
Hope A. Michelsen - Particle Diagnostics Development.....	171
William H. Miller - Reaction Dynamics in Polyatomic Molecular Systems.....	175

Amy S. Mullin - Dynamics of Activated Molecules.....	179
Habib N. Najm - Reacting Flow Modeling with Detailed Chemical Kinetics.....	183
David J. Nesbitt - Spectroscopy, Kinetics and Dynamics of Combustion Radicals.....	187
Daniel Neumark and Stephen Leone – Spectroscopy and Dynamics of Free Radicals.....	191
C. Y. Ng - State-to-state photoionization, photoelectron, and photodissociation of combustion radicals.....	195
Joseph C. Oefelein - Large Eddy Simulation of Turbulence-Chemistry Interactions in Reacting Multiphase Flows.....	199
David L. Osborn - Kinetics and Dynamics of Combustion Chemistry.....	203
Carol A. Parish - A Theoretical Investigation of the Structure and Reactivity of the Molecular Constituents of Oil Sand and Oil Shale.....	207
David S. Perry - The Dynamics of Large-Amplitude Motion in Energized Molecules.....	211
Piotr Piecuch - New Single- and Multi-Reference Coupled-Cluster Methods for High Accuracy Calculations of Ground and Excited States.....	215
Stephen B. Pope & Perrine Pepiot - Investigation of Non-Premixed Turbulent Combustion...	219
Stephen T. Pratt - Optical Probes of Atomic and Molecular Decay Processes.....	223
Kirill Prozument - Chirped-Pulse Fourier Transform Millimeter-Wave Spectroscopy for Dynamics and Kinetics Studies of Combustion-Related Reactions.....	227
Hanna Reisler - Photoinitiated Reactions of Radicals and Diradicals in Molecular Beams.....	231
Klaus Ruedenberg – Accurate Calculations and Analyses of Electronic Structure, Molecular Bonding and Potential Energy Surfaces.....	235
Branko Ruscic - Active Thermochemical Tables.....	237
Trevor Sears - Gas-Phase Molecular Dynamics: High Resolution Spectroscopy and Collision Dynamics of Transient Species.....	243
Ron Shepard - Theoretical Studies of Potential Energy Surfaces and Computational Methods.....	247
Raghu Sivaramakrishnan - Mechanisms and Models for Combustion Simulations.....	251
John F. Stanton - Quantum Chemistry of Radicals and Reactive Intermediates.....	255
Arthur G. Suits - Universal and State-Resolved Imaging Studies of Chemical Dynamics.....	259
James Sutherland - An Update on the Implementation of a Novel Multiscale Simulation Strategy.....	263
Craig A. Taatjes - Elementary Reaction Kinetics of Combustion Species.....	267
Robert S. Tranter - Elementary Reactions of PAH Formation.....	271
Donald G. Truhlar - Variational Transition State Theory.....	275
Angela Violi - Developing a predictive model for the chemical composition of soot nanoparticles: Integrating Model and Experiment.....	279
Albert Wagner - Pressure Dependence of Combustion Reactions: Quantum Inelastic Dynamics On Automatically Generated Potential Energy Surfaces.....	283
Charles K. Westbrook and William J. Pitz and - Kinetic Modeling of Combustion Chemistry.....	287

Margaret S. Wooldridge - Low Temperature Combustion Chemistry and Fuel Component Interactions.....	291
David R. Yarkony - Theoretical Studies of the Reactions and Spectroscopy of Radical Species Relevant to Combustion Reactions and Diagnostics.....	295
Hua-Gen Yu - Gas-Phase Molecular Dynamics: Theoretical Studies in Spectroscopy and Chemical Dynamics.....	299
Judit Zádor - Chemical Kinetics of Elementary Reactions.....	303
Timothy S. Zwier - Isomer-specific Spectroscopy and Pyrolysis of Model Aromatic Fuels ...	307
 Critical Issues for the DOE GPCP Program	
Paul Dagdigian	311
Stephen Klippenstein.....	313
Marsha Lester.....	315
Tianfeng Lu	317
Daniel Neumark.....	319
Cheuk-Yiu Ng.....	321
Ron Shepard.....	323
Albert Wagner.....	325
Margaret Wooldridge.....	327
Timothy Zwier.....	329
 Participant List	 331

Keynote Speaker

Optical Combustion Diagnostics: New Developments and Continuing Challenges

James R. Gord

Air Force Research Laboratory, Aerospace Systems Directorate

Wright-Patterson AFB OH 45433-7541

james.gord@us.af.mil

Advanced measurement techniques that exploit lasers and optics have become well-established tools for characterizing combusting flows [Eckbreth, 1996; Kohse-Höinghaus and Jeffries, 2002; Laurendeau, 2005; Gord et al., 2008; Meyer et al., 2010; Roy et al., 2010]. Such noninvasive measurement approaches are often ideally suited for visualizing complex reacting flows and quantifying key chemical-species concentrations, temperature, and fluid-dynamic parameters. The fundamental information these techniques provide is essential for achieving a detailed understanding of the chemistry and physics of combustion processes.

A tremendous volume of published literature exists documenting the development of laser-based/optical measurement techniques for exploring combustion phenomena and the successful application thereof. A critical review of this literature reveals that much of it involves measurements accomplished in relatively simple combusting flows, such as those encountered in various basic laboratory flames. Although many researchers have increasingly turned their attention to more complicated flows representative of “real-world” systems, most laboratory studies involve simple flames often characterized by one or more of these descriptors: atmospheric-pressure, gaseous-fueled, laminar, temporally and spatially steady, optically thin, axisymmetric, and optically accessible, for example. A great deal has been learned about fundamental combustion phenomena through studies of simple flames that include various premixed, partially premixed, and diffusion systems, such as jet flames, counterflow flames, Hencken and McKenna burners, etc. These flames and more complex burners, such as those studied by numerous groups nationally and internationally in an effort to characterize turbulent combustion phenomena, have emerged as “industry standards” for evaluating new combustion measurement techniques and baselining both experimental and computational research efforts.

The continuing efforts in our group and some others in the community seek to move beyond this established body of scholarly studies and achieve the overarching goal of exploring fundamental combustion phenomena under increasingly realistic conditions encountered in actual systems. Such conditions involve high-pressure, temporally and spatially heterogeneous and evolving turbulent combustion with two-phase flows characteristic of liquid-fueled systems and real-world challenges that include optical thickness, beam steering, static and dynamic combustion instabilities, soot production, turbulence–chemistry interactions, and restricted optical access, to name just a few. The approaches pursued to achieve this goal exploit recent and continuing advances in ultrafast (picosecond/femtosecond) lasers and associated pulse-shaping technology, high-repetition-rate lasers and cameras, and computational methodologies for reducing incredibly large volumes of data and extracting key combustion parameters through detailed physics-based modeling of light–matter interactions as they apply to combustion measurements.

Such efforts are focused on improving the current state-of-the-art through systematic research in each of these eight areas: 1) high data-acquisition bandwidth, 2) measurements in high-pressure combustion, 3) measurements in optically dense sprays characteristic of liquid-fueled combustion, 4) accommodation for limited optical access in practical systems, 5) increased

measurement dimensionality in space and time, 6) measurement simultaneity through coupling of correlated measurement techniques, 7) data reduction and mining for assigning meaning to incredibly large volumes of spatiotemporally evolving data, and 8) physics-based modeling of detailed light–matter interactions for extracting key combustion parameters from optical measurements.

Many of the successful optical measurements achieved to date in combustions flows have been based on the use of conventional continuous-wave and ns-pulsed laser systems, including Q-switched Nd:YAG lasers, excimer lasers, and associated YAG- and excimer-pumped dye lasers. These systems have been the workhorses in most experiments involving such optical-measurement techniques as planar laser-induced fluorescence (PLIF), particle-image velocimetry (PIV), laser-induced incandescence (LII), coherent anti-Stokes Raman scattering (CARS) spectroscopy, and resonant four-wave mixing (RFWM). These laser systems afford high pulse energies required for sheet lighting in planar techniques and for nonlinear interactions such as those in CARS and RFWM. They also provide relatively narrow spectral bandwidths required for spectroscopic studies of key gas-phase combustion species (e.g., OH, CH, NO, CO, etc.).

While the impact of continuous-wave and traditional 10-Hz ns-pulsed lasers systems on the modern science of combustion measurements is undeniable, continuing revolutionary advances in the science and engineering of ultrafast lasers (i.e., ps- and fs-pulsed lasers) and burst-mode lasers (ns and ps duration) have enhanced the capabilities and utility of existing combustion-diagnostic techniques while enabling the development and application of new measurement methodologies previously unachievable.

Myriad benefits stem from the ultrashort ps and fs pulses delivered by modern ultrafast laser systems. These benefits are realized through the time resolution achievable and the temporal duration of optical combustion measurements performed on these timescales. The time resolution afforded by ultrafast laser systems has been exploited through time-resolved measurements to study the kinetics and dynamics of combustion chemistry and energy-transfer processes. Separation in time of various pump and probe pulses has been used to discriminate against

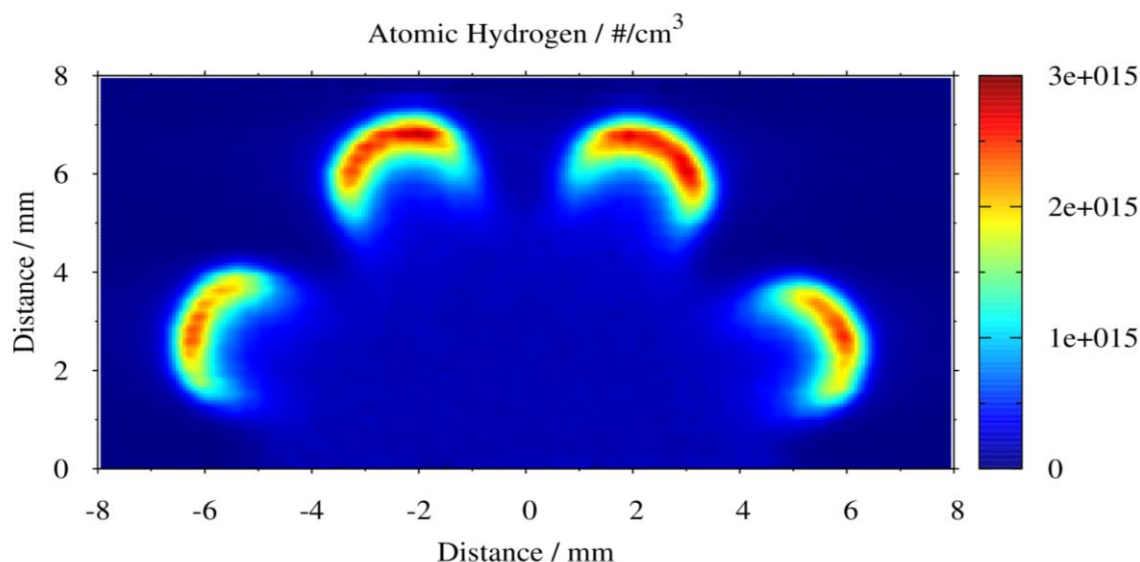


Figure 1. Quantitative, photolytic-interference-free imaging of atomic hydrogen in a premixed hydrogen–air tubular flame by fs two-photon LIF [Hall et al., 2014; Hall et al., 2015].

nonresonant background signals, enhancing measurement sensitivity and selectivity and enabling the detection of key minor-species concentrations. Because of the ultrashort duration of some of these measurements, signals can be acquired that are largely free of collisional and pressure effects [Wrzesinski et al., 2013]. This key feature of ultrafast combustion measurements addresses one of the major limitations of conventional ns-pulsed diagnostics, enabling quantitative measurements of parameters such as temperature and number densities in high-pressure, turbulent flames characteristic of most practical combustion devices. In these systems the chemical and collisional-quenching environment is typically highly inhomogeneous and rapidly changing in both space and time. In addition, ultrashort pulses enable tremendous instantaneous power from laser systems of low-to-moderate average power, allowing previously unimaginable 2D imaging of temperature [Bohlin and Kliewer, 2013] and key combustion species such as H, O, and CO [Kulatilaka et al., 2012]. Figure 1 shows a 2D image of atomic hydrogen achieved by exploiting the high instantaneous power of an amplified fs laser via two-photon LIF with no interfering H produced photolytically from H₂O and CH₃ [Kulatilaka et al., 2012]. Previous measurements with ns lasers were plagued by photolytic O and H production, making quantitative concentration measurements extremely difficult; ps lasers provided significant reduction of these interferences, but photolytic production of O and H was still an issue [Frank et al., 2004, Kulatilaka et al., 2008].

Despite many successful demonstrations of these significant benefits, ps- and fs-laser-based nonlinear spectroscopic approaches often suffer from limited spatial extent for chemical-species imaging and low data-acquisition rates for two-dimensional imaging of temperature and species-concentration fields [Bohlin and Kliewer, 2013]. This inhibits spatiotemporally resolved imaging and prevents high-fidelity comparisons of experimental and numerical data related to turbulent reacting or hypersonic flows. The limited repetition rate or pulse energy of continuously pulsed ps and fs laser systems originates from limited average output power. To overcome the average-power limitation of continuously pulsed lasers, one can utilize burst-mode operation. Burst-mode

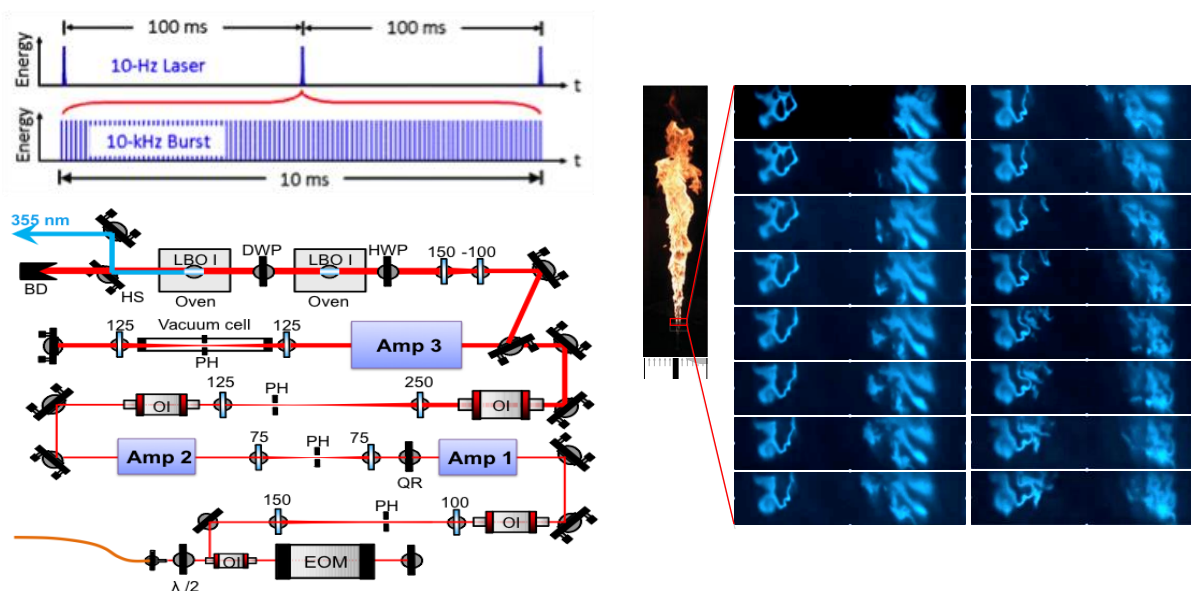


Figure 2. Concept of burst-mode laser operation, producing intermittent but high-speed bursts of laser pulses (top left), optical layout of all-diode-pumped, quasi-continuous burst-mode system (bottom left), and sample imaging of CH₂O fluorescence at the base of a lifted jet diffusion flame collected at 50 kHz (right).

lasers achieve high pulse energy in combination with high-repetition-rate operation by grouping a series of closely spaced pulses into short bursts, thus enabling high pulse peak power and high repetition rate with low average system power. To overcome the low-repetition-rate limitations of commercial, high-energy 100-ps systems and the peak power limitations of high-energy, ns burst-mode laser systems, a high-bandwidth, high-energy (100 J/burst) burst-mode laser of ~100 ps pulse duration has recently been developed by our group and demonstrated with operation at repetition rates of 10 kHz–1 MHz. The laser architecture utilizes both diode- and flashlamp-pumped Nd:YAG amplifiers for amplification of a nearly transform-limited 100-ps oscillator. The compact design is similar to that of previous burst-mode lasers that used narrow-bandwidth ns oscillators but with nearly two-orders-of-magnitude reduction in pulse duration. Figure 2 shows an example pulse train, an optical layout, and sample imaging of CH₂O fluorescence at a rate of 50 kHz. This laser will have wide applicability in an array of nonlinear spectroscopic and imaging applications in high-speed turbulent and unsteady reacting and non-reacting flows.

References

- Bohlin, A., and C.J. Klier, “Communication: Two-dimensional gas-phase coherent anti-Stokes Raman spectroscopy (2D-CARS): Simultaneous planar imaging and multiplex spectroscopy in a single laser shot,” *J. Chem. Phys.* 138, 221101 (2013).
- Eckbreth, A. C. 1996. *Laser Diagnostics for Combustion Temperature and Species*. Amsterdam: Gordon & Breach. 596 pp. 2nd ed.
- Frank, J.H., X.L. Chen, B. D. Patterson, and T. B. Settersten, “Comparison of nanosecond and picosecond excitation for two-photon laser-induced fluorescence imaging of atomic oxygen in flames,” *Appl. Opt.* 43 (12), 2588–2597 (2004).
- Gord, J. R., T. R. Meyer, and S. Roy, “Applications of Ultrafast Lasers for Optical Measurements in Combusting Flows,” *Annu. Rev. Anal. Chem.* 1, 663–687 (2008).
- Hall, C.A., W.D. Kulatilaka, J.R. Gord, and R.W Pitz, “Quantitative atomic hydrogen measurements in premixed hydrogen tubular flames,” *Combust. Flame*, 161, 2924–2932 (2014).
- Hall, C.A., W.D. Kulatilaka, Jiang, N., J.R. Gord, and R.W Pitz, “Minor-species structure of premixed cellular tubular flames,” *Proc. Combust. Inst.*, 35 (1), 1107–1114 (2015).
- Kohse-Höinghaus, K. and J. B. Jeffries. 2002. *Applied Combustion Diagnostics*. New York: Taylor & Francis. 705 pp.
- Kulatilaka, W.D., B.D. Patterson, J.H. Frank, and T.B. Settersten, “Comparison of nanosecond and picosecond excitation for interference-free two-photon laser-induced fluorescence detection of atomic hydrogen in flames,” *Appl. Opt.* 47 (26), 4672–4683 (2008).
- Kulatilaka, W.D., J. R. Gord, V. Katta, and S. Roy, “Photolytic-Interference-Free, Femtosecond Two-Photon Fluorescence Imaging of Atomic Hydrogen,” *Optics Letters* 37, 3051–3053 (2012).
- Laurendeau, N. M. 2005. *Statistical Thermodynamics: Fundamentals and Applications*. New York: Cambridge Univ. Press. 448 pp.
- Linne, M. A. 2002. *Spectroscopic Measurement: An Introduction to the Fundamentals*. New York: Academic. 414 pp.
- Meyer, T. R., M. J. Brear, S. H. Jin, and J. R. Gord, “Formation and Diagnostics of Sprays in Combustion,” in *Handbook of Combustion Volume 2: Combustion Diagnostics and Pollutants*, M. Lacker, F. Winter, and A.K. Agarwal (eds.), Wiley: Hoboken, NJ (2010).
- Roy, S., J.R. Gord, and A.K. Patnaik, “Recent Advances in Coherent Anti-Stokes Raman Scattering Spectroscopy: Fundamental Developments and Applications in Reacting Flows,” *Prog. Energ. Combust. Sci.* 36 (2), 280–306 (2010).
- Wrzesinski, P.J., H. U. Stauffer, W. D. Kulatilaka, J. R. Gord, and S. Roy, “Time-Resolved Femtosecond CARS from 10 to 50 Bar: Collisional Sensitivity,” *Journal of Raman Spectroscopy* 44, 1344–1348, (2013).

*Abstracts
of
Principal Investigator
Presentations*

The Chemical Dynamics Beamline

Musahid Ahmed, Kevin Wilson & Oleg Kostko

Chemical Sciences Division, Lawrence Berkeley National Laboratory
MS 6R2100, 1 Cyclotron Road, Berkeley, CA-94720, mahmed@lbl.gov

Program Scope: The Chemical Dynamics Beamline, located in the Advanced Light Source (ALS) at Lawrence Berkeley National Laboratory (LBNL), is a national user facility providing state-of-the-art experimental resources for visiting scientists and staff to undertake studies of fundamental chemical processes. Much of the work is related to combustion, energy production and utilization, environmental science and chemical reactions on interfaces. Vacuum Ultraviolet (VUV) synchrotron photoionization mass spectrometry on two experimental platforms (molecular beam and aerosol sampling) are applied to a variety of problems of relevance to the Gas Phase Chemical Physics program. A miniature shock tube (Rob Tranter, ANL), pyrolytic reactors (Ralf Kaiser, Hawaii & Barney Ellison, Colorado), and a jet stirred reactor (Steve Leone, LBNL and Nils Hansen Sandia, CRF) have all been incorporated into the molecular beam apparatus. The aerosol mass spectrometer plays a critical role in real time measurements of soot formation chemistry, the results of which are reported by Nils Hansen and Hope Michelson (Sandia, CRF).

Recent Progress and Future Plans:

Formation mechanisms of PAH's- The formation mechanisms of polycyclic aromatic hydrocarbons (PAHs) with indene and naphthalene cores in hydrocarbon-based combustion processes are being examined in collaboration with Ralf Kaiser (Hawaii). This is achieved by simulating the combustion relevant conditions (pressure, temperature, reactant molecules) in a high temperature 'chemical reactor'. For almost half a century, polycyclic aromatic hydrocarbons (PAHs) have been proposed to play a key role in the astrochemical evolution of the interstellar medium (ISM) and in the chemistry of combustion systems. However, even the most fundamental reaction mechanism assumed to lead to the simplest PAH naphthalene—the hydrogen abstraction–acetylene addition (HACA) mechanism—has eluded experimental observation. Here, by probing the phenylacetylene (C_8H_6) intermediate together with naphthalene ($C_{10}H_8$) under combustion-like conditions by photo-ionization mass spectrometry, the very first direct experimental evidence for the validity of the HACA mechanism which so far had only been speculated theoretically is reported. Recently we showed that upon reaction of the naphthyl radical with acetylene, HACA effectively shuts down and does not lead to cyclization of the third aromatic ring, and a new pathway, via ethnyl substitution is operational.

The reaction of the phenyl radical (C_6H_5) with molecular oxygen (O_2) plays a central role in the degradation of poly- and mono- cyclic aromatic radicals in combustion systems which would otherwise react with fuel components to form polycyclic aromatic hydrocarbons (PAH) and eventually soot. In the reaction of phenyl radicals and molecular oxygen at 873 K and 1,003 K, ortho-benzoquinone (*o*- $C_6H_4O_2$), the phenoxy radical (C_6H_5O), cyclopentadienyl radical (C_5H_5), were identified as primary products formed through emission of atomic hydrogen, atomic oxygen and carbon dioxide. Furan (C_4H_4O), acrolein (C_3H_4O) and ketene (C_2H_2O) were also identified as primary products formed through ring opening and fragmentation of the 7-membered ring 2-oxepinoxy radical. Secondary reaction products para-benzoquinone (*p*- $C_6H_4O_2$), phenol (C_6H_5OH), cyclopentadiene (C_5H_6), 2,4-cyclopentadienone (C_5H_4O), vinylacetylene (C_4H_4), and acetylene (C_2H_2) were also identified. We demonstrate by combining the pyrolytic reactor combined with electronic structure calculations that quinoline and isoquinoline can be synthesized via reaction of the 3-pyridyl radical with two acetylene molecules under high temperature conditions representing environments in the inner shells of circumstellar envelopes of carbon stars.

A concerted effort is underway to understand the molecular mass growth processes involving small hydrocarbons and their aromatic (AR) as well as resonance stabilized free radicals (RSFRs) that lead to PAHs in order to successfully mitigate their formation in the combustion of fossil fuels. We are investigating the key reaction between the benzyl radicals (C_7H_7) and acetylene (C_2H_2) to ascertain the ability of this bimolecular reaction to form the prototypical PAH indene. Our investigation aims to elucidate

the branching ratio between the PAH indene and alternative non-bicyclic isomers potentially formed in this process. Future work will be with propargyl (C_3H_3) and allyl (C_3H_5) RSFR's with C2 to C4 hydrocarbons.

Fundamental Processes in the Thermal Cracking of Biomass- Thermochemical processing of biomass, with the goal of producing synthesis gas (CO and H_2) is an important pathway towards the production of renewable fuels. Understanding of this process is incomplete, however, as even the thermolysis chemistry of many of the organic molecules encountered in these processes is poorly understood or completely unknown. To this end, we use a miniature, short residence time flow reactor coupled to synchrotron radiation, computational fluid dynamics and theoretical chemistry to determine the identity of the elementary decomposition pathways in collaboration with Barney Ellison (Colorado), John Daily (Colorado) & John Stanton (Texas). We have focused on a molecule that has proven to be a ubiquitous biomass cracking and combustion intermediate – cyclopentadienone ($C_5H_4=O$), as well as 2,5-dimethylfuran, which is the first legitimate biofuel that we have studied. Specifically, we have determined that $C_5H_4=O$ yields acetylene and vinylacetylene upon thermolysis, but the relative quantities of the two products and chemical mechanisms for these processes are currently being analyzed. Similarly, pyrolysis of 2,5-dimethylfuran leads to an observed set of products rather different from what might be expected based on our earlier work with furan, and indeed are inconsistent with some interpretations already in the literature. A comprehensive pyrolytic and photoionization study on the benzyl radical, $C_6H_5CH_2$ is nearing completion. Pyrolysis of the $C_6H_5CD_2$, $C_6D_5CH_2$, and $C_6H_5^{13}CH_2$ benzyl radicals produces a set of methyl radicals, cyclopentadienyl radicals, and benzynes that are not predicted by a fulvenallene pathway. Explicit searches for the cycloheptatrienyl radical were unsuccessful; there is no evidence for the isomerization of benzyl and cycloheptatrienyl radicals: $C_6H_5CH_2 \leftrightarrow C_7H_7$.

Multiphase Chemistry of Particulate Matter

Significant effort by staff and users of the Chemical Dynamics Beamline has been dedicated to understanding heterogeneous free radical chemistry of hydrocarbon droplets and particles. The overall goal of this work is to better elucidate interfacial reaction mechanisms and rates and to determine how surface reactions might differ from analogous processes in isolated gas phase molecules.

Significant efforts have been devoted to combine two dimensional gas phase chromatography with VUV photoionization mass spectrometry (2DVUVMS). This work (done in collaboration with Allen Goldstein, UC Berkeley) reveals new details about isomer resolved product distributions produced by heterogeneous reactions. GC-VUVMS was used to examine the influence of molecular structure (branched vs. linear) on product formation in the heterogeneous reaction of OH with squalene ($C_{30}H_{50}$, a branched alkene with six C=C double bonds) and linolenic acid ($C_{18}H_{30}O_2$, a linear carboxylic acid with three C=C double bonds). The product distributions reveal how molecular structure govern the formation of products arising from allylic radical intermediates and the formation and decomposition of alkoxy radical species.

Alkoxy radical intermediates play important roles in breaking C-C bonds during a reaction. In addition, intermolecular hydrogen abstraction by alkoxy radicals is quite rapid, leading to the potential of free radical chain chemistry. We have observed a rapid increase in the heterogeneous reaction probability of OH with squalane in the presence of NO and SO_2 . As the OH concentration decreases towards atmospheric densities the effective OH reaction probability exceeds the collision rate indicating rapid free radical chain cycling produced by the $RO_2 \cdot + NO \rightarrow RO \cdot + O_2$ reaction. In the gas phase, peroxy radicals react with NO for form primarily organic nitrates (chain termination) and a small fraction of alkoxy radicals. Thus, from our results it appears that for a heterogeneous reaction the branching ratio to organic nitrates (chain termination) is small mainly forming alkoxy radicals (chain propagation) instead.

DOE sponsored research (2012-2015)

- D. S. N. Parker, R. I. Kaiser, B. Bandyopadhyay, O. Kostko, T. P. Troy, and M. Ahmed, “*Unexpected Chemistry from the Reaction of Naphthyl and Acetylene at Combustion-Like Temperatures*,” *Angew. Chem. Int. Ed.*, (2015, accepted), DOI: [10.1002/anie.201411987](https://doi.org/10.1002/anie.201411987)
- E. C. Browne, J. P. Franklin, M. R. Canagaratna, P. Massoli, T. W. Kirchstetter, D. R. Worsnop, K. R. Wilson, and J. H. Kroll, “*Changes to the Chemical Composition of Soot from Heterogeneous Oxidation Reactions*,” *J. Phys. Chem. A*, DOI: [10.1021/jp511507d](https://doi.org/10.1021/jp511507d) (2015, accepted)
- T. K. Ormond, A. M. Scheer, M. R. Nimlos, D. J. Robichaud, T. P. Troy, M. Ahmed, J. W. Daily, T. L. Nguyen, J. F. Stanton, and G. B. Ellison, “*Pyrolysis of Cyclopentadienone: Mechanistic Insights From a Direct Measurement of Product Branching Ratios*,” *J. Phys. Chem. A*, DOI: [10.1021/jp511390f](https://doi.org/10.1021/jp511390f) (2015, accepted)
- P. T. Lynch, T. P. Troy, M. Ahmed, and R.S. Tranter, “*Probing Combustion Chemistry in a Miniature Shock Tube with Synchrotron VUV Photo Ionization Mass Spectrometry*,” *Anal. Chem.*, DOI: [10.1021/ac5041633](https://doi.org/10.1021/ac5041633) (2015, accepted)
- D. S. N. Parker, R. I. Kaiser, O. Kostko, T. P. Troy, M. Ahmed, A. M. Mebel, and A. G. G. M. Tielens, “*Gas Phase Synthesis of (Iso)Quinoline and Its Role in the Formation of Nucleobases in the Interstellar Medium*,” *Astrophys. J.*, (2015, accepted)
- M. R. Canagaratna, P. Massoli, E. C. Browne, J. P. Franklin, K. R. Wilson, T. B. Onasch, T. W. Kirchstetter, E. C. Fortner, C. E. Kolb, J. T. Jayne, J. H. Kroll, and D. R. Worsnop, “*Chemical Compositions of Black Carbon Particle Cores and Coatings via Soot Particle Aerosol Mass Spectrometry with Photoionization and Electron Ionization*,” *J. Phys. Chem. A.*, DOI: [10.1021/jp510711u](https://doi.org/10.1021/jp510711u) (2015, accepted)
- G. T. Buckingham, T. K. Ormond, J. P. Porterfield, P. Hemberger, O. Kostko, M. Ahmed, D. J. Robichaud, M. R. Nimlos, J. W. Daily, and G. B. Ellison, “*The thermal decomposition of the benzyl radical in a heated micro-reactor: I. Experimental findings*,” *J. Chem. Phys.*, **142**, 044307, DOI: [10.1063/1.4906156](https://doi.org/10.1063/1.4906156) (2015)
- T. Nah, H. Zhang, D. R. Worton, C. Ruehl, B. B. Kirk, A. Goldstein, S. R. Leone, and K. R. Wilson, “*Isomeric Product Detection in the Heterogeneous Reaction of Hydroxyl Radicals with Aerosol Composed of Branched and Linear Unsaturated Organic Molecules*,” *J. Phys. Chem. A*, **118**, 11555, DOI: [10.1021/jp508378z](https://doi.org/10.1021/jp508378z) (2014)
- D. M. Popolan-Vaida, S. R. Leone, and K. R. Wilson, “*Reaction of Iodine Atoms with Submicrometer Squalane and Squalene Droplets: Mechanistic Insights into Heterogeneous Reactions*,” *J. Phys. Chem. A*, **118**, 10688, DOI: [10.1021/jp5085247](https://doi.org/10.1021/jp5085247) (2014)
- M. R. Canagaratna, J. L. Jimenez, J. H. Kroll, Q. Chen, S. H. Kessler, P. Massoli, L. Hildebrandt Ruiz, E. Fortner, L. R. Williams, K. R. Wilson, J. D. Surratt, N. M. Donahue, J. T. Jayne, and D. R. Worsnop, “*Elemental ratio measurements of organic compounds using aerosol mass spectrometry: characterization, improved calibration, and implications*”, *Atmos. Chem. Phys. Discuss*, **14**, 19791, DOI: [10.5194/acpd-14-19791-2014](https://doi.org/10.5194/acpd-14-19791-2014) (2014)
- D. S. N. Parker, R. I. Kaiser, T. P. Troy, O. Kostko, M. Ahmed, and A. M. Mebel, “*Toward the Oxidation of the Phenyl Radical and Prevention of PAH Formation in Combustion Systems*,” *J. Phys. Chem. A.*, DOI: [10.1021/jp509170x](https://doi.org/10.1021/jp509170x) (2014, accepted)
- K. O. Johansson, J. Y. W. Lai, S. A. Skeen, K. R. Wilson, N. Hansen, A. Violi, and H. A. Michelsen, “*Soot Precursor Formation and Limitations of the Stabilomer Grid*,” *Proc. Combust. Inst.*, DOI: [10.1016/j.proci.2014.05.033](https://doi.org/10.1016/j.proci.2014.05.033) (2014, in press)
- D. S. N. Parker, R. I. Kaiser, T. P. Troy, and M. Ahmed, “*Hydrogen Abstraction-Acetylene Addition Revealed*,” *Angew. Chem. Int. Ed.*, **53**, 7740, DOI: [10.1002/anie.201404537](https://doi.org/10.1002/anie.201404537) (2014)
- T. Nah, S. H. Kessler, K. E. Daumit, J. H. Kroll, S. R. Leone, and K. R. Wilson, “*The influence of molecular structure and chemical functionality on the heterogeneous OH-initiated oxidation of unsaturated organic particles*,” *J. Phys. Chem. A*, **118**, 4106, DOI: [10.1021/jp502666g](https://doi.org/10.1021/jp502666g) (2014)
- D. R. Worton, G. Isaacman, D. R. Gentner, T. R. Dallmann, A. W. H. Chan, C. Ruehl, T. W. Kirchstetter, K. R. Wilson, R. A. Harley, and A. H. Goldstein, “*Lubricating oil dominates primary organic aerosol emissions from motor vehicles*,” *Environ. Sci. Technol.*, **48**, 3698, DOI: [10.1021/es405375j](https://doi.org/10.1021/es405375j) (2014)
- N. Hansen, S. A. Skeen, H. A. Michelsen, K. R. Wilson, and K. Kohse-Höinghaus, “*Flame Experiments at the Advanced Light Source: New Insights into Soot Formation Processes*,” *J. Vis. Exp.* **87**, doi:10.3791/51369 (2014)
- K. R. Kolesar, G. Buffaloe, K. R. Wilson, and C. D. Cappa, “*OH-Initiated Heterogeneous Oxidation of Internally-Mixed Squalane and Secondary Organic Aerosol*,” *Environ. Sci. Technol.*, **48**, 3196 (2014)
- H. Zhang, C. Ruehl, A. Chan, T. Nah, D. Worton, G. Isaacman, A. Goldstein, and K. R. Wilson, “*OH- Initiated Heterogeneous Oxidation of Cholestane: A Model System for Understanding the Photochemical Aging of Cyclic Alkane Aerosols*,” *J. Phys. Chem. A*, **117**, 12449 (2013)

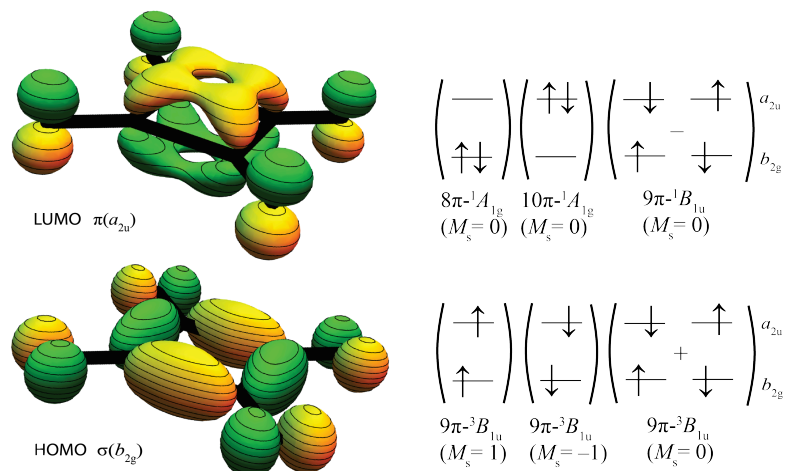
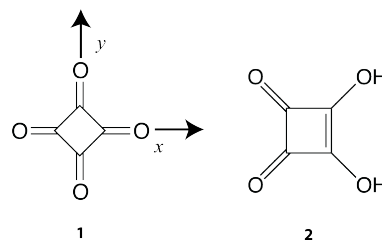
- T. Nah, S. H. Kessler, K. E. Daumit, J. H. Kroll, S. R. Leone and K. R. Wilson, "[OH-initiated oxidation of sub-micron unsaturated fatty acid particles](#)," *Phys. Chem. Chem. Phys.*, **15**, 18649 (2013)
- K. N. Urness, A. Golan, J. W. Daily, M. R. Nimlos, J. F. Stanton, M. Ahmed, and G. B. Ellison, "[Pyrolysis of Furan in a Microreactor](#)," *J. Chem. Phys.*, **139**, 124305 (2013)
- F. Bell, Q. N. Ruan, A. Golan, P. R. Horn, M. Ahmed, S. R. Leone, and M. Head-Gordon, "[Dissociative Photoionization of Glycerol and its Dimer Occurs Predominantly via a Hydrogen-Bonded Ion Complex](#)," *J. Am. Chem. Soc.*, **135**, 14229 (2013)
- A. W. H. Chan, G. Isaacman, K. R. Wilson, D. R. Worton, C. R. Ruehl, T. Nah, D. R. Gentner, T. R. Dallman, T. W. Kirchstetter, R. A. Harley, J. B. Gilman, W. C. Kuster, J. A. de Gouw, J. H. Offenberg, T. E. Kleindienst, Y. H. Lin, C. L. Rubitschun, J. D. Surratt, and A. H. Goldstein, "[Detailed Chemical Characterization of Unresolved Complex Mixtures \(UCM\) in Atmospheric Organics: Insights into Emission Sources, Atmospheric Processing and Secondary Organic Aerosol Formation](#)," *J. Geophys. Res., [Atmos.]* **118**, 6783 (2013)
- C. R. Ruehl, T. Nah, G. Isaacman, D. R. Worton, A. W. H. Chan, K. R. Kolesar, C. D. Cappa, A. H. Goldstein, and K. R. Wilson, "[The influence of molecular structure and aerosol phase on the heterogeneous oxidation of normal and branched alkanes by OH](#)," *J. Phys. Chem. A.*, **117**, 3990 (2013)
- S. A. Skeen, H. A. Michelsen, K. R. Wilson, D. M. Popolan, A. Violi, and N. Hansen, "[Near-threshold Photoionization Mass Spectra of Combustion-Generated High-Molecular-Weight Soot Precursors](#)," *J. Aerosol Sci.*, **58**, 86 (2013)
- L. Lee, P. Wooldridge, T. Nah, K. R. Wilson, and R. Cohen, "[Observation of Rates and Products in the Reaction of NO₃ with Submicron Squalane Aerosol](#)," *Phys. Chem. Chem. Phys.*, **15**, 882 (2013)
- A. Golan, M. Ahmed, A. M. Mebel, and R. I. Kaiser, "[A VUV photoionization study of the multichannel reaction of phenyl radicals with 1,3-butadiene under combustion relevant conditions](#)," *Phys. Chem. Chem. Phys.*, **15**, 341 (2013)
- D. Gentner, G. Isaacman, D. R. Worton, A. W. H. Chan, T. R. Dallmann, L. Davis, S. Liu, D. A. Day, L. M. Russell, K. R. Wilson, R. Weber, A. Guha, R. A. Harley, and A. H. Goldstein, "[Elucidating Secondary Organic Aerosol From Diesel and Gasoline Vehicles Through Detailed Characterization of Organic Carbon Emissions](#)," *PNAS.*, **109**, 18318 (2012)
- A. Golan and M. Ahmed, "[Molecular beam mass spectrometry with tunable vacuum ultraviolet \(VUV\) synchrotron radiation](#)," *J. Vis. Exp.*, **68**, e50164 (2012)
- A. G. Vasiliou, K. M. Piech, B. Reed, X. Zhang, M. R. Nimlos, M. Ahmed, A. Golan, O. Kostko, D. L. Osborn, J. W. Daily, J. F. Stanton, and G. B. Ellison, "[Thermal Decomposition of CH₃CHO Studied by Matrix Infrared Spectroscopy and Photoionization Mass Spectroscopy](#)," *J. Chem. Phys.*, **137**, 164308 (2012)
- G. Isaacman, A. W. H. Chan, T. Nah, D. R. Worsnop, C. R. Ruehl, K. R. Wilson, and A. Goldstein, "[Heterogeneous OH oxidation of motor oil particles causes selective depletion of branched and less cyclic hydrocarbons](#)," *Environ. Sci. Technol.*, **46**, 10632 (2012)
- J. H. Kroll, J. D. Smith, D. R. Worsnop, and K. R. Wilson, "[Characterisation of lightly oxidized organic aerosol formed from the photochemical aging of diesel exhaust particles](#)," *Environ. Chem.*, **9**, 211 (2012)
- F. Zhang, R.I. Kaiser, A. Golan, M. Ahmed and N. Hansen, "[A VUV Photoionization Study of the Combustion-Relevant Reaction of the Phenyl Radical \(C₆H₅\) with Propylene \(C₃H₆\) in a High Temperature Chemical Reactor](#)," *J. Phys. Chem. A.*, **116**, 3541 (2012)
- S. H. Kessler, T. Nah, K. E. Daumit, J. D. Smith, S. R. Leone, C. E. Kolb, D. R. Worsnop, K. R. Wilson, and J. H. Kroll, "[OH-initiated heterogeneous aging of highly oxidized organic aerosol](#)," *J. Phys. Chem. A.*, **116**, 6358 (2012)
- G. Isaacman, K. R. Wilson, A. W. H. Chan, D. R. Worsnop, J. R. Kimmel, T. Nah, T. Hohaus, M. Gonin, J. H. Kroll, D. R. Worsnop, and A. H. Goldstein, "[Improved resolution of hydrocarbon structures and constitutional isomers in complex mixtures using Gas Chromatography-Vacuum Ultraviolet-Mass Spectrometry \(GC-VUV-MS\)](#)," *Anal. Chem.*, **84**, 2335 (2012)
- F. Goulay, A. J. Trevitt, J. D. Savee, J. Bowman, D. L. Osborn, C. A. Taatjes, K. R. Wilson, and S. R. Leone, "[Product Detection of the CH Radical Reaction with Acetaldehyde](#)," *J. Phys. Chem. A.*, **116**, 6091 (2012)
- K. R. Wilson, J. D. Smith, S. H. Kessler, and J. H. Kroll, "[The Statistical Evolution of Multiple Generations of Oxidation Products in the Photochemical Aging of Chemically Reduced Organic Aerosol](#)," *Phys. Chem. Chem. Phys.*, **14**, 1468 (2012)
- D. Ghosh, A. Golan, L. K. Takahashi, A. I. Krylov, and M. Ahmed, "[A VUV Photoionization and Ab Initio Determination of the Ionization Energy of a Gas Phase Sugar \(Deoxyribose\)](#)," *J. Phys. Chem. Lett.*, **3**, 97 (2012)

Theoretical Studies of Elementary Hydrocarbon Species and Their Reactions

Wesley D. Allen and Henry F. Schaefer III
 Center for Computational Quantum Chemistry and Department of Chemistry
 University of Georgia, Athens, GA 30602-2525
 E-mail: wdallen@uga.edu and ccq@uga.edu; Phone: (706) 542-7729

Cyclobutanetetraone: An Unusual Cluster of Low-Lying Electronic States

Cyclobutane-1,2,3,4-tetraone (**1**) is a beautifully symmetric, cyclic species that may be regarded as a tetramer of carbon monoxide. Experimental efforts to synthesize and isolate **1** have not been successful heretofore; nonetheless, the molecule was recently probed by low-temperature photoelectron spectroscopy of the $C_4O_4^-$ anion generated in the gas phase by electrospray ionization of **2**. Remarkably, the photoelectron spectrum of $C_4O_4^-$ provided assignments for either two or three low-lying electronic states of the seemingly simple neutral molecule **1**. The theoretical characterization of **1** has proved difficult due to surprising complexities in its electronic structure. Identifying the electronic ground state and quantifying the singlet-triplet gaps of **1** has turned out to be a treacherous task for theory. Not only have different methods predicted different ground states, but computed energetic spacings have also varied by almost 100 kcal mol⁻¹!



The troublesome electronic structure of cyclobutanetetraone (Figure 1) demands theoretical work using groundbreaking multireference or state-of-the-art high-order single-reference coupled cluster methods. Research in our laboratory over the past several years has developed Mk-MRCC theory into a powerful and practical computational method. This approach is a rigorously size-extensive, state-specific theory that retains the size-consistent property of coupled cluster theory when localized orbitals are used; in addition, Mk-MRCC treats all determinants on an equal footing via the Jeziorski-Monkhurst *ansatz*.

We have optimized the geometric structures of the low-lying states of **1** and computed corresponding vibrational frequencies by means of Mk-MRCCSD/cc-pVQZ, Mk-MRCCSD(T)/cc-pVDZ, and CCSD(T)/cc-pVQZ theory.¹⁴ Systematic focal-point analyses (FPA) were then executed to ascertain final adiabatic electronic excitation energies of **1**, as shown in Table 1. A consistent picture emerges in both the single- and multireference results once the correlation series are pushed to the (T) level. In particular, the ground state of **1** is actually a triplet ($9\pi^{-3}B_{1u}$), while the expected closed-shell singlet candidate ($8\pi^{-1}A_{1g}$) lies over 3 kcal mol⁻¹ higher. The FPA computations reveal that the quadruples effect (Q) brings the $9\pi^{-1}B_{1u}$ and $10\pi^{-1}A_{1g}$ states within 2 kcal mol⁻¹ of $8\pi^{-1}A_{1g}$. The summary conclusion is that **1** has a fascinating cluster of four electronic states lying within a 6 kcal mol⁻¹ range.

Table 1. Adiabatic excitation energies (ΔE_0 , kcal mol⁻¹) of cyclobutanetetraone^a

Method	8 π - ¹ A _{1g}	9 π - ³ B _{1u}	9 π - ¹ B _{1u}	10 π - ¹ A _{1g}
Mk-MRCCSD/cc-pVDZ	0	3.74 ^b	10.81	21.98
Mk-MRCCSD/cc-pVTZ	0	4.10 ^b	10.40	22.98
Mk-MRCCSD/cc-pVQZ	0	4.15 ^b	10.17	22.95
Mk-MRCCSD(T)/cc-pVDZ	0	-3.30 ^b	3.11	3.03
CCSD/cc-pVDZ	0	3.41	c	21.06
CCSD/cc-pVQZ	0	3.82	c	22.08
CCSD(T)/cc-pVDZ	0	-3.61	c	2.26
CCSD(T)/cc-pVQZ	0	-3.50	c	2.69
FPA/CCSDT(Q) ^d	0	-4.34	1.61	1.00

^a Including ZPVE corrections: CCSD(T)/cc-pVQZ values of (-0.62, -1.08) for (9 π -³B_{1u}, 10 π -¹A_{1g}) in single-reference cases; Mk-MRCCSD/cc-pVQZ values of (-0.54, -0.64, -1.18) for (9 π -³B_{1u}, 9 π -¹B_{1u}, 10 π -¹A_{1g}) in multireference cases. ^b Results for M_s = 0 component of the triplet state; the corresponding M_s = 1 values are 3.75, 4.09, 4.15, and -3.33 kcal mol⁻¹, from top to bottom. ^c Not accessible by single-reference coupled-cluster method. ^d Focal-point analysis targeting the complete basis set (CBS) limit of CCSDT(Q) with auxiliary core correlation, relativistic, and DBOC corrections.

Peroxyacetyl Radical: Electronic Excitation Energies, Fundamental Vibrational Frequencies, and Symmetry Breaking in the First Excited State

Fundamental understanding of peroxy radicals (RO₂), key components in the oxidation of organic compounds at low temperatures, is limited by the transient nature of these compounds. Experimental monitoring of peroxy radicals often relies on either the strong, but broad and uninformative, $\tilde{B} \leftarrow \tilde{X}$ transition, or the sharp and weak $\tilde{A} \leftarrow \tilde{X}$ transition. Miller has advanced the use of the latter excitation through cavity ringdown techniques [*Phys. Chem. Chem. Phys.* **2008**, 10, 3955].

The peroxyacetyl radical [CH₃C(O)O₂] is a model compound that is among the most abundant peroxy radicals in the atmosphere. To support spectroscopic studies on this species, we have undertaken a high-level *ab initio* study of the ground (\tilde{X}) and first (\tilde{A}) excited state surfaces of CH₃C(O)O₂.²⁰ The energetics (Figure 2) have been determined using coupled-cluster theory through full triple excitations (CCSDT), extrapolated to the complete basis set (CBS) limit via the focal-point scheme and corrected for vibrational, diagonal Born-Oppenheimer, and relativistic effects. On the ground-state surface, internal rotation of the peroxy terminus yields *cis* and *trans* conformers lying 0.87 kcal mol⁻¹ apart (*cis* < *trans*) with an intervening barrier of 5.14 kcal mol⁻¹ (relative to *trans*). Adiabatic $\tilde{A} \leftarrow \tilde{X}$ electronic excitation energies of 13.96 and 16.04 kcal mol⁻¹ are predicted for the *trans* and *cis* conformers, respectively. The observed *cis* $\tilde{A} \leftarrow \tilde{X}$ excitation energy is within 0.08 kcal mol⁻¹ of our computed value. Interestingly, excitation of the *trans* conformer induces a symmetry-lowering conformational change caused by second-order Jahn-Teller interactions with higher-lying excited states, which we verify using multireference configuration interaction (MRCI) and equation-of-motion coupled-cluster (EOM-CC) computations. This finding resolves the curious absence of an observable $\tilde{A} \leftarrow \tilde{X}$ transition from the *trans* conformer in experimental studies, despite the fact that both conformers have been observed in ground-state

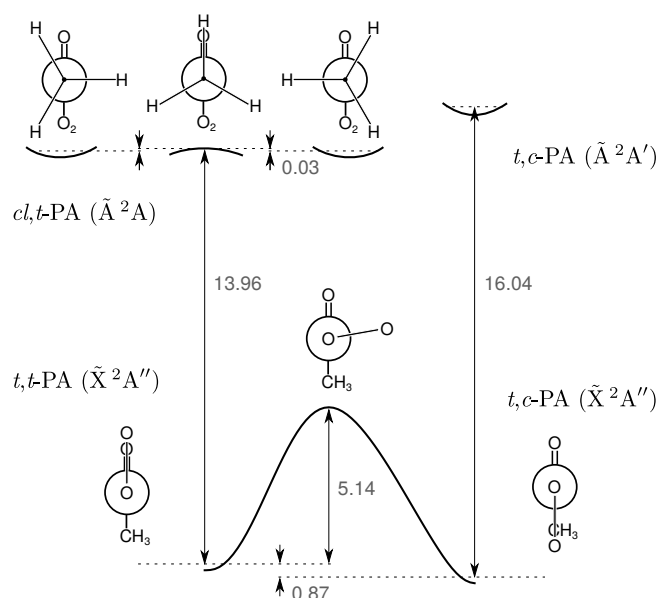


Figure 2. Key energetic relationships (in kcal mol⁻¹) between conformers on the ground and first excited state surfaces of peroxyacetyl radical.

vibrational spectra. Also determined in our study are anharmonic vibrational frequencies for the two ground-state minima, computed using CCSD(T) theory with second-order vibrational perturbation theory (VPT2). The available gas-phase and matrix-isolation IR data are in excellent agreement with our predictions.

Reaction profiles for radical-radical abstraction via multireference coupled cluster theory

Radical-radical hydrogen abstractions in combustion chemistry are disproportionation reactions that are generally exothermic with little or no barrier, yet are underappreciated and poorly studied. Prototypically these reactions begin with two open-shell reactants and end with two closed-shell products, and thus the electronic transformation is intrinsically multireference in nature. Such challenging electronic structure problems have been tackled using our recently developed state-specific multireference coupled cluster methods Mk-MRCCSD and Mk-MRCCSD(T), as well as the companion perturbation theory Mk-MRPT2 and the popular MRCISD, MRCISD+Q, and CASPT2 approaches.¹³ Reaction paths were investigated for five prototypes involving radical-radical hydrogen abstraction: $\text{H} + \text{BeH} \rightarrow \text{H}_2 + \text{Be}$, $\text{H} + \text{NH}_2 \rightarrow \text{H}_2 + \text{NH}$, $\text{CH}_3 + \text{C}_2\text{H}_5 \rightarrow \text{CH}_4 + \text{C}_2\text{H}_4$, $\text{H} + \text{C}_2\text{H}_5 \rightarrow \text{H}_2 + \text{C}_2\text{H}_4$, and $\text{H} + \text{HCO} \rightarrow \text{H}_2 + \text{CO}$. Selected results are plotted in Figures 3 and 4. Full configuration interaction (FCI) benchmark computations for the $\text{H} + \text{BeH}$, $\text{H} + \text{NH}_2$, and $\text{H} + \text{HCO}$ reactions prove that the Mk-MRCCSD(T) potential energy curves display superior accuracy, with mean absolute errors of only $0.2 \text{ kcal mol}^{-1}$. To facilitate studies of combustion kinetics in collaboration with Stephen Klippenstein and Larry Harding at Argonne, energetics for the $\text{CH}_3 + \text{C}_2\text{H}_5$, $\text{H} + \text{C}_2\text{H}_5$, and $\text{H} + \text{HCO}$ reactions were computed at each level of theory with correlation-consistent basis sets (cc-pVXZ, $X = \text{T, Q, 5}$) and extrapolated to the complete basis set (CBS) limit. The rigorous Mk-MRCCSD(T)/CBS results demonstrate unequivocally that these three reactions proceed with no barrier in the entrance channel, contrary to some earlier predictions. Mk-MRCCSD(T) also reveals that the economical CASPT2 method performs well for large interfragment separations but may deteriorate substantially at shorter distances.

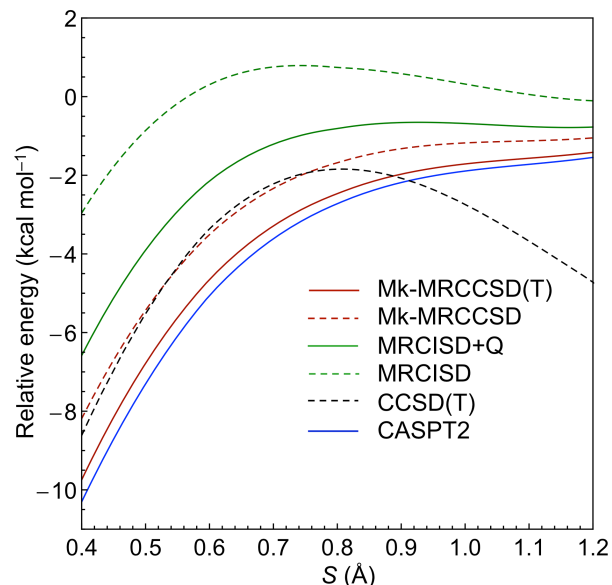


Figure 3. Potential energy curves for the $\text{CH}_3 + \text{C}_2\text{H}_5$ entrance channel computed at numerous levels and extrapolated to the CBS limit. The reaction coordinate S is the difference between C–H distances of the forming and breaking bonds.

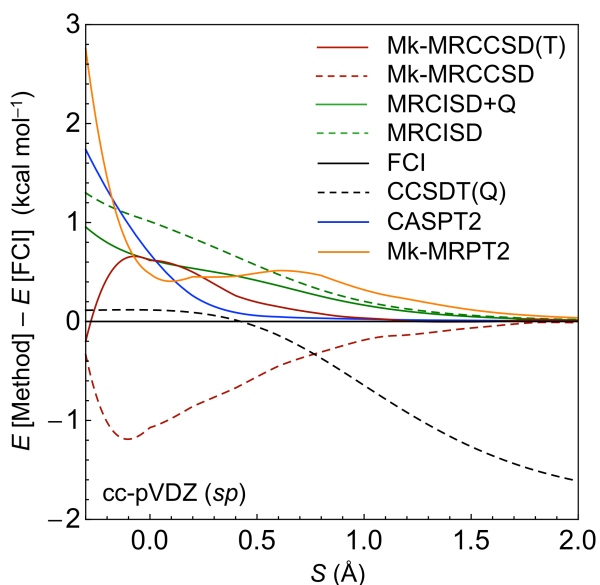


Figure 4. For the entrance channel of $\text{H} + \text{HCO}$, energy deviations are plotted with respect to FCI for different levels of theory with the cc-pVDZ(*sp*) basis set.

Implementing an Explicitly Correlated Hamiltonian in Psi4

Canonical transcorrelated (CT) theory has recently been introduced as an alternative to conventional explicitly correlated F12 methods. In CT theory an effective Hamiltonian is constructed to incorporate explicit electron correlation via similarity transformation of the electronic Hamiltonian; the infinite Baker-Campbell-Hausdorff (BCH) expansion is truncated at second order in perturbation theory. The power of this approach is that it only requires the one- and two-particle reduced density matrices of the reference wave function, and the effective Hamiltonian can be applied to existing electron correlation implementations to obtain energies near the basis set limit. To achieve an

efficient implementation of CT theory in our Psi4 software package, we are developing a new tensor wrapper framework, called *Ambit*, deriving the necessary gradients for molecular properties around the equilibrium geometry, and creating interfaces within Psi4 to allow other developers to utilize these tools. *Ambit* provides the ability to cache tensors to disk and perform efficient tensor stripping to make use of local scratch space.

Recent Publications Supported by DOE

1. S. R. Barua, W. D. Allen, E. Kraka, P. Jerabek, R. Sure, and G. Frenking, "Nearly Degenerate Isomers of C(BH)₂: Cumulene, Carbene, or Carbone?" *Chem. Eur. J.* **19**, 15941 (2013).
2. A. Yu. Sokolov, D. B. Magers, J. I. Wu, W. D. Allen, P. v. R. Schleyer and H. F. Schaefer, "Free Cyclooctatetraene Dianion: Planarity, Aromaticity, and Theoretical Challenges," *J. Chem. Theory Comput.* **9**, 4436 (2013).
3. T. Liang, D. B. Magers, P. L. Raston, W. D. Allen, and G. E. Doublerly, "Dipole Moment of the HOOO Radical: Resolution of a Structural Enigma," *J. Phys. Chem. Lett.* **4**, 3584–3589 (2013).
4. D. S. Hollman, H. F. Schaefer, and E. F. Valeev, "Semi-Exact Concentric Atomic Density Fitting: Reduced Cost and Increased Accuracy Compared to Standard Density Fittings," *J. Chem. Phys.* **140**, 064109 (2014).
5. Q. Fan, H. Feng, W. Sun, Y. Xie, C.-H. Wu, W. D. Allen, and H. F. Schaefer, "The Li⁺-HF van der Waals Minimum and the Barrier to the Deep HF–Li Potential Well," *Mol. Phys.* **112**, 770 (2014).
6. Y. Hao, J. Gu, Y. Guo, M. Zhang, Y. Xie, and H. F. Schaefer, "Spin-Orbit Corrected Potential Energy Surface Features for the I (²P_{3/2}) + H₂O → HI + OH Forward and Reverse Reactions," *Phys. Chem. Chem. Phys.* **16**, 2641 (2014).
7. X. Feng, J. Gu, Q. Chen, Y. Xie, and H. F. Schaefer, "How Small Can a Catenane Be?" *J. Chem. Theory Comput.* **10**, 1511 (2014).
8. S. R. Barua, H. Quanz, M. Olbrich, P. R. Schreiner, D. Trauner, and W. D. Allen, "Polytwistane," *Chem. Eur. J.* **20**, 1638 (2014).
9. G. Li, H. Wang, Q.-S. Li, Y. Xie, and H. F. Schaefer, "The Exothermic HCl + OH• (H₂O) Reaction. Removal of the HCl + OH Barrier by a Single Water Molecule," *J. Chem. Phys.* **140**, 124316 (2014).
10. X. Wang, W. E. Turner, J. Agarwal, and H. F. Schaefer, "Twisted Triplet Ethylene: Interpretation of Rotational and Vibrational Spectra," *J. Phys. Chem.* **118**, 7560 (2014).
11. J. D. Mosley, J. W. Young, J. Agarwal, H. F. Schaefer, P. v. R. Schleyer, and M. D. Duncan, "Structural Isomerization of the Gas Phase 2-Norbornyl Cation Revealed with Infrared Spectroscopy and Computational Chemistry," *Angew. Chem. Int. Ed.* **53**, 5888 (2014).
12. C. Li, J. Agarwal, C.-H. Wu, W. D. Allen, and H. F. Schaefer, "The Intricate Internal Rotation Surface and Fundamental Vibrations of the *n*-Propyl Radical," *J. Phys. Chem. B* **119**, 728 (2015).
13. C. -H. Wu, D. B. Magers, L. B. Harding, S. J. Klippenstein, and W. D. Allen, "Reaction profiles for radical-radical hydrogen abstraction via multireference coupled cluster theory," *J. Chem. Theory Comput.* (2014).
14. A. E. Vaughn, D. S. Greco, C. A. Parish, and W. D. Allen, "Cyclobutanetetraone: An Unusual Cluster of Low-Lying Electronic States," *J. Chem. Theory Comput.* (2014).
15. W. C. McKee, J. Agarwal, H. F. Schaefer, and P. R. Schleyer, "Covalent Hypercoordination: Can Carbon Bind Five Methyl Ligands?" *Angew. Chem. Int. Ed.* **53**, 7875 (2014).
16. M. Zhang, Y. Guo, Y. Xie, and H. F. Schaefer, "Anchoring the Potential Energy Surface for the Br + H₂O → HBr + OH Reaction," *Theoretical Chem. Accounts* **133**, 1513 (2014).
17. T. Zeng, H. Wang, Y. Lu, Y. Xie, H. Wang, H. F. Schaefer, N. Ananth, and R. Hoffmann, "Tuning Spin-States of CR and SiR: A Long Jump with One Leg," *J. Am. Chem. Soc.* **136**, 13388 (2014).
18. Y. Hao, Y. Xie, and H. F. Schaefer, "Features of the Potential Energy Surface for the SiO + OH → SiO₂ + H Reaction: Relationship to Oxygen Isotopic Partitioning During Gas Phase SiO₂ Formation," *RSC Advances* **4**, 47163 (2014).
19. C. M. Leavitt, K. Moore, P. L. Raston, J. Agarwal, G. Moody, C. Shirley, H. F. Schaefer, and G. E. Doublerly, "Liquid Hot NAGMA Cooled to 0.4 Kelvin: Benchmark Thermochemistry of a Gas-Phase Peptide," *J. Phys. Chem. A* **118**, 9692 (2014).
20. A. V. Copan, A. E. Wiens, E. M. Nowara, H. F. Schaefer, and J. Agarwal, *J. Chem. Phys.* **142**, 054303 (2015).

Turbulence-Chemistry Interactions in Reacting Flows

Robert S. Barlow
Combustion Research Facility
Sandia National Laboratories, MS 9051
Livermore, California 94550
barlow@sandia.gov

Program Scope

This program is directed toward achieving a more complete understanding of turbulence-chemistry interactions in gaseous flames and providing detailed measurements for validation of combustion models. In the Turbulent Combustion Laboratory (TCL) simultaneous line imaging of spontaneous Raman scattering, Rayleigh scattering, and two-photon laser-induced fluorescence (LIF) of CO is applied to obtain spatially and temporally resolved measurements of temperature, the concentrations of all major species, mixture fraction, and reaction progress, as well as gradients in these quantities in hydrocarbon flames. The instantaneous three-dimensional orientation of the turbulent reaction zone is also measured by imaging of OH LIF or Rayleigh scattering at 355 nm in two crossed planes, which intersect along the laser axis for the multiscale measurements. These combined data characterize both the thermo-chemical state and the instantaneous flame structure, such that the influence of turbulent mixing on flame chemistry may be quantified. Our experimental work is closely coupled with international collaborative efforts to develop and validate predictive models for turbulent combustion. This is accomplished through our visitor program and through the TNF Workshop series. In recent years the workshop and this program have expanded their scope to address a broad range of combustion modes, including premixed, stratified, partially premixed, and nonpremixed flames. We are also working to extend our quantitative multiscale diagnostics to more complex hydrocarbon fuels. Entry into these new research areas has prompted developments in both hardware and methods of data analysis to achieve unprecedented spatial resolution and precision of multiscale measurements. Within the CRF we collaborate with Jonathan Frank, who applies advanced imaging diagnostics to turbulent flames, and with Joe Oefelein, who performs high fidelity large-eddy simulations (LES) of our experimental flames in order to gain greater fundamental understanding of the dynamics of multi-scale flow-chemistry interactions.

Recent Progress

Raman Spectroscopy of Hydrocarbon Combustion Intermediates

We have been working toward quantitative Raman/Rayleigh measurements in dimethyl ether (DME) flames. Earlier work by Fuest et al. (*Combust. Flame* 159, 2533–2562, 2012) showed that it is essential to account for the contributions of the main hydrocarbon intermediates to the Raman and Rayleigh signals and presented an approximate approach for processing Raman/Rayleigh data from turbulent DME jet flames, based upon an assumed laminar structure. More recently, we have been developing the spectroscopic data base and hardware to enable direct quantitative measurements of multiple hydrocarbons, including DME and its main hydrocarbon intermediates (CH_4 , CH_2O , C_2H_6 , C_2H_4 , and C_2H_2).

The Raman scattering spectrum corresponding to the C-C triple bond vibration (1973.8 cm^{-1}) of acetylene is isolated from that of other species of interest, allowing for a relatively straightforward extension of previously developed methods of data acquisition and processing. This is made possible by the high optical collection efficiency of our system. Fuest et al. (*Combust. Flame*, in press) report measurements of the acetylene in laminar and turbulent jets flames of DME. The temperature dependence of the Raman scattering cross section for acetylene was measured within the range of 300 K to 700 K and then extrapolated to flame temperature using a modified harmonic oscillator model. Figure 1 compares measurements in a laminar jet flame with calculations (Chemkin, Zhou et al. mechanism, multicomponent transport) of an opposed-flow flame at a strain rate selected to match the measured temperature profile. A signal-to-noise ratio of 9 was achieved in the laminar flame where the maximum mole fraction is below 1 percent. Further work is needed to understand the discrepancy between the measured and calculated C_2H_2 profiles.

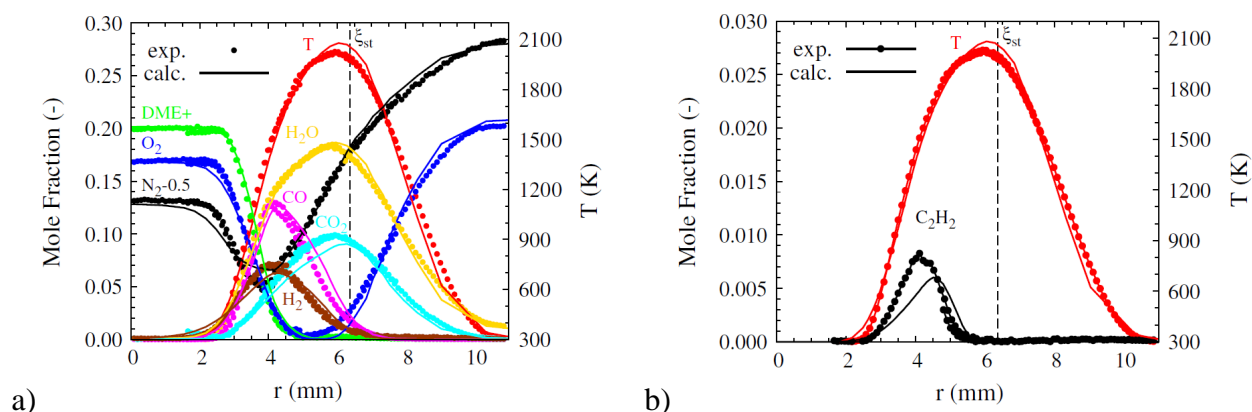


Figure 1. a) Spatial profiles of temperature and major species measured in a laminar partially-premixed DME/air jet flame and calculated in an opposed flow flame with strain rate adjusted to match the width of the measured temperature profile. b) Corresponding profiles of acetylene.

Quantitative interpretation of Raman scattering signals from DME and the other four intermediates listed above is significantly more complex than for acetylene because their spectra overlap in the C-H stretch region ($2700\text{--}3100\text{ cm}^{-1}$) and also interfere to varying degrees with the CO_2 and O_2 Raman signals in the H-C-H bend and C-C stretch regions. Magnotti et al. (JQSRT accepted) report measured high-resolution Raman scattering spectra of DME, CH_4 , C_2H_4 , C_2H_6 , and C_3H_8 at temperatures from 300 K to 860 K, along with preliminary (uncalibrated) measurements of formaldehyde Raman spectra. From these measurements, synthetic spectral libraries were generated in order to allow inclusion of these species in our hybrid matrix inversion method of Raman data processing (Fuest et al., *Proc. Combust. Inst.* 33, 815–822, 2011). Extrapolation of the synthetic spectra to higher temperature is being done based on measurements in laminar flames and comparison with calculations. These flame measurements are being carried out using a recently-developed dual-resolution capability for simultaneous Raman measurements of multiple hydrocarbons. Our second detection system, which was built for the polarization separation and subtraction measurements introduced at the 2014 Contractors Meeting, was reconfigured to acquire measurements of the C-H stretch region of the Raman spectrum using a high-dispersion grating (Fig. 2a). This dual resolution approach yields significantly better spectral separation of the main features of the individual hydrocarbon species, as shown in Fig. 2b.

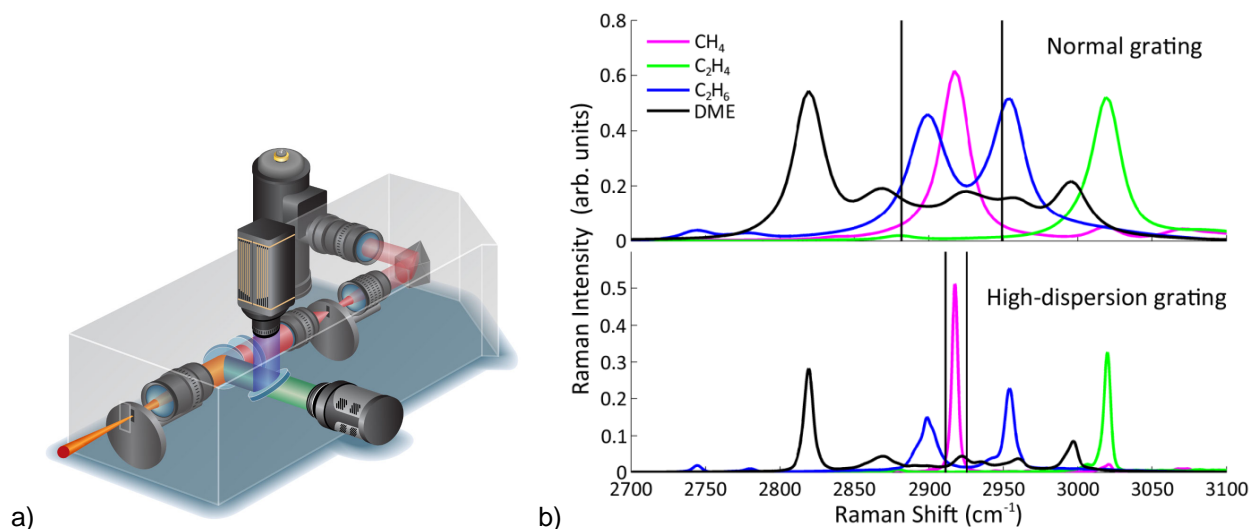


Figure 2. a) Illustration of the second Raman/Rayleigh/LIF detection unit configured with a high-dispersion grating to allow dual-resolution measurements of the C-H stretch region. b) Comparison of Raman spectra of CH₄, C₂H₄, C₂H₆, and DME acquired using the two systems. In both cases the Raman spectra are convolved with the image of our laser beam.

Multi-mode Combustion in Inhomogeneous Piloted Jet Flames

It is common in practical systems to have multiple combustion modes present within a single combustor, so predictive models must be able to handle both premixed-type flames and diffusion-type flames in the same calculation. A new variant of the Sydney piloted burner addresses the need for model test cases that exhibit multimode combustion in a configuration with relatively simple boundary conditions. This new burner has a retractable 4-mm diameter fuel tube within the main tube ($D = 7.5$ mm) that delivers air for partial premixing. The stability of the jet flame is significantly enhanced when the fuel tube is retracted an optimal distance. Raman/Rayleigh/LIF measurements have revealed that the optimally stable flames are characterized by stratified-premixed combustion and low scalar dissipation very close to the burner exit. The resulting additional heat release augments the effect of the pilot and also suppresses the production of turbulence in the near-field shear layer. The mode of combustion then rapidly evolves from a stratified-premixed flame structure toward a partially-premixed diffusion flame structure. This evolution has been tracked by applying double conditioning of species mass fractions on both temperature and the change in mixture fraction across the middle portion of the flame (from 700 K to 1700 K). The evolution to diffusion-type flame structure is essentially complete by $x/D = 10$. The presence of multimode combustion within a relatively compact region of a flame that has relatively simple boundary conditions should make this series of turbulent jet flames an interesting target for combustion models, and the comprehensive data set is already being made available to several modeling groups.

Future Plans

Priorities for the next year are to: i) complete the development hydrocarbon spectral libraries and apply the dual-resolution Raman method to obtain direct single-shot measurements of stable hydrocarbon intermediates along with all major species in the series of turbulent DME jet flames that were developed by J. Frank and previously studied using approximations to account for

hydrocarbon intermediates; ii) obtain additional measurements in the near field of piloted jet flames with inhomogeneous inlets, using our spatial oversampling and wavelet denoising techniques; iii) apply our latest methods to selected cases of the Sydney bluff body flames, which have been an important model test case but have only pointwise scalar data from 1995 and; iv) bring online a programmable pulsewidth Nd:YAG laser that will allow measurements of enclosed flames.

BES Supported Publications (2013 - present)

Dunn, M.J.; Barlow, R.S.; Effects of preferential transport and strain in bluff body stabilized lean and rich premixed CH₄/air flames, *Proc. Combust. Inst.* **2013**, *34*, 1411-1419.

Sweeney, M.S.; Hochgreb, S.; Dunn, M.J.; Barlow, R.S., Multiply conditioned analyses of stratification in highly swirling methane/air flames, *Combust. Flame* **2013**, *160*, 322–334.

Zhou, R.; Balusamy, S.; Sweeney, M.S.; Barlow, R.S.; Hochgreb, S., Flow field measurements of a series of turbulent premixed and stratified methane/air flames, *Combust. Flame* **2013**, *160*, 2017-2028.

Ma, B.; Wang, G.; Magnotti, G.; Barlow, R.S.; Long, M.B., Intensity-ratio and color-ratio thin-filament pyrometry: Uncertainties and accuracy, *Combust. Flame* **2014**, *161*, 908-916.

Rankin, B.A.; Magnotti, G.; Barlow, R.S.; Gore, J.P., Radiation intensity imaging measurements of methane and dimethyl ether turbulent nonpremixed and partially premixed jet flames, *Combust. Flame* **2014**, *161*, 2849–2859.

Fuest, F.; Magnotti, G.; Barlow, R.S.; Sutton, J.A., Scalar structure of turbulent partially-premixed dimethyl ether/air jet flames, *Proc. Combust. Inst.* **2015**, *35*, 1235–1242.

Meares, S.; Prasad, V.N.; Magnotti, G.; Barlow, R.S.; Masri, A.R., Stabilization of piloted turbulent flames with inhomogeneous inlets, *Proc. Combust. Inst.* **2015**, *35*, 1477–1484.

Magnotti, G.; Geyer, D.; Barlow, R.S., Interference-free spontaneous Raman spectroscopy for measurements in rich hydrocarbon flames, *Proc. Combust. Inst.* **2015**, *35*, 3765–3772.

Magnotti, G.; Barlow, R.S., Effects of high shear on the structure and thickness of turbulent premixed methane/air flames stabilized on a bluff-body burner, *Combust. Flame* **2015**, *162*, 100–114.

Barlow, R.S.; Dunn, M.J.; Magnotti, G., Preferential transport effects in premixed bluff-body stabilized CH₄/H₂ flames, *Combust. Flame* **2015**, *162*, 727–735.

Fuest, F.; Barlow, R.S.; Magnotti, G.; Dreizler, A.; Ekoto, I.W., Sutton, J.A., Quantitative acetylene measurements in laminar and turbulent flames using 1D Raman/Rayleigh scattering, *Combust. Flame* (in press).

Magnotti, G.; KC, U.; Varghese, P.L.; Barlow, R.S., Raman spectra of methane, ethylene, ethane, dimethyl ether, formaldehyde and propane for combustion applications, *JQSRT* (accepted).

TNF Workshop Information: <http://www.sandia.gov/TNF>

TNF12 Summary and Proceedings: <http://www.sandia.gov/TNF/12thWorkshop/TNF12.html>

Predictive Large-Eddy Simulation of Supercritical-Pressure Reactive Flows in the Cold Ignition Regime

Josette Bellan

Mechanical and Civil Engineering Department, California Institute of Technology
Pasadena, CA 91125

Josette.Bellan@jpl.nasa.gov

DOE Award Number: **02_GR-ER16107-14-00**

STRIPES award number: **SC0002679**

I. Program Scope

This study addresses issues highlighted in the Basic Energy Needs for Clean and Efficient Combustion of 21st Century Transportation Fuels (DOE BES, 2006) under the topic of Combustion under Extreme Pressure. It is there noted that “the most basic concepts of thermal autoignition” are “based on experience and theory at near atmospheric pressures” and that “as pressure increases significantly..., many of these conceptual pictures begin to change or disappear”. It is also stated “A better description of the coupling and interaction of high pressure flow and molecular transport processes with chemistry is also necessary”, particularly because “Ignition and flame propagation of alternative and renewable fuels, as well as of the changing feed stocks of conventional fossil-based fuels, are very likely to be much different at very high pressures than under the more familiar, lower pressure conditions of current engines.” Recognizing that “Under such (*increasing pressure*) conditions distinctions between gas and liquid phases become moot, new equations of state must be used...”, it is immediately apparent that there must be “a re-examination of the basic assumptions that govern the physics and chemistry related to combustion; and the need for this type of re-examination increases as the combustion pressure increases.” This recognition is also stated under the topic of Multiscale Modeling since due to the new equations of state “The combination of unexplored thermodynamic environments and new physical and chemical fuel properties results in complex interactions among multiphase (*according to the above, the multiphase distinction becomes moot with increasing pressure*) fluid dynamics, thermodynamic properties, heat transfer, and chemical kinetics that are not understood even at a fundamental level.” From the theoretical viewpoint for “systems at high pressure, fluid dynamic time scales can be comparable to chemical time scales.” and therefore “completely diffusion-controlled reactions ... can become important”.

Thus, the objective of this study is the investigation of the coupling among thermodynamics, transport properties, intrinsic kinetics and turbulence under the high-pressure and the relatively (with respect to combustion) low-temperature conditions typical of the auto-ignition regime, with particular emphasis on the manifestation of this coupling on the effective kinetic rate. As planned, we established collaboration with Dr. Joseph Oefelein of the Combustion Research Facility at Sandia Livermore to work together towards implementing the models developed in this research into the high-pressure Large Eddy Simulation (LES) code (named RAPTOR) under development by him at Sandia.

II. Recent Progress

This report contains results obtained during the last year of funding. The focus of the research during this year was to create a reactive flow Direct Numerical Simulation (DNS) database and analyze it *a priori* so as to understand the mixing/turbulence/reaction coupling in the high-

pressure (“high- p ”) regime. To this end, using our model [i], four DNS realizations were created in the configuration of a temporal mixing layer by varying the initial Reynolds number (Re_0), the free-stream pressure and the initial composition of the two streams; only one of the simulation was initiated with the freestream devoid of traces of CO_2 and H_2O (i.e. Exhaust Gas Recirculation (EGR)). The simulations were ran until each reached transition to turbulence and chemical reactions were initiated in each simulation at its respective transitional time. For the simulation at the larger Re_0 , we used smaller amplitudes of the initial perturbations employed to hasten transition, so as to avoid the computation blowing up; the smaller amplitudes result in a delayed momentum thickness growth (Fig. 1a). Ignition corresponds to the time of peak p (Fig. 1b). A higher free-stream pressure results in earlier ignition and higher p at ignition, at same free-stream pressure (p_0) the pressure at ignition is larger when there is no EGR but the ignition time is the same, and the simulation initiated with the larger Re_0 and smaller perturbation achieves ignition later but has a peak p comparable with that of the smaller Re_0 . Ignition produces an abrupt increase in the momentum thickness (Fig. 1a) and for the larger Re_0 layer which was starting to decay due to the smaller initial perturbations, it provides the energy to re-start growing. Both the domain-average positive spanwise vorticity and the enstrophy display timewise peaks indicative of small scale formation and increased flow topological complexity due to the energy added by the ignition (not shown).

As in our previous study focused on mixing [ii], the reactive flow field displays high density-gradient magnitude (HDGM) regions. We believe that the HDGM regions are very important in understanding high- p turbulent combustion and potentially uphill-diffusion-induced phase change. Since the flow is not ergodic, we analyze it at the time of peak p . Figure 2 illustrates conditional averages of the density gradient on the reaction rate for all simulations and shows that the larger is the density gradient, the higher is the reaction rate; also either a larger p_0 or absence of EGR results in higher reaction rates occurring in regions of much higher density gradient magnitude. In Fig. 3 are displayed conditional averages of the species mass fractions for a realization in which there was EGR and the initial uniform mass fractions of CO_2 and H_2O were 0.035 and 0.01, respectively, with otherwise the upper stream being air and the lower stream being C_7H_{16} . Clearly, rather early in the development of the layer ($t^*=30$), before reaction is initiated, in the formed HDGM regions, the mass fractions of CO_2 and H_2O are smaller and larger, respectively, than the initial values. This means that H_2O has experienced uphill diffusion into the HDGM regions and CO_2 has experienced uphill diffusion out of the HDGM regions. We explain this segregation by the fact that since the HDGM regions primarily contain C_7H_{16} and a small amount of O_2 (the amount of C_7H_{16} increases and that of O_2 decreases as one goes deeper into the HDGM regions), the larger C_7H_{16} molecules (molar mass $m=100$ kg/kmol) let the smaller H_2O molecules ($m=18$ kg/kmol) enter the HDGM regions but the molecules as large as

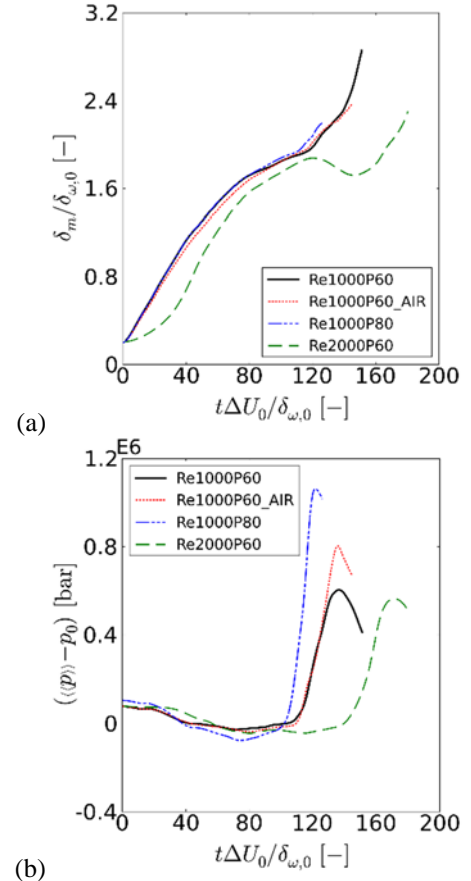


Figure 1. Momentum thickness representing the layer growth (a) and domain-averaged pressure (b), timewise evolution for the four DNS realizations.

those of CO_2 ($m=44$ kg/kmol) cannot diffuse in and must remain outside of the HDGM regions increasing there the CO_2 concentration, i.e. experiencing uphill diffusion outside of the HDGM regions. This picture is confirmed by conditional averages on the density gradient of the angle between the species mass flux and the gradient of that species exhibited in Fig. 4 showing uphill diffusion for H_2O in the HDGM regions but only regular diffusion, except at the largest-magnitude HDGM regions, in those regions for CO_2 . This HDGM phenomenon is the well-known high- p ‘caging’ effect in which due to the high p , the fluid is denser, i.e. the molecules are closer together and thus diffusion into it is impeded. Past ignition and at peak p , Fig. 3 shows that the amount of O_2 decreases being consumed by the reaction, the amount of C_7H_{16} increases (but only very slightly in the largest-magnitude HDGM regions where the combustion is most vigorous) because the consumed fuel not as large as that entrained in the HDGM regions through turbulent mixing, and the amounts of CO_2 and H_2O only imperceptibly increase in the largest-magnitude HDGM regions.

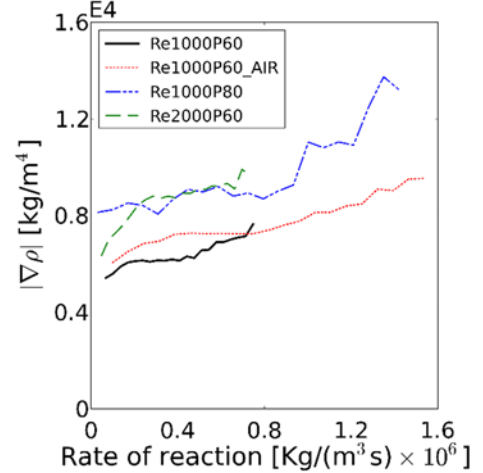


Figure 2. Conditional averages of the density gradient magnitude on the reaction rate at the respective peak pressure for each simulation.

We are currently, computing the activity of the terms in the LES equations to indicate those Subgrid-Scale (SGS) terms which are significant and thus must be modeled. These computations are being done both on a domain-average basis and on a homogeneous-plane average basis. The modeling of these terms will be the next focus of our research.

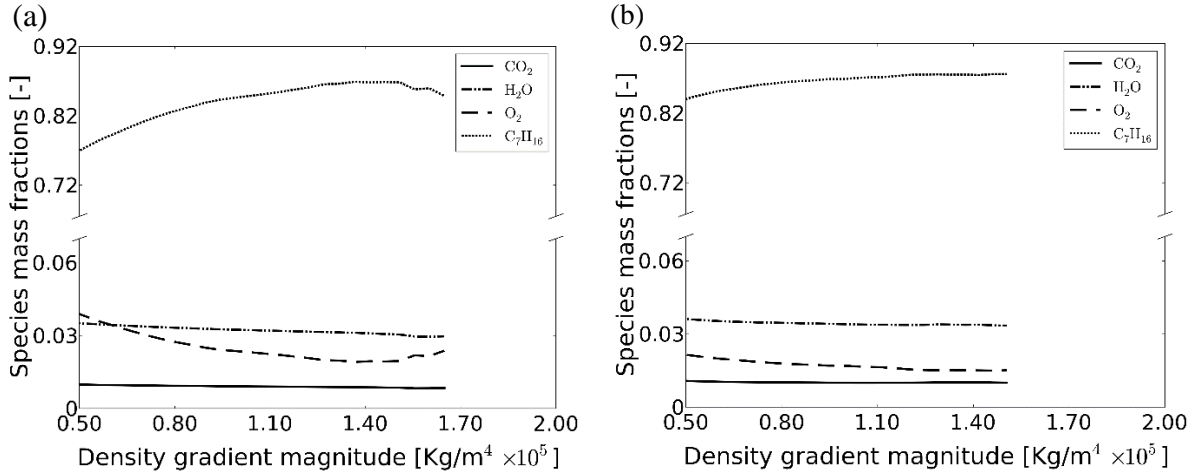


Figure 3. Conditional averages of the species mass fractions on the density gradient magnitude at (a) $t^*=30$ (before ignition) and (b) $t^*=134$ (peak pressure). Simulation Re1000p60.

The PI has continued the collaboration with Dr. Oefelein who will modify RAPTOR once we have developed the methodology of LES for high- p flows.

III. Future Plans

The following activities are planned:

- Finalize the *a priori* reacting-flow analysis and propose subgrid-scale models for the filtered turbulent reaction term.
- Perform an *a posteriori* study.

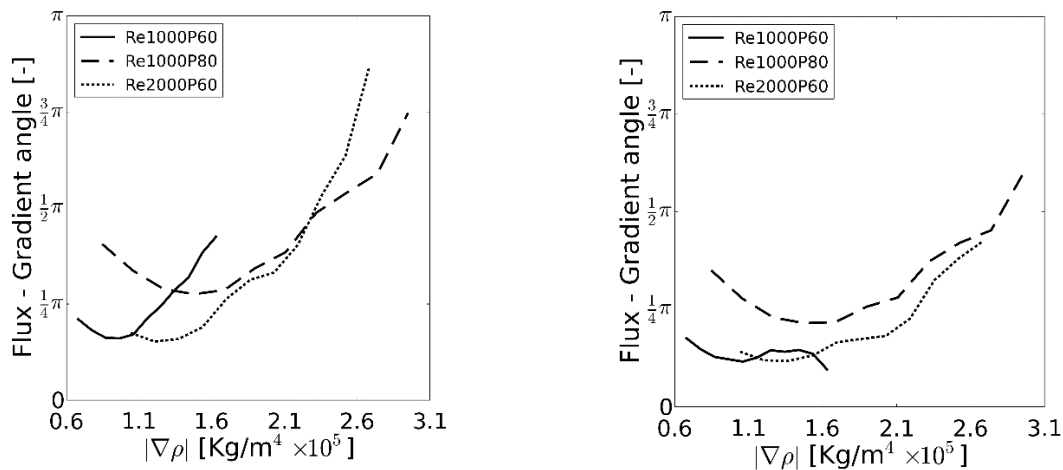


Figure 4. The angle between the flux vector and the gradient of the species for H₂O (left) and CO₂ (right) at the peak pressure time. An angle larger than $\pi/2$ indicates uphill diffusion.

IV. References

- i. Borghesi, G.; Bellan, J., *Proc. of the Comb. Inst.*, 35 **2015** 1537-1547
- ii. Masi, E.; Bellan, J.; Harstad, K.; Okong'o, N. *J. Fluid Mech.* **2013**, 721, 578

V. Publications, presentations and submitted articles supported by this project during 2013- 2015

- [1] Masi, E., Bellan, J., Harstad, K. and Okong'o N., Multi-species turbulent mixing under supercritical-pressure conditions: modeling, Direct Numerical Simulation and analysis revealing species spinodal decomposition, *J. Fluid Mech.*, 721, 578-626, 2013
- [2] Masi, E., Bellan, J. and Harstad, K., Pressure effects from Direct Numerical Simulation of high-pressure multispecies mixing, paper 2013-0711, 51th Aerospace Sciences Meeting, Dallas, TX, 1/7-1/10, 2013
- [3] Borghesi, G. and Bellan, J., Models for the LES equations to describe multi-species mixing occurring at supercritical pressure, paper 2014-0823 presented at the 52nd Aerospace Sciences Meeting, New Harbor, MD, January 13-17, 2014
- [4] Borghesi, G. and Bellan, J., Models for the Large Eddy Simulation equations to describe multi-species mixing occurring at supercritical pressure, *Int. J. Energ. Mat. Chem. Prop.*, 13(5), 435-453, 2014
- [5] Borghesi, G. and Bellan, J., *A priori* and *a posteriori* analysis for developing Large Eddy simulations of multi-species turbulent mixing under high-pressure conditions, accepted for publication, *Phys. Fluids.*, 2015
- [6] Bellan, J., Possible phase formation during high-pressure multi-species jet disintegration, **Keynote Invited Lecture**, ILASS meeting, May 18-21, 2014, Portland, OR.
- [7] Bellan, J., Modeling and numerical simulations of multi-species high-pressure flows, **Invited Plenary Lecture**, 10th International Symposium on Special Topics in Chemical Propulsion, June 2-6, 2014, Poitiers, France
- [8] Borghesi, G. and Bellan, J., Irreversible entropy production rate in high-pressure turbulent reactive flows, *Proc. of the Comb. Inst.*, 35, 1537-1547, 2015
- [9] Borghesi, G. and Bellan, J., *A priori* and *a posteriori* analyses of multi-species turbulent mixing layers at supercritical-p conditions, paper 2015-0162 presented at the 53rd Aerospace Sciences Meeting, Kissimmee, FL., January 5-9, 2015; also presented at the 9th US National Combustion Meeting, Cincinnati, OH., May 17-20, 2015

Towards predictive simulations of soot formation: from surrogate to turbulence

Guillaume Blanquart
Department of Mechanical Engineering
California Institute of Technology
1200 E. California Blvd., Pasadena, CA 91125

Objectives

The combustion of hydrocarbon fuels, including kerosene, gasoline, and diesel, leads to the formation of soot particles which are known to be the source of several health problems and environmental issues.

The objective of the proposed work is to reduce the gap in the present understanding and modeling of soot formation both in laminar and turbulent flames. This effort spans several length scales from the molecular level to large scale turbulent transport. More precisely, the objectives are three fold: 1) develop a *single combined chemical and soot model* validated for all relevant components usually found in real fuel surrogates; 2) develop a framework able to *explain the complete evolution of soot particles* from cluster of PAHs to oxidation of large fractal aggregates; 3) *understand and model the interplay* between unsteady chemistry, differential diffusion, and turbulent transport.

Recent progress

In preparation for the 2014 International Sooting Flames (ISF) workshop, we simulated a large number of flames (from 1D laminar to 3D turbulent flames) in an attempt to evaluate the predictive nature of the recent developments we made in terms of chemistry/PAH/soot modeling.

At the ISF, we were the only group showing contributions to all sections, namely laminar premixed flames, laminar coflow diffusion flames, turbulent diffusion flames, and pressurized flames.

Laminar premixed flames

One-dimensional, burner-stabilized, laminar premixed flames have been used for a long time for the development of PAH and soot models. As co-leader for the ISF workshop, we were in charge of selecting the target flames, collecting the results, and summarizing findings for the laminar premixed flames section. A total of 25 flames covering 6 different burner configurations were selected. In order to help the members of the community simulate these flames and to provide a common basis for comparison between models, we simulated all flames ahead of the workshop and provided an experimentally-consistent, numeri-

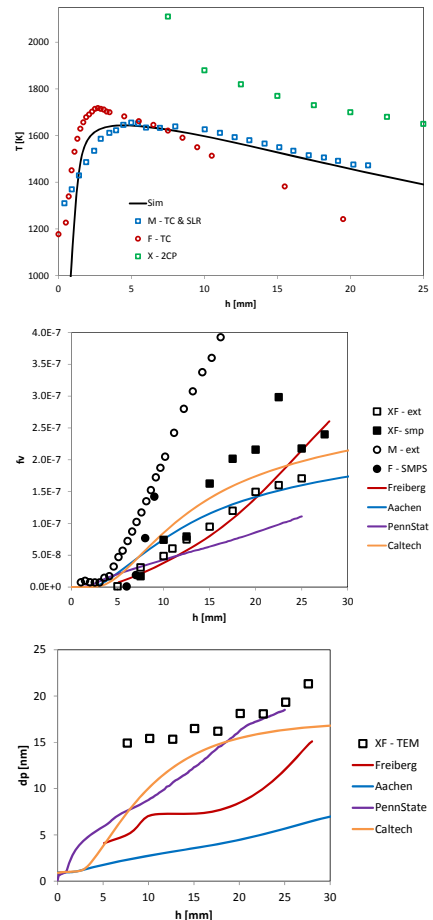


Figure 1. Comparison of the prediction of numerical models by various research groups for one of the laminar premixed target flames (top: temperature, middle: soot volume fraction, bottom: soot particle diameter).

cally-simulated temperature profile for each flame (see Figure 1 for an example). These profiles were used by more than seven research groups in their simulations. Our results indicated that 1) large deviations are often observed between experimentally-measured and numerically-simulated temperature profiles, 2) soot volume fractions are always predicted within a factor of two or three if the “correct” temperature profile is used, and 3) soot particle diameters were only predicted with enough accuracy if aggregates and non-purely spherical particles were considered. More important, we showed that most of the flames investigated exhibit strong two-dimensional effects that have been neglected until now. One of the various implication is an incorrectly predicted gas velocity, and hence residence time which may induce up to a factor of two on the predicted soot volume fraction (see Figure 2).

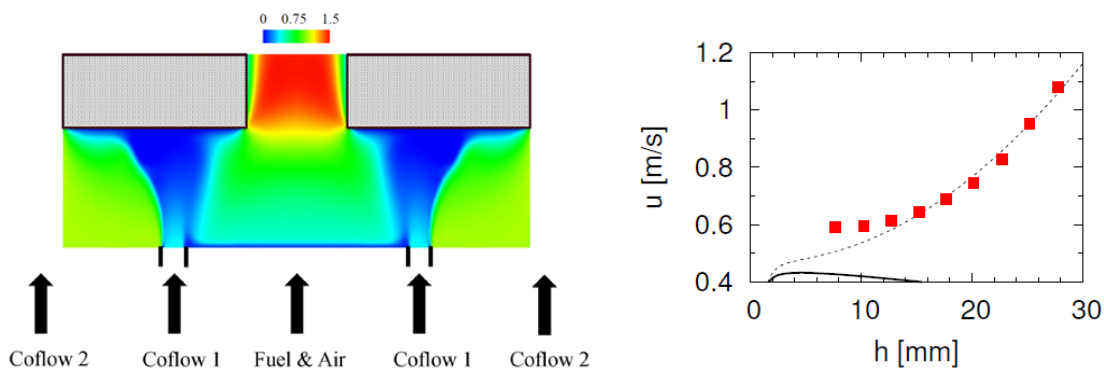


Figure 2. Results of a two-dimensional numerical simulation of the flame shown in Figure 1. Left 2D velocity profile, right: comparison of the centerline velocity (2D sin solid, 1D dashed) with experimental measurements.

Laminar coflow diffusion flames

Coflow diffusion flames present an intermediate configuration in terms of complexity and relevance between laminar premixed flames (previous section) and turbulent diffusion flames (next section). We selected three flames among the ISF target flames and simulated them with our recently improved chemical/soot models. Once again, some deviations we observed between experimentally-observed and numerically simulated temperature profiles were observed (see Figure 3). Consistent with the results of the premixed flames, soot volume fraction was predicted with a factor of two or three on the “wings” of the coflow diffusion flames. Yet, it was always under-predicted along the centerline, showing limitation in our nucleation model and highlighting the need for an improved PAH to soot inception model (see 2012 abstract for details on an ongoing model development in our group).

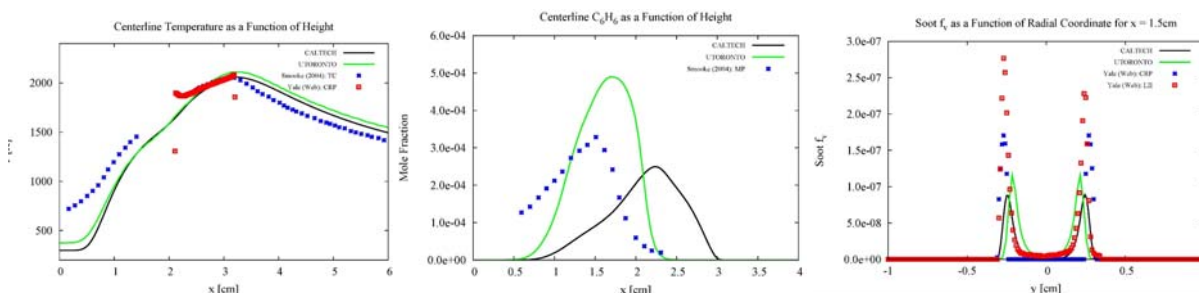


Figure 3. Results of the numerical simulations of one of the coflow diffusion flames. Left: temperature, middle: benzene mole-fractions, and right: soot volume fraction.

Turbulent diffusion flames

Large Eddy Simulations (LES) have been performed on an ethylene/air piloted turbulent non-premixed sooting jet flame to quantify the importance of aromatic chemistry-turbulence interactions. The present flame (also a target for ISF) has been investigated at Sandia National Laboratories by Dr. Shaddix and was selected over other turbulent non-premixed flames, for its relatively large soot yield, high Reynolds number, and well-defined boundary conditions. The numerical simulations relied on a recently-developed relaxation model for PAH chemistry (see 2013 abstract). Comparison between LES and experimental results indicates that the LES predicts the mean soot profile reasonably accurately and that the use of PAH relaxation model was necessary to predict the correct soot yield (see Figure 4). The results also highlighted that the interactions of the slow PAH-chemistry with turbulence had an effect of similar importance as that of the unsteady soot-turbulence interactions.

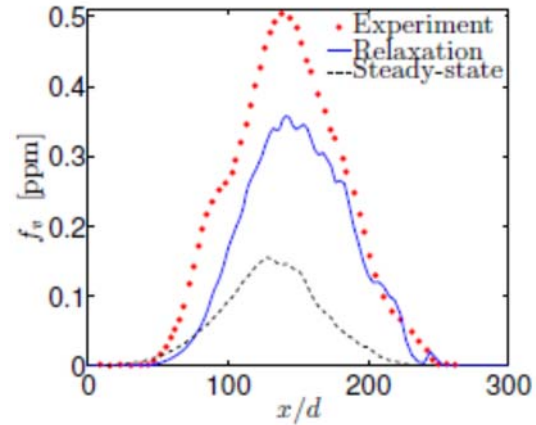


Figure 4. Mean soot volume fraction on the flame centerline.

Additional numerical simulations have been performed on a second ISF target flames, this one investigated experimentally at Adelaide University (Australia). Unlike the piloted ethylene flame from Sandia, the Adelaide flame is a non-piloted jet flame using a mixture of ethylene/hydrogen as fuel. Given the difficulties encountered by other research groups in reproducing the soot volume fraction profiles measured experimentally, we performed a coarse direct numerical simulation (DNS) of the base of the flame. Our preliminary results indicate that differential diffusion effects (partially due to the presence of hydrogen in the fuel) were still present (see Figure 5) and should be included for accurate predictions of this flame.

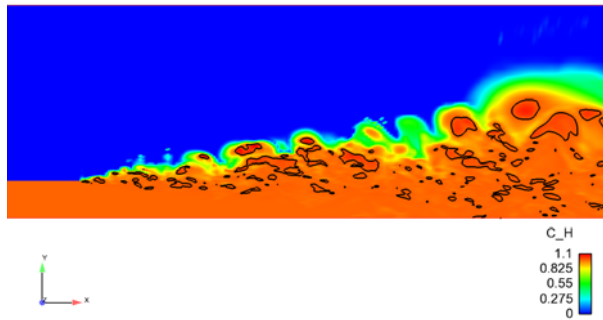


Figure 5. Local carbon-to-hydrogen ratio in the turbulent jet flame of Adelaide. The black iso-contour indicates regions of unusually high ratios due to differential diffusion.

Current and future work

The results of the numerical simulations of the turbulent jet diffusion flame from Adelaide highlighted the need to revisit the treatment of differential diffusion in turbulent flames in general and in particular within the framework of flamelets. More precisely, while the assumption of unity Lewis numbers might be valid for major chemical species (reactants and products), it is not valid for large aromatic species and soot precursors. Preliminary results show this effect might lead to a factor of two on the soot yield. Using experimental and DNS data from the literature, we are currently developing a model to estimate *a priori* the effective/turbulent Lewis numbers for given turbulent conditions. Such model would then be integrated within our current flamelet-based chemistry tabulation and will be tested against various turbulent sooting flames.

Publications

Xuan, Y., Blanquart, G., « *Effects of aromatic chemistry-turbulence interactions on soot formation in a turbulent non-premixed flame* », Proc. Comb. Inst. (2015).

Savard, B., Xuan, Y., Bobbitt, B., Blanquart, G., « *A computationally-efficient, semi-implicit, iterative method for the time-integration of reacting flows with stiff chemistry* », J. Comput. Phys. (2015).

Xuan, Y., Blanquart, G., « *Multi-dimensional flow effects on soot formation in laminar premixed flames* », 9th US Nat. Comb. Meet. (2015).

Burali, N., Xuan, Y., Blanquart, G., « *The validity of the constant non-unity Lewis number assumption in chemically-reacting flows* », 9th US Nat. Comb. Meet. (2015).

Theoretical Studies of Combustion Dynamics (DE-FG02-97ER14782)

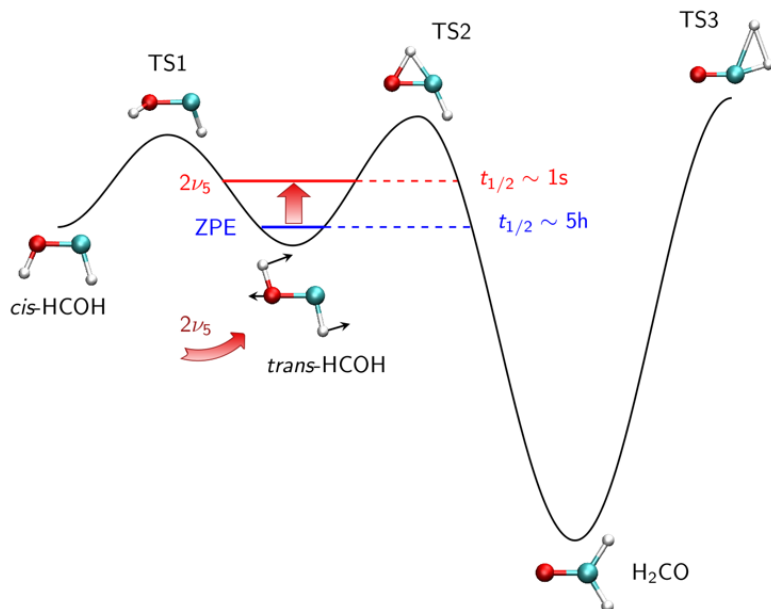
Joel M. Bowman

Cherry L. Emerson Center for Scientific Computation and Department of Chemistry, Emory University Atlanta, GA 30322, jmbowma@emory.edu

Program Scope. The research program, supported by this Department of Energy grant, centers on methods to develop rigorous computational methods to model and gain insight into chemical and physical processes of importance in combustion and issues related to combustion. We have focused in recent years on developing full-dimensional global *ab initio*-based potential energy surfaces (PESs) that describe complex unimolecular and bimolecular reaction that are fits to tens of thousands or more of *ab initio* energies using special polynomial bases that are manifestly invariant with respect to any permutation of like nuclei. Dynamics on these potentials, which may contain multiple minima and saddle points, can be done for long times and can reveal new pathways and mechanisms of chemical reactions. The choice of reaction system to study is always motivated by experiments that challenge and ultimately advance basic understanding of combustion reaction dynamics. Recently, the focus has been on energy transfer in polyatomic hydrocarbons and substituted hydrocarbons, a central area of importance in combustion. The major goal is to go beyond model atom-atom pairwise models of the “non-covalent” interactions that govern energy transfer. Two other areas of research are mode-specific tunneling in unimolecular dissociation and rovibrational energies of polyatomic molecules. Recent Progress in these areas is described next.

Recent Progress: Energy transfer: Ar+allyl, and Ar+HOCO. Energy transfer studies have been initiated in the allyl and HOCO radicals, using full dimensional *ab initio* PESs.^{P24,P25,P27} In the first studies, the collision partner was Ar and an *ab initio* interaction potential was calculated at the MP2/aug-cc-pVTZ level, with counterpoise correction. This interaction potential was represented by a standard sum-of-pairs form and fit to 286 electronic energies. The pairwise fit gave RMS fitting errors of 22 cm⁻¹ for the (negative energy) attractive region, 150 cm⁻¹ for energies up to around 1200 cm⁻¹, and 650 cm⁻¹ for energies up to roughly 8000 cm⁻¹. Thus, this fit is realistic, if not highly precise. Classical trajectory calculations of energy transfer calculations were done for allyl initially non-rotating and highly rotationally excited. The results in the form of ΔE (up and down) distributions for a number of collision energies have been published.^{P24,P25} In addition, a project investigating energy transfer in Ar+HOCO is underway. This project makes use of a global, high-level *ab initio* global potential surface for HOCO and the calculation of the interaction potential. In this case, the goal was to obtain a benchmark quality interaction potential. This was done by using permutationally invariant (PI) fitting to roughly 12 500 CCSD(T)-F12/aug-cc-pVDZ energies. The RMS fitting error is 28 cm⁻¹ for this data set which spans a range from -250 to 12 000 cm⁻¹. The data set was also fit using the pairwise form used for Ar-allyl and novel compact PI form. All three fits were used in preliminary calculations of energy transfer and an initial report of the results has just been accepted for publication as Communication in J. Chem. Phys.^{P27} Development work on more efficient permutationally invariant representations of non-covalent interactions was undertaken with a focus on full dimensional potential energy surfaces for CH₄-H₂O and also CH₄-(H₂O)₂. Excellent progress has been made and described in two recent publications.^{P29,P30} Energy transfer studies in these systems can now be undertaken using extensive classical trajectory or in principle

quantum or mixed classical/quantum methods. **Mode-specific tunneling in unimolecular reactions.** Recent progress in this important research area has been made in the isomerization of trans-HCOH to H₂CO, using a new full-dimensional PES.^{P28} This work was stimulated by previous work,¹⁻³ notably the joint experimental work of Schreiner, Allen, Csaszar and co-workers. The new calculations using a mode-specific theory developed by Wang and Bowman⁴ and predict a large increase in the tunneling rate



upon excitation of the trans-bend mode as shown in the graphic to the left.

Rovibrational energies of polyatomic molecules. The code MULTIMODE has been extended and applied to perform accurate rovibrational calculations of polyatomic molecules. Stuart Carter, the major developer of this code has been working on the code to enable parallel computation, using both Open MP and MPI protocols. This has been largely accomplished with excellent

results.

Future Plans. Further work on energy transfer calculations in both Ar+HOCO and Ar+allyl is planned in a bath of Ar atoms. New calculations of energy transfer of CH₄ in collisions with H₂O and also the water dimer are planned. An existing global potential energy surface for CH₃OH⁵ will be refined to study the unimolecular decomposition dynamics, including mode-specific tunneling. MULTIMODE calculations using this new PES (and dipole moment surface) will be done. This calculations will supplant those already done using an older version of the code and the PES.⁶

REFERECNES

1. P. R. Schreiner, *et al.*, Nature, **453**, 906 (2008).
2. L. Koziol, *et al.* J. Chem. Phys. **128**, 204310 (2008).
3. C. M. Leavitt, C. P. Moradi, J. F. Stanton, and G. E. Douberly, J. Chem. Phys. **140**, 171102 (2014).
4. Y. Wang and J. M. Bowman, J. Chem. Phys. **139**, 154303 (2013).
5. C. Qu and J.M. Bowman, Mol. Phys. **111**, 1964 (2013).
6. J. M. Bowman, X. C. Huang, N. C. Handy, and S. Carter, J. Phys. Chem. A **111**, 7317 (2007).

PUBLICATIONS SUPPORTED BY THE DOE (2012-present)

1. Accurate *Ab Initio* Potential Energy Surface, Thermochemistry, and Dynamics of the Cl(²P, ²P_{3/2}) + CH₄ → HCl + CH₃ and H + CH₃Cl Reactions, G. Czako and J. M. Bowman, J. Chem. Phys. **136**, 044307 (2012).

2. Communication: A Chemically Accurate Global Potential Energy Surface for the HO + CO \rightarrow H + CO₂ Reaction, J. Li, Y. Wang, B. Jiang, J. Ma, R. Dawes, D. Xie, J. M. Bowman, and H. Guo, *J. Chem. Phys.* **136**, 041103 (2012).
3. Large-Amplitude Dynamics in Vinyl Radical: The Role of Quantum Tunneling as an Isomerization Mechanism, A. R. Sharma, J. M. Bowman, and D. J. Nesbitt, *J. Chem. Phys.* **136**, 034305 (2012).
4. Overtone-Induced Dissociation and Isomerization Dynamics of the Hydroxymethyl Radical (CH₂OH and CD₂OH). I. A theoretical Study, E. Kamarchik, C. Rodrigo, J. M. Bowman, H. Reisler, and A. I. Krylov, *J. Chem. Phys.* **136**, 084304 (2012)
5. Mode Selectivity for a “Central” Barrier Reaction: Eight-Dimensional Quantum Studies of the O(³P) + CH₄ \rightarrow OH + CH₃ Reaction on an *Ab Initio* Potential Energy Surface, R. Liu, M. Yang, G. Czako, J. M. Bowman, J. Li, and H. Guo, *J. Phys. Chem. Lett.* **3**, 3776 (2012).
6. Theoretical Study of the Validity of the Polanyi Rules for the Late-Barrier Cl+CHD₃ Reaction, Z. Zhang, Y. Zhou, D. H. Zhang, G. Czako, and J. M. Bowman, *J. Phys. Chem. Lett.* **3**, 3416 (2012).
7. First-Principles Calculations of Rovibrational Energies, Dipole Transition Intensities and Partition Function for Ethylene using MULTIMODE, S. Carter, A. R. Sharma, and J. M. Bowman, *J. Chem. Phys.* **137**, 154301 (2012).
8. Translational Energy Dependence of the Cl+CH₄($v_b=0, 1$) Reactions: A Joint Crossed-Beam and Quasiclassical Trajectory Study, B. Zhang, Kopin L., G. Czako and J. M. Bowman, *Mol. Phys.* **110**, 1617 (2012).
9. Quasi-Classical Trajectory Study of the HO + CO \rightarrow H + CO₂ Reaction on a New *Ab Initio* Based Potential Energy Surface, J. Li, C. Xie, J. Ma, Y. Wang, R. Dawes, D. Xie, J. M. Bowman, and H. Guo, *J. Phys. Chem. A* **116**, 5057 (2012).
10. Quasiclassical Trajectory Study of Fast H-atom Collisions with Acetylene, Y.-C. Han, A. R. Sharma, and J. M. Bowman, *J. Chem. Phys.* **136**, 214313 (2012).
11. Dynamics of the O(³P)+CHD₃($v_{CH} = 0,1$) Reactions on an Accurate *Ab Initio* Potential Energy Surface, G. Czako and J. M. Bowman, *Proc. Natl. Acad. Soc. U.S.A* **109**, 7997 (2012).
12. MULTIMODE Calculations of Rovibrational Energies of C₂H₄ and C₂D₄, S. Carter, J. M. Bowman, and N. C. Handy, *Mol. Phys.* **110**, 775 (2012).
13. Intersystem Crossing and Dynamics in the O(³P)+C₂H₄ Multichannel Reaction: Experiment Validates Theory, B. Fu, Y.-C. Han, J. M. Bowman, L. Angelucci, N. Balucani, F. Leonori, and P. Casavecchia, *Proc. Natl. Acad. Soc. U.S.A.*, **109**, 9733 (2012).
14. Three-State Surface Hopping Calculations of Acetaldehyde Photodissociation to CH₃+HCO on *Ab Initio* Potential Energy Surfaces, B. Fu, Y.-C. Han, and J. M. Bowman, *Faraday Discuss.* **157**, 27 (2012).
15. Dipole Surface and Infrared Intensities for the *cis*- and *trans*-HOCO and DOCO Radicals, X. Huang, R. C. Fortenberry, Y. Wang, J. S. Francisco, T. D. Crawford, J. M. Bowman, and T. J. Lee, *J. Phys. Chem. A* **117**, 6932 (2013).
16. Variational Calculations of Vibrational Energies and IR Spectra of *trans* and *cis*-HOCO Using New *ab initio* Potential Energy and Dipole Moment Surfaces, Y. Wang, S. Carter, and J. M. Bowman, *J. Phys. Chem. A* **111**, 9343 (2013).

17. Classical Trajectory Study of Energy Transfer in Collisions of Highly Excited Allyl Radical with Argon, R. Conte, P. Houston, and J. M. Bowman, *J. Phys. Chem. A* **117**, 14028 (2013).
18. A novel Gaussian Binning (1GB) analysis of vibrational state distributions in highly excited H₂O from reactive quenching of OH* by H₂, R. Conte, B. Fu, E. Kamarchik, and J. M. Bowman, *J. Chem. Phys.* **139**, 044104 (2013).
19. Effects of High Angular Momentum on the Unimolecular Dissociation of CD₂CD₂OH: Theory and Comparisons with Experiment, B. G. McKown, M. Ceriotti, C. C. Womack, E. Kamarchik, L. J. Butler, and J. M. Bowman, *J. Phys. Chem. A* **117**, 10951 (2013).
20. Quasiclassical Trajectory Studies of ¹⁸O(³P) + NO₂ Isotope Exchange and Reaction to O₂ + NO on D₀ and D₁ Potentials, B. Fu, D. H. Zhang, and J. M. Bowman, *J. Chem. Phys.* **139**, 024303 (2013).
21. Energy Disposal and Thermal Rate Constants for the OH+ HBr and OH+DBr Reactions: Quasiclassical Trajectory Calculations on an Accurate Potential Energy Surface, A. G. S. de Oliveira-Filho, F. R. Ornellas, and J. M. Bowman, *J. Phys. Chem. A, Articles ASAP* (2014).
22. Quasiclassical Trajectory Calculations of the Rate Constant of the OH plus HBr -> Br + H₂O Reaction Using a Full-Dimensional Ab Initio Potential Energy Surface Over the Temperature Range 5 to 500 K, A. G. S. de Oliveira, F. R. Ornellas, and J. M. Bowman, *J. Phys. Chem. Lett.* **5**, 706 (2014).
23. Roaming, J. M. Bowman, *Mol. Phys.* **112**, 2516 (2014).
24. Trajectory Study of Energy Transfer and Unimolecular Dissociation of Highly Excited Allyl with Argon, R. Conte, P. L. Houston, and J. M. Bowman *J. Phys. Chem. A* **118**, 7742 (2014).
25. Collisional Energy Transfer in Highly Excited Molecules, P. L. Houston, R. Conte, and J. M. Bowman *J. Phys. Chem. A* **118**, 7758–7775. *J. Phys. Chem. A* 2014, **118**, 7758 (2014).
26. Reaction Dynamics of Methane with F, O, Cl, and Br on ab Initio Potential Energy Surfaces, G. Czako and J. M. Bowman, *J Phys Chem A* **118**, 2839 (2014).
27. Communication: A benchmark-quality, full-dimensional ab initio potential energy surface for Ar-HOCO, R. Conte, P. L. Houston, and J. M. Bowman, *J Chem Phys* **140** 151101 (2014).
28. Bend Excitation Is Predicted to Greatly Accelerate Isomerization of *trans*-Hydroxymethylene to Formaldehyde in the Deep Tunneling Region, Y. Wang and J. M. Bowman. *J. Phys. Chem. Lett.* **6**, 124 (2015).
29. “Plug and play” full-dimensional ab initio potential energy and dipole moment surfaces and anharmonic vibrational analysis for CH₄-H₂O, C. Qu, R. Conte, P. L. Houston, and J. M. Bowman, *Phys Chem Chem Phys.* **17**, 8172 (2015).
30. Permutationally Invariant Fitting of Many-Body, Non-covalent Interactions with Application to Three-Body Methane–Water–Water, R. Conte, C. Qu, and J. M. Bowman, *J. Chem. Theory Comput.* (2015) DOI: 10.1021/acs.jctc.5b00091

Dynamics of Product Branching in Elementary Combustion Reactions: OH + Alkenes and Nitrogen Chemistry

Laurie J. Butler

The University of Chicago, The James Franck Institute

5640 South Ellis Avenue, Chicago, IL 60637

L-Butler@uchicago.edu

I. Program Scope

While the total rate constant for many elementary reactions is well-characterized, understanding the product branching in complex reactions presents a formidable challenge. To gain an incisive probe of such reactions, our experiments investigate the dynamics of the product channels that arise from long-lived radical intermediates along the bimolecular reaction coordinates. Our work¹⁻⁵ uses the methodology developed in my group in the last fourteen years, using both imaging and scattering apparatuses. The experiments generate a particular isomeric form of an unstable radical intermediate along a bimolecular reaction coordinate and study the branching between the ensuing product channels of the energized radical as a function of its internal rotational and vibrational energy under collision-less conditions.

The experiments use a combination of: 1) measurement of product velocity and angular distributions in a crossed laser-molecular beam apparatus, with electron bombardment detection in my lab in Chicago or 2) with tunable vacuum ultraviolet photoionization detection at Taiwan's National Synchrotron Radiation Research Center (NSRRC), and 3) velocity map imaging using state-selective REMPI ionization and single photon VUV ionization of radical intermediates and reaction products. We have implemented tunable VUV photoionization in our imaging apparatus, using difference frequency four-wave mixing to produce photoionization light tunable from 8 to 10.8 eV. In this no-cost extended fourth year of our project, we investigated the photodissociation of $\text{BrCH}_2\text{CH}_2\text{ONO}$ at 193 nm to see if it might generate nascent highly vibrationally excited $\text{CH}_2\text{CH}_2\text{ONO}$ radicals (an important intermediate in the reaction of NO_2 + ethene). It was successful – our experiments measured the branching between primary O-NO fission and C-Br photofission at 193 nm to be 4.28:1. Thus, a sufficient number of $\text{CH}_2\text{CH}_2\text{ONO}$ radicals was produced to allow us to study the competition between two product channels from this radical intermediate, $\text{NO} + \text{oxirane}$ and $\text{NO}_2 + \text{ethene}$. The first results are summarized in Section II.A. We also developed a new theoretical model to predict the energy partitioned to relative kinetic energy when a highly rotationally excited radical dissociates with no exit barrier. The model accurately predicts the velocities measured for the OH and alkene products from highly rotationally excited $\text{C}_3\text{H}_6\text{OH}$ and $\text{C}_2\text{D}_4\text{OH}$ radicals, and it correctly includes the correlation between the velocity of the radical and its rotational angular momentum. These results are described in Section II.B. Section II.C describes results from our collaboration with Y. P. Lee, developing a revised Franck-Condon method to predict the HCl product vibrational energy from the photodissociation of acryloyl chloride at 193 nm that he measured with step-scan FTIR.⁶

II. Recent Progress

A. $\text{CH}_2\text{CH}_2\text{ONO}$ and $\text{BrCH}_2\text{CH}_2\text{O}$ radicals from 193 nm $\text{BrCH}_2\text{CH}_2\text{ONO}$ photodiss'n

While our prior work with Terry Miller showed that the primary photodissociation channel of $\text{BrCH}_2\text{CH}_2\text{ONO}$ at 351 nm is O-NO bond cleavage, we initiated a study at 193 nm to see if we could induce a significant fraction of the molecules to undergo C-Br bond photofission. At 193 nm, $\text{BrCH}_2\text{CH}_2\text{ONO}$ reaches an excited state described by a linear combination of two excited electronic configurations, one repulsive in the repulsive in the O-NO bond, similar to the

S_2 state in alkyl nitrites, and the other repulsive in the C-Br bond, similar to the excited states reached in the 200 nm band of bromoalkanes. Using electron bombardment ionization in the UChicago scattering apparatus, we detected both O-NO and C-Br bond photofission, with a branching ratio of 4.28 to 1. The NO photoproduct is fit in blue line in the upper frame of Fig. 1 while the Br photoproduct is fit in orange line in the lower frame. The $\text{BrCH}_2\text{CH}_2\text{O}$ radicals (co-fragment formed in O-NO photofission) have much higher internal energies than our prior work at 351 nm, so evidence both dissociation to $\text{CH}_2\text{Br} + \text{H}_2\text{CO}$ (as seen in our prior study with Terry) and dissociation to $\text{H} + \text{BrCH}_2\text{CHO}$. The H_2CO signal is fit in purple in Fig. 1 (upper frame) and the signal from the momentum-matched co-fragment CH_2Br is fit in purple in Fig. 2. Dissociative ionization of CH_2Br to Br^+ also contributes to the signal (fit in purple) in the lower frame of Fig. 1. Signal from the $\text{BrCH}_2\text{CH}_2\text{O} \rightarrow \text{H} + \text{BrCH}_2\text{CHO}$ channel appears at several daughter ions of BrCH_2CHO and is, as expected, very close to momentum matched to the NO signal fit in blue in the upper frame of Fig. 1 (as H atom is imparted with most of the recoil velocity).

The C-Br photofission channel gives vibrationally excited $\text{CH}_2\text{CH}_2\text{ONO}$ radicals, so allows us to study the competition between the $\text{NO}_2 + \text{ethene}$ and an $\text{NO} + \text{oxirane}$ product channels. Our G4 calculations on $\text{CH}_2\text{CH}_2\text{ONO}$ shown in Fig. 3 suggest both these channels could be significant. My students just got back from taking a week of data using the scattering apparatus at the NSRRC; the data give evidence for both $\text{NO} + \text{oxirane}$ (the oxirane is detected at parent ion), and $\text{NO}_2 + \text{ethene}$. Interestingly, we also got good data at $m/e = 31$ (HNO^+). We are fitting the data now, but it appears that there is a third primary photodissociation channel, HNO elimination, that produces HNO and bromoacetaldehyde. A fast shoulder on the signal at Br^+ and high kinetic energy signal at vinyoxy may result from photodissociation of this product.

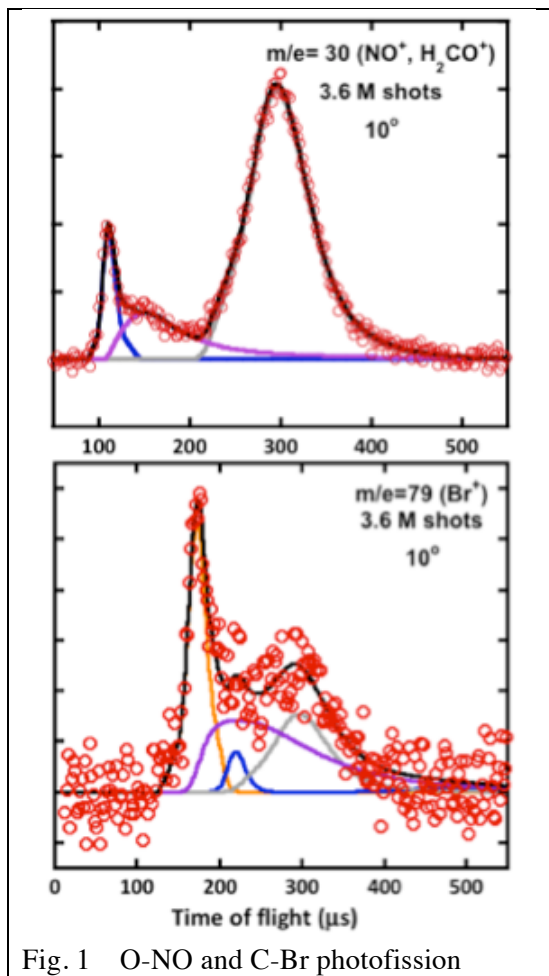


Fig. 1 O-NO and C-Br photofission

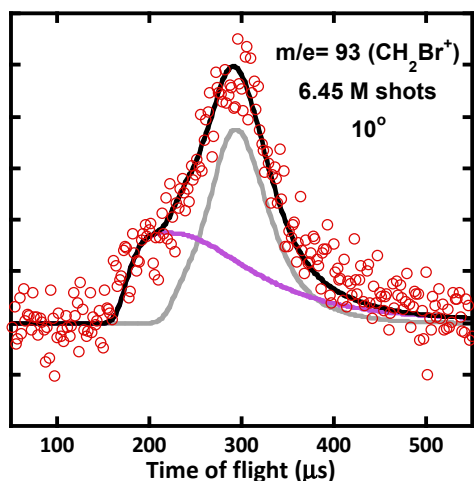


Fig. 2 $\text{BrCH}_2\text{CH}_2\text{O} \rightarrow \text{CH}_2\text{Br} + \text{H}_2\text{CO}$

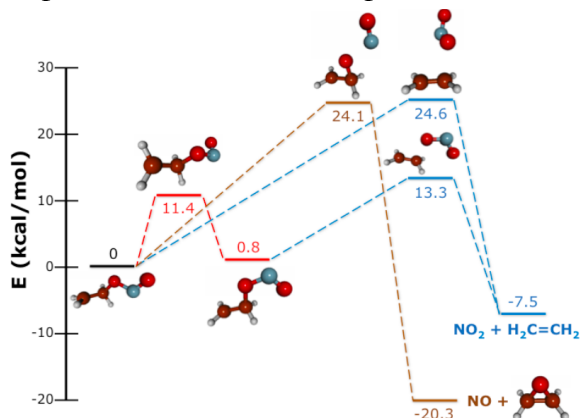


Fig. 3 Some calculated transition states for $\text{CH}_2\text{CH}_2\text{ONO}$

B. Predicting the recoil kinetic energies when rotationally excited radicals dissociate

Our experimental study⁴ last year of the product channels resulting from two radical intermediates, 1-hydroxy-2-propyl and 2-hydroxy-1-propyl, in the reaction of OH with propene motivated a serious effort at predicting the recoil kinetic energies when these radicals dissociate back to OH + propene. Our new modeling paper⁵ details how we make this prediction and assesses its generality by applying it to prior measurements of the dissociation of $\text{CD}_2\text{CD}_2\text{OH}$ radicals to $\text{CD}_2\text{CD}_2 + \text{OH}$. Our model, developed for the dissociation of highly rotationally excited radicals produced photolytically from a halogenated precursor, gives an excellent prediction for the velocities of the radical's dissociation products. Figure 4 shows in green solid line the fit this model gives to the measured velocities of the OH and CD_2CD_2 products from the unimolecular dissociation of highly rotationally excited $\text{CD}_2\text{CD}_2\text{OH}$ radicals. These fits are not the result of an iterative forward-convolution fit, they are predictions from our model with no variable parameters. They properly account for the correlation between velocity of the $\text{CD}_2\text{CD}_2\text{OH}$ radical and its rotational angular momentum, which influences the recoil velocity of the OH from the CD_2CD_2 .

This is an exciting theoretical result. For decades researchers have measured the energy imparted to recoil kinetic energy when radicals dissociate, but comparison of the measured distribution with theory required a global potential energy surface or dynamics-on-the-fly calculations that were only practical for very small molecular systems. Our new model uses the angular momenta of the unstable radicals and the tensor of inertia of each to predict the recoil kinetic energy and angular distributions when hydroxy radicals dissociate to OH + an alkene. We need only propagate the rotational dynamics at the radical's equilibrium geometry and then at the transition state, being careful to preserve the magnitude and direction of the angular momentum vector. The predictions give excellent fits to the data. The only required experimental input is the measured recoil kinetic energies in the C-halogen bond photofission reaction that prepares the highly rotationally excited radical intermediate. As long as the initial photodissociation is via a repulsive excited state and radical dissociates with no barrier beyond the endoergicity, the model we developed accurately predicts the distribution of energies imparted to relative kinetic energy as the radical dissociates; it is particularly good for radicals produced with an angular momentum vector that is not close to an inertial axis.

C. Developing a modified Franck-Condon model for roaming reactions

Y.P. Lee asked us to help him understand the vibrational and rotational distributions that he measured, using step-scan FTIR, for two HCl-photoelimination channels from acryloyl chloride excited at 193 nm. Fig. 5 shows the two pathways we identified for HCl elimination proceeding via internal conversion to the ground electronic state. One HCl

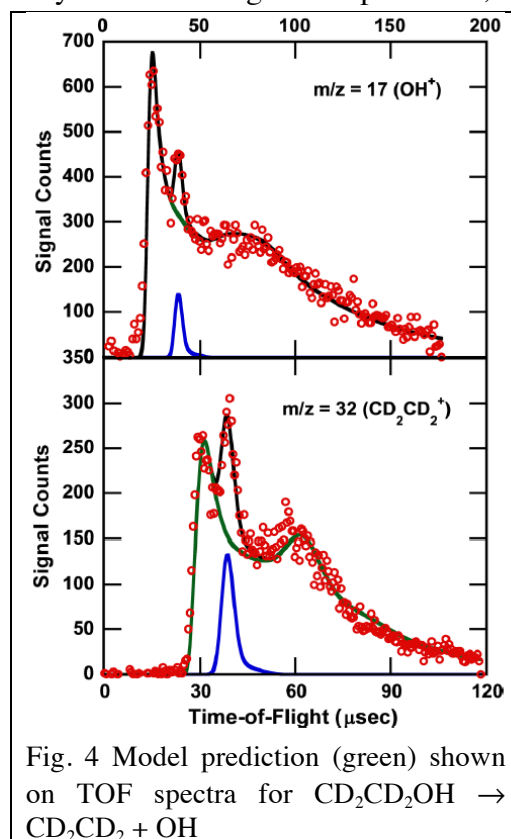
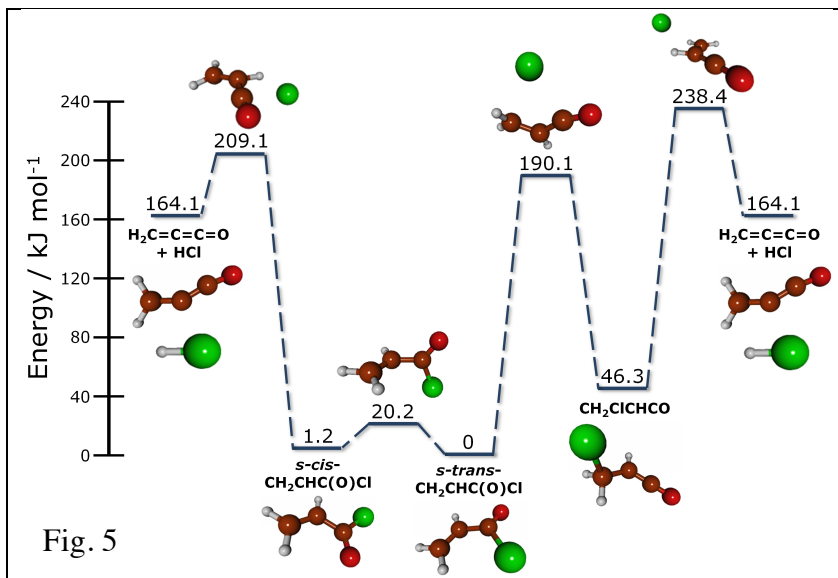


Fig. 4 Model prediction (green) shown on TOF spectra for $\text{CD}_2\text{CD}_2\text{OH} \rightarrow \text{CD}_2\text{CD}_2 + \text{OH}$

elimination channel occurs after a Cl-shift. Using the calculated transition states, our predicted statistical branching ratio of 0.81:0.19 for direct HCl elimination from the *s*-cis conformer: HCl elimination from 3-chloro-1-propen-1-one after the Cl shift agrees very well with the experimental branching of 0.8 : 0.2. To understand the vibrational distribution of the HCl produced in each pathway, a time-honored Franck-Condon analysis, gives a vibrational distribution peaked at far too high an energy because one of the elimination channels occurs via a roaming pathway. My Ph.D. student Preston Scrape identified the correct geometry to make a Franck-Condon prediction for such channels. Noting a broad shoulder along the IRC corresponding to the Cl atom reapproaching the CH₂CHCO, he used the geometry along the IRC when the Cl atom came closest to the center C atom (the IRC is repulsive after this geometry).



This gives an excellent prediction for the most probable HCl vibrational state.

III. Publications Acknowledging DE-FG02-92ER14305 (2012 or later)

1. Photoproduct channels from BrCD₂CD₂OH at 193 nm and the HDO + vinyl products from the CD₂CD₂OH radical intermediate, C. C. Womack, B. J. Ratliff, L. J. Butler, S. -H. Lee, and J. J. Lin, *J. Phys. Chem. A* **116**, 6394-6407 (2012).
2. Effects of high angular momentum on the unimolecular dissociation of CD₂CD₂OH: Theory and comparisons with experiment, B. G. McKown, M. Ceriotti, C. C. Womack, E. Kamarchik, L. J. Butler, and J. M. Bowman, *J. Phys. Chem. A* **117**, 10951-63 (2013).
3. Imaging and scattering studies of the unimolecular dissociation of the BrCH₂CH₂O radical from BrCH₂CH₂ONO photolysis at 351 nm, L. Wang, C. -S. Lam, R. Chhantyal-Pun, M. D. Brynteson, L. J. Butler, and T. A. Miller, *J. Phys. Chem. A*, **118**, 404-416 (2014).
4. Radical Intermediates in the Addition of OH to Propene: Photolytic Precursors and Angular Momentum Effects, M. D. Brynteson, C. C. Womack, R. S. Booth, S.-H. Lee, J. J. Lin, and L. J. Butler, *J. Phys. Chem. A* **118**, 3211-3229 (2014).
5. Predicting the effect of angular momentum on the dissociation dynamics of highly rotationally excited radical intermediates, M. D. Brynteson and L. J. Butler, *J. Chem. Phys.* **142**, 054301 (2015). (Joint funding with NSF.)
6. Two HCl-Elimination Channels and Two CO-Formation Channels Detected with Time-Resolved Infrared Emission upon Photolysis of Acryloyl Chloride [CH₂CHC(O)Cl] at 193 nm, Pei-Wen Lee, Preston G. Scrape, Laurie J. Butler, and Yuan-Pern Lee, *J. Phys. Chem. A*, DOI 10.1021/jp512376a (2015).

Chemical Dynamics and Spectroscopy of Gas Phase Species
Utilizing Velocity Mapped Ion Imaging

David W. Chandler
Combustion Research Facility
Sandia National Laboratory
Livermore, CA 94550
chand@sandia.gov

Program Scope:

The goal of this research program is to generate data that challenges the theoretician's ability to calculate potential energy surfaces and predict dynamics upon them. This is traditionally done through the fields of spectroscopy, chemical dynamics and kinetics. The detailed measurement of atomic and molecular motion on a potential energy surface is what defines the field of chemical dynamics. No matter if the motion is intra-molecular, such as unimolecular dissociation, or inter-molecular, such as inelastic scattering or reactive scattering, one observes dynamics that can test ones ability to obtain an accurate potential energy surface and calculate dynamics upon that surface. In the recent past we have made measurements of collisional energy transfer of both electronically ground state but highly vibrationally excited molecules and electronically excited state but vibrationally ground state molecules. In this period we have finished our measurements and analysis of the collision induced dissociation of highly vibrationally excited NO₂. We will expand these collisional energy transfer studies to lower collision energies where both the study of low energy barriers to reactions can be observed (such as in the O (¹D)+ CH₄ reaction) and low energy resonances can be observed in the scattering (such as in NO + He). These low energy collision experiments are sensitive to the attractive part of the potential energy surfaces in contrast to the higher energy collisions that interrogate the repulsive wall of the system. In addition to these collision studies we have been developing two new spectroscopic capabilities. The first is a dual etalon frequency comb cavity ring down spectroscopy technique that allows one to obtain "high" resolution spectroscopy with low-resolution lasers. This work has been focused on trying to do these experiments in the infrared region of the spectrum where congested spectra make molecular identification difficult. We have also investigated the utility of using velocity mapped ion imaging to perform MHz resolution spectroscopy. We have been able to quantitatively determine line widths down to 10 MHz line widths with this novel use of the velocity-mapped ion imaging (VMII) technique.

Collisional Energy Transfer Studies:

In this last year we have finished our analysis and submitted for publication the work on the collision induced dissociation (CID) of highly vibrationally excited NO₂ by collision with Ar. In this study we excited NO₂ with a single blue photon exciting it in a molecular beam to within 40 cm⁻¹ of its dissociation limit. These highly vibrationally excited (but low rotational excitation) are then crossed with a molecular beam of Ar atoms. A single collision occurs, at a relative collision energy close to 560 cm⁻¹, and the NO₂ molecules that obtain more than 40 cm⁻¹ of energy then dissociate. We use

resonant enhanced (1+1') ionization to state selectively ionize the NO(j) products that are produced in in the collision. By careful analysis of the velocity distributions associated with the different rotational states of NO produced and an analysis of the dynamics of the dissociation of the NO₂ into specific rotational states (measured to be statistical is dissociation is caused by photolysis) one can extract the shape of the energy transfer function of the initial NO₂ + Ar collision. This is a very difficult quantity to extract from any collisional energy transfer process. Only two other set of experiments, one from the group of Dr. Kenny Ni, has claimed to extract this quantity directly from a single collision event and their results disagree with theory by about a factor of about 3 over estimate of the magnitude of the energy transfer. The other set of data is from Dr. Hanna Reisler's group on NO₂ CID and she obtained results similar to ours with a different technique on a slightly different energy range. Our experiments in contrast seem to underestimate the theory by about a factor of 2 and have been submitted as a Frontiers Article in Chem. Phys. Letters.

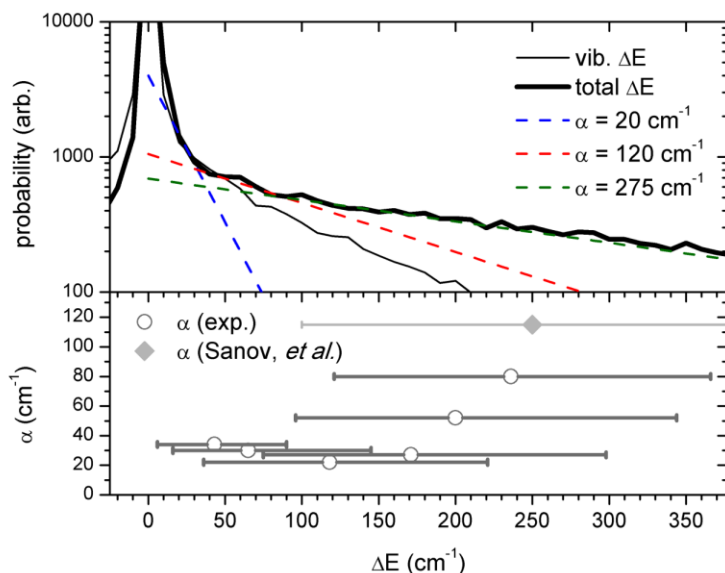


Figure 1: the comparison of our measured collision induced dissociation experiments, Dr. Hanna Reisler's (USC) experiment with our experiment and calculations by Dr. Ahren Jasper (Sandia). Calculations in Figure 1 were actually not performed at the dissociation limit but lower in the potential well. New experiments that can be more directly compared to the theoretical calculations will be performed this summer.

Dual Etalon Frequency Comb Spectroscopy:

First demonstration of this new type of spectrometer was demonstrated utilizing two uncorrelated etalons in the visible portion of the spectrum. We have recently built a monolithic spectrometer from one piece of invar containing two etalons in order to allow signal averaging. The monolithic spectrometer is shown in figure 2. The spectrometer works on the principle that a broadband laser pulse excites both etalons. The etalons are well aligned so that all modes other than the 0,0 mode are minimized. The etalons are not quite the same length therefore the frequencies exiting the etalons are different and have slightly different spacing. As these two outputs are combined on a single photo-detector they interfere and through Fourier analysis of this interference one can observe

the individual frequencies and through this observation one can observe absorption at those frequencies. Efforts to do this in the infrared using an IR OPO as a light source are under way. Sensitive detection of methane is being investigated.

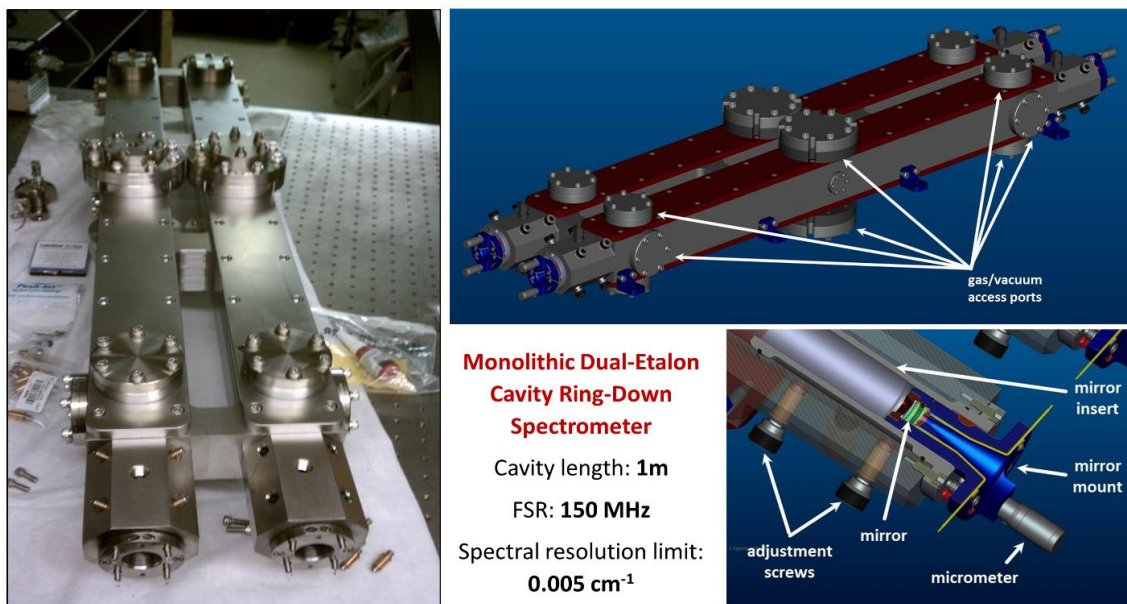


Figure 2: Photograph and schematic of DEFCOM spectrometer showing the two etalons bored out of a single piece of invar.

Utilizing Velocity Mapped Ion Imaging Used for High Resolution Spectroscopy:

When a high-resolution laser is utilized in a resonance enhanced ionization scheme for detection of an atom or a molecule there is the ability to use velocity mapped ion imaging (VMII) to measure the photophysics associated with that transition. This has been demonstrated on Kr atoms. The laser ionization schemes is shown in Figure 3.

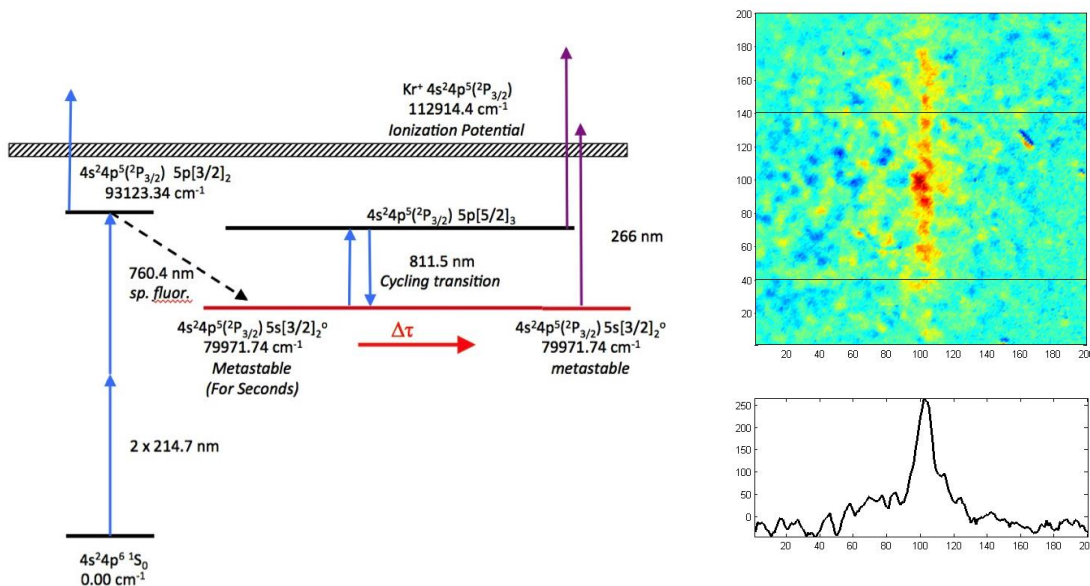


Figure 3: Schematic of laser ionization scheme for Kr atoms.

A difference in the ionization cross section is observed for the two pathways that involve the 266 nm laser light. This difference in ionization cross section can be used to visualize the transition. As different velocity groups Doppler shift themselves into resonance and these velocities are imaged one observes the transition with the resolution of the velocity resolution. For the 811.5 nm transition and Kr atoms we have 3 m/s velocity resolution and this represents a 3 MHz spectral resolution. We observe rabbi cycle broadening, lifetime broadening due to ionization, and can observe measure the laser frequency with this resolution relative to the transition frequency.

Future work:

Collisional Energy transfer of vibrationally hot molecules will be investigated by scattering rotationally hot NO from vibrationally hot NO₂. By exciting the NO₂ a few hundred cm⁻¹ below the dissociation limit the collision will not produce NO from CID but the NO scattered from NO₂ will change rotational state and gain translational energy from vibrational relaxation of the NO₂. By measuring the velocity of the rotationally excited NO one can obtain the energy transfer of specific NO rotational channels and this can be compared directly to calculations.

In a new Velocity Mapped Ion Imaging apparatus we will measure the aligned chemistry of the fundamental H + D₂ reaction. A 532-nm laser beam will be used to align both HBr and D₂ molecules. A UV laser pulse will be used to dissociate the HBr and detect the HD product. It has been shown that this can happen with the 5 nsec of a single laser pulse. In this manner we will be able to measure the reactivity of aligned reagents. This will show a new way forward to investigate the stereochemistry of fundamental reactions.

A merged molecular beam apparatus is being built to investigate low energy collisions with high velocity resolution. This will allow or the study of both low energy entrance barriers and collisional resonances involving both Feschbach and shape resonances.

DEFCOM spectroscopy will be focused on near infrared spectroscopy of molecules in order to be able to utilize faster more sensitive detectors and higher reflectivity mirrors.

VMII will be utilized to image new photo-physical processes including rabbi cycling of atoms and molecules in order to determine absolute transition strengths of transitions between excited electronic states.

Publications 2013 to Present:

- 1) Rotational Alignment of NO (A(2)S+) from Collisions with Ne: Steill, J. D., Kay J. J., Paterson G., Sharples T. R., Klos J., Costen M. L., Strecker K. E., McKendrick K. G., Alexander M. H., Chandler D. W., J. of Phys. Chem. Vol 117 (34), 8163-8174 (2013).
- 2) Determination of the Energy Transfer Function From the Collision Induced Dissociation of NO₂ + Ar. J. D. Steill, A. Jasper, K. E. Strecker, and D. W. Chandler, manuscript submitted Frontier Article CPL 2015.

Petascale Direct Numerical Simulation and Modeling of Turbulent Combustion

Jacqueline H. Chen (PI) and Sgouria Lyra
Sandia National Laboratories, Livermore, California 94551-0969
Email: jhchen@sandia.gov

Program Scope

In this research program we have developed and applied massively parallel three-dimensional direct numerical simulation (DNS) of building-block, laboratory scale flows that reveal fundamental turbulence-chemistry interactions in combustion. The simulation benchmarks are designed to expose and emphasize the role of particular phenomena in turbulent combustion. The simulations address fundamental issues associated with chemistry-turbulence interactions that underly practical combustion devices: extinction and reignition, premixed and stratified flame propagation and structure, flame stabilization in autoignitive coflowing jet flames and reactive jets in crossflow, and flame propagation in boundary layers. In addition to the new understanding provided by these simulations, the resultant DNS data are used to develop and validate predictive mixing and combustion models required in Reynolds-Averaged Navier Stokes (RANS) and large-eddy (LES) simulations.

Recent Progress

In the past year, computer allocations from a DOE Innovative and Novel Computational Impact on Theory and Experiment (INCITE) grant have enabled us to perform several petascale three-dimensional DNS of turbulent flames with detailed chemistry. These DNS studies focused on understanding: 1) turbulent flame propagation in equivalence-ratio stratified methane/air flows, 2) differential diffusion effects on lifted flame stabilization of syngas mixtures in a reacting jet-in-crossflow, and 3) *a posteriori* comparison of a one-dimensional turbulent (ODT) model with DNS of a highly turbulent hydrogen/air counterflow flame with product stratification. Highlights of our accomplishments in the past year are summarized below, followed by a summary of future research directions.

Turbulent flame propagation in equivalence-ratio stratified methane/air flows [1]

Many practical combustion devices involve flame propagation in fuel-air mixtures which are not perfectly mixed. Understanding and developing predictive models for equivalence ratio-stratified combustion physics are important for the design of stratified-charge internal combustion engines as well as lean-burn gas turbine combustion system. Effects of equivalence ratio stratification, in which a flame propagates through an inhomogeneous fuel-air mixture, are investigated using Direct Numerical Simulation (DNS) with a reduced methane-air mechanism. The simulation configuration involves a slot-jet turbulent Bunsen flame that is periodic in the spanwise z -direction (the coordinate system is indicated in Figure 1). One of the runs, Case C2, is a tangentially-stratified Bunsen flame configuration with a mean equivalence ratio of 0.7 shown in Figure 1a with equivalence ratio variation from 0.41-1.0.

The effect of equivalence ratio variation on the local burning intensity is investigated in turbulent flame simulations with complex chemistry. Earlier work showed that flame-normal equivalence ratio gradients affect the propagation speed of laminar flames, due to the effect of equivalence ratio gradients on the molecular transport of radical species and hot products into the reaction zone [2]. Namely, it was observed that *back-supported* flames yield higher propagation speed than flames in a homogeneous mixture, and that flames in a homogeneous mixture yield faster propagation speed than *front-supported* flames.

The effect of equivalence ratio (φ) stratification on flame speed in the present DNS study is analyzed by calculating the conditional average normalized displacement speed ($\rho S_d / \rho_u(\varphi)$) and the strain rate tangential to the flame in case C2, conditioned on $\varphi=0.7$ and $c=0.65$ (progress variable value which is indicative of the location of maximum heat release), and on a range of flame normal mixture fraction gradients $d\xi/dn$. The flame normal vector, $-\nabla c / |\nabla c|$, points towards the reactants, so that a positive (negative) value of $d\xi/dn$ indicates that this fuel-lean flame is front (*back*) supported. The conditionally

averaged displacement speed, colored by the conditionally-averaged tangential strain rate is plotted in Figure 1b, and compared with the displacement speed computed from reactant-to-product counter-flow laminar flame calculations with the same equivalence ratio range as case C2 and a range of imposed strain rates.

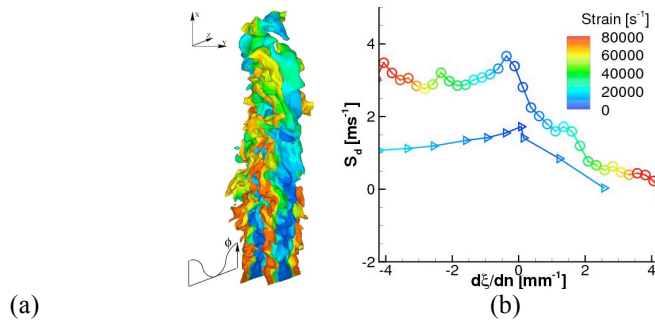


Figure 1. (a) Instantaneous progress variable, $c=0.5$, iso-surface colored by case mixture fraction Z (blue=0, red=1): case C2. (b) Conditionally-averaged displacement speed versus flame-normal mixture fraction gradient. Circles: case C2 at $x/Lx=0.5$ where Lx is the flame height; Triangles: laminar counter-flow flame data.

The turbulent flame exhibits higher average displacement speeds and less sensitivity to mean strain than the laminar flame. This difference may be attributed to the effects of unsteadiness of strain and flame curvature in the turbulent flame, compared to the stationary planar flame front simulated in the laminar counter-flow. However the displacement speed shows an asymmetrical response to flame normal equivalence ratio gradients in both the laminar and turbulent cases, with back supported flames propagating faster compared to front-supported flames at a given tangential strain rate. The similar dependence of flame speed on flame-normal mixture fraction gradient in both the turbulent and laminar cases suggests that the phenomenon is due to the effect of molecular transport from the products that was identified previously in laminar flame studies [2]. Further inspection of the mixture fraction/progress variable cross-dissipation rate conditionally averaged on mixture fraction indicates that there is a tendency for the lean flame to align in a back-supported orientation. This may be a result of the differential propagation mechanism described by Grout et al. [3] and is currently under investigation.

Differential diffusion effects on lifted flame stabilization of syngas mixtures in reacting jet-in-crossflow [4]

Three-dimensional DNS of a transverse syngas fuel jet in a turbulent boundary layer crossflow of air shows the influence of increasing the amount of CO relative to H₂ on the near field flame stabilization. The mean flame anchors at a similar location for the two cases despite the trend suggested by their laminar flame speeds which is higher for the CO-lean condition. To identify local mixtures having preferable mixture conditions for flame anchoring, explosive zones are defined using the chemical explosive mode (CEM) timescale [5]. The explosive zones related to flame stabilization are located in relatively low velocity regions, slightly upstream of the peak heat release rate region. The explosive zones are characterized by excess H transported by differential diffusion with relatively low turbulent mixing intensity or scalar dissipation rate. Based on the balance of scalar flux and differential diffusion, the mixture in the leeward sampling region is classified into three zones. Comparing these three zones with the heat release rate and probable explosive zones, it is found that the differential diffusion predominantly plays an important role in mixture preparation and initiates chemical reactions, followed closely by intense chemical reactions sustained by sufficient mixing owing to the turbulent motion and scalar dissipation rate. Finally, the mechanism of how differential diffusion contributes to mixture preparation is discerned using the Takeno Flame Index computed based on either H₂ or CO mass fraction. The index reveals that H₂ has a significant contribution to premixing, particularly in the explosive zones in the near field of the leeward region, which constitute the flame base. There, a small amount of H₂ is able to diffuse much faster than CO creating a relatively homogeneous mixture, which, together with its

reactivity, helps stabilize a flame at a similar location regardless of the amount of CO present in the fuel.

One-dimensional turbulence modeling of a counterflow flame under intense turbulence and strain with comparison to DNS [6]

The one-dimensional turbulence (ODT) model is applied to a highly turbulent reactant-to-product counterflow configuration and results are compared with recent DNS data [7]. New counterflow configuration specific models were developed to account for 3D dilatation and advection along the 1D line. The model employed solves conservation equations for momentum, energy, and species on a 1D domain corresponding to the line spanning the domain between nozzle orifice centers. The effects of turbulent mixing are modeled via a stochastic process, while the Kolmogorov and reactive length and time scales are explicitly resolved and a detailed chemical kinetic mechanism is used. Comparisons between model and DNS results for spatial mean and fluctuating velocity, temperature, and major and minor species profiles show good agreement. Scatter plots and statistics conditioned on temperature are also compared for heat release rate and all species. Overall, ODT is able to capture the range of results depicted by the DNS. However, conditional statistics in state space show some signs of under-ignition.

Future Work:

Reactive velocity and scalar spectra scaling

Recent results from DNS of turbulent premixed flames reveal that a density change induced by the flame occurring at a characteristic flame scale induces changes to the kinetic energy spectra with a significant deviation from the Kolmogorov scaling, particularly in the high wavenumber range [8]. Furthermore, a dependence of the scaling on a Damköhler number (Da) – ratio of flow time scale to flame time scale – was discerned. A new theoretical framework to study spectral energy balance for variable density flows was proposed that clearly explained the cause of this deviation. However to fully ascertain the proper scaling and to study the balance of energy in the spectral space further DNS spanning a broader range of the relevant parameters, Da and density jump ratio, are proposed. The DNS are being performed in a statistically stationary planar premixed flame configuration. A dimensional analysis will also be performed to understand the importance of the contribution of terms in the balance equations for the velocity and scalar spectrum functions in wavenumber space for combusting flows.

Reactivity controlled compression ignition with thermal inhomogeneities with n-heptane/iso-octane blend

There is currently only a limited fundamental understanding of the nature of combustion in a reactive mixture at high pressure that is conducive to both autoignition and premixed flame propagation. The objective of this study is to perform 3D turbulent DNS of premixed compression ignition (PCI) with a primary reference fuel mixture of n-heptane and iso-octane to quantify the relative roles of autoignition and premixed flame propagation under reactivity controlled compression ignition (RCCI) conditions where thermal and composition stratification are present.

References:

1. E. Richardson and J. H. Chen, (2015) “Analysis of Turbulent Flame Propagation in Equivalence Ratio-Stratified Flow,” *European Combustion Meeting*, Budapest, Turkey.
2. E. S. Richardson, V. E. Granet, A. Eyssartier, J. H. Chen (2010), “Effects of equivalence ratio variation on lean, stratified methane-air laminar counterflow flames,” *Combust. Theory and Model* **14**(6), pp. 775-792.
3. R. W. Grout, N. Swaminathan, R. S. Cant, (2009) *Combust. Theory Model* **13**(5) 823–852.
4. Y. Minamoto, H. Kolla, R. W. Grout, A. Gruber, J. H. Chen, (2015) “Effect of differential diffusion on flame stabilization in a syngas jet in turbulent cross-flow,” *9th U.S. National Combustion Meeting*, Cincinnati, Ohio.
5. T. Lu, C. S. Yoo, J. H. Chen, C. K. Law, (2010), “Three-dimensional direct numerical simulation of a turbulent lifted hydrogen/air jet flame in heated coflow: explosive mode analysis,” *Journal of Fluid Mechanics* **652**:453-481.
6. Z. Jozefik, A. R. Kerstein, H. Schmidt, S. Lyra, H. Kolla, J. H. Chen, (2015) “One-dimensional turbulence modeling of a counterflow flame under intense turbulence and strain with comparison to DNS,” submitted to *Combustion and Flame*.

7. S. Lyra, H. Kolla, B. Coriton, A. Gomez, J.H. Frank & J.H. Chen, (2013) "Extinction phenomena in stratified counterflow H₂/air premixed flames," 8th U. S. National Combustion Meeting, Salt Lake City, Utah.
8. H. Kolla, E. R Hawkes, A. Kerstein, N. Swaminathan, J. H. Chen, (2014) "On velocity and reactive scalar spectra in highly turbulent premixed flames," *J. Fluid Mech.* **754**:456-487.

BES Publications (2013-2015):

1. Y. Yang, H. Wang, S. B. Pope, J. H. Chen, "Large-eddy simulation/probability density function modeling of a non-premixed CO/H₂ temporally evolving jet flame," *Proc. Comb. Inst.* **34** (2013) 1241-1249.
2. N. Chakraborty, H. Kolla, R. Sankaran, E. R. Hawkes, J. H. Chen, and N. Swaminathan, "Determination of 3D quantities related to scalar dissipation rate and its transport from 2D measurements: Direct Numerical Simulation based validation," *Proc. Comb. Inst.* **34** (2013) 1151-1162.
3. C. M. Kaul, V. Raman, E. Knudsen, E. S. Richardson, J. H. Chen, "Large eddy simulation of a lifted ethylene flame using a dynamic nonequilibrium model for subfilter scalar variance and dissipation rate," *Proc. Comb. Inst.* **34** (2013) 1289-1296.
4. O. Chatakonda, E. R. Hawkes, A. Aspden, A. Kerstein, H. Kolla, J. H. Chen, "On the fractal characteristics of low Damkohler number flames," *Combustion and Flame*, **160** (2013) 2422-2433.
5. Y. Yang, S. B. Pope, J. H. Chen, "Empirical low-dimensional manifolds in composition space," *Combustion and Flame*, **160(10)** (2013)1967-1980.
6. D. M. Valiev, M. Zhu, G. Bansal, H. Kolla, C. K. Law, J. H. Chen, "Pulsating instability of externally forced premixed counterflow flame," *Combustion and Flame* **160(2)** (2013) 285-294.
7. H. Zhang, E. R. Hawkes, J. H. Chen, S. Kook, "A numerical study of the autoignition of dimethyl ether with temperature inhomogeneities," *Proc. of the Comb. Inst.* **34(1)** (2013) 803-812.
8. C. S. Yoo, Z. Luo, T. Lu, H. Kim, J. H. Chen, "A DNS study of ignition characteristics of a lean iso-octane/air mixture under HCCI and SACI conditions," *Proc. of the Comb. Inst.* **34(2)** (2013) 2985-2993.
9. A. Gruber, P. Salimath, J. H. Chen, "Direct numerical simulation of laminar flame-wall interaction for a novel H₂-selective membrane / injector configuration" *Intl Journal of Hydrogen Energy* (2014) **39**:5906-5918.
10. A. Bhagatwala, T. Lu, and J. H. Chen, "Direct numerical simulations of HCCI/SACI with ethanol," *Combustion and Flame* (2014) **161**:1826-1841.
11. A. Krisman, J. Tang, E. R. Hawkes, D. Lignell, and J. H. Chen, "A DNS evaluation of mixing models for transported PDF modelling of turbulent nonpremixed flames," *Combustion and Flame* (2014)**161**:2085-2106.
12. Y. Xin, C. S. Yoo, J. H. Chen, C. K. Law, "A DNS study of self-accelerating cylindrical hydrogen-air flames with detailed chemistry," *Proc. Combust. Inst.*, **35** (2015) 753-760.
13. A. Bhagatwala, T. Lu, H. Shen, J. Sutton, J. H. Chen, "Numerical and experimental investigation of turbulent DME jet flames," *Proc. Combust. Inst.*, **35** (2015) 1157-1166.
14. A. Krisman, E. R. Hawkes, M. Talei, A. Bhagatwala, J. H. Chen, "Tribrachial, tetrabrachial and pentabrachial structures in dimethyl ether edge-flames at NTC conditions," *Proc. Combust. Inst.* **35**, (2015) 999-1006.
15. A. Gruber, A. Kerstein, D. Valiev, H. Kolla, J. H. Chen, "Modelling of Mean Flame Shape During Premixed Flame Flashback in Turbulent Boundary Layers," *Proc. Combust. Inst.*, **35** (2015) 1485-1492.
16. R. A. C. Griffiths, J. H. Chen, H. Kolla, R. S. Cant, W. Kollmann, "Three-dimensional topology of turbulent premixed flame interaction," *Proc. Combust. Inst.*, **35** (2015) 1341-1348.
17. Chan, W. L., Kolla, H., Chen, J. H., Ihme, M., "Assessment of model assumptions and budget terms of the unsteady flamelet equations for a turbulent reacting jet-in-crossflow," *Combustion and Flame* (2014) **161**:2601-2613.
18. Bansal, G., Mascarenhas, A. and Chen, J. H., "Direct numerical simulation of autoignition in stratified dimethyl-ether (DME)/Air turbulent mixtures," *Combustion and Flame* (2015) **162**:688-702.
19. Kolla, H., Hawkes, E. R., Kerstein, A. R., Swaminathan, N., Chen, J. H., "On velocity and reactive scalar spectra in highly turbulent premixed flames," *Journal of Fluid Mechanics* (2014) **754**:456-487.
20. Lyra, S., Wilde, B., Kolla, H., Seitzman, J., Lieuwen T., Chen, J. H., "Structure and stabilization of hydrogen-rich transverse jets in a vitiated turbulent flow," *Combustion and Flame*, (2015) **162**:1234-1248.
21. Scholtissek, A., Chan, W. L. Xu, H., Hunger, F., Kolla, H., Chen, J. H., Ihme, M., Class, A., "A multi-scale asymptotic analysis of flamelet equations including tangential diffusion effects for laminar and turbulent flames," *Combustion and Flame* (2015) **162**:1507-1529.
22. S. Kim, M. B. Luong, J. H. Chen, C. S. Yoo, "A DNS study of the ignition of lean PRF/air mixtures with temperature inhomogeneities under high pressure and intermediate temperature," *Combustion and Flame*, (2015) **162**:717-726.

Dynamics and Energetics of Elementary Combustion Reactions and Transient Species

Grant DE-FG03-98ER14879

Robert E. Continetti (rcontinetti@ucsd.edu)

Department of Chemistry and Biochemistry, University of California San Diego
9500 Gilman Drive, La Jolla, CA 92093-0340

I. Program Scope

This research program focuses on experimental studies of transient neutral species and collision complexes relevant to combustion phenomena and fundamental elementary reactions, with the goal of providing benchmarks for state-of-the-art electronic structure and quantum dynamics calculations. Kinematically complete studies of the dissociative photodetachment (DPD) of anion precursors in the form of a photoelectron-photofragment coincidence (PPC) measurement can provide a measure of the dynamics of unimolecular and bimolecular reactions over a wide range of internal and configurational energies, respectively, as shown in the experimental-theoretical study we reported on the $F + H_2O \rightarrow HF + OH$ reaction in collaboration with Hua Guo's group at UNM last year. (DOE Pub. 2) In the last year, new experiments on the $CH_3OH + F \rightarrow HF + CH_3O$ reaction and its isotopologs have been carried out, along with studies of the dissociative excited states of the HOCO radical and aspects of the dissociation mechanism for energized *cis*-HOCO radicals to the OH + CO entrance channel. (DOE Pub. 4) Our measurements of the tunneling rate for cis -HOCO $\rightarrow H + CO_2$ have continued to be of interest as well, and resulted in a collaboration with Al Wagner and colleagues extending in a more quantitative fashion our quasi-1D model for the deep tunneling in that system and applying it to *ab initio* HOCO potential energy surfaces (DOE Pub. 5). In addition, we completed our study of the *tert*-butoxy radical and isomers using photoelectron and PPC spectroscopy as reported in DOE Pub. 6. Final reports on the transition state dynamics of the isotopologs of F-H₂O, the effects of vibrational excitation on F-H₂O and the dynamics of the propiyl radical HC₂CO₂, as discussed in last year's abstract, are also currently in preparation. In the laboratory we are currently bringing the PPC spectrometer back on-line following required maintenance on the cryogenically cooled electrostatic ion beam trap that was necessitated by a failure in December 2014. This will coincide with the commissioning of a cryogenic octupole accumulator trap (COAT) in the ion source that will allow buffer gas cooling of even large polyatomic anions to temperatures < 10 K. In the following sections, recent progress will be reviewed in more detail, followed by a brief discussion of future work.

II. Recent Progress

A. Transition State Dynamics of the $F + HOCH_3 \rightarrow HF + OCH_3$ Reaction

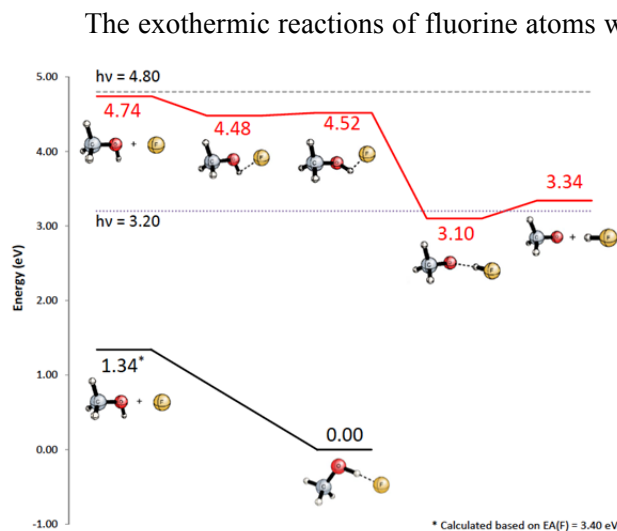


Figure 1. Calculated energetics for the $F + CH_3OH \rightarrow HF + OCH_3$ reaction and the $F^-(CH_3OH)$ anion at the CCSD(T)/aug-cc-pVTZ level of theory.

high accuracy electronic structure calculations, as illustrated by the recent work by Schaefer and co-workers.⁷

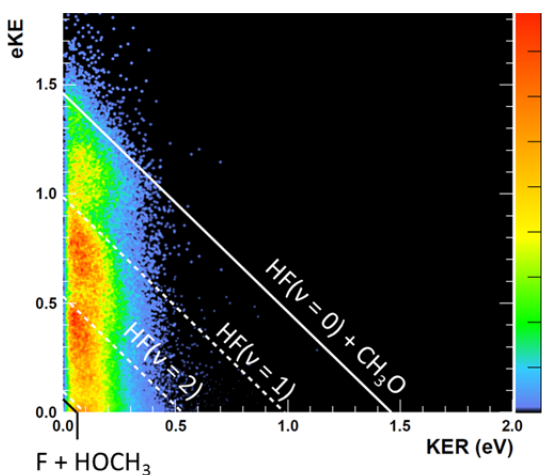


Figure 2. PPC spectrum ($e^- + 2$ momentum-conserving neutrals) for the $F + HOCH_3 \rightarrow HF + OCH_3$ reaction using a photon energy of 4.80 eV. The right most diagonal indicates the maximum kinetic energy (KE_{max}) when the $HF + OCH_3$ products are formed in their vibrational and rotational ground states. The dashed diagonals correspond to vibrational excitation in the HF fragment, while the black diagonal corresponds to the KE_{max} for dissociation to the reactants $F + HOCH_3$.

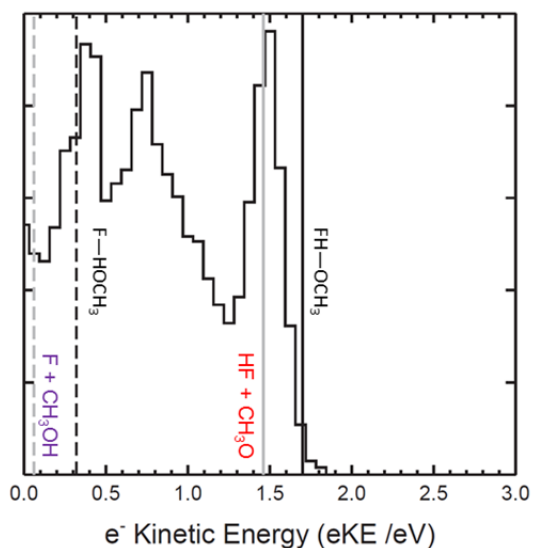


Figure 3. Photoelectron spectrum of the stable ($e^- + 1$ neutral) channel at 4.80 eV (258 nm). The black vertical lines indicate the ZPE corrected, calculated EAs for the entrance (dashed) and exit (solid) complexes. The grey vertical lines correspond to the ZPE corrected, calculated KE_{max} for dissociation to either reactants (dashed) or products (solid) where products are formed in their vibrational and rotational ground states.

The $F^-(CH_3OH)$ anion provides an ideal platform for studying the dynamics on the $F + HOCH_3 \rightarrow HF + OCH_3$ as first illustrated in the photoelectron spectroscopy measurements by Neumark and coworkers more than 20 years ago.⁸ The energetics of photodetachment in this system as well as important stationary points on the neutral potential energy surface are shown in Figure 1. These energetics were provided through a collaboration with Agarwal and Schaefer who have carried out high level calculations (CCSD(T)/aug-cc-pVTZ) at a consistent level of theory for both the anionic and neutral complexes including zero-point-energy corrections.⁹ Figure 1 shows that at a photon energy of 4.80 eV there is sufficient energy to access both reactant (barely) and product channels as well as the submerged barrier separating the entrance and exit channel van der Waals complexes.

We carried out PPC measurements on $F^-(CH_3OH)$, $F^-(CH_3OD)$ and $F^-(CD_3OD)$ at photon energies of 4.80 and 3.20 eV. In these studies we have measured PPC spectra, as well as photoelectron spectra for complexes that appear to be stable or dissociate with exceedingly small kinetic energy release on the 8.4 μs flight time from the laser-ion interaction region to the neutral particle detector at a beam energy of 7 keV. The resulting coincidence spectrum, shown in Figure 2, is dominated by open channels on the product side ($HF + OCH_3 + e^-$) of the neutral potential energy surface. The right most diagonal band corresponds to the calculated energetics, including zero-point energy corrections, for products formed in their ground vibrational and rotational states, in good agreement with experimental data. Additionally, clear banding is observed, consistent with vibrational excitation in the HF product, as indicated by the dashed diagonal lines.

In addition to the dissociative in the coincidence spectrum, a distinct photoelectron spectrum corresponding to a stable channel is observed, shown in Figure 3. The prominent peaks at 1.5 eV and 0.4 eV are assigned to the exit channel ($FH-OCH_3$) and entrance channel ($F-HOCH_3$) van der Waals complexes, respectively. The assignment of the peak near 0.75 eV is less clear, but the implication is that a long-lived metastable complex (a vibrational Feshbach resonance) in the exit channel plays a role. The energetics in Figure 1 are in excellent agreement with the observed exit

channel complex, while the results for the entrance channel complex peak at greater energy than predicted. This observed difference may be a function of the significant geometric difference between the precursor anion and entrance channel complex, possibly requiring vibrational excitation in the anion to facilitate access. This experimental uncertainty can be resolved in the near future with the cryogenic octupole accumulator trap that is being added to the spectrometer. Additional analysis of this system, including a near threshold photoelectron spectrum taken at a photon energy of 3.2 eV, is currently underway.

A. Energetics and Dissociation Dynamics of HOCO and other Oxygenated Radicals

We have continued to study the important combustion intermediate HOCO. In earlier work we measured the barrier for tunneling of *cis*-HOCO and DOCO to H/D + CO₂ over a range of internal energies.¹⁰⁻¹¹ This work motivated a number of theoretical studies, and in the last year in a study led by Dr. Al Wagner (Argonne National Laboratory), a rigorous examination of the quasi-1D tunneling model we introduced in ref. 11 was made using different ab initio potential energy surfaces. This study appeared in the *Journal of Chemical Physics* (DOE Pub. 4), and showed that in spite of its simplicity, the quasi-1D tunneling model provides a useful measure of the properties of the ab initio surfaces in the critical region where tunneling from HOCO to H + CO₂ occurs. A review article of recent progress in studies of the HOCO radical with a focus on contributions by photoelectron and PPC spectroscopies also recently appeared in *Physical Chemistry Chemical Physics* (DOE Pub. 5). In addition to reviewing the earlier studies, this manuscript included a detailed examination of the implications of the PPC experiments on the dynamics for dissociation into the entrance channel OH + CO. We hope that this will promote a more detailed theoretical examination of the *cis* – *trans* isomerization of HOCO and how that couples to the OH + CO entrance channel.

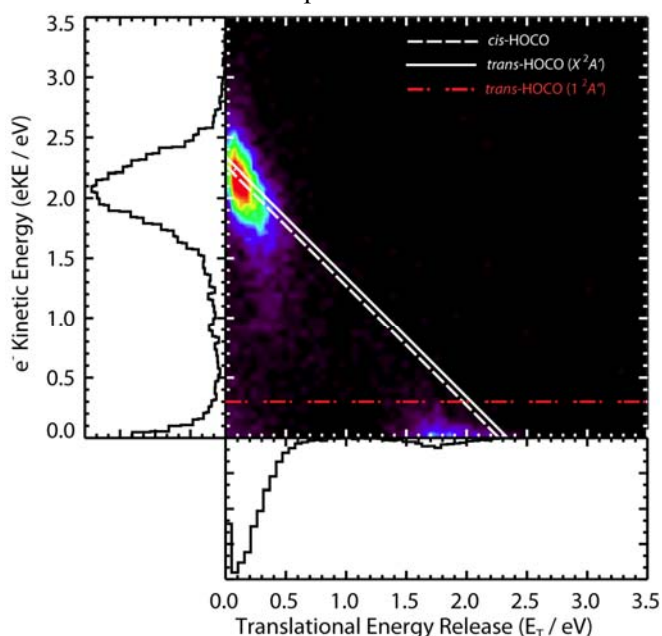


Figure 4. PPC spectrum for the DPD of HOCO to OH + CO at 4.80 eV photon energy. Diagonal lines denote maximum total kinetic energy available for dissociation from *cis*- and *trans*-HOCO while the horizontal line denotes the maximum eKE expected for photodetachment to the $1^2A''$ excited state.

experiments confirmed that the primary stable product is the *tert*-butoxy radical but also detected a small fraction of the alkylhydroxy radical isomer. The carbanion isomer precursor is considerably less stable than the alkoxide in this case, however both can be formed in the high-energy pulsed discharge ion source. A DPD channel was also observed, involving the loss of a methyl radical. This channel can only be the result of two possible reaction pathways: from the carbanion isomer, (a) $(\text{CH}_3)_2\text{COHCH}_2^- + h\nu \rightarrow \text{CH}_3 + \text{CH}_3\text{COHCH}_2$ or *tert*-butoxide, (b) $(\text{CH}_3)_3\text{CO}^- + h\nu \rightarrow \text{CH}_3 + (\text{CH}_3)_2\text{CO}$ (acetone).

We have also extended our studies of HOCO to probe excited state dissociation dynamics focusing in particular on the OH + CO dissociation channel. The DPD of HOCO⁻ at 4.80 eV photon energy reveals two distinct regions of kinetic energy release (E_T), one peaking at < 0.1 eV and the other ~1.7 eV as shown in Figure 4. The peak at high E_T corresponds, by energy conservation with a peak at very low eKE, consistent with photodetachment to a metastable low-lying electronic state of HOCO. These results are qualitatively consistent with stationary point excited state calculations by Li and Francisco that indicate the $1^2A''$ state of *trans*-HOCO lies 1.97 eV above the ground state.¹² Experimental identification of an excited electronic state for HOCO may have important implications for developing new spectroscopic tools for monitoring HOCO in combustion and atmospheric processes.

A study of the photodetachment of *tert*-butoxide with both non-deuterated and deuterated precursors, $(\text{CH}_3)_3\text{CO}^-$ and $(\text{CD}_3)_3\text{CO}^-$ was reported in DOE pub. 6. The

Guided by energetics calculated at the CBS-Q//B3 level of theory, the photoelectron spectra indicated that only a trace of the carbanion isomer was formed. It was concluded, with support from Franck-Condon simulations, that pathway (b) was observed as result of non-Boltzmann internally excited tert-butoxide anion precursors characterized by temperatures up to 1400K along critical C-C stretching modes. This conclusion emphasizes the importance of expanding the PPC spectrometer to include a cryogenically cooled RF accumulator trap to quench vibrational and rotation excitation prior to injection into the EIBT.

III. Current and Future Work

We are currently in the process of bringing the PPC spectrometer back on-line following a major failure in the cryogenic cooling for the electrostatic ion beam trap that necessitated a complete overhaul of closed-cycle He cold head and cryopumps. In addition, we are awaiting the final components for installation of the cryogenic octupole accumulator trap, so that will be brought on line by the middle of this year. This will enable the production of cold ions and will be of immediate use in particular for larger systems like tert-butoxide and the buffer gas cooling of infrared-inactive and rotational modes in all systems prior to injection into the electrostatic ion beam trap. When the spectrometer is brought back on-line, we will demonstrate the effects of vibrational cooling in larger systems like tert-butoxide as well as examining new systems including OH-C₂H₂, OH-C₂H₄ and OH-CH₃ complexes and the OH + NH₃ system.

IV. DOE-supported publications by this project 2012-2015

1. A.W. Ray, B.B. Shen, B.L.J. Poad and R.E. Continetti, *State-resolved predissociation dynamics of the formyloxyl radical*, Chem. Phys. Lett. **592**, 30-35 (2014).
2. R. Otto, J. Ma, A.W. Ray, J.S. Daluz, J. Li, H. Guo and R.E. Continetti, *Imaging dynamics on the F + H₂O → HF + OH potential energy surfaces from wells to barriers*, Science, **343**, 396-399 (2014).
DOE BES Highlight <http://science.energy.gov/bes/highlights/2014/bes-2014-10-d/>
3. R. Otto, A.W. Ray, J.S. Daluz and R.E. Continetti, *Direct IR excitation in a fast ion beam: Application to NO photodetachment cross sections*, EPJ Techniques and Instrumentation **1**:3 (2014).
4. A.F. Wagner, R. Dawes, R.E. Continetti and H. Guo, *Theoretical/experimental comparison of deep tunneling decay of quasi-bound H(D)OCO to H(D)+CO₂*, J. Chem. Phys. **141**, 054304 (2014).
5. C.J. Johnson, R. Otto and R.E. Continetti, *Spectroscopy and dynamics of the HOCO radical*, Phys. Chem. Chem. Phys. **16**, 19091-19105 (2014).
6. B.B. Shen, B.L.J. Poad and R.E. Continetti, *Photoelectron-photofragment coincidence studies of the tert-butoxide anion (CH₃)₃CO, the carbanion isomer (CH₃)₂CH₂COH and corresponding radicals*, J. Phys. Chem. A **118**, 10223-10232 (2014).

V. References

1. Otto, R.; Ma, J.; Ray, A. W.; Daluz, J. S.; Li, J.; Guo, H.; Continetti, R. E., *Science* **2014**, *343*, 396-399.
2. Li, G.; Zhou, L.; Li, Q.-S.; Xie, Y.; Schaefer, H. F., *Phys. Chem. Chem. Phys.* **2012**, *14*, 10891-10895.
3. Li, J.; Dawes, R.; Guo, H., *J. Chem. Phys.* **2012**, *137*, 094304.
4. Li, G.; Li, Q.-S.; Xie, Y.; Schaefer, H. F., *J. Phys. Chem. A* **2013**, *117*, 11979-11982.
5. Nguyen, L.; Li, J.; Dawes, R.; Stanton, J. F.; Guo, H., *J. Phys. Chem. A* **2013**, *117*, 8864-8872.
6. Li, J.; Jiang, B.; Guo, H., *J. Chem. Phys.* **2013**, *138*, 074309.
7. Feng, H.; Randall, K. R.; Schaefer, H. F., *J. Phys. Chem. A* **2015**, *119*, 1636-1641.
8. Bradforth, S.; Arnold, D.; Metz, R. B.; Weaver, A.; Neumark, D. M., *J. Phys. Chem.* **1991**, *95*, 8066-8078.
9. Agarwal, J.; Schaefer, H. F., private communication, **2015**.
10. Johnson, C. J.; Continetti, R. E., *Journal of Physical Chemistry Letters* **2010**, *1*, 1895-1899.
11. Johnson, C. J.; Poad, B. L. J.; Shen, B. B.; Continetti, R. E., *J. Chem. Phys.* **2011**, *134*, 171106.
12. Li, Y. M.; Francisco, J. S., *J. Chem. Phys.* **2000**, *113*, 7963-7970.

Vibrational Dynamics and Dissociation of Ground- and Excited-State Clusters

F.F. Crim
Department of Chemistry
University of Wisconsin–Madison
Madison, Wisconsin 53706
fcrim@chem.wisc.edu

Our research investigates the chemistry of vibrationally excited molecules. The properties and reactivity of vibrationally energized molecules are central to processes occurring in environments as diverse as combustion, atmospheric reactions, and plasmas and are at the heart of many chemical reactions. The goal of our work is to unravel the behavior of vibrationally excited molecules and to exploit the resulting understanding to determine molecular properties and to control chemical processes. A unifying theme is the preparation of a molecule in a specific vibrational state using one of several excitation techniques and the subsequent photodissociation of that prepared molecule. Because the initial vibrational excitation often alters the photodissociation process, we refer to our double-resonance photodissociation scheme as *vibrationally mediated photodissociation*. In the first step, fundamental or overtone excitation prepares a vibrationally excited molecule, and then a second photon, the photolysis photon, excites the molecule to an electronically excited state from which it dissociates. Vibrationally mediated photodissociation provides new vibrational spectroscopy, measures bond strengths with high accuracy, alters dissociation dynamics, and reveals the properties of and couplings among electronically excited states.

Our recent research on vibrational dynamics in clusters has produced new insights into ammonia clusters, one of the prototypical hydrogen-bonded systems. We have determined the dissociation energy of the dimer very precisely ($660 \pm 20 \text{ cm}^{-1}$) and obtained an experimental estimate of the dissociation energy of the trimer ($1600 \pm 100 \text{ cm}^{-1}$). The dynamics we probe show selective coupling of vibrational energy during the dissociation of the dimer. These studies have led us into new studies of ammonia-containing complexes that build on our previous investigations, and we have obtained intriguing results on vibrationally induced isomerization in the complex of ammonia with a substituted phenol.

Ammonia Clusters

The measurements on the ammonia oligomers begin with their formation in a supersonic expansion of ammonia seeded in He followed by infrared laser excitation of their N-H stretching vibrations. Flow of energy from the initially excited N-H stretch dissociates the oligomer to produce vibrationally and rotationally excited ammonia fragments. We detect individual rovibrational states of NH_3 by (2+1) resonance enhanced multiphoton ionization (REMPI) through the \tilde{B} state, as illustrated on the left-hand side of Fig. 1. The right-hand side of the figure shows the infrared-action spectrum obtained by observing NH_3 fragments with one quantum of excitation in the umbrella bending vibration (ν_2). As the lower trace in the figure shows, these features are consistent with the transitions observed in He droplets by Vilesov and coworkers [M. N. Slipchenko, *et al.*, *J. Phys. Chem. A* **111**, 7460 (2007)] and show that excitation of either the symmetric N-H stretch or the antisymmetric N-H stretch initiates vibrational predissociation.

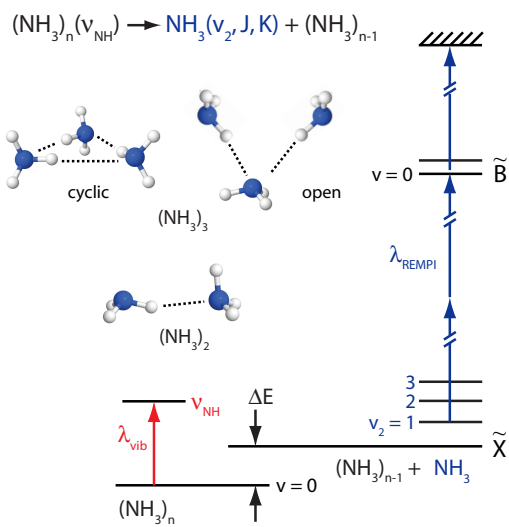
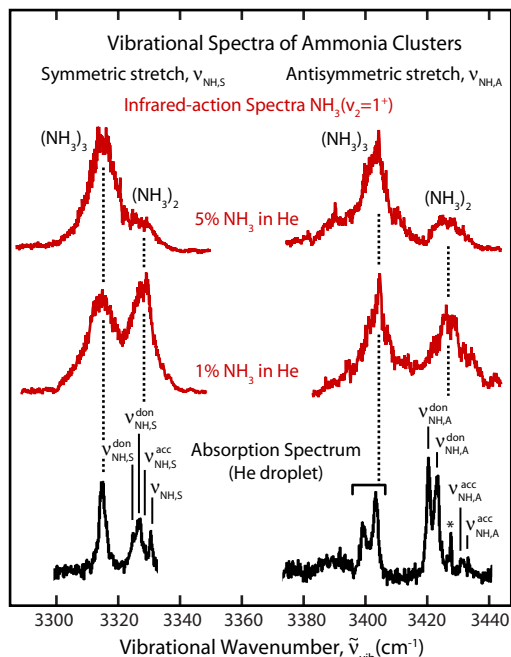


Figure 1



Features corresponding to higher-order clusters appear in the infrared-action spectra in the regions of the intramolecular symmetric N-H stretching vibration ($\nu_{\text{NH},S}$) and the intramolecular antisymmetric N-H stretching vibration ($\nu_{\text{NH},A}$) shown in Fig. 1. The spectra illustrate the influence of expansion conditions on the relative intensities of the features in the spectrum. Because higher seed ratios should favor the formation of larger clusters, the changes between the spectra suggest that the lower energy feature comes from the trimer and that the higher energy feature comes from the dimer, in agreement with the assignments from the He droplet spectra.

Removing an NH_3 fragment from the cyclic trimer, illustrated in Fig. 1, requires breaking two hydrogen bonds. Thus, the dissociation into a monomer and a dimer,



consumes more energy than cleaving the single hydrogen bond of the dimer. As the left hand side of Fig. 2 shows, the trimer feature is prominent in the infrared-action spectrum for detection of $\text{NH}_3(\nu_2 = 1^+, J = 1, K = 0)$ but is essentially absent for detection of $\text{NH}_3(\nu_2 = 3^+, J = 3, K = 0)$. The relative intensities of the dimer and trimer features in the infrared-action spectra depend on the amount of energy available for breaking the hydrogen bonds in the cluster, a quantity that depends on the energy content of the detected fragment. Infrared-action spectra for ammonia fragments with large amounts of internal energy have almost no trimer component because there is not enough energy available to break two bonds in the cyclic trimer and populate the detected state of the NH_3 fragment. By contrast, infrared-action spectra for fragments with low amounts of internal energy have a substantial trimer component.

The right-hand side of the figure shows a quantitative analysis of the trimer contribution compared to that of the dimer in the action spectra. Fitting the two features in the action spectra with Gaussian functions gives a measure of the relative intensity of the dimer and trimer components. The growth in the trimer contribution suggests that fragmentation of the trimer into a monomer and dimer requires an energy of

about 1600 cm^{-1} , a range that is consistent with several theoretical estimates falling within the grey bar in the figure.

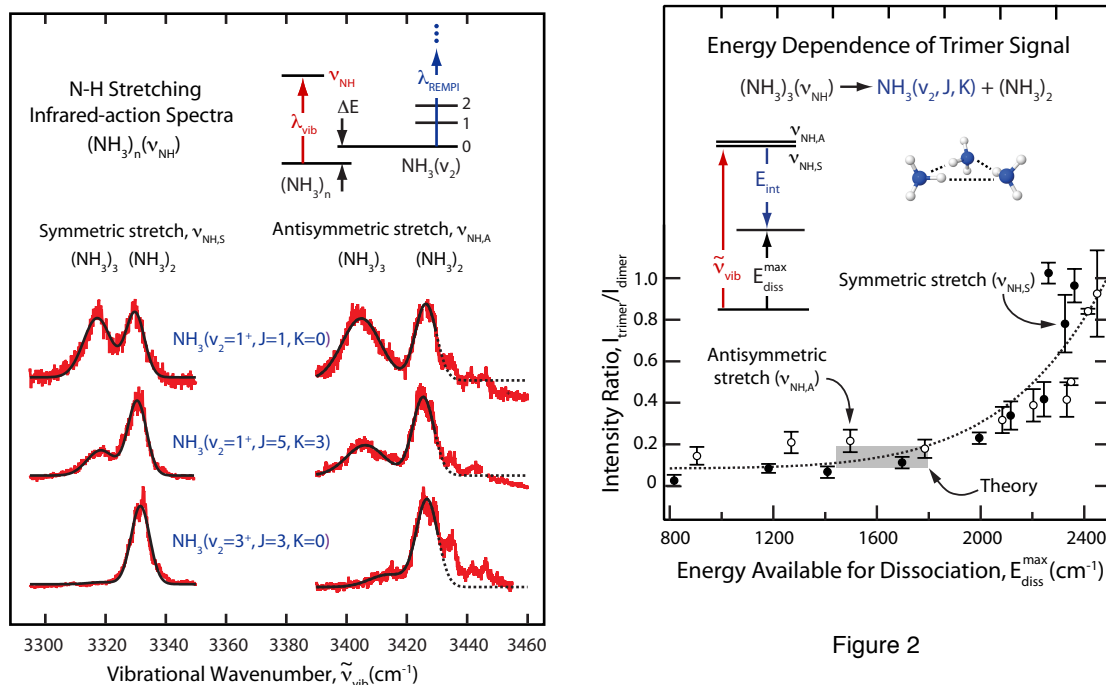
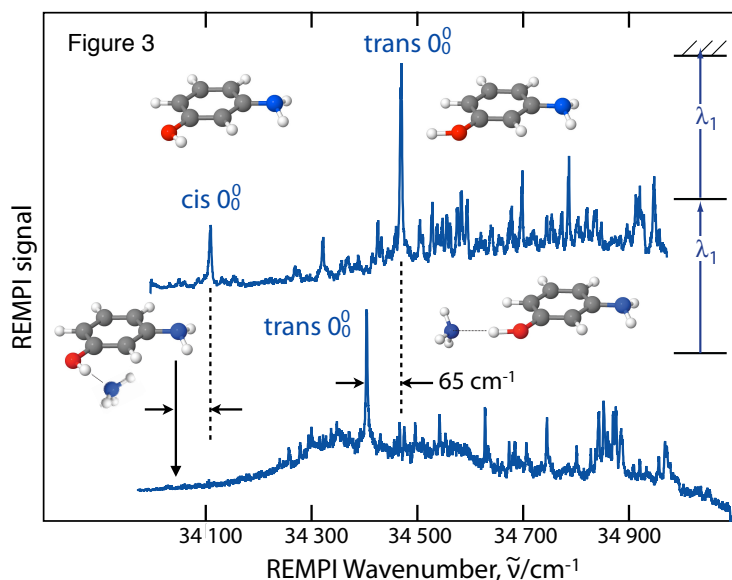


Figure 2

Aminophenol-Ammonia Complexes

We have begun studying the complex of 3-aminophenol with ammonia to understand its bond-strength and its vibrational predissociation as we move toward studying its excited-state dissociation. There are two conformers of 3-aminophenol corresponding to different orientations of the O-H bond. The structures in the top portion of Fig. 3 illustrate the slightly higher energy *cis* conformer and the lower energy *trans* conformer. The spectrum in the top of Fig. 3 is the (1+1) REMPI spectrum of 3-aminophenol with the *cis* and *trans* origins marked. [W. Y. Sohn, *et al.*, Phys. Chem. Chem. Phys. 13, 7006 (2011).] The spectrum in the bottom of the figure is that of the complex, in which the *trans* origin appears about 65 cm^{-1} below that of the bare 3-aminophenol, but the *cis* isomer does not appear, possibly because of interconversion between the two conformers during the formation of the complex. We have recently observed the influence of vibrational excitation on the complex by obtaining the REMPI spectrum after exciting the N-H stretch of the 3-aminophenol in the complex. That action spectrum contains a new feature whose location strongly suggests that it is the origin transition of the *cis* complex. Our preliminary conclusion is that the added vibrational energy induces isomerization of the complex. This observation as well as our detection of a smaller signal upon excitation of the O-H stretch reflects



the coupling of the zero-order stretching state to other motions, likely torsions, that promote isomerization.

Future Directions

We are now in the midst of exploring the influence of vibration on the dynamics of a complex. Our future work goes in two directions. One is similar experiments in other complexes, and the other is to observe the effect of vibrational excitation and the presence of an adduct on the dissociation of electronically excited complexes. We have proven that vibrational excitation of NH₃ drastically alters its dissociation by changing the behavior at a conical intersection. Now we can understand that behavior in different complexes where an adduct will influence the dynamics also.

PUBLICATIONS SINCE 2011 SUPPORTED BY DOE

A. S. Case, C. G. Heid, C. M. Western, and F. F. Crim, *Determining the dissociation threshold of ammonia trimers from action spectroscopy of small clusters*, J. Chem. Phys. **136**, 124310 (2012).

Molecular Reaction Dynamics Across the Phases: Similarities and Differences. F. Fleming Crim, Faraday Discussions **157**, 1 (2012).

Vibrational Predissociation and Vibrationally Induced Isomerization of 3-Aminophenol-Ammonia. Cornelia Heid, Wyatt Merrill, Amanda Case, and F. Fleming Crim, J. Chem. Phys. **142**, 014310 (2015).

Annual Progress Report on project entitled “Theoretical Investigation of Kinetic Processes in Small Radicals” (ER16100)

Millard H. Alexander (mha@umd.edu),
Department of Chemistry and Biochemistry, University of Maryland, College Park, MD 20742-2021
Paul J. Dagdigian (pjdagdigian@jhu.edu),
Department of Chemistry, The Johns Hopkins University of Maryland, Baltimore, MD 21218-2685

Program Scope

Our group studies inelastic and reactive collisions of small molecules, focusing on radicals important in combustion environments. Our goal is the better understanding of kinetic processes that may be difficult to access experimentally. An essential component is the accurate determination and fitting of potential energy surfaces (PESs). We use time-independent (close-coupling) methods to treat the dynamics. We have studied energy transfer (rotationally, vibrationally, and/or electronically inelastic) in small hydrocarbon radicals (CH_2 and CH_3) and the CN radical. We have made a comparison with experimental measurements of relevant rate constants for collisions of these radicals. We have also initiated the calculation of accurate transport properties for collision systems involving a free radical, concentrating on collision pairs relevant to species in a $\text{H}_2/\text{O}_2/\text{He}$ flame. We are presently using these accurate transport properties in 1-dimensional flame simulations.

Personnel

Millard H. Alexander, University of Maryland, Principal Investigator
Paul J. Dagdigian, The Johns Hopkins University, Principal Investigator
Jacek Klos, University of Maryland, Research Assistant Professor
Lifang Ma, University of Maryland, Graduate Research Assistant (Ph.D., 2014)
Qianli Ma, The Johns Hopkins University, Graduate Research Assistant (Ph.D., 2014)

Recent Progress and Future Work

Collisional Relaxation

We have continued to investigate collisional relaxation of methylene (CH_2), a system studied extensively at Brookhaven by the group of Hall and Sears. We previously determined potential energy surfaces (PES's) for the interaction of CH_2 in both its ground X^3B_1 and singlet excited a^1A_1 electronic states with the He atom. By quantum scattering calculations we determined state-to-state integral cross sections for rotationally inelastic transitions and rate constants for total removal of given rotational levels [1,4]. The latter agree well with the Brookhaven results. Vibrational relaxation of the bending mode of $\text{CH}_2(X)$ in collisions with He is two orders of magnitude less efficient than rotational relaxation [14].

We also studied collision-induced internal conversion (CIIC) from the a to the X state of CH_2 , a process mediated by the weak spin-orbit coupling between pairs of accidentally-degenerate rotational levels. Our model is based on coherent mixing of the scattering T -matrix elements for collisional transitions involving the few accidentally degenerate rotational states. [13]. We have employed rate constants for CIIC and rotational energy transfer in a kinetic simulation [3] of the collisional relaxation of $\text{CH}_2(X,a)$ in collisions with He. Figure 1 presents snapshots, following the relaxation of the 8_{18} mixed, nominal a state, studied at Brookhaven. Relaxation proceeds in three steps: (1) rapid equilibration of the two mixed-pair levels [$a(0,0,0)8_{18}$ and $X(0,2,0)9_{37}$, in Fig. 1], (2) fast relaxation within the a state, and (3) slower relaxation among the X -state levels.

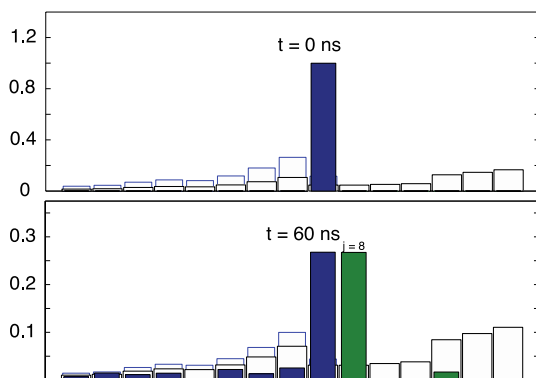


FIG. 1. Rotational distributions of selected singlet (blue) and triplet (green) levels at various times following initial population of the $a(0,0,0) 8_{18}$ mixed level; $p = 2$ Torr, $T = 300$ K. The black rectangular empty boxes denote the relative $T = 300$ K Boltzmann populations. The upper panel indicates the energies of the levels.

Stimulated by our theoretical work on rotational energy transfer in $\text{CH}_3\text{-He}$ collisions [2], Orr-Ewing (Bristol, UK) has applied molecular beam and velocity map imaging to the determination of differential cross sections for scattering of photolytically generated beam of CD_3 with a number of collision partners. REMPI detection of the scattered CD_3 allowed resolution of the rotational angular momentum n , but averaged over a subset of the projection quantum numbers. In a series of studies, Orr-Ewing and his group have determined differential cross sections for collisions of CD_3 with He, H_2 , Ar, and N_2 . We have employed PES's determined by our group for the first 3 collision partners to compute differential cross sections. These agree well with experiment [9,12,16]. We find that the dynamics of collision of the symmetric top CD_3 is richer than that of a diatomic. In collaborative work with Orr-Ewing and van der Avoird (Nijmegen, Netherlands), we have compared the scattering of CD_3 with that of another (nonplanar) symmetric top ND_3 [11].

We have collaborated with Hall and Sears on the study of rotational energy transfer (RET) of $\text{CN}(X)$ in collisions with He and Ar [18]. They have employed frequency modulated transient absorption in a double-resonance, depletion recovery experiment. We carried out quantum scattering calculations for RET of selected rotational levels. Our calculations agree well with measured thermal rate constants, as well as non-thermal Doppler-resolved rate constants. We will investigate collisional depolarization of non-isotropic m distributions.

Transport properties

Modeling combustion involves the prediction of the temporal and spatial dependence of the concentrations of all relevant species, as well as for the calculation of flame velocities. This requires knowledge of rate constants of all the relevant species, as well transport properties. We have been computing accurate transport properties from quantum scattering calculations for collisions of various free radicals. We concluded that: (a) Retention of just the isotropic part of the potential results in errors in transport properties of only a few percent. [The exceptions involve species with a low-lying LUMO, such as $\text{CH}_2(a)$ and BH_3 [8].] (b) Isotropic Lennard-Jones (LJ) 12-6 potentials yield diffusion coefficients with too steep a temperature dependence.

This occurs because the repulsive walls of LJ 12-6 potentials are too steep. (c) Transport property calculations with LJ potentials for radical-radical systems disagree significantly with calculations using accurate potentials.

In current work, we are computing *ab initio* based transport properties for collision pairs relevant to species in a $\text{H}_2/\text{O}_2/\text{He}$ flame, specifically $\text{H}-\text{H}_2\text{O}$ [10], $\text{H}-\text{He}$ [17], $\text{O}-\text{He}$ [17], H_2-He [17], $\text{H}_2\text{O}-\text{He}$ [17], $\text{OH}-\text{He}$ [5], and $\text{H}-\text{O}_2$ [15]. For the latter system ($\text{H}-\text{O}_2$), to accommodate the deep well in the $^2A''$ PES PES's ($^2A''$), we adapted the quantum statistical capture theory of Manolopoulos and co-workers.

We have carried 1-dimensional flame simulations of a freely propagating $\text{H}_2/\text{O}_2/\text{He}$ flame with two sets of transport properties [17]. The first set was based on the conventional parameterized LJ 12-6 potentials, while the second set incorporated exact transport properties for the above collision pairs. A modest increase in laminar flame speeds was seen (Fig. 2), comparable to variations found when employing different models of the chemistry.

We are currently extending our accurate calculation of transport properties to other collision pairs of importance in the combustion of both H_2 and CH_4 . These include $\text{O}-\text{H}_2$, $\text{H}-\text{CO}$, and $\text{H}-\text{CO}_2$. We plan to investigate the CH_3-H system in the near future.

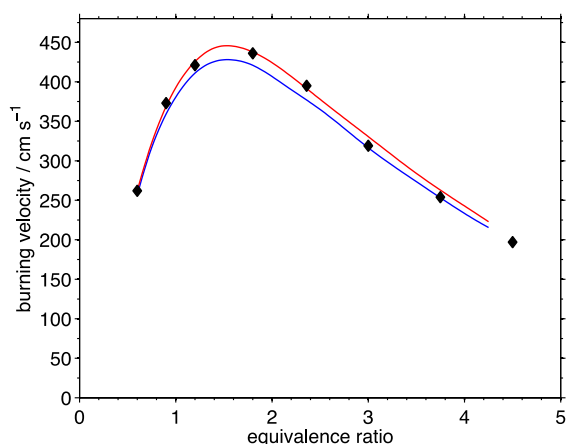


FIG. 2. Laminar flame speed at 1 atm for H_2/O_2 diluted in He with O_2/He dilution ratio of 3.76. The blue and red curves denote calculations with LJ and accurate transport properties, respectively. The black diamonds are experimental data from Kwon and Faeth [Combust. Flame **124**, 590 (2001)].

Interactions with Other Groups and DOE Synergy

Alexander and Dagdigian maintain a close interaction with Hall and Sears at Brookhaven. In addition to our collaborative work on the collisional relaxation of CH_2 , we are collaborating on the Doppler-resolved kinetics and pressure broadening of the CN radical. We are looking forward to comparing our pressure broadening calculations on the $\text{OH } A - X$ transition with forthcoming measurements by Ritchie at Oxford, UK. We have collaborated with Orr-Ewing at Bristol UK on the determination of CD_3 differential cross sections in collisions with a number of species. Alexander has collaborated closely with Chandler at Sandia Livermore on inelastic scattering of the NO radical. Dagdigian's 1-dimensional combustion simulations were facilitated by Sivaramakrishnan at Argonne.

Publications and Submitted Journal Articles Supported by this Project (2011-2015)

1. L. Ma, M. H. Alexander, and P. J. Dagdigian, "Theoretical investigation of rotationally inelastic collisions of $\text{CH}_2(\bar{a})$ with helium," *J. Chem. Phys.* **134**, 154307 (13 pages) (2011)
2. P. J. Dagdigian and M. H. Alexander, "Theoretical investigation of rotationally inelastic collisions of the methyl radical with helium," *J. Chem. Phys.* **135**, 064306 (9 pages) (2011).
3. M. H. Alexander, G. Hall, and P. J. Dagdigian, "The Approach to Equilibrium: Detailed Balance and the Master Equation," *J. Chem. Educ.* **88**, 1538-1540 (2011).
4. L. Ma, M. H. Alexander, and P. J. Dagdigian, "Theoretical investigation of rotationally inelastic collisions of $\text{CH}_2(X)$ with helium," *J. Chem. Phys.* **136**, 224306 (9 pages) (2012).
5. P. J. Dagdigian and M. H. Alexander, "Exact quantum scattering calculation of transport properties for free radicals: $\text{OH}(X^2\Pi)$ -helium," *J. Chem. Phys.* **137**, 094306 (7 pages) (2012).
6. Q. Ma, P. J. Dagdigian, and M. H. Alexander, "Theoretical study of the vibrational relaxation of the methyl radical in collisions with He," *J. Chem. Phys.* **138**, 104317 (10 pages) (2013).
7. P. J. Dagdigian, "Theoretical investigation of collisional energy transfer in polyatomic intermediates," *Int. Rev. Phys. Chem.* **32**, 229-265 (2013).
8. P. J. Dagdigian and M. H. Alexander, "Exact quantum scattering calculations of transport properties: $\text{CH}_2(X^3B_1, a^1A_1)$ -helium," *J. Chem. Phys.* **138**, 164305 (7 pages) (2013).
9. Ondrej Tkáč, A. G. Sage, S. J. Greaves, A. J. Orr-Ewing, P. J. Dagdigian, Q. Ma, and M. H. Alexander, "Rotationally inelastic scattering of CD_3 and CH_3 with He: Comparison of velocity map-imaging with quantum scattering calculations," *Phys. Chem. Chem. Phys.* **140**, 4199-4211 (2013).
10. P. J. Dagdigian and M. H. Alexander, "Exact quantum scattering calculations of transport properties for the $\text{H}_2\text{O}-\text{H}$ system," *J. Chem. Phys.* **139**, 194309 (8 pages) (2013).
11. Ondrej Tkáč, A. J. Orr-Ewing, P. J. Dagdigian, M. H. Alexander, J. Onvlee, and A. van der Avoird, "Collision dynamics of symmetric top molecules: A comparison of the rotationally inelastic scattering of CD_3 and ND_3 with He," *J. Chem. Phys.* **140**, 134308 (10 pages) (2014).
12. Ondrej Tkáč, Q. Ma, C. A. Rusher, S. J. Greaves, A. J. Orr-Ewing, and P. J. Dagdigian, "Differential and integral cross sections for the rotationally inelastic scattering of methyl radicals with H_2 and D_2 ," *J. Chem. Phys.* **140**, 204318 (12 pages) (2014).
13. L. Ma, M. H. Alexander, and P. J. Dagdigian, "Theoretical investigation of intersystem crossing between the a^1A_1 and X^3B_1 states induced by collisions with helium," *J. Chem. Phys.* **141**, 064312 (10 pages) (2014).
14. L. Ma, P. J. Dagdigian, and M. H. Alexander, "Theoretical investigation of the relaxation of the bending mode of $\text{CH}_2(X)$ by collisions with helium," *J. Chem. Phys.* **141**, 214305 (4 pages) (2014).
15. P. J. Dagdigian and M. H. Alexander, "Transport cross sections for systems with deep potential wells," *J. Phys. Chem. A* **118**, 11935-11942 (2014).
16. Ondrej Tkáč, Q. Ma, M. Stei, A. J. Orr-Ewing, and P. J. Dagdigian, "Rotationally inelastic scattering of methyl radicals with Ar and N_2 ," *J. Chem. Phys.* **142**, 014306 (10 pages) (2015).
17. P. J. Dagdigian, "Combustion simulations with accurate transport properties for reactive intermediates," *Comb. Flame* (in press).
18. D. Forthomme, M. L. Hause, H.-G. Yu, P. J. Dagdigian, T. J. Sears, and G. E. Hall, "Doppler-resolved kinetics of saturation recovery," *J. Phys. Chem. A* (in press).

Theory and Modeling of Multiphase Reacting Flow Dynamics in Simulations and Experiments

Rainer N. Dahms
Combustion Research Facility, Sandia National Laboratories
Livermore, CA 94551-0969
Rndahms@sandia.gov

I. Program Scope

This theoretical and modeling effort on multiphase reacting flow dynamics is based on three primary objectives. The first is to establish a physically-based understanding of improved turbulent mixing and combustion models in multiphase flows. Many of the relevant fluid flow processes take place on time and length scales which are not feasible to resolve directly in simulations. Therefore, sophisticated sub-grid scale models have to be developed. This requires a comprehensive understanding of the fundamental processes of the underlying relevant phenomena. In this context, a major focus is the development of more general regimes that incorporate broader ranges of combustion modes and a more complete set of non-dimensional parameters. The second objective is to develop techniques and methods to understand data sets obtained from high-fidelity Large-Eddy simulations (Oefelein) and measurements performed in the Advanced Imaging Laboratory (Frank) and in the Turbulent Combustion Laboratory (Barlow) in a meaningful manner. The fundamental issues of comparing, validating, and understanding advanced combustion data sets will become even more important as we attempt to understand the dynamics of turbulence-flame interactions using data sets that capture the temporal evolution of turbulent flames. The third objective is to understand the implications of the conclusions obtained from well-controlled experiments in the context of advanced power and propulsion systems including gas turbines, automotive engines, and liquid rockets. This effort has to consider the poorly understood effect of elevated pressure on the fundamentals of multiphase combustion phenomena. It builds on the developed theoretical framework, which establishes a meaningful set of major scaling parameters. Combined with the identification of relevant ranges of combustion regimes and non-dimensional parameters in modern transportation and power systems, the framework will serve the general objective of this program to accelerate the development and validation of science-based, predictive computational models for turbulent combustion systems.

II. Recent Progress

Understanding and quantifying multiphase reacting flow phenomena in fundamental experiments and modern transportation and energy systems is widely recognized as a critical research area for future combustion design. The importance to develop a basic science foundation for predictive models has been consistently highlighted over many years in a variety of industry, government, and academic forums including recent DOE workshops such as the *Workshop to Identify Research Needs and Impacts in Predictive Simulations for Internal Combustion Engines (PreSICE)*,¹ and the *Workshop on Clean and Efficient Combustion of 21st Century Transportation Fuels*.² Liquid injection processes largely determine the mixture preparation process which ultimately governs the detailed evolution of chemical kinetic processes and their interaction with the turbulent flow field.

Liquid injection in systems at elevated operating pressures is not well understood. Imaging (such as those performed by Mayer *et al.*)³ has long shown that under some high-pressure conditions, the presence of discrete two-phase flow dynamics may become diminished. Then, the characteristic processes of

primary and secondary atomization, multi-component evaporation, and liquid ligament and drop formation do not occur. As a consequence, the widely acknowledged drop formation and breakup regimes (see Lasheras and Hopfinger⁴), which establish the conceptual foundations of most spray simulation models, do not apply anymore. Modern theory has long lacked a first-principle explanation to understand and quantify the observed phenomena (see a recent review by Cheroudi⁵). Recently, such a theory has been developed that established that the development of such mixing layers is initiated because the multicomponent two-phase interface becomes much wider than the mean free molecular path (see Dahms *et al.*⁶). This theory demonstrated that fuel injection processes in diesel engines are not determined, contrary to conventional wisdom, by classical spray atomization but by diffusion-dominated dense-fluid mixing dynamics without the presence of surface tension at many relevant conditions (see Dahms *et al.*⁷).

Recent studies aimed to understand the dynamics of the transition process from classical sprays to dense-fluid mixing. The performed analysis was built on the previously developed comprehensive framework, based on theories of extended corresponding states, capillary flows, vapor-liquid equilibrium, and Gradient Theory (see for example the pioneering work of van der Waals⁸ and Cahn and Hilliard⁹) to facilitate the calculation of two-phase molecular interface structures. A modified 32-term Benedict-Webb-Rubin equation of state is utilized for the prediction of the pressure-volume-temperature behavior of the liquid phase, saturated vapor mixtures, and gas phase properties. This framework was recently extended to include effects of statistical fluctuations about the average interface molecule number and the presence of significant interfacial free energy forces.

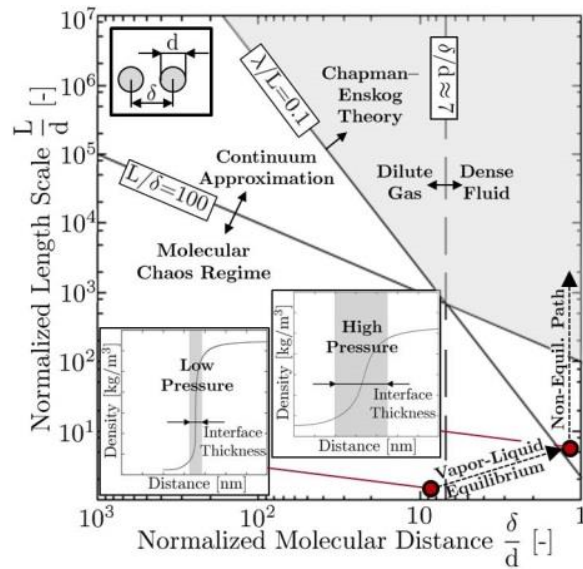


Figure 1: Location of low-pressure and high-pressure gas-liquid interfaces (inset plots) within the regime diagram of microscale flows according to Bird¹⁰. The highlighted area represents the regime where the Navier-Stokes equations are valid and the significance of statistical fluctuations about the average interface molecule number diminishes. The association of the continuum regime with Knudsen-number $Kn < 0.1$ is only valid for dilute gases ($\delta/d > 7$) but not for dense-fluid mixtures at high pressures encountered here (see Dahms *et al.*¹³).

Figure 1 presents the regime diagram of microscale flows according to Bird¹⁰. The diagram is based on the four characteristic length scales of representative molecule size d , mean molecular spacing δ , mean free path λ , and a characteristic length scale L . The regime contains three regime separators. The first is represented by $L/\delta=100$ as the number of molecules within a volume element at which the significance of statistical fluctuations in molecule number diminishes. The second regime separator is represented by the Knudsen number $Kn=\lambda/L=0.1$ below which shear stresses, heat fluxes, and diffusion velocities become linear functions of the gradients in velocity, temperature, and species concentration. The third regime separator is defined by the ratio $\delta/d \approx 7$ as the distinction between dilute gases and dense fluids. These definitions also establish the regime where the Navier-Stokes equations are valid (grey area in Fig. 1). The locations of low-pressure and high-pressure gas-liquid interfaces within the regime diagram are also shown in Fig. 1. Both interfaces are located in the molecular chaos regime and their interfacial dynamics are dictated by substantial statistical fluctuations as a consequence. This analysis illustrates that the association of the continuum regime, where statistical fluctuations of molecule numbers are negligible,

with Knudsen-number $Kn < 0.1$ is only valid in the dilute gas regime but not in the dense-fluid regime encountered here. It also illustrates that the Navier-Stokes equations are not valid under these conditions.

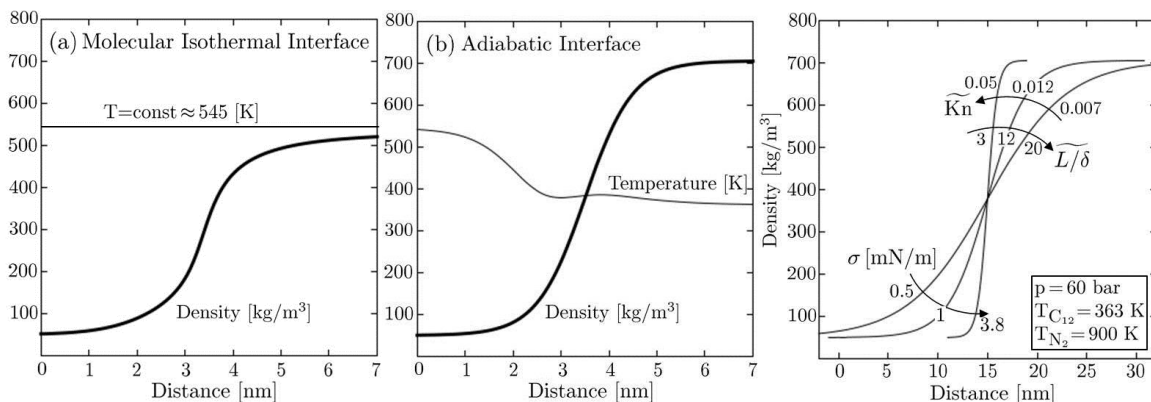


Fig. 2 (left) shows a classical molecular two-phase isothermal interface structure. An adiabatic interface, formed by interfacial gradients when $Kn < 0.1$, is shown in the middle. Figure 2 (right) presents three different interface structures of various stages in the progress of the interface deterioration.

Figure 2 (left) shows the density profile using the molecular isothermal interface assumption according to classical theories of capillary flows. Figure 2 (middle) shows the density profile of an adiabatic interface, formed by the development of internal temperature gradients at low Knudsen numbers ($Kn < 0.1$). Such a temperature distribution across the interface leads to an increased density gradient and an increased density in the compressed liquid phase. Once the interface distinctively departs from the equilibrium state in such a manner, the interfacial region begins to deteriorate as it broadens substantially. This temporal process of interface deterioration is highlighted in Fig. 2 (right). During this process, the interfacial free energy forces σ are calculated using non-equilibrium mean-field thermodynamics. This analysis shows that such free energy forces do not instantly diminish only because the interface has entered the low Knudsen-number regime $Kn < 0.1$. Instead, such forces are shown to gradually decrease over time as the interface continues to broaden. This pathway is also highlighted as the non-equilibrium path in the regime diagram of microscale flows in Fig. 1.

This analysis demonstrates that the fuel injection process close to the injector exit is still affected by capillary forces and physics of molecular chaos. This physical complexity, however, gradually transitions over time, and as the fuel penetrates into the combustion chamber, into a gas-liquid mixing layer without drop formation and evaporation (see Dahms *et al.*¹³).

III. Future Work

All existing simulation models entirely neglect the non-equilibrium two-phase processes discovered here. The presented fundamental finding could carry immense implications for the development of fuel injection models since the inclusion of this discovered physical complexity in simulations promises to significantly improve their predictive capabilities. The fundamental approach described above will be further developed with an emphasis on interrelated areas of research. A close collaboration between the Large-Eddy simulation program and the experimental flow research program will be maintained. A significant effort on the validation and generalization of the proposed theory will be initiated. Such efforts include detailed comparisons to high-speed microscopic imaging at high-pressure conditions, improvements of model accuracy, and the investigation of effects of multi-component fuels on liquid jet breakup regimes and turbulent combustion processes at elevated system pressures. The objective is to develop a predictive first-principle model framework suitable for high-fidelity combustion simulations.

This framework will also increase our understanding of implications, drawn from conclusions obtained from well-controlled fundamental experiments, in the context of general power and propulsion systems including gas turbines, automotive engines, and liquid rockets.

IV. Literature Cited

1. A Workshop to Identify Research Needs and Impacts in Predictive Simulation for Internal Combustion Engines. http://science.energy.gov/~media/bes/pdf/reports/files/PreSICE_rpt.pdf , 2011; Sponsored by the Office of Basic Energy Sciences, Office of Science and the Vehicle Technologies Program, Office of Energy Efficiency and Renewable Energy, U.S. Department of Energy
2. Basic Research Needs for Clean and Efficient Combustion of 21st Century Transportation Fuels. <http://www.osti.gov/scitech/servlets/purl/935428>, 2006; Report of the Basic Energy Sciences Workshop on Clean and Efficient Combustion of 21st Century Transportation Fuels, U.S. Department of Energy.
3. W. Mayer and H. Tamura. Propellant injection in a liquid oxygen/gaseous hydrogen rocket engine. *Journal of Propulsion and Power* 12:1137-1147, 1996.
4. J.C. Lasheras and E.J. Hopfinger. Liquid jet instability and atomization in a coaxial gas stream. *Annu. Rev. Fluid Mech.* 32:275-308, 2000. doi: 10.1146/annurev.fluid.32.1.275
5. B. Chehroudi. Recent experimental efforts on high-pressure supercritical injection for liquid rockets and their implications. *Intl. J. Aerospace Engineering* 2012:1-31, 2012. doi: 10.1155/2012/121802
6. R.N. Dahms, J. Manin, L.M. Pickett, and J.C. Oefelein. Understanding high-pressure gas-liquid interface phenomena in diesel engines. *Proc. Combust. Inst.* 34:1667-1675, 2013. doi: 10.1016/j.proci.2012.06.169
7. R.N. Dahms and J.C. Oefelein. On the transition between two-phase and single-phase interface dynamics in multicomponent fluids at supercritical pressures. *Phys. Fluids* 25, 092103, 2013. doi: 10.1063/1.4820346
8. J.D. van der Waals. Square gradient model. *Verhandel Konink Akad Wetten Amsterdam* 1:8-15, 1893.
9. J.W. Cahn and J.E. Hilliard. Free energy of a nonuniform system. I. Interfacial free energy. *J. Chem. Phys.* 28:258-267, 1958
10. G.A. Bird. *Molecular gas dynamics and the direct simulation of gas flows*. Oxford University Press., 1994.

V. BES Sponsored Publications (2013-2015)

11. R.N. Dahms and J.C. Oefelein. Atomization and dense fluid breakup regimes in liquid rocket engines. *J. Propulsion Power*, 2015. Accepted for publication.
12. R.N. Dahms. Gradient Theory simulations of pure fluid interfaces using a generalized expression for influence parameters and a Helmholtz energy equation of state for fundamentally consistent two-phase calculations. *J. Colloid Interface Sci.* **445**:48-59, 2015. doi: 10.1016/j.jcis.2014.12.069
13. R.N. Dahms and J.C. Oefelein. Non-equilibrium gas-liquid interface dynamics in high-pressure liquid injection systems. *Proc. Combust. Inst.* **35**:1587-1594, 2015. doi: 10.1016/j.proci.2014.05.155
14. R.N. Dahms and J.C. Oefelein. On the transition between two-phase and single-phase interface dynamics in multicomponent fluids at supercritical pressures. *Phys. Fluids* **25**, 092103, 2013. doi: 10.1063/1.4820346
15. R.N. Dahms, J. Manin, L.M. Pickett, and J.C. Oefelein. Understanding high-pressure gas-liquid interface phenomena in diesel engines. *Proc. Combust. Inst.* **34**:1667-1675, 2013. doi: 10.1016/j.proci.2012.06.169
16. J. Manin, M. Bardi, L.M. Pickett, R.N. Dahms, and J.C. Oefelein. Microscopic investigation of the atomization and mixing processes of diesel sprays injected into high pressure and temperature environments. *Fuel* 134:531-543, 2014. doi: 10.1016/j.fuel.2014.05.060

Bimolecular Dynamics of Combustion Reactions

H. Floyd Davis
Department of Chemistry and Chemical Biology
Cornell University
Ithaca, NY 14853-1301
hfd1@Cornell.edu

I. Program Scope:

The aim of this research program is to better understand the mechanisms and product energy disposal in elementary bimolecular reactions fundamental to combustion chemistry. Using the crossed molecular beams method, the angular and velocity distributions of neutral products from single reactive collisions are measured using VUV laser ionization methods.

II. Recent Progress and Future Plans:

Over the past year, a VUV light source employing four-wave mixing of collimated (*i.e.*, unfocussed) nanosecond laser pulses¹ was set up and tested on Endstation 1 at Cornell. This universal crossed molecular beams apparatus was recently moved from LBNL, and is now fully operational in our laboratory. In our original version of this light source, ~0.1 mJ pulses at 9.9 eV (125 nm) were employed for product photoionization.² This made it possible to study reactions forming products with relatively low ionization energies, such as reactions of C₆H₅ (phenyl) radicals with C₃H₆ (propene), C₄H₈ (trans 2-butene),³ and O₂.⁴ However, for systems of interest producing products with higher ionization energies, it is desirable to extend the accessible photon energy range to ~12 eV.

As described in our abstract last year, we developed a technique for producing radiation extending to 13 eV with higher conversion efficiencies than previously reported.⁵ That method involves noncollinear phasematching of focused lasers in laser vaporized mercury (Hg) at room temperature. This approach easily facilitates windowless operation. Furthermore, using noncollinear phasematching, the short wavelength radiation is spatially isolated from the residual UV and visible beams without need for lossy optical elements such as windows, lenses, and gratings.

While the use of noncollinear phasematching is promising for some applications, the efficiency for VUV generation is limited because the incident lasers must be focused. We have therefore devoted considerable effort over the past year to extending the use of *unfocussed* lasers over long (1 meter) interaction lengths for generation light in the 12 eV range. A very promising method employs doubly-resonant frequency tripling of 312 nm light producing 11.9 eV photons. Here, 312 nm corresponds to a two-photon resonance in Hg, while the third photon lies near a Rydberg resonance in Hg. We have found that this scheme facilitates conversion efficiencies within an order of magnitude of that reported earlier by us near 10 eV.¹

Since 104 nm light cannot be transmitted efficiently by any solid material (including lithium fluoride), a completely windowless configuration employing four differential pumping regions was developed, with > 99% of the 312 nm residual beam removed by grazing angle reflection from a custom-made AR coated dielectric mirror. We believe this approach, combined with the schemes

reported earlier, allow us to achieve nearly universal VUV photoionization detection using a single apparatus at 9.5, 9.9, 11.1 and 11.9 eV.

During the upcoming year, we plan to employ this light source for crossed beams studies of reactions of alkyl radicals such as C₂H₅ and C₃H₇ with O₂, and reactions of alkenes such as C₂H₄ and C₃H₆ with OH. The availability of “line tunable” VUV photoionization will be particularly valuable, as the products from these reactions have ionization energies ranging from < 9.5 eV (e.g., CH₂CHOH) to > 11.3 eV (e.g., HO₂).

III. References (Numbers 1-3 are publications since 2012 citing DOE support):

1. D.R. Albert, D.L. Proctor, and H.F. Davis, “High-Intensity Coherent Vacuum Ultraviolet Source Using Unfocussed Commercial Dye Lasers”, *Rev. Sci Instrum.* **84**, 063104 (2013).
2. D.R. Albert and H.F. Davis “Experimental Studies of Bimolecular Reaction Dynamics Using Pulsed Tabletop VUV Photoionization Detection”, invited perspective article, *Phys. Chem. Chem. Phys.* **15**, 14566-14580 (2013).
3. D.R. Albert, M.A. Todt, and H.F. Davis, “Crossed Molecular Beam Studies of Phenyl Radical Reactions with Propene and 2-Butene” *J. Phys. Chem. A* **117**, 13967-13975 (2013).
4. D.R. Albert and H.F. Davis “Collision Complex Lifetimes in the Reaction C₆H₅ + O₂ → C₆H₅O + O”, *J. Phys. Chem. Lett.* **1**, 1107 (2010).
5. M.A. Todt, D.R. Albert, H.F. Davis, “High Intensity VUV and XUV Generation by Noncollinear Phasematching in Laser Vaporized Media”, in preparation.

Exploration and validation of chemical-kinetic mechanisms

Michael J. Davis

Chemical Sciences and Engineering Division
Argonne National Laboratory
Argonne, IL 60439
Email: davis@tcg.anl.gov

The focus of the work is on exploration and theoretical validation of chemical-kinetic mechanisms, which combines global sensitivity analysis with the exploration of the characteristics of the sensitivity analysis over the physical and chemical parameters.

Recent Progress

In collaboration with Liu and Sivaramakrishnan, a project on global sensitivity analysis (GSA) with small sample sizes has been completed. This method was then used to analyze engine simulations in collaboration with Som, Wang, Magnotti, Liu, and Sivaramakrishnan. References [P3] and [P11] have preliminary accounts of both of these papers. As in previous implementations of GSA, the present work uses the results from a set of simulations that differ in the rate coefficients used for each chemical reaction in the model. The sets of rate coefficients in each simulation are random draws from within the ranges of uncertainty of each reaction. In previous work, it was necessary to have large sample sizes to get an accurate set of sensitivities, usually at least a factor of 40 x the number of reactions. For the chemical mechanism used in the engine simulations the number of simulations would have to be at least 36,000 (40 x 914 reactions). Because each engine simulation takes a few processor weeks to complete this would be an excessive amount of computations. The new implementation of GSA can be used with sample sizes between 1/3 and 2 x the number of reactions. It uses the technique of sparse regression developed in the statistical and machine learning literature. It works well because a limited number of reactions have significant sensitivity, although due to difficulties in using small sample sizes in high-dimensional space there is the potential for false positives and false negatives. So some care needs to be exercised in the analysis of the GSA results.

Because of the difficulty with sampling in high-dimensional spaces, a series of 50 constant pressure simulations were performed to validate the sparse GSA procedures. The pressures and initial temperatures and fuel compositions of these simulations sampled the ranges of conditions inside the cylinder during the engine simulations. Sample sizes of 50,000 were used for each of these simulations and GSA was performed from ordinary least squares, i.e. minimization of the first summation in Eq. (2) below. Sparse GSA was then performed on samples of size 800 for each of these 50 conditions. There were a total of 100 runs of this type for each set of conditions, with these samples drawn randomly from the initial set of 50,000. Therefore the total number of sparse GSA runs for the constant pressure simulations was 5000.

All simulations described here were performed with a chemical model for a mixture of n-heptane and methyl butanoate, meant to be a surrogate for a biodiesel fuel. After mechanism reduction this chemical model consists of 166 species and 914 reactions, as described in [P2]. Engine simulations were performed as described in [P6]. The engine simulations lead to a set of ignition delay times, which are fit to the following polynomial model:

$$\tau^{(2)}(\{u_i\}) = \sum_{i=1}^{914} \sum_{k=1}^2 a_{ik} u_i^k + \sum_{j=1}^{r-1} \sum_{r=2}^{914} b_{jr} u_j u_r \quad (1)$$

Sparse regression is accomplished by minimizing the following error:

$$E(\mathbf{c}) = \frac{1}{2} \sum_{k=1}^M \left(t_k - \sum_{j=1}^L c_j g_j(\mathbf{u}_k) \right)^2 + \lambda \sum_{j=1}^L |c_j|, \quad (2)$$

where “g” is shorthand for the function in Eq. (1). The first summation in Eq. (2) leads to ordinary least squares and the second term is a penalty term that results in the sparse regression, because the minimization of Eq. (2) results in a significant number of c’s equal to zero.

Table 1: Sparse sensitivity coefficients for engine simulations compared with 0-D sparse coefficients and full OLS sensitivity coefficients.

Eng ^a	Index ^b	Reaction	0-D Sp ^{c,d}	0-D OL ^{c,e}	Sp S _i ^f	OL S _i ^g
1	831	C7H15O2-2=C7H14OOH2-4	1	1	0.103	0.120
2	836	C7H15O2-4=C7H14OOH4-2	4	3	0.045	0.052
3	873	C7H14OOH2-4O2=NC7KET24+OH	2	4	0.040	0.050
4	723	NC7H16+HO2=C7H15-3+H2O2	3	2	0.037	0.057
5	834	C7H15O2-3=C7H14OOH3-5	5	5	0.032	0.038
6	828	C7H15O2-1=C7H14OOH1-3	6	10	0.023	0.021
7	872	C7H14OOH1-3O2=NC7KET13+OH	8	8	0.019	0.022
8	722	NC7H16+HO2=C7H15-2+H2O2	9	7	0.018	0.026
9	878	C7H14OOH4-2O2=NC7KET42+OH	7	6	0.014	0.028
10	615	MB+OH=H2O+MB3J	11	15	0.013	0.010
11	876	C7H14OOH3-5O2=NC7KET35+OH	10	9	0.009	0.022
12	532	PC4H9=C2H5+C2H4	12	16	0.008	0.009
13	724	NC7H16+HO2=C7H15-4+H2O2	13	12	0.007	0.012

^a Order of sparse sensitivity coefficients from the engine simulations

^b Reaction index

^c Constant pressure runs: P = 82.7 atm, T₀ = 886 K, ϕ₀ = 1.2

^d Sparse sensitivity coefficients from a set of 800 runs, resolved with the quadratic model described in section 2.

^e Ordinary least squares (OLS) with the same quadratic model, based on 50,000 constant pressure runs

^f Sparse sensitivity coefficients for engine simulations for the selected reactions.

^g Sensitivity coefficients for 0-D OLS for the 13 reactions selected from the engine simulations.

GSA results are summarized in Table 1 for the engine simulations and compared to a constant pressure run (labeled “0-D”) whose reaction ordering best matched the engine ordering. As noted above it is important to validate the sparse procedures and the results in Columns 4 and 5 are part of that validation. Comparison of these two columns demonstrates that the sparse GSA and full GSA agree fairly well, although there are some mis-orderings in the sparse case.

The results in columns 4 -7 of Table 1 are extended to the full set of 50 initial conditions in Fig. 1, which shows the average value of the sparse selection vs. the full OLS for the 50 sets of constant pressure runs. The bars on the first 18 points are the rms errors and the line is color-coded based on the fraction of times a reaction appears in the sparse sensitivity analysis. Consider two examples from Fig. 1. The reaction that is most sensitive for the OLS runs is usually the most sensitive for the sparse case. It has an average value of 1.02 (i.e., number one 49 times and number two once). It has an rms error of 0.02 based on these numbers. The reaction that is fifth most sensitive in the OLS calculations at each of the 50 physical initial conditions has an average value of 5.7 in the sparse calculations for the same set of 50 runs and an rms error of 1.46. The distribution for this case is: 4:7, 5:20, 6:12, 7:5, 8:4, 9:2, indicating for example that the fifth most

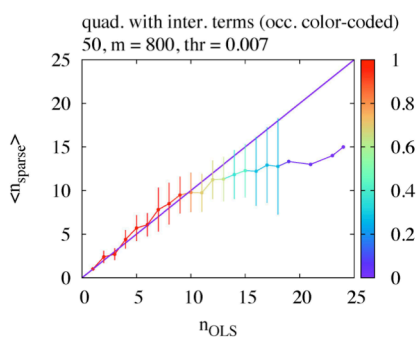


Figure 1. The average values of the sparse selection for 0-D vs. OLS are plotted. The color coding indicates the fraction of reactions chosen.

demonstrates the shift from low-temperature to high-temperature combustion. The two hydrogen/oxygen reactions have their highest sensitivity coefficients in the third column. Two β -scission reactions are evident at the highest temperature as the eleventh and fourteenth most sensitive reactions there, but are not found in the first two columns. Table 2 also demonstrates that several classes of reactions become less common moving through the table as evidenced by

sensitive reaction in the OLS appears as the sixth most sensitive reaction 12 times out of the 50 sets of 800 runs. The coloring in Fig. 1 indicates both the most sensitive and fifth most sensitive reactions in the OLS appear in all 50 sparse cases and that the 10th most sensitive ($n = 10$ on the x-axis) has sparse sensitivity values above 0.007 in 41 out of 50 sparse runs.

Figure 1 makes comparisons based on the relative ordering of the reactions, but the reactions change as the conditions change as emphasized in Table 2. Typical low-temperature combustion chemistry is more prevalent at the lowest temperature studied and less prevalent at the highest temperature studied, where there is more of a mixture of low-temperature and high temperature combustion.

Table 2 shows three of the 50 0-D conditions that we studied. Certain reactions are color-coded based on reaction type. This table lists the top 15 most sensitive reactions, and

Table 2: Sensitivity Coefficients for 0-D simulations: Full OLS values

	$T_0 = 825, P = 81.4 \phi_0 = 2.76^{a,b}$	$T_0 = 886, P = 82.7 \phi_0 = 1.2^{a,c}$	$T_0 = 935, P = 76.1, \phi_0 = 1.16^{a,d}$
1	C7H15O2-2=C7H14OOH2-4	C7H15O2-2=C7H14OOH2-4	NC7H16+HO2=C7H15-3+H2O2
2	C7H15O2-4=C7H14OOH4-2	NC7H16+HO2=C7H15-3+H2O2	C7H15O2-2=C7H14OOH2-4
3	C7H14OOH2-4O2=NC7KET24+OH	C7H15O2-4=C7H14OOH4-2	NC7H16+HO2=C7H15-2+H2O2
4	C7H14OOH4-2O2=NC7KET42+OH	C7H14OOH2-4O2=NC7KET24+OH	C7H14OOH2-4O2=NC7KET24+OH
5	C7H14OOH1-3O2=NC7KET13+OH	C7H15O2-3=C7H14OOH3-5	HO2+HO2=O2+H2O2
6	MB+OH=H2O+MB3J	C7H14OOH4-2O2=NC7KET42+OH	C7H15O2-4=C7H14OOH4-2
7	C7H15O2-2=C7H14OOH2-5	NC7H16+HO2=C7H15-2+H2O2	C7H15O2-3=C7H14OOH3-5
8	NC7H16+HO2=C7H15-2+H2O2	C7H14OOH1-3O2=NC7KET13+OH	OH+OH(+M)=H2O2(+M)
9	C7H14OOH3-5O2=NC7KET35+OH	C7H14OOH3-5O2=NC7KET35+OH	C7H14OOH4-2O2=NC7KET42+OH
10	NC7H16+C7H15O2-3=C7H15-3+C7H15O2H-3	C7H15O2-1=C7H14OOH1-3	C7H14OOH3-5O2=NC7KET35+OH
11	C7H15O2-3=C7H14OOH3-5	HO2+HO2=O2+H2O2	PC4H9=C2H5+C2H4
12	C7H14OOH2-5O2=NC7KET25+OH	NC7H16+HO2=C7H15-4+H2O2	NC7H16+HO2=C7H15-4+H2O2
13	NC7H16+OH=C7H15-3+H2O	OH+OH(+M)=H2O2(+M)	C7H15O2-1=C7H14OOH1-3
14	C7H15O2-2=C7H14OOH2-3	C4H8OOH1-3O2=NC4KET13+OH	C7H15-3=C4H8-1+NC3H7
15	C7H15O2-3=C7H14OOH3-6	MB+OH=H2O+MB3J	C4H8OOH1-3O2=NC4KET13+OH

^aT in degrees Kelvin, P in units of atmospheres

^bWorst lower temperature engine match

^cBest 0-D engine match

^dWorst higher temperature engine match

the color-coding of some of the specific reactions: OH abstraction reactions, RO₂ = QOOH reactions, and the formation of keto-hydroperoxides.

The engine simulations are re-examined in Figure 2. This contour plot shows the rms difference between the engine selection in column 1 of Table 1 and each of the 50 sparse runs. This plot only shows rms errors of 3 and below. Outside these contours the mis-match is higher, with the highest low-temperature mis-match shown in column 1 of Table 2 and the highest mis-match at the higher temperatures in column 3 of Table 2.

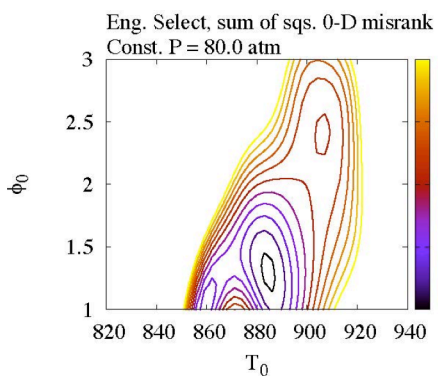


Figure 2. RMS matches between engine selection and 0-D selections. Outside the range of the contours the rms mis-matches are greater than 3.

Figure 2 demonstrates that the engine matches the 0-D well over a relatively narrow range of temperature and that match tends to be better at lower equivalence ratios.

Future Plans

The analysis in Fig. 2 will lead to further study of the chemistry inside the engine cylinder, because it indicates the conditions for which ignition is most sensitive. An effort is underway to automate GSA more fully for the engine simulations, with the goal of generating a full set of sensitivity coefficients in a single day using a large number of processors (the calculations reported here took a few months). In collaboration with Skodje (Colorado), the reaction pathway analysis developed in [P8] will be extended to the engine simulations. A new project on enhanced fitting using dictionary learning developed in the machine learning and statistics community will be initiated.

Publications

1. W. Liu, R. Sivaramakrishnan, M. J. Davis, S. Som, and D. E. Longman, "Development of a Reduced Biodiesel Surrogate Model for Compression Ignition Engine Modeling", Central States Section of the Combustion Institute (2012).
2. W. Liu, R. Sivaramakrishnan, M. J. Davis, S. Som, D. E. Longman and T. F. Lu, "Development of a reduced biodiesel surrogate model for compression ignition engine modeling", Proc. Combust. Inst. 34 401-409 (2013).
3. D. D. Y. Zhou, R. T. Skodje, W. Liu, and M. J. Davis, "Multi-Target Global Sensitivity Analysis of n-Butanol Combustion", Proceedings of the 8th US National Technical Meeting of the Combustion Institute, University of Utah (2013).
4. W. Liu, S. Som, D. D. Y. Zhou, R. Sivaramakrishnan, D. E. Longman, R. T. Skodje, and, M. J. Davis, "The Role of Individual Rate Coefficients in the Performance of Compression Ignition Engine Models", Proceedings of 8th US National Technical Meeting of the Combustion Institute, University of Utah (2013).
5. D. D. Y. Zhou, M. J. Davis, and R. T. Skodje, "Multi-Target Global Sensitivity Analysis of n-Butanol Combustion", J. Phys. Chem. A 117, 3569-3584 (2013).
6. S. Som, W. Liu, D. D. Y. Zhou, G. M. Magnotti, R. Sivaramakrishnan, D. E. Longman, R. T. Skodje, and M. J. Davis, "Quantum Tunneling Affects Engine Performance", J. Phys. Chem. Lett 4, 2021-2025 (2013).
7. Y. Pei, R. Shan, S. Som, T. Lu, D. E. Longman, and M. J. Davis, "Global Sensitivity Analysis of a Diesel Engine Simulation with Multi-Target Functions", Proceedings of the Society of Automotive Engineers (SAE) World Congress, 2014, SAE Paper 2014-01-1117.
8. S. Bai, D. Zhou, M. J. Davis, and R. T. Skodje, "Sum over Histories Representation for Chemical Kinetics", J. Phys. Chem. Lett., 6, 183-188 (2015).
9. D. M. A. Karwat, M. S. Wooldridge, S. J. Klippenstein, and M. J. Davis, "Effects of New Ab Initio Rate Coefficients on Predictions of Species Formed during n-Butanol Ignition and Pyrolysis", J. Phys. Chem. A 119, 543-551 (2015).
10. Y. Pei, M. J. Davis, L. M. Pickett, S. Som, "Engine Combustion Network (ECN): Global sensitivity analysis of Spray A for different combustion vessels", Combustion and Flame (in press).
11. S. Som, Z. Wang, G. M. Magnotti, W. Liu, R. Sivaramakrishnan, and M. J. Davis, "Application of Sparse Sensitivity Analysis to Detailed Chemical Kinetics in High Fidelity Compression-Ignition Engine Simulations", Proceedings of the 9th US National Technical Meeting of the Combustion Institute (2015),

Multiple Coupled Potential Energy Surfaces with Application to Combustion

Richard Dawes

Missouri University of Science and Technology

400 W. 11th Street, Rolla, MO 65409

dawesr@mst.edu

Program Scope: Hydrocarbon combustion involves the dynamics of numerous small radicals such as HO₂, HCO, and HOCO. HOCO is an intermediate in the HO + CO → H + CO₂ reaction which is the last and heat releasing step in hydrocarbon combustion and the subject of many ongoing studies. Accurate calculations of their potential energy surfaces (PESs) are possible using traditional quantum chemistry methods such as MRCI. However, multistate and non-adiabatic processes can be important, and tunneling effects may supersede the more common kinetic or thermodynamic control of rates and branching ratios. Significant fractions of molecular products can also result from radicals roaming far from conventional minimum energy paths and tight transition states. Dynamical calculations for these relatively simple systems are very sensitive to the detailed topography of their global potential energy surfaces (PESs).

This project combines developments in the areas of PES fitting and multistate multireference quantum chemistry to allow spectroscopically and dynamically/kinetically accurate investigations of key molecular systems (such as those mentioned above), many of which are radicals with strong multireference character and have the possibility of multiple electronic states contributing to the observed dynamics. A main goal is to develop general strategies for robustly convergent electronic structure theory for global multichannel reactive surfaces. Combining advances in ab initio methods with automated interpolative PES fitting allows the construction of high-quality PESs incorporating thousands of high level data to be done rapidly through parallel processing on high-performance computing (HPC) clusters. New methods and approaches to electronic structure theory will be developed and tested through applications. Some effort will be applied to the development of Quantum Monte Carlo (QMC) and working to apply these methods in the context of global PESs. The feasibility of capturing a larger fraction of the correlation energy than is possible with traditional electronic structure approaches will be tested on suitable combustion related systems. Strategies will be developed to generate QMC data in the context of a *distributed high-throughput computing* model in which 10s or even 100s of thousands of processors are used.

Recent Progress: This section describes recent progress achieved along various directions of the project occurring over the past 12 months since the last report from April 2014. The initial start date of this project was 07-15-2013.

Non-Born-Oppenheimer molecular dynamics of the spin-forbidden reaction of O(³P) + CO(X¹Σ⁺) → CO₂($\tilde{X}^1\Sigma_g^+$).¹ As reported last year, in 2013 a set of three PESs were developed for this system as well as fully geometry-dependent coupling surfaces. The coupled PESs were used with Ahren W. Jasper (Sandia) in non-Born-Oppenheimer molecular dynamics calculations (NBO MD) of the reaction rate for a range of high temperatures in the high-pressure limit. The total CSDM rate coefficient is 7–35 times larger than the values often used in combustion kinetic models. To make the PESs the method of dynamically-weighted state-averaged CASSCF^{2,3} including electronic 8 states was used as a reference to compute three states at the MRCI/CBS level (1 singlet and 2 triplets). These were iteratively refined into usable fitted

PESs by an automated IMLS-based PES generation scheme running in parallel on an HPC cluster.^{4,5} The dynamically weighted multistate electronic structure calculations were found to be very robust and well-behaved allowing the mean estimated fitting error to be converged to just a few cm^{-1} for the three PESs and even less for the coupling surfaces.

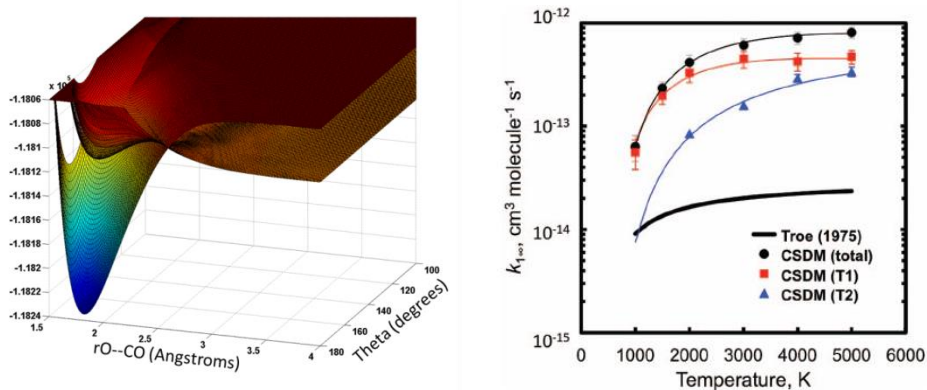


Figure 1. The spin-forbidden chemistry of the $\text{O}({}^3\text{P}) + \text{CO} \rightarrow \text{CO}_2$ reaction is studied using three automatically generated PESs. (at left) Two frustrated triplet states which correlate with ground state $\text{O}({}^3\text{P})$ have shallow wells hanging above the deep singlet CO_2 well. The spin-forbidden reaction occurs via spin-orbit coupling between the surfaces. (at right) The rate of spin-forbidden formation in the high-pressure limit is calculated to be 7-35 times larger than previous models.

In 2014, new experimental data for this system was obtained by Kristie Boering (UC-Berkeley) and co-workers. Those molecular beam experiments produced data for the isotope exchange and electronic quenching processes that occur in the low-pressure limit (CO_2 products are not formed in the absence of stabilizing collisions). Simulating those experiments required extending both the coordinate and energy ranges of the PESs (so that product states could be precisely resolved). This was achieved using the same automated PES generation strategy (restarting the PESs with newly defined limits). Remarkably, robust convergence was obtained in the electronic structure calculations and estimated fitting errors of only a few wavenumbers were again obtained even with the extended ranges (the total energy range of the singlet PES now exceeds 300 kcal/mol). Trajectories calculations by Jasper are in good agreement with the experiments. A limited set of fully quantum calculations were performed by Hua Guo providing some additional insight (fully quantum reactive scattering calculations are challenging due to the deep well depth). The paper is in preparation.

Experimental and theoretical studies of the electronic transitions of MgC. In the 2013 report a previous study of BeC^6 was described in which vibronic calculations were able to help assign and interpret electronic spectra of that system recorded by the group of Michael C. Heaven (Emory). Heaven's efforts to observe similar transitions in MgC have so far been unsuccessful. New vibronic calculations were performed for the MgC system using the dynamically weighted multistate scheme to produce MRCI/CBS quality potential curves. A diabaticization procedure was used along with a DVR method including a complex absorbing potential (CAP) to solve for the vibronic levels and their lifetimes/widths.

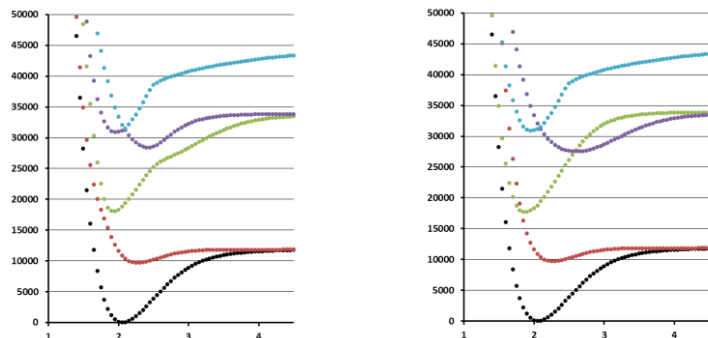


Figure 2. Electronic states of MgC plotted in adiabatic (left) and diabatic representations (right). The zero of the energy is the minimum of the $X^3\Sigma^-$ electronic ground state (shown in black).

Despite difficulties with the experiments, our complete set of theoretical predictions for all bound vibrational and well as vibronic states and lifetimes has been written up and submitted to JCP.

IMLS-PIP fitting. A large set of $\sim 100,000$ high-level multireference data were computed for **methane**.⁷ The IMLS interpolation approach was combined with permutation invariant polynomials (PIP) to fit the 9D PES in a $25,000\text{ cm}^{-1}$ energy range to better than a wavenumber using about 200 local expansions. This was used as a benchmark to assess the accuracy of another fit to the same data set by H. Guo using the NN-PIP method. Guo's fit was found to be very accurate and quick to evaluate. 9D vibrational calculations by T. Carrington confirm that the data is of spectroscopic quality. The lowest levels are systematically $1\text{-}2\text{ cm}^{-1}$ higher than experiment. Having a fit with negligible fitting error permits direct assessment of ab initio methods as well as small corrections. Future plans include testing some small corrections such as relativistic and diagonal Born-Oppenheimer (DBOC). Since the data set is multireference it is also suitable for extension to permit dissociation to $\text{CH}_3 + \text{H}$ and $\text{CH}_2 + \text{H}_2$ and would be useful as a highly accurate PES for dynamics studies. The dissociation energy to $\text{CH}_3 + \text{H}$ was found to be within about 40 cm^{-1} of the best estimates by Ruscic.

The IMLS-PIP approach was applied to a 15D test set of A. F. Wagner and D. L. Thompson composed of $\sim 400,000$ data for **ethyl radical**. This system combines a more complex topography, higher dimensionality and additional permutation symmetry. An initial fit of the lower energy region (below 67 kcal/mol) was obtained with an RMS fitting error of 0.2 kcal/mol using a single PIP expansion. A multi-expansion fit anticipated to provide negligible fitting error over a larger energy range is in progress.

O+H₂O. A set of three global multichannel PESs were produced for the $\text{O}(^3\text{P}) + \text{H}_2\text{O}$ system using explicitly correlated MRCI-F12 in collaboration with the group of H. Guo. The PESs include the $\text{O}(^3\text{P}) + \text{H}_2\text{O}$, $\text{H}_2 + \text{O}_2$, $\text{OH} + \text{OH}$, $\text{H} + \text{HO}_2$ and separated atoms channels. 36 triplet states are degenerate for separated atoms and are included using the dynamically weighted multistate procedure. Fits were obtained by the NN-PIP method of Guo. A paper describing the first classical trajectories study of the dynamics is in preparation.

QMC. We have been developing scripts and testing methods to use multi-configurational trial wavefunctions in VMC/DMC calculations of PECs for small molecules. We have managed to produce highly accurate PECs for CO and N₂ using QMC. The PECs compare well with the best ab initio references and experimental quantities (vibrational levels etc). However, the cost was found not to be competitive with standard electronic structure approaches for small systems. (The scaling with number of electrons is n^3 for QMC so it will certainly be more competitive for larger systems where the e.g. n^7 scaling of traditional methods becomes prohibitive).

We are currently testing QMC methods along the minimum energy dissociation path of ozone. The hope is that QMC can be a useful arbiter in cases where traditional electronic

structure methods are left with uncertainty about the existence or absence of an entrance channel barrier (possibly submerged) as well as more generally the attractiveness of the long-range part of the PES.^{8,9}

Rotationally inelastic scattering. A time-dependent quantum dynamics method called MCTDH was applied to studying inelastic scattering at high collision energies where more typical time-independent calculations (Molscat) become prohibitively expensive. Using an IMLS-based PES for CO+CO constructed for a previous ro-vibrational spectroscopy study,¹⁰ time-independent Molscat calculations (for the low energy range) were combined with time-dependent MCTDH calculations to cover an extended energy range. Where the two approaches overlap, reasonable agreement was obtained between the two.

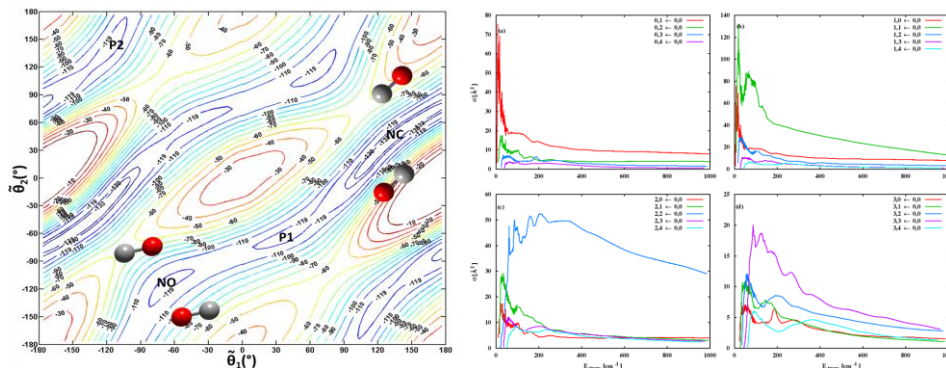


Figure 3. (at left) a plot of the PES for CO-dimer showing low-energy channels for geared motion. (at right) scattering cross-sections for rotational excitation showing increased propensities for equally excited products (possibly imparted by the features of the PES).

The paper describing this study will appear in the special JPC “100 years of combustion chemistry at Argonne” issue.¹¹

References (* denotes publications supported by the DOE)

- ¹ * A. W. Jasper and R. Dawes, *J. Chem. Phys.* **139**, 154313 (2013).
- ² M. P. Deskevich, D. J. Nesbitt and H.-J. Werner, *J. Chem. Phys.* **120**, 7281 (2004).
- ³ R. Dawes, A. W. Jasper, C. Tao, C. Richmond, C. Mukarakate, S. H. Kable, S. A. Reid, *J. Phys. Chem. Lett.* **1**, 641 (2010).
- ⁴ R. Dawes, A. F. Wagner, D. L. Thompson, *J. Phys. Chem. A.* **113**(16) 4709-4721 (2009).
- ⁵ R. Dawes, X.-G. Wang, A. W. Jasper, T. Carrington Jr., *J. Chem. Phys.* **133**, 134304 (2010).
- ⁶ B. J. Barker, I. O. Antonov, J. M. Merritt, V. E. Bondybey, M. C. Heaven, R. Dawes, *J. Chem. Phys.* **137**, 214313 (2012).
- ⁷ * M. Majumder, S. E. Hegger, R. Dawes, S. Manzhos, X.-G. Wang, T. Carrington Jr., J. Li, and H. Guo, *Molecular Physics*, 2015, DOI:10.1080/00268976.2015.1015642
- ⁸ L. B. Harding, S. J. Klippenstein, H. Lischka and R. Shepard, *Theor. Chem. Acc.* **133**, 1429 (2014).
- ⁹ R. Dawes, P. Lolur, A. Li, B. Jiang and H. Guo, *J. Chem. Phys.* **139**, 201103 (2013).
- ¹⁰ R. Dawes, X.-G. Wang and T. Carrington Jr., *J. Phys. Chem. A*, **117**, 7612 (2013).
- ¹¹ * S. Ndengue, R. Dawes and F. Gatti, JPC A, 2015 jp-2015-01022r
- ¹² * J. W. Perry, R. Dawes, A. F. Wagner D. L. Thompson, *J. Chem. Phys.* **139**, 084319 (2013).
- ¹³ * A. F. Wagner, R. Dawes, R. E. Continetti, H. Guo, *J. Chem. Phys.* **141**, 054304 (2014).
- ¹⁴ * P. Lolur, R. Dawes, *J. Chem. Ed.* **91**, 1181 (2014).

Dynamics of Peroxy and Alkenyl Radicals Undergoing Competing Rearrangements in Biodiesel Combustion

Prof. Theodore Dibble (tsdibble@esf.edu)

Chemistry Department, State University of New York- Environmental Science and Forestry
Syracuse, Syracuse, NY 13210

I. Program Scope

The ignition of diesel fuel depends on isomerization of peroxy radicals (ROO•) via a hydrogen shift reaction:



Production of OH radical by chain propagation following reaction (1) contributes to autoignition:



but chain branching (the sequence of reactions 3-6) is critical to autoignition because it produces two OH radicals:



Processes such as reaction (7):



compete with chain branching. Experimentalists face several difficulties in gaining an understanding of this chemistry, and only QOOH species has ever been detected by experiment! This has inspired many computational studies of these processes.

Biodiesel fuel is increasingly being used worldwide. Although we have a fair understanding of the molecular details of the chemistry of peroxy radicals derived from alkanes, biodiesel fuels contain ester and olefin groups which significantly impact the thermodynamics and kinetics of biodiesel ignition.[1] The broader goal of this research is to carry out systematic computational studies of the elementary kinetics of the chemistry of R•, ROO•, QOOH and •OOQOOH compounds that are models for biodiesel ignition.

Carbon-centered radicals such as R• and QOOH can undergo well-known 1,n H-shift reactions, e.g.:



which are known to be able to change the structure of the radical from that initially formed. A competing set of reactions, shown in Scheme 1, can isomerize carbon-centered radicals formed in the vicinity of a double bond. Results from the literature indicate these reactions may compete with 1,n H-shift reactions.[2] We will use computational chemistry to explore the importance of these reactions and analogous cyclization reactions of peroxy radicals in model compounds of biodiesel fuel.

II. Recent Progress

A) Autoignition Mechanism of Methyl Butanoate

We find peroxy radical interconversions of •OOQOOH radicals from methylbutanoate (MB) (•OOQOOH → HOOQOO•) commonly possess the lowest barriers of any unimolecular reaction of these

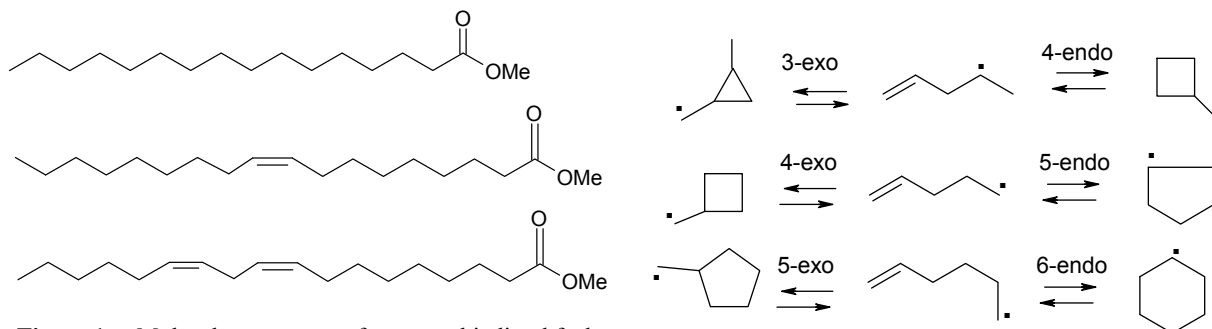


Figure 1. Molecular structures of common biodiesel fuel components: the fatty acid methyl esters (FAMEs) of (from top to bottom) palmitic, oleic, and linoleic acids.

Scheme 1. Examples of exo- and endo-trig reactions.

radicals, despite that they proceed via 8-, 10- and 11-member ring transition states. At temperatures relevant to autoignition, these

peroxy radical interconversions are dominant or significant reaction pathways. This means that $\bullet\text{OOQOOH}$ radicals that were expected to be produced in negligible yields are, instead, major products in the autoignition of methyl butanoate. These reactions have not previously been considered for OOQOOH from MB, and will require revision of models of autoignition of methylbutanoate and other esters.

A harmonic oscillator (HO) treatment of the multiple torsional modes of these large molecules may lead to large errors in computed rate constants. Treating the torsions as separable hindered rotors (HR) provides an approximate correction.[3] From Figure 2, it can be seen that the HR treatment of the torsions leads to much different rate constants than the HO treatment.

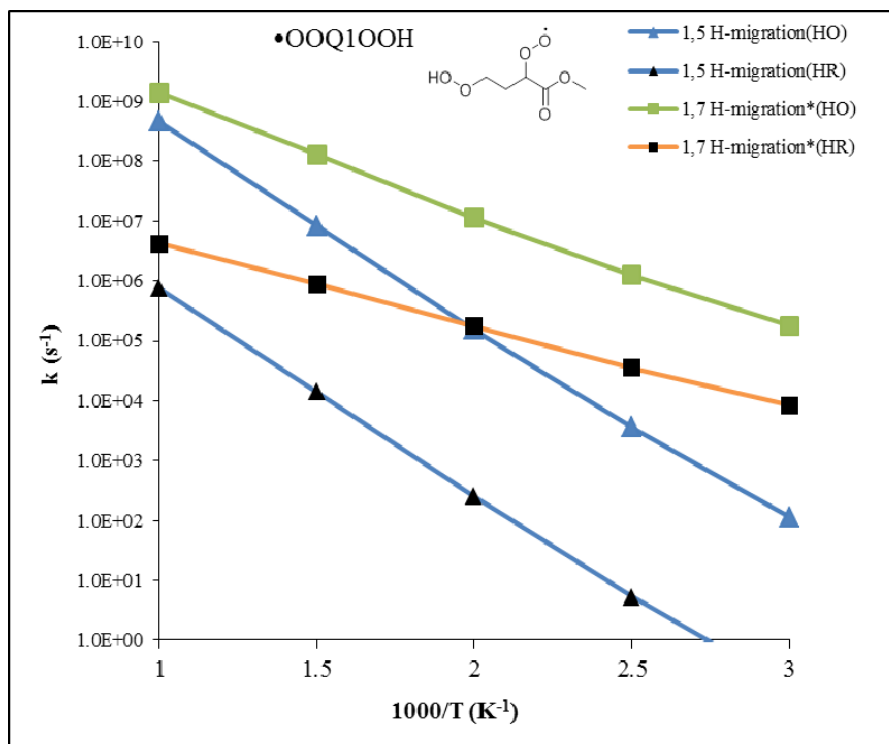


Figure 2. Revised rate constants for the two fastest reactions of $\bullet\text{OOQ1OOH}$ including the 1-D hindered rotor treatment (HR) or using the harmonic oscillator approximation (HO) on both reactants and transition states. The asterisk indicates peroxy radical interconversion: $\bullet\text{OOQOOH} \rightarrow \text{HOOQOO}\bullet$.

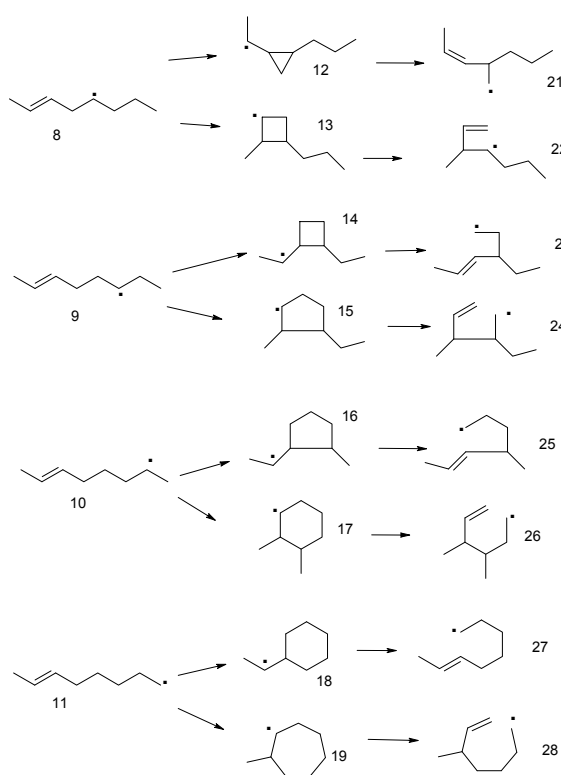
B) Cyclization-Decyclization Reactions of Unsaturated Hydrocarbon Radicals

Cyclization reactions of unsaturated radicals are well known in the organic chemistry literature. The cyclization reactions are labeled *endo* if the radical center of the product is on a carbon *in* the ring, and *exo* if the radical center is not in the ring. We surveyed a broad range of reactions at the CBS-QB3 level of theory, only a few of which are shown below in Scheme 2. The products of cyclization of the *n*-octenyl radicals will potentially decyclize to form branched octenyl radicals (e.g, the reaction 12 → 21 in Scheme 2). In general, branched and straight chain fuels exhibit different ignition behavior. If the chemistry suggested here is important in combustion, and then it needs to be included in kinetic models if those models are to accurately represent combustion behavior.

As can be seen from Table 1, many of the cyclization reactions shown in Scheme 2 possess low barriers, so that these reactions are expected to proceed with high rate constants. Curiously, the decyclization reactions of *exo*-ring systems (e.g, 12→21) have significantly lower barriers than the decyclization reactions of the *endo*-ring system of the same ring size (e.g, 13→22). This result appears consisted across 4-, 5-, and 6-member rings.

Rate constants for these reactions were computed using standard transition state theory using the harmonic oscillator rigid-rotor approximation. These rate constants confirm the importance of many of these reactions in comparison to competing unimolecular reactions. The present work represents a much wider survey of these reactions than has been reported previously.

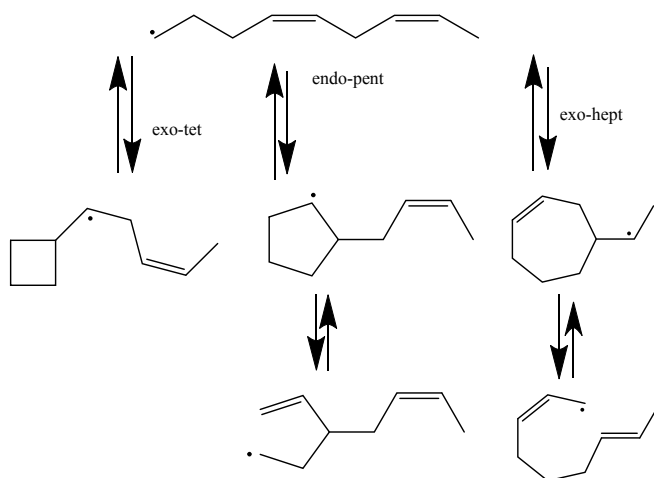
We have also begun looking at radicals



Scheme 2. Examples of *exo* and *endo* cyclization reactions of *n*-octenyl radicals, plus de-cyclization reactions leading to new products.

Table 1. Barrier heights (CBS-QB3 values in kcal/mol at 0 K including zero-point energy) for *endo*- and *exo*-cyclization and decyclization reactions of *n*-octenyl radicals and the products of their cyclization reactions. Numbers correspond to the identity of species in Scheme 2. The notations “c” and “t” after a number corresponds to the *cis* and *trans* isomer, respectively.

Transition State	Reaction type	Forward Barrier	Reverse Barrier
TS_8-12c	<i>exo</i> -trig cyclization	9.1	6.1
TS_8-12t	<i>exo</i> -trig cyclization	9.6	7.0
TS_8-13c	<i>endo</i> -tet cyclization	30.2	24.7
TS_8-13t	<i>endo</i> -tet cyclization	29.0	24.9
TS_9-14c	<i>exo</i> -tet cyclization	14.4	11.0
TS_9-14t	<i>exo</i> -tet cyclization	14.1	12.2
TS_9-15c	<i>endo</i> -pent cyclization	13.6	29.6
TS_9-15t	<i>endo</i> -pent cyclization	14.0	31.6
TS_10-16c	<i>exo</i> -pent cyclization	6.1	20.9
TS_10-16t	<i>exo</i> -pent cyclization	5.9	21.8
TS_10-17c	<i>endo</i> -hex cyclization	6.9	26.1
TS_10-17t	<i>endo</i> -hex cyclization	6.7	27.3
TS_11-18	<i>exo</i> -hex cyclization	7.5	29.3
TS_11-19	<i>endo</i> -hept cyclization	10.8	24.6
TS_12c-21	decyc of 3 member ring	6.2	8.5
TS_12t-21	decyc of 3 member ring	6.3	8.6
TS_13c-22	decyc of 4 member ring	26.3	30.4
TS_13t-22	decyc of 4 member ring	26.9	30.0
TS_14c-23	decyc of 4 member ring	13.1	13.6
TS_14t-23	decyc of 4 member ring	12.7	14.7
TS_15c-24	decyc of 5 member ring	34.1	14.8
TS_15t-24	decyc of 5 member ring	34.2	12.9
TS_16c-25	decyc of 5 member ring	22.1	5.5
TS_16t-25	decyc of 5 member ring	21.7	5.3
TS_17c-26	decyc of 6 member ring	29.6	7.2
TS_17t-26	decyc of 6 member ring	30.0	7.2
TS_18-27	decyc of 6 member ring	50.7	30.1
TS_19-28	decyc of 7 member ring	27.6	13.1



Scheme 3. Selected initial cyclization and subsequent de/cyclization reactions starting from one resonance structure of one isomer of the parent radical.

produced by hydrogen abstraction from di-olefins, such as linoleic acid. The model compound is 2,5-nonadiene with a hydrogen abstracted from one of the carbon atoms. A selection of possible reactions following hydrogen abstract from carbon 9 is shown in Scheme 3. Reactions lead to cyclic radicals, formation of branched species, and formation of allylic radicals starting from non-allylic radicals.

III. Future Work

We will complete our exploration of the barrier heights and thermodynamics of the reactions of dienyl radicals described immediately above. We will also consider C-C bond scission reactions of the various radical isomers. Due to the sheer number of compounds and their size, we are still trying to determine an efficient yet reliable approach to include treatment of hindered rotors in the calculation of rate constants.

IV. References

- [1] Sumathi, R.; Green W. H., *Phys. Chem. Chem. Phys.*, **2003**, *5*, 3402-17.
- [2] Matheu, D.M., Green, W.H., Grenda, J.M. *Int. J. Chem. Kinet.* **2003**, *35*, 95-119.
- [3] Sharma, S.; Raman, S.; Green, W. H. *J. Phys. Chem. A* **2010**, *114*, 5689–5701.

V. Publications and submitted journal articles supported by this project 2010-2014

- Y. Jiao, F. Zhang, and T. S. Dibble. Quantum Chemical Study of Autoignition of Methyl Butanoate, *J. Phys. Chem. A* **2015**, article ASAP. <http://dx.doi.org/10.1021/jp5122118>
- T. S. Dibble, Y. Sha, W. F. Thornton, and F. Zhang. Cis-trans isomerization of chemically activated 1-methylallyl radical and fate of the resulting 2-buten-1-peroxy radical, *J. Phys. Chem. A.* **2012**, *116*, 7603–7614.
- F. Zhang and T. S. Dibble. Impact of Tunneling on hydrogen-migration of n-propylperoxy radical. *Phys. Chem. Chem. Phys.*, **2011**, *13*, 17969-77.
- F. Zhang and T. S. Dibble, Effects of ester and olefin functional groups on kinetics of unimolecular reactions of peroxy radicals, *J. Phys. Chem. A.* **2011**, *115*, 655-663.
- T. S. Dibble and Yue Zeng, Potential energy profiles for the N + HOCO reaction and products of the chemically activated reactions N + HOCO and H + HOCO. *Chem. Phys. Letts.*, **2010**, *495*, 170-174.

Vibrational Spectroscopy of Transient Combustion Intermediates Trapped in Helium Nanodroplets (DE-FG02-12ER16298)

Gary E. Douberly

University of Georgia, Department of Chemistry, 1001 Cedar St., Athens, GA 30602-1546

Program Scope

The objective of this research is to isolate and stabilize transient intermediates and products of prototype combustion reactions. This will be accomplished by Helium nanodroplet isolation (HENDI) spectroscopy, a novel technique where liquid helium nanodroplets freeze out high energy metastable configurations of a reacting system, permitting infrared spectroscopic characterizations of products and intermediates that result from hydrocarbon radical reactions with molecular oxygen and other small molecules relevant to combustion environments. A major aim of this work is to directly observe the elusive hydroperoxyalkyl radical (QOOH) and its oxygen adducts (O₂QOOH), which are important in low temperature hydrocarbon oxidation chemistry.

Recent Projects

Helium Nanodroplet Isolation and Rovibrational Spectroscopy of Hydroxymethylene

Hydroxymethylene H \dot{C} OH and its d₁-isotopologue H \dot{C} OD are isolated in low temperature helium nanodroplets following pyrolysis of glyoxylic acid (Ref 6). Transitions identified in the infrared spectrum are assigned exclusively to the *trans*-conformation based on previously reported anharmonic frequency computations (P. R. Schreiner, *et. al.* Nature **453**, 906 (2008) and L. Koziol, *et. al.* J. Chem. Phys. **128**, 204310 (2008)). For the OH(D) and CH stretches, *a*- and *b*-type transitions are observed, and when taken in conjunction with CCSD(T)/cc-pVTZ computations, lower limits to the vibrational band origins are determined. The relative intensities of the *a*- and *b*-type transitions provide the orientation of the transition dipole moment in the inertial frame. The He nanodroplet data are in excellent agreement with anharmonic frequency computations reported here and elsewhere, confirming an appreciable Ar-matrix shift of the OH and OD stretches and strong anharmonic resonance interactions in the high-frequency stretch regions of the mid-infrared.

Infrared Rovibrational Spectroscopy of OH–C₂H₂ in ⁴He nanodroplets: Parity Splitting due to Partially Quenched Electronic Angular Momentum

Electrophilic addition of the hydroxyl radical to the π bond of acetylene produces, as an intermediate, the carbon-centered 2-hydroxy vinyl radical ($\Gamma_e = A'$; $\text{HC}=\dot{\text{C}}\text{HOH}$). Along the entrance channel to this reaction, a dipole-quadrupole interaction stabilizes a *T*-shaped, hydrogen bonded complex (OH–C₂H₂), whose zero-point level lies ≈ 2.7 kcal·mol⁻¹ below the separated reactants. Moreover, this entrance channel complex is located behind a barrier ≈ 1 kcal·mol⁻¹ above the reactant asymptote. The *T*-shaped OH–C₂H₂ complex is formed in helium droplets via the sequential pick-up and solvation of the monomer fragments (Ref 7). Rovibrational spectra of the *a*-type OH stretch and *b*-type antisymmetric CH stretch vibrations contain resolved parity splitting that reveals the extent to which electronic angular momentum of the OH moiety is quenched upon complex formation. The energy difference between the spin-orbit coupled ²B₁ (*A''*) and ²B₂ (*A'*) electronic states is determined spectroscopically to be 216 cm⁻¹ in helium droplets, which is 13 cm⁻¹ larger than in the gas phase [M. D. Marshall, J. B. Davey, M. E. Greenslade, and M. I. Lester, *J. Chem. Phys.* **121**, 5845 (2004).]. The effect of the helium is rationalized as a difference in the solvation free energies of the two electronic states. This interpretation is motivated by the separation between the *Q*(3/2) and *R*(3/2) transitions in the infrared spectrum of the helium-solvated ²Π_{3/2} OH radical. Despite the expectation of a reduced rotational constant, the observed *Q*(3/2) to *R*(3/2) splitting is *larger* than in the gas phase by ≈ 0.3 cm⁻¹. This observation can be accounted for quantitatively by assuming the energetic separation between ²Π_{3/2} and ²Π_{1/2} manifolds is increased by ≈ 40 cm⁻¹ upon helium solvation.

Reactive Intermediates in ⁴He Nanodroplets: Infrared Laser Stark Spectroscopy of Dihydroxycarbene

Singlet dihydroxycarbene (HO $\dot{\text{C}}$ OH) is produced via pyrolytic decomposition of oxalic acid, captured by helium nanodroplets, and probed with infrared laser Stark spectroscopy (Ref 8). Rovibrational bands in the OH stretch region are assigned to either *trans,trans*- or *trans,cis*-rotamers on the basis of symmetry type, nuclear spin statistical weights, and comparisons to electronic structure theory calculations. Stark spectroscopy provides the inertial components of

the permanent electric dipole moments for these rotamers. The dipole components for *trans,trans*- and *trans,cis*- rotamers are $(\mu_a, \mu_b) = (0.00, 0.68(6))$ and $(1.63(3), 1.50(5))$, respectively. The infrared spectra lack evidence for the higher energy *cis,cis*- rotamer, which is consistent with a previously proposed pyrolytic decomposition mechanism of oxalic acid and computations of HO \ddot{C} OH torsional interconversion and tautomerization barriers.

Ongoing Work and Future Plans

Vibrational-Torsional Coupling Revealed in the Infrared Spectrum of He-Solvated *n*-Propyl Radical

The *n*-propyl and *i*-propyl radicals were generated in the gas phase via pyrolysis of *n*-butyl nitrite ($\text{CH}_3(\text{CH}_2)_3\text{ONO}$) and *i*-butyl nitrite ($\text{CH}_3\text{CH}(\text{CH}_3)\text{CH}_2\text{ONO}$) precursors, respectively. Nascent radicals were promptly solvated by a beam of He nanodroplets, and the infrared spectra of the radicals were recorded in the C-H stretching region. In addition to three vibrations of *n*-propyl previously measured in an Ar matrix, we observe many unreported bands between 2800 and 3150 cm^{-1} , which we attribute to propyl radicals. The C-H stretching modes observed above 2960 cm^{-1} for both radicals are in excellent agreement with anharmonic frequencies computed using VPT2. Between 2800 and 2960 cm^{-1} , however, the spectra of *n*-propyl and *i*-propyl radicals become quite congested and difficult to assign due to the presence of multiple anharmonic resonances. Computations reveal the likely origin of the spectral congestion to be strong coupling between the high frequency C-H stretching modes and a lower frequency torsional motion, which modulates quite substantially a through-space hyperconjugation interaction.

Instrumentation Development

We have modified our pyrolysis source to increase the upper temperature that can be achieved in our experiments. With the higher temperature, the range of precursor systems that can be pyrolyzed to create radicals has been vastly expanded. This involves incorporating a resistively heated silicon carbide (SiC) tube, similar to those reported by P. Chen and co-workers and B. Ellison and co-workers that can be heated up to ~ 2100 K. Because the pick-up efficiency of the He droplets is quite large, for example, compared to the molecular densities needed for matrix isolation spectroscopy, we can work in a regime where we can isolate transient species while

minimizing secondary reactions within the pyrolysis source, such as recombination reactions between two radicals. We have successfully used this source to generate, for example, a continuous, high-purity sample of Cl radicals, which have been doped into helium droplets. We are preparing a manuscript describing the spectroscopy of the Cl-HCl complex, which is a prototype system for studying the kinetic couplings of several low-lying potential energy surfaces.

Publications acknowledging DOE support (2012-present):

1. Paul L. Raston, Tao, Liang and Gary E. Douberly, "Infrared spectroscopy and tunneling dynamics of the vinyl radical in ^4He Nanodroplets" *Journal of Chemical Physics*, **138**, 174302 (2013). Published: May 7, 2013.
2. Paul L. Raston, Jay Agarwal, Justin M. Turney, Henry F. Schaefer III and Gary E. Douberly, "The Ethyl Radical in Superfluid Helium Nanodroplets: Rovibrational Spectroscopy and Ab Initio Computations" *Journal of Chemical Physics*, **138**, 194303 (2013). Published: May 21, 2013.
3. Alexander M. Morrison, Paul L. Raston and Gary E. Douberly, "Rotational Dynamics of the Methyl Radical in Superfluid ^4He nanodroplets" *Journal of Physical Chemistry A* **117**, 11640-11647 (2013). Published: November 21, 2013.
4. Christopher P. Moradi, Alexander M. Morrison, Stephen J. Klippenstein, C. Franklin Goldsmith and Gary E. Douberly, "Propargyl + O_2 Reaction in Helium Droplets: Entrance Channel Barrier or Not?" *Journal of Physical Chemistry A* **117**, 13626-13635 (2013). Published: December 19, 2013.
5. Christopher M. Leavitt, Christopher P. Moradi, Bradley W. Acrey and Gary E. Douberly, "Infrared Laser Spectroscopy of the Helium-Solvated Allyl and Allyl Peroxy Radicals" *Journal of Chemical Physics* **139**, 234301 (2013). Published: December 21, 2013.
6. Christopher M. Leavitt, Christopher P. Moradi, John F. Stanton and Gary E. Douberly "Communication: Helium Nanodroplet Isolation and Rovibrational Spectroscopy of Hydroxymethylene" *Journal of Chemical Physics* **140**, 171102 (2014). Published: May 5, 2014.
7. Gary E. Douberly, Paul L. Raston, Tao Liang and Mark D. Marshall, "Infrared Rovibrational Spectroscopy of $\text{OH}-\text{C}_2\text{H}_2$ in ^4He nanodroplets: Parity Splitting due to Partially Quenched Electronic Angular Momentum" *Journal of Chemical Physics* **142**, 134306 (2015). Published: April 3, 2015.
8. Bernadette M. Broderick, Laura McCaslin, Christopher P. Moradi, John F. Stanton and Gary E. Douberly "Reactive Intermediates in ^4He Nanodroplets: Infrared Laser Stark Spectroscopy of Dihydroxycarbene" *Journal of Chemical Physics* **142**, (2015). Accepted: April 1, 2015.

Spectroscopic and Dynamical Studies of Highly Energized Small Polyatomic Molecules

Robert W. Field
Massachusetts Institute of Technology
Cambridge, MA 02139
rwfield@mit.edu

I. Program Scope

The fundamental goal of the program is to develop the experimental techniques, diagnostics, interpretive concepts, spectrum-assignment strategies, and pattern-recognition schemes needed to reveal and understand how large-amplitude motions are encoded in the vibration-rotation energy level structure of small, gas-phase combustion-relevant polyatomic molecules. We are focusing our efforts on unimolecular isomerization and dissociation reactions in the prototypical acetylene system, including the acetylene \rightleftharpoons vinylidene isomerization on the S_0 ground electronic surface, the *cis* \rightleftharpoons *trans* conformational isomerization on the S_1 excited state surface, and the photodissociation at around 47000 cm^{-1} , which gains oscillator strength from the S_1 surface, but is believed to be mediated by coupling to triplet electronic states. Work has been extended to characterization of atmospherically relevant molecules such as SO_2 .

II. Recent Progress

A. Calculation of Franck-Condon Intensities in Acetylene and a Simplified Model for the Intra-Polyad Intensity Patterns

We have recently published a full-dimensional calculation of Franck-Condon intensity factors for the $\tilde{A}-\tilde{X}$ transition in acetylene in the harmonic normal-mode basis [4,5]. These calculations have explained a number of previously misunderstood observations in the vibronic intensities obtained in IR-UV double resonance experiments, and they provide predictions for the best strategies to observation of highly-excited local bending states on the S_0 surface that sample the acetylene \rightleftharpoons vinylidene isomerization coordinate.

Although the harmonic normal-mode basis calculation provides qualitative agreement with experiment, the results are not fully quantitative. However, we have shown [3] that when experimentally-determined interactions between the \tilde{A} -state bending levels are taken into account, near-quantitative agreement is reached between the calculated transition intensities and the observed dispersed fluorescence (DF) and stimulated emission pumping (SEP) spectra (Figure 1). This work led to the formulation of a new model for describing Franck-Condon propensities for systems undergoing linear-to-bent geometry changes upon electronic excitation. For emission from the ground vibrational level of the \tilde{A} state, there is a simplifying set of Franck-Condon propensity rules that gives rise to only one zero-order bright state per conserved vibrational polyad of the \tilde{X} state. Unfortunately, when the upper level involves excitation in the highly admixed *ungerade* bending modes, ν_4' and ν_6' , the simplifying Franck-Condon propensity rule breaks down—as long as the usual polar basis (with ν and l quantum numbers) is used to describe the degenerate bending vibrations of the \tilde{X} state—and the intrapolyad intensities result from complicated interference patterns between many zero-order bright states.

We have shown that, when the degenerate bending levels are instead treated in the Cartesian two-dimensional harmonic oscillator basis (with ν_x and ν_y quantum numbers), the propensity for *only one* zero-order bright state (in the Cartesian basis) is restored, and the intrapolyad intensities are simple to model, as long as corrections are made for anharmonic interactions. In the Cartesian basis, the problem is simplified, because the out-of-plane component of the trans-bend (ν_4'') overlaps with a -axis rotation of the trans-bent \tilde{A} -state molecule, so as a result of Eckart conditions it does not contribute to the vibrational Franck-Condon overlap. As a result of *trans* \rightleftharpoons *cis* isomerization in the \tilde{A} state, intrapolyad emission patterns from overtones of ν_4' and ν_6' evolve as quanta of trans bend (ν_3') are added, so the emission intensities are not only relevant to the ground-state acetylene \rightleftharpoons vinylidene isomerization, they are also a direct reporter of isomerization in the electronically excited state.

B. FID-detected MODR schemes for rapid assignment of LIF spectra

We have recently published a paper [1] outlining new approaches millimeter-wave/optical double resonance spectroscopy and evaluating their capability in a study of the perturbed spectrum of the \tilde{C} -state of SO_2 . We have provided a unified treatment for free induction decay (FID)-detected double-resonance techniques that have been described previously by different research groups. Most importantly, we have demonstrated the ability to multiplex these experimental techniques using frequency-agile millimeter-wave technology, which helps to overcome one of the major drawbacks of existing double-resonance spectroscopy implementations—the fact that

previous implementations require the acquisition of many full spectrum double-resonance scans to build up a large enough data set to begin spectral analysis. Fig. 2 shows the results of a single multiplexed double-resonance scan on a high-lying predissociated vibrational level of the \tilde{C} -state of SO_2 .

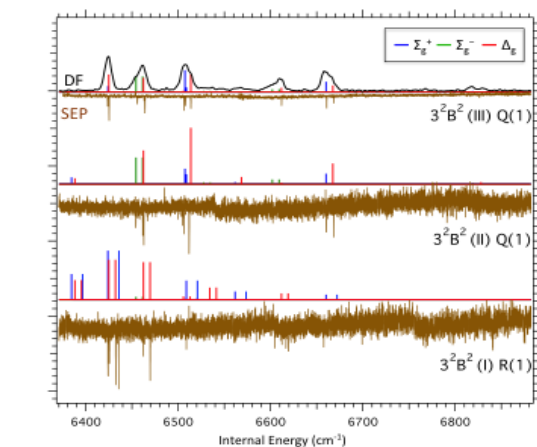


Figure 1. The SEP spectra from $J'=1$ intermediate levels of the three different $K'=1$ stacks of the 3^2B^2 polyad of the \tilde{A} state (labeled with Roman numerals in order of increasing energy) into the $\{N_s, N_{res}\}=\{0,10\}$ pure bending polyad set of the \tilde{X} state are displayed as downward-directed peaks. The eigenstate compositions of the SEP intermediates are taken from experimentally-determined fits to the observed polyad structure. The DF spectrum from 3^2B^2 $K'=1$ Q(1) is shown for comparison at the top of the figure. Also shown as upward stick spectra are the intensities obtained from the Cartesian propensity model. The stick spectrum is colored according to the symmetry of the lower level (see legend).

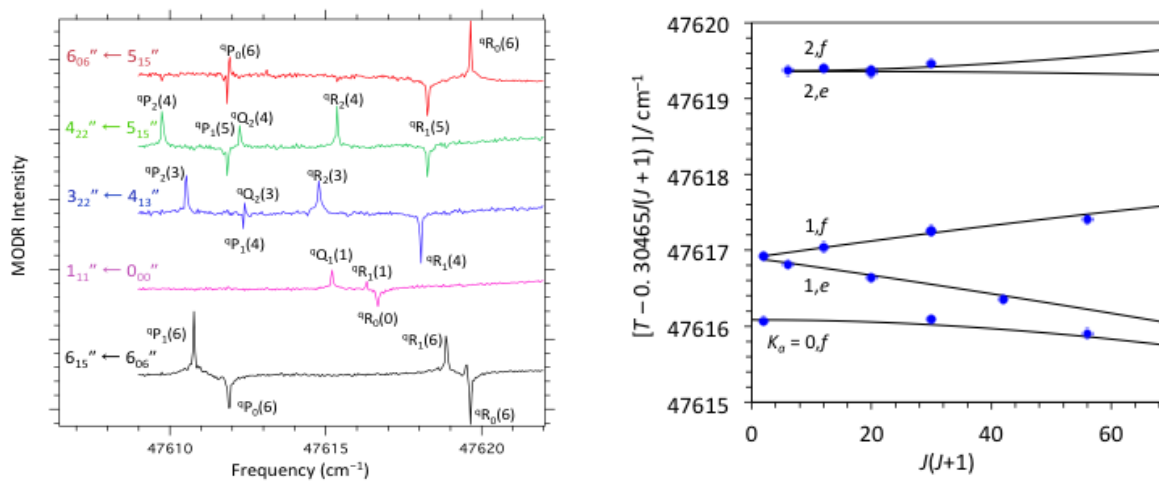


Figure 2. Multiplexed MODR spectrum of the predissociated band of \tilde{C} -state SO_2 at 47616 cm^{-1} . A complete set of low- J rotational term levels can be determined from the five MODR spectra shown in the left panel, which were recorded simultaneously in a single scan of the dye laser. The right panel shows a reduced term value plot of the observed rotational levels. Curves through the data are from an effective rotational fit.

C. Direct observation of the b_2 vibrational levels of \tilde{C} -state SO_2

The \tilde{C} state of SO_2 has a small barrier at the C_{2v} geometry, so it prefers non-equivalent bond lengths (C_s geometry). The barrier causes a staggering in the antisymmetric stretch overtones with even vs. odd vibrational quanta. We have made the first direct observation (via IR-UV double-resonance) of the low-lying odd (b_2) levels, which allows us to characterize the asymmetry directly. The results are analyzed in terms of a diabatic vibronic coupling model with the 2^1A_1 state. One interesting result is that the tunneling staggering increases as quanta of bending (ν_2) are added, which provides evidence for an approach to a conical intersection between the \tilde{C} 1B_2 state and 2^1A_1 state, theoretically predicted to occur at a bond angle of $\sim 150^\circ$. Figure 3 shows the ν_3' staggering as a function of ν_1' and ν_3' .

D. H-atom fluorescence detection of predissociated S_1 acetylene: investigation of the dissociation mechanism

A hydrogen-atom fluorescence detection scheme has been developed to study the predissociation mechanism(s) of S_1 acetylene. Using the new scheme, H-atom action spectra of S_1 acetylene are recorded in

the 47100-47300 cm^{-1} region. The signal-to-noise ratio of our spectra is superior to that of conventional REMPI-detected H-atom action spectra. We have observed vibrational level-dependent predissociation rates, as well as line broadening in the H-atom spectra compared with laser-induced fluorescence spectra in the same energy region. Our observations support the proposed T_3 doorway-mediated predissociation mechanism of S_1 acetylene.

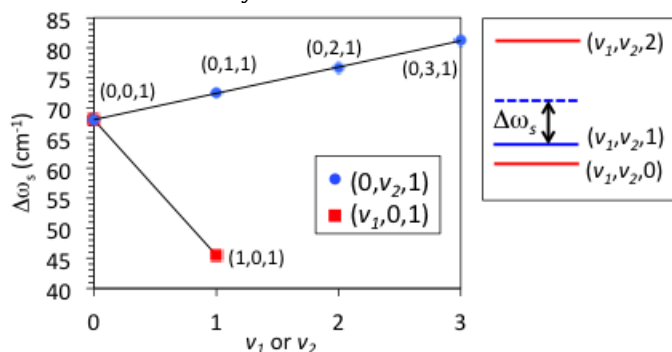


Figure 3. The staggering parameter, $\Delta\omega_s = [E(v_1, v_2, 2) - E(v_1, v_2, 0)]/2 + E(v_1, v_2, 1)$ is plotted for \tilde{C} -state SO_2 as a function of v_1 and v_2 . The parameter is related to the effective barrier height at the C_{2v} geometry. It increases linearly with v_2 as the \tilde{C} -state PES approaches a conical intersection with the 2^1A_1 potential.

In our experiment, the photolysis pump beam (150 $\mu\text{J}/\text{pulse}$, 0.04 cm^{-1} spectral width) and the H-atom probe beam (205.14 nm, ~ 1 mJ/pulse, 0.1 cm^{-1} spectral width) counter-propagate and are focused to cross a supersonic beam of 13% $\text{C}_2\text{H}_2/\text{Ar}$ mixture in the vacuum chamber (10^{-6} torr). The photolysis photon dissociates the molecule into $\text{C}_2\text{H} (^2\Sigma^+) + \text{H}$ fragments. The H-atoms are excited into 3s and 3d atomic levels by the probe beam (10 ns delay) via a two-photon process. Fluorescence from the H-atoms (3s,3d \rightarrow 2p at 656.3nm) is detected with a photomultiplier tube. From Fig. 4, it is clear that the S/N ratio of the H-atom fluorescence detection scheme is superior to that of REMPI.

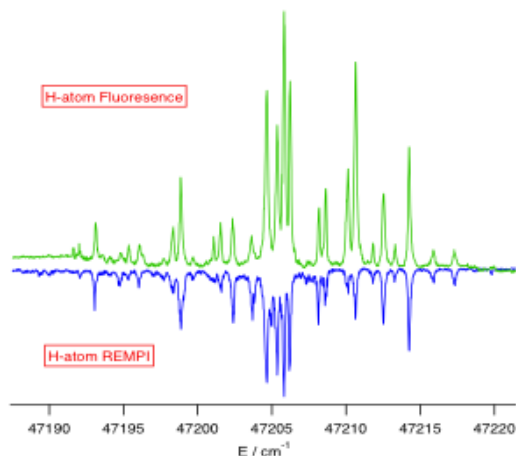


Figure 4. Comparison of s/n ratio between the H-atom fluorescence-detected action spectrum (top) and conventional REMPI-detected action spectrum (bottom).

As Fig. 5 shows, the 1^13^2 state dissociates less rapidly than the other two states, as evidenced by a much smaller H-atom/LIF signal ratio. Compared to the other two states, the 1^13^2 state has fewer quanta of excitation in *trans*-bending mode 3, which is known to be a promoting mode for S_1/T_3 intersystem-crossing (ISC). Since triplet states are known to be involved in the predissociation of S_1 acetylene and S_1/T_3 interaction is believed to be the rate-determining step, the 1^13^2 state dissociates less rapidly than the other two states, even though they lie close in energy. Our observations support the T_3 doorway-mediated predissociation mechanism of S_1 acetylene.

In addition, we have also observed the variation of H-atom yield as a function of rotational quantum number, as well as the broadening of several peaks in the H-atom action spectra (but not in the LIF). The broadened portions of the peaks in the H-atom spectra are unresolved triplet-character eigenstates, which are better sampled in the H-atom channel than in the LIF, because triplet states dissociate readily but they do not fluorescence as rapidly.

III. Future Work

To compare the relative importance of modes 4 and 6 in promoting acetylene S_1 predissociation, we propose using our H-atom fluorescence detection scheme in action spectra of the 3^44^1 and 3^46^1 levels and compare them to their respective LIF spectra. Mode 4 (torsion) had been proposed to be another promoting mode of S_1/T_3 interaction (thus presumably of predissociation as well), but there has been no consensus

about its importance. Note that, due to Franck-Condon selection rules, IR-UV double resonance is needed to probe those two states.

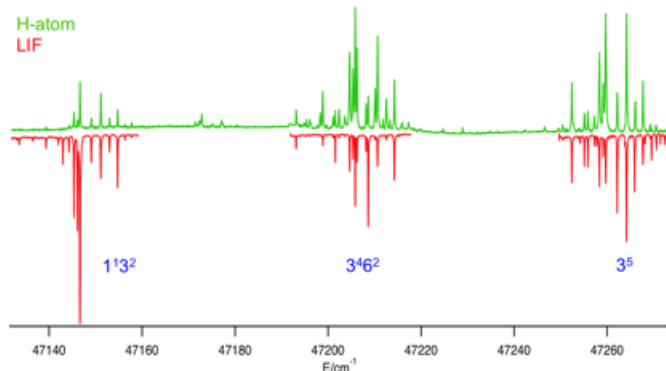


Figure 5. Comparison of H-atom fluorescence-detected action spectra and laser-induced fluorescence spectra (LIF) of the same energy region. The vibrational assignments are given at the bottom in blue.

To investigate the line-broadening mechanisms in the H-atom spectra, we plan an experiment where the delay between the pump and H-atom probe beam is increased to 50-100 ns. With a longer pump-probe delay, we expect to see narrowing, as well as a small shift in the center of gravity of the originally broader peaks in the H-atom channel. This experiment will provide information about the background triplet states, such as their energies relative to the S_1 state, the parity of those states, and, ultimately, their role in acetylene predissociation.

IV. Publications supported by this project 2013–2015

1. G. B. Park, C. C. Womack, A. R. Whitehill, J. Jiang, S. Ono, R. W. Field. "Millimeter-wave optical double resonance schemes for rapid assignment of perturbed spectra, with applications to the \tilde{C}^1B_2 state of SO_2 " *The Journal of Chemical Physics*, **142**, 144201 (2015).
2. G. B. Park, R. W. Field. "Edge effects in chirped-pulse Fourier transform microwave spectra" *The Journal of Molecular Spectroscopy*, **312**, 54 (2015).
3. G. B. Park, J. H. Baraban, A. H. Steeves, R. W. Field "Simplified Cartesian basis model for intrapolyad emission intensities in the bent-to-linear electronic transition of acetylene." *Journal of Physical Chemistry A*, **2015**, 857 (2015).
4. G. B. Park. "Full dimensional Franck-Condon factors for the acetylene $\tilde{A}^1A_u-\tilde{X}^1\Sigma_g^+$ transition. I. Method for calculating polyatomic linear—bent vibrational intensity factors and evaluation of calculated intensities for the *gerade* vibrational modes in acetylene." *The Journal of Chemical Physics*, **141**, 134304 (2014).
5. G. B. Park, J. H. Baraban, R. W. Field. "Full dimensional Franck-Condon factors for the acetylene $\tilde{A}^1A_u-\tilde{X}^1\Sigma_g^+$ transition. II. Vibrational overlap factors for levels involving excitation in *ungerade* modes." *The Journal of Chemical Physics*, **141**, 134305 (2014).
6. P. B. Changala. "Reduced dimension rovibrational variational calculations of the S_1 state of C_2H_2 . I. Methodology and implementation." *J. Chem. Phys.* **140**, 024312 (2014).
7. P. B. Changala, J. H. Baraban, J. F. Stanton, A. J. Merer, R. W. Field. "Reduced dimension rovibrational variational calculations of the S_1 state of C_2H_2 . II. The S_1 rovibrational manifold and the effects of isomerization." *J. Chem. Phys.* **140**, 024313 (2014).
8. K. Prozument, G. B. Park, R. G. Shaver, A. K. Vasiliou, J. M. Oldham, D. E. David, J. S. Muentner, J. F. Stanton, A. G. Suits, G. B. Ellison, R. W. Field. "Chirped-pulse millimeter-wave spectroscopy for dynamics and kinetics studies of pyrolysis reactions." *Physical Chemistry Chemical Physics*, **16**, 15739, (2014).
9. J. Jiang, J. H. Baraban, G. B. Park, M. L. Clark, R. W. Field. "Laser-Induced Fluorescence Study of the S_1 State of Doubly-Substituted ^{13}C Acetylene and Harmonic Force Field Determination." *Journal of Physical Chemistry A*, **117**, 13696, (2013).
10. K. Prozument, R. G. Shaver, M. A. Ciuba, J. S. Muentner, G. B. Park, J. F. Stanton, H. Guo, B. M. Wong, D. S. Perry, R. W. Field. "A new approach toward transition state spectroscopy." *Faraday Discussions* **163**, 33 (2013).
11. H. Lee, J. H. Baraban, R. W. Field, J. F. Stanton. "High-Accuracy Estimates for the Vinylidene-Acetylene Isomerization Energy and the Ground State Rotational Constants of $:C=CH_2$ " *J. Phys. Chem. A* **117**, 11679-11683 (2013).

Quantitative Imaging Diagnostics for Reacting Flows

Jonathan H. Frank
Combustion Research Facility
Sandia National Laboratories
Livermore, CA 94551-0969
jhfrank@sandia.gov

Program Scope

The primary objective of this project is the development and application of quantitative laser-based imaging diagnostics for studying the interactions of fluid dynamics and chemical reactions in reacting flows. Imaging diagnostics provide temporally and spatially resolved measurements of species, temperature, and velocity distributions over a wide range of length scales. Multi-dimensional measurements are necessary to determine spatial correlations, scalar and velocity gradients, flame orientation, curvature, and connectivity. Current efforts in the Advanced Imaging Laboratory focus on studying the detailed structure of both isolated flow-flame interactions and turbulent flames. The investigation of flow-flame interactions is of fundamental importance in understanding the coupling between transport and chemistry in turbulent flames. These studies require the development of imaging diagnostic techniques to measure key species in the hydrocarbon-chemistry mechanism as well as mixture fraction, rates of reaction and dissipation. Recent studies on flow-flame interactions have focused on localized extinction and re-ignition as well as effects of stratification. Diagnostic development includes efforts to extend measurement capabilities to a broader range of flame conditions and combustion modes, including combustion of hydrocarbon fuels beyond methane and stratified premixed combustion. A major thrust continues to be the development and application of diagnostic capabilities for measuring the temporal evolution of turbulent flames using high-repetition rate imaging techniques. A series of studies on the fluid dynamics of turbulent flames are underway using three-dimensional high-speed measurements of the velocity field.

Recent Progress

High-speed imaging of turbulent flame dynamics and structure

We are using high-repetition rate imaging to probe the dynamics and structure of interactions between turbulent flows and flames. We have developed a capability for high-repetition rate tomographic particle image velocimetry (TPIV) measurements in turbulent flames. The TPIV technique provides volumetric, three-component velocity field measurements that enable determination of the complete velocity gradient tensor. Recently, we used this capability to measure the 3-D structure and temporal evolution of the strain rate field in turbulent partially-premixed jet flames with localized extinction.

High-repetition rate TPIV is combined with OH-LIF imaging measurements using the experimental configuration in Fig. 1a to measure the transient response of the high-temperature reaction zone of flames to interactions with high strain rate regions of the flow field. The sequence of 10-kHz measurements in Fig. 1b shows the temporal evolution of the velocity, compressive principal strain rate, and OH-LIF fields during localized extinction event in a turbulent partially-premixed dimethyl ether (DME)/air jet flame. The velocity and OH-LIF signal are displayed in the central plane, and the compressive strain rate is represented by blue

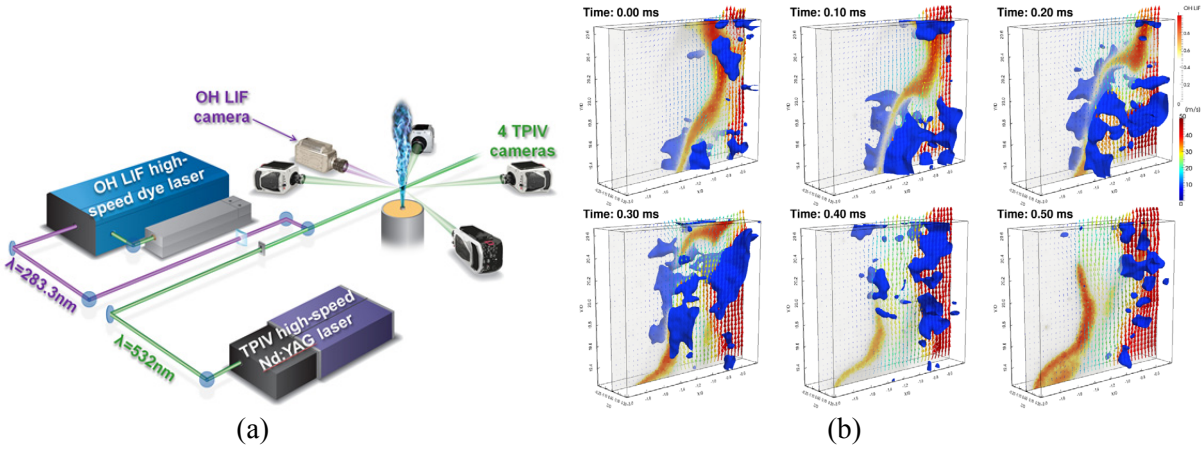


Fig. 1: (a) Experimental configuration for simultaneous high-speed tomographic PIV and OH-LIF imaging measurements, (b) Time sequence of TPV and OH-LIF measurements at 10 kHz in a turbulent partially-premixed DME/air jet flame at $y/D = 20$. Jet axis is near the right-hand side of the probe volume. Blue surfaces are isosurfaces of the compressive strain rate for $s_3 = -15,000 \text{ s}^{-1}$. Velocity vectors are shown in the same plane as the OH-LIF images (1 out of 16 in-plane vectors displayed).

isosurfaces at $s_3 = -15,000 \text{ s}^{-1}$. The onset of extinction occurs at time $t = 0.20 \text{ ms}$ and is identified by the formation of a discontinuity in the contour of the OH-LIF signal. The image sequence shows large structures with high compressive strain rates in the region of localized extinction. These structures remain coherent and coupled to the reaction zone until extinction occurs. As the flame approaches extinction, the high-temperature reaction zone becomes thinner. Once the flame is locally quenched, the strain rate decreases and the large coherent structures break apart. These compressive strain rates are an order of magnitude greater than the extinction strain rate for a laminar counterflow flame with the same composition. Analysis of many sequences shows that intermittent regions of high compressive strain do not always cause extinction since there is a requisite interaction time for the strain to induce extinction.

To understand the effects of combustion on the turbulent flow field, we are conducting comparative studies of turbulent non-reacting flows and flames. Figure 2a shows a time sequence of strain rate isosurfaces in a turbulent air jet and partially-premixed methane/air jet flame with jet exit Reynolds numbers of approximately 13,000. The strain rate field in the flame consists of elongated regions of high strain rate that are concentrated in a narrow region of the shear layer between the high velocity jet and the low-velocity coflow. In contrast, the regions of high strain rate in the turbulent air jet are more fragmented and distributed over a broader portion of the flow field. These results are consistent with the lower entrainment rates of the jet flame. In both flows, regions of high strain appear in intermittent bursts, which we have studied using a cluster analysis. Figure 2b shows time sequences of the number of strain rate clusters as a function of the strain rate threshold, $|s_{thrs}|$, for the air jet and jet flame. The narrow peaks in the time traces indicate intermittent bursts of high strain regions. Burst durations are on the order of the flow residence time in the probe volume. Overall, the air jet shows significantly greater numbers of clusters at intermediate strain rates, corresponding to the more fragmented structure of the strain rate field. The combustion induces a strain field with greater connectivity.

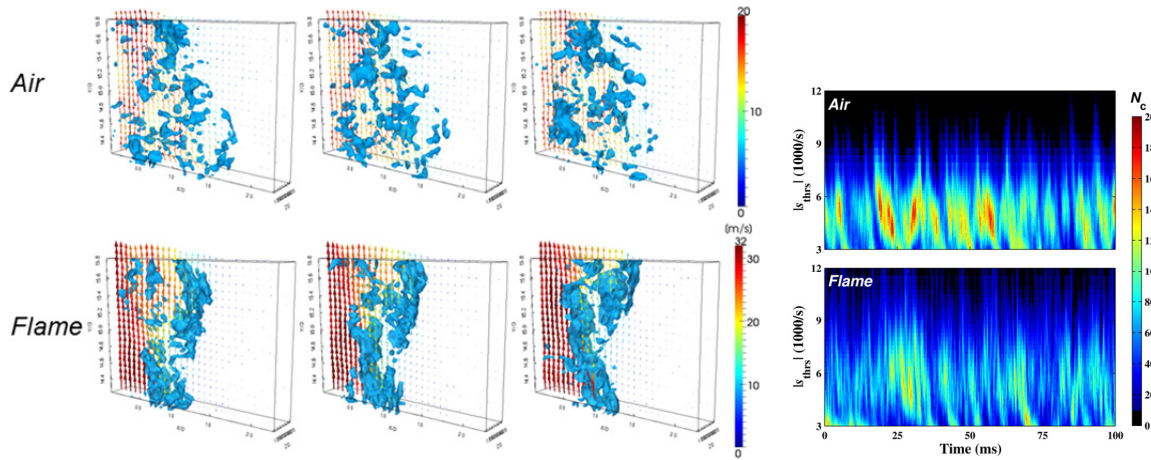


Fig. 2: (a) Time sequences of velocity and strain rate in a turbulent air jet and partially-premixed CH_4/air jet flame with comparable jet exit Reynolds numbers. Inter-frame time is $100 \mu\text{s}$. Measurements at $y/D = 15$ with the jet axis near the left-hand side of the $16.5 \text{ mm} \times 12.3 \text{ mm} \times 2.5 \text{ mm}$ probe volume. Blue surfaces are isosurfaces of the strain rate norm for $|s| = 7,000 \text{ s}^{-1}$. (b) Time sequences of the number of clusters, N_c , in the strain rate field as a function of strain rate threshold.

The effects of combustion on the structure of the strain rate tensor were investigated using an analysis of the principal strain rates, s_1 , s_2 and s_3 , which are defined such that $s_1 \geq s_2 \geq s_3$. The maximum and minimum principal strain rates, s_1 and s_3 , correspond to the most extensive and compressive strain rate components, respectively. The ratios of the three principal strain rates along with the sign of the intermediate strain rate, s_2 , provide insight into the local structure of the strain rate field. The local state of the strain rate field was determined from the relative ratios of the three principal strain rates, $s_1/s_2:1:s_3/s_2$. According to previous studies, the most probable ratios in isotropic turbulence are approximately 3:1:-4. In the presence of shear, the relative strain rate ratios s_1/s_2 and s_3/s_2 tend to increase, indicating a more planar strain field in turbulent shear flows than in isotropic turbulence. In the turbulent jet flames of our studies, the most probable values of strain rate ratios were approximately 8:1:-9. These ratios signify that the extensive and compressive strain rates dominate over the intermediate strain rate. Large strain rates in the reacting and non-reacting turbulent jets are preferentially sheet-forming with a single axis of compressive strain and two axes of extensive strain. Probability density functions of the strain rate ratios conditioned on high strain rate regions, $|s| > 5|s|'$, show a shift in the most probable value of strain rate ratios approaching those found in isotropic turbulence.

Turbulent partially-premixed DME/air jet flames

We continue to develop joint experimental and computational studies of a series of piloted partially-premixed DME/air jet flames that have differing degrees of localized extinction and are target flames for the TNF Workshop. In recent studies, we performed comparisons of velocity, OH-LIF, and CH_2O -LIF imaging measurements with large eddy simulations by C. Hasse (T. U. Freiberg) that used an LES flamelet-progress variable approach (LES-FPV). Comparisons were facilitated by including simulations of the OH-LIF and CH_2O -LIF signals in the flamelet library and using these results within the LES calculation. Overall, the simulations showed good agreement with the measured downstream evolution of the velocity, OH, and CH_2O distributions. Experimentally observed intermittent gaps between the OH and CH_2O distributions were captured by the LES-FPV calculations. The separation of these species varies as a function of strain rate, which is captured within the flamelet library. We continue to investigate this issue further. We are also refining the formaldehyde LIF measurements and

performing high-speed imaging measurements to study dynamics of localized extinction and re-ignition. An initial coupling of velocity, OH-LIF, and CH₂O-LIF measurements with complementary species and temperature measurements by R. Barlow (Sandia) has been performed and further analysis is planned. Plans for the next phase of coupling experiments with simulations include high-fidelity LES performed at Sandia by J. Oefelein.

Future Plans

The investigation of the structure and dynamics of flow-flame interactions in turbulent non-premixed, premixed, and stratified modes of combustion will remain a major thrust in our research program. In the near term, we plan to study the effects of combustion on the strain rate and vorticity fields in flames with and without localized extinction. Our planned high-speed imaging effort includes optimization of TPIV analysis and further evaluation of uncertainties, methods for noise reduction, and the development of efficient methods for analyzing large sets of imaging data. We will expand our high-speed imaging studies to turbulent counterflow flames and develop a joint experimental and computational investigation with LES calculations performed by J. Oefelein. This collaboration will include the development of a framework for comparing measurements and simulations of turbulent flame dynamics.

Plans for developing and improving diagnostic capabilities include continued investigations of x-ray diagnostic techniques, the development of simultaneous velocity and temperature measurements by combining PIV and 2-D CARS in collaboration with C. Kliewer (Sandia), and the quantification of CH₂O-LIF measurements. Improved CH₂O-LIF measurements are needed to understand formaldehyde transport in turbulent DME flames and to resolve discrepancies in the formaldehyde concentrations that are predicted by different chemical kinetic mechanisms.

BES-supported publications and submitted journal articles (2013-present)

B. Coriton, J.H. Frank, A. Gomez, "Effects of strain rate, turbulence, reactant stoichiometry and heat losses on the interaction of turbulent premixed flames with stoichiometric counterflowing combustion products," *Combust. Flame*, **160**, 2442-2456 (2013).

B. Coriton, A.M. Steinberg, J.H. Frank, "High-speed tomographic PIV and OH PLIF measurements in turbulent reactive flows," *Exp. Fluids*, **55**, 1-20 (2014).

J.H. Frank, A. Sharvorkiy, H. Bluhm, B. Coriton, E. Huang, D.L. Osborn, "In-situ soft x-ray absorption spectroscopy of flames," *Appl. Phys. B*, **117**, 493-499 (2014).

B. Coriton, J.H. Frank, "High-speed tomographic PIV measurements of strain rate intermittency and clustering in turbulent partially premixed jet flames," *Proc. Combust. Inst.*, **35**, 1243-1250 (2015).

B. Coriton, M. Zendejdel, S. Ukai, A. Kronenburg, O.T. Stein, S-K Im, M. Gamba, J.H. Frank, "Imaging measurements and LES-CMC modeling of a partially-premixed turbulent dimethyl ether/air jet flame," *Proc. Combust. Inst.*, **35**, 1251-1258 (2015).

A.M. Steinberg, B. Coriton, J.H. Frank, "Influence of combustion on principal strain-rate transport in turbulent premixed flames," *Proc. Combust. Inst.*, **35**, 1287-1294 (2015).

J. Weinkauff, P. Trunk, J. H. Frank, M.J. Dunn, A. Dreizler, B. Böhm, "Investigation of flame propagation in a partially premixed jet by high-speed stereo PIV and acetone PLIF," *Proc. Combust. Inst.*, **35**, 3773-3781 (2015).

S. Popp, F. Hunger, S. Hartl, D. Messig, B. Coriton, J. H. Frank, F. Fuest, C. Hasse, "LES flamelet-progress variable modelling and measurements of a turbulent partially-premixed dimethyl ether jet flame," *Combust. Flame*, submitted.

Computer-Aided Construction of Chemical Kinetic Models

William H. Green
Department of Chemical Engineering, M.I.T.
Cambridge, MA 02139
whgreen@mit.edu

I. Program Scope

The combustion chemistry of even simple fuels can be extremely complex, involving hundreds or thousands of kinetically significant species. The most reasonable way to deal with this complexity is to use a computer not only to numerically solve the kinetic model, but also to construct the kinetic model in the first place. Because these large models contain so many numerical parameters (e.g. rate coefficients, thermochemistry) one never has sufficient data to uniquely determine them all experimentally. Instead one must work in “predictive” mode, using theoretical values for many of the numbers in the model, and as appropriate refining the most sensitive numbers through experiments. Predictive chemical kinetics is exactly what is needed for computer-aided design of combustion systems based on proposed alternative fuels, particularly for early assessment of the value and viability of proposed new fuels. Our research effort is aimed at making accurate predictive chemical kinetics practical; this is a challenging goal which necessarily includes a range of science advances. Our research spans a wide range from quantum chemical calculations on individual molecules and elementary-step reactions, through the development of improved rate/thermo calculation procedures, the creation of algorithms and software for constructing and solving kinetic simulations, the invention of methods for model-reduction while maintaining error control, and finally comparisons with experiment. Many of the parameters in the models are derived from quantum chemistry, and the models are compared with experimental data measured in our lab or in collaboration with others.

II. Recent Progress

A. Elucidating Interesting Chemistry

1. Sulfur and Nitrogen chemistry

We recently added the capability to model organosulfur and organonitrogen chemistry to the Reaction Mechanism Generator (RMG), and computed many [a] of the needed thermochemical and rate parameters using quantum chemistry (typically at the CBS-QB3 level, but more recently using the CCSD(T)-F12a method to achieve higher accuracy in enthalpies and barrier heights). While our database surely does not include all the chemistry of sulfur and nitrogen species yet, and some of the rate parameters have fairly large error bars, we were able to construct fairly good models for a variety of systems:

- 1) Gas Phase Pyrolysis of several dialkyl sulfides (RSR).[b] Interestingly, we have recently found that tertiary alkyl sulfides follow a very different reaction path than primary and secondary sulfides, reacting primarily via thiols (RSH) rather than thioaldehydes (RCHS). Our computer-generated detailed models for sulfide pyrolysis are in quantitative agreement with multiple experiments.
- 2) Reactions of dihexyl sulfide (RSR) in supercritical water [c]. While (as usual) the water mostly acts as an inert solvent, we found that thioaldehyde (RCHS) intermediates react rapidly with the water, altering the product distribution significantly.
- 3) Pyrolysis of ethyl nitrite (RONO) in a Chen-type flash pyrolysis nozzle [8]. The original model predictions were inconsistent with the experimental data measured by Suits and Field, but the discrepancy was resolved by considering a roaming-radical reaction.
- 4) Selective oxidation of alkenes by N_2O . [d] Ab initio rates are in agreement with experiments by Klavs Jensen’s group.

- 5) Pyrolysis and ignition of ethyl amine (RNH_2). Model is in semi-quantitative agreement with experiments by Hanson and Davidson.

2. Hydrocarbon ignition/combustion

Together with Stephen Klippenstein, Michael Burke, and Franklin Goldsmith we have made a significant advance in understanding phase 1 ignition, which we find is actually is two stages: an exponential growth phase we call stage 1A followed by a more complicated phase where the chemistry is nonlinear we call stage 1B. Both stages are sensitive to only a handful of reactions, suggesting that it may be possible to understand and model low-temperature ignition without recourse to the very large kinetic models used currently, and indeed for alkanes we are able to write simple analytical expressions for ignition delay in terms of a few rate parameters.[e] We are currently pursuing a similar approach to understand phase 2 ignition chemistry.

For several years we have been developing a detailed model for the synthetic jet fuel JP-10, which is a fused ring tricyclic molecule. There were several technical issues which had to be overcome, for example how to compute the rates of intramolecular disproportionation of the biradical intermediates, and how to estimate the thermochemistry and reaction rates of a variety of bicyclic intermediates. This year we completed that study, developing a model which accurately predicts the pyrolysis and high-temperature oxidation/ignition of this complicated fuel.[11]

For several years we have been measuring and computing the chemistry of vinyl radical (C_2H_3), which is the key species at the branch point between clean combustion (to CO_2) and soot formation. Very recently we directly measured the rate coefficient for vinyl + butadiene, a proposed route to benzene formation, which is an order of magnitude slower than published estimates.[f]

3. Criegee Intermediate Chemistry

In recent years we measured and computed several reactions of the smallest Criegee Intermediate CH_2OO . [6,g,h] This year we measured and so corrected [h] the too-high rate of the $\text{CH}_2\text{OO} + \text{CH}_2\text{OO}$ reaction reported in a paper published in *Nature Chemistry*.

B. Methodology for Computer-Aided Kinetic Modeling

A major focus of this research project continues to be the development of advanced methods for automatically constructing, reducing, and solving combustion simulations.[1,4] We are constantly adding functionality and additional types of chemistry to the open-source Reaction Mechanism Generator (RMG) software package. We are in the process of distributing a new version of RMG including S,N,Si chemistry in addition to the C,H,O chemistry in the prior release.

This computer-aided kinetic modeling approach is having a broad impact. With the Brezinsky group we modeled how alkene chemistry depends on the position of the double bond, an issue relevant to biodiesel combustion.[10] We continue to distribute the mechanism construction software to many research groups, and to train and support the new users. In the past two years researchers from Chicago, Belgium, China, France, Germany, Japan, and Saudi Arabia have visited my group for training in how to use the RMG software. Several companies are also now using the software, several energy and petrochemical companies but also other industries including Intel and Proctor & Gamble. Developers outside of my research group have begun to add functionality to this open-source software; among the most active developers are researchers at Northeastern University and the University of Ghent. These independently funded external efforts leverage the funding provided by this program.

C. Quantum Calculations of Reaction Rates and Thermochemistry

Historically, the accuracy of rate and equilibrium calculations for combustion were almost always limited by the uncertainties in the computed potential energy surface, due to the need to use approximate electronic structure methods and small basis sets. Modern quantum chemistry methods, such as explicitly-correlated coupled-cluster methods (e.g. CCSD(T)-F12) have made it practical to significantly reduce

these errors in computed PES's and molecular enthalpies. As the energy calculations improve, we find that the accuracy of our equilibrium and rate calculations is now often limited by other aspects of the overall calculation. This has led us (and many others, including Don Truhlar and Stephen Klippenstein) to invest significant efforts in improving on the traditional rate and thermochemistry computation methodology, which is based on several approximations which are not really accurate.

Over the past two years we focused on developing an alternative method for rate calculations, which avoids many of the approximations associated with traditional TST calculations. We created and distributed an efficient software implementation [i] of the new RPMD method for computing reaction rates. We demonstrated that RPMD is an attractive way for computing accurate rates and isotope-effects for systems too large for exact quantum rate calculations (i.e. bigger than H+CH₄), but small enough that constructing a fairly accurate full-dimensional PES is practical. To test and demonstrate the new rate-calculation method we used this new software, often in collaboration with Hua Guo, to compute rate coefficients for several reactions of the type X + CH₄ (e.g. X=OH, O, Cl, H, D, Mu).[2,3,5,7] Overall, the tests demonstrated that RPMD is relatively easy to use and that it is pretty accurate; its main drawback is that it requires a full PES, not just the PES at/near the stationary points required by conventional transition state theory (TST).

We recently found that the RPMD method also works well for barrierless insertion reactions.[9] It would be interesting to see if this method will also work well for roaming radical reactions.

During our calculations of this relatively small set of relatively simple reactions, we ran into several cases where there are unexpectedly large differences between the rate computed by RPMD and by a standard TST approach.[5,7,j] It appears that the anharmonic shape of the PES near the saddle point leads to pretty large (~ factor of 4) errors in rates computed using the conventional canonical variational transition-state-theory. Anharmonicity is apparently even more important for rate calculations than previously appreciated, and methodology for dealing with this needs improvement.

III. References

- a. Caleb A Class, Jorge Aguilera-Iparraguirre, William H Green, "A kinetic and thermochemical database for organic sulfur and oxygen compounds", *Phys. Chem. Chem. Phys.* (2015, accepted).
- b. R Van de Vijver, NM Vandewiele, AG Vandeputte, KM Van Geem, M-F Reyniers, WH Green, GB Marin, "Rule-based ab initio kinetic model for alkyl sulfide pyrolysis", *Chem. Eng. J.* (2014, in press) [doi:10.1016/j.cej.2014.10.067](https://doi.org/10.1016/j.cej.2014.10.067)
- c. Yuko Kida, Caleb A Class, Anthony J Concepcion, Michael T Timko, William H Green, "Combining Experiment and Theory to Elucidate the Role of Supercritical Water in Sulfide Decomposition", *Phys. Chem. Chem. Phys.* **16**, 9220-9228 (2014).
- d. Stephen G Newman, Kyoungmi Lee, Jianghuai Cai, Lu Yang, William H Green, Klavs F Jensen, "Continuous Thermal Oxidation of Alkenes by Nitrous Oxide in a Packed Bed Reactor", *Ind. Eng. Chem. Res.* (2015, in press). DOI: 10.1021/ie504129e
- e. Shamel S. Merchant, C. Franklin Goldsmith, Aäron G. Vandeputte, Michael P. Burke, Stephen J. Klippenstein and William H. Green, "Understanding low-temperature first-stage ignition delay: Propane", *Combustion & Flame* (2015, submitted).
- f. ZJ Buras, EE Dames, SS Merchant, G Liu, RMI Elsamra, WH Green, "Kinetics and Products of Vinyl + 1,3-Butadiene, a Potential Route to Benzene", *J. Phys. Chem. A* (submitted)
- g. Zachary J Buras, Rehab MI Elsamra, Amrit Jalan, Joshua E Middaugh, William H Green, "Direct Kinetic Measurements of Reactions between the Simplest Criegee Intermediate CH₂OO and alkenes", *J. Phys. Chem. A* **118**, 1997-2006 (2014).
- h. ZJ Buras, RMI Elsamra, WH Green, "Direct Determination of the Simplest Criegee Intermediate (CH₂OO) Self Reaction Rate", *J. Phys. Chem. Lett.* **5**, 2224-2228 (2014).

- i. Y.V. Suleimanov, J.W. Allen, and W.H. Green, "RPMDrate: bimolecular chemical reaction rates from ring polymer molecular dynamics", *Comp. Phys. Comm.* **184**(3), 833-840 (2013).
- j. Gonzalez-Lavado, J.C. Corchado, Y.V. Suleimanov, W.H. Green, J. Espinosa-Garcia, "Theoretical Kinetics Study of the $O(^3P) + CH_4/CD_4$ Hydrogen Abstraction Reaction: The Role of Anharmonicity and Quantum Mechanical Effects", *J. Chem. Phys. A* **118**, 3243-3252 (2014).

IV. Publications and submitted journal articles supported by this DOE program 2013-2015

1. G.R. Magoon and W.H. Green, "Design and implementation of a next-generation software system for on-the-fly quantum and force field calculations in automated reaction mechanism generation", *Computers in Chemical Engineering* **52**, 35-45 (2013).
2. Y. Li, Y.V. Suleimanov, M.-H. Yang, W.H. Green, and H. Guo, "Ring Polymer Molecular Dynamics Calculations of Thermal Rate Constants for the $O(^3P) + CH_4 \rightarrow OH + CH_3$ Reaction: Contributions of Quantum Effects", *Journal of Physical Chemistry Letters* **4**, 48 (2013).
3. Y. Li, Y.V. Suleimanov, J. Li, W.H. Green, and H. Guo, "Rate coefficients and kinetic isotope effects of the $X + CH_4 \rightarrow CH_3 + HX$ ($X = H, D, Mu$) reactions from ring polymer molecular dynamics", *Journal of Chemical Physics* **138**, 094307 (2013).
4. Edward Blurock, Federique Battin-Leclerc, Tiziano Faravelli, and William H. Green, "Automatic generation of detailed mechanisms" in *Cleaner Combustion: Developing Detailed Chemical Kinetic Models*, ed. by F. Battin-Leclerc, J. Simmie, and E. Blurock (Springer-Verlag, London, 2013).
5. J.W. Allen, W.H. Green, Y. Li, H. Guo, and Y.V. Suleimanov, "Full dimensional quantum rate coefficients and kinetic isotope effects from ring polymer molecular dynamics for a seven-atom reaction $OH + CH_4 \rightarrow CH_3 + H_2O$ ", *J. Chem. Phys.* **138**, 221103 (2013).
6. A. Jalan, J.W. Allen, and W.H. Green, "Chemically activated formation of organic acids in reactions of the Criegee intermediate with aldehydes and ketones", *Phys. Chem. Chem. Phys.* **15**, 16841-16852 (2013).
7. Y. Li, Y.V. Suleimanov, W.H. Green, and H. Guo, "Quantum Rate Coefficients and Kinetic Isotope Effect for the Reaction $Cl + CH_4 \rightarrow HCl + CH_3$ from Ring Polymer Molecular Dynamics", *Journal of Physical Chemistry A* **118**, 1989-1996 (2014).
8. Kirill Prozument, Yury V Suleimanov, Beat Buesser, James M Oldham, William H Green, Arthur G Suits, Robert W Field, "A signature of roaming dynamics in the Thermal Decomposition of Ethyl Nitrite: Chirped-Pulse Rotational Spectroscopy and Kinetic Modeling", *J. Phys. Chem. Lett.* **5**, 3641-3648 (2014)
9. Yury V Suleimanov, Wendi J Kong, Hua Guo, William H Green, "Ring-polymer molecular dynamics: Rate coefficient calculations for energetically symmetric (near thermoneutral) insertion reactions ($X + H_2 \rightarrow HX + H(X = C(^1D), S(^1D))$)", *J. Chem. Phys.* **141**, 244103 (2014)
10. A. Fridlyand, S.S. Goldsborough, K. Brezinsky, S.S. Merchant, and W.H. Green, "Influence of the Double Bond Position on the Oxidation of Decene Isomers at High Pressures and Temperatures", *Proceedings of the Combustion Institute* **35**, 333-340 (2015).
11. Connie W. Gao, Aäron Vandeputte, Nathan W. Yee, William H. Green, Robin E. Bonomi, Gregory R. Magoon, Hsi-Wu Wong, Oluwayemisi O. Oluwole, David K. Lewis, Nick M. Vandewiele, Kevin Van Geem "JP-10 combustion studied with shock tube experiments and modeled with automatic reaction mechanism generation", *Combustion & Flame* (2015, accepted)

Quantum Dynamics of Elementary Chemical Reactions

Hua Guo (hquo@unm.edu)

Department of Chemistry and Chemical Biology, University of New Mexico, Albuquerque, NM 87131

Program scope

To understand the quantum dynamics of elementary chemical reactions in the gas phase.

Recent progress

We continue to push for the application of the ring-polymer molecular dynamics (RPMD) method for computing rate coefficients for gas phase bimolecular reactions. Recent collaborations with Yury Suleimanov in Bill Green's group at MIT have explored the applicability of this method in complex-forming reactions.¹⁻² Our tests on several simple insertion reactions showed that the RPMD method is capable of yielding accurate rate coefficients.

One of our major research activities has been the development of accurate multi-dimensional global potential energy surfaces (PESs) for elementary chemical reactions. Using our recently proposed permutation invariant polynomial-neural network (PIP-NN) approach,³⁻⁴ we have constructed PESs for tetra-atomic,⁵⁻⁷ penta-atomic,⁸⁻¹¹ and hexa-atomic systems.¹² The PIP-NN approach uses low-order PIPs of the Morse variable of internuclear distances¹³⁻¹⁴ as symmetry functions, which replacing the coordinates as the input layer of the NN. It rigorously enforces the permutation symmetry, and is simple to implement and efficient to evaluate. The root mean square error (RMSE) of the fitting is typically on the order of a few meV or less. In a recent implementation for the acetylene-vinylidene isomerization PES, for example, the RMSE was less than 10 cm⁻¹ and the calculated highly excited vibrational levels approached spectroscopic accuracy.⁷ In another application, the reactive PES for the NH₄ system was developed with an RMSE of 27 cm⁻¹, which includes not only the hydrogen abstraction channel, but also the hydrogen exchange channel.⁸

These high fidelity fits of high-level ab initio points allowed us to examine various issues in molecular spectroscopy and reaction dynamics of elementary reactions. In addition to the classical unimolecular process mentioned above (isomerization between HCCH and H₂CC),⁷ we have recently reported an accurate PES for the simplest Criegee intermediate (CH₂OO).¹⁰ The ro-vibrational energy levels and intensities calculated on this PES were found to agree with experiment very well,^{10, 15} which helped us to understand the vibrational dynamics of this elusive species. On the reaction dynamics side, we have focused on mode specificity of both bi and uni-molecular reactions. For uni-molecular processes, we investigated the HOCO/HCO₂ → H + CO₂ dissociation reactions and their deuterated counterpart facilitated by tunneling,¹⁶⁻¹⁸ in collaboration with Al Wagner at Argonne and Bob Continetti at UCSD. The bimolecular systems include the X + H₂O ↔ HX + OH (X=F, Cl)¹⁹⁻²² and the H + NH₃ ↔ H₂ + NH₂ reactions.²³⁻²⁴ We have also examined mode specificity of some ion-molecule reactions,²⁵ using accurate PESs.^{6, 9} The observed mode specificity and product energy disposal in these reactions can be largely explained by the recently proposed Sudden Vector Projection model,²⁶⁻²⁹ which has been successfully used to predict mode specificity and bond selectivity in gas phase and gas-surface reactions.³⁰ Figure 1 shows the cover of J. Chin. Chem. Soc. on our featured review on the SVP model applied to the X + CH₄ → HX + CH₃ reactions.

In addition to the dynamics of reactions mentioned above, we have explored the dynamics of photodissociation of several prototypical systems. In collaboration with David Yarkony at Johns Hopkins, the non-adiabatic dynamics in ammonia has been systematically elucidated.³¹⁻³³ In particular, we have

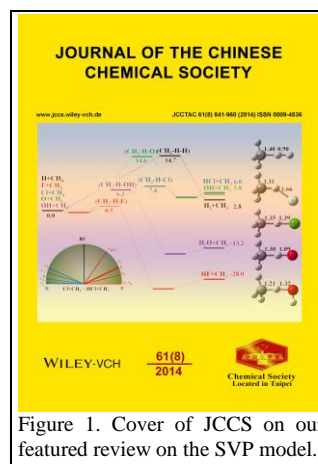


Figure 1. Cover of JCCS on our featured review on the SVP model.

computed the OH(A/X) branching ratio with the parent molecule in ground and excited vibrational levels prior to photolysis, using highly accurate coupled PESs. Excellent agreement with experimental results has been achieved, as shown in Fig. 2. The resolution of the NH₂ internal states in our model allows a re-interpretation of the experimental data.³³ In addition, we have teamed up with Richard Dawes at Missouri University of Science and Technology to resolve the controversy concerning the measured absorption spectra in the UV photodissociation of the simplest Criegee intermediate (CH₂OO).³⁴

To achieve the ultimate state-to-state characterization of bimolecular reactions, we have devoted some effort to development of new methodologies. In particular, we have implemented a transition state wave packet (TSWP) approach to state-to-state reaction dynamics recently proposed by Uwe Manthe and coworkers.³⁶ This TSWP method has been demonstrated to be accurate and efficient in computing the integral and differential cross sections for a prototypical atom-diatom reaction (H + D₂ → HD + D).³⁷ It has recently been extended to the J=0 state-to-state dynamics of the H + H₂O → H₂ + OH reaction,³⁸ and F + H₂O → HF + OH reaction.³⁹

Finally, we have been involved in several other PES,⁴⁰ spectroscopic,⁴¹ kinetic,⁴²⁻⁴³ and dynamic studies.⁴⁴⁻⁴⁸ Some of the studies are collaborations with Gabor Czako, Richard Dawes, Joaquin Espinosa-Garcia, Kopin Liu, Z. Sun, Al Viggiano, Minghui Yang, and Daiqian Xie. The details of these studies are not provided here due to space limitations.

Future plans

In the next year, we plan to continue to pursue our proposed research in the areas of chemical dynamics and kinetics. The focus will be placed on the following areas: i). further develop an efficient method to obtain state-to-state scattering information for bimolecular reactions involving four atoms; ii). to construct accurate PESs for such reactions, and iii). to perform quantum scattering and quasi-classical trajectory calculations on these PESs.

References (* indicates DOE funded work in the past year):

- *1 Y. Li, Y. V. Suleimanov and H. Guo, *J. Phys. Chem. Lett.* **5**, 700 (2014).
- *2 Y. V. Suleimanov, W. J. Kong, H. Guo and W. H. Green, *J. Chem. Phys.* **141**, 244103 (2014).
- 3 B. Jiang and H. Guo, *J. Chem. Phys.* **139**, 054112 (2013).
- 4 J. Li, B. Jiang and H. Guo, *J. Chem. Phys.* **139**, 204103 (2013).
- 5 J. Li, J. Chen, D. H. Zhang and H. Guo, *J. Chem. Phys.* **140**, 044327 (2014).
- *6 A. Li and H. Guo, *J. Phys. Chem. A* **118**, 11168 (2014).
- *7 H. Han, A. Li and H. Guo, *J. Chem. Phys.* **141**, 244312 (2014).
- 8 J. Li and H. Guo, *Phys. Chem. Chem. Phys.* **16**, 6753 (2014).
- *9 A. Li and H. Guo, *J. Chem. Phys.* **140**, 224313 (2014).
- *10 J. Li, S. Carter, J. M. Bowman, R. Dawes, D. Xie and H. Guo, *J. Phys. Chem. Lett.* **5**, 2364 (2014).
- *11 M. Majumder, S. E. Hegger, R. Dawes, S. Manzhos, X.-G. Wang, T. Carrington Jr., J. Li and H. Guo, *Mol. Phys.* **in press**, DOI: [10.1080/00268976.2015.1015642](https://doi.org/10.1080/00268976.2015.1015642) (2015).
- *12 J. Li, J. Chen, D. Xie, D. H. Zhang and H. Guo, (to be published).
- 13 Z. Xie and J. M. Bowman, *J. Chem. Theo. Comp.* **6**, 26 (2010).
- 14 B. J. Braams and J. M. Bowman, *Int. Rev. Phys. Chem.* **28**, 577 (2009).
- *15 M. Nakajima, Q. Yue, J. Li, H. Guo and Y. Endo, *Chem. Phys. Lett.* **621**, 129 (2015).
- *16 J. Wang, J. Li, J. Ma and H. Guo, *J. Chem. Phys.* **140**, 184314 (2014).
- *17 A. F. Wagner, R. Dawes, R. E. Continetti and H. Guo, *J. Chem. Phys.* **141**, 054304 (2014).
- *18 L. Zou, J. Li, H. Wang, J. Ma and H. Guo, *J. Phys. Chem. A* **in press**, doi: [10.1021/jp512557k](https://doi.org/10.1021/jp512557k) (2015).
- *19 H. Song, J. Li and H. Guo, *J. Chem. Phys.* **141**, 164316 (2014).

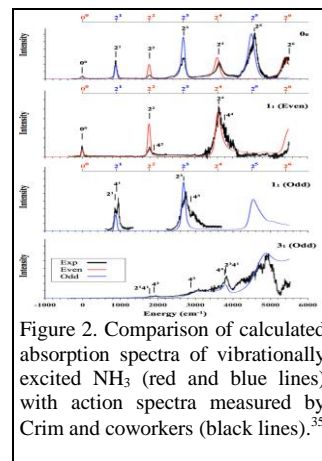


Figure 2. Comparison of calculated absorption spectra of vibrationally excited NH₃ (red and blue lines) with action spectra measured by Crim and coworkers (black lines).³⁵

- *20 J. Li, H. Song and H. Guo, *Phys. Chem. Chem. Phys.* **17**, 4259 (2015).
- *21 H. Song and H. Guo, *J. Phys. Chem. A* **119**, 826 (2015).
- *22 J. Li, J. C. Corchado, J. Espinosa-García and H. Guo, *J. Chem. Phys.* **142**, 084314 (2015).
- *23 H. Song, J. Li, M. Yang, Y. Lu and H. Guo, *Phys. Chem. Chem. Phys.* **16**, 17770 (2014).
- *24 H. Song and H. Guo, *J. Chem. Phys.* **141**, 244311 (2014).
- *25 S. G. Ard, A. Li, O. Martinez, N. S. Shuman, A. A. Viggiano and H. Guo, *J. Phys. Chem. A* **118**, 11485 (2014).
- 26 B. Jiang and H. Guo, *J. Chem. Phys.* **138**, 234104 (2013).
- 27 B. Jiang and H. Guo, *J. Am. Chem. Soc.* **135**, 15251 (2013).
- 28 B. Jiang, J. Li and H. Guo, *J. Chem. Phys.* **140**, 034112 (2014).
- *29 J. Li and H. Guo, *J. Phys. Chem. A* **118**, 2419 (2014).
- *30 H. Guo and B. Jiang, *Acc. Chem. Res.* **47**, 3679 (2014).
- *31 C. Xie, J. Ma, X. Zhu, D. H. Zhang, D. R. Yarkony, D. Xie and H. Guo, *J. Phys. Chem. Lett.* **5**, 1055 (2014).
- *32 J. Ma, C. Xie, X. Zhu, D. R. Yarkony, D. Xie and H. Guo, *J. Phys. Chem. A* **118**, 11926 (2014).
- *33 C. Xie, X. Zhu, J. Ma, D. R. Yarkony, D. Xie and H. Guo, *J. Chem. Phys.* **142**, 091101 (2015).
- *34 R. Dawes, B. Jiang and H. Guo, *J. Am. Chem. Soc.* **137**, 50 (2015).
- 35 A. Bach, J. M. Hutchison, R. J. Holiday and F. F. Crim, *J. Chem. Phys.* **116**, 9315 (2002).
- 36 R. Welsch, F. Huarte-Larrañaga and U. Manthe, *J. Chem. Phys.* **136**, 064117 (2012).
- *37 B. Zhao, Z. Sun and H. Guo, *J. Chem. Phys.* **140**, 234110 (2014).
- *38 B. Zhao, Z. Sun and H. Guo, *J. Chem. Phys.* **141**, 154112 (2014).
- *39 B. Zhao and H. Guo, *J. Phys. Chem. Lett.* **6**, 676 (2015).
- *40 B. Alday, R. Johnson, J. Li and H. Guo, *Theo. Chem. Acc.* **133**, 1540 (2014).
- *41 J. Gao, A. K. Thomas, R. Johnson, H. Guo and J. K. Grey, *Chem. Mater.* **26**, 4395 (2014).
- *42 S. G. Ard, J. J. Melko, O. Martinez, V. G. Ushakov, A. Li, R. S. Johnson, N. S. Shuman, H. Guo, J. Troe and A. A. Viggiano, *J. Phys. Chem. A* **118**, 6789 (2014).
- *43 J. J. Melko, S. G. Ard, R. S. Johnson, N. S. Shuman, H. Guo and A. A. Viggiano, *J. Phys. Chem. A* **118**, 8141 (2014).
- *44 B. Jiang and H. Guo, *J. Chin. Chem. Soc.* **61**, 841 (2014).
- *45 R. Liu, F. Wang, B. Jiang, G. Czakó, M. Yang, K. Liu and H. Guo, *J. Chem. Phys.* **141**, 074310 (2014).
- *46 Y. Li, Z. Sun, B. Jiang, D. Xie, R. Dawes and H. Guo, *J. Chem. Phys.* **141**, 081102 (2014).
- *47 Y. Wang, J. Li, H. Guo and M. Yang, *Theo. Chem. Acc.* **133**, 1555 (2014).
- *48 W. Xie, L. Liu, Z. Sun, H. Guo and R. Dawes, *J. Chem. Phys.* **142**, 064308 (2015).

Gas-Phase Molecular Dynamics: High Resolution Spectroscopy and Collision Dynamics of Transient Species

Gregory E. Hall

Chemistry Department, Brookhaven National Laboratory

Upton, NY 11973-5000

gehall@bnl.gov

Program Scope

This research is carried out as part of the Gas-Phase Molecular Dynamics program in the Chemistry Department at Brookhaven National Laboratory. Chemical intermediates in the elementary gas-phase reactions involved in combustion chemistry are investigated by high resolution spectroscopic tools. Production, reaction, and energy transfer processes are investigated by transient, double resonance, polarization and saturation spectroscopies, with an emphasis on technique development and connection with theory, as well as specific molecular properties.

Recent Progress

A. Speed-dependent kinetics of saturation recovery

Rotational energy transfer within the ground vibrational level of CN ($X^2\Sigma^+$) has been investigated by Doppler-resolved saturation recovery transient spectroscopy.[1] A single rotational state from a thermal ensemble of CN (X) radicals was bleached by a visible, ns dye laser pulse. The prompt depletion and collisional recovery of population was monitored with single-collision time resolution and Doppler-resolved spectral resolution using transient frequency modulation (FM) spectroscopy on the $A^2\Pi - X^2\Sigma^+$ (1-0) band. The kinetics of saturation recovery kinetics for selected rotational states in $v=0$ is isomorphic to the thermalization of a single level populated in an otherwise empty manifold of rotational states, an experimentally challenging initial condition to generate for ground state molecules. Thermal rate constants for population recovery (analogous to total removal rate constants in a more conventional single level kinetics measurement) were determined for selected rotational states colliding with He and Ar. The values of the thermal rate constants are consistent with quantum scattering calculations,[1-2] but up to a factor of 2 slower than reported in earlier work, [3-4] and with a qualitatively different rotational state dependence. Despite the thermal velocity distribution of the inert collision partner and the lack of velocity selection in the saturation step, the Doppler spectrum of the depletion shows rapid translational cooling below room temperature during early stages of the recovery. This is a consequence of the non-thermal averaging of speed-dependent relaxation cross sections for Doppler-selected velocity groups, in

competition with velocity randomizing collisions.[1] Comparisons with new quantum scattering calculations on Ar + CN(X) by P. Dagdigian have been essential, and the differences between He and Ar collision partners have also been investigated by quasiclassical trajectory calculations, focusing on the behavior of CN in high rotational states.

B. Saturation Transfer and Depolarization in CN (X)

The saturation recovery measurements made with parallel and perpendicular polarization of bleach and probe beams can be combined in different linear combinations to give both transient depletion of population and transient alignment of the hole. The population relaxation probes the rotational energy transfer, and the alignment relaxation is sensitive to elastic depolarization and inelastic polarization transfer. The alignment of the depletion signals from low rotational states of CN were additionally found

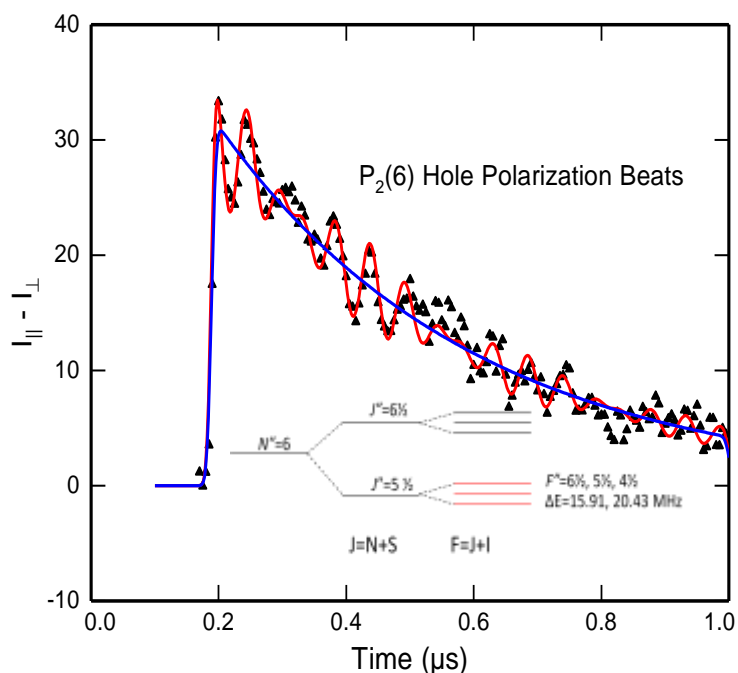


Figure 1. Hyperfine polarization quantum beats in CN (X) depletion recovery. Unresolved hyperfine levels of a single J state are initially aligned by linearly polarized depletion, then dephase.

partially saturated excitation by linearly polarized light. The phases, frequencies and relative magnitudes of the oscillations are fixed by known hyperfine constants of the CN(X) state and angular momentum coupling factors, with no detectable collisional damping.

After accounting for the periodic hyperfine depolarization, the initial relative rates of alignment decay and population depletion recovery probe the effect of elastic depolarization, *i.e.*, collisions that change M without changing J . The elastic depolarization rates are determined to be smaller than the inelastic

to display polarization quantum beats at the frequencies of the CN (X) state hyperfine splittings, as shown in Figure 1. This may at first seem startling, since the oscillations can be considered as a coherent evolution of the molecules that are missing from an otherwise thermal and incoherent ensemble. On further consideration, however, the initial alignment of the hole must be complementary to the aligned excited state molecules, and the calculated (red line) fit to the quantum beat pattern shown in Figure 1 requires as adjustable parameters only the overall amplitude and decay rate shown in blue, and an initial alignment amplitude resulting from

rotational energy transfer rates for low J states, and become increasingly negligible at higher J states of $\text{CN}(X, v=0)$, in good qualitative accord with quantum scattering calculations performed by Paul Dagdigian as part of this collaboration.

Future Work

A. Intersystem crossing in CH_2 induced by O_2 ($^3\Sigma_g^-$)

The collision-induced intersystem crossing (ISC) between singlet a and triplet X states of CH_2 , induced by nonreactive singlet collision partners is dominated by a gateway state mechanism involving a few pairs of accidentally perturbed rotational levels with mixed singlet/triplet character. Interaction of triplet O_2 with singlet CH_2 can proceed by a spin-allowed mechanism, not dependent on accidental perturbations. The complicated potential surfaces of CH_2O_2 furthermore connect multiple low-energy product channels including energetically accessible singlet and triplet states of the Criegee intermediate. We have measured quenching kinetics of selected rotational states of singlet CH_2 in samples containing controlled amounts of ketene photolytic precursor, Ar and O_2 in order to investigate the reversible ISC process. In the absence of O_2 , the relaxation is double exponential, with distinguishable kinetics for *ortho* and *para* states of CH_2 , a mark of the stronger coupling of *para* states with the more nearly isoenergetic (030) vibrational level of the X^3B_2 state of CH_2 . The interaction of singlet CH_2 with molecular O_2 accesses an excited triplet state of CH_2O_2 , which intersects the lowest triplet surface, leading nonreactively to O_2 + triplet CH_2 . The initial decay rate of selected rotational states of CH_2 is accelerated by O_2 , but the relative amplitude of the slow decay is also enhanced by O_2 , suggesting a continued role for reversible population of vibrationally excited triplet CH_2 in the overall mechanism. Kinetic modeling studies are in progress, as are spectroscopic searches for infrared probe transitions suitable for monitoring vibrationally excited triplet methylene, as discussed in the abstract of T. Sears.

B. Sub-Doppler saturation recovery in CN radicals

Future studies with sub-Doppler saturation recovery kinetics, probed by independently tunable sub-Doppler probe spectroscopy can more directly address the conditions under which velocity changing collisions contribute to pressure broadened line shapes, and modify the Doppler-shift-selected relaxation rates. Preliminary work performed with one laser, split into counterpropagating amplitude modulated bleach and frequency modulated probe beams, has shown that the dark recovery rate of a sub-Doppler bleach signal is dominated by rotationally inelastic collisions, at least for low rotational states. One-color saturation spectroscopy is generally sensitive to the collision dynamics on both upper and lower potential energy surfaces, complicating the interpretation of the saturation recovery kinetics. The use of hyperfine crossover resonances, (a three-level, one color, double resonance condition) selectively isolates upper or

lower state effects, but only for low rotational states where crossover resonances have significant intensity, and only for the Doppler-free velocity group near line-center. Using an independently tunable and rapidly extinguished bleach laser will allow analogous measurements of sub-Doppler saturation recovery for different velocity groups and any rotational state, and specifically sensitive to either *A* state or *X* state collisions, for example, with pump laser saturation on the (2-0) band and the probe laser measurement by either gain on the (2-1) band or absorption on the (1-0) band of the red *A-X* system. Having access to a range of rotational states will be important, as the relative contribution of velocity changing collisions is expected to increase as the rotational spacing increases and the inelastic cross sections decrease. Comparison with scattering calculations on realistic potentials will be an important part of the program.

Cited References

- [1] D. Forthomme, M.L. Hause, H.G. Yu, P.J. Dagdigian, T.J. Sears, G.E. Hall, *J. Phys. Chem. A* ASAP (2015).
- [2] F. Lique, A. Spielfiedel, N. Feautrier, I.F. Schneider, J. Klos, M.H. Alexander, *J. Chem. Phys.* 132 (2010) 024303.
- [3] R. Fei, H.M. Lambert, T. Carrington, S.V. Filseth, C.M. Sadowski, *J. Chem. Phys.* 100 (1993) 1190-1201.
- [4] R. Fei, D.E. Adelman, T. Carrington, C.H. Dugan, S.V. Filseth, *Chem. Phys. Lett.* 232 (1995) 547-553.

Publications supported by this project since 2013

- Argon-induced pressure broadening, shifting and narrowing in the CN $A^2\Pi - X^2\Sigma^+$ (1-0) band, D. Forthomme, C. P. McRaven, T. J. Sears, and G. E. Hall. *J. Phys. Chem. A* **117**, 11837-46 (2013). <http://dx.doi.org/10.1021/jp4030359>
- Temperature-dependent, nitrogen-perturbed line shape measurements in the $\nu_1+\nu_3$ band of acetylene using a diode laser referenced to a frequency comb, M. J. Cich, D. Forthomme, C. P. McRaven, G. V. Lopez, G. E. Hall, T. J. Sears, A. W. Mantz, *J. Phys. Chem. A* 117, 13908-13918 (2013). <http://dx.doi.org/10.1021/jp408960e>
- Collinear two-color saturation spectroscopy in CN *A-X* (1-0) and (2-0) bands, D. Forthomme, C. P. McRaven, T. J. Sears, and G. E. Hall, *J. Molec. Spectrosc.* **296**, 36-42 (2014) <http://dx.doi.org/10.1016/j.jms.2013.12.006>
- Frequency Comb-Referenced Spectroscopy in the $\nu_1 + \nu_3$ Region of Acetylene, M.J. Cich, D. Forthomme, G.E. Hall, C.P. McRaven, T.J. Sears, S. Twagirayezu, *The 13th Biennial HITRAN Conference (HITRAN13), Harvard-Smithsonian Center for Astrophysics, Cambridge, MA, USA*, 23-25 June, 2014. <http://dx.doi.org/10.5281/zenodo.11181>
- Frequency-comb referenced spectroscopy of ν_4 and ν_5 hot bands in the $\nu_1+\nu_3$ combination band of C_2H_2 , S. Twagirayezu, M. J. Cich, T. J. Sears, C. P. McRaven, and G. E. Hall, *J Molec. Spectrosc.* (submitted, 3/2015)
- Doppler-Resolved Kinetics of Saturation Recovery, D. Forthomme, M. L. Hause, H.-G. Yu, P. J. Dagdigian, T. J. Sears and G. E. Hall, *J. Phys. Chem. A.* (in press, 2015)

Flame Chemistry and Diagnostics

Nils Hansen

Combustion Research Facility, Sandia National Laboratories, Livermore, CA 94551-0969

Email: nhansen@sandia.gov

SCOPE OF THE PROGRAM

In this program, we seek to understand the detailed chemistry of combustion through a unique scheme of diagnostics development and experimental studies of simple flames. Our goal is to provide reliable experimental data on the chemical composition of laboratory-scale model flames through state-of-the-art diagnostics. The experiments are designed to serve as benchmarks for the development and validation of detailed chemical kinetic models. In particular, we study laminar premixed flames, which are stabilized on a flat-flame burner under a reduced pressure of ~15-30 Torr and laminar opposed-flow diffusion flames at low and atmospheric pressure. We implement mainly mass spectrometry and our experimental data in the form of species identification and quantification serve as stringent tests for the development and validation of any detailed chemical kinetic mechanisms. Over the past years, the overall objective of this program has been to elucidate the chemistry of soot precursors and the formation of unwanted byproducts in incomplete combustion in flames fueled by hydrocarbons and oxygenates. Studying this complex combustion chemistry with an unprecedented level of detail requires determining the chemical structures and concentrations of species sampled from sooting or nearly-sooting model flames.

PROGRESS REPORT

Soot Precursor Formation and Limitations of the Stabilomer Grid: Collaborating with the groups of H.A. Michelsen (Sandia), K.R. Wilson (Berkeley), and A. Violi (Michigan) we have gained new insight into the mechanisms of PAH growth and soot formation. The experimental approach involves aerosol-mass spectrometry in conjunction with vacuum-ultraviolet photoionization of volatile species vaporizing from particles sampled from an Ar-diluted C₂H₂/O₂ counter-flow diffusion flame at nearly atmospheric pressure (700 Torr). The aerosol mass spectra contain a large distribution of peaks, highlighting the importance of small building blocks and odd-carbon numbered species. A variety of chemical species were detected that, based on the traditional classification of PAHs by their thermodynamic stability, were unexpected. Also, the experimental results suggested that species of higher masses can build up concentration ahead of species of lower masses, suggesting that a single monotonic growth mechanism is not enough to describe PAH formation processes.

Combustion Chemistry of Alcohols: Experimental and Modeled Structure of a Premixed 2-Methylbutanol Flame: In a collaborative effort together with the group of Sarathy (KAUST), we

determined the experimental and modeled structure of a flame fueled by 2-methylbutanol. In the experiment, a total of 55 species were identified and subsequently quantitative mole fraction profiles as function of distance from the burner surface were determined and compared to an independently assembled detailed flame chemistry model to assess its predictive capabilities. Discrepancies between experimental and modeling results were used to suggest areas where improvement of the kinetic model would be needed.

Formation of Oxygenated and Hydrocarbon Intermediates in Premixed Combustion of 2-Methylfuran: We have collaborated with the group of Kohse-Höinghaus (Bielefeld) to determine the detailed chemical structure of a premixed laminar 2-MF flame. Mole fraction profiles of 60 intermediate, reactant, and product species were measured in order to assess the pollutant potential of this possible next-generation biofuel. Special emphasis was paid towards the fuel's ability to form aromatic and oxygenated intermediates during incomplete combustion processes, with the latter species representing a variety of different classes including alcohols, ethers, enols, ketones, aldehydes, acids, and ketenes. Whenever possible the experimental data were compared to the results of model calculations, but it should be noted that many newly detected species were not included in the calculations. The experimental data provided guidance towards development of a next-generation 2-MF combustion chemistry model.

Dimethyl ether (DME) Low-Temperature Oxidation in a Jet-Stirred Reactor: In collaboration with the groups of Jasper (Sandia), Leone (Berkeley), Yu (Princeton), Sarathy (KAUST), Dagaut (Orleans), Taatjes (Sandia), and Kohse-Höinghaus (Bielefeld) we reported the detection and identification of the keto-hydroperoxide hydroperoxymethyl formate (HPMF) and other partially oxidized intermediate species arising from the low-temperature (540 K) oxidation of dimethyl ether (DME). These observations were made possible by coupling a jet-stirred reactor with molecular-beam sampling capabilities, operated near atmospheric pressure, to a reflectron time-of-flight mass spectrometer that employs single-photon ionization via tunable synchrotron-generated vacuum-ultraviolet radiation. We showed that the theoretical characterization of multiple conformeric structures of some intermediates is required when interpreting the experimentally observed ionization thresholds.

OUTLOOK

Low-Temperature Oxidation in a Jet-Stirred Reactor: We will continue to explore the reaction network of low-temperature oxidation processes by using the above mentioned jet-stirred reactor with molecular-beam sampling capabilities. Our work on DME will continue with efforts to provide quantitative mole fraction profiles as function of the reactor temperature of the previously identified intermediates. This information is critically needed to improve the combustion chemistry models for low-temperature oxidation. Future work will focus on the low-temperature oxidation of *n*-pentane. Preliminary

mass spectra were recorded and the data reduction, *i.e.* species identification and quantification, is currently work in progress.

Experimental Studies on the Molecular-Growth Chemistry of Soot Precursors in Combustion Environments: With benzene formation in combustion processes now well understood, the objective of this part of the research program has shifted towards the molecular-growth chemistry from small combustion intermediates to larger PAH's. The underlying chemistry will be investigated by a combination of different experiments. The centerpiece of all experiments is a simple, *i.e.* laminar, premixed or opposed-flow flame, and analyzing the chemical composition of such model flames will provide guidance and benchmarks needed to improve and test theoretical models describing soot-formation chemistry with predictive capabilities. We plan to investigate the chemical composition of these flames in unprecedented detail by flame-sampling mass spectrometry with electron ionization (EI), resonance-enhanced multiphoton ionization (REMPI), single-photon VUV ionization, and gas chromatography (GC/MS).

Although our current set-up allows for a pressure between 30 and 700 Torr, sampling from sooting flames at atmospheric pressure will eventually lead to clogging of the small opening (a few μm) in the microprobe. We therefore propose to rebuild the mass spectrometer and to add an additional stage of pumping.

The systems proposed to study are flames fueled by allene/propyne (C_3H_4), and the C_4 fuels, butane and *iso*-butane (C_4H_{10}), 1-butene and *iso*-butene (C_4H_8), 1,3-butadiene (1,3- C_4H_6), and n-pentane (C_5H_{12}). These fuels are of special interest, because these molecules are potential precursors for the resonance-stabilized propargyl, allyl, and *i*- C_4H_5 radicals. Contributions towards PAH growth via resonantly stabilized free radicals should be enhanced in these flames, thus making them a perfect test case for further model development.

PUBLICATIONS ACKNOWLEDGING BES SUPPORT 2013-PRESENT

1. C. K. Westbrook, B. Yang, T. A. Cool, N. Hansen, K. Kohse-Höinghaus, "Photoionization Mass Spectrometry and Modeling Study of Premixed Flames of Three Unsaturated $\text{C}_5\text{H}_8\text{O}_2$ Esters", *Proc. Combust. Inst.*, **2013**, 34(1), 443-451.
2. A. W. Jasper and N. Hansen, "Hydrogen-Assisted Isomerizations of Fulvene to Benzene and of Larger Cyclic Aromatic Hydrocarbons", *Proc. Combust. Inst.*, **2013**, 34(1), 279-287.
3. S. A. Skeen, B. Yang, H. A. Michelsen, J. A. Miller, A. Violi, N. Hansen, "Studies of Laminar Opposed-Flow Diffusion Flames of Acetylene at Low Pressures with Photoionization Mass Spectrometry", *Proc. Combust. Inst.*, **2013**, 34(1), 1067-1075.
4. N. J. Labbe, V. Seshadri, T. Kasper, N. Hansen, P. Oßwald, K. Kohse-Höinghaus, P. R. Westmoreland, "Flame Chemistry of Tetrahydropyran as a Model Heteroatomic Biofuel", *Proc. Combust. Inst.*, **2013**, 34(1), 259-267.
5. S. A. Skeen, H. A. Michelsen, K. R. Wilson, D. M. Popolan, A. Violi, N. Hansen, "Near-Threshold Photoionization Mass Spectra of Combustion-Generated High-Molecular-Weight Soot Precursors", *J. Aerosol Sci.*, **2013**, 58(1), 86-102.

6. N. Hansen, S.S. Merchant, M. R. Harper, W. H. Green, "The Predictive Capability of an Automatically Generated Combustion Chemistry Mechanism: Chemical Structures of Premixed *iso*-Butanol Flames", *Combust. Flame*, **2013**, 160(11), 2343-2351.
7. N. Hansen, S. A. Skeen, H. A. Michelsen, K. R. Wilson, K. Kohse-Höinghaus, "Flame Experiments at the Advanced Light Source: New Insights into Soot Formation Processes", *J. Vis. Exp.*, **2014**, 87, e51369, doi:10.3791/51369
8. F. N. Egolfopoulos, N. Hansen, Y. Ju, K. Kohse-Höinghaus, C. K. Law, F. Qi, "Advances and Challenges in Experimental Research of Combustion Chemistry in Laminar Flames", *Prog. Energy Combust. Sci.*, **2014**, 43(1), 36-67.
9. S. M. Sarathy, P. Oßwald, N. Hansen, K. Kohse-Höinghaus, "Alcohol Combustion Chemistry", *Prog. Energy Combust. Sci.*, *Prog. Energy Combust. Sci.*, **2014**, 44(1), 40-102.
10. J. Krüger, J. Koppmann, P. Nau, A. Brockhinke, M. Schenk, N. Hansen, U. Werner, K. Kohse-Höinghaus, *From Precursors to Pollutants: Some Advances in Combustion Chemistry Diagnostics*, *Eurasian Chem. Technol. J.*, **2014**, 16(2-3), 91-105.
11. A. Nawdiyal, N. Hansen, T. Zeuch, L. Seidel, F. Mauß, "Experimental and Modelling Study of Speciation and Benzene Formation Pathways in Premixed 1-Hexene Flames", *Proc. Combust. Inst.*, **2015**, 35(1), 325-332.
12. N. Hansen, M. Braun-Unkhoff, T. Kathrotia, A. Lucassen, B. Yang, "Understanding the Reaction Pathways in Premixed Flames Fueled by Blends of 1,3-Butadiene and n-Butanol", *Proc. Combust. Inst.*, **2015**, 35(1), 771-778.
13. A. Lucassen, S. Park, N. Hansen, S.M. Sarathy, "Combustion Chemistry of Alcohols: Experimental and Modeled Structure of a Premixed 2-Methylbutanol Flame", *Proc. Combust. Inst.*, **2015**, 35(1), 813-820.
14. M. Schenk, N. Hansen, H. Vieker, A. Beyer, A. Gölzhäuser, K. Kohse-Höinghaus, "PAH Formation and Soot Morphology in Flames of C₄ Fuels", *Proc. Combust. Inst.*, **2015**, 35(2), 1761-1769.
15. D. Felsmann, K. Moshhammer, J. Krüger, A. Lackner, A. Brockhinke, T. Kasper, T. Bierkandt, E. Akyildiz, N. Hansen, A. Lucassen, P. Oßwald, M. Köhler, G.A. Garcia, L. Nahon, P. Hemberger, A. Bodi, T. Gerber, K. Kohse-Höinghaus, "Electron Ionization, Photoionization and Photoelectron/Photoion Coincidence Spectroscopy in Mass-Spectrometric Investigations of a Low-Pressure Ethylene/Oxygen Flame", *Proc. Combust. Inst.*, **2015**, 35(1), 779-786.
16. K. O. Johansson, J. Y. W. Lai, S. A. Skeen, K. R. Wilson, N. Hansen, A. Violi, H. A. Michelsen, "Soot Precursor Formation and Limitations of the Stabilomer Grid", *Proc. Combust. Inst.*, **2015**, 35(2), 1819-1826.
17. K. Moshhammer, A. Lucassen, C. Togbé, K. Kohse-Höinghaus, N. Hansen, "Formation of Oxygenated and Hydrocarbon Intermediates in Premixed Combustion of 2-Methylfuran", *Z. Phys. Chem.*, **2015**, in press
18. O. P. Korobeinichev, I. E. Gerasimov, D. A. Knyazkov, A. G. Shmakov, T. A. Bolshova, N. Hansen, C. K. Westbrook, G. Dayma, B. Yang, "An Experimental and Kinetic Modeling Study of Premixed Laminar Flames of Methyl Pentanoate and Methyl Hexanoate", *Z. Phys. Chem.*, **2015**, in press
19. K. Moshhammer, A. W. Jasper, D. M. Popolan-Vaida, A. Lucassen, P. Dievart, H. Selim, Hatem, A. J. Eskola, C. A. Taatjes, S. R. Leone, S. M. Sarathy, Y. Ju, P. Dagaut, K. Kohse-Höinghaus, N. Hansen, "Detection and Identification of the Keto-Hydroperoxide (HOOCH₂OCHO) and other Intermediates during Low-Temperature Oxidation of Dimethyl Ether", *J. Phys. Chem. A*, **2015**, in press
20. H. Selim, S. Mohamed, A. Lucassen, N. Hansen, S. M. Sarathy, "Effect of the Methyl Substitution on the Combustion of Two Methylheptane Isomers: Flame Chemistry Using VUV Photoionization Mass Spectrometry", *Energy Fuels*, **2015**, in press

Kinetics and Spectroscopy of Combustion Gases at High Temperatures

R. K. Hanson, C. T. Bowman
Department of Mechanical Engineering, Stanford University
Stanford, CA 94305-3023

rkhanon@stanford.edu, ctbowman@stanford.edu

I. Program Scope

This program involves two complementary activities: (1) development and application of cw laser absorption methods for the measurement of concentration time-histories and fundamental spectroscopic parameters for species of interest in combustion; and (2) shock tube studies of reaction kinetics relevant to combustion. Species recently investigated in the spectroscopic portion of the research include formaldehyde and acetaldehyde. New diagnostics developments include the first use of CW Cavity Enhanced Absorption Spectroscopy (CEAS) for ultra-sensitive species detection in a shock tube, applied here to CH₄, C₂H₂ and CO. Recent reaction kinetics work has advanced on two fronts. First, we have made direct high-temperature shock tube/laser absorption measurements of the reaction rate constants for OH + aldehydes and alcohols, including formaldehyde, acetaldehyde, propionaldehyde, n-butyraldehyde, ethanol, and tert-butanol. Second, we have investigated the decomposition of cyclohexene, which is commonly used in single-pulse shock tube studies as a chemical thermometer.

II. Recent Progress: Spectroscopy

Cavity Enhanced Absorption Spectroscopy (CEAS)

A new technique for ultra-sensitive species detection in a shock tube has been developed, applied here to IR active species. As a primary example, the concentration of CO was monitored using mid-IR quantum cascade laser absorption near 4.56 μm , targeting the R(13) transition of the CO fundamental rovibrational band. The implementation of the CO laser absorption diagnostic was combined with an off-axis CEAS setup. CEAS uses a pair of highly reflective CaF₂ mirrors (98.9% reflectivity at 4.56 μm) to form an optical cavity in the shock tube, thereby increasing the effective path length for absorption measurements. The transmitted beams after each reflection are collected with a lens onto a single TE-cooled photovoltaic HgCdTe detector. The beams are arranged in an off-axis pattern (a narrow ellipse with the short axis aligned with the shock tube longitudinal direction) to suppress the mode-cavity coupling noise. Usually the laser is rapidly scanned by varying the injection current using a 50 kHz sinusoidal waveform, to further suppress the coupling noise while also eliminating the influence from broadband interference absorption and thermal emission. Under typical experimental conditions, a minimum detectable absorbance of 2×10^{-3} can be achieved, which corresponds to a detection limit of 0.11 ppm at 1500 K and 1.5 atm. See Figure 1.

Using this method, a direct measurement for the rate constant of the acetone dissociation reaction ($\text{CH}_3\text{COCH}_3 = \text{CH}_3\text{CO} + \text{CH}_3$) was conducted behind reflected shock waves. By investigating the clean pyrolysis of less than 20 ppm acetone in argon, the current experiment eliminated the influence from secondary reactions and temperature change. For the first time, the acetone dissociation rate constant (k_1) was directly measured over 5.5 orders of magnitude with a high degree of accuracy: k_1 (1004 – 1494 K, 1.6 atm) = $4.39 \times 10^{55} \text{ T}^{-11.394} \exp(-52140\text{K}/\text{T}) \pm 24\% \text{ s}^{-1}$ as shown in Figure 2. This result was seen to agree with most previous studies, and has bridged the gap between their temperature and pressure conditions. The current work serves to illustrate the significant potential of using the CEAS technique in shock tube kinetics studies.

II. Recent Progress: Chemical Kinetics

Rate Constant Measurements of the Reactions of C1-C4 Aldehydes with OH

The overall rate constants for the reactions of hydroxyl radicals with a series of aldehydes, including formaldehyde (Figure 3), acetaldehyde (Figure 4), propionaldehyde and n-butyraldehyde, were

studied under pseudo-first-order conditions behind reflected shock waves at temperatures of 950 - 1400 K and pressures of 1 - 2 atm. OH radicals were produced by rapid thermal decomposition of tert-butyl hydroperoxide, and OH time-histories were monitored by narrow-linewidth UV laser absorption near 306.7 nm. The overall rate constants were inferred by fitting simulated OH profiles to the measured OH time histories using detailed mechanisms, though the OH decay was nearly first-order.

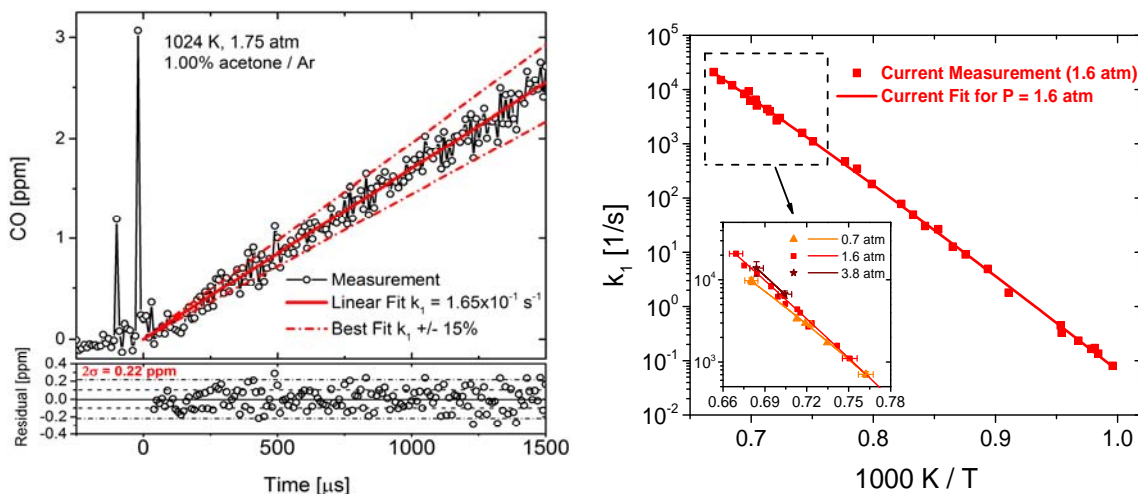


Figure 1 (left). Example CO time-history in the pyrolysis of acetone/Ar mixtures: a low temperature case of 1.00% acetone/Ar at 1024 K, 1.75 atm. Figure 2 (right). Arrhenius plot for the reaction $\text{CH}_3\text{COCH}_3 = \text{CH}_3\text{CO} + \text{CH}_3$. Both figures adapted from Wang et al. in press.

No pressure dependence was observed in these measurements. The measured rate constant for the formaldehyde + OH reaction is consistent with previous experimental studies. For C2-C4 aldehydes + OH, this study provides the first direct rate constant measurement at high temperatures. More general rate constant expressions covering a much wider temperature range (200 - 1600 K) were also determined by combining current measurements with existing low temperature data in the literature.

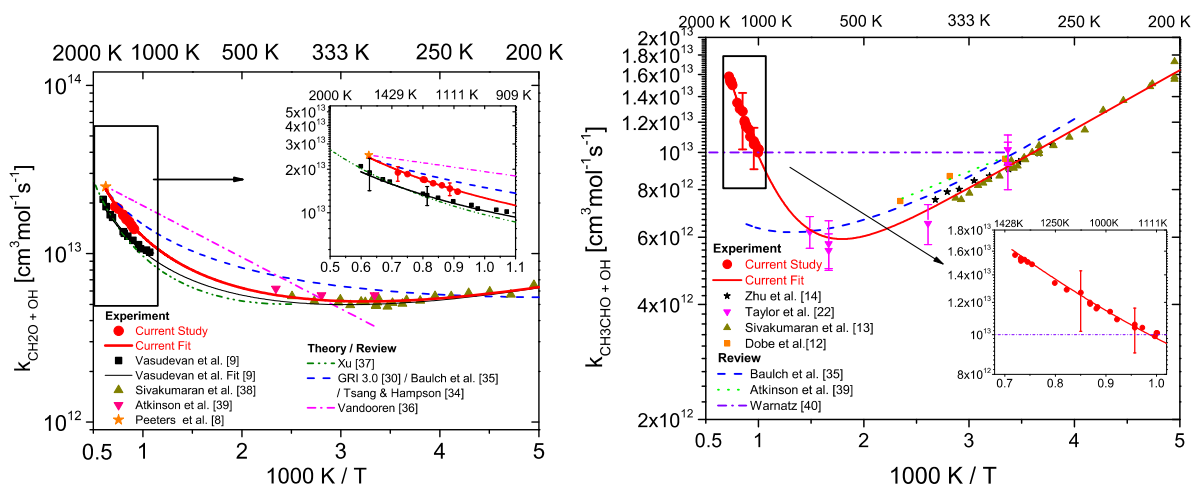


Figure 3 (left). Arrhenius plot of $\text{CH}_2\text{O} + \text{OH} = \text{products}$. Figure 4 (right). Arrhenius plot of $\text{CH}_3\text{CHO} + \text{OH} = \text{products}$. Both figures adapted from Wang et al. (2015).

Rate Constant Measurement of the Reaction of $\text{CH}_2\text{O} + \text{H}$

The rate constant of the H-abstraction reaction of formaldehyde (CH_2O) by hydrogen atoms (H), $\text{CH}_2\text{O} + \text{H} = \text{H}_2 + \text{HCO}$, has been studied behind reflected shock waves using a sensitive mid-IR laser absorption diagnostic for CO, over temperatures of 1304 - 2006 K and at pressures near 1 atm. $\text{C}_2\text{H}_5\text{I}$ was used as an H-atom precursor and 1,3,5-trioxane as the CH_2O precursor, to generate a well-controlled $\text{CH}_2\text{O}/\text{H}$ reacting system. By designing the experiments to maintain relatively constant H-atom concentrations, the current study significantly boosted the measurement sensitivity of the target reaction and suppressed the influences of interfering reactions. The measured $\text{CH}_2\text{O} + \text{H}$ rate constant can be expressed in modified Arrhenius form as $k_{\text{CH}_2\text{O}+\text{H}}$ (1304 – 2006 K, 1 atm) = $3.43 \times 10^6 (\text{T}/\text{K})^{2.34} \exp(-1508 \text{ K}/\text{T}) \text{ cm}^3 \text{ mol}^{-1} \text{ s}^{-1}$, with uncertainty limits estimated to be +18/-26%. See Figure 5. A transition-state-theory (TST) calculation, using the CCSD(T)-F12/VTZ-F12 level of theory, is in good agreement with the shock tube measurement and extended the temperature range of the current study to 200 - 3000 K, over which a modified Arrhenius fit of the rate constant can be expressed as $k_{\text{CH}_2\text{O}+\text{H}}$ (200 – 3000 K) = $5.86 \times 10^3 (\text{T}/\text{K})^{3.13} \exp(-762 \text{ K}/\text{T}) \text{ cm}^3 \text{ mol}^{-1} \text{ s}^{-1}$.

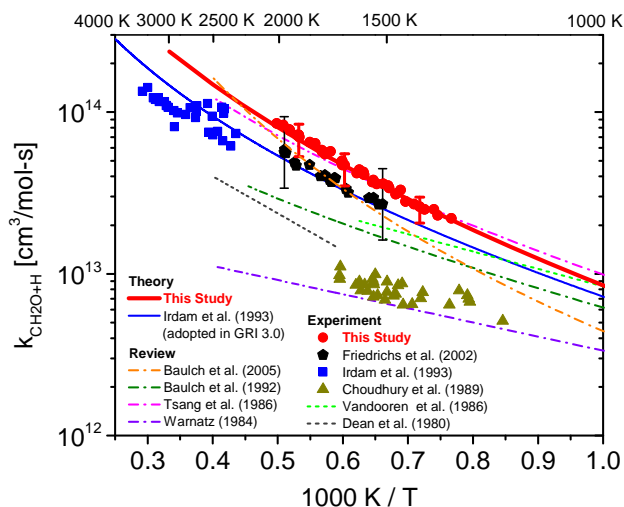


Figure 5. Arrhenius plot for the rate constant of $\text{CH}_2\text{O} + \text{H}$ between 1000 - 4000 K

III. Future Work

Spectroscopic experimental work continues on a development of the multi-color IR-UV aldehyde laser absorption diagnostic; exploration of mid- and far-IR detection of acetylene and larger alkenes (e.g., propene, n-butene and i-butene), respectively, and development of the CEAS method for ultra-sensitive species detection. Reaction kinetics studies will focus on measurement of the rate constants for the reactions of methyl radicals + aldehydes, and formation pathways of aldehydes during the oxidation of oxygenate fuel components.

IV. Major Publications Attributed to this Grant 2012-2015

1. S. Wang, K. Sun, D. F. Davidson, J. B. Jeffries, R. K. Hanson, "Shock Tube Measurement of Acetone Dissociation using Cavity-Enhanced Absorption Spectroscopy of CO," J. Physical Chemistry A, in press.
2. S. Wang, E. E. Dames, D. F. Davidson, R. K. Hanson, "Reaction Rate Constant of $\text{CH}_2\text{O}+\text{H} = \text{HCO}+\text{H}_2$ Revisited: A Combined Study of Direct Shock Tube Measurement and Transition State Theory Calculation," J. Physical Chemistry A, in press.
3. S. Wang, D. F. Davidson, R. K. Hanson, "High Temperature Laser Absorption Diagnostics for CH_2O and CH_3CHO and Their Application to Shock Tube Kinetics Studies," Combustion and Flame 160 (2013) 1930-1938, DOI 10.1016/j.combustflame.2013.05.004.
4. S. Wang, D. F. Davidson, R. K. Hanson, "High Temperature Measurements for the Rate Constants of C1-C4 Aldehydes with OH in a Shock Tube," Proceedings of the Combustion Institute 35 (2015) 473-480, DOI 10.1016/j.proci.2014.06.112.
5. I. Stranic, G. A. Pang, R. K. Hanson, D. M. Golden, C. T. Bowman, "Shock Tube Measurements of the tert-Butanol + OH Reaction Rate and the tert-C₄H₈OH Radical beta-Scission Branching Ratio Using Isotopic Labeling," Journal of Physical Chemistry A 117 (2013) 4777-4784, DOI 10.1021/jp402176e.
6. I. Stranic, G. A. Pang, R. K. Hanson, D. M. Golden, C. T. Bowman, "Shock Tube Measurements of the Rate Constant for the Reaction Ethanol + OH," Journal of Physical Chemistry A 118 (2014) 822-828, DOI 10.1021/jp410853f.
7. I. Stranic, D. F. Davidson, R. K. Hanson, "Shock Tube Measurements of the Rate Constant for the Reaction Cyclohexene \rightarrow Ethylene + 1,3-Butadiene," Chemical Physics Letters 584 (2013) 18-23, DOI 10.1016/j.cplett.2013.07.067.
8. K.-Y. Lam, D.F. Davidson and R.K. Hanson, "A Shock Tube Study of $\text{H}_2+\text{OH} \rightarrow \text{H}_2\text{O}+\text{H}$ using Laser Absorption," Int. J. Chem. Kinetics 45 (2013) 363-373, DOI 10.1002/kin.20771. (With additional support from NSF.)
9. K.-Y. Lam, D. F. Davidson, R. K. Hanson, "High-Temperature Measurements of the Reactions of OH with small Methyl Esters: Methyl Formate, Methyl Acetate, Methyl Propanoate, and Methyl Butanoate," J. Phys. Chem. A 116 (2012) 12229-12241, DOI 10.1021/jp310256j.
10. K.-Y. Lam, D.F. Davidson and R.K. Hanson, "High Temperature Measurements of the Reaction of OH with a Series of Ketones: Acetone, 2-Butanone, 3-Pentanone and 2-Pentanone," J. Phys. Chem. A 116 (2012), 5549-5559, DOI 10.1021/jp303853h.
11. G.A. Pang, R. K. Hanson, D. M. Golden and C. T. Bowman, "Experimental Determination of the High-Temperature Rate Constant for the Reaction of OH with sec-Butanol," J. Phys. Chem. A, 116 (2012), 9607-9613, DOI 10.1021/jp306977e.
12. G. A. Pang, R. K. Hanson, D. M. Golden and C. T. Bowman, "High-Temperature Rate Constant Determination for the Reaction of OH with iso-Butanol," J. Phys. Chem. A 116 (2012) 4720-4725, DOI 10.1021/jp302719j.
13. G.A. Pang, R.K. Hanson, D.M. Golden and C.T. Bowman, "Rate Constant Measurements of the Overall Reaction of $\text{OH}+1\text{-Butanol} \rightarrow \text{Products}$ from 900 to 1200K," J. Phys. Chem. A 116 (2012) 2475-2483, DOI 10.1021/jp211885p. (With additional support from DOE-EFRC.)
14. G.A. Pang, "Experimental determination of rate constants for reactions of the hydroxyl radical with alkanes and alcohols," Ph.D. Thesis, Mechanical Engineering Dept. Stanford University, CA (2012).
15. K.-Y. Lam, W. Ren, Z. Hong, D.F. Davidson and R.K. Hanson, "Shock Tube Measurements of 3-Pentanone Pyrolysis and Oxidation," Comb. and Flame 159 (2012) 3251-3263, DOI 10.1016/j.combustflame.2012.06.012.

Theoretical Studies of Potential Energy Surfaces

Lawrence B. Harding
Chemical Sciences and Engineering Division
Argonne National Laboratory, Argonne, IL 60439
harding@anl.gov

Program Scope

The goal of this program is to calculate accurate potential energy surfaces for both reactive and non-reactive systems. Our approach is to use state-of-the-art electronic structure methods (CASPT2, MR-CI, CCSD(T), etc.) to characterize multi-dimensional potential energy surfaces. Depending on the nature of the problem, the calculations may focus on local regions of a potential surface or may cover the surface more globally. A second aspect of this program is the development of techniques to fit multi-dimensional potential surfaces to convenient, global, analytic functions suitable for use in dynamics calculations.

Recent Progress

Nitromethane Decomposition:

This year in, collaboration with Klippenstein, Jasper, Ruscic and Tranter, we completed a combined theoretical/experimental study of the decomposition of nitromethane, focusing on the competition between direct dissociation to methyl radical plus NO_2 and the roaming-type isomerization to methyl nitrite, followed by dissociation of the nitrite. High level electronic

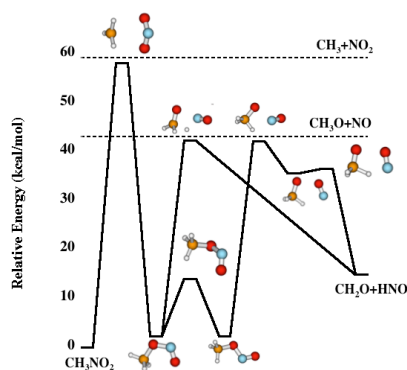


Figure 1

The branching ratios between roaming isomerization and direct dissociation of nitromethane were calculated using both statistical and dynamical approaches. Rigid body trajectories (RBT) were employed for the dynamical calculations. The RBT calculations required fitting quasirandom, six dimensional, grids of approximately 90,000, (7o,10e)-CASPT2/aug-cc-pvdz energies to an analytic, potential function of nine Morse variables. One dimensional correction potentials were then developed along MEP's for nitrogen addition and cis oxygen addition to correct for limitations in the size of the basis set, the size of the active space and geometry relaxation.

Figure 2 illustrates the interaction energy between the rigid CH_3 and NO_2 fragments on the roaming dividing surface separating CH_3NO_2 from CH_3ONO . The plotting plane here contains

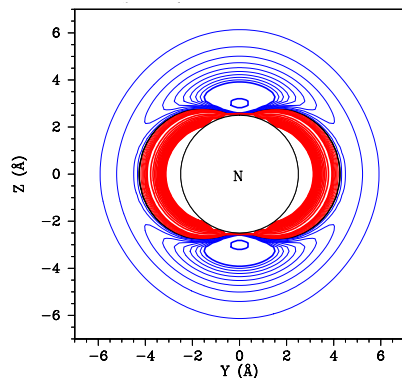


Figure 2 the nitrogen atom and is perpendicular to the C_2 axis of NO_2 . The blue contours depict regions with energies below that of the $\text{CH}_3 + \text{NO}_2$ asymptote. The roaming saddle points correspond to the symmetrical minima directly above and below the nitrogen atom. Note that in this plot the roaming saddle points appear as minima because the reaction coordinate is perpendicular to the plotting coordinates. The plot illustrates that although there are well defined first order saddle points for roaming, there is a considerable range of orientations and separations for which the roaming can take place at energies below the asymptotic energy of $\text{CH}_3 + \text{NO}_2$. Indeed purely attractive roaming paths exist even in the plane of the NO_2 fragment. A proper evaluation of the roaming flux must consider the full range of paths as is done in both the present RBT and statistical theory calculations.

The calculated branching ratio between roaming and direct dissociation is shown in Figure 3 along with the previous theoretical results of Homayoon et al¹. The results show good agreement

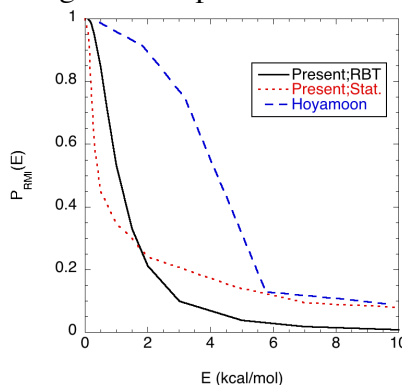


Figure 3 between the statistical and RBT calculations with the statistical calculation overestimating the branching at high energies and underestimating at low energies. The full dimensional trajectory calculations of Homayoon et al¹ show significantly more roaming than the present calculations. This is surprising because, owing to a combination of lower level electronic structure calculations and errors in the fitting of the nine dimensional potential energy surface, their zero point corrected roaming saddle point lies 0.23 kcal/mol above the radical asymptote rather than 1 kcal/mole below as in the present calculations. Presumably most, if not all, of the roaming in the Homayoon et al¹ calculations come from trajectories violating zero point conservation in the roaming region. The present RBT calculations avoid this problem as only the low frequency transitional modes are treated classically. The high frequency conserved modes are treated as harmonic oscillators (including zero point). This is a general problem in the application of full dimensional trajectory calculations to threshold phenomena such as roaming.

Roaming Mechanisms for Decomposition of Aldehydes:

Recently reported photodissociation experiments⁴ led to the conclusion that the roaming mechanism is more important for ethyl aldehyde than for acetaldehyde. We have characterized roaming saddle point for the series acetaldehyde, ethyl aldehyde, iso-propyl aldehyde and tert-butyl aldehyde. The saddle point energies, relative to the corresponding radical asymptotes, are -1.2, -2.3, -3.2 and -3.9 kcal/mol respectively. Thus as the size of the roaming fragments increase, long range, dispersion forces lower the energies of the saddle points thus increasing the importance of the roaming mechanisms.

Future Plans

We plan to continue our studies of R+O₂ reactions including ³CH₂+O₂ and roaming radical pathways.

Acknowledgement: This work was performed under the auspices of the Office of Basic Energy Sciences, Division of Chemical Sciences, Geosciences and Biosciences, U.S. Department of Energy, under Contract DE-AC02-06CH11357.

References:

- (1) Z. Homayoon and J. M. Bowman, J. Phys. Chem. A **117**, 11665 (2013)
- (2) R. S. Zhu, P. Raghunath and M. C. Lin, J. Phys. Chem. **117**, 7308 (2013)
- (3) M. Isegawa, F. Li, S. Maeda and K. Morokuma, J. Chem. Phys. **140**, 244310 (2014)
- (4) P.-Y. Tsai, K.-C. Hung, H.-K. Li and K.-C. Lin, J. Phys. Chem. Lett **5**, 190 (2014)

PUBLICATIONS (2012 - Present):

Bi-fidelity Fitting and Optimization

R. L. Miller, L. B. Harding, M. J. Davis, and S. K. Gray, J. Chem. Phys. **136**, 074102(2012)

Theoretical Determination of the Rate Coefficient for the HO₂+HO₂→ H₂O₂+O₂ Reaction: Adiabatic Treatment of Anharmonic Torsional Effects

D. D. Y. Zhou, K. Han, P. Zhang, L. B. Harding, M. J. Davis and R. T. Skodje
J. Phys. Chem. A **116**, 2089-2100 (2012)

Shock Tube Explorations of Roaming Radical Mechanisms: The Decomposition of Isobutane and Neopentane

R. Sivaramakrishnan, J. V. Michael, L. B. Harding and S. J. Klippenstein
J. Phys. Chem. A **116**, 5981-5989 (2012)

Separability of Tight and Roaming Pathways for Molecular Decomposition

L. B. Harding, S. J. Klippenstein, and A. W. Jasper
J. Phys. Chem. A **116**, 6967-6982 (2012)

A Quantitative Explanation for the Apparent Anomalous Temperature Dependence of OH + HO₂ → H₂O + O₂ through Multi-Scale Modeling

M. P. Burke, S. J. Klippenstein, L. B. Harding, Proc. Comb. Inst. **34**, 547-555 (2013)

Unconventional Peroxy Chemistry in Alcohol Oxidation: The Water Elimination Pathway

O. Welz, S. J. Klippenstein, L. B. Harding, C. A. Taatjes, J. Zador
J. Phys. Chem. Letters **4**, 350-354 (2013)

Rate Constant and Branching Fraction for the $\text{NH}_2 + \text{NO}_2$ Reaction

S. J. Klippenstein, L. B. Harding, P. Glarborg, Y. Gao, H. Hu, P. Marshall
J. Phys. Chem. A **117**, 9011 (2013)

Predictive Theory for the Addition Insertion Kinetics of $^1\text{CH}_2$ Reacting with Unsaturated Hydrocarbons

D. Polino, S. J. Klippenstein, L. B. Harding, Y. Georgievski
J. Phys. Chem. A **117**, 12677-12692 (2013)

Comparison of Multireference Configuration Interaction Potential Energy Surfaces for $\text{H} + \text{O}_2 \rightarrow \text{HO}_2$: The Effect of Internal Contraction

L. B. Harding, S. J. Klippenstein, H. Lischka, R. Shepard
Theoretical Chemical Accounts **133**,1429 (2013)

Secondary Channels in the Thermal Decomposition of monomethylhydrazine (CH_3NHNH_2)

P. Zheng, S. J. Klippenstein, L. B. Harding, H. Sun, C. K. Law
RSC Advances **4**, 62951 (2014)

Electronic States of the Quasilinear Molecule Propargylene (HCCCH) from Negative Ion Photoelectron Spectroscopy

D. L. Osborn, K. M. Vogelhuber, S. W. Wren, E. M. Miller, Y.-J. Lu, A. S. Case, L. Sheps, R. J. McMahon, J. F. Stanton, L. B. Harding, B. Ruscic, W. C. Lineberger
J. Amer. Chem. Soc. **136**, 10361 (2014)

Predictive A Priori Pressure-Dependent Kinetics

A.W. Jasper, K. M. Pelzer, J. A. Miller, E. Kamarchik, L. B. Harding, S. J. Klippenstein
Science **346**, 1212 (2014)

Resolving Some Paradoxes in the Thermal Decomposition Mechanism of Acetaldehyde

R. Sivaramakrishnan, J. V. Michael, L. B. Harding, S. J. Klippenstein
J. Phys. Chem. A (in press)

Temperature and Pressure-Dependent Rate Coefficients for the Reaction of Vinyl Radical with Molecular Oxygen

F. C. Goldsmith, L. B. Harding, Y. Georgievski, J. A. Miller, S. J. Klippenstein
J. Phys. Chem. A (submitted)

Thermal Dissociation and Roaming Isomerization of Nitromethane: Experiment and Theory

C. Annesley, J. Randazzo, S. J. Klippenstein, L. B. Harding, A. Jasper, Y. Georgievski, B. Ruscic, R. S. Tranter
J. Phys. Chem. A (submitted)

Theory of Electronic Structure and Chemical Dynamics

Martin Head-Gordon, William A. Lester Jr., and William H. Miller

Chemical Sciences Division, Lawrence Berkeley National Laboratory and Department of Chemistry, University of California, Berkeley, California 94720. mhg@cchem.berkeley.edu, walester@lbl.gov, millerwh@berkeley.edu

Scope of the Project: To expand knowledge of transient species such as radicals relevant to combustion chemistry and other areas including catalysis, new theoretical methods are needed for reliable computer-based prediction of their properties. The two main areas of relevant theory are electronic structure methods and techniques for chemical dynamics. Within electronic structure theory, focus centers on the development of new density functional theory methods and new wave function theories. Examples of current activity include the introduction of combinatorial design strategies for density functionals, and new approaches to orbital optimized wave function methods. In chemical dynamics, recent progress and planned activity centers on the development of tractable semi-classical dynamics approaches that can address non-adiabatic processes. The focus is on turning semi-classical theory into a practical way of adding quantum effects to classical molecular dynamics simulations of large, complex molecular systems. Newly developed theoretical methods, as well as existing approaches, are employed to study prototype radical reactions, often in collaboration with experimental efforts. These studies help to deepen understanding of the role of reactive intermediates in diverse areas of chemistry. They also sometimes reveal frontiers where new theoretical developments are needed in order to permit better calculations in the future.

Recent Progress

Due to length limitations, only a selection of projects can be summarized here.

Density functionals. Head-Gordon and co-workers have been seeking the limit of transferable accuracy that can be achieved with generalized gradient approximations (GGA's) and corrections for long-range dispersion interactions. They introduced a novel "survival of the most transferable" (SOMT) procedure to achieve this goal. SOMT is a combinatorial design protocol that involves training a very large numbers of functionals using roughly half the data, and then selecting the functional that performs best on the remaining data (with the fewest parameters). A new range-separated hybrid van der Waals corrected GGA functional was trained based on the SOMT protocol. The functional, named ω B97X-V, contains only 10 parameters (e.g. versus 15 for the 2008 functional, ω B97X-D, or about 30 for M06-2X) and reduces RMS errors in non-bonded interactions by about 40% relative to ω B97X-D, while matching its performance for thermochemistry. The SOMT approach is in principle extensible to the much more difficult problem of designing a meta GGA (MGGA). The major challenge is an astronomical increase in the dimension of the search space. Making reasonable choices about which parameters to consider to include or exclude, it increases from roughly 2^{16} in the case of the ω B97X-V functional to approximately 2^{40} in the case of the meta GGA. A partial search of the MGGA functional space has led to the very recent development of the B97M-V functional, which has only 12 adjustable parameters (vs 34 for M06-L, which is in the same class). On some 2500 test cases, B97M-V is able to reduce the RMS errors of the best existing alternative MGGA's by nearly 30% for thermochemistry and nearly 50% for non-bonded interactions.

Semi-classical dynamics. It has been well established for many years that semi-classical (SC) theory provides a very good description of essentially *all* quantum effects in molecular dynamics, and the outstanding challenge has been to what extent one can implement it efficiently enough to make it routinely useful. Recent progress by Miller included the most accurate and efficient approach to date for implementing the SC initial value representation (IVR) for molecular dynamics. The key to the efficiency is in use of a time-dependent Monte Carlo sampling function for evaluating the phase space average over initial conditions of classical trajectories that are the 'input' to the SC theory. Efforts were also begun at finding a general and dynamically consistent way for treating the electronic and nuclear degrees of freedom in non-adiabatic processes by classical molecular dynamics. The two

essential steps for this are (1) to find a consistent way for describing the electronic (as well as nuclear) degrees of freedom by classical mechanics (currently by the Meyer-Miller (MM) ‘electronic oscillator’ model), and (2) to be able to extract quantum state information for the electronic states from such a description, where the ‘symmetrical quasi-classical’ (SQC) model was used. Both of these approaches have a long history but have never been used in concert before in this way. They have given remarkably good results for a series of standard non-adiabatic problems, even being able to describe ‘quantum coherence’ effects within a standard classical MD simulation.

Computational studies of chemical properties and reactivity. (i) In collaboration with experimental measurements from the Ahmed and Leone groups at LBNL, the photodissociation of glycerol has been explored. The key intermediate is a triplex between vinyl alcohol radical cation, water and formaldehyde. (ii) Stimulated by experiments of Leone and collaborators, the reaction of methylidyne (CH) with acrolein (CH₂CHCHO) was studied using various *ab initio* and Diffusion Monte Carlo methods. In agreement with experiment, the dominant product channel was found to be the formation of C₄H₆ systems + H with leading products of furan + H and 1,3-butadienal + H. (iii) A collaborative study between the Lester and Frenklach groups employing uncertainty quantification (UQ) to improve quantum chemical predictions by using the Bound-to-Bound Data Collaboration Framework has been completed, showing promise for problem-specific improvement of double hybrid density functionals.

Future Plans: (i) Density functionals: The new combinatorial design approach will be extended to range separated hybrid van der Waals functionals in the meta GGA class. This offers the possibility of significantly higher accuracy than either ω B97X-V or B97M-V, possibly without many if any additional parameters. A further possible extension is to double hybrid functionals, possibly including orbital optimization. (ii) Semiclassical dynamics: It is planned to further pursue the recent work that has proved so encouraging for having a general and robust classical simulation model for treating electronically non-adiabatic processes, including further investigation of the fundamental theoretical model, as well as to its application to specific processes. (iii) Computational studies of chemical properties and reactivity: It is planned to characterize the reaction pathways associated with the Criegee intermediate, CH₃CHOO, by combining diffusion Monte Carlo (DMC) with *ab initio* molecular dynamics simulations. Other potential systems of interest include energetics, spectroscopy, and dynamics of RO₂ radicals in the context of low temperature reactions, and larger polycyclic aromatic hydrocarbon species, and their ions, including clustering effects.

Recent Publications Citing DOE Support (2012-2015)

- Austin, B. M., Zubarev, D. Yu., Lester, Jr., W. A. “Quantum Monte Carlo and Related Approaches” *Chem. Rev.* **2012** 112, 263-288. DOI: 10.1021/cr2001564
- Azar, R. J. and M. Head-Gordon, “An Energy Decomposition Analysis for Intermolecular Interactions from an Absolutely Localized Molecular Orbital Reference at the Coupled- Cluster Singles and Doubles Level” *J. Chem. Phys.*, **2012**, 136, 024103. DOI: 10.1063/1.3674992
- Azar, R. J., P.R. Horn, E.J. Sundstrom, and M. Head-Gordon, “Useful Lower Limits to Polarization Contributions to Intermolecular Interactions Using a Minimal Basis of Localized Orthogonal Orbitals: Theory and Analysis of the Water Dimer” *J. Chem. Phys.*, **2013**, 138, 084102. DOI: 10.1063/1.4792434
- Bell, F., Q. N. Ruan, A. Golan, P. R. Horn, M. Ahmed, S. R. Leone, and M. Head-Gordon, “Dissociative Photoionization of Glycerol and its Dimer Occurs Predominantly via a Ternary Hydrogen-Bridged Ion-Molecule Complex” *J. Am. Chem. Soc.*, **2013**, 135, 14229- 14239. DOI: 10.1021/ja405511v
- Cotton, S. J. and Miller, W. H. “Symmetrical Windowing for Quantum States in Quasi-Classical Trajectory Simulations” *J. Phys. Chem. A* **2013**, 117, 7190-7194. DOI: 10.1021/jp401078u
- Cotton, S. J. and Miller, W. H., “Symmetrical Windowing for Quantum States in Quasi-Classical Trajectory Simulations: Application to Electronically Non-Adiabatic Processes” *J. Chem. Phys.* **2013**, 139, 234112.1-9. DOI: 10.1063/1.4845235

- Cotton, S. J., Igumenshchev, K. and Miller, W. H., “Symmetrical Windowing for Quantum States in Quasi-Classical Trajectory Simulations: Application to Electron Transfer” *J. Chem. Phys.* **2014**, 141, 084104.1-14. DOI: 10.1063/1.4893345
- Edwards, D. E., You, X., Zubarev, D. Yu., Lester, Jr., W.A., Frenklach, M., “Thermal Decomposition of Graphene Armchair Oxyradical” *Proc. Combust. Inst.* **2013** 34, 1759. DOI: 10.1016/j.proci.2012.05.031
- Edwards, D. E., Zubarev, D. Y., Packard, A., Lester Jr., W. A., Frenklach, M. “Interval Prediction of Molecular Properties in Parametrized Quantum Chemistry” *Phys. Rev. Lett.* **2014** 112, 253003/5/. DOI: 10.1103/PhysRevLett.112.253003
- Edwards, D. E., Zubarev, D., Lester, Jr., W. A., Frenklach, M., “Pathways to Soot Oxidation: Reaction of OH with Phenanthrene Radicals” *J. Phys. Chem. A* **2014**, 118, 8606-8613. DOI: 10.1021/jp5033178
- Goldey, M. and M. Head-Gordon, “Separate Electronic Attenuation Allows a Spin-Component Scaled Second Order Møller-Plesset Theory to be Effective for Both Thermochemistry and Non-Covalent Interactions” *J. Phys. Chem. B*, **2014**, 118, 6519-6525. DOI: 10.1021/jp4126478
- Goldey, M. B. and M. Head-Gordon, “Convergence of Attenuated Second Order Møller-Plesset Perturbation Theory Towards the Complete Basis Set Limit” *Chem. Phys. Lett.*, **2014**, 608, 249-254. DOI: 10.1016/j.cplett.2014.05.092
- Goldey, M., A. D. Dutoi and M. Head-Gordon, “Attenuated Second Order Moller-Plesset Theory: Assessment and Performance in the aug-cc-pVTZ Basis” *Phys. Chem. Chem. Phys.*, **2013**, 15, 15869-15875. DOI: 10.1039/c3cp51826d
- Goldey, M., R. A. DiStasio, Jr., Y. Shao, and M. Head-Gordon, “Shared Memory Multi Processing Implementation of Resolution-of-the-Identity Second Order Møller-Plesset Perturbation Theory with Attenuated and Unattenuated Results for Intermolecular Interactions between Larger Molecules” *Mol. Phys.*, **2014**, 112, 836-843. DOI: 10.1080/00268976.2013.869363
- Goldey, M. and M. Head-Gordon, “Attenuating Away the Errors in Inter and Intra-Molecular Interactions from Second Order Møller-Plesset Calculations in the Small aug-cc-pVDZ Basis Set” *J. Phys. Chem. Lett.*, **2012**, 3, 3592-3598. DOI: 10.1021/jz301694b
- Horn, P.R., E.J. Sundstrom, T. Baker and M. Head-Gordon, “Unrestricted Absolutely Localized Molecular Orbitals for Energy Decomposition Analysis: Theory and Applications to Intermolecular Interactions Involving Radicals” *J. Chem. Phys.*, **2013**, 138, 134119. DOI: 10.1063/1.4798224
- Huang, Y.-H., M. Goldey, M. Head-Gordon, and G. J. O. Beran, “Achieving High Accuracy Intermolecular Interactions Through Coulomb-Attenuated Dispersion Corrected Second Order Møller-Plesset Theory” *J. Chem. Theory Comput.*, **2014**, 10, 2054-2063. DOI: 10.1021/ct5002329
- Kurlancheek, W., R. Lochan, K. V. Lawler, and M. Head-Gordon, “Exploring the Competition Between Localization and Delocalization of the Neutral Soliton Defect in Polyenyl Chains With the Orbital Optimized Second Order Opposite Spin Method” *J. Chem. Phys.* **2012**, 136, 054113. DOI: 10.1063/1.3679658
- Lambrecht, D. S., L. McCaslin, S. S. Xantheas, E. Epifanovsky, and M. Head-Gordon, “Refined Energetic Ordering for Sulfate-Water (N=3-6) Clusters Using High-Level Electronic Structure Calculations” *Mol. Phys.*, **2012**, 110, 2513-2521. DOI: 10.1080/00268976.2012.708442
- LeDell, E., Prabhat, Zubarev, D. Yu., Austin, B. M., Lester, Jr., W. A. “Classification of Nodal Pockets in Many-Electron Wave Functions via Machine Learning” *J. Math. Chem.* **2012** 50, 2043-2050. DOI: 10.1007/s10910-012-0019-5
- Li, B. and Miller, W. H., “A Cartesian Classical Second-Quantized Many-Electron Hamiltonian, for Use with the Semiclassical Initial Value Representation” *J. Chem. Phys.* **2012**, 137, 154107.1-7. DOI: 10.1063/1.4757935
- Li, B., Levy, T. J., Swenson, D. W. H., Rabani, E. and Miller, W. H., “A Cartesian Quasi- Classical Model to Nonequilibrium Quantum Transport: The Anderson Impurity Model” *J. Chem. Phys.* **2013**, 138, 104110.1-6. DOI: 10.1063/1.4793747
- Li, B., Miller, W. H., Levy, T. J., and Rabani, E., “Classical Mapping for Hubbard Operators: Application to the Double-Anderson Model” *J. Chem. Phys.* **2014**, 140, 204106.1-7. DOI: 10.1063/1.4878736
- Li, B., Wilner, E. Y., Thoss, M., Rabani, E., and Miller, W. H., “A Quasi-Classical Mapping Approach to Vibrationally Coupled Electron Transport in Molecular Junctions” *J. Chem. Phys.* **2014**, 140, 104110.1-7. DOI: 10.1063/1.4867789
- Mardirossian, N., D.S. Lambrecht, L. McCaslin, S.S. Xantheas, and M. Head-Gordon, “The Performance of Current Density Functionals for Sulfate-Water Clusters” *J. Chem. Theory Comput.*, **2013**, 9, 1368-1380. DOI: 10.1021/ct4000235

- Mardirossian, N. and M. Head-Gordon “Characterizing and Understanding the Remarkably Slow Basis Set Convergence of Several Minnesota Density Functionals for Intermolecular Interaction Energies” *J. Chem. Theor. Comput.*, **2013**, 9, 4453-4461. DOI: 10.1021/ct400660j
- Mardirossian, N. and M. Head-Gordon, “ ω B97X-V: A 10 Parameter Range Separated Hybrid Density Functional Including Non-Local Correlation, Designed by a Survival of the Fittest Strategy” *Phys. Chem. Chem. Phys.*, **2014**, 16, 9904-9924. DOI: 10.1039/c3cp54374a
- Mardirossian, N., and M. Head-Gordon, “Exploring the Limit of Accuracy for Density Functionals Based on the Generalized Gradient Approximation: Local, Global Hybrid and Range-Separated Hybrids With and Without Dispersion Corrections” *J. Chem. Phys.*, **2014**, 140, 18A527. DOI: 10.1063/1.4868117
- Mardirossian, N. and M. Head-Gordon, “Mapping the genome of meta-generalized gradient approximation density functionals: The search for B97M-V”, *J. Chem. Phys.* 142, 074111 (2015); (32 pages) <http://dx.doi.org/10.1063/1.4907719>
- Miller, W. H., “A Journey Through Chemical Dynamics” *Annu. Rev. Phys. Chem.* **2014**, 65, 1- 19. DOI: 10.1146/annurev-physchem-040513-103720
- Miller, W. H., “Note: Another Resolution of the Identity for Two-Electron Integrals” *J. Chem. Phys.* **2012**, 136, 216101.1-2. DOI: 10.1063/1.4728027
- Miller, W. H., “Perspective: Quantum or Classical Coherence?” *J. Chem. Phys.* **2012**, 136, 210901.1-6. DOI: 10.1063/1.4727849
- Peverati, R. and M. Head-Gordon, “Orbital Optimized Double Hybrid Density Functionals” *J. Chem. Phys.*, **2013**, 139, 024110. DOI: 10.1063/1.4812689
- Small, D. W. and M. Head-Gordon, “A Fusion of the Closed-Shell Coupled Cluster Singles and Doubles Method and Valence-Bond Theory for Bond Breaking” *J. Chem. Phys.*, **2012**, 137, 114103. DOI: 10.1063/1.4751485
- Small, D. W., K. V. Lawler, and M. Head-Gordon, “Coupled Cluster Valence Bond Method: Efficient Implementation and Application to Extended Acene Oligomers” *J. Chem. Theor. Comput.*, **2014**, 10, 2027-2040. DOI: 10.1021/ct500112y
- Stück, D. and M. Head-Gordon, “Regularized Orbital Optimized Second Order Perturbation Theory” *J. Chem. Phys.*, **2013**, 139, 244109. DOI: 10.1063/1.4851816
- Tao, G, and Miller, W. H., “Time-Dependent Important Sampling in Semiclassical Initial Value Representation Calculations or Time Correlation Functions. III. A State-Resolved Implementation to Electronically Non-Adiabatic Dynamics” *Mol. Phys.* **2013**, 111, 1987- 1993. DOI: 10.1063/1.4793747
- Tao, G. and Miller, W. H., “Time Dependent Importance Sampling in Semiclassical Initial Value Representation Calculations for Time Correlation Functions. II A Simplified Implementation” *J. Chem. Phys.* **2012**, 137, 124105.1-7. DOI: 10.1063/1.4752206
- Wang Z., Zubarev, D. Yu., Lester, W. A. Jr. “Quantum Monte Carlo Investigation of the H-shift and O₂-loss Reactions of Cis-2-Butene-1-Peroxy Radical” *Theor. Chem. Accs.* **2014** 133, 1541. DOI: 10.1007/s00214-014-1541-2
- Zubarev, D. Yu., Austin, B. M., Lester, Jr., W. A. “Practical Aspects of Quantum Monte Carlo for the Electronic Structure of Molecules” in *Practical Aspects of Computational Chemistry: Methods, Concepts and Applications*, J. Leszczynski and M. K. Shukla, Eds., Springer, **2012**, 255-292.
- Zubarev, D. Yu., Austin, B. M., Lester, Jr., W. A. “Quantum Monte Carlo for the X-Ray Absorption Spectrum of Pyrrole at the Nitrogen K-Edge” *J. Chem. Phys.* **2012** 136, 144301/5/. DOI: 10.1063/1.3700803
- Zubarev, D. Yu., Frenklach, M., Lester, Jr., W. A. “From Aromaticity to Self-Organized Criticality in Graphene” *Phys. Chem. Chem. Phys.* **2012** 14, 12075-12078. (Communication). DOI: 10.1039/c2cp41675a
- Zubarev, D. Yu., Lester, Jr., W. A. “Beyond a Single Solvated Electron: Hybrid Quantum Monte Carlo and Molecular Mechanics Approach” ACS Symposium Series *Advances in Quantum Monte Carlo*, **2012** 1094, 201-206.
- Zubarev, D. Yu., You, X., Frenklach, M., Lester, Jr., W. A. “Delocalization Effects in Pristine and Oxidized Graphene Substrates” in *Advances in the Theory of Quantum Systems in Chemistry and Physics* (P. E. Hoggan, E. J. Brändas, J. Maruani, P. Piecuch, and G. Delgado-Barrio, Eds.), Progress in Theoretical Chemistry and Physics, **2012**, 22, Springer, Dordrecht, Chapter 29, p. 553-569.

Laser Studies of Combustion Chemistry

John F. Hershberger

Department of Chemistry and Biochemistry
North Dakota State University
NDSU Dept. 2735, PO Box 6050
Fargo, ND 58108-6050
john.hershberger@ndsu.edu

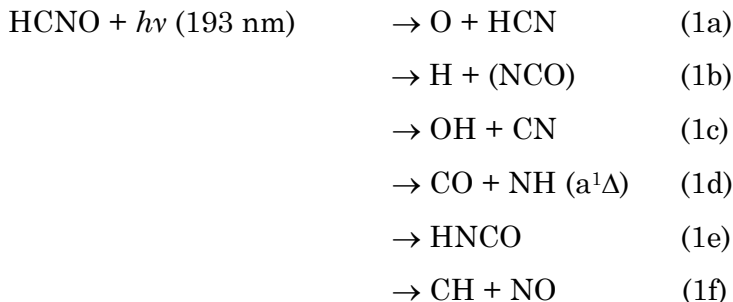
Time-resolved infrared diode laser absorption is used in our laboratory to study the kinetics and product channel dynamics of chemical reactions of importance in the gas-phase combustion chemistry of nitrogen-containing species. This program is aimed at improving the kinetic database of reactions crucial to modeling of combustion processes, with emphasis on NO_x chemistry. When feasible, we perform quantitative measurement of both total rate constants and product branching ratios.

1) HCNO Photochemistry

In previous years, we have extensively studied the kinetics of radical-molecule reactions involving HCNO, fulminic acid, which is produced in combustion chemistry primarily by the HCCO + NO reaction. In the last two years, we have studied the photochemistry of this molecule. We have determined the following UV absorption cross sections for HCNO:

$$\begin{aligned}\sigma(193 \text{ nm}) &= (5.65 \pm 0.48) \times 10^{-19} \text{ cm}^2 \text{ molecule}^{-1}. \\ \sigma(248 \text{ nm}) &= (1.52 \pm 0.15) \times 10^{-19} \text{ cm}^2 \text{ molecule}^{-1}. \\ \sigma(266 \text{ nm}) &= 1.42 \times 10^{-19} \text{ cm}^2 \text{ molecule}^{-1}.\end{aligned}$$

We then used infrared spectroscopy to detect and quantify several product species, including HCN, DCN, CO₂, CO, DCN, NH, and HNCO. Last year's (2014) report described measurements of the 248-nm photolysis yields. Subsequently, we have extended the measurements to 193 nm. At 193 nm, the following channels are energetically possible:

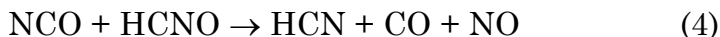


Channels (1a)-(1e) were accessible at 248 nm, but (1f) is not; it requires a higher energy photon.

In order to suppress and/or redirect secondary chemistry, additional reagents were often added. Details are given in the relevant publications, but briefly, reactive species such as CN, NCO, and CH can react with HCNO, producing some of the same products as we detect. CH is a particular problem, as it is highly reactive, and the products of CH + HCNO are unknown. We first showed that channel (1f) is insignificant by including ^{15}NO in the reaction mixture. Under those conditions, the following reactions occur:



We then detect the double labeled $^{15}\text{N}^{15}\text{NO}$ molecule by infrared spectroscopy. We found no transient signal attributable to $^{15}\text{N}^{15}\text{NO}$, indicating that channel (1f) is very minor. Based on an upper limit for a detectable transient signals, and consideration of the branching ratios into (2a) and (3a), we estimated an upper limit for $\phi_{1f} < 0.02$. At that point, we can use the same techniques used in our previous study at 248-nm to deal with other secondary reactions. For example, if channel (1b) is active, any NCO produced can react with HCNO:

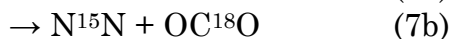
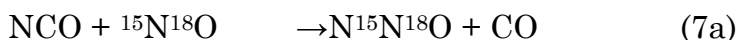


which would interfere with our HCN detection experiment. Addition of NO reagent can suppress this reaction, as NCO+NO is fast and does not produce HCN. CN radicals in channel (1c) are more problematic, however:



By including ^{15}NO reagent, the HCN produced in reaction (6) is HC ^{15}N . Our infrared probe then detects unlabeled HCN, which then entirely originates from photolysis channel (1a).

To quantify channel (1b), we included $^{15}\text{N}^{18}\text{O}$ reagents, resulting in the following:



We then detect the OC ^{18}O molecule. CO $_2$ can also be produced by



But this produces double-labeled CO_2 , which is spectroscopically distinct.

To quantify channel (1c), we detected DCN produced upon addition of C_2D_6 :



Results are as follows:

Quantum Yields for HCNO Photolysis at 248 and 193nm

Product Channel	$\phi(248 \text{ nm})$	$\phi(193\text{nm})$
O + HCN	0.39 ± 0.07	0.38 ± 0.04
H + (NCO)	0.21 ± 0.04	0.07 ± 0.02
CN + OH	0.16 ± 0.04	0.21 ± 0.03
NH + CO	0.05 ± 0.03	0.09 ± 0.04
HNCO	0.05 ± 0.02	0.02 ± 0.01
CH + NO		< 0.02
Total	0.86	0.77

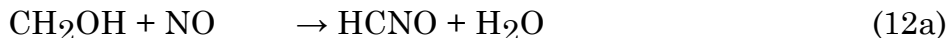
As can be seen, the primary difference between the 193 nm and 248 nm yields is that channel (1b), H + (NCO), is much less important at 193 nm, while channel (1d), NH+CO, is somewhat more important.

2) Reactions of Hydroxymethyl Radical

In last year's report, we noted that the CN radical primarily abstracts an alkyl hydrogen atom when it reacts with methanol:



Where we found that the yield of (11a) is ~0.8-0.9, while that of (11b) is only ~0.08. This reaction therefore represents a clean source of hydroxymethyl (CH_2OH), using ICN as a CN precursor at 248 or 266 nm. CH_2OH can then react with NO, as follows:





One previous experimental study found a fairly high rate constant, $2.5 \times 10^{-11} \text{ cm}^3 \text{ molecule}^{-1} \text{ s}^{-1}$, but only at 1 atm pressure. Rate constants at lower pressure are unknown; it is therefore possible that the collisionally stabilized adduct (12e) dominates. We are currently using transient infrared spectroscopy and ab initio calculations to study the product channels of this reaction. Preliminary experimental results indicate that no HCNO or HCN is formed, but a modest yield of HNO and a significant yield of HNCO is formed. Ab initio calculations show that the adduct (12e) may readily be formed, but high barriers must be crossed in order to form at least some of the bimolecular product channels. In particular, the hydrogen migration to form ONCHOH₂, which would dissociate to form (12a), appears to be a high energy process. Surprisingly, a more complex multistep pathway leading to channel (12d) appears to have accessible barriers. Experimental work to quantify the HNCO product yield is ongoing.

References

1. P. Pagsberg, J. Munk, C. Anastasi, and V. Simpson, *J. Phys. Chem.* 93, 5162 (1989).

Students/postdocs involved in project: Wenhui Feng, Erik Janssen.

Publications acknowledging DOE support (2012-present)

1. "Kinetics of the O + ICN Reaction", W. Feng and J.F. Hershberger, *J. Phys. Chem. A* 116, 4817 (2012).
2. "Product Channels of the CN + HCNO Reaction", W. Feng and J.F. Hershberger, *J. Phys. Chem. A* 116, 10285 (2012).
3. "Experimental and Theoretical Study of the Product Channels of the C₂H + NO Reaction", W. Feng and J.F. Hershberger, *J. Phys. Chem. A* 117, 3585 (2013).
4. "Quantification of the 248 nm Photolysis Products of HCNO (Fulminic Acid)", W. Feng and J.F. Hershberger, *J. Phys. Chem. A* 118, 829 (2014).
5. "Kinetics of CN Reactions with Alcohols", E. Janssen and J.F. Hershberger, *Chem. Phys. Lett.* 625, 26 (2015).
6. "Product Channels in the 193 nm Photodissociation of HCNO", W. Feng and J.F. Hershberger, *J. Phys. Chem. A*, submitted.

Breakthrough Design and Implementation of Electronic and Vibrational Many-Body Theories

So Hirata (principal investigator: DE-FG02-11ER16211)

Department of Chemistry, University of Illinois at Urbana-Champaign,
600 South Mathews Avenue, Urbana, IL 61801
sohirata@illinois.edu

Program Scope

Predictive chemical computing requires hierarchical many-body methods of increasing accuracy for both electrons and vibrations. Such hierarchies are established, at least conceptually, as configuration-interaction (CI), many-body perturbation (MP), and coupled-cluster (CC) methods, which all converge at the exact limit with increasing rank of a hierarchical series. These methods can generate results of which the convergence with respect to various parameters of calculations can be demonstrated and which can thus be predictive in the absence of experimental information.

The wide use of the hierarchical electronic and vibrational many-body methods has, however, been hindered (1) by the immense cost of *executing* the calculations with these methods and, furthermore, the nonphysical rapid increase of the cost with increasing system or computer size; in other words, the conventional matrix-algebra-based algorithms of these methods are fundamentally non-scalable, (2) by the complexity and cost of *developing* some of the high-rank members of these methods, and (3) by the slow convergence of electronic energies and wave functions with respect to one-electron basis set sizes, which further drives up the cost of execution. For applications to large molecules and solids, the additional difficulties arise by the lack of (4) size consistency in some methods (whose energies and other observables scale non-physically with size) and of (5) efficient methods that work for metallic and superconducting states as well as for electronic and/or vibrational strong correlation.

We aim to address all of these difficulties for electrons and vibrations with a view to establishing accurate and systematic computational methods for condensed-phase systems, which go beyond the usual density-functional approximations for electrons and harmonic approximation for vibrations.

Recent Progress

Publications

Twenty (20) papers have resulted from this award since 2012, acknowledging this DOE support. They include a Feature Article in *Journal of Physical Chemistry A* with a cover art, an account in *Account of Chemical Research*, and a review in *International Reviews in Physical Chemistry*. One book chapter in *Annual Reviews of Physical Chemistry* has also resulted from this project. There are nine (9) additional papers that resulted from another DOE (SciDAC) support, acknowledging the latter. These two projects are mutually beneficial, but distinct from each other.

Research Highlights I. Electronic Structure Theory

Size-consistency theorems.⁷ Why do variational electron-correlation methods such as truncated CI methods tend to be non-size-consistent (non-size-extensive)? Why are size-consistent (size-extensive) methods such as MP and CC methods nonvariational? We conjecture that the variational and size-consistent properties are mutually exclusive in an *ab initio* electron-correlation method (which thus excludes the Hartree–Fock and density-functional methods). We have analyzed key examples (truncated and full CI as well as variational and projection CC methods) that support the truth of this conjecture.

Monte Carlo explicitly correlated MP2.⁸ In collaboration with J. Zhang and E. F. Valeev (Virginia Tech), we have proposed a stochastic algorithm that can compute the basis-set-incompleteness correction to the second-order many-body perturbation (MP2) energy of a polyatomic molecule. It evaluates the sum of two-, three-, and four-electron integrals over an explicit function of electron-electron distances by a Monte Carlo (MC) integration at an operation cost per MC step increasing only quadratically with size.

The method can reproduce the corrections to the MP2/cc-pVTZ energies of H₂O, CH₄, and C₆H₆ within a few mE_h after several million MC steps. It circumvents the resolution-of-the-identity approximation to the nonfactorable three-electron integrals usually necessary in the conventional explicitly correlated (R12 or F12) methods.

The aforementioned F12 method is based on the so-called “V” formula that is not variational with respect to the form of the correlation factor. It gives F12 corrections to total energies that are accurate, but F12 corrections to relative energies are found to be less reliable. We are thus extending this MC-MP2-F12 method to a variational (“VBX”) formula, which gives more accurate F12 energy differences. Our preliminary work shows that there are tens of up to six-electron integrals, which are to be evaluated brute-force by MC integration.

Research Highlights II. Vibrational Structure Theory

Stochastic XVSCF.² We have developed a stochastic algorithm based on an Metropolis MC integration for the size-extensive vibrational self-consistent field methods, XVSCF(n) and XVSCF[n], for anharmonic molecular vibrations. The new MC-XVSCF methods substitute stochastic evaluations of a small number of high-dimensional integrals of functions of the potential energy surface (PES), which is sampled on demand, for diagrammatic equations involving high-order anharmonic force constants. This algorithm obviates the need to evaluate and store any high-dimensional partial derivatives of the potential and can be applied to the fully anharmonic PES without any Taylor-series approximation in an intrinsically parallelizable algorithm. The MC-XVSCF methods reproduce deterministic XVSCF calculations on the same Taylor-series PES in all energies, frequencies, and geometries. Calculations using the fully anharmonic PES evaluated on the fly with electronic structure methods report anharmonic effects on frequencies and geometries of much greater magnitude than deterministic XVSCF calculations, reflecting an underestimation of anharmonic effects in a Taylor-series approximation to the PES.

Stochastic XVMP2.⁴ A new quantum Monte Carlo (QMC) method for anharmonic vibrational zero-point energies and transition frequencies is developed, which combines the diagrammatic vibrational many-body perturbation theory based on the Dyson equation with MC integration. The infinite sums of the diagrammatic and thus size-consistent first- and second-order anharmonic corrections to the energy and self-energy are expressed as sums of a few m - or $2m$ -dimensional integrals of wave functions and a PES (m is the vibrational degrees of freedom). Each of these integrals is computed as the integrand (including the value of the PES) divided by the value of a judiciously chosen weight function evaluated on demand at geometries distributed randomly but according to the weight function via the Metropolis MC algorithm. In this way, the method completely avoids cumbersome evaluation and storage of high-order force constants necessary in the original formulation of the vibrational perturbation theory; it furthermore allows even higher-order force constants essentially up to an infinite order to be taken into account in a scalable, memory-efficient algorithm. The diagrammatic contributions to the frequency-dependent self-energies that are stochastically evaluated at discrete frequencies can be reliably interpolated, allowing the self-consistent solutions to the Dyson equation to be obtained. This method, therefore, can compute directly and stochastically the transition frequencies of fundamentals and overtones as well as their relative intensities as pole strengths, without fixed-node errors that plague some QMC. It is shown that, for an identical PES, the new method reproduces the correct deterministic values of the energies and frequencies within a few cm^{-1} and pole strengths within a few thousandths. With the values of a PES evaluated on the fly at random geometries, the new method captures a noticeably greater proportion of anharmonic effects.

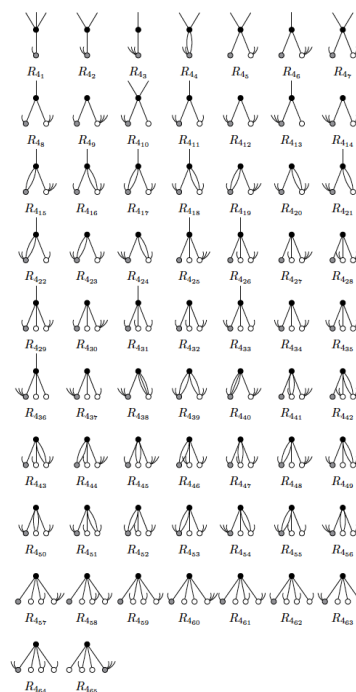
Normal-ordered vibrational Hamiltonian.³ The molecular electronic Hamiltonian has evolved from the first-quantized to second-quantized form, and then to the third and most advanced, normal-ordered form, which is equivalent to

$$\begin{aligned} \hat{a}_i \hat{a}_j \hat{a}_k^\dagger \hat{a}_l^\dagger &= \{\hat{a}_i \hat{a}_j \hat{a}_k^\dagger \hat{a}_l^\dagger\} + \overline{\{\hat{a}_i \hat{a}_j \hat{a}_k^\dagger \hat{a}_l^\dagger\}} + \overline{\{\hat{a}_i \hat{a}_j \hat{a}_k^\dagger \hat{a}_l^\dagger\}} \\ &\quad + \overline{\{\hat{a}_i \hat{a}_j \hat{a}_k^\dagger \hat{a}_l^\dagger\}} + \overline{\{\hat{a}_i \hat{a}_j \hat{a}_k^\dagger \hat{a}_l^\dagger\}} \\ &\quad + \overline{\{\hat{a}_i \hat{a}_j \hat{a}_k^\dagger \hat{a}_l^\dagger\}} + \overline{\{\hat{a}_i \hat{a}_j \hat{a}_k^\dagger \hat{a}_l^\dagger\}} \\ &= \{\hat{a}_i \hat{a}_j \hat{a}_k^\dagger \hat{a}_l^\dagger\} + \delta_{ik} \{\hat{a}_j \hat{a}_l^\dagger\} + \delta_{il} \{\hat{a}_j \hat{a}_k^\dagger\} \\ &\quad + \delta_{jk} \{\hat{a}_i \hat{a}_l^\dagger\} + \delta_{jl} \{\hat{a}_i \hat{a}_k^\dagger\} + \delta_{ik} \delta_{jl} + \delta_{il} \delta_{jk} \end{aligned}$$

Normal ordering of the quartic force constant operator.

the corresponding Feynman–Goldstone diagrammatic form. Not only do normal ordering and associated Wick’s theorem expedite the evaluation of the expectation values of operators, they also serve as a rigorous mathematical basis of size-consistency arguments. Whereas normal ordering for boson creation and annihilation operators and second-quantized (but not normal-ordered) vibrational Hamiltonians are well documented, a normal-ordered vibrational Hamiltonian does not seem to be fully discussed in the literature. Here, we present the most compact form of such a Hamiltonian for anharmonic molecular vibrations on a Taylor-series PES in the style of the normal-ordered electronic counterpart¹ widely used in deriving equations of *ab initio* electronic structure theories. We then demonstrate how it can be used to rapidly define XVSCF methods and XVMP methods using the Møller–Plesset partitioning of the Hamiltonian.

XVCC and EOM-XVCC. Diagrammatically size-consistent and basis-set-free vibrational coupled-cluster (XVCC) theory for both zero-point energies and transition frequencies, the latter through the equation-of-motion (EOM) formalism, is defined for an n th-order Taylor-series PES. Quantum-field-theoretical tools (the rules of normal-ordered second quantization³ and Feynman–Goldstone diagrams) for deriving their working equations are established. The equations of XVCC and EOM-XVCC including up to the m th-order excitation operators are derived and implemented with the aid of computer algebra in the range of $1 \leq m \leq 8$. The calculated zero-point energies and frequencies of fundamentals, overtones, and combinations as well as Fermi-resonant modes display rapid and nearly monotonic convergence with m towards the exact values for the PES. The theory with the same excitation rank as the truncation order of the Taylor-series PES ($m = n$) seems to strike the best cost-accuracy balance, achieving the accuracy of a few tenths of cm^{-1} for transitions involving $(m - 3)$ modes and of a few cm^{-1} for those involving $(m - 2)$ modes. The relationships between XVCC and the vibrational coupled-cluster theories of Prasad and coworkers and of Christiansen and coworkers as well as the XVSCF and XVMP2 theories are also elucidated. The manuscript is being finalized for publication.



Diagrams of the R_4 amplitude equation of EOM-CCSDTQ.

Publications of This DOE Grant Sponsored Research (2012–Present)

1. M. R. Hermes and S. Hirata, *International Reviews in Physical Chemistry* (in press, 2015), “**Diagrammatic theories of anharmonic molecular vibrations.**”
2. M. R. Hermes and S. Hirata, *The Journal of Chemical Physics* **141**, 244111 (2014) (11 pages), “Stochastic algorithm for size-extensive vibrational self-consistent field methods on fully anharmonic potential energy surfaces.”
3. S. Hirata and M. R. Hermes, *The Journal of Chemical Physics* **141**, 184111 (2014) (7 pages), “Normal-ordered second-quantized Hamiltonian for molecular vibrations.”
4. M. R. Hermes and S. Hirata, *The Journal of Chemical Physics* **141**, 084105 (2014) (17 pages), “Stochastic many-body perturbation theory for anharmonic molecular vibrations.”
5. S. Hirata, K. Gilliard, X. He, J. Li, and O. Sode, *Accounts of Chemical Research* **47**, 2721-2730 (2014), “**Ab initio molecular crystal structures, spectra, and phase diagrams.**”
6. S. Hirata, X. He, M. R. Hermes, and S. Y. Willow, *The Journal of Physical Chemistry A* **118**, 655-672 (2014) [an invited Feature Article], “**Second-order many-body perturbation theory: An eternal frontier.**”
7. S. Hirata and I. Grabowski, *Theoretical Chemistry Accounts* **133**, 1440 (2014) (9 pages) [Thom Dunning Special Issue], “On the mutual exclusion of variationality and size consistency.”

8. S. Y. Willow, J. Zhang, E. F. Valeev, and S. Hirata, *The Journal of Chemical Physics (Communications)* **140**, 031101 (2014) (4 pages), “Stochastic evaluation of explicitly correlated second-order many-body perturbation energy.”
9. S. Y. Willow, M. R. Hermes, K. S. Kim, and S. Hirata, *Journal of Chemical Theory and Computation* **9**, 4396-4402 (2013), “Convergence acceleration of parallel Monte Carlo second-order many-body perturbation calculations using redundant walkers.”
10. M. R. Hermes and S. Hirata, *The Journal of Chemical Physics* **139**, 034111 (2013) (21 pages), “Second-order many-body perturbation expansions of vibrational Dyson self-energies.”
11. M. R. Hermes and S. Hirata, *The Journal of Physical Chemistry A* **117**, 7179-7189 (2013) [Joel M. Bowman Festschrift], “First-order Dyson coordinates and geometry.”
12. S. Y. Willow, K. S. Kim, and S. Hirata, *The Journal of Chemical Physics* **137**, 204122 (2012) (5 pages), “Stochastic evaluation of second-order many-body perturbation energies.”
13. K. Yagi, M. Keçeli, and S. Hirata, *The Journal of Chemical Physics* **137**, 204118 (2012) (16 pages), “Optimized coordinates for anharmonic vibrational structure theories.”
14. R. D. Thomas, I. Kashperka, E. Vigen, W. Geppert, M. Hamberg, M. Larsson, M. af Ugglas, V. Zhaunerchyk, N. Indriolo, K. Yagi, S. Hirata, and B. J. McCall, *Astrophysical Journal* **758**, 55 (2012), “Dissociative recombination of vibrationally cold CH_3^+ and interstellar implications.”
15. M. R. Hermes, M. Keçeli, and S. Hirata, *The Journal of Chemical Physics* **136**, 234109 (2012) (17 pages), “Size-extensive vibrational self-consistent field method with anharmonic geometry corrections.”
16. G. J. O. Beran and S. Hirata, *Physical Chemistry Chemical Physics* **14**, 7559-7561 (2012) [Guest Editorial in Special Issue on “Fragment and Localized Orbital Methods in Electronic Structure Theory”], “**Fragment and localized orbital methods in electronic structure theory**,” (Top 10 most read in May, 2012).
17. S. Hirata and Y.-Y. Ohnishi, *Physical Chemistry Chemical Physics* **14**, 7800-7808 (2012) [Special Issue on “Fragment and Localized Orbital Methods in Electronic Structure Theory”], “Thermodynamic limit of the energy density in a crystal,” (A Hot Article)
18. Y.-Y. Ohnishi and S. Hirata, *Chemical Physics* **401**, 152-156 (2012) [Debashis Mukherjee Special Issue], “Charge-consistent redefinition of Fock integrals.”
19. S. Hirata, *Theoretical Chemistry Accounts* **131**, 1071 (2012) (4 pages) [an introductory article in the 50th Anniversary Issue], “**Electronic structure theory: Present and future challenges**.”
20. S. Hirata, M. Keçeli, Y.-Y. Ohnishi, O. Sode, and K. Yagi, *Annual Reviews of Physical Chemistry* **63**, 131-153 (2012), “**Extensivity of energy and size-consistent electronic and vibrational structure methods for crystals**.”

Publications of Other DOE Grant Sponsored Research (2013–Present)

21. T. Yamada and S. Hirata, *Theoretical Chemistry Accounts* (submitted, 2015), “Instability theorems for degenerate Hartree-Fock wave functions.”
22. S. Hirata, M. R. Hermes, J. Simons, and J. V. Ortiz, *Journal of Chemical Theory and Computation* (in press, 2015), “General-order many-body Green's function method.”
23. S. Y. Willow, K. S. Kim, and S. Hirata, *Physical Review B (Rapid Communications)* **90**, 201110(R) (2014) (5 pages), “Brueckner-Goldstone quantum Monte Carlo for correlation energies and quasiparticle energy bands of one-dimensional solids.”
24. Z. Kou and S. Hirata, *Theoretical Chemistry Accounts* **133**, 1487 (2014) (9 pages) [Isaiah Shavitt Special Issue], “Finite-temperature full configuration interaction.”
25. X. He, S. Ryu, and S. Hirata, *The Journal of Chemical Physics* **140**, 024702 (2014) (7 pages), “Finite-temperature second-order many-body perturbation and Hartree-Fock theories for one-dimensional solids: An application to Peierls and charge-density-wave transitions in conjugated polymers.”
26. S. Y. Willow and S. Hirata, *The Journal of Chemical Physics* **140**, 024111 (2014) (7 pages), “Stochastic, real-space, imaginary-time evaluation of third-order Feynman-Goldstone diagrams.”
27. J. Li, O. Sode, G. A. Voth, and S. Hirata, *Nature Communications* **4**, 2647 (2013) (7 pages), “A solid-solid phase transition in carbon dioxide at high pressures and intermediate temperatures.”
28. S. Hirata and X. He, *The Journal of Chemical Physics* **138**, 204112 (2013) (13 pages), “On the Kohn-Luttinger conundrum.”
29. S. Y. Willow, K. S. Kim, and S. Hirata, *The Journal of Chemical Physics* **138**, 164111 (2013) (5 pages), “Stochastic evaluation of second-order Dyson self-energies.”

Generalized Van Vleck Variant of Multireference Perturbation Theory

Mark R. Hoffmann
University of North Dakota
Chemistry Department
Grand Forks, ND 58202-9024
Email: mhoffmann@chem.und.edu

I. Project Scope

There is a continuing need to develop new, cutting edge theoretical and computational electronic structure methods to support the study of complex potential energy surfaces (PESs). While standard methods of computational chemistry are usually adequate for studying the ground electronic states of molecular species near their equilibrium geometries, reaction intermediates, transition states and excited states generally require advanced methods that take into account their multiconfigurational nature. Multireference (MRPT) and quasidegenerate (QDPT) perturbation theories have been demonstrated to be efficient and effective for the description of electron correlation in essentially arbitrarily complex molecules. Recent work demonstrated that the mathematically robust and physically correct structures in our MRPT, called Generalized van Vleck Perturbation Theory (GVVPT), are amenable to highly efficient algorithms. Specifically, second- and third-order approximations of GVVPT (i.e., GVVPT2 and GVVPT3) utilize routines in common with our efficient macroconfiguration-based, configuration-driven MRCISD¹. Consequently, theoretical and computational development can proceed by first addressing the structurally simpler equivalent CI problem. Chemical problems that are not addressed readily by other theoretical methods become accessible to MRPT or QDPT: problems such as the descriptions of large regions of excited electronic state PESs of polyatomics, especially when the characters of the excited states are doubly excited relative to the ground state, and the characterizations of multiple PESs of the same symmetry in close proximity. Within the scope of this grant, we apply these theoretical techniques primarily to combustion-relevant Group 15 and 16 oxides, and to develop their descriptions of derivative and spin-orbit nonadiabatic couplings.

II. Recent Progress

A.1. GVVPT2 Molecular Derivatives and Nonadiabatic Coupling Terms. The fully variational Lagrangian functional formalism² provided, in past reporting periods, the framework to construct analytical formulas for GVVPT2^{3, LoP1} and MRCISD⁴ molecular gradients and nonadiabatic coupling terms. Efforts to scale-up beyond transformation-based approaches, to iterative techniques, continue to be faced with puzzling convergence issues that manifest themselves in the need to use unfeasibly large Lanczos or Arnoldi subspaces. In the past year, our analysis shows that the source of the instability is either due to the use of numerical techniques appropriate to convex surfaces (e.g. the Lagrangian multiplier approach or, equivalently, constrained variational approach) to an inherently non-convex surface⁵ or due to particularly large near-null spaces⁶. It appears that this class of problem has not been previously addressed (or at least not widely discussed) in the molecular electronic structure literature. In words, the problem is that none of the wave function parameters (with the exception of the rather trivial configuration amplitudes of the effective Hamiltonian) are stationary with respect to energy. This contrasts strongly with the situation in MRCISD, in which the MCSCF parameters are non-stationary (with respect to the MRCISD energy), but the CI amplitudes are not only stationary but strict minima.

Efforts to understand the topology of the space of wave function parameters for GVVPT2 has led to the development of randomized single valued decomposition⁷ approaches to electronic structure. In completed studies, we have shown that randomized SVD produces meaningful and accurate solutions for an asymptotically stable (in the Lyapunov sense) series, such as produced by garden-variety, closed-shell MP2 or even by a quartically confined hydrogen atom. Work is underway to develop programs to support the large-scale (i.e., high dimensionality) vector spaces of relevance to GVVPT2.

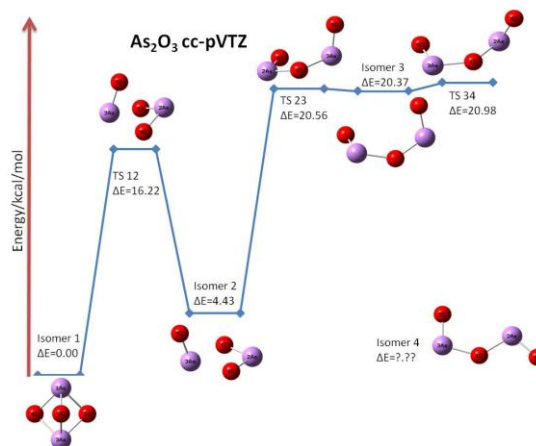
A.2. Relativistic Effects. Two types of relativistic effects are considered within the scope of this project.

One is the scalar (or spin-free) contribution and the other is spin-orbit coupling. The standard approach starts with approximations to the spin-free relativistic Hamiltonian (such as the second-order Douglas-Kroll-Hess (DKH) approximation or the zero-order regular approximation (ZORA)), and grafts onto such calculations spin-orbit coupling (often using some approximation to the Breit-Pauli operator). This protocol, while useful in many respects, is not entirely satisfactory.⁸ In past reporting periods, we realized a spin-free exact two-component (X2C)⁹ within our GVVPT2 approach.¹⁰ We have used it successfully on some highly problematic first- and second-row transition metal dimers (including the ever popular Cr₂). In particular, we have generated the first-ever complete potential energy curves of the lowest three states of Y₂, which correlate to the same asymptotic atomic states. Work during the preceding year examined ground- and low-lying potential energy curves of Ni₂ and has begun on the very challenging lanthanoid dimers. Our implementation of sf-X2C for MCSCF and GVVPT2 appears robust and, unless some hitherto unsuspected problem arises, can be considered completed.

The situation with spin-dependent relativistic effects is much less clear. Evidence suggests that a partitioning that is reminiscent of Douglas-Kroll-Hess, but with a different unperturbed operator, produces quite satisfactory results in low order.⁹ In the past two years, work has been refocused on producing an effective one-electron spin-orbit operator that is obtained from the Douglas-Kroll-Hess-like representation of spin dependence. It is conjectured that an effective one-electron spin-orbit operator can be developed that is related to the full spin-dependent DKH-like treatment in much the same manner that atomic mean field integrals¹¹ (AMFI) are derived from the Breit-Pauli operator will be efficacious. Calculation of the true one-electron contribution (i.e., essentially the pVp-type integral with the scalar product replaced by a vector product) using efficient Obara-Saika recursion has been refined in the preceding year for our software platform. Issues with attaining accuracy of the p×V×p integrals, comparable to pVp, have delayed progress. Particular attention is paid to the symmetry properties, as the effective one-electron integrals that include the two-electron contributions through AMFI, will have the same symmetries.

B.1. Selenium Oxides GVVPT2 calculations on the monoselenium oxides (SeO, SeO₂ and SeO₃) and some of their dimers (Se₂O₃ and Se₂O₅) were completed earlier in the study and the results published.^{LoP3} These studies are complete, and wait either for experimental validation or further investigation should a discrepancy be found.

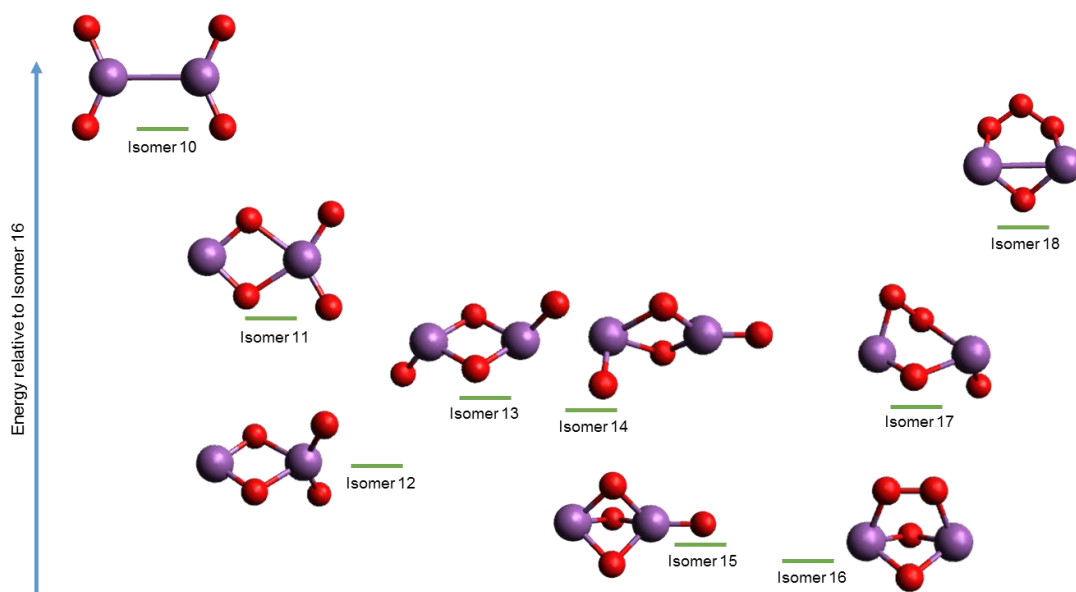
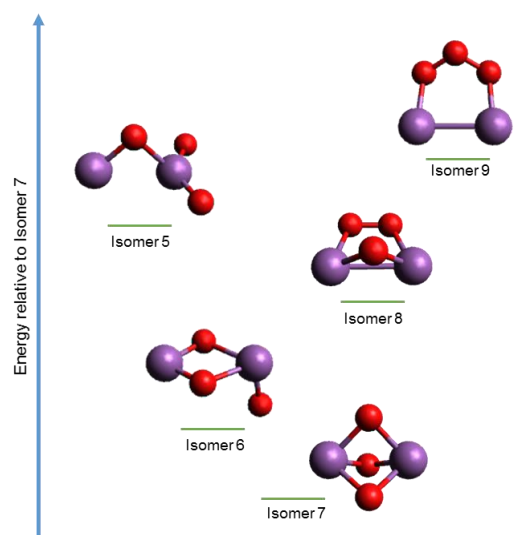
B.2. Arsenic Oxides Based on the completed selenium oxide work, and earlier work on nitrogen oxides, studies of plausible oxides containing one or two arsenic were performed.^{LoP4} The studies followed much the same protocol as did the selenium oxides study. Specifically, geometries were optimized as the B3LYP level, with verification of suitability against GVVPT2 and CR-CC(2,3)¹² for a select number of compounds, followed by single point energy calculations using GVVPT2, with comparison with CR-CC(2,3) for a number of the more traditionally bound isomers.



The active orbitals for the dimeric arsenic oxides were divided into two subgroups. The high (single point) energy occupied orbitals and the low energy unoccupied orbitals comprised the two groups. The model space was generated by allowing all one and two electron excitations from the first to the second group. This procedure, which used our macroconfiguration-based configuration generation program, allowed us to generate a small active space than nonetheless spanned the most important configurations of a large number of orbitals. Specifically, the energy calculations of the isomers and transition states of As₂O₃ used 20 active orbitals (i.e., the 2s and 2p of O, and the 4s and 4p of As) which contained 28 electrons (28e, 20o)

that were distributed as $G_1 = (13-18a_1 5a_2 6-9b_1 11-13b_2)$, in C_{2v} symmetry for isomer 1 (see Figure on previous page), $23-31a' 10-14a''$, in C_s symmetry for isomer 2, or simply $32-45a$ in C_1 symmetry) and $G_2 = (19-20a_1 6a_2 10b_1 14-15b_2)$, in C_{2v} symmetry, $32-35a' 15-16a''$, in C_s symmetry, or simply $46-51a$ in C_1 symmetry). For isomer 4 of As_2O_3 , the MCSCF calculation used 17 active orbitals (i.e., the 2p of O, and the 4s and 4p of As) which contained 22 electrons (22e, 17o) that were distributed as $G_1 = (27-33a' 9-12a'')$ and $G_2 = (34-38a' 13a'')$, while in the GVVPT2 treatment, the oxygen 2s dominated molecular orbitals were correlated which introduced three additional orbitals into the GVVPT2 occupied space ($24-26a''$, in C_s symmetry). GVVPT2 calculations were then performed allowing all one- and two-electron excitations from all active orbitals plus those from the lower energy occupied orbitals (i.e., “core”) to the higher energy unoccupied orbitals (i.e., “virtual”). Excitations from the core to the active, as well as all semi-internal excitations, were also allowed at the GVVPT2 stage.

B.3. Antimony Oxides The study of Sb_mO_n ($m=1,2; n=1, 3, 5$) was a major focus during the preceding year. The studies followed the protocol developed for Se_mO_n and As_mO_n . To begin, calculations validating the adequacy of B3LYP DFT geometries, relative to GVVPT2, CR-CC(2,3) and the few experimental results available, for select compounds were performed. Again, it was found that B3LYP geometries were quite reasonable and were used for the remainder of the calculations. The SDB-aug-cc-pVTZ basis set was used for antimony atoms and the corresponding aug-cc-pVTZ for oxygen atoms. SbO and SbO_2 were unremarkable, with bond lengths of 1.821 and 1.834 Å, respectively. In comparison, the corresponding bond lengths in arsenic were 1.637 and 1.644 Å. However, the relatively large size of Sb led to a marked difference in the case of the trioxides. Namely, SbO_3 shows pronounced elongation of the Sb–O bonds (to over 1.9 Å), to the extent that an O_2 moiety (with bond length of 1.504 Å) is seen to form. Since the dominant bonding motifs in the diantimony oxides (as was the case for selenium oxides and arsenic oxides) are arrangements of 2 and 3 oxygens attached to a metalloid center, the formation of pseudo-molecular O_2 provides more varied structures than found for the lighter elements. Moreover, increased proclivity to form Sb–Sb bonds is also observed.



III. Future Work

We expect continued progress in both the advancement of nuclear derivative and relativistic effects for GVVPT2 and MRCISD in applications to primarily Group 15 and 16 oxides. The highest priority vis-à-vis GVVPT2 continues to be resolution of the scale-up issue for gradients, which has proven itself to be a surprisingly difficult problem. Progress on scale-up of determination of the GVVPT2 nonadiabatic coupling matrix elements should follow rapidly, since the response matrix is identical between GVVPT2 gradients and nonadiabatic couplings. Using the in-house configuration-driven UGA code, spin-dependent Douglas-Kroll-Hess-like effective one-electron spin-orbit coupling matrix elements will be optimized for use in our program suite (“undmol”). Together with the recently realized inclusion of spin-free exact two-component (X2C) treatment of kinematic effects, robust relativistic MRCISD and GVVPT2 computer programs, appropriate for much of the periodic table, will be pursued. As production computer codes become available, we intend to refine the As_mO_n potential energy surfaces, but foresee continued emphasis on the Sb_mO_n surfaces. All-electron relativistic calculations will replace earlier work using ECPs. Similarly, our studies on O_3 , HO_3 and the $NO+NO$ surfaces, which were examined earlier by us at the GVVPT2 level using energy only calculations, will be re-examined as the new spin-orbit and nonadiabatic coupling codes become available. Once GVVPT2 derivative codes are optimized, an interface to the quasi-classical Newton-X dynamics code will be built. Plans are to consider dynamical and kinematical features of the surfaces.

IV. References

- ¹ W. Jiang, Y. G. Khait, and M. R. Hoffmann, *J. Phys. Chem. A* **113**, 4374 (2009).
- ² T. Helgaker and P. Jørgensen, *Adv. Quantum Chem.* **19**, 183 (1988); *Theor. Chim. Acta* **75**, 111 (1989).
- ³ D. Theis, Y. G. Khait, and M. R. Hoffmann, GVVPT2 energy gradient using a Lagrangian formulation, *J. Chem. Phys.* **135**, 044117 (2011).
- ⁴ Y. G. Khait, D. Theis, and M. R. Hoffmann, *Mol. Phys.* **108**, 2703 (2010).
- ⁵ A. Y. Azimov and R. N. Gasimov, *Cybern. Syst. Anal.* **38**, 412 (2002).
- ⁶ M. Byckling and M. Huhtanen, *SIAM J. Sci. Comput.* **36**, A88 (2014).
- ⁷ N. Halko, P. G. Martinsson and J. A. Tropp, arXiv:09094061v2 [math.NA] (2010).
- ⁸ W. Liu, *Mol. Phys.* **108**, 1679 (2010).
- ⁹ Z. Li, Y. Xiao, and W. Liu, *J. Chem. Phys.* **137**, 154114 (2012).
- ¹⁰ P. K. Tamukong, M. R. Hoffmann, Z. Li, and W. Liu, *J. Phys. Chem. A* **118**, 1489 (2014).
- ¹¹ B. A. Hess, C. M. Marian, U. Wahlgren, and O. Gropen, *Chem. Phys. Lett.* **251**, 365 (1996).
- ¹² P. Piecuch, M. Wloch, J. R. Gour, and A. Kinal, *Chem. Phys. Lett.* **418**, 467 (2006).

V. Publications and Submitted Journal Articles Supported by this Project 2012-2014

- ^{LoP1} Y. G. Khait, D. Theis, and M. R. Hoffmann, Nonadiabatic coupling terms for the GVVPT2 variant of multireference perturbation theory, *Chem. Phys.* **401**, 88 (2012).
- ^{LoP2} T. J. Dudley, J. J. Howard, and M. R. Hoffmann, Generalized Van Vleck Perturbation Theory Study of Chlorine Monoxide, *AIP Conf. Proc.* **1504**, 582 (2012).
- ^{LoP3} R. M. Mokambe, J. M. Hicks, D. Kerker, W. Jiang, D. Theis, Z. Chen, Y. G. Khait, and M. R. Hoffmann, GVVPT2 Multireference Perturbation Theory Study of Selenium Oxides, *Mol. Phys.* **111**, 1078 (2013).
- ^{LoP4} J. Hicks, Theoretical Studies of Oxides Relevant to the Combustion of Fossil Fuels, M.S. Thesis, Grand Forks, December 2013.

Theoretical Methods for Pressure Dependent and Electronically Nonadiabatic Kinetics

Ahren W. Jasper
Combustion Research Facility, Sandia National Laboratories
Livermore, CA 94551-0969
ajasper@sandia.gov

I. Program Scope

Elementary chemical kinetics calculations aid in the interpretation of experimental rate measurements and inform the development of comprehensive and detailed models of combustion. The predictive accuracy of chemical kinetics calculations is improving and generally approaching so-called “kinetic accuracy,” defined as a factor of 2 in the calculated rate coefficient. This term may be compared with the 1990s realization of “chemical accuracy” (~1 kcal/mol) in thermochemistry, when calculated thermochemistry began to be accurate enough to be used alongside experimental values. A similar situation is emerging in chemical kinetics thanks to ongoing improvements in computational power and theoretical methods. The principal goal of this project is to develop and validate new theoretical methods designed to broaden the applicability and improve the accuracy of theoretical chemical kinetics and to aid in the realization of kinetic accuracy for applications throughout combustion. The model developments we are presently focused on are: (1) predicting pressure dependence in elementary reactions using detailed master equation models of energy transfer informed by classical trajectories, (2) characterizing spin-forbidden kinetics using both multistate trajectory methods and statistical theories, and (3) predicting anharmonic vibrational properties for polyatomic molecules at combustion temperatures via Monte Carlo phase space integration.

II. Recent Progress

The pressure-dependent unimolecular kinetics of $\text{CH}_4 + \text{He}$ and $\text{C}_2\text{H}_3 + \text{He}$ were calculated in collaboration with Harding, Miller, and Klippenstein (Argonne). This work involved a combination of quantum chemistry, transition state theory, classical trajectory, and master equation methods. A detailed model for the collisional energy transfer function $P(E, J; E', J')$ was developed, which, unlike the well known single exponential down model, features: explicit angular momentum dependence, “long tail” collisions in both ΔE and ΔJ , and nonseparability of ΔE and ΔJ . The information required to parameterize such a model was obtained by calculating low-order moments of P using classical trajectories, against which the parameters of the model for P were optimized. Calculated rate coefficients obtained via this first-principles approach agreed with available experimental values within ~20%, which is similar to the reported accuracy of the experimental rates.

In other work, $P(E, J; E' = 97\% \text{ of the dissociation threshold of } \text{NO}_2, J' = 0)$ for $\text{NO}_2 + \text{Ar}$ was calculated as part of a joint theoretical/experimental study with Dave Chandler (Sandia). Both determinations of P showed biexponential (“long tail”) behavior, although the theoretical value for the long tail range parameter (275 cm^{-1}) was ~3x larger than the experimental value. The source of this discrepancy is unclear and may be related to the calculations’ neglect of excited electronic states.

We have used direct dynamics trajectories to study collisional energy transfer for $\text{CH}_4 + \text{He}$, Ne , and H_2 , $\text{C}_2\text{H}_5 + \text{He}$, and $\text{C}_2\text{H}_6 + \text{He}$. These results were used to test the accuracy of the pairwise approximation for the interaction potential. We further tested the accuracy of using pairwise interaction potentials obtained for $\text{CH}_4 + \text{M}$ for systems larger than methane, i.e., we tested the accuracy of using methane’s interaction parameters as universal $\text{C}_x\text{H}_y + \text{M}$ interaction parameters. For the saturated and lightly unsaturated systems we considered, results obtained using the universal $\text{C}_x\text{H}_y + \text{M}$ potentials were found to agree with direct dynamics results within the statistical uncertainties of

the calculations. The resulting universal potentials are very efficient relative to direct dynamics and may be used to study systems with dozens of C atoms.

We used the universal $C_xH_y + M$ potentials to evaluate Troe's collision efficiency (and an approximation to it) for seven atomic and diatomic baths and for molecules and radicals as large as octane. In total, 266 systems were studied, including normal, branched, cyclic, and unsaturated hydrocarbon molecules, as well as hydrocarbon radicals interacting with the seven baths. These collision efficiencies are simple functions of the first moment of the energy transferred in deactivating collisions, $\langle \Delta E_d \rangle$. We also considered the *rotational* collision efficiency for several systems by calculating the first moment of the angular momentum transferred in deactivating collisions, $\langle \Delta J_d \rangle$. Trends in the collision efficiencies with respect to the bath gas, its temperature, and the size and chemical structure of the hydrocarbon target were quantified and discussed.

We have carried out direct dynamics collisional energy transfer trajectory calculations, where the potential energy surface was calculated using MP2 and double- ζ basis sets. The quality of the MP2 potentials was validated by comparing cuts through the interaction potential with those from higher-level quantum chemistry methods and then optimizing details of the basis set and/or scaling the correlation energy. This MP2-based approach accurately reproduces anisotropies in the interaction potentials while remaining efficient enough for the trajectory calculations. This approach is particularly useful for systems with strongly anisotropic interaction potentials, such as $CH_4 + H_2O$. Collisional energy transfer for the $CH_4 + H_2O$ system was studied in detail, and the results for this bath were compared with those for atomic and diatomic baths. The collision efficiency of water relative to argon was found to depend on temperature and to vary from 3 at 300 K to 7 at 2000 K. We found that water completely equilibrated rotations only at low temperatures, and that none of the other baths completely equilibrated rotations at any of the temperatures considered. Nonetheless, low-pressure rate coefficients calculated using a model that assumes statistically equilibrated rotations were shown to be accurate at combustion temperatures. At low temperatures and for He, however, weak-collider-in- J effects were found to reduce the predicted low-pressure-limit rate coefficients by a factor of 2.

Several methods for predicting Lennard-Jones parameters for use as transport parameters in chemical kinetics models and for calculating collision rates in elementary kinetics were tested. The "one-dimensional minimization" method was found to be both accurate and efficient. In this method, the two interacting species are randomly oriented with respect to one another, and the interaction potential is minimized for this fixed orientation. The process is repeated for several orientations, and the resulting set of minimum energies and optimized center-of-mass separations are then averaged to obtain the Lennard-Jones parameters. Collision rates predicted using this method agree well with those based on tabulated parameters (typically within $\sim 10\%$) for a wide variety of systems.

Dilute gas binary diffusion coefficients of H, H_2 , and 4 n-alkanes in N_2 were calculated "exactly" (but within the classical approximation) using full-dimensional classical trajectories and the $C_xH_y + N_2$ potentials described above. The calculated diffusion coefficients were found to agree with Manion's (NIST) measured values for the n-alkanes in N_2 to within a few percent. Diffusion coefficients are often approximated using Lennard-Jones parameters in combustion models, and the exact classical results were used to test the severity of this approximation for such applications. For most systems at combustion temperatures, the Lennard-Jones approximation is likely accurate within $\sim 15\%$. For weakly interacting systems, however, more realistic treatments of the repulsive wall are required. For systems at low temperatures, the neglect of anisotropy may introduce non-negligible errors.

With Richard Dawes (MST), the high-pressure limit rate coefficient for the spin-forbidden reaction $O + CO \rightarrow CO_2$ was characterized in detail using a combination of high-level ab initio calculations, diabatic potential energy surface fitting, and electronically nonadiabatic trajectory calculations. The dynamic weighted MRCI method with a large basis set and near full valence active space was used to characterize the lowest-energy singlet and two lowest-energy triplet surfaces. The interpolated moving least squares (IMLS) method was used to fit accurate global analytic representations of the MRCI surfaces along with geometry-dependent calculated spin-orbit coupling

surfaces. The coherent switches with decay of mixing (CSDM) semiclassical trajectory method was then used to calculate spin-forbidden rate coefficients corresponding to the high pressure limit. Dynamical details of the coupled-state trajectories were used to analyze the appropriateness of typical assumptions appearing in spin-forbidden statistical models. A semiclassical statistical theory that includes models for electronic decoherence and multidimensional electronic transitions was developed and applied to this system. The rates obtained via the new statistical theory agree quantitatively with the CSDM results, so long as consistent thresholds are used, whereas a Landau-Zener-based statistical rate differs by $\sim 2\times$.

Efficient and accurate strategies for performing classical Monte Carlo phase space integrals (MCPSI) for calculating vibrational properties at combustion temperatures have been developed. We quantified that classical phase space integration could be done more efficiently using natural (z -matrix, curvilinear) coordinates instead of Cartesian normal mode coordinates. The classical MCPSI results are fairly accurate at combustion temperatures and can be made quantitative via simple Pitzer-Gwinn corrections to the classical anharmonic partition functions. To better enable practical MCPSI calculations for large molecular systems, we have approximated the full-dimensional phase space integral via a hierarchy of expressions based on so-called “ n -mode intrinsic” state densities. The 2-mode (pairwise) intrinsic state density, for example, is defined for a pair of vibrational coordinates as the vibrational state density not represented by the convolution of the one-dimensional state densities for each of the coordinates. The low-order state densities used to define the intrinsics are evaluated via MCPSI and contain all of the anharmonicity within the modes considered, and so the method may be applied to nonlocal motions such as torsions. The full-dimensional state density is then approximated via convolutions of the intrinsic state densities. We found that very accurate full-dimensional anharmonic state densities could be recovered by considering only pairwise intrinsic state densities. The computational cost scales much better with respect to the size of the system via this pairwise approximation relative to full-dimensional MCPSI.

III. Future Work

We will continue the development and application of predictive models for pressure-dependent chemical kinetics. These calculations require the development of both direct dynamics and fitted potential surface strategies for accurately describing the full-dimensional target-bath systems. We will extend the types of species considered to include those with halogen and oxygen atoms. Enhanced energy transfer for halogens and alcohols has been reported, and the trajectory studies will be used to elucidate the dynamical mechanisms of these enhancements. Several applications to combustion-relevant systems will be carried out. This work continues the collaboration with Miller and Klippenstein at Argonne.

The MCPSI method for calculating vibrational anharmonicity will continue to be applied and developed. We will focus on systems where the accuracy of existing vibrational anharmonicity approaches is not known, such as those involving constrained torsions and rings. We will also adapt our curvilinear n -mode MCPSI strategies for calculating classical fluxes through transition state dividing surfaces, where care must be taken when projecting out the curvilinear reaction coordinate.

We propose to continue to develop and validate theoretical methods for studying electronic state transitions in chemistry. We will continue to use short-time multistate trajectories to calculate improved spin-forbidden transition probabilities that, unlike the Landau-Zener approximation, include multidimensional dynamical and (de)coherence effects. These multidimensional transition probabilities will be used in statistical calculations, where complex reactions with competing spin-forbidden and spin-allowed pathways can be accurately studied.

IV. AITSTME

The AITSTME project (PI: Klippenstein, Argonne) is part of the Predictive Theory and Modeling component of the Materials Genome Initiative and supports the integration of several

chemical kinetics codes actively being developed at Argonne and Sandia. We have used our AITSTME funding to develop two published codes. `DINT` (sandia.gov/~ajasper/dint/) is a general trajectory code capable of nonadiabatic trajectory calculations (including those for the spin-forbidden kinetics) as well as collisional energy transfer calculations. `OneDMin` (sandia.gov/~ajasper/onedmin/) is a code for efficiently approximating Lennard-Jones parameters from full-dimensional interaction potentials via the “one-dimensional minimization” method described. In the next year, we will continue to develop several codes, with the AITSTME-funded goals of generalizing and documenting them such that they can usefully be made available online.

V. Publications supported by this project since 2013

1. **Multidimensional effects in nonadiabatic statistical theories of spin-forbidden kinetics: A case study of $^3\text{O} + \text{CO} \rightarrow \text{CO}_2$.** A. W. Jasper, *J. Phys. Chem. A*, submitted.
2. **Determination of the collisional energy transfer distribution responsible for the collision-induced dissociation of NO_2 with Ar.** J. D. Steill, A. W. Jasper, and D. W. Chandler, *Chem. Phys. Lett.*, submitted.
3. **The kinetics of propargyl radical decomposition.** S. J. Klippenstein, J. A. Miller, and A. W. Jasper, *J. Phys. Chem. A*, submitted.
4. **Thermal dissociation and roaming isomerization of nitromethane: Experiment and theory.** C. J. Annesley, J. B. Randazzo, S. J. Klippenstein, L. B. Harding, A. W. Jasper, Y. Georgievski, and R. S. Tranter, *J. Phys. Chem. A*, submitted.
5. **Detection and identification of the keto-hydroperoxide ($\text{HOOCH}_2\text{OCHO}$) and other intermediates during low-temperature oxidation of dimethyl ether.** K. Moshhammer, A. W. Jasper, S. M. Popolan-Vaida, A. Lucassen, P. Dievert, H. Selim, A. J. Eskola, C. A. Taatjes, S. R. Leone, S. M. Sarathy, Y. Ju, P. Dagaut, K. Kohse-Höinghaus, and N. Hansen, *J. Phys. Chem. A*, online (2015).
6. **Ab initio variational transition state theory and master equation study of the reaction $(\text{OH})_3\text{SiOCH}_2 + \text{CH}_3 \rightarrow (\text{OH})_3\text{SiOC}_2\text{H}_5$.** D. Nurkowski, S. J. Klippenstein, Y. Georgievskii, M. Verdicchio, A. W. Jasper, J. Akroyd, S. Mosbach, and M. Kraft, *Z. Phys. Chem.*, online (2015).
7. **“Third-body” collision efficiencies for combustion modeling: Hydrocarbons in atomic and diatomic baths.** A. W. Jasper, C. M. Oana, and J. A. Miller, *Proc. Combust. Inst.*, 35, 197 (2015).
8. **Predictive a priori pressure dependent kinetics.** A. W. Jasper, K. M. Pelzer, J. A. Miller, E. Kamarchik, L. B. Harding, and S. J. Klippenstein, *Science*, 346, 1212-1215 (2014).
9. **First-principles binary diffusion coefficients for H, H_2 , and four normal alkanes + N_2 .** A. W. Jasper, E. Kamarchik, J. A. Miller, and S. J. Klippenstein, *J. Chem. Phys.*, 141, 124313 (2014).
10. **Lennard-Jones parameters for combustion and chemical kinetics modeling from full-dimensional intermolecular potentials.** A. W. Jasper and J. A. Miller, *Combust. Flame* 161, 101 (2014).
11. **The collision efficiency of water in the unimolecular reaction $\text{CH}_4 (+ \text{H}_2\text{O}) \rightarrow \text{CH}_3 + \text{H} (+ \text{H}_2\text{O})$: One-dimensional and two-dimensional solutions of the low-pressure-limit master equation.** A. W. Jasper, J. A. Miller, and S. J. Klippenstein, *J. Phys. Chem. A* 117, 12243 (2013).
12. **Non-Born–Oppenheimer molecular dynamics of the spin-forbidden reaction $\text{O}(^3\text{P}) + \text{CO}(X^1\Sigma^+) \rightarrow \text{CO}_2(X^1\Sigma_g^+)$.** A. W. Jasper and R. Dawes, *J. Chem. Phys.* 139, 154313 (2013).
13. **Anharmonic vibrational properties from intrinsic n -mode state densities.** E. Kamarchik and A. W. Jasper, *J. Phys. Chem. Lett.* 4, 2430 (2013).
14. **Anharmonic state counts and partition functions for molecules via classical phase space integrals in curvilinear coordinates.** E. Kamarchik and A. W. Jasper, *J. Chem. Phys.* 138, 194109 (2013).
15. **Hydrogen-assisted isomerizations of fulvene to benzene and of larger cyclic aromatic hydrocarbons.** A. W. Jasper and N. Hansen, *Proc. Combust. Inst.* 34, 279 (2013).

Probing the Reaction Dynamics of Hydrogen-Deficient Hydrocarbon Molecules and Radical Intermediates via Crossed Molecular Beams

Ralf I. Kaiser

Department of Chemistry, University of Hawai'i at Manoa, Honolulu, HI 96822

ralfk@hawaii.edu

1. Program Scope

The major goals of this project are to explore experimentally in crossed molecular beams experiments the reaction dynamics and potential energy surfaces (PESs) of hydrocarbon molecules and their corresponding radical species, which are relevant to combustion processes. The reactions are initiated under single collision conditions by crossing two supersonic reactant beams containing radicals and/or closed shell species under a well-defined collision energy and intersection angle. By recording angular-resolved time of flight (TOF) spectra, we obtain information on the reaction products, intermediates involved, branching ratios of competing reaction channels, reaction energetics, and on the underlying reaction mechanisms. These data are of crucial importance to comprehend the formation of two key classes of molecules in combustion processes: resonantly stabilized free radicals (RSFRs) and (substituted) polycyclic aromatic hydrocarbons (PAHs).

2. Recent Progress

2.1. Formation of Resonantly Stabilized Free Radicals (RSFRs) in Crossed Beams

We expanded our studies on the formation of resonantly stabilized free radicals (RSFR) and explored the C_6H_5 and C_7H_7 potential energy surfaces (PES) via the reactions of dicarbon molecules with C_4H_6 (1-butyne, 2-butyne, 1,2-butadiene) [P14] and C_4H_6 isomers (isoprene, 1-methyl-1,3-butadiene) [P13, P15], respectively, under single collision conditions. Besides the synthesis of the aromatic *and* resonantly stabilized free benzyl ($C_6H_5CH_2$) radical [P13], these reactions revealed the synthesis of acyclic doublet radicals, which are isomers of the thermodynamically more stable phenyl and benzyl radicals, respectively. These studies were conducted in collaboration with Prof. Mebel (Florida International University) to investigate these bimolecular reactions computationally. The experimental and computational studies on the formation of resonantly stabilized free radicals (RSFR) under single collision conditions have been reviewed in P28.

2.2. Formation of (Methylsubstituted) Bicyclic Aromatic Molecules in Crossed Beams

Considering our unique capabilities to synthesize bicyclic PAH molecules indene (C_9H_8), naphthalene ($C_{10}H_8$), and dihydronaphthalene ($C_{10}H_{10}$) via reactions of the phenyl radical (C_6H_5) with unsaturated C3 (methylacetylene, allene) and C4 hydrocarbons (vinylacetylene, 1,3-butadiene) under single collision conditions, we have expanded our studies to the next level and investigated the formation of (di)methyl-substituted PAHs with indene and naphthalene cores (Figure 1) [P12, P16, P17, P19-P22, P24, P27, P30]. For this, we generated intense supersonic beams of meta and para tolyl (2- and 4-methylphenyl) radicals ($C_6H_4CH_3$) via photodissociation of m- and p-chlorotoluene (2- and 4-chlorotoluene) at 193 nm and probed the reactions with unsaturated C3 to C5 hydrocarbons. The bimolecular reactions of these phenyl-type radicals with C4 and C5 hydrocarbons were found to synthesize polycyclic aromatic hydrocarbons (PAHs) with naphthalene and 1,4-dihydronaphthalene cores in exoergic and *entrance barrier-less* reactions under single collision conditions. The reaction mechanism involves the initial formation of a van-der-Waals complex and addition of the phenyl-type radical to the C1 position of a vinyl-type group through a *submerged barrier*. Our investigations suggest that in the hydrocarbon reactant, the vinyl-type group must be in conjugation to a $-C\equiv CH$ or $-HC=CH_2$ group to form a *resonantly stabilized free radical (RSFR) intermediate*, which eventually isomerizes to a cyclic intermediate followed by hydrogen loss and aromatization (PAH formation). The studies were conducted in collaboration with Prof. Mebel (Florida International University) and Prof. Morakuma (Emory) to investigate the bimolecular reactions computationally.

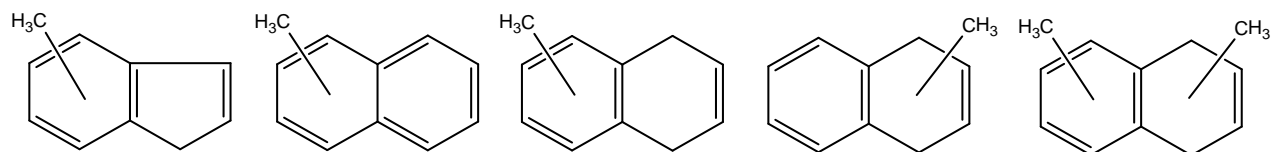


Figure 1: (Di)methylsubstituted PAHs with indene, naphthalene, and dihydronaphthalene cores formed in the reactions of phenyl-type radicals with C3 to C4 hydrocarbons.

2.3. Destruction of Aromatic Molecules - Photoionization Studies at the ALS

To yield further insights into the chemistry of the phenyl radical – the key growth species leading to PAH formation - under combustion relevant conditions, it is important to unravel not only the molecular growth pathways from reactions with (unsaturated) hydrocarbons, but also the destruction pathways of the phenyl radical upon reaction with molecular oxygen. Here, we expanded our collaboration with Musa Ahmed (LBNL) at the Chemical Dynamics Beamline and probed the outcome of the key reactions of the phenyl radical degradation by molecular oxygen in a high temperature ‘chemical reactor’ (P23). The reaction is conducted in a supersonic molecular beam through reaction of pyrolytically generated phenyl radicals (C_6H_5) with oxygen inside a heated silicon carbide tube (‘chemical reactor’). The products formed are then photoionized by vacuum ultraviolet (VUV) light from the Advanced Light Source at various photon energies from 7 to 11 eV to record photoionization efficiency (PIE) curves. Based on known PIE curves of known/calibrated isomers, the recorded PIE curves are then simulated to extract the nature of the products formed and their branching ratios over a range of combustion-relevant reaction vessel temperatures and pressures to extract the overall reaction channels.

2.4. Growth of Aromatic Molecules - Photoionization Studies at the ALS

Despite the popularity of the HACA mechanism in PAH formation, this mechanism has not been verified experimentally to date under controlled experimental conditions. Exploiting a ‘chemical reactor’ to simulate combustion conditions, we exposed for the first time that the HACA mechanism can produce the prototype PAHs naphthalene ($C_{10}H_8$) (P18), indene (C_9H_8), and acenaphthylene ($C_{12}H_8$) (P26) via reactions of phenyl (C_6H_5), benzyl ($C_6H_5CH_2$), and naphthyl radicals ($C_{10}H_7$) with acetylene (Figure 2). Note that neither anthracene nor phenanthrene have been detected as products of the reaction of naphthyl radicals with acetylene proposing that the HACA mechanisms is much less ‘versatile’ toward the formation of more complex PAHs than previously postulated thus opening up alternative reaction pathways such as a vinylacetylene-mediated synthesis of complex PAHs in combustion flames (P21). Our experiments at the Advanced Light Source have been also expanded to elucidate the formation of nitrogen-substituted aromatic molecules such as pyridine (P29) and (iso)quinoline (P25) as their simplest representatives.

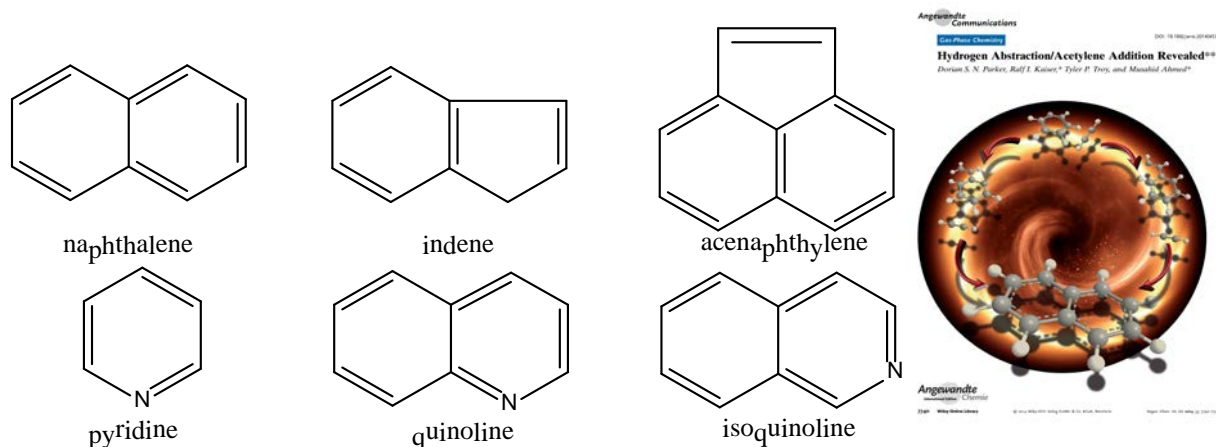


Figure 2: Structures of PAHs and nitrogen-bearing aromatic systems synthesized in the pyrolytic reactor.

3. Future Plans

We are planning to explore the formation of tricyclic PAHs carrying six- and five-membered rings such as anthracene/phenanthrene and fluorene under single collision conditions via reactions of bicyclic aromatic radicals like naphthyl and indenyl with C2 to C4 hydrocarbons (acetylene, methylacetylene, allene, vinylacetylene) in collaboration with Prof. Mebel. Further, we continue the elucidation of the destruction (oxidation) of PAH-based radicals such as naphthyl and indenyl in the pyrolysis reactor in collaboration with Musa Ahmed (LBNL) at the Chemical Dynamics Beamline.

4. Acknowledgements

This work was supported by US Department of Energy (Basic Energy Sciences; DE-FG02-03-ER15411).

5. Publications Acknowledging DE-FG02-03ER15411 (1/2012 – now)

- P1** A.V. Wilson, D.S.N. Parker, F. Zhang, R.I. Kaiser, *Crossed Beam Study of the Atom-Radical Reaction of Ground State Carbon (C^3P_j) with the Vinyl Radical (C_2H_3 , X^2A')*. Physical Chemistry Chemical Physics 14, 477-481 (2012).
- P2** R.I. Kaiser, X. Gu, F. Zhang, P. Maksyutenko, *Crossed Beams Reactions of Methylidyne [$CH(X^2\Pi)$] with D2-Acetylene [$C_2D_2(X^1\Sigma_g^+)$] and of D1-Methylidyne [$CD(X^2\Pi)$] with Acetylene [$C_2H_2(X^1\Sigma_g^+)$]*. Physical Chemistry Chemical Physics 14, 575-588 (2012).
- P3** R.I. Kaiser, D.S.N. Parker, M. Goswami, F. Zhang, V. Kislov, A.M. Mebel, *Crossed Beam Reaction of Phenyl and D5-Phenyl Radicals with Propene and Deuterated Counterparts – Competing Atomic Hydrogen and Methyl Loss Pathways*. Physical Chemistry Chemical Physics 14, 720-729 (2012).
- P4** D.S.N. Parker, F. Zhang, R.I. Kaiser, V. Kislov, A.M. Mebel, A.G.G.M. Tielens, *Low Temperature Formation of Naphthalene and Its Role in the Synthesis of PAHs in the Interstellar Medium*. Proceedings National Academy of Sciences USA (PNAS) 109, 53-58 (2012).
- P5** D.S.N. Parker, F. Zhang, Y. S. Kim, R. I. Kaiser, A. Landera, A. M. Mebel, *On the Formation of Phenylacetylene (C_6H_5CCCH) and D5-Phenylacetylene (C_6D_5CCCH) Studied under Single Collision Conditions*. Physical Chemistry Chemical Physics 14, 2997-3003 (2012).
- P6** F. Zhang, R.I. Kaiser, A. Golan, M. Ahmed, N. Hansen, *A VUV Photoionization Study of the Combustion-Relevant Reaction of the Phenyl Radical (C_6H_5) with Propylene (C_3H_6) in a High Temperature Chemical Reactor*. The Journal of Physical Chemistry A 116, 3541-3546 (2012).
- P7** R.I. Kaiser, D.S.N. Parker, F. Zhang, A. Landera, V.V. Kislov, A.M. Mebel, *Formation of PAHs and their Derivatives under Single Collision Conditions - The 1,4-Dihydronaphthalene Molecule as a Case Study*. The Journal of Physical Chemistry A 116, 4248-4258 (2012).
- P8** A. Golan, M. Ahmed, A. M. Mebel, R.I. Kaiser, *A VUV Photoionization Study on the Formation of Primary and Secondary Products in the Reaction of the Phenyl Radical with 1,3-Butadiene under Combustion Relevant Conditions*. Physical Chemistry Chemical Physics 15, 341-347 (2013).
- P9** B.B. Dangi, D.S.N. Parker, R.I. Kaiser, A. Jamal, A.M. Mebel, *A Combined Experimental and Theoretical Study on the Gas Phase Synthesis of Toluene under Single Collision Conditions*. Angew. Chemie Int. Ed. 52, 7186-7189 (2013).
- P10** B.B. Dangi, S. Maity, R.I. Kaiser, A.M. Mebel, *A Combined Crossed Beam and Ab Initio Investigation of the Gas Phase Reaction of Dicarbons (C_2 ; $X^1\Sigma_g^+/a^3\Pi_u$) with Propene (C_3H_6 ; X^1A')*. The Journal of Physical Chemistry A 117 11783-11793 (2013).
- P11** D.S.N. Parker, T. Yang, R. I. Kaiser, A. Landera, A. M. Mebel, *On the Formation of Ethynylbiphenyl ($C_{14}D_5H_5$; $C_6D_5C_6H_4CCH$) Isomers in the Reaction of D5-Phenyl Radicals (C_6D_5 ; X^2A_1) with Phenylacetylene ($C_6H_5C_2H$; X^1A_1) Under Single Collision Conditions*. CPL 595, 230-236 (2014).
- P12** D.S.N. Parker, B. B. Dangi, R.I. Kaiser, A. Jamal, M.N. Ryazantsev, K. Morokuma, A. Korte, W. Sander, *An Experimental and Theoretical Study on the Formation of 2-Methylnaphthalene ($C_{11}H_{10}/C_{11}H_3D_7$) in the Reactions of the Para-Tolyl (C_7H_7) and Para-Tolyl-d7 (C_7D_7) with Vinylacetylene (C_4H_4)*. The Journal of Physical Chemistry A, 118, 2709-2718 (2014).
- P13** B.B. Dangi, D.S.N. Parker, T. Yang, R.I. Kaiser, A.M. Mebel, *Gas Phase Synthesis of the Benzyl Radical ($C_6H_5CH_2$)*, Angew. Chemie Int. Ed. 53, 4608-4613 (2014).

- P14** D.S.N. Parker, S. Maity, B.B. Dangi, R.I. Kaiser, T. Labrador, A. M. Mebel, *Understanding the Chemical Dynamics of the Reactions of Dicarbon with 1-Butyne, 2-Butyne, and 1,2-Butadiene – Toward the Formation of Resonantly Stabilized Free Radicals*. Physical Chemistry Chemical Physics 16, 12150-12163 (2014).
- P15** B. B. Dangi, D.S.N. Parker, R.I. Kaiser, A.M. Mebel, *An Experimental and Theoretical Investigation of the Formation of C₇H₇ Isomers in the Bimolecular Reaction of Dicarbon Molecules with 1,3-Pentadiene*, Chem. Phys. Lett. 607 92-99 (2014).
- P16** T. Yang, D.S.N. Parker, B. Dangi, R.I. Kaiser, V.V. Kislov, A.M. Mebel, *Crossed Beam Reactions of the Reaction of Phenyl (C₆H₅; X²A₁) and D5-Phenyl Radical (C₆D₅; X²A₁) with 1,2-Butadiene (H₂CCCHCH₃; X¹A')*, The Journal of Physical Chemistry A 118, 4372–4381 (2014).
- P17** B.B. Dangi, T. Yang, R.I. Kaiser, A.M. Mebel, *Reaction Dynamics of the 4-Methylphenyl Radical (C₆H₄CH₃; p-Tolyl) with Isoprene (C₅H₈) - Formation of Dimethyldihydronaphthalenes*. Physical Chemistry Chemical Physics 16, 16805-16814 (2014).
- P18** D.S.N. Parker, R.I. Kaiser, T. Troy, M. Ahmed, *Hydrogen Abstraction Acetylene Addition Revealed!* Angew. Chemie Int. Edition 53, 7440-7444 (2014).
- P19** R.I. Kaiser, B.B. Dangi, T. Yang, D.S.N. Parker, A.M. Mebel, *Reaction Dynamics of the 4-Methylphenyl Radical (p-Tolyl) with 1,2-Butadiene (1-Methylallene) – Are Methyl Groups purely Spectators?* The Journal of Physical Chemistry A 118, 6181-6190 (2014).
- P20** D.S.N. Parker, B. B. Dangi, R.I. Kaiser, A. Jamal, K. Morokuma, *Formation of 6-Methyl-1,4-Dihydronaphthalene in the Reaction of the Para-Tolyl Radical with 1,3-Butadiene under Single Collision Conditions*. The Journal of Physical Chemistry A 118, 12111-12119 (2014).
- P21** R.I. Kaiser, D.S.N. Parker, A.M. Mebel, *Reaction Dynamics in Astrochemistry: Low Temperature Pathways to Polycyclic Aromatic Hydrocarbons (PAHs) in the Interstellar Medium (ISM)*. Annu. Rev. Physical Chemistry 66, 43-67 (2015).
- P22** T. Yang, L. Muzangwa, D.S.N. Parker, R. I. Kaiser, A.M. Mebel, *Synthesis of 2- and 1-Methyl-1,4-Dihydronaphthalene Isomers studied via the Crossed Beam Reactions of Phenyl Radicals (C₆H₅) with 1,3-Pentadiene (CH₂CHCHCHCH₃) and Isoprene (CH₂C(CH₃)CHCH₂)*. Physical Chemistry Chemical Physics, 17, 530-540 (2015).
- P23** D.S.N. Parker, R.I. Kaiser, T. P. Troy, O. Kostko, M. Ahmed, A.M. Mebel, *Toward the Oxidation of the Phenyl Radical and Prevention of PAH Formation in Combustion Systems*. The Journal of Physical Chemistry A (in press 2015).
- P24** T. Yang, D.S.N. Parker, B. B. Dangi, R. I. Kaiser, A.M. Mebel, *Formation of 5- and 6-Methyl-1H-Indene (C₁₀H₁₀) via the Reactions of the Para-Tolyl Radical (C₆H₄CH₃) with Allene (H₂CCCH₂) and Methylacetylene (HCCCH₃) under Single Collision Conditions*. Physical Chemistry Chemical Physics (in press 2015).
- P25** D.S.N. Parker, R.I. Kaiser, O. Kostko, T.P. Troy, M. Ahmed, A.M. Mebel, A.G.G.M. Tielens, *On the Synthesis of (Iso)Quinoline in Circumstellar Envelopes and Its Role in the Formation of Nucleobases in the Interstellar Medium*. The Astrophysical Journal (in press 2015).
- P26** D.S.N. Parker, R.I. Kaiser, O. Kostko, T.P. Troy, M. Ahmed, *Unexpected Chemistry from the Reaction of Naphthyl plus Acetylene Molecules*. Angewandte Chemie – International Edition (in press 2015).
- P27** L.G. Muzangwa, R.I. Kaiser, T. Yang, D.S.N. Parker, A.M. Mebel, A. Jamal, K. Morokuma, *A Crossed Molecular Beam and Ab Initio Study on the Formation of 6- and 7-Methyl-1,4-Dihydronaphthalene (C₁₁H₁₂) via the Reaction of Meta-Tolyl (C₇H₇) with 1,3-Butadiene (C₄H₆)*. Phys. Chem. Chem. Phys. (revised version submitted 2015).
- P28** A.M. Mebel, R.I. Kaiser, *Formation of Resonantly Stabilized Free Radicals via the Reactions of Atomic Carbon, Dicarbon, and Tricarbon with Unsaturated Hydrocarbons: Theory and Crossed Molecular Beams Experiments*. (submitted 2015).
- P29** D.S.N. Parker, R.I. Kaiser, O. Kostko, T.P. Troy, M. Ahmed, A.H.H, Chang. *On the Formation of Pyridine in the Interstellar Medium*. (submitted 2015).
- P30** T. Yang, L. Muzangwa, R.I. Kaiser, A. Jamal, K. Morokuma, *A Combined Crossed Molecular Beam and Theoretical Investigation of the Reaction of the Meta-Tolyl Radical with Vinylacetylene - Toward the Formation of Methylnaphthalenes*. (submitted 2015).

DYNAMICAL ANALYSIS OF HIGHLY EXCITED MOLECULAR SPECTRA

Michael E. Kellman

Department of Chemistry, University of Oregon, Eugene, OR 97403

kellman@uoregon.edu

PROGRAM SCOPE:

Highly excited vibration-rotation dynamics of small molecular species, including those approaching the threshold of reaction, are crucial to understanding fundamental processes important for combustion. Our goal is to develop theoretical tools to analyze spectra and dynamics of these highly excited systems. A persistent theme is the use of effective spectroscopic fitting Hamiltonians to make the link between experimental data and theoretical dynamical analysis. A recent new line of research has begun to explore small quantum systems (such as a single combustion molecule) in interaction with a quantum environment. There are three main areas currently under investigation. (I) The role of bifurcations and the birth of new modes in bifurcations from the low energy normal modes (II) Quantum dynamics of small systems entangled with an environment, divided into two main areas: (A) Quantum thermodynamics, free energy, and the entropy of the universe; and (B) Environmental monitoring and measurement in competition with thermalization. I address each of these below.

RECENT PROGRESS AND FUTURE PLANS. Our current research is pursuing the three main areas described above, with a natural division into I, IIA, and IIB.

I. CRITICAL POINTS BIFURCATION ANALYSIS OF EFFECTIVE SPECTROSCOPIC HAMILTONIANS.

This work continues with Dr. Vivian Tyng. Ref. 2 was done in collaboration with DOE Combustion PI Hua Guo of the University of New Mexico.

Our emphasis on the critical points bifurcation analysis of effective spectroscopic Hamiltonians has continued in recent years [2,5]. In a project conducted with Dr. Vivian Tyng, we are completing our first bifurcation analysis for a rotation-vibration effective Hamiltonian, using a recent spectroscopic Hamiltonian for CO₂ fit to experimental data.

We have in hand the successful critical points analysis of rotation-vibration dynamics of CO₂ on the effective Hamiltonian fit to experimental data. The analysis gives relatively simple, intelligible dynamics, comparable to but significantly extending what has been obtained with pure vibrational dynamics. At $J = 0$ there is only the bifurcation tree of normal modes and Fermi resonance modes. Then, as J increases, we find a principal "Coriolis mode" that bifurcates out of one of the Fermi resonance modes at very low J , with further finer branching of the tree into Coriolis modes with increasing J .

The challenge to completing this work has been the physical interpretation of the results of the critical points analysis. What is the physical nature of the rotation-vibration motion in the new bifurcation rotation-vibration "modes" of the molecule? The natural starting point is the standard picture of the rotation-vibration motion of a symmetric top. In the new Coriolis modes of CO₂

determined in the bifurcation analysis, things will be somewhat but not altogether different from the symmetric top; and also with some similarities to the asymmetric top.

II. QUANTUM DYNAMICS OF SMALL MOLECULAR SYSTEMS ENTANGLED WITH AN ENVIRONMENT.

We have focused for many years on the dynamics of highly excited molecular systems in isolation. This has been necessary to achieve significant advances in understanding the dynamics of strongly coupled, anharmonic molecules. Recently we have begun to turn our attention to embedding these systems in an environment. This inevitably is essential to understanding the behavior of highly excited molecules in the combustion context. A proper full quantum description requires treatment of “entanglement” (in a strictly defined quantum sense) of the system in some kind of environment, described quantum mechanically in terms of a Hamiltonian operator, with system-environment interaction. The behavior of small quantum entangled systems is of great interest in many areas of fundamental and applied physics and physical chemistry. The particular questions we have begun investigating fall first in the domain of “quantum thermodynamics” of small molecular systems; and then more generally in the domain of “monitoring of the system by the environment” including both “measurement” and “thermalization.” Quantum thermodynamics is of obvious relevance to combustion systems, where small molecular species are embedded in a thermal, in general non-equilibrium environment. Environmental monitoring is less familiar and is detailed below. With former postdoc George Barnes, now at Siena College, one paper has been published in *J. Chem. Phys.* [3] and another is near completion [4]. A paper is in progress with graduate student Philip Lotshaw [6].

IIA. QUANTUM THERMODYNAMICS

Thermal behavior in a small quantum entangled system-environment.

In the first of these papers [3], simulations were performed of a small quantum system interacting with a quantum environment. The system consists of various initial states of two harmonic oscillators coupled to give normal modes. The environment is “designed” by its level pattern to have a thermodynamic temperature. A random coupling causes the system and environment to become entangled in the course of time evolution. We examine the time-dependent quantum behavior of various initially prepared pure states as the oscillator system interacts with the quantum environment. The total system + environment “universe” is in a pure state described by the density matrix ρ_{se} . The statistical behavior of the system is described by the reduced density matrix (RDM) $\rho_s = \text{Trace } \rho_{se}$. Visual insight into the dynamics of the system is obtained by examining spatial density distributions of the system RDM ρ_s .

Approach to a Boltzmann distribution is observed, and effective fitted temperatures close to the designed temperature are obtained. All initial pure states of the system are driven to equilibrium at very similar rates, with quick loss of memory of the initial state. The time evolution of the von Neumann entropy is calculated as a measure of equilibration and of quantum coherence and gives reasonable results. This is gratifying, but not unexpected. The next topic goes well beyond these “classical thermodynamics” results.

Entropy of the universe, free energy, and the second law.

In a paper nearing completion with Dr. Barnes [4], we are investigating the fundamental meaning of the second law of thermodynamics in the context of quantum thermodynamics. The well-known standard statement of the second law in “classical thermodynamics” is that the entropy of the universe is always increasing in a spontaneous process: $\Delta S_{\text{univ}} > 0$. The problem with this is that the standard quantum definition of entropy due to von Neumann yields $S^{\text{vN}} = 0$ for a pure quantum state. That means if we consider a small system-environment “universe” to be in a pure quantum state, as is the case in our simulations, the von Neumann entropy of the universe $S^{\text{vN}}_{\text{univ}}$ is always zero! This seems like a perverse state of affairs. We take the view that there is an obvious conflict with standard “classical” thermodynamics. To our surprise, this conflict does not seem to have been addressed widely in the small-systems quantum thermodynamics community. We have devised an alternative definition of the entropy of the universe that has the potential to be in accord with the second law. For a model quantum system becoming entangled with a quantum environment, we perform simulations of time dependent dynamics. We have tested the new definition of the entropy of the universe against the standard thermodynamic relation $\Delta F_{\text{sys}} = -T \Delta S_{\text{univ}}$, calculating the properties of the system using the reduced density matrix and standard von Neumann entropy. Good agreement between the two sides is obtained, showing the compatibility of a definition of entropy for the pure state of a universe with the statements of the second law and the concept of free energy.

Excess entropy production in time-dependent quantum states.

As stated above, for reasonable systems the free energy change and the change in the entropy of the universe match well via the approximate equality $\Delta F_{\text{sys}} = -T \Delta S_{\text{univ}}$ in the simulations, in accord with standard thermodynamics. This raises the interesting question of whether it is possible to have deviations in quantum systems from this “classical” thermodynamic behavior. The reason for suspecting this might be the case is that classical thermodynamics is based on the notion of the microcanonical ensemble, which is predicated upon a fixed, well-defined energy (or energy shell). However, in quantum mechanics it is of course possible to have time-dependent states which do not have a well-defined energy i.e. have an energy uncertainty ΔE governed by the time-energy uncertainty relation. One might therefore suspect that time-dependent states would have behavior in which the entropy of the universe deviates from the “classical microcanonical” relation $\Delta F_{\text{sys}} = -T \Delta S_{\text{univ}}$. In simulations we have found that this is indeed the case, with excess entropy production i.e. $T \Delta S_{\text{univ}} > -\Delta F_{\text{sys}}$. We have found that this is indeed the case. Moreover, we find a near-linear relation between the excess entropy production and the quantum energy uncertainty i.e. $\Delta S_{\text{univ}(\text{excess})} \sim \Delta E$. This work is now being prepared for publication [6]. An interesting future question is the following. In situations where there is a mismatch between the entropy change ΔS_{univ} and the free energy change $-\Delta F_{\text{sys}}$, which quantity serves as the true measure of spontaneity? We are working to define model systems where there might be a mismatch and where this question can be answered computationally.

IIB. ENVIRONMENTAL MONITORING AND MEASUREMENT IN COMPETITION WITH THERMALIZATION IN SMALL MOLECULES IN A THERMAL ENVIRONMENT.

Work in the foundations of quantum mechanics in recent years has focused on the “quantum measurement problem.” This is the question of why we see certain “real-world” outcomes instead of bizarre outcomes that nonetheless are perfectly reasonable within the basic quantum formalism. The outstanding exemplar of this is the “Schrodinger cat” which is always observed to be either dead or alive, rather than in some superposition of both dead and alive. The

explanation that has emerged invokes the idea of “decoherence” of the system as it becomes entangled with the environment (e.g. the recent widely-used book “Decoherence and the Quantum-to-Classical Transition” by M. Schlosshauer). Thus, an initial superposition Dead + Alive becomes entangled with the environment and decoheres into Dead and Alive entangled branches of system + environment. In effect, the environment, through random interactions with the system, essentially monitors or measures the system.

An aspect of this which has received very little attention involves competition between thermalization and measurement by the environment. Thus, a system in a certain superposition has some degrees of freedom that become thermalized, while other degrees of freedom remain unthermalized and essentially in the process of environmental monitoring maintain their initial “form” or “structure.” We are investigating this competition in simulations of small molecules in a thermal environment – e.g. H₂O in a hot environment, a model with an obvious relation to combustion systems. Generally, nonlinear molecular systems with strong resonance couplings, such as coupled stretch normal modes in 2:2 resonance, or 2:1 Fermi resonance systems, have marked phase space structure, including stable and unstable modes born in bifurcations. There are many examples of these species of relevance in combustion that are good candidates for investigation in our simulations.

Recent papers, published or referenced above, related to DOE supported research:

1. G.L. Barnes and M.E. Kellman, “Visualizing the Zero Order Basis of the Spectroscopic Hamiltonian,” J. Chem. Phys. 136, 024114 (2012).
2. J. Ma, D. Xu, H. Guo, V. Tyng, and M.E. Kellman, “Isotope effect in normal-to-local transition of acetylene bending modes” J. Chem. Phys. 136, 014304 (2012).
3. G.L. Barnes and M.E. Kellman, “Time Dependent Quantum Thermodynamics of a Coupled Quantum Oscillator System in a Small Thermal Environment,” J. Chem. Phys. 139, 214108 (2013).
4. G.L. Barnes and M.E. Kellman, “Quantum Thermodynamics, Entropy of the Universe, Free Energy, and the Second Law” manuscript in preparation.
5. V. Tyng and M.E. Kellman, “Rotation-Vibration Dynamics of CO₂ from the Effective Spectroscopic Hamiltonian” manuscript in preparation.
6. P. Lotshaw and M.E. Kellman, “Excess Entropy Production in Time-Dependent Quantum Thermodynamics of Molecular Systems” manuscript in preparation.

Time-Resolved Optical Diagnostics

Christopher J. Kliewer (PI)
Combustion Research Facility, Sandia National Laboratories
P.O. Box 969, MS 9055
Livermore, CA 94551-0969
cjkliw@sandia.gov

Program Scope

This program focuses on the development of innovative laser-based techniques for measuring temperature and concentrations of important combustion species as well as the investigation of fundamental physical and chemical processes that directly affect quantitative application of these techniques. Our development efforts focus on crossed-beam approaches such as time-resolved nonlinear wave-mixing. A critical aspect of our research includes the study of fundamental spectroscopy, energy transfer, and photochemical processes. This aspect of the research is essential to the development of accurate models and quantitative application of techniques to the complex environments encountered in combustion systems. These investigations use custom-built tunable picosecond (ps) and commercial femtosecond lasers, which enable efficient nonlinear excitation, provide high temporal resolution for pump/probe studies of collisional processes, and are amenable to detailed physical models of laser-molecule interactions.

Recent Progress

In the previous year, we have extended our recent developments of both multidimensional and supercontinuum based coherent anti-Stokes Raman spectroscopy (CARS) measurements. Accurate time- and spatially resolved measurement of temperature remains a critical focus of combustion diagnostics. The local temperature field and gradient not only govern chemical reaction rates but also physical quantities such as gas expansion and heat transfer. CARS has been applied for concentration measurements and ro-vibrational thermometry in gas-phase applications for more than three decades, and is often held as the gold standard optical technique for the non-intrusive determination of temperature in

gas-phase systems, but the technique has only recently been extended from point-wise measurement to multi-dimensional spatially correlated measurements in our lab.

ID-CARS imaging of head-on- quenching flame wall interactions: Extending CARS measurements to single-laser-shot imaging modalities allows for the measurement of spatially correlated data, such as the instantaneous thermal gradient. Further, one of the key advantages of the coherent nature of the CARS signal is the ability to probe very near to scattering interfaces such as a burner nozzle or wall. Whereas linear optical techniques such as filtered Raleigh/Raman scattering may provide excellent thermometry and species concentrations in combustion, these techniques fail near scattering objects such as a burner surface, near a wall, or in sooting environments. In collaboration with Prof. Andreas Dreizler (TU Darmstadt) we have continued the study the flame-wall interaction by time-resolved probing of turbulent

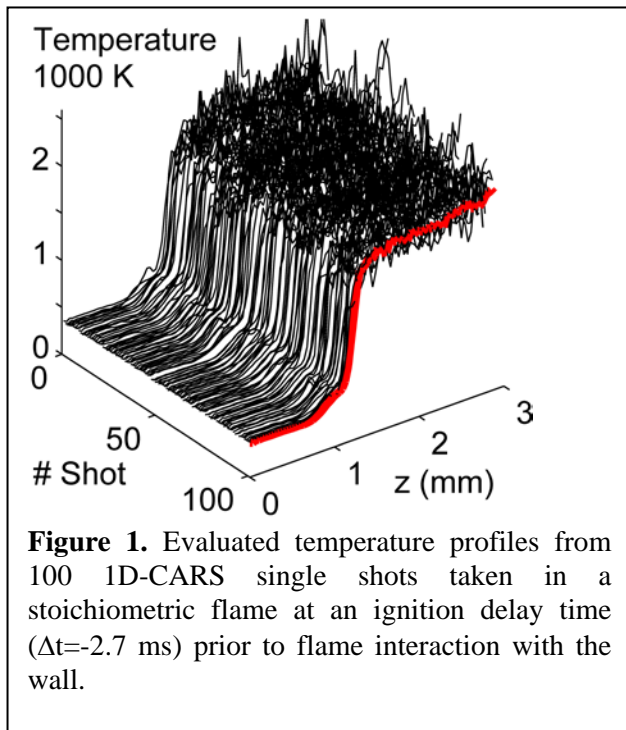


Figure 1. Evaluated temperature profiles from 100 ID-CARS single shots taken in a stoichiometric flame at an ignition delay time ($\Delta t = -2.7$ ms) prior to flame interaction with the wall.

combusting flows impinging and quenching upon a metal surface. Both steady-state and time-resolved ignition delay studies were performed to study fluctuations of the instantaneous thermal gradient upon surface quenching of the combustion reaction in a Reynolds number 5,000 turbulent methane / air flame impinging on a cool steel surface. This data benchmark will greatly guide model development and understanding of interaction of flames with walls for the head-on-quenching canonical configuration.

Ultrabroadband CARS for combustion studies: Over the years, many complex dual-pump CARS schemes have been developed with the aim of detecting up to a few molecular species simultaneously, specific to the laser frequencies employed. Similarly, CARS schemes have been developed to simultaneously probe more than one manifold of a molecule, such as the pure-rotational and Q-branch of N_2 with the aim of improved accuracy in mode-specific thermometry. Last year, we demonstrated a capability for crossed beam ultrabroadband CARS, allowing for high spatial and spectral resolution, and the simultaneous detection of pure-rotational, and vibrational O-, Q-, and S-branches of any molecules present in significant concentration ($>1\%$) with Raman-active transitions up to 4200 cm^{-1} . The 45 femtosecond output of our laser is sent through a hollow-core fiber filled with Argon inducing a significant amount of spectral broadening primarily through self phase modulation. This pulse is then compressed to $\sim 7\text{ fs}$ using negatively chirped optics. The two-beam CARS phase matching scheme

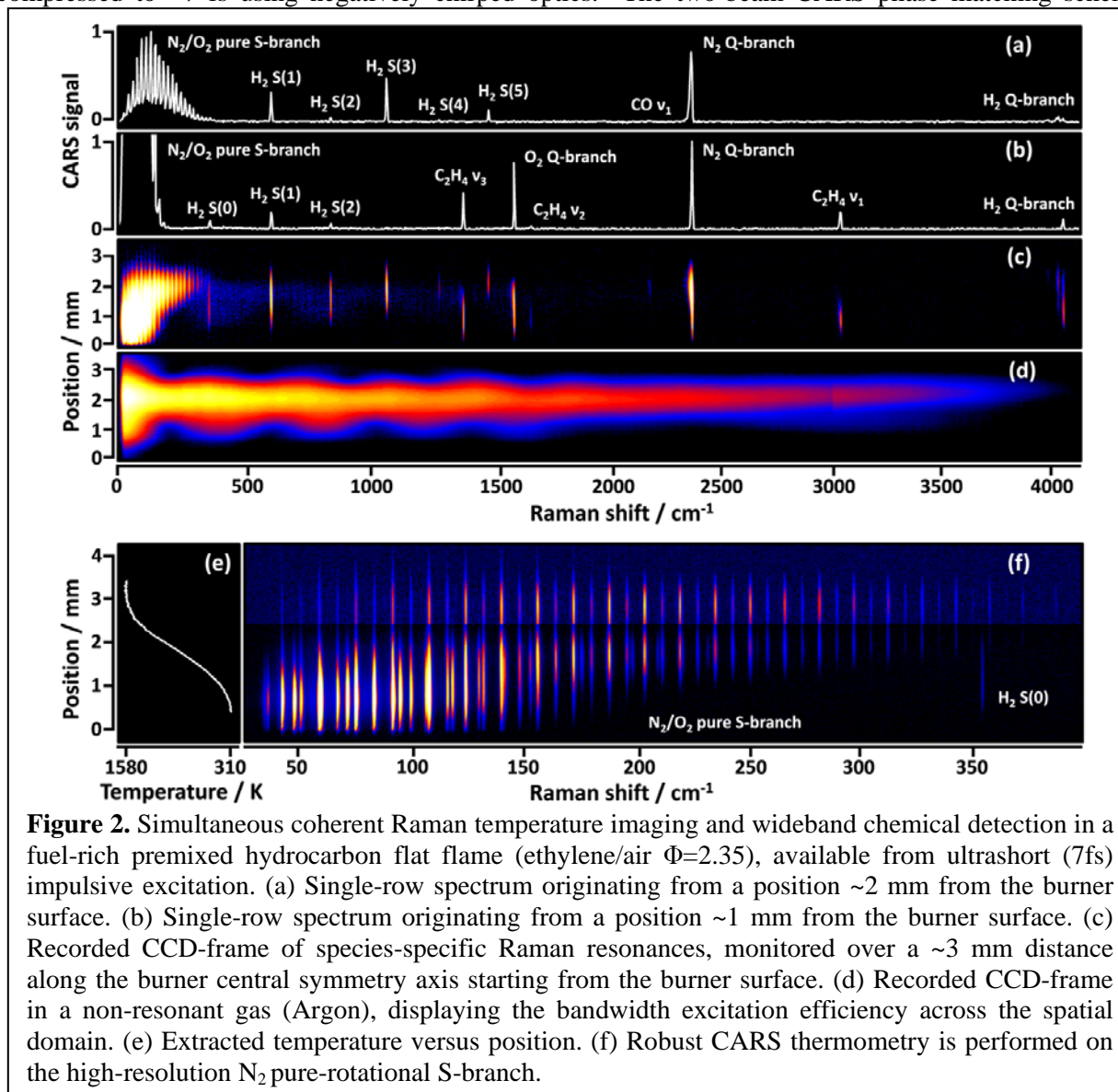


Figure 2. Simultaneous coherent Raman temperature imaging and wideband chemical detection in a fuel-rich premixed hydrocarbon flat flame (ethylene/air $\Phi=2.35$), available from ultrashort (7fs) impulsive excitation. (a) Single-row spectrum originating from a position $\sim 2\text{ mm}$ from the burner surface. (b) Single-row spectrum originating from a position $\sim 1\text{ mm}$ from the burner surface. (c) Recorded CCD-frame of species-specific Raman resonances, monitored over a $\sim 3\text{ mm}$ distance along the burner central symmetry axis starting from the burner surface. (d) Recorded CCD-frame in a non-resonant gas (Argon), displaying the bandwidth excitation efficiency across the spatial domain. (e) Extracted temperature versus position. (f) Robust CARS thermometry is performed on the high-resolution N_2 pure-rotational S-branch.

ensures that the ultrashort pump and Stokes fields are automatically overlapped temporally, while allowing for the high spatial resolution of a crossed probe technique. Recently, we have performed ultrabroadband CARS measurements in a standardized sooting flat flame, and some of these results are shown in Figure 2. These measurements served two purposes. Firstly, we demonstrated that the supercontinuum-based CARS technique can be applied in a flame to measure many species simultaneously. Secondly, the measurements served to benchmark the new technique against a known standard flame, to assign a level of accuracy and precision to the method and spectral fitting routines.

Future Work

Measurements of side-wall-quenching flame-wall interactions. Head-on-quenching and side-

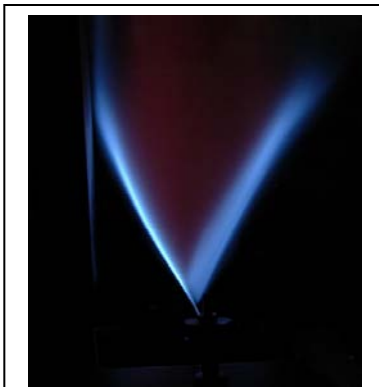


Figure 3. Photograph of the rod stabilized V-shaped flame impinging on a metal wall.

wall quenching are the two canonical configurations for studying flame-wall interactions for which significant efforts have been made in the numerical simulation community. Having successfully demonstrated a benchmarking thermometry dataset for head-on-quenching within the thermal boundary layer using the fs/ps 1D-CARS technique, we will continue to the second canonical burner configuration for assessing flame-wall interactions. In further collaboration with Andreas Dreizler (Darmstadt, Germany) we will probe a side-wall-quenching process as a function of ignition delay time to assess flame structures and fluctuations within the thermal boundary layer of this second important class of quenching induced by flame-wall interactions. Figure 3 shows a photograph of the flame to be studied in this collaboration. A V-shaped flame produced by a rod-stabilized burner will impinge on a cooled steel wall. Varying amounts of turbulence will be studied at Reynolds number $Re=5,000$ by insertion of a turbulence grid in the jet nozzle consisting of small diameter holes. While 1D-CARS measurements in the wall-normal

direction were sufficient for studying the head-on-quenching configuration, the implementation of 2D-CARS will be required in this side-wall-quenching system.

Multiplexing 2D-CARS with particle imaging velocimetry (PIV). With the recent development of the first 2D-CARS measurements in our lab, our plan is to begin multiplexing the diagnostic with other techniques to gain access to joint statistics not previously attainable, such as the instantaneous thermal field and flow field obtained by combining 2D-CARS with PIV measurements, respectively. While other attempts have been made in the past to measure these two scalar fields simultaneously, none have the accuracy and precision achievable in CARS measurements. Collaborating with Dr. Jonathan Frank (CRF, Sandia), we will perform joint PIV and 2D-CARS in turbulent DME flames of current interest in Jonathan's lab. Planar CARS measurements before and after the addition of the PIV seeding particles will ensure the negligible effects of the seed particles on the combustion process. Initially, we will utilize the four time synchronized picosecond YAG lasers in our lab to provide four PIV frames per 2D-CARS frame. Although, in the future these diagnostics may be employed at multi-kHz repetition rates with upgraded laser repetition rate. The datasets garnered will serve as benchmarks of high accuracy for comparison to numerical simulations of turbulent combustion, and will thus aid in the endeavor to understand interactions between flame turbulence and chemistry.

Direct measurement of N_2 -Fuel and N_2 - H_2O broadening coefficients. With the successful development of the time-domain technique for acquiring high-accuracy S-branch broadening coefficients, demonstrated thus far for the N_2 - N_2 and N_2 - H_2 collisional systems, we propose to continue the collaboration with Per-Erik Bengtsson of Lund University, Sweden, to tackle the relative paucity of broadening coefficient data in the literature for air-fuel collisional systems. Initial studies will focus on the collisional broadening of N_2 and O_2 when perturbed by DME, ethane, ethylene, propane, and propylene. Accurate broadening models must be developed for these collisional environments, especially at elevated pressures. We will alter our current time-domain CARS code to implement these new

linewidth libraries and test the validity of the model in our newly constructed high-pressure, high-temperature cell.

Collaborative implementation of 2-beam 1D and 2D fs/ps rotational CARS (Collaboration with Barlow). With the implementation of our hybrid fs/ps rotational CARS system and the continued development of both 1D and 2D rotational CARS, opportunity to leverage the technique for other programs within the CRF exists. In general, the combined Rayleigh/Raman measurements performed in Rob Barlow's lab are not capable of probing near a burner surface or bluff body because of scattering of the laser beams interfering with the Rayleigh measurement. However, accurate measurements of thermal boundary layers on burner surfaces are needed in order to understand mechanisms of flame stabilization and provide boundary conditions for computational simulations. We plan initial experiments to obtain single-laser-shot 1D and possibly 2D temperature measurements close to the bluff body flame stabilizer in the annular premixed burner recently constructed in his laboratory. Access to the region within 5 mm of the surface is not possible with the current setup, but in the 2-beam CARS arrangement, the instantaneous temperature field may be acquired to within microns of the surface.

Improved precision in species concentration measurements for ultrabroadband CARS. While we have demonstrated high accuracy and surprisingly good precision (< 1% fluctuations) in thermometry utilizing supercontinuum-based CARS, the ultimate purpose of developing this technique is for enhanced simultaneous relative species concentration measurements. There is still significant room for improvement in the precision of relative species concentration measurements, for which the single-laser-shot precision varies depending on the separation of Raman transition frequencies. We plan to implement a simultaneous referencing technique for monitoring the single-shot nonlinear excitation profile of the chaotic supercontinuum source. This will be implemented in one of two ways. The nonresonant signal may be separated through polarization and used as a single-laser shot reference of the excitation bandwidth. Alternatively, the pump/Stokes and probe beams could be refocused into a high pressure cell filled with a nonresonant gas such as Argon. The single-shot spectrum taken in this gas may serve as a reference for the nonlinear excitation profile.

Journal publications supported by this BES project (2013-2015)

1. A. Bohlin and C. J. Kliewer, "Communication: Two-dimensional gas-phase coherent anti-Stokes Raman spectroscopy (2D-CARS): Simultaneous planar imaging and multiplex spectroscopy in a single laser shot," *J. Chem. Phys.* **138**, 221101 (2013).
2. A. Bohlin, B. D. Patterson, and C. J. Kliewer, "Simplified two-beam rotational CARS signal generation demonstrated in 1D," *J. Chem. Phys.* **138**, 081102 (2013).
3. S. P. Kearney, D. J. Scoglietti, and C. J. Kliewer, "Hybrid femtosecond/picosecond rotational coherent anti-Stokes Raman scattering temperature and concentration measurements using two different picosecond-duration probes," *Opt. Express* **21**, 12327-12339 (2013).
4. B. D. Patterson, Y. Gao, T. Seeger, and C. J. Kliewer, "Split-probe hybrid femtosecond/picosecond rotational CARS for time-domain measurement of S-branch Raman linewidths within a single laser shot," *Opt. Lett.* **38**, 4566-4569 (2013).
5. A. Bohlin and C. J. Kliewer, "Two-beam ultrabroadband coherent anti-Stokes Raman spectroscopy for high resolution gas-phase multiplex imaging," *Appl. Phys. Lett.* **104**, 031107 (2014).
6. A. Bohlin and C. J. Kliewer, "Diagnostic imaging in flames with instantaneous planar coherent Raman spectroscopy," *J. Phys. Chem. Lett.* **5**, 1243-1248 (2014).
7. A. Bohlin and C. J. Kliewer, "Single-shot hyperspectral coherent Raman planar imaging in the range 0-4200 cm⁻¹," *Appl. Phys. Lett.* **105**, 161111 (2014).
8. A. Bohlin, M. Mann, B.D. Patterson, A. Dreizler, C. J. Kliewer, "Development of two-beam femtosecond/picosecond one-dimensional rotational coherent anti-Stokes Raman spectroscopy: time-resolved probing of flame wall interactions," *Proc. Combust. Inst.* **35**, 3723-3730 (2015).
9. A. Bohlin and C. J. Kliewer, "Direct Coherent Raman Temperature Imaging and Wideband Chemical Detection in a Hydrocarbon Flat Flame," *J. Phys. Chem. Lett.* **6**, 643-649 (2015)

THEORETICAL CHEMICAL KINETICS

Stephen J. Klippenstein
Chemical Sciences and Engineering Division
Argonne National Laboratory
Argonne, IL, 60439
sjk@anl.gov

Program Scope

The focus of this program is the theoretical estimation of the kinetics of elementary reactions of importance in combustion chemistry. The research involves a combination of *ab initio* electronic structure calculations, variational transition state theory (TST), classical trajectory simulations, and master equation calculations. We apply these methods to reactions of importance in various aspects of combustion chemistry including (i) polycyclic aromatic hydrocarbon (PAH) formation, (ii) hydrocarbon oxidation, and (iii) NO_x chemistry. The specific reactions studied are generally motivated by our interactions with combustion modeling efforts. We are also interested in a detailed understanding of the limits of validity of and, where feasible, improvements in the accuracy of specific implementations of transition state theory. Detailed comparisons with experiment and with other theoretical methods are used to explore and improve the predictive properties of the transition state theory models. Dynamics simulations are performed as a means for testing the statistical assumptions, for exploring reaction mechanisms, and for generating theoretical estimates where statistical predictions are clearly inadequate. Master equation simulations are used to study the pressure dependence of the kinetics and to obtain phenomenological rate coefficients for use in kinetic modeling.

A new component of this effort involves the development of an expert state-of-the-art, open-source, user-friendly *ab initio* transition-state-theory-based master equation (AITSTME) software package for predicting the thermal kinetics of gas phase reactions. Separate funding for this effort is provided by the Predictive Theory and Modeling Component of the Materials Genome Initiative.

Recent Progress

Formalism:

PAPER: Our recent AITSTME program development efforts focussed on exploring, expanding, and improving the utility of the PAPER (Predictive Automated Phenomological Elementary Rates) program package. New features were added related to the treatment of hot reactions and of energy transfer. Testing through numerous applications helped resolve various difficulties. Various minor improvements were designed to improve the input and outputs. The proper treatment of species that become unstable at high temperatures is unclear. We are currently exploring the feasibility of internal eigensystem based extrapolations as a means for directly producing the requisite artificial rate constants. This code is now a central part of essentially all of our applications studies and its major improvements in utility have led us (together with Mebel) to grand new visions for PAH kinetics modeling.

2DME: We have also now developed and implemented a two-dimensional master equation (2DME) approach (with Jasper, Harding, and Miller). Our code implementing this formalism

was built off our old VariFlex software package (rather than PAPER) because VariFlex already includes the requisite framework for evaluating quantities at the E and J resolved level. An initial application of this approach, which was performed as part of the Argonne-Sandia Consortium on High Pressure Combustion Chemistry, demonstrated the utility of coupling trajectory simulations of the collisional kernel for transition in energy and angular momentum, with the 2DME. Completely a priori predictions for the pressure dependence of the $\text{CH}_3 + \text{H}$, $\text{C}_2\text{H}_2 + \text{H}$, and C_2H_3 dissociation reactions were found to agree with the extant experimental data to within 20%. We are currently in the process of improving this 2DME code to facilitate its routine use. A further application to the $\text{H} + \text{O}_2 (+\text{M})$ recombination, which is perhaps the most important recombination reaction in combustion, suggests unexpected deviations from prior models, while still accurately reproducing the experimental data. These revisions may have important ramifications for extrapolation of combustion models outside their validation range.

C₂H₅OH Uncertainty: In collaboration with Zheng (USTC), global uncertainty and sensitivity analysis was applied to the propagation of the uncertainties from the input parameters (e.g., barrier heights, frequencies, and collisional energy transfer parameters) to the rate constants computed with the AITSTME method for the decomposition of ethanol. This case study provides a systematic exploration of the effect of temperature and pressure on the parametric uncertainties in RRKM/master equation calculations for a prototypical single-well multiple-channel dissociation. Notably, the competition between dissociation to the lower energy channel and collisional excitation has dramatic effects on the predicted uncertainties for the rate to form the higher energy products, with uncertainties of a factor of 100 or more predicted for lower pressures. These large uncertainties are related to the need for large-scale single collision induced transitions in energy in order to produce the higher energy products in the low pressure limit.

Hydrocarbon Growth Studies:

C₃H₃ Dissociation: The importance of propargyl radical to hydrocarbon growth in high temperature environments is related to its exceptional thermal and chemical stability, which results in remarkably high concentrations in the steady-state environment of flames. The increased importance of the propargyl radical relative to other resonantly stabilized radicals is related to the difficulty of further dehydrogenation of propargyl. Nevertheless, its thermal decomposition may still provide the dominant loss channel and a proper delineation of propargyl's role in combustion chemistry requires accurate estimates for its decomposition kinetics.

In collaboration with Jasper and Miller, we have studied C_3H_3 dissociation kinetics with the ab initio transition state theory based master equation (AITSTME) method. The potential energy surface (PES) for the decomposition of propargyl was first mapped at a high level of theory (building on earlier work of Mebel) with a combination of coupled cluster and multireference perturbation calculations. Variational transition state theory was then used to predict the microcanonical rate coefficients, which are subsequently implemented within the multiple-well multiple-channel master equation. The sensitivity of the thermal rate predictions to the energy transfer parameters was explored. The predictions for the thermal decomposition rate coefficient are in good agreement with the limited experimental data. Modified Arrhenius representations of the rate constants are reported for utility in combustion modeling.

Xylyl Dissociation: Xylyl radical chemistry plays a dominant role in the overall combustion chemistry of xylene, an important aromatic surrogate molecule in real fuels. In collaboration with Cavallotti (Milan) and Sivaramakrishnan and Michael, we explored the decomposition of o-xylyl radicals both theoretically and experimentally. A PES for the decomposition of o-xylyl as well as for isomerization to its meta and para isomers was determined at the CBS-QB3//M06-2X/6-311+G(d,p) level. The full PES is composed of 20 wells connected by 32 transition states. Master equation simulations were performed to determine channel specific rate constants for the decomposition of o-, m-, and p-xylyl for a wide range of temperatures and pressures. The simulations predict that the main products of decomposition are o-xylylene + H, p-xylylene + H, styrene + H, phenyl + C₂H₄ and fulvenallene + CH₃, with H channels accounting for about 80% of the decomposition products. It was also found that ortho-meta-para isomerization is a fast process, with a rate that is competitive with that of decomposition.

Future Directions

Our future work will continue to focus on (i) the further development of PAPER and (ii) the application of this code to the prediction of the kinetics for reactions of key importance in combustion chemistry. Our various applications will continue to involve coupling with state-of-the-art electronic structure methods in collaboration with Harding and detailed comparisons with experiment as available.

Various new code development efforts are planned. In collaboration with Jasper, we are currently improving our implementation of the 2-dimensional master equation and of its coupling with codes for performing trajectory simulations of energy transfer. We are also exploring the feasibility of developing master equations that describe the conversion of internal energy through a sequence of multiple bimolecular reactions. Further considerations of anharmonic torsional, linear bending, and umbrella modes and their coupling are also planned. Currently, we are developing a method for treating the coupling of torsional and umbrella motions with the transitional modes for barrierless reactions. We have recently implemented a direct conversion of the partition functions evaluated with the PAPER package into standard polynomial representations of the thermodynamic data, which will facilitate a planned exploration of anharmonic effects on the thermodynamic properties for the full set of core combustion species.

The current ease of converting ab initio data to phenomenological rate coefficients has led Mebel and myself to a grand vision of mapping the full PAH kinetics for the first few rings. Most prior ab initio kinetics work for PAHs has devoted considerable effort to mapping out the potential energy surfaces, but then generally considered high pressure kinetics estimates, at best. The first stage of our effort will simply involve the conversion of all this detailed PES data into meaningful kinetic estimates via the PAPER program package. Further work will explore refinements of the various AITSTME models to improve the accuracy of their predicted kinetics. As a first step in this project we are collaborating with Mebel on a detailed study of the role of the HACA mechanism in the conversion from one to two rings. Harding, Jasper, Miller, and Sivaramakrishnan are also contributing to this effort.

DOE Supported Publications, 2013-Present

1. **A Quantitative Explanation for the Apparent Anomalous Temperature Dependence of OH + HO₂ = H₂O + O₂ through Multi-Scale Modeling**, M. P. Burke, S. J. Klippenstein, L. B. Harding, *Proc. Comb. Inst.* **34**, 547-555 (2013).

2. **Rate Constant and Branching Fraction for the $\text{NH}_2 + \text{NO}_2$ Reaction**, S. J. Klippenstein, L. B. Harding, P. Glarborg, Y. Gao, H. Hu, P. Marshall, *J. Phys. Chem. A* **117**, 9011-9022 (2013).
3. **Reformulation and Solution of the Master Equation for Multiple-Well Chemical Reactions**, Y. Georgievskii, J. A. Miller, S. J. Klippenstein, *J. Phys. Chem. A* **117**, 12146-12154 (2013).
4. **Low Temperature Rate Coefficients for the Reaction $\text{CN} + \text{HC}_3\text{N}$?** S. C. Sid Ely, S. B. Morales, J.-C. Guillemin, S. J. Klippenstein, I. R. Sims, *J. Phys. Chem. A* **117**, 12155-12164 (2013).
5. **Predictive Theory for the Addition and Insertion Kinetics of $^1\text{CH}_2$ Reacting with Unsaturated Hydrocarbons**, D. Polino, S. J. Klippenstein, L. B. Harding, Y. Georgievskii, *J. Phys. Chem. A* **117**, 12677-12692 (2013).
6. **Propargyl + O_2 Reaction in Helium Droplets: Entrance Channel Barrier or Not?** C. P. Moradi, A. M. Morrison, S. J. Klippenstein, C. F. Goldsmith, G. E. Douberly, *J. Phys. Chem. A* **117**, 13626-13635 (2013).
7. **Comparison of Multireference Configuration Interaction Potential Energy Surfaces for $\text{H} + \text{O}_2 \rightarrow \text{HO}_2$: The Effect of Internal Contraction**, L. B. Harding, S. J. Klippenstein, H. Lischka, R. Shepard, *Theor. Chem. Acc.* **133**, 1429 (2013).
8. **Chemical Kinetics and Mechanisms of Complex Systems: A Perspective on Recent Theoretical Advances**, S. J. Klippenstein, V. S. Pande, D. G. Truhlar, *J. Am. Chem. Soc.* **136**, 528-546 (2014).
9. **Predictive *A Priori* Pressure Dependent Kinetics**, A. W. Jasper, K. M. Pelzer, J. A. Miller, E. Kamarchik, L. B. Harding, S. J. Klippenstein, *Science* **346**, 1212-1215 (2014).
10. **Secondary Channels in the Thermal Decomposition of Monomethylhydrazine (CH_3NHNH_2)** P. Zhang, S. J. Klippenstein, L. B. Harding, H. Y. Sun, C. K. Law, *RSC Advances* **4**, 62951-62964 (2014).
11. **Pressure-Dependent Branching in the Reaction of $^1\text{CH}_2$ with C_2H_4 and other Reactions on the C_3H_6 Potential Energy Surface**, L.-L. Ye, Y. Georgievskii, S. J. Klippenstein, *Proc. Comb. Inst.* **35**, 223-230 (2015).
12. **The Role of Prompt Reactions in Ethanol and Methylformate Low-Pressure Flames**, N. J. Labbe, R. Sivaramakrishnan, S. J. Klippenstein, *Proc. Comb. Inst.* **35**, 447-455 (2015).
13. **Effects of New *Ab Initio* Rate Coefficients on Predictions of Species Formed During *n*-Butanol Ignition**, D. M. A. Karwat, M. S. Wooldridge, S. J. Klippenstein, M. J. Davis, *J. Phys. Chem. A* **119**, 543-551 (2015).
14. **Hydrolysis of Ketene Catalyzed by Formic Acid: Modification of Reaction Mechanism, Energetics, and Kinetics with Organic Acid Catalysis**, M. K. Louie, J. S. Francisco, M. Verdicchio, S. J. Klippenstein, A. Sinha, *J. Phys. Chem. A* ASAP, DOI: 10.1021/jp5076725 (2015).
15. ***Ab Initio* Variational Transition State Theory and Master Equation Study of the Reaction $(\text{OH})_3\text{SiOCH}_2 + \text{CH}_3 = (\text{OH})_3\text{SiOC}_2\text{H}_5$** , D. Nurkowski, S. J. Klippenstein, Y. Georgievskii, M. Verdicchio, A. W. Jasper, J. Akroyd, S. Mosbach, M. Kraft, *Zeit. Phys. Chem.*, *in press* (2015).
16. **The 2014 KIDA Network for Interstellar Chemistry**, V. Wakelam, J.-C. Loison, E. Herbst, B. Pavone, A. Bergeat, K. Beroff, M. Chabot, A. Faure, W. D. Geppert, D. Gerlich, P. Gratier, N. Harada, K. M. Hickson, P. Honvault, S. J. Klippenstein, S. D. LePicard, G. Nyman, M. Ruaud, S. Schlemmer, I. R. Sims, D. Talbi, J. Tennyson, R. Wester, *Astrophys. J. Supp.*, *in press* (2015).
17. **Resolving Some Paradoxes in the Thermal Decomposition Mechanism of Acetaldehyde**, R. Sivaramakrishnan, J. V. Michael, L. B. Harding, S. J. Klippenstein, *J. Phys. Chem. A*, ASAP, DOI: 10.1021/acs.jpca.5b01032 (2015).
18. **Kinetics of Propargyl Radical Dissociation**, S. J. Klippenstein, J. A. Miller, A. W. Jasper, *J. Phys. Chem. A*, *in press* (2015).

ARGONNE-SANDIA CONSORTIUM ON HIGH-PRESSURE COMBUSTION CHEMISTRY

Stephen J. Klippenstein (PI), Michael J. Davis, Lawrence B. Harding, Joe V. Michael,
James A. Miller, Branko Ruscic, Raghu Sivaramakrishnan, Robert S. Tranter
Chemical Sciences and Engineering Division, Argonne National Laboratory, Argonne, IL, 60439

sjk@anl.gov

Craig A. Taatjes (PI), Ahren W. Jasper, David L. Osborn, Leonid Sheps, Judit Zádor
*Combustion Research Facility, Mail Stop 9055, Sandia National Laboratories
Livermore, CA 94551-0969*

cataatj@sandia.gov

Program Scope

The goal of this project is to explore the fundamental effects of high pressure (P) on the chemical kinetics of combustion and to use that knowledge in the development of accurate models for combustion chemistry at the high pressures of current and future engines. We design and implement novel experiments, theory, and modeling to probe high-pressure combustion kinetics from elementary reactions, to submechanisms, to flames. The work focuses on integrating modeling, experiment, and theory (MET) through feedback loops at all levels of chemical complexity. We are currently developing and testing the methodology for small alkanes, alcohols, and ethers as key prototype fuels. The consortium expands and enhances collaborations between Argonne's Dynamics in the Gas Phase Group and the Combustion Chemistry Group in Sandia's Combustion Research Facility.

Recent Progress

High-Repetition Rate Shock Tube (HRRST): Based on experience gained in initial experimental campaigns at the Advanced Photon Source (APS) and Advanced Light Source (ALS) a number of modifications to the HRRST have been made. These include a new differentially pumped interface between the HRRST and a new Kasedorf TOF-MS. The former facilitates replacement of the nozzle that forms the end of the shock tube. An additional sensor close to the nozzle more precisely measures the incident shock velocity close to the nozzle, allowing mass spectra from many experiments to be accurately aligned temporally prior to signal averaging. The new TOF-MS allows the mass spectra to be acquired at 150 kHz (up to ~ 200 amu with a mass resolution of ~ 1300), tripling the temporal resolution available from the original instrument, which will result in more accurate kinetic measurements in the crucial first 100 μs of reaction. Finally, the HRRST and new TOF-MS have been mounted on independent frames that incorporate the key electronics. These have been designed to fit into the tight spaces at the ALS and simplify shipping and setup of the equipment. A recent publication [23] discusses the analysis of PIMS data acquired at the ALS, including a discussion of the number of spectra that have to be averaged to obtain sufficient S/N for peaks of various intensities.

Oxidation Chemistry of Ethers. The radical chain-branching chemistry of QOOH species is critical to our understanding of low- T autoignition. QOOH is a carbon-centered radical intermediate formed by internal H abstraction in peroxy species (RO_2), following the oxidation of a fuel radical (R). In an effort to focus on the effects of fuel structure on reactivity, we have initiated studies of the low- T autoignition chemistry of linear, cyclic, and branched ether compounds. We have collected preliminary photoionization mass spectrometry (PIMS) data on the oxidation of tetrahydrofuran (THF), 2-methyl THF (2MTHF), and 3-methyl THF (3MTHF), at pressures ranging from 10 Torr to 2 atm (cf. Fig. 1). The experiments reveal rich oxidation chemistry with many competing reaction channels, such as HO_2 and OH elimination, β -scission and ring-opening

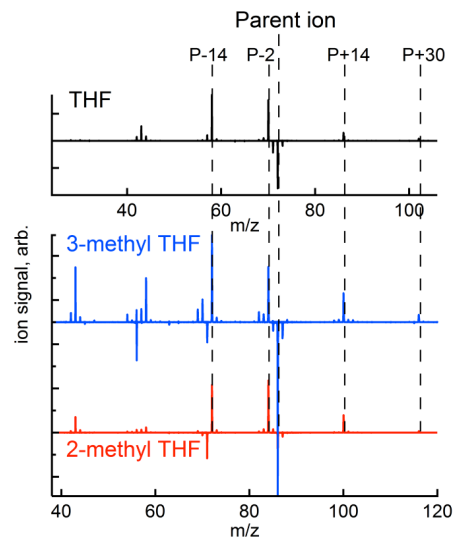


Fig. 1: Time-resolved ion signals in the oxidation of THF, 2MTHF, and 3MTHF at $P = 10$ Torr, $T = 600$ K. The mass scale for THF is shifted by 14 amu to align the parent ion peaks. Four analogous product ions are highlighted: P-14 (formed by β -scission), P-2 (HO_2 elimination), P+14 (OH elimination), and P+30 (most likely by QOOH oxidation pathways).

pathways, and evidence of QOOH oxidation pathways. In particular, we identified product ions at the mass of parent compound + 30 amu in the reactions of all three cyclic ethers we studied. These products, which have P -dependent yields, likely arise from second O_2 addition to QOOH and can therefore be used as sensitive probes of QOOH + O_2 chemistry. We also performed the first PIMS experiments on the oxidation of dimethyl ether (DME) for P up to 1 atm and T up to 650 K. The oxidation chemistry is dominated by the formation of QOOH ($\bullet CH_2OCH_2OOH$) and its decomposition, mainly producing formaldehyde and OH. Several minor products (methyl formate, formic acid, and $HOCH_2OOH$) are also observed. Complementary master-equation based theoretical work is nearing completion.

Propane Oxidation. We completed an extensive experimental and computational investigation of propane oxidation in the low- T autoignition regime (*J. Phys. Chem. A*, submitted). Using time-resolved tunable VUV PIMS at the ALS, we identified numerous reaction intermediates and stable products of n - and i -propyl radical oxidation at $P = 4$ Torr and $T = 530 - 670$ K. Of these, we measured absolute concentration time profiles for nine chemical species, including the first time-resolved measurements of four different reaction channels that form oxygenated products acetone, propanal, oxetane, and methyloxirane, all in conjunction with the OH radical. To aid in the interpretation of our experimental results, we extended the recently developed multi-scale informatics (MSI) approach, which treats theoretical and experimental uncertainties on an even footing, to the relatively complex case of propane oxidation. This powerful modeling method combines diverse sets of experimental and computational results (our MPIMS data, earlier measurements of propyl radical decays and OH and HO_2 production, *ab initio* electronic structure calculations, and master equation kinetics) to optimize a propane oxidation mechanism that includes primary and secondary chemistry. The newly optimized mechanism reconciles earlier discrepancies in the measured OH yields from propane oxidation, suggests a previously unrecognized role for QOOH + O_2 chemistry in low temperature OH observations, and identifies the recombinations reactions of propyl peroxy (RO_2) radicals, as the main gateway processes to the secondary chemistry in propane oxidation under these conditions.

OH + 2-butene. We undertook a combined experimental and theoretical study of the reaction of OH with 2-butene, the smallest alkene with structural isomers (*J. Phys. Chem. A*, submitted). Using laser-induced fluorescence OH detection, we probed the complex P - and T -dependent competition between multiple reaction channels in the “intermediate” temperature regime (400 – 800 K) for $P = 1 - 20$ atm. Our experiments served as benchmarks for master equation-based chemical kinetics calculations (cf. Fig. 2), which used *ab initio* calculated OH + 2-butene potential energy surfaces.

D + C_3H_8 , OH + $C_3H_8/n-C_4H_{10}/iso-C_4H_{10}$. In high temperature combustion chemistry, H/OH + fuel abstraction reactions are often the dominant fuel-destruction steps, leading to the formation of a fuel radical and either H_2 or H_2O as the co-product. The vast majority of experimental studies of these reactions have probed the decay of the radical reactant to obtain total bimolecular rate constants. In recent work, we used atomic resonance absorption spectrometry (ARAS) to probe product H-atoms in the reactions of D with C_3H_8 , and OH with C_3H_8 , $n-C_4H_{10}$, and $i-C_4H_{10}$ at high temperatures (>900 K) in a shock tube. Kinetic simulations indicated that the H-atom profiles are sensitive to the abstraction rate constant at a specific C-H bond, thereby allowing for the determination of channel-specific abstraction rate constants. In combination with prior published total rate constants, the present results yield direct experimental determinations of abstraction branching ratios.

Decomposition of Nascent Radicals: The rates of formation and decay of radicals is central to the modeling of global combustion properties. Standard kinetic modeling presumes that the formation and decay of the radicals are decoupled, with decomposition occurring from a thermal ensemble on a timescale that is longer than that for internal energy relaxation. However, at high temperatures, and/or for radicals that are formed rovibrationally hot (via exothermic reactions, for example) a significant fraction of the radicals will dissociate during the timescale for internal energy relaxation. This “directly dissociative” fraction can have a significant effect on the overall kinetics. For example, abstraction by H or OH from formaldehyde produces excited HCO, which can either be collisionally

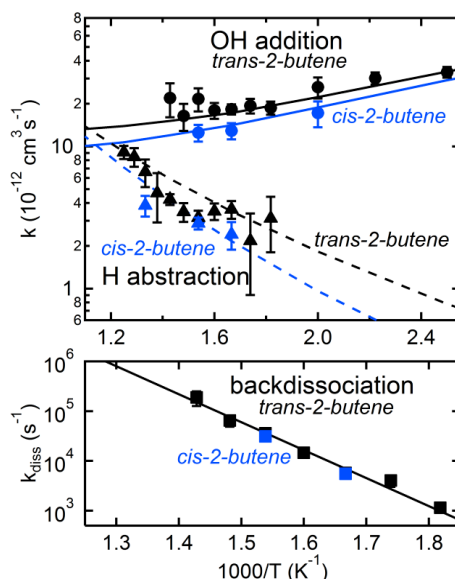


Fig 2. Measured (symbols) and calculated (lines) high- P limit rate coefficients for H abstraction, OH addition, and backdissociation in the reaction of OH with cis-2-butene and trans-2-butene.

thermalized or alternatively, directly decompose to H + CO. The inclusion of a direct decomposition fraction for formaldehyde abstraction reactions can have large consequences because of the important role of HCO in combustion modeling. Theoretical calculations have been performed to quantify the probability of direct dissociation of HCO when it is formed ro-vibrationally excited from hydrogen abstractions in OH and H + CH₂O. These direct dissociation probabilities were then included in combustion models to simulate laminar flame speeds of simple C₁-C₂ fuels. Preliminary modeling results indicate that flame speed predictions are sensitive to the newly considered hot direct decomposition of HCO, with significantly increased flame speeds predicted. These results indicate the need to revisit descriptions of radical decompositions in current combustion models, and in studies of the elementary reaction kinetics of HCO at high temperatures. Theory/modeling studies are in progress to characterize these effects for a set of combustion relevant weakly bound radicals (C₂H₃, C₂H₅, CH₂OH, etc.).

A Priori Predictive Pressure Dependence: We have developed and applied a completely a priori procedure for predicting the pressure dependence of reaction rates. The procedure involves a coupling of trajectory simulations of the collisional induced transitions in energy, E , and angular momentum, J , with solutions to the 2-dimensional master equation (in E and J) employing ab initio transition state theory predictions for the microcanonical rate constants. A priori results for the CH₄ and C₂H₃ systems were found to agree with the experimental data to within their error bars for a wide range of conditions.

Future Directions

High- P PIMS Construction. The main challenge to extending time-resolved PIMS to elevated pressures is that higher sample P must be coupled with higher reactant dilution, because reactant concentrations must remain low to avoid radical-radical processes. In contrast to low- P experiments, the relative mole fraction of reactants at high P must be on the order of ppb, pushing the sensitivity limits of conventional mass spectrometry. We have recently designed and begun the construction of an improved high- P MPIMS apparatus, based on an innovative mass spectrometer design. In the new apparatus, photoionization occurs in a high-density region of the supersonic sampling expansion, followed by gentle electrostatic ion guides that afford high ion collection efficiency without inducing additional molecular collisions. We expect the new apparatus to be constructed and commissioned at Sandia this summer, and to be coupled to the Advanced Light Source within a year, with an anticipated factor of ~100 increase in detection sensitivity over the current high-pressure PIMS prototype.

Low-Temperature Autoignition Chemistry. We plan to continue our studies of autoignition chemistry aimed at understanding the relationship between fuel structure and reactivity. We will broaden the recent propane and butane oxidation experiments to larger branched alkanes, neo-pentane and iso-octane, in an effort to improve the fidelity of ignition models for traditional fuels. The QOOH reaction pathways often produce cyclic ethers and other oxygenated species in combination with hydroxyl radicals. The complementary methods of laboratory-based OH LIF detection and synchrotron-based MPIMS will help elucidate these competing QOOH pathways.

Ethers are an important class of potential biofuels and additives, which also commonly arise as intermediates in the overall fuel oxidation. Thus, we are planning to examine the pyrolytic and oxidative chemistry at elevated pressures for a variety of dioxanes and methylated furans. These experiments will be performed with both the HRRST and with PIMS and LIF detection in flow reactors. In the case of cyclic ethers, we plan to use partially deuterated THF, which will allow us to distinguish between the many possible internal H shifts and β -scission pathways. Similarly, the use of deuterated DME will help identify some of the reaction products by separating overlapping ion signals. In addition, we will probe the OH and HO₂ radical products from DME, THF, and methyl-substituted THF oxidation to complement the PIMS data. An HRRST study of the high pressure pyrolysis of DME will pay particular attention to the kinetic role of roaming radical pathways.

Radical Abstractions: We plan to extend our technique for obtaining channel specific rate constants in H-atom abstractions to simple oxygenated molecules. We also envision that this technique will directly probe the nascent decompositions of the radicals. Abstraction using a thermal source for OH-radicals (TBHP) or O-atoms (O₃) will be used as a means to form the radical of interest in the shock tube. H/D/O-ARAS and/or OH-multipass absorption will then be used to make time-resolved measurements of the radical decomposition. Experiment, theory, and modeling will be used to probe the relevance of direct decompositions of weakly bound radicals in combustion kinetics.

DOE Supported Publications, 2013-Present

1. **Uncertainty Propagation in the Derivation of Phenomenological Rate Coefficients from Theory: A Case Study of Propyl Radical Oxidation**, C. F. Goldsmith, A. S. Tomlin, S. J. Klippenstein, *Proc. Comb. Inst.* **34**, 177-185 (2013).

2. **Unimolecular Dissociation of Hydroxypropyl and Propoxy Radicals**, J. Zádor, J. A. Miller, *Proc. Comb. Inst.* **34**, 519-526 (2013).
3. **Studies of Laminar Opposed-Flow Diffusion Flames of Acetylene at Low Pressures with Photoionization Mass Spectrometry**, S. A. Skeen, B. Yang, H. A. Michelsen, J. A. Miller, A. Violi, N. Hansen, *Proc. Comb. Inst.* **34**, 1067-1075 (2013).
4. **Unconventional Peroxy Chemistry in Alcohol Oxidation – The Water Elimination Pathway**, O. Welz, S. J. Klippenstein, L. B. Harding, C. A. Taatjes, J. Zádor, *J. Phys. Chem. Lett.* **4**, 350-354 (2013).
5. **Determining Phenomenological Rate Coefficients from a Time-Dependent, Multiple-Well Master Equation: “Species Reductions” at High Temperatures**, J. A. Miller, S. J. Klippenstein, *Phys. Chem. Chem. Phys.* **15**, 4744-4753 (2013).
6. **The Dissociation of Propyl Radicals and Other Reactions on a C₃H₇ Potential**, J. A. Miller, S. J. Klippenstein, *J. Phys. Chem. A* **117**, 2718-2727 (2013).
7. **Lennard-Jones Parameters for Combustion and Chemical Kinetics Modeling from Full-Dimensional Intermolecular Potentials**, A. W. Jasper, J. A. Miller, *Combust. Flame* **161**, 101-110 (2013).
8. **A Miniature High Repetition Rate Shock Tube**, R. S. Tranter, P. T. Lynch, *Rev. Sci. Instr.* **84**, 094102 (2013).
9. **Direct Measurements of Rate Constants for the Reactions of CH₃ Radicals with C₂H₆, C₂H₄, and C₂H₂ at High Temperatures**, S. L. Peukert, N. J. Labbe, R. Sivaramakrishnan, J. V. Michael, *J. Phys. Chem. A* **117**, 10228-10238 (2013).
10. **Low-Temperature Combustion Chemistry of n-Butanol: Principal Oxidation Pathways of Hydroxybutyl Radicals**, O. Welz, J. Zádor, J. D. Savee, L. Sheps, D. L. Osborn, C. A. Taatjes, *J. Phys. Chem. A*, **117**, 11983–12001 (2013).
11. **The Collision Efficiency of Water in the Unimolecular Reaction CH₄ (+H₂O) → CH₃ + H (+H₂O): One-Dimensional and Two-Dimensional Solutions of the Low-Pressure-Limit Master Equation**, A. W. Jasper, J. A. Miller, S. J. Klippenstein, *J. Phys. Chem. A* **117**, 12243-12255 (2013).
12. **First-Principles Binary Diffusion Coefficients for H, H₂, and Four Normal Alkanes + N₂**, A. W. Jasper, E. Kamarchik, J. A. Miller, S. J. Klippenstein, *J. Chem. Phys.*, **141**, 124313:1-12 (2014).
13. **Photoionization Mass Spectrometric Measurements of Initial Reaction Pathways in Low-Temperature Oxidation of 2,5-dimethylhexane**, B. Rotavera, J. Zádor, O. Welz, L. Sheps, A. M. Scheer, J. D. Savee, M. A. Ali, T. S. Lee, B. A. Simmons, D. L. Osborn, A. Violi, C. A. Taatjes, *J. Phys. Chem. A* **118**, 10188-10200 (2014).
14. **UV Absorption Probing of the Conformer-Dependent Reactivity of a Criegee Intermediate CH₃CHOO**. L. Sheps, A. M. Scully, K. Au, *Phys. Chem. Chem. Phys.* **16**, 26701-26706 (2014).
15. **Predictive *A Priori* Pressure Dependent Kinetics**, A. W. Jasper, K. M. Pelzer, J. A. Miller, E. Kamarchik, L. B. Harding, S. J. Klippenstein, *Science*, **346** 1212-1215 (2014).
16. **High Temperature Rate Constants for H/D + n-C₄H₁₀ and i-C₄H₁₀**, S. L. Peukert, R. Sivaramakrishnan, J. V. Michael, *Proc. Comb. Inst.* **35**, 171-179 (2015).
17. **Adventures on the C₃H₅O potential energy surface: OH + propyne, OH + allene and related reactions**, J. Zádor, J. A. Miller, *Proc. Comb. Inst.* **35**, 181-188 (2015).
18. **“Third-body” Collision Efficiencies for Combustion Modeling: Hydrocarbons in Atomic and Diatomic Baths**, A. W. Jasper, C. M. Oana, J. A. Miller, *Proc. Comb. Inst.* **35**, 197-204 (2015).
19. **Toward a Quantitative Understanding of the Role of Non-Boltzmann Reactant Distributions in Low-Temperature Oxidation**, M. P. Burke, C. F. Goldsmith, Y. Georgievskii, S. J. Klippenstein, *Proc. Comb. Inst.* **35**, 205-213 (2015).
20. **Effect of Non-Thermal Product Energy Distributions on Ketohydroperoxide Decomposition Kinetics**, C. F. Goldsmith, M. P. Burke, Y. Georgievskii, S. J. Klippenstein, *Proc. Comb. Inst.* **35**, 283-290 (2015).
21. **Probing the Low-Temperature Chain-Branching Mechanism for n-Butane Autoignition Chemistry via Time Resolved Measurements of Ketohydroperoxide Formation in Photolytically Initiated n-C₄H₁₀ Oxidation**, A. J. Eskola, O. Welz, J. Zádor, I. O. Antonov, L. Sheps, J. D. Savee, D. L. Osborn, C. A. Taatjes, *Proc. Comb. Inst.* **35**, 291-298 (2015).
22. **Direct Observation and Kinetics of a Hydroperoxyalkyl Radical (QOOH)**. J. D. Savee, E. Papajak, B. Rotavera, H. Huang, A. J. Eskola, O. Welz, L. Sheps, C. A. Taatjes, J. Zádor, D. L. Osborn, *Science*, **347**, 643-646 (2015).
23. **Probing Combustion Chemistry in a Miniature Shock Tube with Synchrotron VUV-Photoionization Mass Spectrometry**, P. T. Lynch, M. Ahmed, T. P. Troy, R. S. Tranter, *Anal. Chem.* **87**, 2345–2352 (2015).

Theoretical modeling of spin-forbidden channels in combustion reactions

Anna I. Krylov

Department of Chemistry, University of Southern California,
Los Angeles, CA 90089-0482; krylov@usc.edu

1 Scope of the project

The goal of our research is to develop predictive theoretical methods, which can provide crucial quantitative data (e.g., rate constants, branching ratios, heats of formation), identify new channels and refine reaction mechanisms. Specifically, we are developing tools for computational studies of spin-forbidden and non-adiabatic pathways of reactions relevant to combustion, and applying these tools to study electronic structure, reactions, and spectroscopy of open-shell and electronically excited species involved in these processes.

2 Summary of recent major accomplishments

During the past year, we conducted several computational studies of open-shell and electronically excited species. The common theme in these studies is interactions between states of different character and intersections between the corresponding potential energy surfaces. We also continued to develop and benchmark computational methods for modeling electronic structure and spectroscopy of open-shell species. Particular emphasis was placed on determining spectroscopic signatures of transient species, to facilitate comparisons with experimental data. In 2014-2015, the DOE support was acknowledged in two papers.^{1,2} Two manuscripts are in the final stage of preparation. Some of the recent results are highlighted below.

2.1 Formalism and computer codes for calculating spin-orbit couplings for EOM-CC wave functions

We have developed a formalism and an implementation for calculating spin-orbit couplings (SOCs) within EOM-CCSD (equation-of-motion coupled-cluster methods with single and double substitutions) for the following variants of EOM-CCSD: EOM-CC for excitation energies (EOM-EE), EOM-CC with spin-flip (EOM-SF), EOM-CC for ionization potentials (EOM-IP) and electron attachment (EOM-EA). We employ a perturbative approach in which SOCs are computed as matrix elements of the respective part of the Breit-Pauli Hamiltonian using zero-order non-relativistic wave functions. We follow the expectation-value approach rather than the response theory formulation for property calculations. Both the full two-electron treatment and the mean-field approximation (a partial account of the two-electron contributions) have been implemented and benchmarked using several small molecules containing elements up to the fourth row of the periodic table. The benchmark results illustrate excellent performance of the perturbative treatment and the mean-field approximation (see Table 1). When used with an appropriate basis set, the errors against experiment are below 5%. The findings regarding basis set requirements are in agreement with

previous studies. The impact of different correlation treatment in zero-order wave functions was analyzed. Overall, EOM-IP-CCSD, EOM-EA-CCSD, EOM-EE-CCSD, and EOM-SF-CCSD wave functions yield SOCs which agree well with each other (and with the experimental values when available). Using an EOM approach that provides a more balanced description of the target states yields more accurate results. The manuscript presenting this work is finalized for publication. The code will be released in the upcoming 4.3 release of Q-Chem.

Table 1: Spin-orbit splittings (cm^{-1}) in selected doublet radicals computed by various EOM-CCSD methods using cc-pCVTZ.

System	Exp. ^a	EOM-EA		EOM-IP ^b		EOM-EE ^b	
		1el+2el	SOMF	1el+2el	SOMF	1el+2el	SOMF
CF	77.1	76.28	74.93	78.66	79.32	77.00	76.48
O ₂ ⁺	200.3	204.17	201.37	194.86	195.60	195.13	193.70
NO	123.1	124.16	122.12	122.11	122.74	121.85	120.90
PO	224.0	232.97	232.21	215.96	216.52	223.87	223.76
NS	222.9	227.93	226.84	242.28	242.85	231.46	231.09
PS	321.9	330.44	330.01	327.76	328.35	327.92	328.11

^a Experimental values are taken from Klein and Gauss, J. Chem. Phys. **129** 194106 (2008).

^b ROHF reference.

2.2 Dyson orbitals and absolute cross sections for photoionization

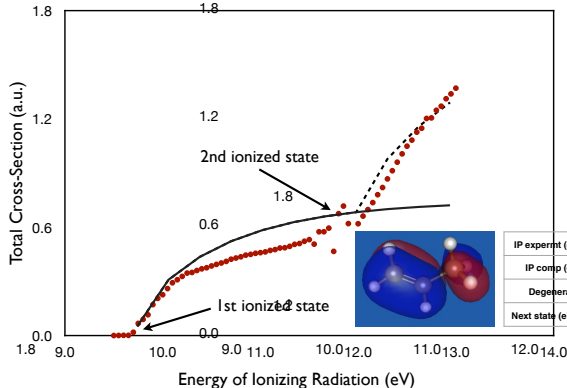


Figure 1: Absolute photoionization cross section for propene. Two states are accessed in this energy range. Theoretical values (solid and dashed black lines) are in excellent agreement with the experimental measurements (red dots). In most cases that we investigated, the theoretical curves are within 20% from the experimental ones, however, several systems show much larger discrepancies. We are currently investigating what are the reasons for disagreement.

Dyson orbital is a one-electron quantity “connecting” N and $N-1$ electron states:

$$\phi^d(1) = \sqrt{N} \int \Psi^I(1, 2, \dots, N) \Psi^F(2, \dots, N) d2 \dots dN \quad (1)$$

It is a rigorous generalization of a Koopmans picture to correlated many-electron wave functions. Qualitatively, Dyson orbital describes the state of an ionized electron. Quantitatively, it enters the expressions for photoelectron transition matrix elements that define total and differential cross sections. We developed a production-level efficient code for computing Dyson orbitals using various EOM-CC wave functions. We also performed extensive benchmarks of absolute photoionization cross sections against an experimental database (Dr. Osborn, private communication) using our simple model for cross sections (matrix elements between Dyson orbitals and a plane wave describing the outgoing electron). We computed cross sections for more than 100 closed-shell molecules. Overall, the agreement is rather good, however, several cases show larger discrepancies. One

obvious limitation of the model, which we plan to address in a near future, is including ionization via resonances.

2.3 Insights into non-adiabatic couplings

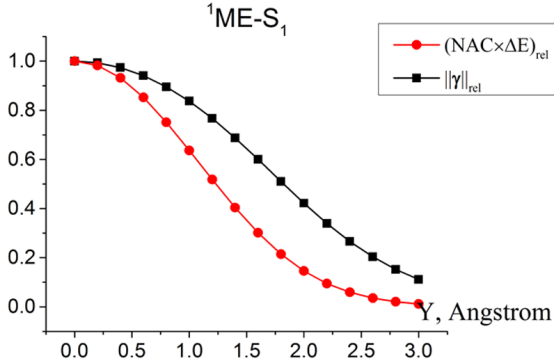


Figure 2: $\|\gamma\|$ and interstate couplings ($\text{NAC} \cdot \Delta E$) computed using CASSCF wave functions between the ^1ME (multi-exciton, ^1TT) and S_1 states in a stacked ethylene dimer. The respective values are normalized to their values at the perfectly stacked geometry. As the fragments are displaced along the short molecular axis, the states acquire their pure asymptotic character and become formally doubly excited with respect to each other. The coupling decreases accordingly. As expected, large values of $\|\gamma\|$ are required for large couplings. However, finer variations in couplings may be lost.

Non-adiabatic coupling (NAC) matrix elements are required for computing rates of non-adiabatic transitions. Since NAC is a one-electron operator, it can be computed from one-particle transition density matrix:

$$\frac{1}{E_I - E_J} \langle \Psi_I | H^x | \Psi_J \rangle = \frac{1}{\Delta_{IJ}} \sum_{pq} H_{pq}^x \gamma_{pq}^{IJ} \leq \frac{1}{\Delta_{IJ}} \|H^x\| \cdot \|\gamma^{IJ}\| \quad (2)$$

where

$$\gamma_{pq}^{IJ} \equiv \langle \Psi_I | p^+ q | \Psi_J \rangle \quad (3)$$

We realized that $\|\gamma\|$, norm of transition one-particle transition density matrix, can be used as a crude proxy for NAC,² owing to the Cauchy-Schwartz inequality above. More generally, $\|\gamma\|$ quantifies the degree of one-electron character in the $I \rightarrow F$ transition and can be exploited to monitor changes in the states upon structural changes (Fig. 2). This tool has been used to investigate the effect of morphology on singlet fission rates. It also provides a simple metric for analyzing the type of an electronic transition.²

2.4 Multiple potential energy surfaces and conical intersections

Accurate description of conical intersections is a challenging task for electronic structure methods as it requires balanced description of interacting states. Using a simple model system, PSB3, we investigated the performance of various approaches in the vicinity of a conical intersection,¹ see Fig. 3 (left). We considered multi-reference methods, such as CASSCF, MR-CI with and without Davidson correction, various flavors of MR-PT, as well as spin-flip methods. We found that a balanced description of dynamical and non-dynamical correlation is essential for reproducing the location and energy of conical intersections. As illustrated in Fig. 3 (right), dynamical correlation stabilizes the S_1 state along the entire path and, also, stabilizes the S_0 energy of all structures relative to the equilibrium cis and trans structures. While it is not surprising that the CASSCF surfaces are quite far from the reference MR-CISD(Q), the discrepancies between various MR-PT methods are disconcerting. Overall, the performance of XMCQDPT2 is solid, whereas the CASPT2 methods exhibit artifacts in the regions of exact degeneracies. EOM-SF-CCSD provides a qualitatively accurate description of the two PES, however, the triples correction (dT) is needed for quantitatively accurate profiles that are in good agreement with MRCISD+Q.

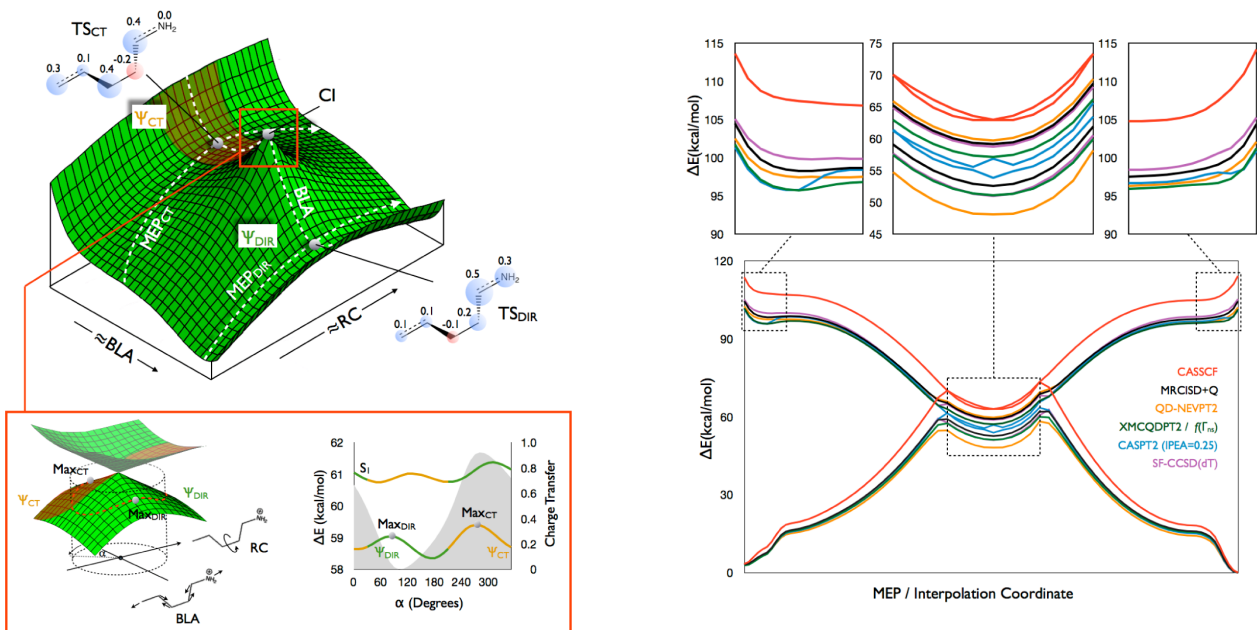


Figure 3: Left: Schematic two-dimensional cut of the ground-state potential energy surface of PSB3. The two coordinates can be described as bond length alternation (BLA) and the C2-C3 twisting reaction coordinate (RC). Around the intersection, the wave function changes its character from charge-transfer (brown) to diradical (green). Three different paths around the intersection (dashed lines) are shown by the dashed lines on the surface. Right: CASSCF (red), MRCISD+Q (black), QD-NEVPT2 (orange), XMCQDPT2 (green), CASPT2 (blue), and SF-CCSD(dT) (violet) energy profiles along the composite CASSCF path comprising MEP_{CIS} , CI seam, and MEP_{TRANS} . The insets show an expansion of the 10 points nearest to each of the cis- and trans-PSB3 structures and of the CI seam.

3 Current developments and future plans

Currently, we are improving the methodology for calculating cross sections from Dyson orbitals by developing tools for including resonance channels. We are also investigating the sources of discrepancies between theory and experiment. This is conducted in collaboration with the experimental groups (Kaiser, Osborn) and theoreticians (Stanton). Other projects include computational studies of several radicals relevant to combustion and spin-forbidden channels in the reactions of oxygen with unsaturated hydrocarbons.

References

- [1] S. Gozem, F. Melaccio, A. Valentini, M. Filatov, M. Huix-Rotllant, N. Ferre, L.M. Frutos, C. Angeli, A.I. Krylov, A.A. Granovsky, R. Lindh, and M. Olivucci, On the shape of multireference, EOM-CC, and DFT potential energy surfaces at a conical intersection, *J. Chem. Theory Comput.* **10**, 3074 (2014).
- [2] S. Matsika, X. Feng, A.V. Luzanov, and A.I. Krylov, What we can learn from the norms of one-particle density matrices, and what we can't: Some results for interstate properties in model singlet fission systems, *J. Phys. Chem. A* **118**, 5188 (2014).

SPECTROSCOPY AND DYNAMICS OF REACTION INTERMEDIATES IN COMBUSTION CHEMISTRY

Marsha I. Lester
Department of Chemistry
University of Pennsylvania
Philadelphia, PA 19104-6323
milester@sas.upenn.edu

I. Program Scope

The hydroxyl radical, a key oxidant in combustion, is generally detected by laser-induced fluorescence on the $A^2\Sigma^+ - X^2\Pi$ band system. Sensitive, state-selective ionization detection of OH radicals offers additional advantages, and thus this laboratory is expanding its efforts to develop and apply a robust 1+1' ionization scheme that combines OH A-X excitation with VUV ionization via autoionizing Rydberg states. Carbonyl oxides, important intermediates in tropospheric hydrocarbon oxidation and some combustion reactions, are also being examined to determine their intrinsic stability and explore dynamical pathways involving multiple potential energy surfaces that result from UV excitation. Lastly, reactive intermediates produced in low temperature combustion of alkanes, including QOOH, are being investigated using novel spectroscopic and dynamical methods.

II. Recent Progress

A. Velocity map imaging studies related to Criegee intermediates

Our initial velocity map imaging (VMI) study focused on the photodissociation of CH_2I_2 at 248 nm,¹ which is of renewed interest because subsequent reaction of CH_2I photofragments with O_2 is being utilized to generate the simplest Criegee intermediate CH_2OO for laboratory studies.² In our VMI study, the $I^*(^2P_{1/2})$ products are detected by 2+1 REMPI at 313 nm; background one-color I^* signal from 313 nm photolysis/ionization alone is subtracted. The resultant image arising from 248 nm photolysis is reconstructed to obtain the velocity and angular distributions of the I^* products as well as the corresponding kinetic energy release to products and anisotropy parameter. The dominant feature in the total kinetic energy distribution has a sizable breadth and average translational energy of 2100 cm^{-1} , which corresponds to only 14% of the available energy. This leaves the remaining 86% channeled into the internal excitation of the CH_2I cofragment, where $\langle E_{\text{int}} \rangle = 12,700 \text{ cm}^{-1}$ ($36.3 \text{ kcal mol}^{-1}$). This is in accord with a previous investigation of IR emission from CH_2I fragments produced with a combination of I and I^* cofragments.³ Depending on experimental conditions, some internal excitation of the CH_2I fragments could be carried over into CH_2OO in a near thermo-neutral process.⁴

Our next VMI study focused on the UV photodissociation dynamics of the simplest Criegee intermediate CH_2OO .^{5,6} Initially, we characterized the velocity and angular distributions of O^1D photofragments following UV excitation of jet-cooled CH_2OO on the $B^1A' \leftarrow X^1A'$ transition at 308, 330, and 360 nm.⁵ A representative image and corresponding total kinetic energy release (TKER) distribution resulting from 360 nm photolysis is shown in Figure 1. The anisotropic angular distributions observed at each wavelength are indicative of prompt dissociation, which is rapid compared with the ps timescale for rotation of the Criegee intermediate. The

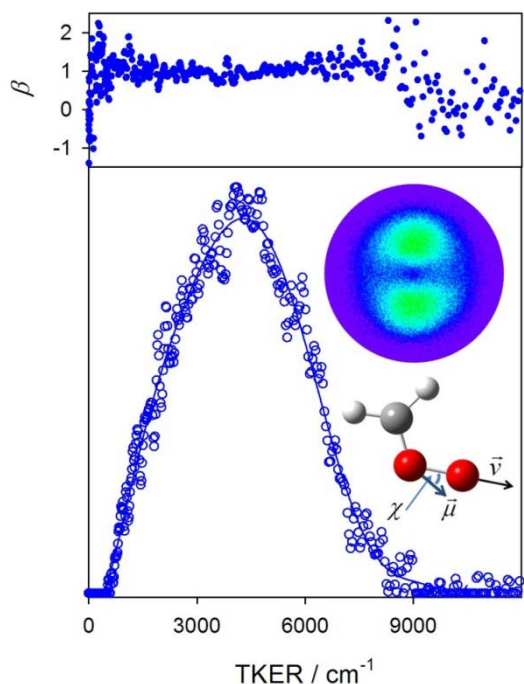


Figure 1 Velocity map image with derived total kinetic energy release (TKER) and anisotropy parameter (β) distributions for O^1D products resulting from photolysis of CH_2OO at 360 nm. The angle χ between the TDM of CH_2OO and the recoil velocity of the O-atom fragment is evaluated from the anisotropy parameter.

X^1A' to the excited B^1A' state will result in dissociation via multiple coupled potentials to two spin-allowed product channels: $H_2CO X^1A_1 + O^1D$ and $H_2CO a^3A'' + O^3P$. This prompted our experimental VMI study of the higher energy $H_2CO a^3A'' + O^3P$ channel.⁸ Again, anisotropic angular distributions of the O^3P products are obtained at 330 and 350 nm, indicative of rapid (sub-ps) dissociation, along with broad and unstructured total kinetic energy distributions that reflect the internal excitation of the $H_2CO a^3A''$ co-fragment. A harmonic normal mode analysis indicates that the CH_2 wag and C-O stretch modes of the $H_2CO a^3A''$ fragment will be significantly excited upon dissociation. The termination of the TKER distribution at each UV wavelength establishes the energy required to yield $H_2CO a^3A'' + O^3P$ products of ca. 76 kcal mol⁻¹, corresponding to a threshold excitation of 378 nm. This, in turn, is utilized with the singlet-triplet spacings in formaldehyde and oxygen atoms to deduce the energy required to reach the $H_2CO X^1A_1 + O^1D$ asymptotic limit. The latter provides an upper limit for the dissociation energy from $CH_2OO X^1A'$ to $H_2CO X^1A_1 + O^1D$ of $D_0 \leq 49$ kcal mol⁻¹, which is in good accord with theoretical predictions.

Scanning the UV excitation laser, while detecting O^1D or O^3P products, yields action spectra. The O^3P action spectrum⁸ for CH_2OO peaks at shorter wavelength (~ 330 nm) and falls off more rapidly on the long wavelength side than the previously reported CH_2OO B-X absorption spectrum under similar jet-cooled conditions.⁶ These spectral changes arise from the close proximity of the energetic threshold for the $H_2CO a^3A'' + O^3P$ product channel at 378 nm. Modeling suggests that the O^3P product yield steadily increases toward shorter wavelength over

experimentally derived anisotropy parameter β also yields the orientation of the transition dipole moment (TDM) with respect to the O^1D recoil along the O-O bond axis. Complementary electronic structure calculations yield a theoretically derived TDM orientation in good accord with experiment, showing that the angular distribution of the O^1D products is a reflection of the $\pi^* \leftarrow \pi$ character of the electronic transition associated with the COO group.

The TKER distributions indicate a high degree of vibrational excitation in the H_2CO products, originating from changes in the equilibrium structure for $CH_2OO X^1A'$ compared to $H_2CO X^1A_1$. In particular, a harmonic normal mode analysis suggests significant C-O stretch excitation. After accounting for the different excitation energies, the TKER distributions are found to have a common termination, providing an initial estimate for the $CH_2OO X^1A'$ dissociation energy ($D_0 \leq 54$ kcal mol⁻¹). Some rotational excitation of the $H_2CO X^1A_1$ fragments is also anticipated based on an impulsive model, which would lower this estimate.

In a collaborative theoretical study, Samanta et al.⁷ predicted that electronic excitation of CH_2OO

the region spanned by the UV absorption spectrum of CH₂OO, thereby distorting the shape of the O³P action spectrum. On the other hand, the O¹D action spectrum⁵ appears to follow the absorption spectrum of jet-cooled CH₂OO more closely,⁶ indicating that H₂CO X¹A₁ + O¹D is the dominant product channel.

Analogous VMI experiments are in progress on the UV photodissociation dynamics of a prototypical alkyl-substituted Criegee intermediate CH₃CHOO, yielding both CH₃CHO X¹A' + O¹D and CH₃CHO a³A + O³P products. Again, anisotropic angular and TKER distributions are obtained, in accord with rapid (sub-ps) photodissociation dynamics and vibrationally excited CH₃CHO products. In this case, an even more pronounced threshold for the onset of O³P products is observed at ca. 320 nm.

B. A new spectroscopic window on hydroxyl radicals using UV+VUV resonant ionization

Recently, we demonstrated a new 1+1' resonance enhanced multiphoton ionization (REMPI) scheme for detection of OH X²Π radicals utilizing a broad range of intermediate A²Σ⁺ (ν=1, 2) levels.^{9,10} Subsequent fixed-frequency VUV excitation at 118 nm (10.5 eV) accesses the OH [A³Π, 3d], ν=0 Rydberg state prior to rapid Auger decay and ionization. This REMPI scheme has already been utilized for detection of OH X²Π products from unimolecular decay of energized Criegee intermediates.^{11,12} In addition, a very recent VMI study is using this 1+1' ionization scheme to obtain the kinetic energy release to OH products following IR activation of *syn*-CH₃CHOO.¹³

III. Future Work

Future studies will expand our investigation of the 1+1' REMPI detection scheme for OH X²Π radicals. The planned research focuses on understanding the ionization step by separating the VUV excitation and autoionization processes using tunable VUV radiation and photoelectron velocity map imaging. We also plan to utilize this novel OH detection scheme in VMI studies of photochemical and unimolecular reactions. Ongoing studies of carbonyl oxides will explore the dissociation dynamics of methyl-substituted Criegee intermediates upon UV excitation. Lastly, a new line of research is being initiated to generate and stabilize QOOH intermediates in a pulsed supersonic expansion.

IV. References

1. J. H. Lehman, H. Li and M. I. Lester, *Chem. Phys. Lett.* **590**, 16-20 (2013).
2. O. Welz, J. D. Savee, D. L. Osborn, S. S. Vasu, C. J. Percival, D. E. Shallcross and C. A. Taatjes, *Science* **335**, 204 (2012).
3. S. L. Baughcum and S. R. Leone, *J. Chem. Phys.* **72**, 6531 (1980).
4. E. P. F. Lee, D. K. W. Mok, D. E. Shallcross, C. J. Percival, D. L. Osborn, C. A. Taatjes and J. M. Dyke, *Chem. Eur. J.* **18**, 12411 (2012).
5. J. H. Lehman, H. Li, J. M. Beames and M. I. Lester, *J. Chem. Phys.* **139**, 141103 (2013).
6. J. M. Beames, F. Liu, L. Lu and M. I. Lester, *J. Am. Chem. Soc.* **134**, 20045-48 (2012).
7. K. Samanta, J. M. Beames, M. I. Lester, and J. E. Subotnik, *J. Chem. Phys.* **141**, 134303 (2014).
8. H. Li, Y. Fang, J. M. Beames, and M. I. Lester, *J. Chem. Phys.*, submitted (2015).
9. J. M. Beames, F. Liu, M. I. Lester and C. Murray, *J. Chem. Phys.* **134**, 241102 (2011).
10. J. M. Beames, F. Liu, and M. I. Lester, *Mol. Phys.* **112**, 897-903 (2014).

11. J. M. Beames, F. Liu, L. Lu, and M. I. Lester, *J. Chem. Phys.* **138**, 244307 (2013).
12. F. Liu, J. M. Beames, A. M. Green, and M. I. Lester, *J. Phys. Chem. A* **118**, 2298–2306 (2014).
13. F. Liu, J. M. Beames, A. S. Petit, A. B. McCoy, and M. I. Lester, *Science* **345**, 1596-1598 (2014).

V. Publications supported by this project (2012-2015)

1. K. Samanta, J. M. Beames, M. I. Lester, and J. E. Subotnik, “Quantum dynamical investigation of the simplest Criegee intermediate CH₂OO and its O-O photodissociation channels”, *J. Chem. Phys.* **141**, 134303 (2014).
2. J. H. Lehman and M. I. Lester, “Dynamical outcomes of quenching: Reflections on a conical intersection”, *Ann. Rev. Phys. Chem.* **65**, 537-55 (2014).
3. J. M. Beames, F. Liu, and M. I. Lester, “1+1' resonant ionization of OH radicals via the A²Σ⁺ state: Insights from direct comparison with A-X fluorescence detection”, *Mol. Phys.* **112**, 897-903 (2014).
4. J. H. Lehman, H. Li, J. M. Beames and M. I. Lester, “Communication: Ultraviolet photodissociation dynamics of the simplest Criegee intermediate CH₂OO”, *J. Chem. Phys.* **139**, 141103 (2013).
5. J. H. Lehman, H. Li and M. I. Lester, “Ion imaging studies of the photodissociation dynamics of CH₂I₂ at 248 nm”, *Chem. Phys. Lett.* **590**, 16-20 (2013).
6. J. H. Lehman, M. I. Lester, J. Kłos, M. H. Alexander, P. J. Dagdigian, D. Herráez-Aguilar, F. J. Aoiz, M. Brouard, H. Chadwick, T. Perkins, and S. A. Seamans, “Electronic quenching of OH A²Σ⁺ induced by collisions with Kr atoms”, *J. Phys. Chem. A* **117**, 13481-90 (2013).
7. J. H. Lehman, M. I. Lester, and D. H. Yarkony, “Reactive quenching of OH A²Σ⁺ by O₂ and CO: Experimental and nonadiabatic theoretical studies of H- and O-atom product channels”, *J. Chem. Phys.* **137**, 094312 (2012).

Computational Flame Diagnostics for Direct Numerical Simulations with Detailed Chemistry of Transportation Fuels

Tianfeng Lu

Department of Mechanical Engineering
University of Connecticut, Storrs, CT 06269-3139
tlu@engr.uconn.edu

I. Program Scope

The goal of the proposed research is to create computational flame diagnostics that are rigorous numerical algorithms to detect critical flame features, including ignition, local extinction/re-ignition, and premixed reaction fronts and non-premixed flamelet, and to understand the underlying physicochemical processes controlling limit flame phenomena, flame stabilization, turbulence-chemistry interactions and pollutant emissions etc. Diagnostics based on chemical explosive mode analysis (CEMA) [i] are performed for direct numerical simulations (DNS) of a variety of turbulent flames using non-stiff reduced mechanisms for transportation fuels (collaboration with J.H. Chen at Sandia) to extract salient physical information from the complex flow fields.

II. Recent Progress

A. *Reduced mechanisms and reduction methods for engine fuels*

Reduced mechanisms for a variety of engine fuels, including ethanol, DME, n-dodecane have been developed for high-fidelity flame simulations, including both large eddy simulations (LES) and DNS, at engine-relevant conditions. The reduction is primarily based on directed relation graph (DRG), sensitivity analysis and analytically solved linearized quasi steady state approximations. Chemical stiffness is dynamically removed such that the highly efficient explicit solvers can be employed in DNS [ii]. Specifically, a 28-species reduced mechanism is developed for ethanol/air with NO_x formation and was applied in Sandia's 2-D and 3-D DNS of HCCI and spark assisted compression ignition (SACI) [7]. A reduced mechanism for DME with 30 transported species is developed [9] and employed in Sandia's DNS of laminar and turbulent lifted flames, temporal jet flame, and homogeneous charge compression ignition (HCCI). A 106-species skeletal mechanism for *n*-dodecane is developed and employed in RANS and LES of lifted diesel spray flames in collaboration with S. Som at Argonne National Laboratory and employed by other research groups in the engine combustion network (ECN).

Rigorous error control is critical for model reduction methods while the challenges result from the highly nonlinear couplings among different reaction pathways. While the DRG method can effectively control the worst case error in skeletal mechanisms, error propagation in further reduced models can be highly complex. A linearized error propagation (LEP) model based on Jacobian analysis is developed to quantify the reduction error propagating into high concentration species due to the elimination of the species in low concentrations. The reduction is based on 0-D steady-state perfectly stirred reactors (PSR) involving both ignition and extinction states. Validation result in Fig. 1 shows that the LEP based reduction method can effectively control the worst case errors in major species of interest. Furthermore, it is shown that the skeletal mechanism derived from PSR can be extended to more complex flames in that the PSR S-curve covers both ignition and extinction chemistry.

To achieve high efficiency in flame simulations, DAC methods based on DRG are developed to expedite time integration of chemically reacting systems based on the DRG method [3,5,11,13]. DAC is integrated with the Strang splitting scheme and a second order accuracy in time-integration is achieved and demonstrated in 1-D freely propagating premixed laminar flames of methane-air. Speedup factors of about 30 are achieved for simulations of HCCI combustion of iso-octane/air in a partially stirred reactor [3].

DRG-based DAC is further extended to the method of species time scale and rate analysis (TSRA) by modeling error propagation in major species. The TSRA method is applied to auto-ignition of methane-air and *n*-heptane-air mixtures over a wide range of initial temperatures and pressures. Ignition is accurately predicted, including the negative temperature coefficient (NTC) behavior for *n*-heptane.

Multicomponent diffusion is involved in most practical combustion devices. For high-fidelity flame simulations, multicomponent diffusion models involve inversion of linear problems and can be highly time consuming when the number of species is large. A systematic strategy is developed to reduce multicomponent diffusion models by accurately accounting for the species whose diffusivities are important for flame responses, while approximating the diffusivities of the less important species [11]. The reduced models are investigated in planar premixed flames, counterflow diffusion flames, and ignition of droplet flames, showing significantly higher accuracy than that of the mixture-averaged model, while the computational cost was reduced by a factor of approximately 5 compared with the detailed multicomponent model for an *n*-heptane with 88 species.

C. Computational flame diagnostics

A bifurcation analysis (BA) is developed based on the description of extinction and ignition states as bifurcation points on the S-curves of steady state combustion, and the reactions important to ignition and extinction are identified based on their normalized contributions to the bifurcation points, defined as the bifurcation index (BI) [8]. BA is based on the full Jacobian of ordinary differential equations obtained for 0-D reactors and spatially discretized reacting flows. For 2-D and 3-D flame simulations, the full Jacobian becomes too large such that BA is not feasible. In such cases, CEMA is applied by focusing on the chemical Jacobian and the responses of the chemical properties of local mixtures to different flame features [10]. Both BA and CEMA are based on eigen-analyses to decouple the interactions among different processes.

Identification of ignition and premixed fronts using CEMA are investigated in [i, 1, 10, 12], and extinction behaviors of 1-D laminar counterflow flames and a 3-D DNS of turbulent non-premixed ethylene-air flame [iii] are investigated with CEMA to systematically identify local flame features involved during local extinction and re-ignition. Results on laminar flames show that mixtures in the reaction zone start to show explosive behavior, characterized by a

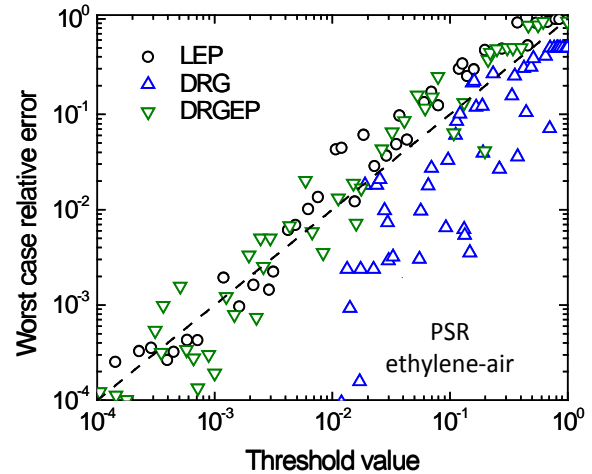


Figure 1. Worst case relative error in target species in PSR for 1-30atm, $\phi=1$, $T_{in} = 1000K$, calculated using local skeletal models for ethylene-air based on USC-Mech II, derived with LEP, DRG, and DRGEP, respectively.

positive eigenvalue of the chemical Jacobian, when the flame approaches extinction, while only non-explosive mixtures are present in strongly burning flames at low strain rates. Thus the presence of explosive mixtures is a necessary condition to detect flame extinction. This criterion is employed to study the DNS data in [iii]. Local flame features, including strongly burning non-premixed, near-extinction, post-extinction and premixed front zones are identified and shown in Fig. 2 and compared with 1-D premixed and non-premixed flamelets.

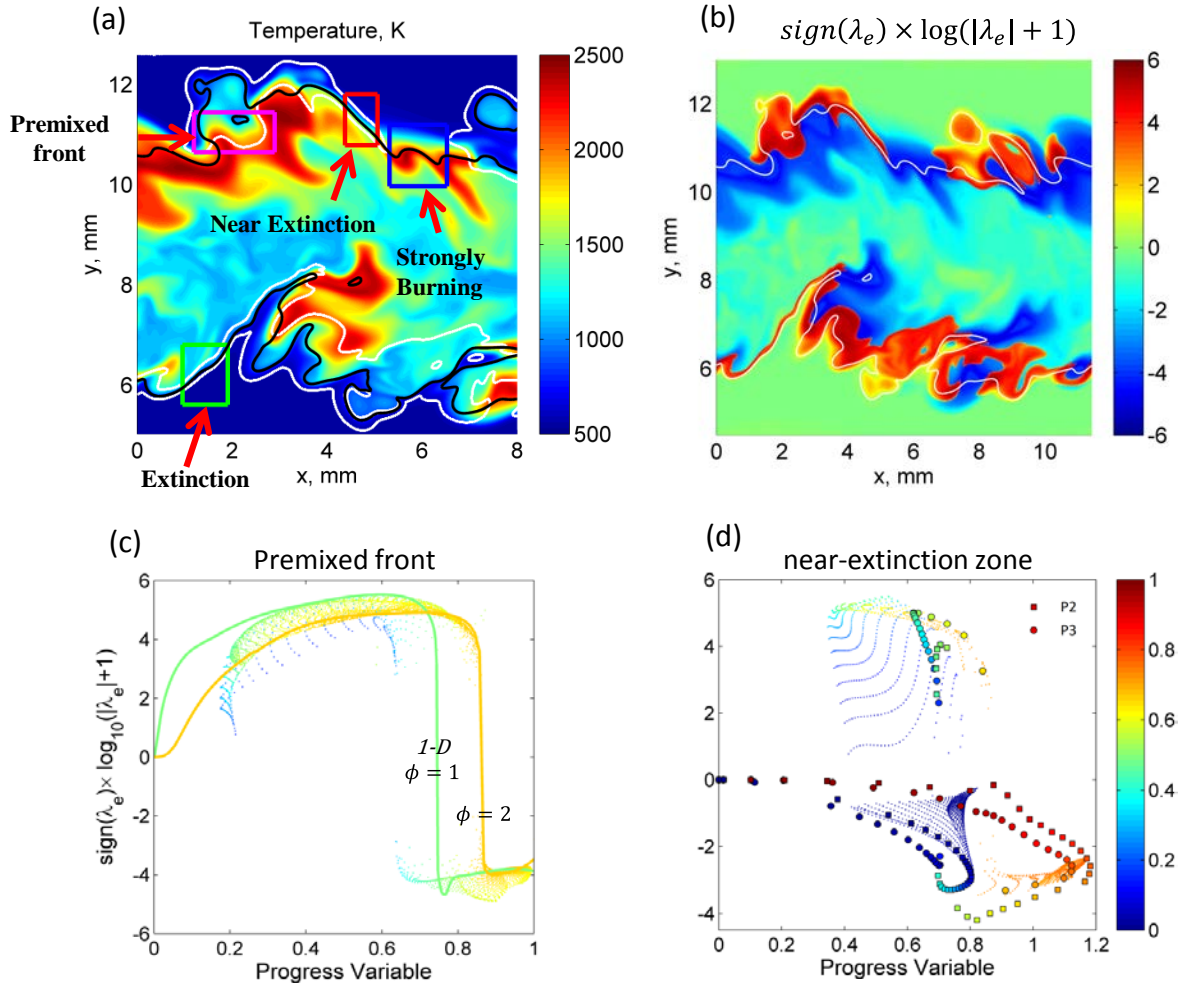


Figure 2. a) Isocontour of temperature, b) reciprocal explosive mode timescale, λ_e , c) scatter of λ_e vs. progress variable in the premixed front zone, the pink box in a), and d) scatter of λ_e vs. progress variable in the near-extinction zone, the red box in a), on the 2-D center plane at $t = 0.2 \text{ ms}$. The white isoline in b) indicates the stoichiometric surface. The solid lines in c) are unstrained 1-D premixed flame solutions, showing the presence of local premixed fronts in the DNS data. The large symbols in d) indicate 1-D non-premixed flame solutions, showing the signature of non-premixed near-extinction flamelets.

CEMA based diagnostics are also performed on Sandia's 3-D DNS of a lifted DME jet flame at elevated pressure. Results show that non-premixed flames at strongly turbulent conditions can involve complex flame features, including local premixed fronts and local extinction and re-ignition, as also observed in the DNS in Fig. 2. CEMA-based diagnostics therefore provide reliable criteria to identify different flames features for adaptive combustion modeling.

References

- i. T. Lu, C.S. Yoo, J.H. Chen, C.K. Law, *J. Fluid Mech.*, 2010 652 (1) 45–64.
- ii. T. Lu, C. K. Law, *Prog. Energy Combust. Sci.* 2009, 35(2), 192-215.
- iii. D.O. Lignell, J.H. Chen, H.A. Schmutz, *Combust. Flame* 2011, 158 (5) 949-963

Journal papers funded by this grant

1. M.B. Luong, Z. Luo, T.F. Lu, S.H. Chung, C.S. Yoo, "Direct numerical simulations of the ignition of lean primary reference fuel/air mixtures under HCCI condition," *Combustion and Flame*, 160 (10) 2038–2047, 2013.
2. S.M. Sarathy, S. Park, B. Weber, W. Wang, P. Veloo, A.C. Davis, C. Togbe, C.K. Westbrook, O. Park, G. Dayma, Z. Luo, M.A. Oehlschlaeger, F. Egolfopoulos, T.F. Lu, W.J. Pitz, C.J. Sung, P. Dagaut, "A comprehensive experimental and modeling study of iso-pentanol combustion," *Combustion and Flame*, 160 (12) 2712-2728, 2013.
3. Z. Ren, Y. Liu, T.F. Lu, L. Lu, O.O. Oluwole, G.M. Goldin, "The use of dynamic adaptive chemistry and tabulation in reactive flow simulations," *Combustion and Flame*, 161 (1) 127–137, 2014.
4. Z. Ren, H. Yang, T.F. Lu, "Effects of Small-Scale Turbulence on NO_x Formation in Premixed Flame Fronts," *Fuel*, 115 241–247, 2014.
5. Z. Ren, C. Xu, T.F. Lu, M.A. Singer, "An Operator Splitting Scheme with Dynamic Adaptive Chemistry for Reactive Flow Simulations," *Journal of Computational Physics*, 263 19–36, 2014.
6. Z. Luo, S. Som, S.M. Sarathy, M. Plomer, W.J. Pitz, D.E. Longman, T.F. Lu, "Development and Validation of an n-Dodecane Skeletal Mechanism for Diesel Spray-Combustion Applications," *Combustion Theory and Modeling*, 18 (2) 187-203, 2014.
7. A. Bhagatwala, J.H. Chen, T.F. Lu, "Direct numerical simulations of HCCI/SACI with ethanol," *Combustion and Flame*, 161 (7) 1826-1841, 2014.
8. R. Shan, T.F. Lu, "A Bifurcation Analysis for Limit Flame Phenomena of DME/air in Perfectly Stirred Reactors," *Combustion and Flame*, 161 (7) 1716-1723, 2014.
9. A. Bhagatwala, T.F. Lu, H. Shen, J.A. Sutton, J.H. Chen, "Numerical and experimental investigation of turbulent DME jet flames," *Proceedings of the Combustion Institute*, 35(2) 1157-1166, 2015.
10. M.B. Luong, T.F. Lu, S.H. Chung, C.S. Yoo, "Direct numerical simulations of the ignition of a lean biodiesel/air mixture with temperature and composition inhomogeneities at high pressure and intermediate temperature," *Combustion and Flame*, 161(11) 2878–2889, 2014.
11. Y.X. Xin, W.K. Liang, W. Liu, T.F. Lu, C.K. Law, "A Reduced Multicomponent Diffusion Model," *Combustion and Flame*, 162(1) 68-74, 2015.
12. M.B. Luong, G.H. Yu, T.F. Lu, S.K. Chung, "Direct numerical simulations of ignition of a lean n-heptane/air mixture with temperature and composition inhomogeneities relevant to HCCI and SCCI combustion," *Combustion and Flame*, submitted.
13. Z. Lu, L. Zhou, Z. Ren, T.F. Lu, K.H. Luo, "Transient simulations of an n-heptane spray flame with dynamic adaptive chemistry," *Combustion Theory and Modeling*, submitted.

Advanced Nonlinear Optical Methods for Quantitative Measurements in Flames

Robert P. Lucht

School of Mechanical Engineering, Purdue University

West Lafayette, IN 47907-2088

Lucht@purdue.edu

I. Program Scope

Nonlinear optical techniques such as laser-induced polarization spectroscopy (PS), resonant wave mixing (RWM), and electronic-resonance-enhanced (ERE) coherent anti-Stokes Raman scattering (CARS) are techniques that show great promise for sensitive measurements of transient gas-phase species, and diagnostic applications of these techniques are being pursued actively at laboratories throughout the world. The objective of this research program is to develop and test strategies for quantitative concentration and temperature measurements using nonlinear optical techniques in flames and plasmas. We have continued our fundamental theoretical and experimental investigations of these techniques. We have also initiated both theoretical and experimental efforts to investigate the potential of femtosecond (fs) laser systems for sensitive and accurate measurements in gas-phase media. Our initial efforts have been focused on fs CARS, although the systems will be useful for a wide range of future diagnostic techniques involving two-photon transitions. In the last year we have demonstrated the acquisition of single-shot temperature measurements at data rates of 5 kHz in highly turbulent, swirl-stabilized methane-air flames. The fs CARS measurements exhibited high signal-to-noise ratios and temperatures were extracted from nearly every laser shot. We have also extended the dynamic range of the system by using a two-channel detection scheme.

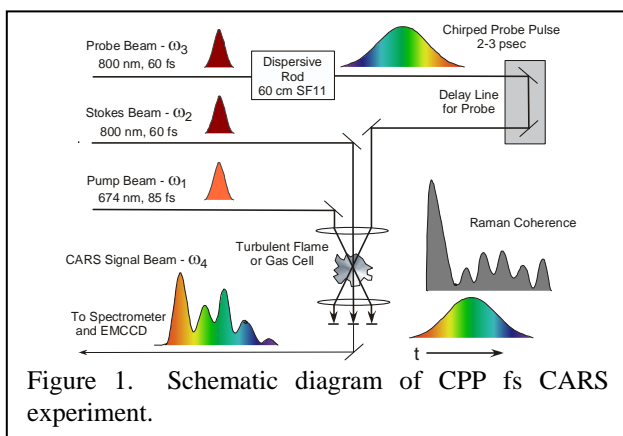
Over the past year we have continued our two-color PS measurements. We developed and optimized a new laser system for the two-color PS measurements of nitric oxide featuring two injection-seeded optical parametric generator/pulsed dye amplifier (OPG/PDA) systems, both operating near 452 nm. Collision-induced resonances were clearly observed with this system. The effects of different buffer gases on the generation of the collision-induced resonances was investigated and a numerical code for calculation of the two-color PS spectra developed.

We are investigating the physics of both fs CARS and two-color PS by direct numerical integration (DNI) of the time-dependent density matrix equations for the resonant interaction. Significantly fewer restrictive assumptions are required using this DNI approach compared with the assumptions required to obtain analytical solutions. We are concentrating on the accurate simulation of two-photon processes, including Raman transitions, where numerous intermediate electronic levels contribute to the two-photon transition strength. We have made significant progress in the last year on modeling two-color PS of atomic hydrogen, and are obtaining good agreement between experiment and modeling. We have also developed a code for the modeling of two-color PS signals, including the generation of collision-induced resonances.

II. Recent Progress

A. Femtosecond CARS Calculations and Experiments

The single-shot, chirped-pulse-probe (CPP) fs CARS system for temperature measurements is shown in Fig. 1. Fs CARS offers several major potential advantages compared with nanosecond (ns) CARS; i.e., CARS as usually performed with nanosecond pump and Stokes lasers. These potential advantages include an elimination of collisional effects in the signal generation and the capability of performing real-time temperature and species measurements at data rates of 1 kHz or greater as compared to 10-50 Hz for ns CARS. Our Coherent ultrafast laser system operates at 5 kHz with a fundamental pulse width of 60 fs and energy of over 2 mJ. The fundamental 800-nm pulse is Fourier-transform-limited to within a few percent. The fundamental 800-nm beam is used as the probe beam



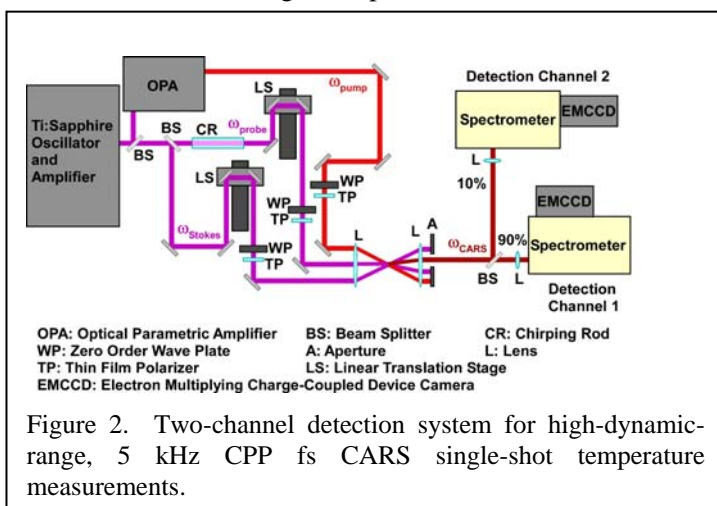
for our CPP fs CARS experiments. The greatly increased pulse energy of the chirped-pulse-probe beam results in a significant increase in the signal-to-noise ratio of the single-pulse measurements.

The fundamental 800-nm pulse is Fourier-transform-limited to within a few percent. The fundamental 800-nm beam is used as the probe beam for our chirped-pulse-probe (CPP) fs CARS experiments as shown in Fig. 1. The greatly increased pulse energy of the chirped-pulse-probe beam results in a significant increase in the signal-to-noise ratio

of the single-pulse measurements. During the past year we continued our analysis of single-laser-shot temperature measurements acquired at a data rate of 5 kHz in a highly turbulent, swirl-stabilized burner that has been characterized extensively at DLR Stuttgart. Measurements were performed for a so-called “stable” case and for a case with significant thermoacoustic instabilities. The CARS temperature measurements are in good agreement with previous single-shot Raman scattering measurements in the same flame. A microphone was used to record pressure pulsations in the burner. Simultaneous acoustic measurements enabled phase-synchronization of the fs CARS measurements with the thermo-acoustic pulsations in the burner. The rapid accumulation of statistically-converged datasets also supported a phase conditioned statistical analysis to study the time-evolving thermo-chemical state over the course of a thermoacoustic cycle. The CARS measurements are described in P3 and in a pair of articles in preparation for submission to Combustion and Flame.

The measurements in the DLR burner were quite successful in that on virtually every laser shot the signal level was high enough and the signal was clean enough such that a temperature could be determined by least squares fitting of theoretical spectra to the experimental spectra. However, in regions of the burner where cold gas pockets were present the CARS signal was high enough to saturate the EMCCD detector. To address this problem we borrowed a spectrometer and EMCCD camera from Andor and set up a two-channel detection system featuring a 90%T/10%R beamsplitter as shown in Fig. 2. When the gas in the CARS probe volume was hot (>1000K), the signal in detection channel 1 was analyzed to determine the temperature. When the gas in the CARS probe volume was cold (<1000K), the signal in detection channel 2 was analyzed to determine the temperature. The experimental system and measurements in a hydrogen jet diffusion flame are discussed in paper P5.

We have also begun to perform CPP fs CARS measurements of fuel species. We performed



measurements of methane, ethylene, and propane, and mixtures of these gases at room temperature for a range of pressures up to 10 bars. Measurements of methane and nitrogen in a swirling nonreacting flow were also performed by tuning the OPA pump beam output wavelength to 640 nm so that the central Raman frequency shift was midway between N_2 (2330 cm^{-1}) and CH_4 (2914 cm^{-1}). The results of those measurements and the best-fit theoretical spectrum are shown in Fig. 3. The methane spectral

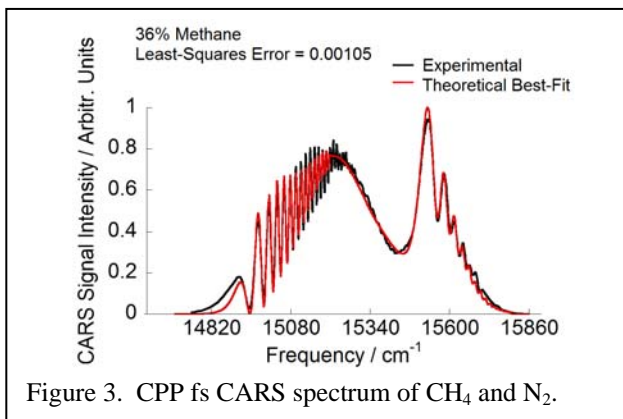


Figure 3. CPP fs CARS spectrum of CH₄ and N₂.

radiation from OPGs is then amplified using two separate pulse dye amplifier stages. During the last year we continued our experiments on two-color, single-photon PS of NO. An energy level diagram for the generation and detection of collision-induced resonances is shown in Fig. 4, and experimental spectra are shown in Figs. 5 and 6 for measurements of two-color NO PS for the buffer gases helium and argon, respectively. The spectrum shown in Fig. 5 clearly shows transitions resulting from the

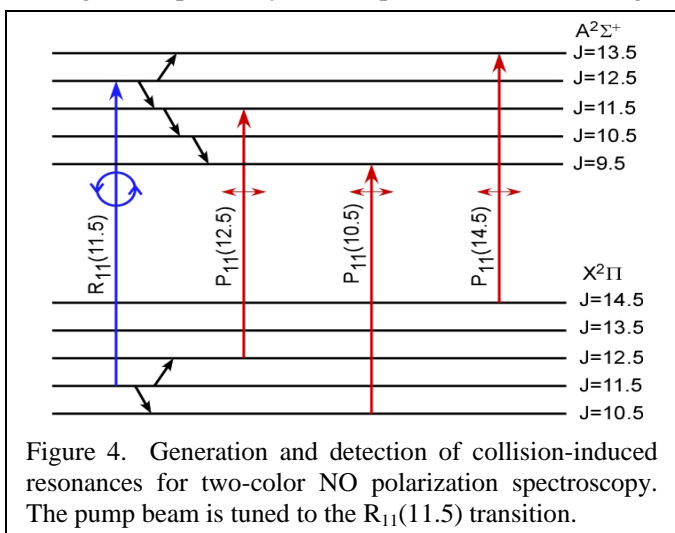


Figure 4. Generation and detection of collision-induced resonances for two-color NO polarization spectroscopy. The pump beam is tuned to the R₁₁(11.5) transition.

model does a very good job of simulating the experimental spectrum

B. Polarization Spectroscopy and Six-Wave Mixing: Experiments and Modeling Efforts

We developed and have continued to apply a new experimental apparatus for high-spectral-resolution PS measurements. The system features two OPG stages that injection seeded at the idler wavelength and pumped by the 355-nm third harmonic radiation from an injection-seeded Nd:YAG laser. The signal

radiation from OPGs is then amplified using two separate pulse dye amplifier stages. During the last year we continued our experiments on two-color, single-photon PS of NO. An energy level diagram for the generation and detection of collision-induced resonances is shown in Fig. 4, and experimental spectra are shown in Figs. 5 and 6 for measurements of two-color NO PS for the buffer gases helium and argon, respectively. The spectrum shown in Fig. 5 clearly shows transitions resulting from the transfer of anisotropy in the Zeeman state distribution during rotational transfer in either the lower or upper electronic levels for the transition. The helium atom is light enough that it cannot alter the direction of the rotation significantly during a collision. For collisions with argon, however, the intensity of the collision-induced resonances is significantly decreased compared to the case of helium buffer gas.

We are continuing our collaborative efforts with Dr. Thomas B. Settersten at Sandia's Combustion Research Facility on six-wave mixing (6WM) spectroscopy and PS of atomic hydrogen.

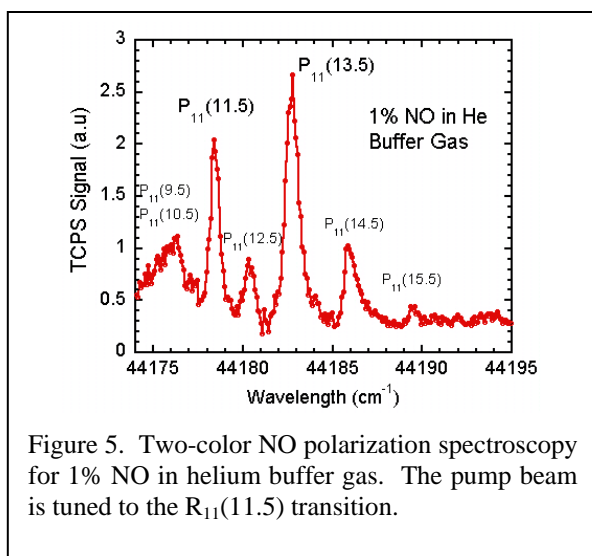


Figure 5. Two-color NO polarization spectroscopy for 1% NO in helium buffer gas. The pump beam is tuned to the R₁₁(11.5) transition.

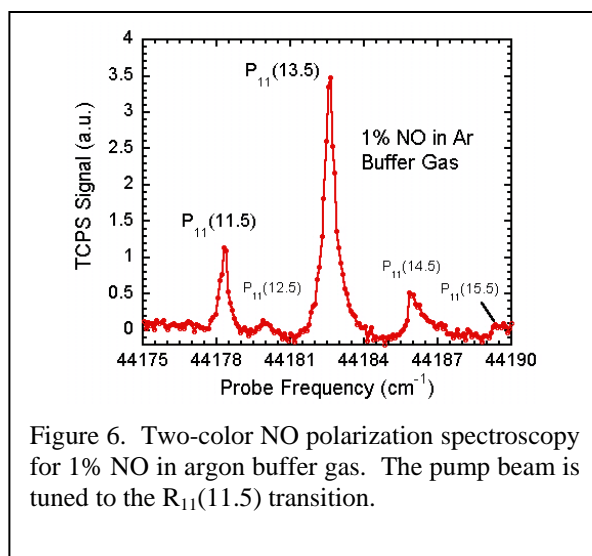


Figure 6. Two-color NO polarization spectroscopy for 1% NO in argon buffer gas. The pump beam is tuned to the R₁₁(11.5) transition.

III. Future Work

We will continue to perform fs CARS experiments in our laboratory using the Coherent ultrafast laser system. Our studies of temperature measurements using CPP fs CARS will continue. We continue to investigate the effect of laser system parameters on the CPP fs CARS spectrum to improve the temperature accuracy of the technique. We will explore the potential for using CPP fs CARS for accurate concentration measurements for hydrocarbon species and other polyatomic molecules, a very hard species to measure using ns CARS. We plan to design and fabricate a high-temperature, high-pressure furnace for fundamental studies of temperature and species measurements.

Our investigation of the physics of single-photon, two-color PS for species such as NO, and two-photon, two-color PS and 6WM for species such as CO will continue. We have developed a new experimental apparatus for these measurements and collected extensive line shape and concentration data for atomic hydrogen, and are in the process of investigating collision-induced resonances for two-color PS of NO. We will be able to explore collisional effects on the PS and 6WM processes in much more detail using a low-pressure cell filled with NO and different buffer gases. We will continue to use the density matrix code to gain insight into the physics of the PS and 6WM processes.

In the future we plan to introduce a dual-pump CARS variant of the technique for sensitive detection of three or more species along with the temperature measurement from both pure rotational and vibrational CARS. We plan to combine the two-beam pure rotational CARS with a dual-beam CARS system where the vibrational spectra for H₂ and N₂ are detected simultaneously.

IV. Refereed publications and submitted journal articles supported by this project 2013-2015

- P1. D. R. Richardson, R. P. Lucht, S. Roy, W. D. Kulatilaka, and J. R. Gord, "Chirped-Probe-Pulse Femtosecond Coherent Anti-Stokes Raman Scattering Concentration Measurements," *Journal of the Optical Society of America B* **30**, 188-196 (2013).
- P2. A. Satija and R. P. Lucht, "Development of a New Combined Pure Rotational and Vibrational Coherent Anti-Stokes Raman Scattering (CARS) System," *Optics Letters* **38**, 1340-1342 (2013).
- P3. C. N. Dennis, C. D. Slabaugh, I. G. Boxx, W. Meier, R. P. Lucht, "Femtosecond Coherent Anti-Stokes Raman Scattering Thermometry at 5 kHz in a Gas Turbine Model Combustor," *Proceedings of the Combustion Institute* **35**, 3731-3738 (2015). DOI: 10.1016/j.proci.2014.06.063
- P4. A. Satija, S. Yuan, S. V. Naik, and R. P. Lucht, "Vibrational Coherent Anti-Stokes Raman Scattering (VCARS) Thermometry and 1-D Numerical Simulations in CH₄/H₂/Air Partially-Premixed Flames," *International Journal of Hydrogen*, accepted for publication (2015).
- P5. C. N. Dennis, A. Satija, and R. P. Lucht, "High Dynamic Range Thermometry at 5 kHz in Hydrogen-Air Diffusion Flame using Chirped-Probe-Pulse Femtosecond Coherent Anti-Stokes Raman Scattering," *Journal of Raman Spectroscopy*, submitted for publication (2015).

V. PhD theses completed by students supported by this project 2011-2013

- T1. Clareta N. Dennis, "Applications of Femtosecond Coherent Anti-Stokes Raman Scattering in Combustion," **Ph.D. Thesis**, Purdue University, West Lafayette, December 2014.

Theoretical studies of chemical reactions related to the formation and growth of polycyclic aromatic hydrocarbons and molecular properties of their key intermediates

Alexander M. Mebel

Department of Chemistry and Biochemistry, Florida International University
Miami, Florida 33199. E-mail: mebela@fiu.edu

Program Scope

In this project, we investigate complex chemical mechanisms of PAH formation, growth, and oxidation via theoretical studies of their critical elementary reactions. Our primary objectives include (i) to unravel reaction mechanisms through detailed, accurate, and reliable calculations of pertinent potential energy surfaces (PESs); (ii) to compute rate constants for individual reaction steps and total absolute reaction rate constants and product branching ratios depending on reaction conditions, such as collision energy or temperature and pressure; (iii) to characterize molecular, energetic, and spectroscopic parameters of various possible reaction intermediates and products including their enthalpies of formation, geometric structure, vibrational frequencies and rotational constants, as well as photoionization and photoexcitation spectra. To achieve these goals, we employ chemically accurate density functional and ab initio calculations (using CCSD(T)/CBS, G3, and explicitly correlated methods) of the PESs of these reactions which are then utilized for statistical (TST and RRKM/Master Equation) computations of absolute reaction rate constants and product branching ratios.

Recent Progress

Formation of methyl-substituted naphthalene, dihydronaphthalene, and indene. In a series of works combining theoretical calculations of potential energy surfaces and experimental crossed molecular beams studies in R. Kaiser's group, we investigated the formation of methyl-substituted naphthalene, dihydronaphthalene, and indene molecules via the reactions of tolyl radicals with C_4H_4 , C_4H_6 , and C_5H_8 , and of phenyl radical with C_5H_8 . For instance, the bimolecular reactions of phenyl-type radicals with the C4 and C5 hydrocarbons vinylacetylene and (methyl-substituted) 1,3-butadiene have been found to synthesize PAHs with naphthalene and 1,4-dihydronaphthalene cores in exoergic and entrance barrierless reactions under single-collision conditions. The reaction mechanism involves the initial formation of a van der Waals complex and addition of a phenyl-type radical to the C1 position of a vinyl-type group through a submerged barrier. Investigations suggest that in the hydrocarbon reactant, the vinyl-type group must be in conjugation with a $-C\equiv CH$ or $-HC=CH_2$ group to form a resonantly stabilized free radical intermediate, which eventually isomerizes to a cyclic intermediate followed by hydrogen loss and aromatization (PAH formation). Also, the reactions of para-tolyl radicals with C_3H_4 isomers allene and methylacetylene can produce methyl-indenes after overcoming moderate barriers in the entrance channel.

Roaming dynamics in radical addition-elimination reactions. We have studied PESs for the reactions of chlorine atoms with butenes, the dynamics of which was probed experimentally in crossed beams by A. Suits' group. The joint experimental and theoretical work has shown that these reactions involve formation of a transient strongly bound intermediate and the Cl addition-HCl elimination pathway occurs from an abstraction-like Cl-H-C geometry rather than a conventional three-center or four-center transition state. The access to this geometry is attained by roaming excursions of the Cl atom from the initially formed adduct. In effect, the alkene π cloud serves to capture the Cl atom and hold it, allowing many subsequent opportunities for the energized intermediate to find a suitable approach to the abstraction geometry. These bimolecular

roaming reactions are closely related to the roaming radical dynamics recently discovered to play an important role in unimolecular reactions.

Oxidation of graphene-edge six- and five-member rings by molecular oxygen. To gain qualitative and quantitative understanding of oxidation processes of large polycyclic aromatics, soot particles, and graphene edges, we carried out a theoretical study of the pyrenyl-O₂ reaction system in collaboration with M. Frenklach's group. Possible reaction pathways and their energetics were investigated using high-level G3-type ab initio calculations. The results were utilized in RRKM-Master-Equation calculations of rate coefficients and relative product yields at temperatures and pressures relevant to combustion. Finally, the deduced oxidation mechanisms of six- and five-member rings and the computed rate coefficients were employed in kinetic Monte-Carlo simulations of oxidation of a graphene "molecule" evolving in flame-like environments. The results of the ab initio calculations show that the reaction of the pyrenyl radical or of a pyrenyl radical-like structure in a larger PAH or a graphene sheet with two oxygen molecules is most likely to produce the phenanthryl radical, $C_{16}H_9 + 2O_2 \rightarrow C_{14}H_9$ (phenanthryl) + CO + O + CO₂, i.e., to destroy one six-member ring and form an arm-chair edge with a radical site on it. A C₁₅H₉-like radical with one five-member ring resulting from the reaction with a first O₂ molecule would undergo oxidation with a second oxygen molecule attacking the five-member ring, which completely erases the five-member ring, rather than to be subjected to an H₂/H assisted isomerization moving the radical site to a six-member ring. Therefore, two consequent oxidation reactions are not expected to produce relatively unstable structures with two five-member rings next to each other; such structures indeed are not usually observed in experiment. Among the major findings from the Monte-Carlo simulations are the following: The oxidation system exhibits two basic pathways, thermal decomposition and regeneration of oxyradicals. Their competition is temperature dependent, with the former dominating at higher and the latter at lower temperatures. The overall oxidation of the graphene substrate is computed to be time dependent, with the initial rates consistent with the known experimental data.

Future Plans

During sabbatical leave at the Argonne National Lab, the PI's collaboration with S. Klippenstein and other members of S. Pratt's group led to initiation of a research project aimed on the generation of reliable temperature- and pressure-dependent rate constants for various mechanisms of PAH formation and growth. Potential energy surfaces and molecular parameters for the reactions producing naphthalene and indene computed by the PI's group or taken from the literature are utilized in RRKM-Master Equation calculations of rate constants at temperatures and pressures relevant to combustion using the latest version of the PAPER code developed by Klippenstein and coworkers. The rate constants will be included in the latest combustion models in collaboration with R. Sivaramakrishnan and J. Miller. Within this project, we will first explore all possible pathways to the two-ring PAHs, naphthalene and indene, and then eventually extend the studies to the formation of smaller RSFR, the first aromatic ring, a further PAH growth, and PAH oxidation. In the meantime, we will continue the calculations of PESs for oxidation of large aromatic radicals (for instance, oxidation of pyrenyl with OH) and our collaborations with R. Kaiser's and M. Ahmed's groups on the studies of combustion-relevant bimolecular reactions in crossed beams and in the pyrolytic reactor at LBNL, and with A. Suits' group on the roaming dynamics of Cl reactions with hydrocarbons.

DOE/BES sponsored publications (2012-2015)

1. Kaiser R.I., Goswami M., Zhang F., Parker D., Kislov V.V., Mebel A.M., Aguilera-Iparraguirre J., Green W.H., "Crossed Beam Reaction of Phenyl and D5-Phenyl Radicals with

- Propene and Deuterated Counterparts – Competing Atomic Hydrogen and Methyl Loss Pathways”, *Phys. Chem. Chem. Phys.*, 2012, 14, 720-729.
2. Parker D.S.N., Zhang F., Kaiser R.I., Landera A., Kislov V.V., Mebel A.M., Tielens A.G.G.M., “Low Temperature Formation of Naphthalene and its Role in the Synthesis of PAH in the Interstellar Medium”, *Proc. Nat. Acad. Sci.*, 2012, 109, 53-58.
 3. Parker D.S.N., Zhang F., Kim Y.S., Kaiser R.I., Landera A., Mebel A.M., “On the Formation of Phenylacetylene ($C_6H_5C\equiv CCH$) and D5-Phenylacetylene ($C_6D_5C\equiv CCH$) Studied under Single Collision Conditions”, *Phys. Chem. Chem. Phys.*, 2012, 14, 2997-3003.
 4. Zhou C.-W., Kislov V.V., Mebel A.M., “The Reaction Mechanism of Naphthyl Radicals with Molecular Oxygen. I. A Theoretical Study of the Potential Energy Surface”, *J. Phys. Chem. A*, 2012, 116, 1571–1585.
 5. Kislov V.V., Mebel A.M., Aguilera-Iparraguirre J., Green W.H., “The Reaction of Phenyl Radical with Propylene as a Possible Source of Indene and Other Polycyclic Aromatic Hydrocarbons: An Ab Initio/RRKM-ME Study”, *J. Phys. Chem. A*, 2012, 116, 4176-4191.
 6. Kaiser R.I., Parker D.S.N., Zhang F., Landera A., Kislov V.V., Mebel A.M., “PAH Formation under Single Collision Conditions - Reaction of Phenyl Radical and 1,3-Butadiene to Form 1,4-Dihydronaphthalene”, *J. Phys. Chem. A*, 2012, 116, 4248-4258.
 7. Mebel A.M., Landera A., “Product branching ratios in photodissociation of phenyl radical: A theoretical Ab initio/RRKM study”, *J. Chem. Phys.*, 2012, 136, 234305 (9 pp.).
 8. Kaiser R.I., Mebel A.M., Golan A., Ahmed M., “A VUV Photoionization Study on the Formation of Primary and Secondary Products in the Reaction of the Phenyl Radical with 1,3-Butadiene under Combustion Relevant Conditions”, *Phys. Chem. Chem. Phys.*, 2013, 15, 341-347.
 9. Kislov V.V., Sadovnikov A.I., Mebel A.M., “Formation Mechanism of Polycyclic Aromatic Hydrocarbons Beyond the Second Aromatic Ring”, *J. Phys. Chem. A*, 2013, 117, 4794-4816.
 10. Dangi B.B., Parker D.S.N., Kaiser R.I., Jamal A., Mebel A.M., “A Combined Experimental and Theoretical Study on the Gas-Phase Synthesis of Toluene under Single Collision Conditions”, *Angew. Chem., Int. Ed.*, 2013, 52, 7186-7189.
 11. Dangi B.B., Maity S., Kaiser R.I., Mebel A.M., “A Combined Crossed Beam and Ab Initio Investigation of the Gas Phase Reaction of Dicarbon Molecules (C_2 ; $X^1\Sigma_g^+/a^3\Pi_u$) with Propene (C_3H_6 ; X^1A'): Identification of the Resonantly Stabilized Free Radicals 1- and 3-Vinylpropargyl”, *J. Phys. Chem. A*, 2013, 117, 11783–11793.
 12. Wang Q., Dyakov Y.A., Wu D., Zhang D., Jin M., Liu F., Liu H., Hu Z., Ding D., Mineo H., Teranishi Y., Chao S.D., Lin S.H., Kosheleva O.K., Mebel, A. M., “Ionization/dissociation processes of methyl-substituted derivatives of cyclopentanone in intense femtosecond laser field”, *Chem. Phys. Lett.*, 2013, 586, 21–28.
 13. Parker D.S.N., Yang T., Kaiser R.I., Landera A., Mebel A.M., “On the formation of ethynylbiphenyl ($C_{14}D_5H_5$; $C_6D_5C_6H_4C\equiv CCH$) isomers in the reaction of D5-phenyl radicals (C_6D_5 ; X^2A_1) with phenylacetylene ($C_6H_5C_2H$; X^1A_1) under single collision conditions”, *Chem. Phys. Lett.*, 2014, 595-596, 230-236.
 14. Dangi B.B., Parker D.S.N., Yang T., Kaiser R.I., Mebel A.M., “Gas-phase synthesis of the benzyl radical ($C_6H_5CH_2$)”, *Angew. Chem., Int. Ed.*, 2014, 53, 4608–4613.
 15. Joalland B., Shi Y., Kamasah A., Suits A.G., Mebel A.M., “Roaming Dynamics in Radical Addition-Elimination Reactions”, *Nature Communications*, 2014, 5, Article number: 4064, doi:10.1038/ncomms5064

16. Parker D.S.N., Maity S., Dangi B.B., Kaiser R.I., Landera A., Mebel A.M., “Understanding the Chemical Dynamics of the Reactions of Dicarbon with 1-Butyne, 2-Butyne, and 1,2-Butadiene – Toward the Formation of Resonantly Stabilized Free Radicals”, *Phys. Chem. Chem. Phys.*, 2014, 16, 12150-12163.
17. Yang T., Parker D.S.N., Dangi B.B., Kaiser R.I., Kislov V.V., Mebel A.M., “Crossed Beam Reactions of the Phenyl (C_6H_5 ; X^2A_1) and D5-Phenyl Radical (C_6D_5 ; X^2A_1) with 1,2-Butadiene ($H_2CCCHCH_3$; X^1A')”, *J. Phys. Chem. A*, 2014, 118, 4372-4381.
18. Dangi B.B., Parker D.S.N., Kaiser R.I., Belisario-Lara D., Mebel A.M., “An Experimental and Theoretical Investigation of the Formation of C_7H_7 Isomers in the Bimolecular Reaction of Dicarbon Molecules with 1,3-Pentadiene”, *Chem. Phys. Lett.*, 2014, 607, 92-99.
19. Dangi B.B., Yang T., Kaiser R.I., Mebel A.M., “Reaction Dynamics of the 4-Methylphenyl Radical ($C_6H_4CH_3$; p-Tolyl) with Isoprene (C_5H_8) - Formation of Dimethyldihydronaphthalenes”, *Phys. Chem. Chem. Phys.*, 2014, 16, 16805-16814.
20. Kaiser R.I., Dangi B.B., Yang T., Parker D.S.N., Mebel A.M., Korte A., Sander W., “Reaction Dynamics of the 4-Methylphenyl Radical (p-Tolyl) with 1,2-Butadiene (1-Methylallene) – Are Methyl Groups Purely Spectators?”, *J. Phys. Chem. A*, 2014, 118, 6181-6190.
21. Ribeiro J.M., Mebel A.M., “Reaction Mechanism and Product Branching Ratios of the $CH + C_3H_8$ Reaction: A Theoretical Study”, *J. Phys. Chem. A*, 2014, 118, 9080-9086.
22. Joalland B., Shi Y., Estillore A., Kamasah A., Mebel A.M., Suits A.G., “Dynamics of Chlorine Atom Reactions with Hydrocarbons: Insights from Imaging the Radical Product in Crossed Beams (Feature Article)”, *J. Phys. Chem. A* 2014, 118, 9281-9295.
23. Kislov V.V., Singh R.I., Edwards D.E, Mebel A.M., Frenklach M., “Rate coefficients and product branching ratios for the oxidation of phenyl and naphthyl radicals: A theoretical RRKM-ME study”, *Proc. Int. Combust. Inst.* 2015, 1861-1869.
24. Kaiser R.I., Parker D.S.N., Mebel A.M., “Reaction Dynamics in Astrochemistry: Low-Temperature Pathways to Polycyclic Aromatic Hydrocarbons in the Interstellar Medium”, *Ann. Rev. Phys. Chem.* 2015, 66, 43-47.
25. Yang T., Muzangwa L., Parker D.S.N., Kaiser R.I., Mebel A.M., “Formation of 2- and 1-Methyl-1,4-Dihydronaphthalene Isomers via the Crossed Beam Reactions of Phenyl Radicals (C_6H_5) with Isoprene ($CH_2C(CH_3)CHCH_2$) and 1,3-Pentadiene ($CH_2CHCHCHCH_3$). *Phys. Chem. Chem. Phys.* 2015, 17, 530-540.
26. Muzangwa L., Yang T., Parker D.S.N., Kaiser R.I., Mebel A.M., Jamal A., Ryazantsev M., Morokuma K., “A Crossed Molecular Beam and Ab Initio Study on the Formation of 5- and 6-Methyl-1,4-Dihydronaphthalene ($C_{11}H_{12}$) via the Reaction of Meta-Tolyl (C_7H_7) with 1,3-Butadiene (C_4H_6)”, *Phys. Chem. Chem. Phys.* 2015, 17, 7699-7706.
27. Yang T., Parker D.S.N., Dangi B.B., Kaiser R.I., Mebel A.M., “Formation of 5- and 6-methyl-1H-indene ($C_{10}H_{10}$) via the reactions of the para-tolyl radical ($C_6H_4CH_3$) with allene (H_2CCCH_2) and methylacetylene ($HCCCH_3$) under single collision conditions”, *Phys. Chem. Chem. Phys.* 2015, Advance Article, DOI: 10.1039/C4CP04288C.
28. Ribeiro J.M., Mebel A.M., “Reaction mechanism and rate constants of the $CH+CH_4$ reaction: a theoretical study”, *Mol. Phys.* 2015, in press, DOI:10.1080/00268976.2015.1019584.
29. Parker D.S.N., Kaiser R.I., Troy T.P., Kostko O., Ahmed M., Mebel A.M., “Toward the Oxidation of the Phenyl Radical and Prevention of PAH Formation in Combustion Systems”, *J. Phys. Chem. A* 2015, Articles ASAP, DOI: 10.1021/jp509170x.

FLASH PHOTOLYSIS-SHOCK TUBE STUDIES

Joe V. Michael

Chemical Sciences and Engineering Division
Argonne National Laboratory, Argonne, IL 60439
E-mail: jmichael@anl.gov

The scope of the program is to measure, with the ANL flash photolysis reflected shock tube technique, high-temperature thermal rate constants for use in high temperature combustion. This year we have concentrated on reactions where [H] is a product and is measured by atomic resonance absorption spectrometry (ARAS).

In recent studies from this laboratory [1], it was shown that the highly sensitive H-ARAS technique can be used to directly determine bimolecular rate constants by observing the formation of product H-atoms. Unstable radicals, that can decompose to give atomic species like H ($T > 1000\text{K}$), can be formed as a product of these bimolecular reactions. H-atom formations from radicals are nearly instantaneous, and they will therefore be a marker for the rate-limiting reaction of interest.

Using this approach, unambiguous rate constants determinations were obtained [1,2] for difficult to isolate "slow" H-abstractions in $\text{CH}_3 + \text{CH}_3\text{OH}/\text{C}_2\text{H}_6$.



In either of these cases the formation of H-atoms from either CH_3O or CH_2OH dissociations, giving $\text{CH}_2\text{O} + \text{H}$ in (1) or C_2H_5 giving $\text{C}_2\text{H}_4 + \text{H}$ in (2), allows direct determinations for k_1 and k_2 because the radical dissociations ($\text{CH}_2\text{OH}/\text{CH}_3\text{O}$ in reaction (1) and C_2H_5 in reaction (2)) are instantaneous (at $T > 1000\text{ K}$) in comparison to the slow, rate-limiting methyl abstractions. As mentioned earlier, reaction (1) and (2) are abstractions.

The technique described above was also used to measure rate constants for,



In reaction (3), H-atoms are formed from two competing processes at high temperatures ($>1000\text{ K}$); addition-elimination to directly form C_3H_6 as a co-product and abstraction to form CH_4 and C_2H_3 with the rapid dissociation of vinyl being the ultimate source for H-atoms. The measured experimental rate constants for the sum of the two processes are in remarkably good agreement with recent theoretical predictions [3]. Interestingly, in the case of $\text{CH}_3 + \text{C}_2\text{H}_2$ the measured H-atoms are a direct marker for the addition-elimination process on the C_3H_5 PES and in good agreement with theory [4]. These

experimental determinations for reactions (3) and (4) are also the first direct determinations at combustion relevant temperatures (>1000 K).

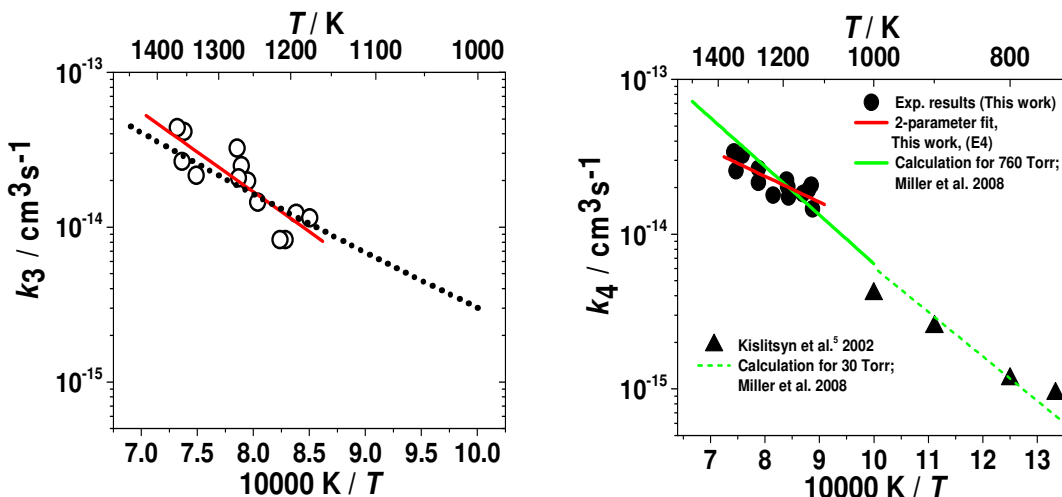


Figure 1: [○] – k_3 from present experiments Figure 2: [●] – k_4 from present experiments [...] - Theory from ref. 3. [—] – Theory from ref. 4.

The above-described method can also be applied to measure channel-specific rate constants for OH radical abstractions. The caveat in the measurements is that in these simple alkanes at high temperatures, specific alkyl radicals (formed by abstraction) instantaneously dissociate to either an H-atom and an alkene or a CH_3 radical and an alkene. Measurements of H-atoms therefore lead to a channel specific rate constant measurement. The additional constraint of total rate constant measurements made in earlier studies [5,6] then allows unambiguous direct determinations of branching ratios in high temperature abstractions. This approach is amenable for probing not just OH + Alkanes but other classes of abstractions such as H + Alkanes and CH_3 + Alkanes. In these higher barrier abstractions non-Arrhenius effects and kinetic isotope effects are expected to be more pronounced, and thereby render Tully's indirect technique less accurate. In the present study, we have used measurements of H-atoms in reactions of OH + C_3H_8 , n- C_4H_{10} , iso- C_4H_{10} , and D + C_3H_8 , coupled with total rate constant measurements in prior studies [5,6,7] (under similar experimental conditions) to directly determine site-specific experimental abstraction branching ratios. The present branching ratio measurements are compared to previous experimental and theoretical estimates and also provide a basis for probing existing rate rules [6,8] for OH + Alkanes and H + Alkanes.

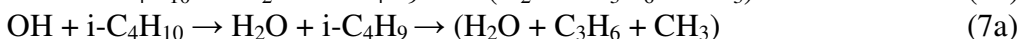
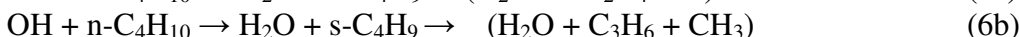
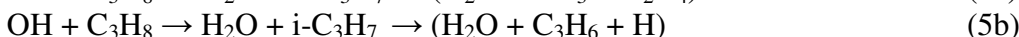
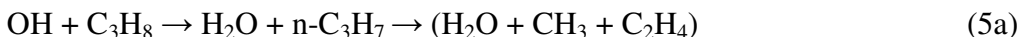
Abstraction at the two sites in simple alkanes such as C_3H_8 (primary and secondary sites), n- C_4H_{10} (primary and secondary sites), and i- C_4H_{10} (primary and tertiary sites) are known to produce unstable radicals that lead to H-atoms at only one unique site. For example, abstraction at the secondary site in C_3H_8 leads to i- C_3H_7 that instantaneously dissociates only to C_3H_6 and H-atoms, while abstraction at the primary site forms n- C_3H_7 that dissociates exclusively to CH_3 + C_2H_4 at typical combustion conditions [3]. Similarly, abstraction at the primary site in n- C_4H_{10} and the tertiary site in i- C_4H_{10} produce the n- C_4H_9 and t- C_4H_9 radicals respectively, and these exclusively dissociate to H-atoms and

the corresponding alkenes [9]. The other abstraction sites in n-C₄H₁₀ and i-C₄H₁₀, the secondary and the primary sites respectively, form the s-C₄H₉ and i-C₄H₉ radicals that dissociate only to CH₃-radicals and the corresponding alkenes.

Consequently, with prior knowledge of total abstraction rate constants in these molecules, H-atom product measurements can be used to obtain site specific rate constants, and, therefore, site specific branching ratios. This technique has been applied in the present study for H-atom abstractions by OH from C₃H₈, n-C₄H₁₀, and i-C₄H₁₀. With OH-multipass absorption as the diagnostic, total rate constants for the reactions



were measured [5] at high temperatures (800-1300 K). As discussed earlier, there are two unique abstraction sites in these molecules that lead to,



Measuring H-atom formation in the present study, using H-atom ARAS as the diagnostic, leads to unambiguous determinations for the site-specific rate constants; k_{5b} , k_{6a} , and k_{7b} . These site-specific rate constants in combination with the total rate constant constraints, under similar experimental conditions as the earlier experimental studies [5], provides direct determinations of the site-specific branching ratios in reactions 5, 6, and 7. The same concepts can also be applied to H-abstractions by D-atoms which represent surrogates for H + Alkanes at high temperatures and in the present case it could be unambiguously applied to D + C₃H₈.

References

1. S.L. Peukert and J.V. Michael, J. Phys. Chem. A 2013, 117, 10186.
2. S.L. Peukert, N.J. Labbe, R. Sivaramakrishnan, J.V. Michael, J. Phys. Chem. A 2013, 117, 10228.
3. J.A. Miller, S.J. Klippenstein, J. Phys. Chem. A 2013, 117, 2718.
4. J.A. Miller, J. P. Senosiain, S.J. Klippenstein, Y. Georgievskii, J. Phys. Chem. A 2008, 112, 9429.
5. R. Sivaramakrishnan, N.K. Srinivasan, M.-C. Su, J.V. Michael, Proc. Combust. Inst. 2009, 32, 107.
6. R. Sivaramakrishnan, J.V. Michael, J. Phys. Chem. A 2009, 113, 5047.
7. R. Sivaramakrishnan, J.V. Michael, B. Ruscic, Int. J. Chem. Kin. 2012, 44, 194.
8. S.L. Peukert, R. Sivaramakrishnan, J.V. Michael, Proc. Combust. Inst. 2015, 35, 171.
9. V.D. Knyazev, I.R. Slagle, J. Phys. Chem. 1996, 100, 5318.

PUBLICATIONS FROM DOE SPONSORED WORK FROM 2013-2015

- *High Temperature Rate Constants for H/D + Methylformate and Methylacetate*, S. Peukert, R. Sivaramakrishnan, M.-C. Su, and J.V. Michael, Proc. Combust. Inst. **34**, 463-471 (2013).
- *High Temperature Shock Tube and Theoretical Studies on the Thermal Decomposition of Dimethyl Carbonate and its Bimolecular Reactions with H and D -Atoms*, S. Peukert, R. Sivaramakrishnan and J.V. Michael, J. Phys. Chem. A, **117**, 3718-3728 (2013)
- *High Temperature Shock Tube Studies on the Thermal Dissociation of O₃ and the Reaction of Dimethyl Carbonate with O-atoms*, S. Peukert, R. Sivaramakrishnan, and J.V. Michael, J. Phys. Chem. A, **117**, 3729-3738 (2013).
- *High Temperature Shock Tube and Modeling Studies on the Reactions of Methanol with D-Atoms and CH₃-Radicals*, S.L. Peukert and J.V. Michael, J. Phys. Chem. A **117**, 10186-10195 (2013).
- *Direct Measurements of Rate Constants for the Reactions of CH₃ radicals with C₂H₆, C₂H₄, and C₂H₂ at High Temperatures* S.L. Peukert, N.J. Labbe, R. Sivaramakrishnan, J.V. Michael, J. Phys. Chem. A **117**, 10228-10238 (2013).
- *High Temperature Rate Constants for H/D + n-C₄H₁₀ and i-C₄H₁₀*, S.L. Peukert, R. Sivaramakrishnan, and J.V. Michael, Proc. Combust. Inst., **35**, 171-179 (2015).
- *Resolving some paradoxes in the thermal decomposition mechanism of acetaldehyde*, R. Sivaramakrishnan, J. V. Michael, L. B. Harding, S. J. Klippenstein, In Press, Festschrift for Lawrence B. Harding, Joe V. Michael, Albert F. Wagner - 100 Years of Combustion Kinetics at Argonne, J. Phys. Chem. A, **119** (2015) doi: 10.1021/acs.jpca.5b01032
- *Shock tube and theoretical studies on the thermal decomposition of iso-propanol and its reaction with D-atoms*, S.L. Peukert, R. Sivaramakrishnan, S.J. Klippenstein, and J.V. Michael, J. Phys. Chem. A, In preparation (2015).
- *The Decomposition Kinetics of Xylyl Radicals*, D. Polino, C. Cavallotti, R. Sivaramakrishnan, S.J. Klippenstein, and J.V. Michael, J. Phys. Chem. A, preparation (2015).

Particle Diagnostics Development

H. A. Michelsen

Sandia National Labs, MS 9055, P. O. Box 969, Livermore, CA 94551
hamiche@sandia.gov

I. Program Scope

Combustion processes often produce solid carbon particles, i.e., soot. These particles may be oxidized to form gas-phase species or released into the exhaust stream, where they can be coated with liquid coatings. These coatings can be comprised of any of a number of components, including unburned fuel, lube oil, sulfuric acid, water, and other combustion by-products.¹ The research program described here focuses on the development and use of diagnostics for soot particles in combustion environments and combustion exhaust plumes. The goal of this work is *in situ* measurements of volume fraction, size, composition, and morphology of combustion-generated particles with fast time response and high sensitivity. Measurement techniques are targeted for studies of soot formation and evolution and must be versatile enough to probe particles throughout their entire life cycle. Techniques are being developed for detection and characterization of particles in combustion environments from incipient particles that are 2-10 nm in diameter and composed of condensed large organic species to mature soot particles composed of aggregates of carbonaceous primary particles resembling polycrystalline graphite. Diagnostics are also being developed for chemical studies of growth, pyrolysis, and oxidation within combustors and characterization of inhomogeneous particles in exhaust streams.

II. Recent Progress

Our work has focused on developing a detailed understanding of the chemical and physical mechanisms that influence the applicability of laser-based, x-ray, and mass spectrometric techniques for soot detection and characterization under a wide range of conditions. In recent work, we have developed, refined, and applied a range of diagnostic methods to investigate the formation, evolution, and oxidation of soot in atmospheric premixed flat and laminar diffusion flames.

We are also working on a SISGR project led by Prof. Angela Violi to develop a validated predictive multiscale model to describe the chemical composition of soot nanoparticles in premixed and diffusion flames. This project closely couples experimental investigations of soot precursors and incipient particle characteristics with the development of a predictive model for the chemical composition of soot nanoparticles. The co-investigators on the project are Prof. Angela Violi (University of Michigan) for model development and Drs. Hope Michelsen (Sandia) and Nils Hansen (Sandia) in collaboration with Dr. Kevin Wilson (LBNL ALS) for experimental investigations.

A. Characterizing the Effects of Soot Morphology on Laser-Induced Incandescence

Clean, mature soot is composed of small “primary” particles of polycrystalline graphite 10-50 nm in diameter covalently bound into dendritic aggregates of varying size with branched-chain structures typically characterized by fractal dimensions of 1.7-1.9. Mature soot absorbs strongly and broadly across optical wavelength regions and is refractory with a sublimation temperature of ~4000 K. Less mature soot maintains some of its original hydrocarbon characteristics and includes significant hydrogen content. Laser-induced incandescence (LII) is a diagnostic technique that has been used extensively to measure soot-particle abundances and physical properties under a wide range of conditions. The implementation of LII exploits the refractory nature of the soot particles and involves heating soot particles in an intense laser field to temperatures as high as 4000 K and measuring the resulting incandescence from the hot particles. The signal magnitude is related to the particle volume fraction or mass. It is also nonlinearly dependent on the particle temperature. While laser absorption is responsible for heating the particle, conductive cooling is the dominant cooling mechanism under non-vacuum conditions when sublimation can be ignored. The balance of heating and cooling mechanisms determines particle temperature, which controls LII signal as a function of time. When a pulsed laser system is used to heat the particles, the LII signal decay rate after the laser pulse is often used to infer a primary-particle size, assuming that cooling is dominated by conduction, which is determined by the surface area to volume ratio. This approach requires a firm understanding of conductive-cooling rates and their dependence on particle size.

We have employed a cw-laser system (rather than a nanosecond pulsed laser system) for particle heating to study the effects of aggregation on conductive cooling and LII signal production.² The cw-laser

instrument is sensitive enough to detect single particles drifting through the laser beam over a time scale of $\sim 10 \mu\text{s}$. This approach enables classification of particles by size (via LII signal magnitude) and thus characterization of LII signal time evolution as a function of particle size. We generated soot in a co-flow diffusion flame with a fractal dimension of ~ 1.9 . We size selected particles using a differential mobility analyzer (DMA). Particles with a single charge that make it through the DMA at a particular voltage will be smaller than particles with a double charge, which in turn will be smaller than particles with a triple charge. We also coated size selected particles with an oleic acid coating, which caused the aggregates to restructure (i.e., collapse), increasing their fractal dimension to a value of ~ 2.4 . We sent these particles through a thermal denuder, which removes the coating while maintaining the fractal dimension at ~ 2.4 .

Aggregation effects modify the average particle-surface area available to interact directly with the bath gas and thus influence conductive-cooling rates. Shielding of some primary particles within an aggregate by other primary particles is predicted to cause large aggregates to have lower effective surface areas per primary particle than smaller aggregates.³ Restructured aggregates also have lower effective surface areas than fresh, dendritic particles.⁴ Our work indicates that this reduction in surface area decreases the conductive-cooling rate, which increases the net-heating rate when the particles enter the laser beam. The effect on LII signal is demonstrated in Fig. 1a, which shows that the leading edge of the LII signal moves to earlier times with increasing particle size and fractal dimension. We have developed a model that solves the energy- and mass-balance equations for particle temperature and size as a function of time and predicts LII signal using a modified Planck function. Results are demonstrated in Fig. 1a. The model also reproduces the scattering signal that was recorded simultaneously with the LII temporal profiles, as shown in Fig. 1b. In order to reproduce the experimental results with the model, we assumed a distribution of surface area exposure for the primary particles within an aggregate. In addition, reproducing the scattering signal required incorporating a mechanism for particle expansion during sublimation. Restructured particles expanded more vigorously than dendritic particles.

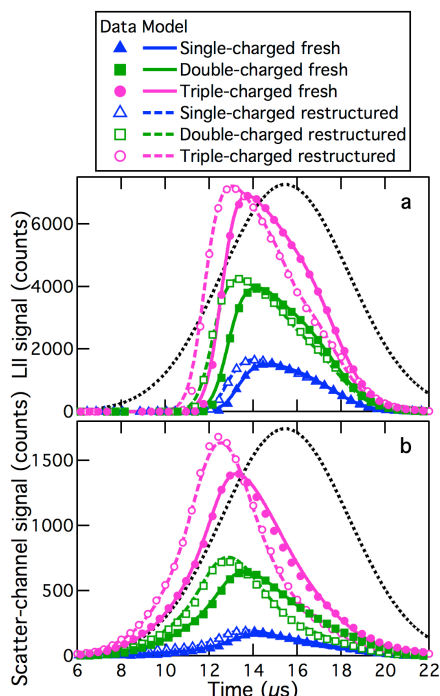


Figure 1. Measured and modeled temporal profiles. Modeled (a) LII and (b) scattered temporal profiles (lines) are compared with average measured (a) LII and (b) temporal profiles (symbols) for fresh and restructured soot. The measured profiles represent averages from 50 particles for each case. The laser-particle interaction profile (dotted line), used as input to the model, is also shown and is scaled to the top of the graph.

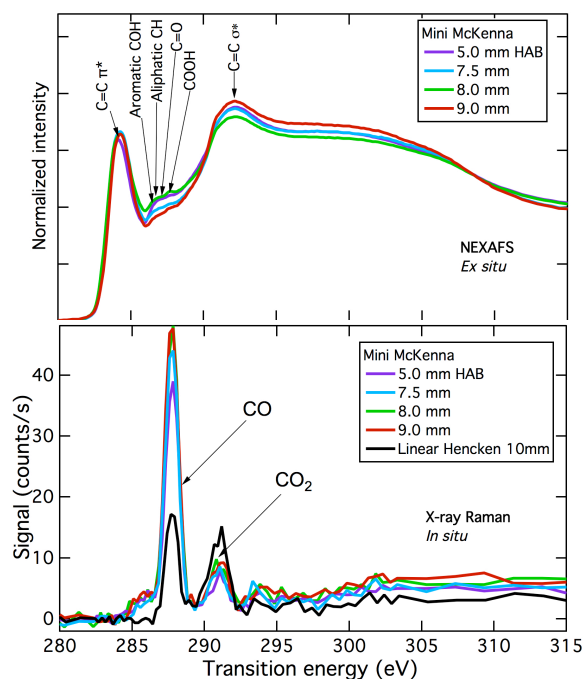


Figure 2. X-ray spectra recorded at the carbon K edge. Top panel: NEXAFS spectra were recorded on soot samples collected from an atmospheric ethylene-air premixed flat flame at selected heights above the burner (HABs). Signatures of functional groups are labeled. Bottom panel: X-ray Raman spectra were recorded *in situ* in the flame produced by the same burner. The spectra are compared with a spectrum recorded in a laminar diffusion flame from a linear Hencken burner.

B. Probing Soot Formation, Graphitization, and Oxidation Using X-Ray Diagnostics

Measurements of soot-particle size, morphology, fine structure, and composition form the foundation for our understanding of soot formation, graphitization, and oxidation in combustors and the basis for predictive soot-chemistry models. Numerous experimental techniques have been developed to probe the evolution of these parameters, but many of these methods involve extractive sampling, which leads to large perturbations of the chemistry under investigation. There is a need for diagnostics that can be used to characterize particles formed in the combustor without resorting to extractive sampling. We have initiated a collaboration with Drs. Ich Tran and Tony Van Buuren (LLNL) to exploit x-ray techniques for *in situ* measurements of soot physical and chemical characteristics. We are using Small-Angle X-ray Scattering (SAXS) for particle size, Wide-Angle X-ray Scattering (WAXS) for particle fine structure, and spontaneous X-ray Raman Spectroscopy (XRS) for particle composition information. We are comparing these diagnostics to techniques using extractive sampling, such as Scanning Mobility Particle Sizer (SMPS) measurements for particle size, Transmission Electron Microscopy (TEM) for particle fine structure, and Near-Edge X-ray Absorption Fine-structure Spectroscopy (NEXAFS) and Aerosol Mass Spectrometry (AMS) for particle composition information. We are also collaborating with ALS beamline scientists Drs. Zhu, Hexemer, and Schaible for SAXS/WAXS and Stanford Synchrotron Radiation Lightsources (SSRL) beamline scientists Drs. Weng, Nordlund, and Sokaras for XRS.

We have designed and built several burners to study soot formation, graphitization, and oxidation under premixed and diffusion-controlled conditions. These burners were designed for compatibility with x-ray diagnostics, given constraints of synchrotron hutch, beam, and detector configurations. Figure 2a shows *ex situ* NEXAFS spectra recorded on soot samples collected from an ethylene-fueled premixed flat flame produced by a mini-McKenna burner, a smaller version of a common research burner. The spectra were recorded at the carbon K edge and demonstrate features indicative of aromatic and aliphatic hydrocarbons and oxygen-containing functional groups. The results suggest that aromaticity increases and oxygenation decreases with increasing height above the burner (HAB), which is consistent with oxygen depletion and particle graphitization as the flame evolves. Such measurements are more powerful if made *in situ* without perturbing the flame. Figure 2b shows *in situ* XRS spectra recorded with the same flame configuration as that used to generate the soot probed by the NEXAFS spectra shown in Fig 2a. These spectra were recorded on Beamline 6-2 at the SSRL using the Si(111) monochromator, which delivers photons at ~ 6.5 keV with a flux of 2×10^{13} photons/s and energy resolution of 0.85 eV.⁵ The detector was a Johann-type crystal spectrometer 40 spherically bent and diced Si(110) crystals positioned on a 1-m Rowland circle and subtending a solid angle of 1.9% of 4π sr.⁵ The signal was recorded on a silicon drift detector that was used to reduce background by spectrally discriminating against diffuse scatter. Because both the incident beam and signal were in the hard x-ray regime, the experiment could be performed at atmospheric pressure without excessive loss of signal. The photon energy of the incident beam was scanned, and the detection wavelength was fixed. The transition energy is recorded as the energy difference between the incident and detected photons.

The most striking features in the spectra shown in Fig. 2b are those attributable to gas-phase CO and CO₂ in the flame. This result is similar to the measurements of NEXAFS spectra recorded in a low-pressure methane diffusion flame by Frank et al.⁶ Figure 2b demonstrates that CO and CO₂ increase with increasing HAB as the combustion moves toward completion. The underlying features of the soot particles and precursors are difficult to discern in these spectra, but there is some evidence of aromatic hydrocarbons at ~ 287 eV, in the shoulder of the CO peak. This feature is not obvious in the spectrum taken in a diffusion flame. This observation requires more investigation for confirmation.

III. Future Work

Future work will refine and expand on the x-ray measurements demonstrated in Fig. 2. We will continue to develop laser-based diagnostics that can be used to probe particle size, morphology, and composition and apply these *in situ* diagnostics to study soot evolution and oxidation in flames. These diagnostics will be complemented by *ex situ* diagnostics, such as AMS, TEM, and SMPS, making an effort to deploy all of these diagnostics on selected combustion systems. Our goal is to eventually apply these diagnostics to combustion systems at higher pressure with an emphasis on working with the modeling community to facilitate model development and validation.

IV. References

1. (a) Kittelson, D. B., Engines and nanoparticles: A review. *J. Aerosol Sci.* **1998**, *29* (5/6), 575-588; (b) Lighty, J. S.; Veranth, J. M.; Sarofim, A. F., Combustion aerosols: Factors governing their size and composition and implications for human health. *J. Air Waste Manage. Assoc.* **2000**, *50* (9), 1565-1618.
2. Bambha, R. P.; Michelsen, H. A., Effects of aggregate morphology on size and laser-induced incandescence and scattering from black carbon (mature soot). *J. Aerosol Sci.* **2015**, submitted.
3. Filippov, A. V.; Zurita, M.; Rosner, D. E., Fractal-like aggregates: Relation between morphology and physical properties. *J. Colloid Interface Sci.* **2000**, *229*, 261-273.
4. Bambha, R. P.; Dansson, M. A.; Schrader, P. E.; Michelsen, H. A., Effects of volatile coatings on the laser-induced incandescence of soot. *Appl. Phys. B* **2013**, *112* (3), 343-358.
5. Sokaras, D.; Nordlund, D.; Weng, T.-C.; Alonso Mori, R.; Velikov, P.; Wenger, D.; Garachtchenko, A.; George, M.; Borzenets, V.; Johnson, B.; Qian, Q.; Rabedeau, T.; Bergmann, U., A high resolution and large solid angle x-ray Raman spectroscopy end-station at the Stanford Synchrotron Radiation Lightsource. *Rev. Sci. Instrum.* **2012**, *83*, 043112.
6. Frank, J. H.; Shavorskiy, A.; Bluhm, H.; Coriton, B.; Huang, E.; Osborn, D. L., In situ soft X-ray absorption spectroscopy of flames. *Appl. Phys. B* **2014**, *117*, 493-499.

V. Publications and submitted journal articles supported by this project 2013-2015

1. R. P. Bambha and H. A. Michelsen, " Effects of aggregate morphology and size on laser-induced incandescence and scattering from black carbon (mature soot)", *J. Aerosol Sci.*, submitted (2015).
2. H. A. Michelsen, C. Schulz, G. J. Smallwood, and S. Will, " Laser-induced incandescence: Particulate diagnostics for combustion, atmospheric, and industrial applications ", *Progress Energy Combust. Sci.*, submitted (2015).
3. A. Nanthamornphong, K. Morris, D. W. I. Rouson, and H. A. Michelsen, "A case study: Agile development in the Community Laser-Induced Incandescence Modeling Environment (CLiME)", *Comput. Sci. Eng.* **16(3)**, 36-46 (2014).
4. K. O. Johansson, J. Y. W. Lai, S. A. Skeen, K. R. Wilson, N. Hansen, A. Violi, and H. A. Michelsen, "Soot precursor formation and limitations of the stablomer grid", *Proc. Combust. Inst.* **35**, 1819-1826 (2015).
5. X. López-Yglesias, P. E. Schrader, and H. A. Michelsen, "Effects of soot maturity on its absorption cross section and thermal-accommodation coefficient", *J. Aerosol Sci.* **75**, 43-64 (2014).
6. N. Hansen, S. A. Skeen, H. A. Michelsen, K. R. Wilson, and K. Kohse-Höinghaus, "Flame experiments at the Advanced Light Source: New insights into soot formation processes", *Journal of Visualized Experiments (JoVE)* **87**, e51369 (2014).
7. R. P. Bambha, M. A. Dansson, P. E. Schrader, and H. A. Michelsen, "Effects of volatile coatings on the laser-induced incandescence of soot", *Appl. Phys. B* **112(3)**, 343-358 (2013).
8. R. P. Bambha, M. A. Dansson, P. E. Schrader, and H. A. Michelsen, "Effects of volatile coatings and coating removal mechanisms on the morphology of graphitic soot", *Carbon* **61**, 80-96 (2013).
9. F. Goulay, P. E. Schrader, X. López-Yglesias, and H. A. Michelsen, "A dataset for validation of models of laser-induced incandescence from soot: Temporal profiles of LII signal and particle temperature", *Appl. Phys. B* **112(3)**, 287-306 (2013).
10. J. M. Headrick, P. E. Schrader, and H. A. Michelsen, "Radial-profile and divergence measurements of combustion-generated soot focused by an aerodynamic-lens system", *J. Aerosol Sci.* **58**, 158-170 (2013).
11. S. A. Skeen, H. A. Michelsen, K. R. Wilson, D. M. Popolan, A. Violi, and N. Hansen, "Near-threshold photoionization mass spectra of combustion-generated high-molecular-weight soot precursors", *J. Aerosol Sci.* **58**, 86-102 (2013).
12. S. A. Skeen, B. Yang, H. A. Michelsen, J. A. Miller, A. Violi, and N. Hansen, "Studies of laminar opposed-flow diffusion flames of acetylene at low pressures with photoionization mass spectrometry", *Proc. Combust. Inst.* **34**, 1067-1075 (2013).

Reaction Dynamics in Polyatomic Molecular Systems

William H. Miller

Department of Chemistry, University of California, and
Chemical Sciences Division, Lawrence Berkeley National Laboratory
Berkeley, California 94720-1460
millerwh@berkeley.edu

I. Program Scope

The goal of this program is the development of theoretical methods and models for describing the dynamics of chemical reactions, with specific interest for application to polyatomic molecular systems of special interest and relevance. There is interest in developing the most rigorous possible theoretical approaches and also in more approximate treatments that are more readily applicable to complex systems.

II. Recent Progress

Effort in recent years has focused on finding ways to add quantum mechanical effects to classical molecular dynamics (MD) simulations, which are now so ubiquitously applied to all types of dynamical processes in complex molecular systems, e.g., chemical reactions in clusters, nanostructures, molecules on or in solids, bio-molecular systems, etc. Since quantum effects in *transitions between different electronic states* can obviously be very significant, one of the most important applications of semiclassical (SC) approaches¹⁻³ is to these non-adiabatic processes. The first approach that allowed both nuclear and electronic degrees of freedom (DOFs) to be treated by SC, or even classical methods, in a unified and completely consistent fashion was the model introduced by Meyer and Miller⁴ (MM), in which each electronic state is characterized by a classical DOF (a harmonic oscillator). [Stock and Thoss⁵ (ST) later showed this to be an *exact representation* of a vibronic system.] A variety of applications of this approach has demonstrated its usefulness.⁶⁻⁸

In the MM model each electronic state k is characterized by a pair of classical action-angle variables (n_k, q_k) , and if (\mathbf{P}, \mathbf{R}) are the nuclear momenta and coordinates, the MM classical Hamiltonian for the nuclear and electronic degrees of freedom is

$$H(\mathbf{P}, \mathbf{R}, \mathbf{n}, \mathbf{q}) = \frac{\mathbf{P}^2}{2\mu} + \sum_{k=1}^F n_k H_{kk}(\mathbf{R}) + 2 \sum_{k < k'=1}^F \sqrt{(n_k + \gamma)(n_{k'} + \gamma)} \cos(q_k - q_{k'}) H_{kk'}(\mathbf{R}) \quad (1)$$

where, as indicated, the $F \times F$ diabatic electronic matrix $\{H_{kk'}(\mathbf{R})\}$ is a function of the nuclear coordinates and assumed to come from many-electron ‘quantum chemistry.’ (There is an equivalent adiabatic version of this Hamiltonian, but the diabatic version is somewhat simpler to describe.) The electronic and nuclear dynamics are determined by computing classical trajectories from this Hamiltonian (by integrating Hamilton’s equations) for electronic and

nuclear degrees of freedom. This was the primary goal of the MM approach: to have a consistent dynamical description of electronic and nuclear degrees of freedom that treated them in an equivalent framework.

The parameter γ in Eq. (1) was at first equal to 0 in MM's heuristic derivation of this Hamiltonian, but on the basis of semiclassical considerations (a Langer-like modification) they then took it to be $\frac{1}{2}$, effectively providing the zero point energy of each electronic degree of freedom. Stock later found⁹ in some of his applications that better results were obtained by choosing $\gamma < \frac{1}{2}$ (suggesting a 'best value' of $\sim 1/4$), so as to incorporate only a fraction of the zero point energy. Within the quasi-classical approach we take it to be an empirical parameter with a value between 0 and $\frac{1}{2}$; there is theoretical justification for choosing it to be $(\sqrt{3}-1)/2 \sim 0.366$, a value we find to give good results in our symmetrical windowing treatment.

The most significant recent development to the topic has been to realize that a modified version of the venerable 'quasi-classical' (QC) model for state-to-state quantum transitions provides a surprisingly good description of electronically non-adiabatic processes using the MM model for the electronic DOFs. The new aspect of the QC approach is that the initial, as well as the final, values of the classical action variables are 'quantized' (approximately) by assigning their corresponding classical action variables to histogram 'boxes', an approach referred to as *symmetrical* quasi-classical (SQC). It is straightforward to apply this approach to any molecular system for which a classical molecular dynamics simulation is feasible.

More details of this MM/SQC approach are described in ref. 10, which also presents the results of its application to a number of examples that demonstrate its performance. These were presented in last year's abstract. Since then, application has been made to a spin-boson-like model¹¹ of electron transfer, also with excellent results¹². It is especially noteworthy that the 'Marcus inverted region' of electron transfer is described correctly by the MM/SQC approach, something that a number of other classical-like models have a difficulty with. Fig. 1a corresponds to the symmetric case (energetic bias $\epsilon = 0$). In Fig. 1b the non-adiabatic coupling is held fixed at $\Delta = 5 \times 10^{-5}$ (at the lower end in Fig. 1a), and the energetic bias ϵ is varied in order to illustrate the ET rate dependence on exothermicity/bias and the inverted regime known from Marcus Theory. Again, the MM/SQC calculations show excellent agreement with MT—here, over about 3 orders of magnitude variation in ET rates.

Application has also been made to a model¹³ of coupled proton-electron transfer in a condensed phase. A reduced density matrix (RDM) approach was used in ref. 13 to calculate the explicit time-dependence of the donor state populations (rather than to calculate thermal rate constants); to demonstrate the effectiveness of the MM/SQC approach, $P_{2 \leftarrow 1}(t)$ is calculated for each of four models a-d, respectively, treated in ref. 13. The MM/SQC results shown in Figs. 2a and 2b show nearly perfect agreement with the RDM results, while those in Figs. 2c and 2d exhibit some deviation from the RDM results, but are still in reasonable qualitative agreement (the population differences being ~ 10 -20% at most). One has to assume that these deviations are due to the limitations of the MM/SQC approach, but the RDM methodology is also not exact, so one cannot necessarily rule out the possibility that part of the discrepancy is attributable to the limitations of the RDM technique. In any event, the MM/SQC approach does a reasonable job overall of capturing the characteristics of the PCET dynamics exhibited by these models.

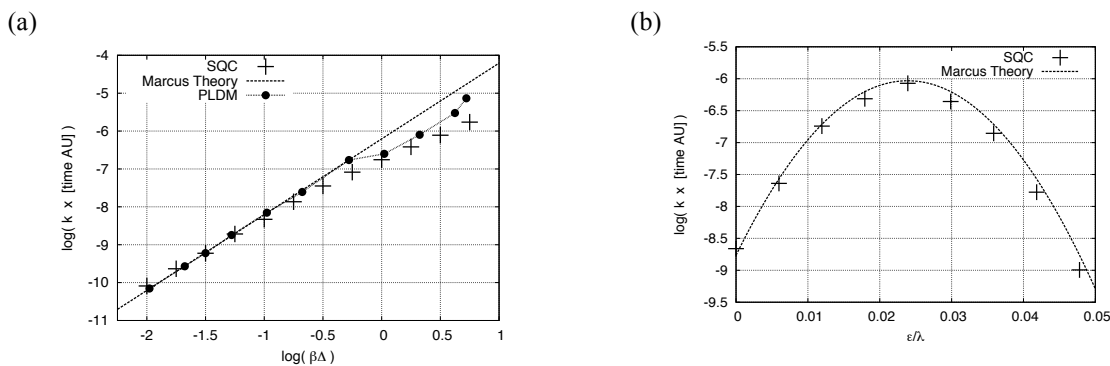


Figure 1: (a) MM/SQC electron transfer (ET) rates (+) versus Marcus Theory (MT) rates (--) and PLDM (partial linearized density matrix) results (•) of ref.11. The non-adiabatic coupling Δ is varied keeping a fixed energetic bias $\epsilon = 0$. (b) same as (a) but with fixed non-adiabatic coupling Δ while varying energetic bias ϵ to illustrate the rate inversion predicted by Marcus Theory. (The PLDM result of ref 11 is not displayed since it is essentially in exact agreement with Marcus Theory.)

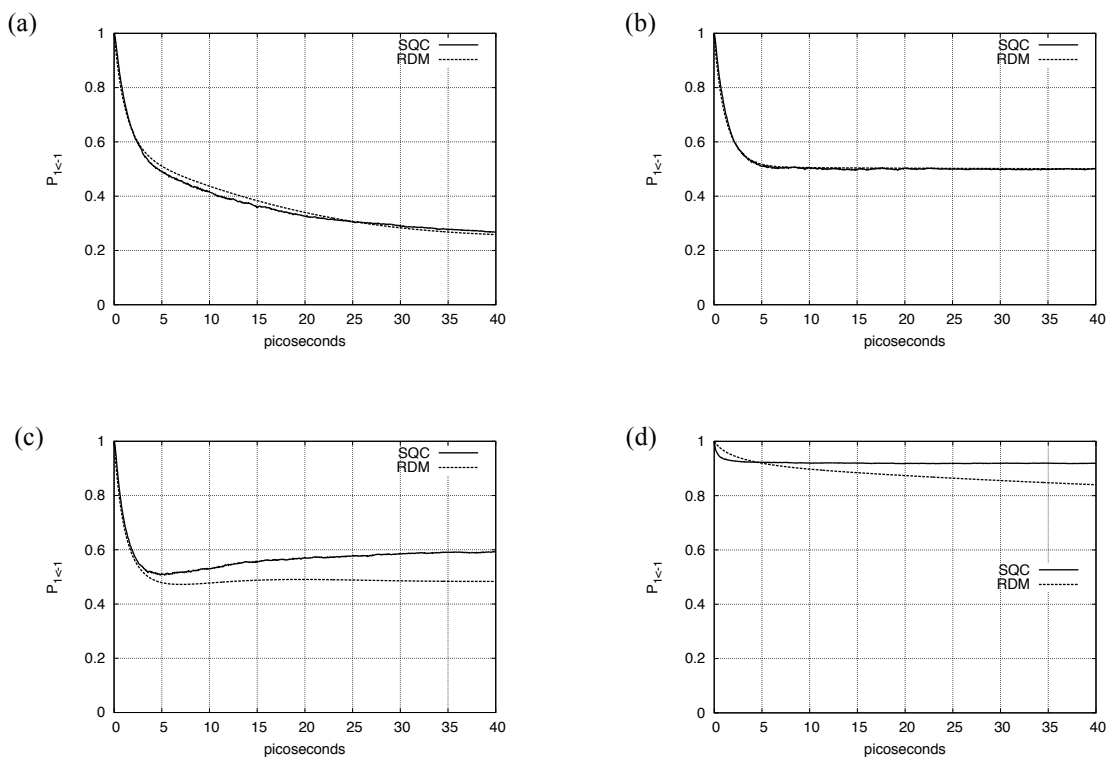


Figure 2: Time-dependent survival probability $P_{2\leftarrow 1}(t)$ of the upper/donor electronic state (state 1) while it decays to the acceptor state (state 2) after photoexcitation from the ground state (state 0) for the proton-coupled electron transfer (PCET); MM/SQC results (—), reduced density matrix (RDM) results (--) of ref. 13.

III. Future Plans

Since this quasi-classical model has proved quite reliable for describing electronically non-adiabatic dynamics in these simple model problems, work is in progress to extend its application to more general and complex non-adiabatic processes.

References

1. For reviews, see W. H. Miller, *Adv. Chem. Phys.* **25**, 69-177 (1974); **30**, 77-136 (1975).
2. W. H. Miller, *J. Chem. Phys.* **53**, 1949-1959 (1970).
3. For reviews, see (a) W. H. Miller, *J. Phys. Chem. A* **105**, 2942-2955 (2001); (b) W. H. Miller, *Proceedings of the National Academy of Sciences*, **102**, 6660-6664 (2005); (c) W. H. Miller, *J. Chem. Phys.* **125**, 132305.1-8 (2006).
4. H. D. Meyer and W. H. Miller, *J. Chem. Phys.* **71**, 2156-2169 (1979).
5. G. Stock and M. Thoss, *Phys. Rev. Lett.* **78**, 578-581 (1997).
6. G. Stock and M. Thoss, *Adv. Chem. Phys.* **134**, 243 (2005).
7. W. H. Miller, *J. Phys. Chem.* **113**, 1405-1415 (2009).
8. D. F. Coker and L. Xiao, *J. Chem. Phys.* **102**, 496-510 (1995).
9. G. Stock, *J. Chem. Phys.* **103**, 2888-2902 (1995).
10. S. J. Cotton and W. H. Miller, *J. Chem. Phys.* **139**, 234112.1-9 (2013).
11. P. Huo, T.F. Miller III, and D.F. Coker, *J. Chem. Phys.* **139**, 151101.1-4 (2013).
12. S. J. Cotton, K. Igumenshchev, and W.H. Miller, *J. Chem. Phys.* **141**, 084104.1-10 (2014).
13. C. Venkatarahman, A.V. Soudackov, and S. Hammes-Schiffer, *J. Chem. Phys.* **131**, 154502.1-11 (2009).

IV. 2012 - 2014 DOE Publications

1. W. H. Miller, Perspective: Quantum or Classical Coherence?, *J. Chem. Phys.* **136**, 210901.1-6 (2012).
2. W. H. Miller, Another Resolution of the Identity for Two-Electron Integrals, *J. Chem. Phys.* **136**, 216101.1-2 (2012).
3. G. Tao and W. H. Miller, Time Dependent Importance Sampling in Semiclassical Initial Value Representation Calculations for Time Correlation Functions. II A Simplified Implementation, *J. Chem. Phys.* **137**, 124105.1-7 (2012).
4. B. Li and W. H. Miller, A Cartesian Classical Second-Quantized Many-Electron Hamiltonian, for Use with the Semiclassical Initial Value Representation, *J. Chem. Phys.* **137**, 154107.1-7 (2012).
5. B. Li, T. J. Levy, D. W. H. Swenson, E. Rabani and W. H. Miller, A Cartesian Quasi-Classical Model to Nonequilibrium Quantum Transport: The Anderson Impurity Model, *J. Chem. Phys.* **138**, 104110.1-6 (2013).
6. G. Tao and W. H. Miller, Time-Dependent Importance Sampling in Semiclassical Initial Value Representation Calculations for Time Correlation Functions. III. A State-Resolved Implementation to Electronically Non-Adiabatic Dynamics, *Mol. Phys.* **111**, 1987-1993 (2013).
7. S. J. Cotton and W. H. Miller, Symmetrical Windowing for Quantum States in Quasi-Classical Trajectory Simulations, *J. Phys. Chem. A* **117**, 7190-7194 (2013).
8. S. J. Cotton and W. H. Miller, Symmetrical Windowing for Quantum States in Quasi-Classical Trajectory Simulations: Application to Electronically Non-Adiabatic Processes, *J. Chem. Phys.* **139**, 234112.1-9 (2013).
9. W. H. Miller, A Journey Through Chemical Dynamics, *Annu. Rev. Phys. Chem.* **65**, 1-19 (2014).
10. B. Li, E. Y. Wilner, M. Thoss, E. Rabani and W. H. Miller, A Quasi-Classical Mapping Approach to Vibrationally Coupled Electron Transport in Molecular Junctions, *J. Chem. Phys.* **140**, 104110.1-7 (2014).
11. B. Li, W. H. Miller, T. J. Levy and E. Rabani, Classical Mapping for Hubbard Operators: Application to the Double-Anderson Model, *J. Chem. Phys.* **140**, 204106.1-7 (2014).
12. S. J. Cotton, K. Igumenshchev and W. H. Miller, Symmetrical Windowing for Quantum States in Quasi-Classical Trajectory Simulations: Application to Electron Transfer, *J. Chem. Phys.* **141**, 084104.1-14 (2014).

Dynamics of Activated Molecules

Amy S. Mullin

Department of Chemistry and Biochemistry, University of Maryland

College Park, MD 20742

mullin@umd.edu

I. Program Scope

We investigate the microscopic mechanisms for inelastic collisions of molecules with large amounts of internal energy using high-resolution transient IR absorption probing. Collisional energy transfer is ubiquitous in gas-phase chemistry and impacts overall reaction rates and branching ratios. This is particularly true for high energy molecules that are more likely to undergo chemical transformations. Currently, there are no first-principle theories of collisional energy transfer for high energy molecules and the lack of fundamental knowledge often results in cursory and insufficient treatments in reactive models. A goal of my research program is to gain new insights into the microscopic details of relatively large complex molecules at high energy as they undergo quenching collisions and redistribute their energy. This data provides important benchmarks for the development of new models that account for energy partitioning in molecular collisions.

We use state-resolved transient IR absorption to characterize the energy transfer pathways that are responsible for the collisional cooling of high energy molecules. Direct probing of high energy molecules is challenging due to their transient nature, poorly defined spectral signatures and high state densities. Our approach is to develop a molecular level understanding by focusing instead on the small energy-accepting bath molecules that undergo collisions with high energy molecules. We measure the population changes for individual rotational and vibrational states that are induced by collisions and the nascent translational temperatures of the scattered molecules. With this technique, we have performed in-depth spectroscopic studies that provide a greater understanding of high energy molecules and their collisional energy transfer. In the past decade, we made a major stride forward by developing the means to characterize the transient behavior for the full range of rotational states for the scattered molecules.[1] Previous measurements had been limited to only the highest energy states, thereby giving information about the “strongest” collisions. Having eyes to also see the so-called “weak” collisions gives us access to characterize the entire energy transfer distribution with unprecedented detail.

In the current grant period, we have made use of new experimental capabilities based on incorporating two new generation mid-IR light sources into our high-resolution transient absorption spectrometers.[2] One is a tunable optical parametric oscillator (OPO) and the other is a quantum cascade laser (QCL). The OPO and QCL offer a number of advantages for high resolution transient IR absorption studies. They provide continuous and broad tuning ranges, a high degree of frequency and amplitude stability and relatively high output powers. Our IR tuning range now covers $\lambda=2.5\text{-}3.9\ \mu\text{m}$ (OPO) and $4.2\text{-}4.5\ \mu\text{m}$ (QCL and lead salt diode), thereby providing the tools needed to investigate more complex molecules that quench high energy molecules. This year we have investigated collisional energy transfer for which methane and ammonia are quenchers of high energy molecules. For both of these studies we have used highly vibrationally excited pyrazine ($\text{C}_4\text{H}_4\text{N}_2$, $E=38000\ \text{cm}^{-1}$) as a benchmark donor molecule, thereby enabling comparisons of different quencher gases previously studied in our laboratories.

Our ability to measure the full distribution of scattered molecules allows us to ask fundamental questions about the underlying molecular features that are responsible for observed energy transfer behavior. In the past year, we have targeted 3 studies: 1) a full characterization of the vibration-to-rotation/translation energy transfer pathway for pyrazine(E)/methane collisions, 2) determination of the dynamics for vibration-to-vibration energy transfer in pyrazine(E)/methane collisions and 3) transient IR absorption detection of ammonia. Our recent progress in these studies is described below.

II. Recent Progress

A. Collisions of high energy molecules and methane: pyrazine ($E=38000\text{ cm}^{-1}$) + CH_4

Methane is the simplest hydrocarbon and knowledge of its energy transfer dynamics will lead to a greater understanding of hydrocarbon energy flow in combustion. We have measured the state-resolved scattering dynamics for methane/pyrazine(E) collisions using high-resolution transient IR absorption at $\lambda=3.3\text{ }\mu\text{m}$ using the output of a cw OPO. Vibrationally excited pyrazine is prepared by pulsed 266 nm light. Nascent rotational and translational energy profiles for scattered methane molecules were measured for the ground vibrationless state (0000), and for two vibrationally excited bending states, ν_2 at 1533 cm^{-1} (0100) and ν_4 at 1311 cm^{-1} (0001). The IR probe transitions involve one-quantum excitation of the ν_3 asymmetric stretch (Fig. 1a). The primary quenching pathway involves (pyrazine vibration)-to-(methane rotation/translation) energy transfer, denoted here as (V-RT). Quantitative rate measurements for combined elastic and inelastic collisions show that the (V-RT) pathway accounts for 93% of methane/pyrazine(E) collisions, while the individual (V-V) pathways each account for 3-4% of collisions.

Despite being the simplest hydrocarbon, methane's IR spectroscopy requires some explanation. When methane does not rotate or vibrate, it is a spherical top with rotational energies given by $BJ(J+1)$. For all other ro-vibrational states, vibration-rotation coupling and centrifugal distortion of spherical symmetry split the $(2J+1)^2$ degeneracy, resulting in numerous states for each J and numerous IR transitions. Nuclear spin statistics lead to groups of states with A, E and F type symmetry. Each rotational state is identified by J and a symmetry number. Transient IR probing involves one quantum absorption of the ν_3 stretching mode.

Vibration-to-Rotation/Translational Energy Transfer: Nascent J -dependent translational energy distributions were determined from measurements of transient Doppler-broadened line profiles of CH_4 (0000) as shown in Fig 1b-d. Fractional absorption data were collected at $t=1\text{ }\mu\text{s}$ following pyrazine excitation for a number of states with $J=0-15$ (up to $E_{\text{rot}}=1250\text{ cm}^{-1}$). Transient signals for low- J states (with thermal population at 300 K) show negative-going depletion at line center and positive-going appearance

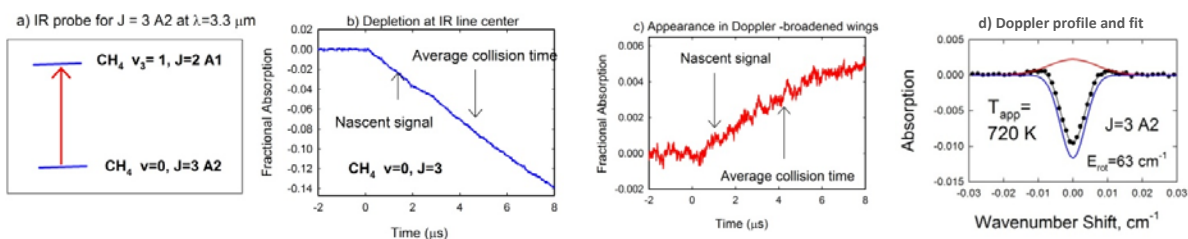


Fig. 1. Wavelength-dependent transient IR absorption signals for CH_4 $J=3$ following collisions with highly vibrationally excited pyrazine ($E=38000\text{ cm}^{-1}$). Ro-vibrational transitions of the ν_3 asymmetric stretch at $\lambda=3.3\text{ }\mu\text{m}$ are used to probe rotational states of CH_4 (0000). Nascent Doppler-broadened line profiles yield J -specific translational energies and populations.

of scattered molecules in the Doppler-broadened wings. The nascent appearance temperatures (center of mass frame) range from 530 K to 780 K for methane states with $J=0-15$ (Fig 2a). No significant J -dependence is observed for this range of J states. The nascent rotational distribution of scattered methane (0000) has a temperature of $T_{\text{rot}}=480\text{ K}$ (Fig. 2b), showing that methane gains modest amounts of rotational energy through collisions with high energy pyrazine. The nascent recoil energy measurements show that the V-RT pathway occurs via an impulsive mechanism with the majority of product energy in the form of translation. The modest rotational energy gains are likely correlated to the spherical shape of methane and its relatively small moment of inertia. IR fluorescence studies report that the average energy transfer value for methane/pyrazine(E) collisions is 6 times larger than with neon. Our state resolved data show that both translational and rotational energy contribute to the enhanced quenching efficiency of methane relative to that for collisional quenching by atoms of comparable mass and attractive interactions.

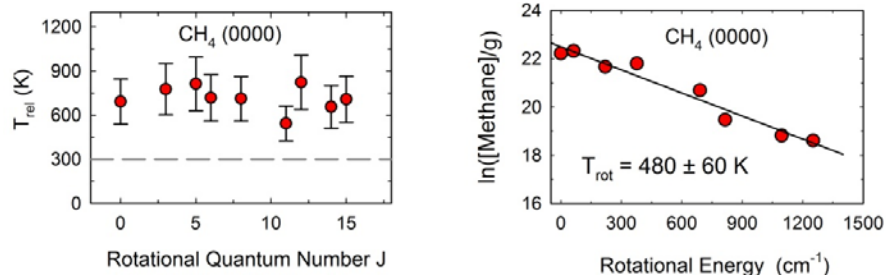


Fig. 2. Nascent translational and rotational energy distributions for scattered methane (0000) immediately following collisions with pyrazine ($E=37,900\text{ cm}^{-1}$).

Vibration-to-Vibration Energy Transfer: We have also measured the extent to which vibration-to-vibration energy transfer takes place in quenching collisions of pyrazine(E) with methane. Our studies so far have focused on the ν_2 and ν_4 bending modes of methane. Lack of transient signals for the ν_1 and ν_3 states suggest minor contributions from collisions that excite the higher frequency stretching modes in methane. Scattering profiles for the excited bending modes were measured for the $J=6$ state of (0100) and a number of rotational states for (0001). The nascent translational energy distributions for both vibrational states have temperatures of $T=244\text{-}348\text{ K}$ (Fig 3). The data for the (0100) state do not exhibit any J -dependent trends. It is clear from these results that vibrational excitation of methane from collisions with pyrazine(E) takes place without any appreciable translational energy release.

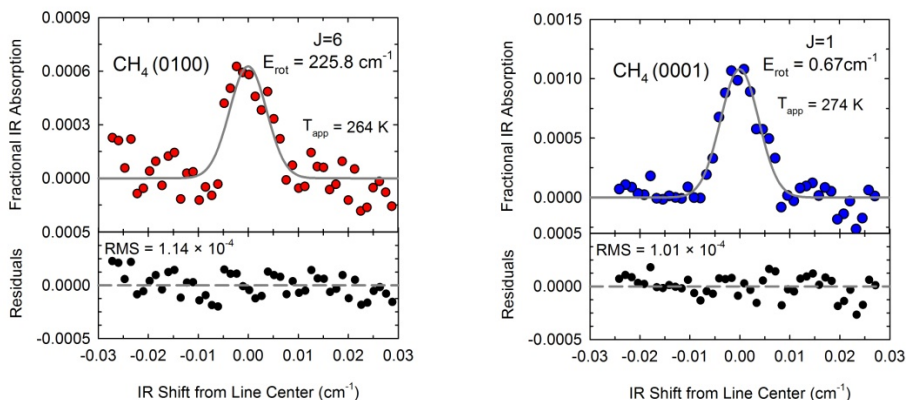


Fig. 3. Nascent Doppler-broadened line profiles for vibrationally excited bending modes of scattered methane.

The nascent rotational distribution for vibrationally excited methane in the (0001) state has a rotational temperature of $T_{\text{rot}}=233\text{ K}$, showing that essentially no rotational energy is exchanged in (V-V) collisions. The initial (0000) rotational distribution at 300 K is mapped onto the vibrationally excited state with only minor ΔE_{rot} values, if any. Together, the low values of recoil and rotational energy provide strong evidence for near-resonant (V-V) energy transfer that occurs via long-range attractive interactions. Both of the methane vibrational modes have energies that are nearly resonant with pyrazine. The pyrazine ν_{12} vibrational mode at 1522 cm^{-1} [3] is close to the methane (0100) mode at 1533 cm^{-1} while the pyrazine ν_{21} mode at 1337 cm^{-1} is close to the methane (0001) mode at 1311 cm^{-1} .

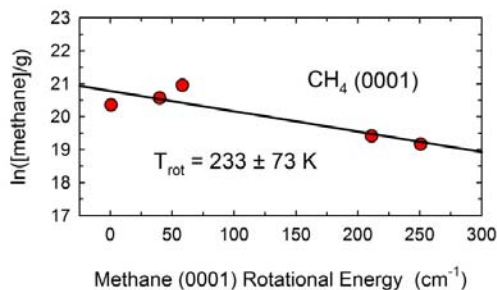


Fig. 4. Nascent rotational distribution for vibrationally excited scattered methane (0001) following collisions with pyrazine(E).

Comparisons of the methane/pyrazine(E) scattering dynamics to those of CO₂, HOD and DCl with pyrazine reveal a number of similarities: the (V-RT) pathway is the primary energy transfer channel; the angular momentum (not rotational energy) of the scattered energy-acceptor molecules is a key indicator for predicting J-dependence of recoil energy.

B. High-resolution transient detection of ammonia as an energy quencher

A new set of studies are now underway to investigate collisional energy transfer of high energy molecules with ammonia. One of our goals is to learn about energy transfer mechanisms for more complex molecules beyond diatomic and triatomic molecules, for which vibrational modes are expected to play an increasingly important role. Ammonia gives us the opportunity to explore how vibrational energy loss pathways in high energy are affected by the presence of a dipole moment in energy acceptor. We are interested in learning how near-resonant energy transfer, product branching ratios and collision rate constants are affected.

III. Future Work

Our future goals include writing up our methane results and our recent studies on HCl collisions. We will continue our studies on the energy transfer dynamics in collisions of highly excited molecules with NH₃. We are also interested in establishing the importance of energy resonance effects in the relaxation of highly excited molecules. We will do this by studying collisions of sequentially-deuterated methane.[4]

IV. References

1. D. K. Havey, Q. Liu, Z. Li, M. Elioff and A. S. Mullin, *J. Phys. Chem. A* 111, 13321-13329 (2007)
2. G. Echibiri, M. Smarte, W. Walters and A. S. Mullin, *Optics Express*, 22, 14885-14895 (2014)
3. Billes, F.; Mikosch, H.; Holly, S. *J. Mol. Struct. (THEOCHEM)* 423, 225 (1998)
4. T. Shimanouchi, *NBS Nat. Stand. Ref. Data Ser.* 39 (1972)

V. Publications supported by this project 2012-2015

1. J. Du, N. A. Sassin, D. K. Havey, K. Hsu and A. S. Mullin, "Full energy gain profiles of CO₂ from collisions with highly vibrationally excited molecules. II. Energy dependent pyrazine (E=32700 and 37900 cm⁻¹) relaxation" *J. Phys. Chem. A* 117, 12104-12115 (2013)
2. G. Echibiri, M. Smarte, W. Walters and A. S. Mullin, "Performance of a high-resolution mid-OR optical parametric oscillator transient absorption spectrometer" *Optics Express*, 22, 14885-14895 (2014); selected for publication in *Virtual Journal for Biomedical Optics (VJBO)*
3. J. Du, D. K. Havey, S. W. Teitelbaum and A. S. Mullin, "Full energy gain profiles of CO₂ from collisions with highly vibrationally excited molecules. III. 2-Methylpyridine, 2,6-dimethylpyridine and 3,5-dimethylpyridine (E~38500 cm⁻¹) relaxation" in preparation.
4. M. Smarte, G. Echibiri, W. Walters, J. Cleveland and A. S. Mullin, "Unusual isotope effects in collisions of pyrazine (E) + HCl and DCl: Role of strong interactions", in preparation.

Reacting Flow Modeling with Detailed Chemical Kinetics

Habib N. Najm

Sandia National Laboratories
P.O. Box 969, MS 9051, Livermore, CA 94551
hnnajm@sandia.gov

I. Program Scope

The goal of this research program is to improve fundamental understanding of reacting flow, thereby advancing the state of the art in predictive modeling of combustion. The work involves:

- Developing numerical methods for the efficient solution of reacting flow systems of equations with detailed kinetics and transport, massively parallel codes for computing large scale reacting flow with detailed kinetics, and techniques for analysis of multidimensional reacting flow.
- Using computations to investigate the structure and dynamics of flames using detailed chemical kinetics.
- Developing numerical methods for uncertainty quantification (UQ) in reacting flow computations.
- Estimation of uncertain chemical model parameters, and calibration/validation of reacting flow models, based on experimental data and computational predictions.
- UQ studies in computations of chemical systems and reacting flow.

In the following, recent progress and future plans in this overall area are discussed.

II. Recent Progress

A. Statistical Inference of Reaction Rate Coefficients

In order to construct meaningful probability density functions (PDFs) on uncertain Arrhenius-rate parameters of chemical kinetic mechanisms, in the absence of actual data from previous measurements but given other constraint information in the form of moments on parameters, we had developed in recent years a general “data free inference” (DFI) computational strategy to infer uncertain parameters given constraints in lieu of data. DFI is a computational strategy rooted in the maximum entropy principle (MaxEnt) and relying on an approximate Bayesian computation (ABC) approach to enforce constraints of interest. We have so far published demonstrations of DFI for the inference of parameters of a simple single-step global methane-air model given nominal values and error bars on these parameters. Elsewhere, we extended the method to use summary statistics on functions of the parameters.

We have recently applied DFI for the inference of kinetic rate parameters in an H_2 - O_2 mechanism. Specifically, we have focused to begin with on the Arrhenius rate parameters of one reaction, R_2 : $H+O_2 \rightarrow OH+O$, relying on published summary statistics on the reaction rate $k(T)$ over a range of initial temperature. The experiment [MHB90] employed shock-tube ignition measurements of OH concentration over time, over a range of initial conditions. Based on sensitivity of OH to other rate constants, we included the uncertainty in the pre-exponential rate constant of the reaction R_1 : $OH+H_2 \rightarrow H_2O+H$ as a nuisance parameter. This is a challenging application of DFI, given the fact that we’re trying to replicate details in the fitting of high-dimensional experimental data. Even with coarse sampling over the relevant initial temperature range and associated time histories, there is a lot of data, rendering the DFI Markov chain on data space high-dimensional and therefore computationally challenging. Thus, we spent significant effort on speeding up the algorithm. This included construction of a mixed Padé-Legendre polynomial surrogate for $[OH](t, T_0, k_1, k_2)$ to allow fast evaluation of predicted OH time response. Given observed robust nearly-Gaussian posteriors, we also employed importance sampling and Gauss-Hermite quadrature for evaluation of the summary statistics for any proposed data set, thereby avoiding an inner Markov chain on model parameters. Overall, these improvements lead to orders of magnitude in speedup of the algorithm. Given the structure of available information on uncertainty in $\ln k(T)$ from the experiment, the application of DFI to this problem lead to the need for significant regularization, which we achieved by imposing strict informative priors on a subset of the parameters. This allowed inference of uncertain parameters resulting in statistics on $\ln k(T)$

that match given summary statistics from the experiment. Nonetheless, this degree of regularization is not desirable. We are continuing to work on this going forward in an effort to explore avenues allowing a lower degree of regularization and less informative priors.

B. Estimation of Model Error in Chemical Models

Working with K. Sargsyan, we extended our earlier demonstrations for estimation of model error in the context of model-to-model calibration, to encompass methane-air mixture ignition over a range of initial temperature and equivalence ratio. We calibrated a single-step irreversible global reaction for methane oxidation in air, based on predictions of ignition time, relative to corresponding predictions from GRImech3.0. The broad range of initial conditions exposed the shortcomings of the simple model, thereby exhibiting a significant degree of model error. Our embedded model error approach, relying on a density estimation setting, provided desired results. Specifically, uncertainty in calibrated model parameters translated into a range of uncertainty in predicted ignition time that is consistent with the discrepancy from the detailed model, in an ℓ_2 -sense, over the range of initial conditions. We also extended the construction to allow for data noise. In this way, we demonstrated calibration of benchmark polynomial forward models with synthetic noisy data from more complex models, while estimating both model-error and data-noise induced uncertainty in model parameters and associated uncertain predictions. We demonstrated the ability of the method to disambiguate between these two sources of error, where, in the limit of large amounts of data, or small data noise, we observe the decay of the data-noise induced uncertainty, being left with the non-decaying model-error component. Demonstrations of this capability in chemical models is pending.

C. Uncertainty Quantification in Large Eddy Simulation of Turbulent Combustion

Working with J. Oefelein and G. Lacaze we have continued to work on UQ in large-eddy simulation (LES) of turbulent combustion. We focused on a turbulent non-premixed hydrocarbon flame stabilized on a bluff-body, and considered uncertainty in the Smagorinsky coefficient and the turbulent Prandtl and Schmidt numbers. Input uncertainties were modeled using polynomial chaos expansions (PCEs) and propagated through the LES computations using sparse-quadrature sampling. Random sampling of the resulting PCEs was used to obtain marginal joint distributions of output quantities of interest (QoIs). The PCEs were also used to estimate global sensitivity coefficients for various QoIs on the three LES parameters. The resulting probability densities and sensitivity indices provided insight into the mechanics of the flow field and the LES solver. This study also indicated the need for higher degrees of precision in the estimation of QoIs that are turbulent statistics, as errors due to finite sample size translate into non-smooth behavior in the input-output map and present a challenge for accurate representation of uncertainty using PCEs.

We also worked jointly with Lacaze and Oefelein on the statistical calibration of a 2-step chemical model for n-dodecane oxidation to be used in LES computations. We used a reference detailed mechanism [NPP14] for n-dodecane, with 255 species and 2,289 reactions as the basis for calibration. The Arrhenius parameters of one of the reactions in the 2-step model, namely the reaction step accounting for incomplete oxidation of n-dodecane into CO, were written as functions of equivalence ratio and temperature, and the parameters defining this functional dependence were the object of calibration. We built a polynomial chaos (PC) surrogate model for ignition time predictions from the 2-step model, and used it in statistical model-to-model calibration relative to the detailed model predictions, thereby providing estimation of the parameters of interest with quantified uncertainty. These will be used subsequently for associated LES predictions of Diesel engine injection, with quantified uncertainty. The current implementation relies on conventional data-error noise structures, and does not account for model error. Future implementations will account for model-error as outlined above.

D. Chemical Model Reduction under Uncertainty

Chemical model reduction methods rely on a starting detailed mechanism as a reference/gold-standard, in relation to which simplified mechanisms are judged. Yet, given uncertainties in detailed chemical models of complex fuels, it is clear that some accounting for uncertainty is required in the analysis and reduction strategies. We have recently brought together chemical model analysis and reduction methods that make use of computational singular perturbation (CSP) analysis, and UQ methods, to address this issue. Our approach relies on random sampling of prescribed uncertain parameters of the detailed model. For every such sample, the conventional deterministic CSP model analysis and reduction strategy is run, arriving at a simplified mechanism. Assembling all samples,

we arrive at an estimated probability for each reaction to be included in the simplified model. Thus, given chosen thresholds on these probabilities, we arrive at the sought-after simplified model accounting for uncertainty. We have developed algorithms and software for handling the analysis and reduction for large numbers of samples, and have demonstrated the performance of the algorithm on both methane and n-butane detailed mechanisms. Further work is in progress to produce a spectrum of simplified mechanisms of different degrees of fidelity, and to develop reliable error measures accounting for uncertainty in parameters of both detailed and simplified models.

III. Future Plans

A. Intrusive UQ in Chemical Systems

We have previously addressed the question of stability of intrusive UQ methods in chemical systems from multiple perspectives. We demonstrated the utility of a positivity-preserving filtering approach that employs iterative reduction of the probability of negative states when it exceeds a given threshold, thereby stabilizing time integration of the stochastic Galerkin system. This method, however, had limited utility outside a narrow range of operating conditions. We also outlined an alternate approach that pursues positivity at specific quadrature points. The evaluation of this approach is in progress. In the meantime, we envision utility of yet another approach that we plan to evaluate going forward. Specifically, we aim to address the problem by detecting spurious positive eigenvalues, and then adaptively modifying the source term of the chemical system so as to eliminate them. The hope is that this approach, by targeting more finely-tuned adjustment of the source term, may be more globally effective in stabilizing the computations. The essential guide for identifying spurious positive eigenvalues is our observation in previous work that there is a connection between the sampled eigenvalues of the uncertain system and non-spurious eigenvalues of the stochastic Galerkin system. This relationship provides a potential means of identifying the unwanted spurious positive eigenvalues.

B. Dynamical Analysis in Stochastic Chemical Systems

Stochastic chemical systems are of interest in applications ranging from biology to catalytic gas kinetics at nano-structured surfaces. Conventional methods for dynamical analysis and model reduction in continuum level chemical systems are, however, not applicable in micro/nano-scale stochastic chemical systems, as necessary Jacobian eigenanalysis tools are stymied by the stochastic nature of the chemical source terms. Accordingly, there is interest in the development of an adequate framework for analysis and reduction of stochastic chemical systems. We have outlined in previous work initial steps along this path, where we used random dynamical system theory to reformulate stochastic differential equations in a manner that allowed the definition and quantification of stochastic slow manifolds. Going forward, we plan to develop means of projecting stochastic source terms onto underlying nominal slow manifold structures, allowing potential means of selectively eliminating fast stochastic processes. Developing an appropriate geometrical structure for both fast and slow subspaces, and corresponding means of projection onto these subspaces, will enable generalized analysis and reduction of stochastic chemical systems.

C. Estimation of Model Error in Chemical Systems

Our formulation for estimation of model error has been demonstrated in both noise-free and noisy data environments, in the context of algebraic model problems. We also demonstrated the construction with noise-free data from a detailed chemistry model, which was used to estimate model error in a simple/global chemistry model for methane-air ignition. The next challenge is to extend the chemical model demonstration to the noisy-data context, where detailed model predictions will be corrupted by noise for algorithm demonstration purposes. Our present demonstrations with noisy data in algebraic model problems have relied on computational efficiencies realized due to the linearity of the fit model in the parameters, a property that will not be generally true for the chemical context. We will address this challenge relying either on approximate Bayesian computation or on marginalized likelihoods with one-dimensional kernel density estimation (KDE) procedures.

D. UQ in LES of Turbulent Combustion

Going forward in the LES-UQ context, we have two main near-term goals. To begin with, we will extend the current work by addressing the matter of sampling noise in the estimation of turbulent flow statistics. Establishing

a requisite order for estimation of PC surrogates with good accuracy for turbulent flow statistics needs to be done in a context where sampling errors are well understood and are small enough. This will be done employing extensive averaging over longer time horizons, which will require significant computational resources. Second, we will extend the current n-dodecane model-to-model calibration to include model error, thereby allowing calibration with meaningful levels of predictive uncertainty in ignition time over requisite ranges of operating conditions.

E. Statistical Inference of Reaction Rate Constants

We will extend our current demonstration of DFI in H_2 - O_2 chemistry to deal with the need for significant regularization via informative priors. This situation is possibly the result of a number of issues including the degree of information in the available statistics, the degree of uncertainty in nuisance parameters, the number of operating conditions and data points, or the structure of the high-dimensional markov chain monte carlo (MCMC) procedure. We are in the process of examining these issues, and will explore potential remedies where appropriate.

F. Chemical Model Reduction under Uncertainty

We will continue current developments on model reduction under uncertainty, focusing on n-butane kinetics. This demonstration will involve significant computational challenges, in terms of: (1) run/analysis times for large numbers of random samples; (2) establishing convergence and robust reduction results; and (3) in conducting *a-posteriori* error-estimation studies.

IV. References

- [MHB90] D.A. Masten, R.K. Hanson, and C.T. Bowman. Shock tube study of the reaction $H + O_2 \rightarrow OH + O$ using oh laser absorption. *Journal of Physical Chemistry*, 94:7119–7128, 1990.
- [NPP14] K. Narayanaswamy, P. Pepiot, and H. Pitsch. A chemical mechanism for low to high temperature oxidation of n-dodecane as a component of transportation fuel surrogates. *Combustion and Flame*, 161:867–884, 2014.

V. BES-Supported Published/In-Press Publications [2013-2015]

- [1] X. Han and H.N. Najm. Dynamical structures in stochastic chemical reaction systems. *SIAM J. Appl. Dyn. Systems*, 13(3):1328–1351, 2014.
- [2] K.S. Kedia, C. Safta, J. Ray, H.N. Najm, and A.F. Ghoniem. A second-order coupled immersed boundary-SAMR construction for chemically reacting flow over heat-conducting Cartesian grid-confirming solid. *J. Comput. Phys.*, 272:408–428, 2014.
- [3] M. Khalil, G. Lacaze, J.C. Oefelein, and H.N. Najm. Uncertainty quantification in LES of a turbulent bluff-body stabilized flame. *Proceedings of the Combustion Institute*, 35:1147–1156, June 2015.
- [4] H.N. Najm, R.D. Berry, C. Safta, K. Sargsyan, and B.J. Debusschere. Data Free Inference of Uncertain Parameters in Chemical Models. *Int. J. for Uncertainty Quantification*, 4(2):111–132, 2014.
- [5] H.N. Najm and M. Valorani. Enforcing Positivity in Intrusive PC-UQ Methods for Reactive ODE Systems. *J. Comput. Phys.*, 270:544–569, 2014.
- [6] J. Prager, H.N. Najm, K. Sargsyan, C. Safta, and W.J. Pitz. Uncertainty Quantification of Reaction Mechanisms Accounting for Correlations Introduced by Rate Rules and Fitted Arrhenius Parameters. *Combustion and Flame*, 160:1583–1593, 2013.
- [7] J. Prager, H.N. Najm, and J. Zádor. Uncertainty Quantification in the *ab initio* Rate-Coefficient Calculation for the $CH_3CH(OH)CH_3 + OH \rightarrow CH_3C^*(OH)CH_3 + H_2O$ Reaction. *Proc. Comb. Inst.*, 34:583–590, 2013.
- [8] K. Sargsyan, H. N. Najm, and R. Ghanem. On the Statistical Calibration of Physical Models. *International Journal for Chemical Kinetics*, 47(4):246–276, 2015.

Spectroscopy, Kinetics and Dynamics of Combustion Radicals

Grant No. DE-FG02-09ER16021

Annual Progress Report, David J. Nesbitt

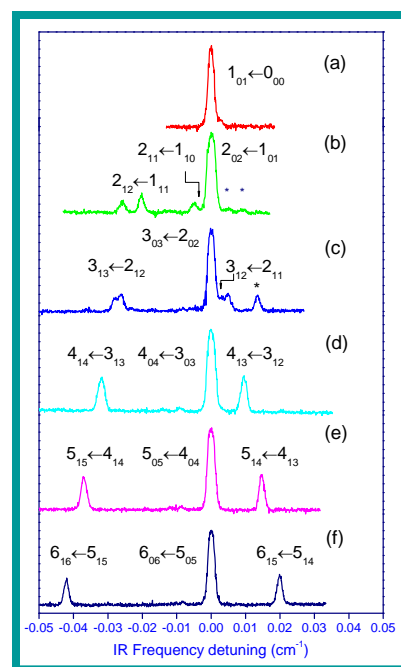
djn@jila.colorado.edu, April 1, 2015

*JILA, University of Colorado and National Institute of Standards and Technology, and
Department of Chemistry and Biochemistry, University of Colorado, Boulder, Colorado*

This report summarizes the results from our research program for elucidation of spectroscopy, kinetics and structural dynamics of combustion radicals. The experimental apparatus is based on the powerfully synergistic combination of i) high resolution IR difference frequency light generation, ii) slit discharge sources for formation of jet cooled radicals, and iii) high sensitivity detection with direct laser absorption methods near the quantum shot noise limit. The key advantage of such methods is that such highly reactive radical transients can be made at relatively high pressures/temperatures characteristic of combustion conditions, and yet with the resulting reactive species cooled within several mm (5-10 μ s) down to $T \approx 10$ -15K in the slit supersonic expansion for maximal spectroscopic simplification. Selected highlights from work over the last year are summarized below.

I. Propargyl Radical: Sub-Doppler Rovibrational/Spin-Rotation Spectroscopy

The formation of benzene molecules from reaction of two propargyl radical (H_2CCCH) has been recently observed in synchrotron based VUV photoionization mass spectrometry in low pressure flames, which showcases the special importance of such C_3 propargyl radical species in the early growth stages to form larger aromatic structures. This provides particular motivation for detailed understanding of the high resolution spectroscopy and dynamics of propargyl radical, in order to facilitate both unambiguous identification and direct laser based concentration measurements in further experimental studies of such aggregation processes. We have obtained first sub-Doppler infrared spectra of jet cooled propargyl radical in the CCH stretch region, based on formation and rapid cooling in a slit supersonic jet discharge source. The extensive delocalization of this unpaired electron over the entire radical framework proves to be a particularly interesting issue, which has attracted attention from both theoretical and experimental perspectives. The localization or delocalization of this unpaired electron result in electronic structure corresponding to either the propargyl form ($\text{H}_2\text{C}-\text{C}\equiv\text{CH}$) or the nominally allenyl form ($\text{H}_2\text{C}=\text{C}=\text{CH}$), with a paired electron localized at the methylenic or acetylenic carbon atom, respectively. However, there is evidence that a more balanced intermediate resonance structure [$\text{H}_2\text{C}-\text{C}\equiv\text{CH} \leftrightarrow \text{H}_2\text{C}=\text{C}=\text{CH}$] may be the appropriate description for this system, for which the probability density distribution of the unpaired electron can influence the geometry of the radical and vice versa. In our present study, the rovibrational transitions of the acetylenic CH stretching mode of propargyl radical in the vicinity of 3326 cm^{-1} has been investigated in a discharge slit jet expansion under supersonically cooled conditions and with sub-Doppler resolution ($\sim 60 \text{ MHz}$). The density of collisions in the slit jet

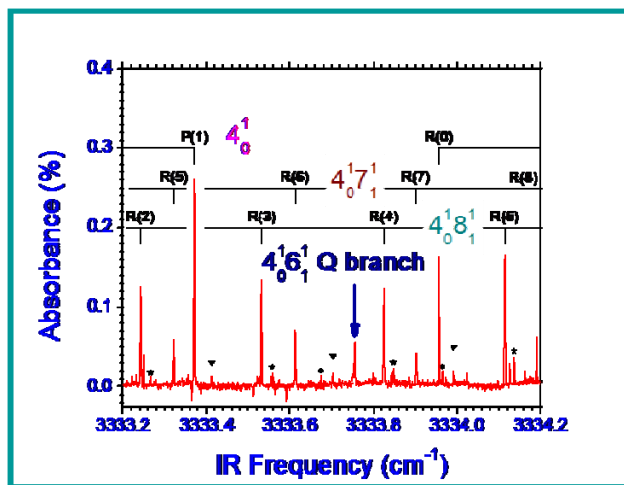


discharge expansion result in efficient rotational cooling of the hot propargyl radical down to the lowest two para/ortho nuclear spin states $K_a=0, 1$, with fully Boltzmann distributions in J well characterized by $T_{\text{rot}} = 17$ K. Sub-Doppler resolution in the slit jet expansion geometry permits first glimpses into fine-structure electron spin-rotation dynamics in propargyl radical for the C–H stretching mode, as well as partial hyperfine information on Fermi contact interactions for the two sets of distinguishable H nuclei. By way of example, a cascaded P branch view of rotational asymmetry doublet and spin-rotation structure are shown in the figure below, centering on the $K_a = 0 \leftarrow 0$ transitions for each J . The spin rotation structure is fully resolved at low J and merges into an inhomogeneously fine and hyperfine structure broadened line with increasing J . Due to indistinguishability of the methylenic H atoms, the nuclear spin statistical weights are 3:1 for $K_a = 0:1$, respectively, which makes transitions in the $K_a = 0 \leftarrow 0$ manifold predominant.

II. Spectroscopy and Dynamics of Jet-cooled Polyynes in a Slit Supersonic Discharge: Sub-Doppler Infrared Studies of Diacetylene HCCCCH

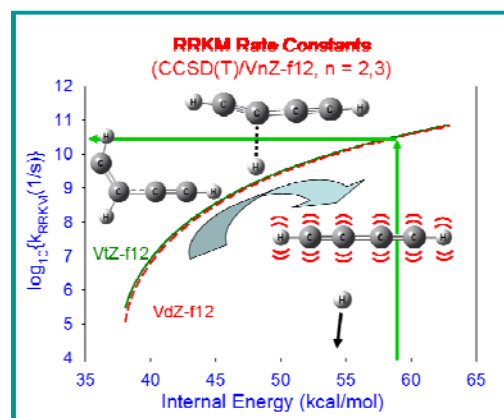
Fundamental, bending ($\nu_6, \nu_7, \nu_8, \nu_9$), and CC-stretch (ν_2, ν_3) hot band spectra in the antisymmetric CH stretch (ν_4) region near 3330 cm^{-1} have been observed and analyzed for jet cooled diacetylene ($\text{HC}\equiv\text{C}-\text{C}\equiv\text{CH}$) under sub-Doppler conditions. Diacetylene is generated *in situ* in the throat of a pulsed supersonic slit expansion by discharge dissociation of acetylene to form ethynyl ($\text{C}\equiv\text{CH}$) + H, followed by radical attack ($\text{HC}\equiv\text{CH} + \text{C}\equiv\text{C}-\text{H}$) to form $\text{HC}\equiv\text{C}-\text{C}\equiv\text{CH} + \text{H}$. The combination of i) sub-Doppler line widths and ii) absence of spectral congestion permit rotational structure and Coriolis interactions in the ν_4 CH stretch fundamental to be observed and analyzed with improved precision. Of particular dynamical interest, the spectra reveal diacetylene formation in highly excited internal vibrational states. Specifically, multiple $\Pi \leftarrow \Pi$ and $\Delta \leftarrow \Delta$ hot bands built on the ν_4 CH stretch fundamental are observed, due to doubly degenerate bending vibrations [cis $\text{C}\equiv\text{C}-\text{H}$ bend (ν_6), trans $\text{C}-\text{C}\equiv\text{C}$ bend (ν_7), trans $\text{C}\equiv\text{C}-\text{H}$ bend (ν_8) and cis $\text{C}-\text{C}\equiv\text{C}$ bend (ν_9)], as well as a heretofore unobserved $\Sigma \leftarrow \Sigma$ band assigned to excitation of the ν_2 or $2\nu_3$ CC stretch. Boltzmann analysis yields populations consistent with a universally cold rotations ($T_{\text{rot}} \approx 15 \pm 5$ K) and yet *superthermal* vibrations ($T_{\text{vib}} \approx 85\text{-}430$ K), the latter range of which is quite anomalously high for the high collision densities in a slit jet expansion. In order to elucidate a possible physical mechanism for this excess vibrational excitation, high level *ab initio*

MOLPRO/CCSD(T) calculations have been pursued with explicitly correlated basis sets (VnZ-f12; $n=2,3$) and extrapolated to the complete basis set (CBS) limit. The results suggest that this extensive hot band structure observed arises from i) highly exothermic $\text{CCH} + \text{HCCH}$ addition to yield a strongly bent HCCHCCH radical intermediate ($\Delta H = -62.6$ kcal/mole), followed by ii) rapid fragmentation over a submerged transition state barrier ($\Delta H = -18.9$ kcal/mole) to form vibrationally hot diacetylene + H products ($\Delta H = -25.6$ kcal/mol), and consistent with



crossed molecular beam studies by Kaiser et al.¹ In further support, RRKM fragmentation rates for this complex are calculated, which exceed collision frequencies in the slit jet expansion and suggest near unity quantum efficiency for diacetylene formation.

Diacetylene ($\text{H-C}\equiv\text{C-C}\equiv\text{CH}$), the smallest member of the polyynes family, represents an ubiquitous species in combustion/pyrolysis chemistry. What makes these linear polyynes so chemically interesting is the fact that they form so readily via chain reaction addition with CCH ethynyl radical, e.g., i) $\text{HC}\equiv\text{CH} + \text{C}\equiv\text{CH} \rightarrow [\text{H-C}\equiv\text{C(H)-C}\equiv\text{CH}] \rightarrow \text{H-C}\equiv\text{C-C}\equiv\text{CH} + \text{H}$, augmented by ii) $\text{H} + \text{HCCH} \rightarrow \text{H}_2 + \text{CCH}$. It is worth noting here that the intermediate species of reaction i) is not a high energy transition state but rather an extremely stable radical adduct, > 60 kcal/mol lower in energy than $\text{HCCH} + \text{CCH}$ reactants, with little or no barrier and therefore resulting in insertion on nearly every collision. This process can therefore continue by subsequent exothermic attack of CCH into one of the diacetylene CC bond, which then forms even higher order polyynes such as triacetylene, tetraacetylene, etc. Indeed, such chain reaction kinetics are extremely rapid under non-oxidizing flame conditions, and therefore diacetylene is thought to be a crucial intermediate in the formation of soot particles. The fundamental anti-symmetric CH stretching mode (ν_4) and its many hot combination bands in the region of 3333 cm^{-1} of di-acetylene (C_4H_2) have been reinvestigated under sub-Doppler jet cooled conditions in a pulsed supersonic slit discharge. Single quantum hot bands ($\Pi \leftarrow \Pi$) due to all 4 degenerate bending vibrations (specifically, the cis $\text{C}\equiv\text{C-H}$ bend (ν_6), trans $\text{C-C}\equiv\text{C}$ bend (ν_7), trans $\text{C}\equiv\text{C-H}$ bend (ν_8) and cis $\text{C-C}\equiv\text{C}$ bend (ν_9)) are observed in conjunction with the ν_4 CH stretch fundamental and successfully analyzed. In addition, a clear $\Sigma \leftarrow \Sigma$ hot band built on the strong ν_4 fundamental is observed and unambiguously assigned to single quantum excitation of the low frequency C-C symmetric stretch (ν_3). Furthermore, the combination of i) sub-Doppler line widths and ii) absence of spectral congestion in the slit jet permit weak Coriolis perturbation structure in the ν_4 CH stretch fundamental to be observed and analyzed for the first time. The observation of such extensive hot band structure even under jet cooled slit conditions underscores the presence of highly non-equilibrium dynamics in rovibrational degrees of freedom, with a cold rotational temperature ($T_{\text{rot}} = 15\text{ K}$) common to all lower states and yet a highly *superthermal* vibrational temperature on the order of 358(16) K. From a dynamical perspective, a simple Boltzmann population analysis suggests that effective vibrational “temperatures” to be over > 20-25-fold higher than rotation. Indeed, such dramatic levels of bend excitation can be ascribed to i) a highly bent precursor HCCCCH framework, which, as suggested by *ab initio* MOLPRO (CCSD(T)/vdz-f12) calculations, tend to funnel energy selectively into low frequency bending coordinates, augmented by ii) far less efficient cooling of vibrations vs. rotations in the normal 2D pinhole expansion.



III. Symmetric CH Stretch Spectroscopy of Jet-cooled Hydroxymethyl Radical

Hydroxyalkyl radicals, $\bullet\text{ROH}$, represent some of the simplest oxyhydrocarbon radical species and yet crucial intermediates in combustion and atmospheric chemistry models. The simplest of these, hydroxymethyl ($\bullet\text{CH}_2\text{OH}$), is predicted to have a slightly non-planar

equilibrium structure with a low barrier across a C_s transition state due to OH internal rotation.²⁻⁴ Of particular dynamical interest is the evidence for strong coupling between the CH_2 flip and COH torsional coordinate, which makes the spectra challenging to analyze without complete rotational resolution yet also provides potentially much more informative with respect to isomerization barrier heights. From a simple freshman chemistry perspective, this coupling arises from valence electron repulsion of radical and lone pair orbitals, amplified by a “soft” barrier between sp^2 and sp^3 hybridization of the C radical center. Hydroxymethyl radical, CH_2OH , plays a critically role as a reactive intermediate in combustion. In addition to fundamental combustion processes, hydroxymethyl radical is an important intermediate for oxidative reactions occurring in the troposphere. For example, atmospheric scrubbing reactions of alkanes, alkenes, and alcohols all involve hydroxymethyl radical as a reactive intermediate. We have made substantial progress with spectral searches for CH_2OH in the symmetric CH_2 stretch region in a methanol doped He/Ne discharge. At sub-Doppler resolution, CH_2OH reveals a surprisingly intense spectrum, with typical S/N of 20:1, and $K_a = 0 \leftarrow 0$ A-type rotational assignments, which provide first precision molecular constants for this oxyradical species. The transitions are fit to a Watson A-reduced symmetric top Hamiltonian to yield first precision experimental values for the ground state rotational constants as well as improved values for the symmetric stretch rotational constants and vibrational band origin. The results both complement and substantially augment previous spectral efforts⁵ as well as offer high resolution predictions for astronomical detection of CH_2OH radical in the mm-wave region.

Papers published:

1) Chih-Hsuan Chang, Grant T. Buckingham, and David J. Nesbitt, “**Sub-Doppler Spectroscopy of *trans*-HOCO Radical in the OH Stretching Mode,**”

Papers submitted:

2) Chih-Hsuan Chang and David J. Nesbitt, “**Spectroscopy and dynamics of jet cooled polyynes in a slit supersonic discharge: Sub-Doppler infrared studies of diacetylene HCCCCH,**” J. Phys. Chem. A (Al Wagner, Joe Michel, Festschrift).

3) Chih-Hsuan Chang, Melanie A. Roberts, David J. Nesbitt, “**Spin-rotation structure of propargyl radical in the supersonic slit jet discharge.**” (J. Chem. Phys.)

Papers in preparation:

4) Chih-Hsuan Chang and David J. Nesbitt, “**Sub-Doppler infrared spectroscopy and formation dynamics of slit jet cooled triacetylene (HCCCCCH): the ν_5 antisymmetric CH stretch,**” (J. Chem. Phys.)

5) Chih-Hsuan Chang, Grant T. Buckingham, Fang Wang, David J. Nesbitt, “**High resolution spectroscopy of jet cooled phenyl radical: The ν_1 and ν_2 a_1 symmetry C-H stretching modes.**” (J. Chem. Phys.)

References:

- ¹ R. I. Kaiser, F. Stahl, P. V. Schleyer, and H. F. Schaefer, Phys. Chem. Chem. Phys. **4**, 2950 (2002).
- ² C. S. Dulcey and J. W. Hudgens, Bull. Soc. Chim. Belg. **92**, 583 (1983).
- ³ C. S. Dulcey and J. W. Hudgens, J. Chem. Phys. **84**, 5262 (1986).
- ⁴ R. D. Johnson and J. W. Hudgens, J. Phys. Chem. **100**, 19874 (1996).
- ⁵ L. Feng, J. Wei, and H. Reisler, J. Phys. Chem. A **108**, 7903 (2004).

Spectroscopy and Dynamics of Free Radicals

Stephen R. Leone and Daniel M. Neumark

Lawrence Berkeley National Laboratory and Departments of Chemistry and Physics, University of California, Berkeley, California 94720 (510) 643-5467 srl@berkeley.edu, 510-642-3502
dmneumark@berkeley.edu

Scope of the Project: In this program a diverse approach to researching combustion chemistry is taken by applying a variety of techniques to study radical spectroscopy and dynamics. It is motivated in part by the need to develop and refine reaction mechanisms for combustion as more fuel variations are explored and combustion under various temperature and pressure regimes is considered. This experimental program characterizes key properties of free radicals including bond dissociation energies, orbital energetics, electron affinities, spectroscopy of low-lying electronic states, primary photochemistry, and reaction dynamics. Laser spectroscopic methods and vacuum ultraviolet (VUV) light from the Chemical Dynamics Beamline of the Advanced Light Source are used to selectively investigate individual processes involved in formation and reaction of radicals. These studies facilitate a detailed understanding of the role of free radicals in reaction mechanisms that govern diverse processes such as low-temperature autoignition, the oxidation of aromatic hydrocarbons, and the growth of complex molecules such as PAH's in flames.

Recent Progress

Experimental investigations using synchrotron photoionization mass spectrometry considered several reactions of CH and C₂H with straight-chain molecules that result in formation of cyclic species. Specifically, it was found that the reaction between CH and acrolein proceeds *via* addition and H-loss to yield C₄H₄O products with an isomeric composition of (60 ± 12)% 1,3-butadienal and (17 ± 10)% furan (cyclic compound). Moreover, further evidence has been obtained that shows cyclization reactions compete favorably with direct H-loss that gives straight-chain products. For example, the reaction of CH with 1,3-butadiene, which has a structural motif identical to that of acrolein, yields cyclopentadiene in an analogous pathway to the furan formation in the CH + acrolein reaction. In addition, recent work showed that C₂H reacts with 1,3-butadiene to give approximately 57±30% fulvene (a five-membered ring cyclic isomer of C₆H₆).

Utilizing synchrotron photoionization mass spectrometry, the reaction of I atoms with squalene and squalane sub-micron aerosol droplets explored the reactivity of C=C double bonds in the heterogeneous phase. Because of uphill energetics, the I atom reaction rates in the gas phase with both saturated and unsaturated hydrocarbons are vanishingly small (via either H abstraction or I addition). In the heterogeneous aerosol phase, there is also no evidence of product formation for I atoms with squalane droplets (no C=C bonds). In contrast, squalene droplets (6 C=C bonds) react with I atoms, most likely by I addition to the double bond, followed by radical abstraction with neighboring molecules. The reactive uptake coefficient for I atoms with squalene, $\gamma_{eff} = (1.20 \pm 0.52) \times 10^{-4}$, is three orders of magnitude greater than the limit placed on the reaction with squalane. The increased reactivity is attributed to trapping, diffusion, and consequent reactivity in the unsaturated particles due to multiple interactions in the aerosol phase.

The kinetics and products of model heterogeneous reaction systems of OH + Oleic acid, linoleic acid, linolenic acid, each containing 1, 2, 3, C=C double bonds, respectively, are investigated to explore further the reactivity of droplets composed of unsaturated molecules. The acid molecules are similar in structure to long chain alkyl esters found in biodiesel fuel and can represent model systems to examine the fundamental heterogeneous reactions between hydrocarbon droplets and gas phase radicals and molecules. In a 10% mixture of O₂ in N₂ in the flow reactor, the effective reactive uptake coefficients (γ_{eff}) are all larger than unity (measured by the loss of the parent aerosol molecules), providing clear evidence for particle-phase chain chemistry. Values of γ_{eff} for oleic, linoleic and linolenic acid are 1.72 ± 0.08 , 3.75 ± 0.18 and 5.73 ± 0.14 , respectively.

A high temperature (500-1100 K) jet stirred reactor system has recently been constructed and interfaced for the first time to the sampling cone and time-of-flight mass spectroscopy arrangement of the Sandia flame apparatus at the Advanced Light Source. This experimental

arrangement presents a unique approach to monitor chemical transformations with tunable photoionization spectroscopy in well-defined conditions comparable to those in combustion engines. Oxidation studies of n-butane, partially deuterated n-butane and dimethyl ether have revealed new insights into the oxidation mechanism of these species. In addition to corroborating the observations of previous experiments at the synchrotron in China, which showed production of a ketohydroperoxide intermediate species in the n-butane oxidation reaction, the use of deuterated butane in the experiments performed here provides potential evidence for the Korcek mechanism of decomposition of the intermediate ketohydroperoxide species into acid, ketone and aldehyde pairs, via the observation of the fully deuterated acetone product.

Recently, a table-top soft x-ray transient absorption method utilizing high-harmonic generation to produce XUV and soft x-ray pulses with sub-40 fs duration has been applied to capture ultrafast gas-phase photochemical dynamics of radicals. The technique has been applied to probe the formation and electronic structure of halomethyl radicals, CH_2Br and CH_2I , from the UV photodissociation of dihalomethanes, CH_2IBr and CH_2I_2 . The investigated radicals are the simplest of the haloalkyl radicals (R-CX , $\text{X}=\text{Br},\text{I}$), which can act as key reactive intermediates in combustion chemistry or in the case of CH_2I as a precursor for a Criegee intermediate. The transient soft x-ray spectra of these radicals reveal spectroscopic transitions corresponding to the frontier singly-occupied molecular orbitals (SOMO) and lowest unoccupied molecular orbitals (LUMO) of the radicals via the 3d and 4d core orbitals of Br and I, respectively. In this way, a key new result is the measurement of the SOMO-LUMO splittings in radical species.

In the second component of this program, the spectroscopy and dynamics of free radicals that play a key role in combustion are investigated using three complementary, state-of-the-art experiments. Slow Electron Velocity-Map Imaging of cryogenically cooled anions (cryo-SEVI) yields precise electron affinities, vibrational frequencies, and term values of low-lying states for radicals that are generated by negative ion photodetachment. Negative ion photodetachment also forms the basis of the fast radical beam (FRBM) instrument, in which neutral free radicals generated in this manner are photodissociated, with the kinetic energy and angular distributions of the various photofragment channels analyzed using sophisticated coincidence detection techniques. The photodissociation processes of radicals generated by flash pyrolysis are investigated using a molecular beam instrument with a rotating mass spectrometer as a detector.

Highly resolved photoelectron spectra of the α - and β - naphthyl radicals have recently been measured on the cryo-SEVI instrument, yielding new spectroscopic information on the ground and low-lying states of these polycyclic aromatic hydrocarbon radicals. Preliminary results have been obtained for the anthracenyl radical, as well.

The photodissociation of thiophenoxy radicals was investigated at 248 nm (5.0 eV), 193nm (6.4eV), and 157nm (7.9eV) on the FRBM instrument. There are two major competing dissociation channels leading to $\text{SH} + \text{C}_6\text{H}_4$ (o-benzyne) and $\text{CS} + \text{C}_5\text{H}_5$ (cyclopentadienyl) with a minor contribution of $\text{S} + \text{C}_6\text{H}_5$ (phenyl). Dissociation proceeds by internal conversion from the initially prepared excited state to the ground electronic state followed by statistical dissociation. Calculations show that SH loss involves a single isomerization step followed by simple bond fission. For both SH and S loss, C-S bond cleavage proceeds without an exit barrier. By contrast, the CS loss pathway entails multiple transition states and minima as it undergoes five-membered ring formation and presents a small barrier with respect to products.

Three-body dissociation of ozone at 193 and 157 nm was also investigated on the FRBM instrument. Dalitz plots¹⁰ show how the translational energy released in photodissociation is partitioned among the three fragments. At both wavelengths, but more noticeably at 157 nm, the plots comprise three spots centered on the symmetry axes. Events along those axes correspond to equal energy partitioning in two of the recoiling O atoms, consistent with a synchronous concerted mechanism in which the two O-O bonds in ozone dissociate symmetrically and at the same time.

The photodissociation of the phenyl radical was re-investigated on the molecular beam instrument. In previous work, it was found that at 248 nm, the only observed channel was production of C_6H_4 (ortho-benzyne) + H, the lowest energy channel. At 193 nm, however, an additional channel, $\text{C}_4\text{H}_3 + \text{C}_2\text{H}_2$, was observed and found to be the dominant channel. However, recent calculations by Mebel and co-workers¹³ have shown that if dissociation at 193 nm is a statistical ground state process, then very little of this isomer should be produced and H-atom loss

should dominate. With this in mind, the photodissociation of C_6H_5 was revisited to see how sensitive the product branching was to experimental conditions. Source conditions in the flash pyrolysis radical source were optimized to reduce the internal temperature of the radicals, and the experiment was run at considerably lower photodissociation laser fluences to minimize the likelihood of two-photon processes. Under these conditions, both channels were still observed at 193 nm, but it was found that the H-atom channel was in fact dominant, with branching between the two channels consistent with the expected results for statistical ground state dissociation.

Future Plans: In future experiments, a laser system and apparatus is being introduced to produce 275-300 eV photons, which will access the carbon K shell directly and allow the investigation of fundamental hydrocarbon radicals such as CH_3 , allyl, and phenyl without the need for a halogen tag. By utilizing UV-pump, soft x-ray probe transient absorption spectroscopy in the 275-285 eV range, the spectral signature of vibrationally-excited radical produced by photodissociation will be investigated and the “hot band” character of the core-to-SOMO transitions in the x-ray spectra will be revealed. In this way, radical spectroscopy will provide fertile ground for assessing the first carbon K edge dynamics experiments in the ultrafast regime. In complementary future experiments, time-resolved x-ray photoelectron spectroscopy will also be used to track the core level electronic structure and ultrafast dissociation dynamics of molecules like CH_3I through I 4d core-ionization. While the ground state potential of the I 4d⁻¹ inner shell vacancy state may be estimated by theory, x-ray transitions from repulsive excited dissociative states to excited core hole states are completely uncharacterized. The energetics and dynamics of these transitions will reveal the effect of fundamental chemical processes such as bond-breaking on the core-level electronic structure.

The three instruments available to the second part of the effort will provide an integrated experimental platform for the study of free radical spectroscopy and dissociation experiments. During the coming year, the cryo-SEVI instrument will generate high resolution spectra for larger polycyclic aromatic hydrocarbon radicals, RO_2 species, and other radicals whose photodissociation dynamics will be investigated on the FRBM and molecular beam instruments. A “soft ionization” electron impact ionizer has recently been installed on the molecular beam instrument in order to reduce dissociative ionization; this will facilitate interpretation of radical photodissociation experiments. FRBM experiments will focus on the photodissociation of the t-butyl peroxy radical, as part of our programmatic goal to map out the spectroscopy and dissociation dynamics of radicals that play a key role in low temperature combustion and autoignition.

Recent Publications Citing DOE Support (2012-2015)

- K. Moshhammer, A. W. Jasper, D. M. Popolan-Vaida, A. Lucassen, P. Diévar, H. Selim, A. J. Eskola, C. A. Taatjes, S. R. Leone, S. M. Sarathy, Y. Ju, P. Dagaut, K. Kohse-Höinghaus, and N. Hansen, “Detection and identification of keto-hydroperoxide ($HOOCH_2OCHO$) and other intermediates during low-temperature oxidation of dimethyl ether”, *J. Phys. Chem. A*, in press (2015)
- M. L. Weichman, J. B. Kim and Daniel M. Neumark, “Slow Photoelectron Velocity-Map Imaging Spectroscopy of the ortho-Hydroxyphenoxide Anion”, *J. Phys. Chem. A*, DOI: 10.1021/acs.jpca.5b00768, (2015)
- M. L. Weichman, J. B. Kim, J. A. DeVine, D. S. Levine and D. M. Neumark, “Vibrational and Electronic Structure of the α - and β -naphthyl Radicals via Slow Photoelectron Velocity-Map Imaging”, *J. Am. Chem. Soc.*, 137, 1420, (2015)
- A. R. Attar, L. Piticco, and S. R. Leone, “Core-to-valence spectroscopic detection of the CH_2Br radical and element-specific photodissociation dynamics of CH_2IBr ”, *J. Chem. Phys.*, 141, 164308 (2014)
- J. F. Lockyear, M. Fournier, I. R. Sims, J.-C. Guillemin, C. A. Taatjes, D. L. Osborn and S. R. Leone, “Formation of fulvene in the reaction of C_2H with 1,3-butadiene”, *Int. J. Mass. Spectrom.*, in press (2014)
- T. Nah, S. H. Kessler, K. E. Daumit, J. H. Kroll, S. R. Leone, and K. R. Wilson, “Influence of molecular structure and chemical functionality on the heterogeneous OH-initiated oxidation of unsaturated organic particles”, *J. Phys. Chem. A*, 118, 4106 (2014)
- D. M. Popolan-Vaida, K. R. Wilson, and S. R. Leone, “Reaction of I atoms with sub-micron squalane and squalene droplets: mechanistic insights into heterogeneous reactions”, *J. Phys. Chem. A*, 118, 10688 (2014)
- N. Cole-Filipiak, M. Shapero, B. Negru and D. M. Neumark, “Revisiting the Photodissociation Dynamics of the Phenyl Radical”, *J. Chem. Phys.*, 141, 104307, (2014)

- M. Ryazanov, A. Harrison, G. Wang, P. Crider and D. M. Neumark, “Investigation of 3-fragment Photodissociation of O_3 at 193.4 and 157.6 nm by Coincident Measurements”, *J. Chem. Phys.*, **140**, 234304, (2014)
- J. F. Lockyear, O. Welz, J. D. Savee, F. Goulay, A. J. Trevitt, C. A. Taatjes, D. L. Osborn and S. R. Leone, “Isomer Specific Product Detection in the Reaction of CH with Acrolein”, *J. Phys. Chem. A*, **117**, 11013 (2013)
- A. J. Trevitt, M. B. Prendergast, F. Goulay, J. D. Savee, D. L. Osborn, C. A. Taatjes and S. R. Leone, “Product Branching Fractions of the CH plus Propene Reaction from Synchrotron Photoionization Mass Spectrometry”, *J. Phys. Chem. A*, **117**, 6450, (2013)
- J. Bouwman, M. Fournier, I. R. Sims, S. R. Leone and K. R. Wilson, “Reaction Rate and Isomer-Specific Product Branching Ratios of $C_2H + C_4H_8$: 1-Butene, cis-2-Butene, trans-2-Butene, and Isobutene at 79 K”, *J. Phys. Chem. A*, **117**, 5093, (2013)
- E. R. Hosler and S. R. Leone, “Characterization of Vibrational Wave Packets by Core-Level High-Harmonic Transient Absorption Spectroscopy”, *Phys. Rev. A*, **88**, 023420, (2013)
- S. D. Chambreau, J. B. Liu, G. L. Vaghjiani, C. J. Koh, A. Golan, O. Kostko and S. R. Leone, “Thermal decomposition mechanisms of ionic liquids by direct dynamics simulations and vacuum ultraviolet photoionization mass spectrometry”, *Abstracts of Papers of the Am. Chem. Soc.*, **245**, 206-PHYS, (2013)
- T. Nah, M. Chan, S. R. Leone and K. R. Wilson, “Real Time in Situ Chemical Characterization of Submicrometer Organic Particles using Direct Analysis in Real Time Mass Spectrometry”, *Anal. Chem.*, **85**, 2087, (2013)
- T. Nah, S. H. Kessler, K. E. Daumit, J. H. Kroll, S. R. Leone and K. R. Wilson, “OH-initiated oxidation of sub-micron unsaturated fatty acid particles”, *Phys. Chem. Chem. Phys.*, **115**, 18649, (2013)
- A. W. Harrison, J. S. Lim, M. Ryazanov, G. Wang, S. Gao and D. M. Neumark, “Photodissociation Dynamics of the Thiophenoxy Radical at 248, 193, and 157nm”, *J. Phys. Chem. A*, **117**, 11970, (2013)
- N. C. Cole-Filipiak, B. Negru, G. M. P. Just, D. Park and D. M. Neumark, “Photodissociation Dynamics of the Methyl Perthyl Radical at 248 nm via Photofragment Translation Spectroscopy”, *J. Chem. Phys.*, **138**, 054301, (2013)
- S. H. Kessler, T. Nah, K. E. Daumit, J. D. Smith, S. R. Leone, C. E. Kolb, D. R. Worsnop, K. R. Wilson and J. H. Kroll, “OH-Initiated Heterogenous Aging of Highly Oxidized Organic Aerosol”, *J. Phys. Chem. A*, **116**, 6358 (2012)
- J. Bouwman, F. Goulay, S. R. Leone and K. R. Wilson, “Bimolecular Rate Constant and Product Branching Ratio Measurements for the Reaction of C_2H with Ethene and Propene at 79 K”, *J. Phys. Chem. A*, **116**, 3907 (2012)
- F. Goulay, A. J. Trevitt, J. D. Savee, J. Bouwman, D. L. Osborn, C. A. Taatjes, K. R. Wilson and S. R. Leone, “Product Detection of the CH Radical Reaction with Acetaldehyde”, *J. Phys. Chem. A*, **116**, 6091, (2012)
- G. M. P. Just, B. Negru, D. Park and D. M. Neumark, “Photodissociation of Isobutene at 193 nm”, *Phys. Chem. Chem. Phys.*, **14**, 675, (2012)

State-to-state photoionization, photoelectron, and photodissociation of combustion radicals

Cheuk-Yiu Ng

Department of Chemistry, University of California, Davis, California 95616

E-mail Address: cyng@ucdavis.edu

I. Program Scope:

High-resolution vacuum ultraviolet (VUV) photoionization and photoelectron spectroscopy has a distinguished history of providing accurate spectroscopic and energetic data for neutral molecules and their cations. Through the cation thermochemical cycle, ionization energies (IEs) and 0 K appearance energies (AEs) of dissociative photoionization processes thus obtained, can provide 0 K bond dissociation energies (D_0 's) and 0 K heats of formation (ΔH_{f0}° 's) for both neutrals and cations. This program is aimed to provide the most accurate spectroscopic and thermochemical data with quantified uncertainties for key combustion radicals to serve as experimental benchmarks for the further development of more accurate quantum computation packages. We plan to coordinate with the Thermochemical Network (TN) approach to establish comprehensive values for the Active Thermochemical Tables (ATcT) and to devote our experimental effort for the measurement of radical systems that are identified as weak links by the ATcT analysis. The high-resolution rotationally resolved photoionization and photoelectron spectra obtained for key combustion intermediates should allow the design of more reliable detection schemes of these radicals in mechanistic chemical studies by using the VUV photoionization mass spectrometric techniques.

II. Recent Progress:

We have recently demonstrated a high-resolution photoelectron spectroscopic method based on VUV laser velocity-map imaging (VMI) measurements of threshold photoelectrons (TPEs). This VUV-VMI-TPE method achieves a photoelectron resolution comparable to that observed in pulsed field ionization-photoelectron (PFI-PE) measurements. Since VUV-VMI-TPE measurements can be made using a relatively high dc electric field, its detection sensitive is believe to be higher than the PFI-PE scheme.

A. VUV-VMI-TPE measurements of CH_2Cl and CH_2Br

By employing the VUV-VMI-TPE method, we have measured the high-resolution photoelectron spectra of chloromethyl (CH_2Cl) and bromomethyl (CH_2Br) radicals. The halogenated methyl radicals play an important role in catalytic depletion of the ozone layer. In the earth troposphere, CH_2Cl and CH_2Br radicals are generated by the atmospheric reactions between hydroxyl radical (OH) and CH_3Cl and CH_3Br , which are generated by marine organisms in the ocean and subsequently released into the atmosphere.

The simulation of the VUV-VMI-TPE spectra for CH_2Cl^+ is consistent with the selection rules: $\Delta K_a = \text{odd}$ and $\Delta K_c = \text{even and odd}$; and gives a rotational temperature of 40K for the CH_2Cl sample. The simulation also gives the $\text{IE}(\text{CH}_2\text{Cl}) = 70546 \pm 4 \text{ cm}^{-1}$ ($8.7466 \pm 0.0005 \text{ eV}$). A similar simulation exercise for the VUV-VMI-TPE origin band for CH_2Br^+ yields the $\text{IE}(\text{CH}_2\text{Br}) = 69464 \pm 4 \text{ cm}^{-1}$ ($8.6124 \pm 0.0005 \text{ eV}$). The analysis of the VUV-VMI-TPE spectra of CH_2Cl and CH_2Br also provides the C-Cl and C-Br stretching frequencies for CH_2Cl and CH_2Br to be 1040 ± 2 and $844 \pm 2 \text{ cm}^{-1}$, respectively. We have also obtained IE predictions at the CCSDTQ/CBS level of

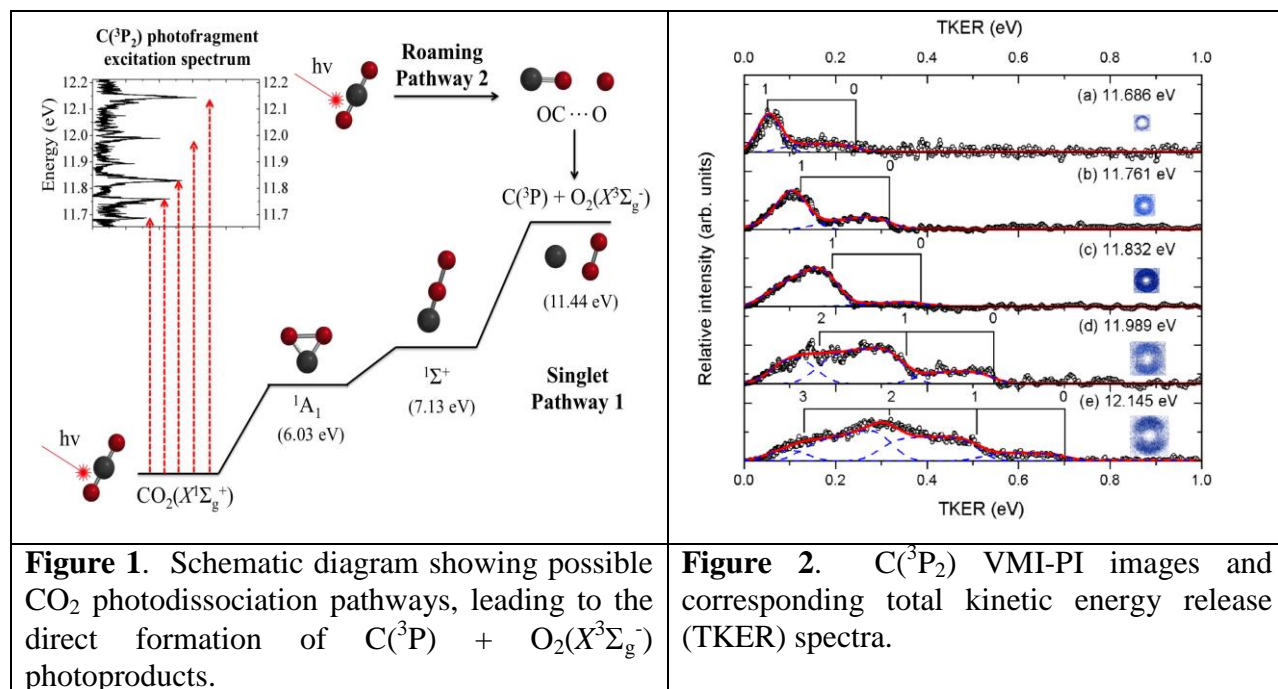
theory. IE predictions: $\text{IE}(\text{CH}_2\text{Cl}) = 8.767 \text{ eV}$ and $\text{IE}(\text{CH}_2\text{Br}) = 8.611 \text{ eV}$. This work is being prepared for publication.

B. Development of the VUV-VUV-VMI-PI apparatus

When a polyatomic molecule absorbs a photon at a VUV range of $\geq 7 \text{ eV}$, but below its IE, photodissociation is usually the major decay pathway. Since the detection of neutral photofragments by mass spectrometric techniques necessitates the ionization of the photofragments prior to their detection, the attainable detection sensitivity for neutral photofragments is significantly lower than that achieved by the direct detection of photoions. As a result, the investigations of molecular photodissociation processes in the VUV range have received much less attention than photoionization and photoelectron studies. Even for simple atmospheric molecules, such as CO , N_2 , and CO_2 , the photoproduct branching ratios measured as a function of VUV photodissociation energy were mostly unavailable previously.

During the past three years, we have developed a VUV-VUV-VMI-PI apparatus and demonstrated that the VUV photodissociation of simple gaseous molecules can be investigated to the state-to-state detail by employing the two-color VUVI photodissociation-pump and VUVII photoionization-probe approach. The VUV-VUV-VMI-PI apparatus consists of a supersonic molecular beam production system, a VMI detection system, and two independently tunable VUV lasers. When one of the photofragments is an atom ($\text{X} = \text{N}, \text{C}, \text{and O}$), high detection sensitivities of these atomic photoproducts can be achieved via the VUV-UV or VUV-VIS ($1 + 1'$) photoionization or the VUV-excited autoionizing-Rydberg method. The direct determination of spin-orbit state distributions of atomic photoproducts, such as $\text{C}(^3\text{P}_{2,1,0})$ and $\text{O}(^3\text{P}_{2,1,0})$, has been demonstrated. Highly sensitive state-selected detection of molecular photofragments can also be achieved via the two-color UV-VUV or VIS-VUV photoionization method.

C. Discovery of the $\text{C} + \text{O}_2$ channel in VUV photodissociation of CO_2



Carbon dioxide (CO_2) is a final product in hydrocarbon combustion, and is known to play an important role in the Earth's atmosphere as a major greenhouse gas, which is related to global

warming. In a recent experiment by employing the VUV-VUV-VMI-PI apparatus, we have discovered that O_2 can be produced directly in VUV photodissociation of CO_2 . Figure 1 shows the schematic potential energy diagram and ball stick model (C: grey; O: red) of the dissociation pathways leading to the formation of $C(^3P) + O_2(X^3\Sigma_g^-)$ photoproducts. The singlet ground state potential energy pathway (Pathway 1) is predicted to be a feasible pathway by *ab initio* calculations to involve the formation a cyclic [$c-CO_2(^1A_1)$] and a linear [$COO(^1\Sigma^+)$] intermediates situated at 6.03 and 7.13 eV above the $CO_2(X^1\Sigma_g^+)$ ground state. Pathway 2 illustrates the roaming mechanism. The photoexcitation of CO_2 is indicated by the upward pointing arrows to CO_2 absorption bands manifested by the $C(^3P_2)$ photofragment excitation spectrum in the energy range of 11.655 to 12.212 eV (upper inset of Fig. 1).

Figure 2 shows the total kinetic energy release (TKER) distributions for the formation of $C(^3P) + O_2(X^3\Sigma_g^-; v)$ converted from the VMI-PI images of $C(^3P_2)$ (shown in the insets of individual TKER spectra). The simulations (red curves in Fig. 2) indicate that the threshold energies observed are consistent with the known thermochemical threshold of 11.44 eV for the formation of the $C(^3P) + O_2(X^3\Sigma_g^-)$ channel. Furthermore, the measured TKER spectra indicate that $O_2(X^3\Sigma_g^-)$ photofragments are formed in $v = 0-3$ states with significant rotational excitation.

III. Research plan

With the advances in experimental methodologies and the significant increase of usable vacuum ultraviolet (VUV) laser intensities achieved in our laboratory, we plan to perform high-resolution photoionization, photoelectron, and photodissociation studies of selected oxygen-containing hydrocarbon radical species, including alkyloxy radicals (RO), alkylperoxy radicals (ROO), hydroperoxyalkyl radicals (QOOH), and Creigee intermediates. These radicals are known to play a central role in the low-temperature oxidation of hydrocarbons and combustion of biofuels. The chemistry of ROO and QOOH radicals are believed to be responsible for the chain branching and engine knock, which is a limiting factor on the efficiency of internal combustion engines. Our first experimental effort will be focused on VUV laser PFI and VMI measurements of methoxy radical (CH_3O), phenoxy radical (C_6H_5O), hydroxymethyl radical (CH_2OH), hydroperoxyl radical (HOO), methylperoxy radical (CH_3OO), ethylperoxy radical (C_2H_5OO), CH_2OO , and CH_3CHOO . Since the IR spectra for many of these species, such as CH_3O , CH_2OH , CH_3OO , CH_2OO , and CH_3CHOO , are also known, these radicals are excellent candidates for IR-VUV-PFI and IR-VUV-VMI measurements, which are expected to yield rotationally resolved state-to-state PFI-PE and PFI-PI spectra of these radicals. In addition to yielding highly precise thermochemical and spectroscopic data for these radical systems, the high-resolution PFI and VMI studies should also provide reliable spectroscopic information on photoionization transitions for designing sensitive detection schemes for the identification of these radicals in mechanistic chemical studies by using photoionization mass spectrometric techniques.

IV. Publications acknowledged the support of DOE (2012-present)

1. Hong Gao, Yang Pan, Lei Yang, Jingang Zhou, C. Y. Ng, and W. M. Jackson, "Time-sliced velocity-map ion imaging studies of the photodissociation of NO in the extreme vacuum ultraviolet (EUV) region", *J. Chem. Phys.* **136**, 134302 (2012).
2. X. Shi, H. Huang, B. Jacobson, Y.-C. Chang, Q.-Z. Yin, and C. Y. Ng, "A high-resolution photoionization and photoelectron study of ^{58}Ni using a vacuum ultraviolet laser", *Astrophys. J.* **747**, 20 (2012).
3. Hong Gao, Yu Song, Lei Yang, Xiaoyu Shi, Qing-Zhu Yin, Cheuk-Yiu Ng, and William M. Jackson, "Branching ratio measurements of the predissociation of $^{12}C^{16}O$ by time-slice

- velocity imaging in the energy region from 108,000 to 110,500 cm^{-1} ”, *J. Chem. Phys.* **137**, 034305 (2012).
4. Y.-C. Chang, Y. Xu, Z. Lu, H. Xu, and C. Y. Ng, “Rovibrationally selected ion-molecule collision study using the molecular beam vacuum ultraviolet laser pulsed field ionization-photoion method: charge transfer reaction of $\text{N}_2^+(X; v^+ = 0-2, N^+ = 0-9) + \text{Ar}$ ”, *J. Chem. Phys.* **137**, 104202 (2012).
 5. Hong Gao, Zhou Lu, Lei Yang, Jingang Zhou, and C. Y. Ng, “Communication: A vibrational study of propargyl cation using the vacuum ultraviolet laser velocity-map imaging photoelectron method”, *J. Chem. Phys.* **137**, 161101 (2012).
 6. Yuntao Xu, Bo Xiong, Yih Chung Chang, and C. Y. Ng, “Communication: Rovibrationally selected absolute total cross sections for the reaction $\text{H}_2\text{O}^+(X^2B_1; v_1^+v_2^+v_3^+ = 000; N^+_{Ka+Kc+}) + \text{D}_2$: Observation of the rotational enhancement effect”, *J. Chem. Phys.* **137**, 241101 (2012).
 7. Yih-Chung Chang, Huang Huang, Zhihong Luo, and C. Y. Ng, “Communication: A vibrational study of titanium dioxide cation using the vacuum ultraviolet laser pulsed field ionization-photoelectron method”, *J. Chem. Phys.* **138**, 041101 (2013).
 8. H. Huang, Y. C. Chang, Z. Luo, X. Shi, C.-S. Lam, K.-C. Lau, and C. Y. Ng, “Rovibrationally selected and resolved two-color laser photoionization and photoelectron study of cobalt carbide cation”, *J. Chem. Phys.*, **138**, 094301 (2013).
 9. H. Gao, Y. Song, W. M. Jackson, and C. Y. Ng, “Communication: State-to-state photodissociation study of $^{12}\text{C}^{16}\text{O}$ by the VUV-VUV pump-probe Time-Slice Velocity-Map Imaging Photoion Method”, *J. Chem. Phys.* **138**, 191102 (2013).
 10. Y. Xu, B. Xiong, Y.-C. Chang, and C. Y. Ng, “Translational, rotational, and vibrational energy effects on the chemical reactivity of water cation $\text{H}_2\text{O}^+(X^2B_1)$ in the collision with deuterium molecule D_2 ”, *J. Chem. Phys.* **139**, 024203 (2013).
 11. Y. Song, H. Gao, Y.-C. Chang, Z. Lu, C. Y. Ng, and W. M. Jackson, “Photodissociation of CO_2 between 13.540 eV and 13.678 eV”, *Phys. Chem. Chem. Phys.* **16**, 563 (2014).
 12. A. Li, Y. Li, H. Guo, K.-C. Lau, Y. Xu, B. Xiong, Y. C. Chang, and C. Y. Ng, “Communication: The origin of rotational enhancement effect for the reaction of $\text{H}_2\text{O}^+ + \text{H}_2 (\text{D}_2)$ ”, *J. Chem. Phys.* **140**, 011102 (2014).
 13. Cheuk-Yiu Ng, “State-to-state spectroscopy and dynamics of ions and neutrals by photoionization and photoelectron methods”, *Ann. Rev. Phys. Chem.* **65**, 197-224 (2014).
 14. Z. Luo, Z. Zhang, H. Huang, Y.-C. Chang, and C. Y. Ng, “Communication: State-to-State Photoionization and Photoelectron Study of Vanadium Methylidyne Radical (VCH)”, *J. Chem. Phys.* **140**, 181101 (2014).
 15. Z. Lu, Y.-C. Chang, H. Gao, Y. Benitez, Y. Song, C. Y. Ng, and W. M. Jackson, “Communication: Direct measurements of nascent $\text{O}({}^3\text{P}_{0,1,2})$ fine-structure distributions and branching ratios of correlated spin-orbit resolved product channels $\text{CO}(\tilde{a}^3\Pi; v) + \text{O}({}^3\text{P}_{0,1,2})$ and $\text{CO}(\tilde{X}^1\Sigma^+; v) + \text{O}({}^3\text{P}_{0,1,2})$ in VUV photodissociation of CO_2 ”, *J. Chem. Phys.* **140**, 231101 (2014).
 16. Z. Lu, Y.-C. Chang, Q.-Z. Yin, C. Y. Ng, and W. M. Jackson, Evidence for direct molecular oxygen production in CO_2 photodissociation”, *Science* **346**, 61 (2014).

Large Eddy Simulation of Turbulence-Chemistry Interactions in Reacting Flows

Joseph C. Oefelein, Anthony Ruiz, Guilhem Lacaze
Combustion Research Facility, Sandia National Laboratories
Livermore, CA 94551-0969
oefelei@sandia.gov

Program Scope

Application of the Large Eddy Simulation (LES) technique within the Diagnostics and Reacting Flows program at the CRF is based on two primary objectives. The first is to establish a set of high-fidelity first-principles computational benchmarks that identically match the geometry and operating conditions of selected experimental target flames. The second is to establish a scientific foundation for advanced model development that effectively bridges the gap between the idealized jet flame processes studied under this program and application relevant processes exhibited at the device scale. The goal is to provide direct one-to-one correspondence between measured and modeled results at conditions unattainable using Direct Numerical Simulation (DNS) by performing a series of detailed simulations that progressively incorporate the fully coupled dynamic behavior of reacting flows with detailed thermodynamics, transport, chemistry, and realistic spectra of turbulence. Our primary focal point is the series of flames that have been studied as part of the Experimental Reacting Flow Research program in collaboration with Barlow and Frank. This represents a direct extension of joint activities being pursued as part of the *International Workshop on Measurement and Computation of Turbulent (Non)premixed Flames* [1] (i.e., the “TNF Workshop”). Complementary information from highly specialized LES calculations, combined with detailed laser-based measurements, provide new opportunities to understand the central physics of turbulence-chemistry interactions in realistic parameter spaces and for the development of accurate predictive models for turbulent combustion. After achieving an adequate level of validation, results from high-fidelity LES provide fundamental information that cannot be measured and a strong link between theory, experiments, and relevant applications. The insights gained provide a basic science foundation for development of models and simulation techniques for state-of-the-art transportation, propulsion, and power devices such as internal combustion engines (e.g., reciprocating, gas turbine, liquid rockets).

Recent Progress

Understanding turbulent scalar mixing in the context of LES still presents many challenges. This is largely due to the fact that calculations of a given flow are performed over a wide range of resolutions, and the unsteady “structural” evolution of the flow varies significantly as a function of resolution. It becomes unclear, under these circumstances, how to quantitatively determine what the optimal resolution is that adequately reproduces the correct resolved-scale structural dynamics for a given combustion closure. Finding this optimum (e.g., the balance between computational cost and resolution) is compounded by the fact that most flows of interest are highly inhomogeneous. Thus, a variety of different scales, at different locations in the flow, come into play. As part of an effort to investigate these issues, we have recently performed a detailed analysis of the flow topologies and turbulence scales in the jet-in-cross-flow experiment of Su and Mungal [2]. The analysis was performed using LES over a progressive set of spatial and temporal resolutions with well controlled boundary conditions. This enabled quantitative agreement with the first and second moments of turbulence statistics measured in the experiment. A major focal point was the comprehensive characterization of key turbulence scales and their evolution. Time-resolved probes were used with long sampling periods to obtain maps of the integral scales, Taylor microscales, and turbulent kinetic energy spectra. Scalar-fluctuation scales were also quantified. In the near-field, coherent structures were identified, both in physical and spectral space. Along the jet centerline, turbulence scales were shown to grow according to a classical one-third power law. However, the derived maps of turbulence scales reveal strong inhomogeneities in the flow. From the modeling perspective, these insights are useful toward determining optimal resolution requirements, which in turn will improve numerical predictions in

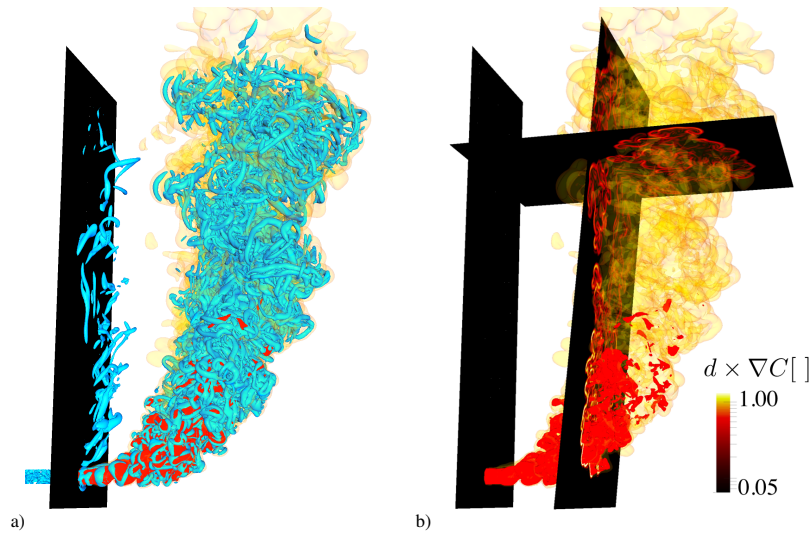


Figure 1. Instantaneous three-dimensional LES showing the structural characteristics of the flow field. a) The blue isocontour represents $Q = 0.02$, the red represents $C = 0.25$, and yellow represents $C = 0.01$. b) Cutting planes are colored by ∇C (with red and yellow isocontours the same as a).

similar types of flow. Details related to this study are given by Ruiz, Lacaze, and Oefelein [2]. A concise summary is given here as follows.

The experiment is performed at atmospheric pressure and ambient temperature in an updraft wind tunnel with air as the cross-flow fluid and nitrogen mixed with acetone as the jet fluid. The cross-flow is laminar upstream of the jet, with a peak velocity of 2.96 m/s. The diameter of the jet nozzle is $d = 4.53$ mm, and the length of the injector tube is $70 d$, which is long enough for a fully developed turbulent boundary layer to form. The bulk jet velocity is 16.9 m/s, which produces a velocity ratio of 5.7, and jet Reynolds number is 5000. The jet is seeded with approximately 10-percent of acetone by volume for diagnostic purposes. To seed the acetone vapor into the jet flow, the jet fluid is passed through a bubbler containing liquid acetone. During the experimental runs, the acetone level in the bubbler and the seeding efficiency slowly diminishes. Even though the post-processing procedure of the raw PLIF signals accounts for this concentration drift, the penetration of the jet turns out to be sensitive to this drift through small changes in momentum-flux ratio. Thus, we account for this in the LES using a multicomponent treatment of the equation of state, thermodynamics, and transport properties. LES was performed using the mixed dynamic Smagorinsky model with the RAPTOR code developed by Oefelein [4]. Turbulence statistics (mean and RMS of velocity and scalar-mixing) were found to be independent of the LES filter width with a uniform grid spacing of $d/15$ and a domain size of $(L_x/d, L_y/d, L_z/d) = (33, 33, 40)$. The total grid density used was 190×10^6 cells and statistics were acquired using a sampling period of 20 flow-through times.

Figure 1 shows the instantaneous three-dimensional structure of the flow field from LES (in the same orientation as given by Su and Mungal [2]). In 1a), the blue isocontour represents a “Q-criterion” value of $Q = 0.02$, the red isocontour represents a concentration of $C = 0.25$, and the yellow isocontour represents $C = 0.01$. The Q-criterion is the second invariant of the velocity gradient tensor. Positive isosurfaces of Q identify flow regions containing more vorticity than strain. This essentially filters out the vorticity sheets to reveal the underlying coherent structures. A wide range of turbulence scales are captured by the simulation, especially along the jet trajectory. Coherent structures also form in the boundary layer downstream of the jet. This shows that even though the boundary layer is initially laminar, vortical structures develop in the disturbed portion downstream. Figure 1b) shows cutting planes colored by the gradient in concentration, ∇C , along with the same red and yellow isocontours shown in Fig. 1a). The cutting planes are located at $y/d = 20$ and $x/d = 7$. The $x/d = 7$ plane has an inclination angle of 5-degrees. Strong gradients are observed in the near-field, especially at the interface between the jet and the cross-flow, which shows a convoluted shape. In the wake region, the footprint of the counter-rotating vortex-pair is observed with two distinct alleys in the $x/d = 7$ plane (the two lobes of the kidney shape cross this plane). In the $y/d = 20$ plane, broadband mixing can be observed, with stronger gradients present at the outer envelope of the jet.

LES and experimental measurements of mean velocity, mean concentration, Reynolds stress tensor, and the turbulent scalar flux have been compared and errors have been quantified. Figure 2 shows an example of the agreement with the experimental data. Here, the time-averaged profiles of velocity magnitude in the jet center plane are shown. The detailed validation and corresponding analysis confirm that LES is a good instrument for predicting complex three-

dimensional turbulent flows. After achieving a detailed level of validation, further analysis was performed to extract key turbulence scales, their origin, and dynamic evolution in the flow. Measuring these types of quantities is currently not attainable using experimental diagnostics due to constraints in resolution. Four quantities were mapped: 1) integral scales, 2) Taylor microscales, 3) turbulent energy spectra, and 4) scalar gradient thicknesses. The dynamic quantities (1-3) exhibited a similar spatial evolution. These scales were observed to first grow at various rates before breakdown of the jet turbulence, then a one-third power law was observed along the jet trajectory and consistently within the wake. For the scalar fluctuations and gradients (4), the observed trend was different. A sharp linear evolution of the gradient thickness occurred before the complete destabilization of the jet. This was followed by a secondary, almost constant evolution further downstream, which indicates that excessive stretching of the mesh from the injection point to the far-field can introduce significant errors in the mixing field by filtering out key turbulent flow structures present in the wake of the jet.

Observations such as those made above highlight the need to understand how LES represents various flow structures as a function of resolution. Similarly, the insights gained can be used to design more optimal grids that resolve the relevant flow structures correctly. For example, the trajectory of the jet can be estimated using the momentum flux ratio. An optimal initial grid size at the injector exit can be determined that is fine enough to resolve the vorticity thickness. Then, if scalar transport is not the dominant focal point, one may use a 1/3 power law to stretch the grid to make it consistent with the evolution of turbulent flow structures in the wake of the jet. If scalar transport is important and scalar gradients must be captured, a stretching rate smaller than $(y/d)^{1/3}$ is required to maintain good resolution of scalar fields. Smaller cells, however, should be placed at the outer edge of the jet to capture the interaction between the jet and the cross-flow, which gives rise to small vortical structures that inject energy into the TKE spectrum.

Future work on this topic will focus on two aspects: 1) using coarser grid sizes, we will study the impact of filtering *a posteriori* on the resolved scales of turbulence, their interaction, and the subsequent errors on turbulent mixing predictions, and 2) we will devise an optimal mesh with local cell sizes following the spatial evolution of turbulence scales using the maps derived in the current work. This will enable one to determine whether the same level of accuracy can be obtained at a significantly lower cost. Similar analyses under reacting flow conditions would also bring crucial insights into the effects of LES filtering on the predictive accuracy of different classes of combustion closures.

Future Plans

We will continue to use the foundational approach and framework described above with emphasis placed on three interrelated areas of research: 1) Maintain close coordination between LES and the experimental reacting flow research program with emphasis on the collaborative activities of the TNF Workshop to advance our fundamental understanding of turbulent reacting flows. 2) Maintain a significant effort in the development of quality assessment and uncertainty quantification (UQ) techniques for LES aimed at understanding and controlling the myriad of errors that complicate the development and validation of predictive models. 3) Continue to develop advanced models and simulation techniques aimed at accurate prediction of flame behavior across a broad range of combustion modes, regimes, and fuels. Tasks related to research area 1 will be pursued through close collaborations with Barlow and Frank et al. following the proposed series of experiments outlined in their respective abstracts. Tasks related to research area 2 will be pursued through close collaborations with Najm et al. (e.g., see Najm's abstract). Tasks related to research area 3 will continue to focus on advanced model development in a manner that effectively bridges the gap between the idealized jet flame processes studied under this program and application relevant processes exhibited at the device scale.

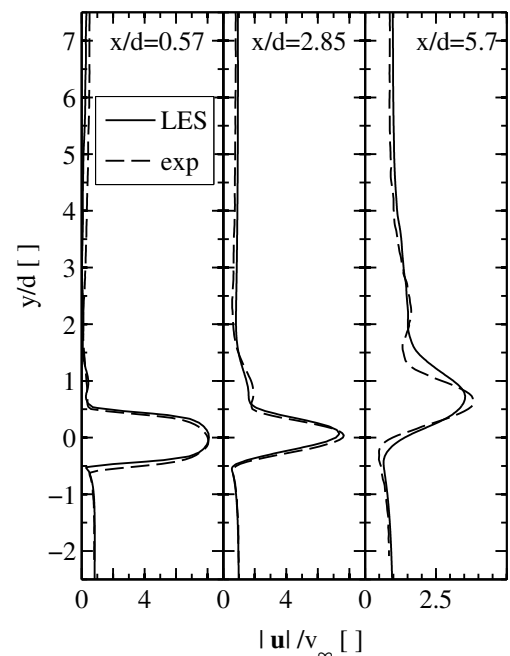


Figure 2. Time-averaged profiles of the velocity magnitude in the jet center plane.

Literature Cited

- [1] R. S. Barlow. International workshop on measurement and computation of turbulent (non)premixed flames. www.sandia.gov/TNF, 1996-2014. Sandia National Laboratories, Combustion Research Facility, Livermore, California.
- [2] L. K. Su and M. G. Mungal. Simultaneous measurements of scalar and velocity field evolution in turbulent crossflowing jets. *Journal of Fluid Mechanics*, 513:1–45, 2004.
- [2] A. M. Ruiz, G. Lacaze, and J. C. Oefelein. Dynamics and evolution of flow topologies and turbulence scales in a jet-in-cross-flow. *Physics of Fluids*, 2015. In Print.
- [4] J. C. Oefelein. Large eddy simulation of turbulent combustion processes in propulsion and power systems. *Progress in Aerospace Sciences*, 42(1):2–37, 2006.

BES Sponsored Publications (2013–Present)

- [1] A. M. Ruiz, G. Lacaze, J. C. Oefelein, R. Mari, B. Cuenot, L. Selle, and T. Poinot. A numerical benchmark for high-reynolds number supercritical flows with large density gradients. *AIAA Journal*, 2015. Submitted.
- [2] A. M. Ruiz, G. Lacaze, and J. C. Oefelein. Dynamics and evolution of flow topologies and turbulence scales in a jet-in-cross-flow. *Physics of Fluids*, 2015. In Print.
- [3] R. N. Dahms and J. C. Oefelein. Atomization and dense fluid breakup regimes in liquid rocket engines. *Journal of Propulsion and Power*, 2015. In Print.
- [4] G. Lacaze, A. Misdariis, A. Ruiz, and J. C. Oefelein. Analysis of high-pressure diesel fuel injection processes using LES with real-fluid thermodynamics and transport. *Proceedings of the Combustion Institute*, 35:1603–1611, 2015.
- [5] R. N. Dahms and J. C. Oefelein. Non-equilibrium gas-liquid interface dynamics in high-pressure liquid injection systems. *Proceedings of the Combustion Institute*, 35:1587–1594, 2015.
- [6] M. Khalil, G. Lacaze, J. C. Oefelein, and H. N. Najm. Uncertainty quantification in LES of a turbulent bluff-body stabilized flame. *Proceedings of the Combustion Institute*, 35:1147–1156, 2015.
- [7] J. Quinlan, J. McDaniel, T. Drozda, G. Lacaze, and J. Oefelein. A priori analysis of flamelet-based modeling for a dual-mode scramjet combustor. *50th AIAA/ASME/SAE/ASEE Joint Propulsion Conference and Exhibit, Paper 2014-3743*, July 28-30 2014. Cleveland, Ohio.
- [8] J. Manin, M. Bardi, L. M. Pickett, R. N. Dahms, and J. C. Oefelein. Microscopic investigation of the atomization and mixing processes of diesel sprays injected into high pressure and temperature environments. *Fuel*, 134:531–543, 2014.
- [9] J. Oefelein, G. Lacaze, R. Dahms, A. Ruiz, and A. Misdariis. Effects of real-fluid thermodynamics on high-pressure fuel injection processes. *SAE International Journal of Engines*, 7(3):1–12, 2014.
- [10] R. N. Dahms and J. C. Oefelein. On the transition between two-phase and single-phase interface dynamics in multicomponent fluids at supercritical pressures. *Physics of Fluids*, 25(092103):1–24, 2013.
- [11] G. Lacaze and J. C. Oefelein. Modeling high density gradient flows at supercritical pressures. *49th AIAA/ASME/SAE/ASEE Joint Propulsion Conference and Exhibit, Paper 2013-3717*, July 15-17 2013. San Jose, California.
- [12] R. N. Dahms and J. C. Oefelein. Theory and analysis of liquid-oxygen–hydrogen interface dynamics in liquid rockets at supercritical pressures. *49th AIAA/ASME/SAE/ASEE Joint Propulsion Conference and Exhibit, Paper 2013-3716*, July 15-17 2013. San Jose, California.
- [13] J. C. Oefelein. Large eddy simulation of complex thermophysics in advanced propulsion and power systems. *Proceedings of the 8th Joint Meeting of the US Sections of the Combustion Institute, Invited Plenary Presentation and Paper*, May 19-22 2013. Park City, Utah.
- [14] J. C. Oefelein, R. N. Dahms, G. Lacaze, and A. M. Ruiz. Modeling and numerical treatment of liquid injection processes at high-pressure supercritical conditions. *Proceedings of the Fourteenth International Conference on Numerical Combustion*, April 8-10 2013. Society of Industrial and Applied Mathematics (SIAM), San Antonio, Texas.
- [15] R. N. Dahms, J. Manin, L. M. Pickett, and J. C. Oefelein. Understanding high-pressure gas-liquid interface phenomena in diesel engines. *Proceedings of the Combustion Institute*, 34:1667–1675, 2013.
- [16] L. Lu, P. M. Najt, T.-W. Kuo, V. Sankaran, and J. C. Oefelein. A fully integrated linear eddy and chemistry agglomeration method with detailed chemical kinetics for studying the effect of stratification on HCCI combustion. *Fuel*, 105:653–663, 2013.

KINETICS AND DYNAMICS OF COMBUSTION CHEMISTRY

David L. Osborn

Combustion Research Facility, Mail Stop 9055, Sandia National Laboratories

Livermore, CA 94551-0969

dlosbor@sandia.gov

PROGRAM SCOPE

The goal of this program is to elucidate mechanisms of elementary combustion reactions through the use of multiplexed optical spectroscopy and mass spectrometry. We developed a technique known as time-resolved multiplexed photoionization mass spectrometry (MPIMS), which is used to sensitively and selectively probe unimolecular and bimolecular reactions. This work is in collaboration with Craig Taatjes, Leonid Sheps and has been utilized through collaboration by many scientists from other institutions in the US and abroad. The Sandia-designed MPIMS instrument utilizes tunable vacuum ultraviolet light from the Advanced Light Source synchrotron at Lawrence Berkeley National Laboratory for sensitive, isomer-specific ionization of reactant and product molecules sampled from chemical reactions.

As a complementary approach, we utilize time-resolved Fourier transform spectroscopy (TR-FTS) to probe multiple reactants and products with broad spectral coverage ($> 1000 \text{ cm}^{-1}$), moderate spectral resolution (0.1 cm^{-1}), and a wide range of temporal resolution (ns – ms). The inherently multiplexed nature of TR-FTS makes it possible to simultaneously measure product branching ratios, internal energy distributions, energy transfer, and spectroscopy of radical intermediates. Together with total rate coefficients, this additional information provides further constraints upon and insights into the potential energy surfaces that control chemical reactivity. Because of its broadband nature, the TR-FTS technique provides a global view of chemical reactions and energy transfer processes that would be difficult to achieve with narrow-band, laser-based detection techniques.

RECENT PROGRESS

Isomer-resolved mass spectrometry

The multiplexed chemical kinetics photoionization mass spectrometer operates both at Sandia National Laboratories (using a discharge lamp to create VUV radiation), and at the Chemical Dynamics Beamline of the Advanced Light Source (ALS) synchrotron of LBNL. The chemical reactor is based on the Gutman design,¹ which allows the study of photodissociation and bimolecular reactions at pressures of 1 – 10 Torr and temperatures of 300 – 1000 K.

During past 3-year period, we have applied this apparatus to a broad array of chemical problems, including studies of biofuel oxidation, reactions relevant to Saturn's moon Titan, the chemistry of carbonyl oxides (Criegee Intermediates), autoignition chemistry, and fundamental studies of photoionization dynamics and absolute cross sections.

Direct observation and kinetics of a hydroperoxyalkyl radical (QOOH)

Autoignition chemistry as a part of low-temperature combustion is critical to improved efficiency and lower pollution in all advanced engine concepts, be they spark ignition (gasoline), compression ignition (diesel), or stratified charge compression ignition (SCCI) engines. The need to have predictive models of this process requires experimental knowledge of how the chemical mechanisms in autoignition are influenced by pressure, temperature, and fuel structure. For decades, hydroperoxyalkyl radicals, known as •QOOH radicals, have been known to be

pivotal reaction intermediates in autoignition, in which their unimolecular or bimolecular reactions control whether chain termination, propagation, or branching will dominate in low-temperature combustion. However, no $\bullet\text{QOOH}$ radical had ever been detected directly, and this lack of direct probing had hampered efforts to understand their chemistry.

Why are $\bullet\text{QOOH}$ radicals so hard to detect? These molecules are formed from peroxy radicals ($\text{ROO}\bullet$) via internal H atom abstraction that converts the oxygen-centered peroxy radical to a carbon centered $\bullet\text{QOOH}$ radical. For many hydrocarbons, the $\text{ROO}\bullet$ isomer is more stable than the $\bullet\text{QOOH}$ isomer, but the latter is much more reactive. Therefore $\bullet\text{QOOH}$ radicals usually have very low steady-state concentrations despite being key reactive intermediates.

We have detected a $\bullet\text{QOOH}$ radical in the Cl-initiated oxidation of cycloheptadiene ($c\text{-C}_7\text{H}_{10}$), measured its photoionization spectrum, and the kinetics of its formation and consumption via reactions with O_2 .² This particular hydrocarbon represents a class of unsaturated, conjugated hydrocarbons, of which 1,3-butadiene ($\text{H}_2\text{C}=\text{CH}-\text{CH}=\text{CH}_2$) and isoprene (2-methyl 1,3-butadiene) are smaller analogs. Because cycloheptadiene can form resonance stabilized $\text{R}\bullet$ and $\bullet\text{QOOH}$ radicals, but the $\text{ROO}\bullet$ radical is not resonance stabilized, this $\bullet\text{QOOH}$ radical is more stable than its peroxy radical isomers. We have shown that this $\bullet\text{QOOH}$ is present in sufficient concentration to detect, and that the rate coefficient for its reaction with O_2 is 3-4 orders of magnitude smaller than the few known $\bullet\text{QOOH} + \text{O}_2$ analogs. This study combined experiments at the ALS and Sandia with electronic structure and master equation modeling of the reaction in collaboration with Judit Zádor.

Threshold photoelectron spectrum of the benzyl radical ($\text{C}_6\text{H}_5\text{-CH}_2$)

The benzyl radical is a resonance stabilized radical involved in the combustion of toluene and other aromatic species. Benzyl radical was formed by the pyrolysis of bibenzyl in a microtubular reactor at the VUV beamline of the Swiss Light Source, and interrogated with imaging photoelectron photoion coincidence spectroscopy. We have recently published a new threshold photoelectron spectrum that contains contributions from at least three electronic states of the benzyl cation.³ The $\tilde{X}^+ (^1\text{A}_1) \leftarrow \tilde{X} (^2\text{B}_1)$, $\tilde{a}^+ (^3\text{B}_2) \leftarrow \tilde{X} (^2\text{B}_1)$, and $\tilde{A}^+ (^1\text{B}_2) \leftarrow \tilde{X} (^2\text{B}_1)$ are clearly identified and the singlet-triplet splitting of benzyl cation is measured to be 1.928(7) eV.

Photoelectron spectroscopy provides access to both optically allowed and optically forbidden states of the cation, and hence provides a more complete view of electronic and vibrational structure for comparison with high-level ab initio calculations. In collaboration with Judit Zádor, we have calculated the lowest 5 electronic states in the singlet and triplet manifolds, and computed Franck-Condon factors (FCF) to simulate the photoelectron spectrum. Although the lowest two electronic states are simulated perfectly (within our resolution), the next two electronic states are more difficult, perhaps due to the influence of low-frequency internal rotors that are not well treated in FCF calculations using Cartesian normal modes (the straightforward and standard approach). In collaboration with Kent Ervin, University of Nevada, Reno, we are attempting to model these spectra with a more realistic treatment of free and nearly free rotors using a new approach developed UNR.

CRF-PEPICO (Combustion Reactions Followed by Photoelectron Photoion Coincidence Spectroscopy)

We and others have made great use of photoionization spectroscopy as a tool for quantitative chemical analysis in complex chemical environments such as flames and time-evolving chemical reactions. Coupled with time-of-flight mass spectrometry (or other

multiplexed mass spectrometry), the technique provides an efficient method to sort a chemical mixture first by m/z ratio, and further by ionization energy and spectral shape at each m/z ratio for isomer identification. However, all techniques have their limits, and in some cases, mixtures of three or more isomers can be difficult or impossible to quantify by this technique.

In the absence of resonances, the photoionization spectrum is essentially the integral of the photoelectron spectrum of a molecule. Detecting peaks in a photoelectron spectrum provides a better molecular fingerprint than the thresholds of a photoionization spectrum. However, photoelectron spectroscopy (where only electrons are detected) has rarely been applied to mixtures of neutral species because it is difficult to correlate multiple overlapping photoelectron spectra with each cation present in a system. For most of the reactions we study, this approach would be hopeless due to the large number of molecular species present.

Photoelectron photoion coincidence (PEPICO) spectroscopy is one solution to this problem, providing an independent photoelectron spectrum for each cation m/z ratio. In collaboration with Prof. Bálint Sztáray of the University of the Pacific, we have recently shown⁴ that modern imaging PEPICO spectroscopy can be used to separate mixtures of many components with significantly increased fidelity compared to photoionization spectroscopy.

We have built a new set of ion / electron optics designed to provide velocity map imaging of both cations and electrons in PEPICO, but with several new goals that have not traditionally been a focus of PEPICO instruments: 1) high mass resolution, 2) high dynamic range, 3) a large number of individually addressable electrodes providing focusing flexibility. We have tested this new concept at the Swiss Light Source in collaboration with Andras Bodi and Patrick Hemberger. The initial results are promising, in that we have obtained time-resolved kinetics signals that provide 2nd order rate coefficients in agreement with literature values, and our concept for rejection of false coincidences seems to be successful.

Future Plans

These prototype experiments will soon be completed, after which we will begin construction of the CRF-PEPICO spectrometer for use at Sandia and the Advanced Light Source, which should enable better molecular fingerprints to help resolve chemical reaction mechanisms that are beyond our capabilities at present.

BES-sponsored publications, 2013 – present

- 1) Threshold photoelectron spectrum of the benzyl radical, J. D. Savee, J. Zádor, P. Hemberger, B. Sztáray, A. Bodi, and D. L. Osborn, *Mol. Phys.* **In press** DOI: 10.1080/00268976.2015.1021398 (2015).
- 2) Chlorine atom-initiated low-temperature oxidation of prenol and isoprenol: The effect of C=C double bonds on the peroxy radical chemistry in alcohol oxidation, O. Welz, J. D. Savee, D. L. Osborn, and C. A. Taatjes, *Proc. Combust. Inst.* **35**, 401 (2015).
- 3) Direct observation and kinetics of a hydroperoxyalkyl radical (QOOH), J. D. Savee, E. Papajak, B. Rotavera, H. Huang, A. J. Eskola, O. Welz, L. Sheps, C. A. Taatjes, J. Zador, and D. L. Osborn, *Science* **347**, 643 (2015).
- 4) Photoionization Mass Spectrometric Measurements of Initial Reaction Pathways in Low-Temperature Oxidation of 2,5-Dimethylhexane, B. Rotavera, J. Zador, O. Welz, L. Sheps, A. M. Scheer, J. D. Savee, M. A. Ali, T. S. Lee, B. A. Simmons, D. L. Osborn, A. Violi, and C. A. Taatjes, *J. Phys. Chem. A* **118**, 10188 (2014).
- 5) Correction to Facile Rearrangement of 3-oxoalkyl radicals is evident in low-temperature gas-phase oxidation of ketones, A. M. Scheer, O. Welz, D. Y. Sasaki, D. L. Osborn, and C. A. Taatjes, *J. Am. Chem. Soc.* **136**, 8486 (2014).
- 6) Synchrotron photoionization study of mesitylene oxidation initiated by reaction with Cl (²P) or O(³P) radicals, M. Y. Ng, J. Nelson, C. A. Taatjes, D. L. Osborn, and G. Meloni, *J. Phys. Chem. A* **118**, 3735 (2014).
- 7) Probing the low-temperature chain-branching mechanism of *n*-butane autoignition chemistry via time-resolved measurements of ketohydroperoxide formation in photolytically initiated *n*-C₄H₁₀ oxidation, A. J. Eskola, O. Welz, J. Zador, I. O. Antonov, L. Sheps, J. D. Savee, D. L. Osborn, C. A. Taatjes, *Proc. Combust. Inst.* **35**, 291 (2015).
- 8) Influence of temperature and resonance-stabilization on the ortho- effect in cymene oxidation, B. Rotavera, A. M. Scheer, H. Huang, D. L. Osborn, and C. A. Taatjes, *Proc. Combust. Inst.* **35**, 543 (2015).

- 9) In situ soft X-ray absorption spectroscopy of flames, J. H. Frank, A. Shavorskiy, H. Bluhm, B. Coriton, E. Huang, and D. L. Osborn, *Appl. Phys. B* **117**, 493 (2014).
- 10) Electronic states of the quasilinear molecule propargylene (HCCCH) from negative ion photoelectron spectroscopy, D. L. Osborn, K. M. Vogelhuber, S. W. Wren, E. M. Miller, Y. J. Lu, A. S. Case, L. Sheps, R. J. McMahon, J. F. Stanton, L. B. Harding, B. Ruscic, and W. C. Lineberger, *J. Am. Chem. Soc.* **136**, 10361 (2014).
- 11) Low-Temperature Combustion Chemistry of Novel Biofuels: Resonance-Stabilized QOOH in the Oxidation of Diethyl Ketone, A. M. Scheer, O. Welz, J. Zádor, D. L. Osborn and C. A. Taatjes, *Phys. Chem. Chem. Phys.* **16**, 13027 (2014).
- 12) Rate Coefficients of C1 and C2 Criegee Intermediate Reactions with Formic and Acetic Acid Near the Collision Limit: Direct Kinetics Measurements and Atmospheric Implications, O. Welz, A. J. Eskola, L. Sheps, B. Rotavera, J. D. Savee, A. M. Scheer, D. L. Osborn, D. Lowe, A. M. Booth, P. Xiao, M. A. H. Khan, C. J. Percival, D. E. Shallcross, and C. A. Taatjes, *Angew. Chem.* **53**, 4547 (2014).
- 13) A coordinated investigation of the combustion chemistry of diisopropyl ketone, a prototype for biofuels produced by endophytic fungi, J.W. Allen, A.M. Scheer, C. Gao, S.S. Merchant, S.S. Vasu, O. Welz, J.D. Savee, D.L. Osborn, C. Lee, S. Vranckx, Z. Wang, F. Qi, R.X. Fernandes, W.H. Green, M.Z. Hadi, and C.A. Taatjes, *Combustion and Flame* **161**, 711 (2014).
- 14) Synchrotron photoionization mass spectrometry measurements of product formation in low-temperature n-butane oxidation: towards fundamental understanding of autoignition chemistry and $n\text{-C}_4\text{H}_9 + \text{O}_2 / s\text{-C}_4\text{H}_9 + \text{O}_2$ reactions, A. J. Eskola, O. Welz, J. D. Savee, D. L. Osborn, and C. A. Taatjes, *J. Phys. Chem. A* **117**, 12216 (2013).
- 15) Low-temperature combustion chemistry of n-butanol: principal oxidation pathways of hydroxybutyl radicals, O. Welz, J. Zador, J. D. Savee, L. Sheps, D. L. Osborn, and C. A. Taatjes, *J. Phys. Chem. A* **117**, 11983 (2013).
- 16) Isomer specific product detection in the reaction of CH with acrolein, J. F. Lockyear, O. Welz, J. D. Savee, F. Goulay, A. J. Trevitt, C. A. Taatjes, D. L. Osborn, and S. R. Leone, *J. Phys. Chem. A* **117**, 11013 (2013).
- 17) Mass-resolved isomer-selective chemical analysis with imaging photoelectron photoion coincidence spectroscopy, A. Bodi, P. Hemberger, D. L. Osborn, and B. Sztaray, *J. Phys. Chem. Lett.* **4**, 2948 (2013).
- 18) Product branching fractions of the CH + propene reaction from synchrotron photoionization mass spectrometry, A. J. Trevitt, M. B. Prendergast, F. Goulay, J. D. Savee, D. L. Osborn, C. A. Taatjes, and S. R. Leone, *J. Phys. Chem. A* **117**, 6450 (2013).
- 19) Regional and global impacts of Criegee intermediates on atmospheric aerosol formation, C. J. Percival, O. Welz, A. J. Eskola, J. D. Savee, D. L. Osborn, D. O. Topping, D. Lowe, S. R. Utembe, A. Bacak, G. McFiggans, M. C. Cooke, P. Xiao, A. T. Archibald, M. E. Jenkin, R. G. Derwent, I. Riipinen, D. W. K. Mol, E. P. F. Lee, J. M. Dyke, C. A. Taatjes, and D. E. Shallcross, *Faraday Discussions* **165**, 45 (2013).
- 20) Absolute photoionization cross-section of the vinyl radical, J. D. Savee, J. F. Lockyear, S. Borkar, A. J. Eskola, O. Welz, C. A. Taatjes, and D. L. Osborn, *J. Chem. Phys.* **139**, 056101 (2013).
- 21) Facile rearrangement of 3-oxoalkyl radicals is evident in low-temperature gas-phase oxidation of ketones, A. M. Scheer, O. Welz, D. Y. Sasaki, D. L. Osborn, and C. A. Taatjes, *Journal of the American Chemical Society* DOI: 10.1021/ja405892y (2013).
- 22) Absolute photoionization cross-sections of selected furanic and lactonic potential biofuels, J. Czekner, C. A. Taatjes, D. L. Osborn, and G. Meloni, *International Journal of Mass Spectrometry* **348**, 39 (2013).
- 23) Directly measuring reaction kinetics of QOOH—a crucial but elusive intermediate in hydrocarbon autoignition, J. Zador, H. Huang, O. Welz, J. Zetterberg, D. L. Osborn, and C. A. Taatjes, *Physical Chemistry Chemical Physics* **15**, 10753 (2013).
- 24) Direct measurements of conformer-dependent reactivity of the Criegee intermediate CH_3CHOO , C. A. Taatjes, O. Welz, A. J. Eskola, J. D. Savee, A. M. Scheer, D. E. Shallcross, B. Rotavera, E. P. F. Lee, J. M. Dyke, D. K. W. Mol, D. L. Osborn, and C. J. Percival, *Science* **340**, 177 (2013).
- 25) Formation of dimethylketene and methacrolein by reaction of the CH radical with acetone, F. Goulay, A. Derakhshan, E. Maher, A. J. Trevitt, J. D. Savee, A. M. Scheer, D. L. Osborn, and C. A. Taatjes, *Physical Chemistry Chemical Physics* **15**, 4049 (2013).
- 26) Synchrotron photoionization measurements of fundamental autoignition reactions: Product formation in low-temperature isobutane oxidation, A. J. Eskola, O. Welz, J. D. Savee, D. L. Osborn, and C. A. Taatjes, *Proc. Combust. Inst.*, **34**, 385 (2013).
- 27) Low-temperature combustion chemistry of biofuels: Pathways in the low-temperature (550 – 700 K) oxidation chemistry of isobutanol and tert-butanol, O. Welz, J. D. Savee, A. J. Eskola, L. Sheps, D. L. Osborn, and C. A. Taatjes, *Proc. Combust. Inst.*, **34**, 493 (2013).

References

¹ I. R. Slagle and D. Gutman, *J. Am. Chem. Soc.* **107**, 5342 (1985).

² See publication #3

³ See publication #1

⁴ A. Bodi, P. Hemberger, D. L. Osborn, and B. Sztaray, *J. Phys. Chem. Lett.* **4**, 2948 (2013).

Program Title: A Theoretical Investigation of the Structure and Reactivity of the Molecular Constituents of Oil Sand and Oil Shale

Principle Investigator: Carol Parish

Address: Department of Chemistry, University of Richmond, Richmond, VA 23227
cparish@richmond.edu

PROGRAM SCOPE

Our work focuses on the theoretical characterization of the gas phase structures, energies and reactivities of the molecular constituents of asphaltenes contained in oil sand and oil shale. Asphaltenes represent an untapped source of hydrocarbon fuel in North America; however, information about the molecular nature of these deposits has only recently become available. Theoretical and experimental evidence suggests that asphaltenes are composed of aromatic molecules that contain 4-10 fused ring cores, with alkyl chain arms extending from the core. Sulfur and nitrogen are also present. Very little is known about the reaction pathways, combustion efficiency and reactivity of these heteroaromatic species. We are currently characterizing the combustion and pyrolysis reaction channels available to asphaltene constituents such as thiophene and methyl thiophene.

RECENT PROGRESS - FY 2014 HIGHLIGHTS

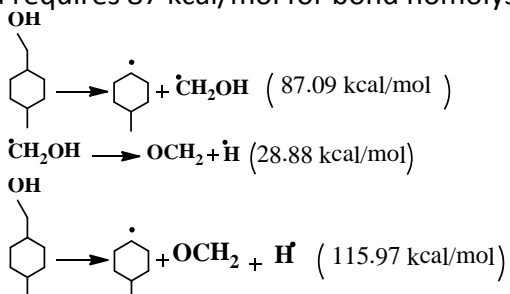
Ground and low-lying valence excited states of didehydrothiophene diradicals: A multireference comparison study

High-level multireference theories (MCSCF, MRCISD, MRCISD+Q and MRAQCC at ccpVdz and ccpVtz levels) using an active space of 8 eight electrons (for 2,5DDTH) and ten electrons in eight orbitals (for all other isomers), CAS(8,8) and CAS(10,8), were employed to investigate the ground and low-lying excited states of all four didehydrothiophenes (DDTHs). Both state averaged and single state reference MCSCF wave functions were used for high symmetrical structures, C_{2v} . These computational methods consistently predict the singlet state as the ground state and with a singlet-triplet (S-T) adiabatic energy gap of 15-23 kcal/mol indicative of through bonds coupling. The 2,3-DDTH presents the highest S-T splitting energies of 23.53 kcal/mol at MRAQCC/ccpVtz. The remaining DDTHs have quite similar S-T splitting energies \sim 16 kcal/mol at MRAQCC/ccpVtz. A comparison between different multireference methods reveals a competitive performance between MRAQCC and MR-CISD+Q. The lowest energy isomer is 2,3-didehydrothiophene on the basis of the computed total electronic energies (MRAQCC/ccpVtz and MRCISD+Q/ccpVtz) and the CCSD(T)/6-311++G(3df,2p) single points energies of the MRAQCC/ccpVtz optimized geometries. The 2,3-DDTH isomer has the strongest C-C bond, close to ethyne C-C triple bond. However, an examination of the electronic structure and NBO analysis show 2,3 and 2,5-DDTH to have the lowest and highest diradical character, respectively. Similar to o-benzyne, the latter can be considered a strained alkyne. In general,

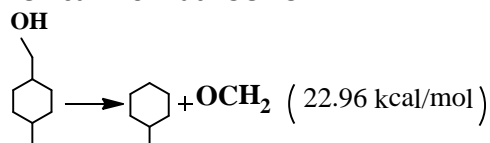
the singlet-triplet splitting energies of all didehydrothiophenes are smaller than in the benzyne suggesting them to be more reactive systems. This work is in preparation for submission to the *Journal of Physical Chemistry A*.

A First Principle Study of the Thermal Decomposition of (4-Methylcyclohexane)methanol, $C_8H_{15}OH$ – Is the Formation of Formaldehyde a Possibility?

On January 9, 2014 (4-methylcyclohexane)methanol (4-MCHM) was inadvertently released into the Elk River in Charleston, West Virginia. Very little is known about the effect of MCHM on human health and initial news reports suggested that MCHM breaks down to form formaldehyde. We have investigated the probable initial steps of the thermal decomposition pathways of 4-MCHM and examined possible formation of formaldehyde using various quantum chemical methods such as B3LYP/6-311++G(d,p), MP2/6-311++G(d,p), CCSD(T)/6-31G(d,p), G3B3, G4, G4MP2 and CBS-QB3. For the reaction, $\cdot CH_2OH \rightarrow CH_2O + H\cdot$, the W1BD theory was also employed. The C-C bond rupture between the cyclohexane ring and the methanol group in 4-MCHM is a predicted precursor of the thermal decomposition of 4-MCHM and requires 87 kcal/mol for bond homolysis at CS-QB3 level.



The production of formaldehyde and methylcyclohexyl arising from the decomposition of 4-MCHM is found to be endothermic ($\Delta H_f = 115 \text{ kcal/mol}$) and is unlikely to occur at ambient temperature without any specific catalyst. The enthalpy of the decomposition reaction of the 4-methylcyclohexylmethanol in 4-methylcyclohexane and formaldehyde stable species is about 23 kcal mol^{-1} at 298.15K.



The total atomization energy at 0K and enthalpy of formation of 4-MCHM at 298.15K calculated at the same level of theory (CBS-QB3) amount to 2555 and -322 kcal/mol, respectively. This work is in preparation for submission to the *Journal of Physical Chemistry A*.

Singlet Oxygen (2+4) Cycloaddition to Heteroaromatic Compounds

The 2+4 cycloaddition reactions of singlet molecular oxygen ($^1\Delta_g$) with a series of aromatic heterocyclic compounds were investigated at both the MP2/6-311++G(d, p) and B3LYP/6-311++G(d, p) levels of theory. Several factors related to heteroaromatic ring structure were determined to affect the activation energy of the cycloaddition and the stability of the corresponding endoperoxide products. Such factors include: (1) the position of methyl substitution; (2) the number of methyl substituents; (3) the alkyl chain length of substituents; (4) the electronic structure of substituents and; (5) the type of heteroatom in the ring. In total, fourteen 2+4 cycloaddition routes were examined and in each case the mechanism is concerted. The order of reactivity toward O_2 ($^1\Delta_g$) was determined to be: 2,3,4,5-tetramethylthiophene > 2,3,5-trimethylthiophene > 2,5-dimethylthiophene > 2-methylthiophene > 2-ethylthiophene > 2-propylthiophene > 3-methylthiophene > thiophene > benzothiophene > dibenzothiophene; and furan > pyrrole > thiophene > benzene. The stability of the endoperoxide products follows a similar trend. Each of the reaction pathways is initiated by the formation of a pre-reactive complex, formed by a van der Waals interaction between a C atom on the ring and an O atom on O_2 . To the best of our knowledge, this type of VDW pre-reactive complex has not been identified in previous studies of cycloaddition reactions of singlet oxygen with arenes.

Jahn-Teller Stabilization in POSS Cations: Octatert-butyl and Octachloro silsesquioxanes $Si_8O_{12}(C(CH_3)_3)_8^+$ and $Si_8O_{12}Cl_8^+$

Polyoligomeric silsesquioxanes (POSS) are molecules containing a rigid, cubic inorganic core Si_8O_{12} with Si atoms attached to organic or inorganic peripheral groups. These compounds have found many applications in polymer chemistry as they impart thermal stability when mixed with organic polymers to form nanostructured organic-inorganic hybrids. We have investigate the symmetry breaking mechanism in cubic octatert-butyl silsesquioxane and octachloro silsesquioxane monocations ($Si_8O_{12}(C(CH_3)_3)_8^+$ and $Si_8O_{12}Cl_8^+$) applying density functional theory (DFT) and group theory. Under O_h symmetry, these ions possess $^2T_{2g}$ and 2E_g electronic states and undergo different symmetry breaking mechanisms. The ground states of $Si_8O_{12}(C(CH_3)_3)_8^+$ and $Si_8O_{12}Cl_8^+$ belong to the C_{3v} and D_{4h} point groups and are characterized by Jahn-Teller stabilization energies of 3959 and 1328 cm^{-1} ; respectively, at the B3LYP/def2-SVP level of theory. The symmetry distortion mechanism in $Si_8O_{12}Cl_8^+$ is Jahn-Teller type, whereas in $Si_8O_{12}(C(CH_3)_3)_8^+$ the distortion is a combination of both Jahn-Teller and pseudo-Jahn-Teller effects. The distortion force acting in $Si_8O_{12}(C(CH_3)_3)_8^+$ is mainly localized on one Si-(tert-butyl) group while in $Si_8O_{12}Cl_8^+$ it is concentrated on the oxygen atoms. In these ionic compounds, the main distortion forces acting on the Si_8O_{12} core arise from the coupling between the electronic

state and the vibrational modes; identified as $9t_{2g}+1e_g+3a_{2u}$ for the $\text{Si}_8\text{O}_{12}(\text{C}(\text{CH}_3)_3)_8^+$ and $1e_g+2e_g$ for $\text{Si}_8\text{O}_{12}\text{Cl}_8^+$. This work has been published in the *Journal of Physical Chemistry A*.

FUTURE WORK

Work is currently underway to characterize the electrocyclizations of penta-, hepta- and octa-diyne as well as the ground and excited states of heteroaromatic diradicals such as thiophene, fulvene and pyrrole. We are also pursuing a complete characterization of the singlet and triplet surfaces of the electrocyclization reaction of (Z)-hexa-1,3,5-triene leading to *p*-benzyne as well as a characterization of the endo and exo-dig radical cyclization reactions.

PUBLICATIONS

1. “Jahn-Teller Stabilization in POSS Cations”, Jules Tshishimbi Muya, Arnout Ceulemans, Gopinadhanpillai Gopakumar and Carol A. Parish*, *Journal of Physical Chemistry A*, **2015**, *accepted 4/1/15*.
2. “Mechanisms for the reaction of thiophene and methylthiophene with singlet and triplet molecular oxygen,” Xinli Song, Matthew G. Fanelli, Justin M. Cook, Furong Bai and Carol A. Parish*, *Journal of Physical Chemistry A*, **2012** *116*, 4934-4946.

PUBLICATIONS - NOT RELATED TO THE PROJECT

1. “A Conservative Isoleucine to Leucine Mutation Causes Major Rearrangements and Cold-Sensitivity in KlenTaq1 DNA Polymerase,” Eugene Y. Wu*, Amanda R. Walsh, Emma C. Materne, Emily P. Kornberg, Bryan Zielinski, Bill Miller III, Lily Mawby, Erica Modeste, Carol Parish, Wayne M. Barnes and Milko B. Kermekchiev, *Biochemistry*, **2014**, *54*, 881-889.
2. “Molecular Dynamics Study of the Opening Mechanism for DNA Polymerase I”, Bill Miller III, Carol A. Parish* and Eugene Wu*, *PLOS Computational Biology*, **2014**, *10*, e1003961.
3. “Halogen bonding in DNA base pairs,” Anna J. Parker, John Stewart, Kelling Donald* and Carol Parish*, *Journal of the American Chemical Society*, **2012** *134*, 5165-5172.
4. “Evidence that the kinesin light chain contains tetratricopeptide repeat units.” Sally Q. Fisher, Meredith Weck, Jenna E. Landers, Jeffrey Emrich, Shana A. Middleton, Jordan Cox, Lisa N. Gentile and Carol A. Parish*, *Journal of Structural Biology*, **2012**, *177*, 602-612.
5. “Challenging Disciplinary Boundaries in the First-Year: A New Introductory Integrated Science Course for STEM Majors”, Gentile, L.*; Caudhill, L.; Fetea, M.; Hill, A.; Hoke, K.; Lawson, B.; Lipan, O.; Kerckhove, M.; Parish, C.; Stenger, K.; Szajda, D., *Journal of College Science Teaching*, **2012**, *41(5)*, 24-30.

The Dynamics of Large-Amplitude Motion in Energized Molecules

David S. Perry, Principal Investigator
Department of Chemistry, The University of Akron
Akron OH 44325-3601
DPerry@UAkron.edu

I. Program Scope

Chemical reactions involve large-amplitude nuclear motion along the reaction coordinate that serves to distinguish reactants from products. Some reactions, such as roaming reactions and reactions proceeding through a loose transition state, involve more than one large amplitude degree of freedom. In principle, the exact quantum nuclear dynamics may be calculated, but such calculations are limited by practical considerations to a few degrees of freedom. Thus in larger systems, one must define the active degrees of freedom and separate them in some way from the other degrees of freedom. In this project, we use large-amplitude motion in bound model systems to investigate the coupling of large-amplitude degrees of freedom to other nuclear degrees of freedom [1-13]. This approach allows us to use the precision and power of high-resolution molecular spectroscopy to probe the specific coupling mechanisms involved, and to apply the associated theoretical tools. In addition to slit-jet spectra at the University of Akron [5, 7], this project involves collaboration with Michel Herman of the Université Libre de Bruxelles [1, 6], and with Brant Billinghurst at the Canadian Light Source (CLS) [12].

II. Recent Progress

A. Vibrational Conical Intersections

In this work, sets of seven conical intersections between vibrationally adiabatic surfaces have been found in both CH_3OH and CH_3SH , but arranged in very different patterns in the two molecules (Fig. 1). The implications for spectroscopy and dynamics are discussed.

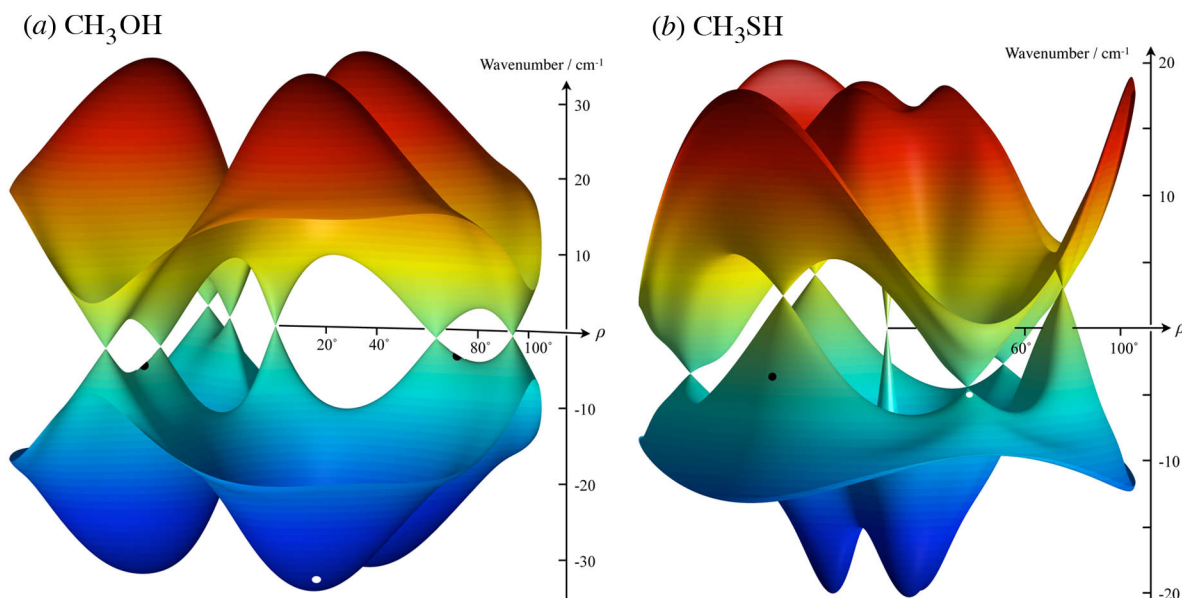


Fig. 1. Relative model frequencies of the two asymmetric CH stretch vibrations in (a) methanol and (b) methyl mercaptan, represented as surfaces in the 2-dimensional coordinate space of the COH bend angle ρ and the torsional angle γ . The model (Eq. (1)) was fit to *ab initio* frequencies (CCSD(T)/aug-cc-pVTZ) computed at geometries optimized with respect to the other ten internal coordinates. To enhance viewability, the large variations of the average frequency $\bar{\nu}^{0\gamma}$ and of the underlying electronic energy $U^{0\gamma}$ are suppressed. The locations of the global minima in the electronic potential are indicated by white dots, and the torsional saddle points by black dots.

Conical intersections (CIs) between electronic potential energy surfaces are widespread throughout electronic spectroscopy and are responsible for ultrafast electronic relaxation in diverse circumstances. Whereas these electronic surfaces represent the adiabatic separation of electronic and nuclear motions under the Born-Oppenheimer approximation, it is also possible in some cases to make an (approximate) adiabatic separation of fast and slow vibrational motions. In such cases, the motion of the high frequency vibrations, which might include hydride stretches, can be solved quantum mechanically at each molecular geometry along the low-frequency, large-amplitude torsional or bending coordinates. These slower motions are then solved in the effective potential that is the sum of the electronic potential plus the variation of the high-frequency vibrational energies in the large-amplitude space.

In the electronic context, the 1st-order Jahn-Teller effect necessarily results in a CI at the symmetric geometry. Zwanziger and Grant¹ studied $E \otimes e$ systems in which both 1st- and 2nd-order Jahn-Teller couplings are present, the former scaling linearly with the deviation ρ from the C_{3v} reference geometry and the latter scaling quadratically. They showed that there are necessarily four CIs between the coupled electronic surfaces, one at the C_{3v} reference geometry and three more at distorted geometries of C_s symmetry at the values of ρ where the magnitudes of the linear and quadratic couplings become equal.

This same formalism applies also to the purely vibrational context, where the adiabatic separation is not between degenerate Born-Oppenheimer electronic states and a degenerate vibrational mode, but now between a high frequency degenerate vibrational state in the electronic ground state and a pair of large-amplitude low-frequency modes [11]. Specifically, we consider the vibronic surfaces formed by considering the energies of the asymmetric CH stretch vibrations as a function of the torsional angle γ and the CXH bend angle ρ , where X = O, S. The C_{3v} reference geometry occurs at $\rho = 0$ where the CXH group is linear. In this reference geometry, the two asymmetric CH stretch vibrations become degenerate (E), and the large-amplitude coordinates ρ and γ together become a degenerate CXH bending coordinate (e). One significant difference encountered when applying the $E \otimes e$ formalism to these vibrationally adiabatic surfaces is that the equilibrium geometry is now far from the C_{3v} reference geometry ($\rho = 71^\circ$ in CH_3OH and $\rho = 83^\circ$ in CH_3SH) rather than close to it as is typically the case for Jahn-Teller coupling between electronic surfaces. We follow Viel and Einfeld's treatment of the electronic Jahn-Teller effect, which includes higher-order coupling terms.² The adiabatic energies of the two asymmetric CH stretches are

$$E_{\pm} = (V^{0\gamma} + U^{0\gamma}) + (V^{3\gamma} + U^{3\gamma}) \cos 3\gamma + (V^{6\gamma} + U^{6\gamma}) \cos 6\gamma \\ \pm \left\{ (W^{1\gamma})^2 + (W^{2\gamma})^2 + (W^{4\gamma})^2 + 2W^{1\gamma}(W^{2\gamma} + W^{4\gamma}) \cos 3\gamma + 2W^{2\gamma}W^{4\gamma} \cos 6\gamma \right\}^{\frac{1}{2}}. \quad (1)$$

Here the Fourier parameters $U^{m\gamma}$ describe the electronic potential, $V^{m\gamma}$ describe the diagonal parts of the CH vibrational Hamiltonian, and the $W^{m\gamma}$ represent the 1st- 2nd- and 4th-order Jahn-Teller couplings. Each of these Fourier parameters is a high-order power series in ρ . This analytical form (Fig. 1) fits the *ab initio* data with an RMS error $< 0.4 \text{ cm}^{-1}$. Thus classic Jahn-Teller theory provides an excellent description of the global adiabatic behavior of the CH stretch vibrations, providing a beautiful conceptual link between the domains of vibrational and electronic spectroscopy.

Fig. 1 reveals the presence of seven conical intersections in each molecule, one occurring in the C_{3v} reference geometry ($\rho = 0^\circ$). In methanol, six additional CIs occur in eclipsed conformations (C_s) at $\rho = 62^\circ$ and 92° . The three CI's at $\rho = 62^\circ$ are close to the torsional saddle point at $\rho = 71^\circ$, within the range of the zero-point COH bending amplitude, and therefore accessible to the dynamics at relatively low energies. The pattern is very different in CH_3SH , where CIs occur in both staggered and eclipsed conformations. Remarkably, the staggered CIs are almost coincident with the three equivalent minima of the electronic potential.

When the dimensionality of the low-frequency coordinate space is 3 or more, then the CIs become seams or hyper-seams of CIs. When the methanol CO stretch coordinate r_{CO} is included along

with γ and ρ to form a 3-dimensional low-frequency coordinate space, we find that the CI's at $\rho = 62^\circ$ and 92° belong to the same seam of CIs. A significant length of the seam is accessible to the dynamics in the lowest quantum states of the large-amplitude motion.

These conical intersections illuminate the role of geometric phase in methanol. Since four CIs are enclosed by the MEP for a 2π torsional rotation, the Zwanziger and Grant theorem¹ predicts a geometric phase of +1 in agreement with the findings of Xu *et al.*³ One might also consider additional adiabatic paths enclosing an odd number of CIs, say 1 or 3, which would have geometric phase of -1. However, rather than following an adiabatic path when it approaches the eclipsed geometry, there is reason to believe that the system will likely follow a diabatic path, jumping between the two surfaces in Fig. 1(a). Following the limiting cases of Xu *et al.*³, there are three qualitatively different diabatizations, each of which corresponds to a different geometric phase.

The CIs have the potential to impact both unimolecular and intermolecular dynamics. In methanol, Xu *et al.*³ have shown that the vibrational characters of the ν_2 and ν_9 CH stretches change sharply over a small range of the torsional angle near the eclipsed conformation. The presence of nearby CIs explains this behavior and will allow quantitative predictions of non-adiabatic processes (surface hopping) near the eclipsed geometry. In general, in the context of either intramolecular or collision-induced dynamics, the CIs provide a connection between the vibrationally adiabatic surfaces. Therefore, one should expect acceleration of energy transfer processes in localized regions around the CIs. Just as electronic conical intersections are now known to be ubiquitous throughout electronic spectroscopy, vibrational conical intersections may also be widespread, consequently impacting the vibrational dynamics in diverse chemical systems.

B. Six-Fold Internal Rotation

CH_3NO_2 is a benchmark system for nearly free internal rotation in a 6-fold potential and for the coupling to other small-amplitude vibrations. Since many internal rotor states are populated at room temperature, CH_3NO_2 offers an opportunity to study a manifold of large-amplitude states built on the CH stretches. As noted above, such combination states hold the key to unlocking the interactions between large- and small-amplitude degrees of freedom. Rotationally resolved infrared spectra of CH_3NO_2 have been recorded using Far-infrared Beamline at Canadian Light Source on a high resolution Bruker IFS 125HR spectrometer. The observed infrared spectra, in the range 400 - 1000 cm^{-1} , are recorded at a nominal resolution of 0.00096 cm^{-1} . Together with previous spectra from EMSL at the Pacific Northwest National Laboratory, high-resolution spectra of five bands have been obtained: the in-plane NO_2 wag (475.2 cm^{-1}), the out-of-plane NO_2 wag (604.9 cm^{-1}), NO symmetric bend (657.1 cm^{-1}) for CN-stretch and at for CN-stretch (917.2 cm^{-1}), and the NO asymmetric stretch (1582.9 cm^{-1}). Our first paper on the 475.2 cm^{-1} band has now appeared on-line [12], and others are in preparation.

C. Two-Dimensional Large-Amplitude Motion and Coupling to CH Stretches

In molecules with two large-amplitude vibrations (LAV), the LAV's are coupled both to each other and to the other small-amplitude vibrations (SAV) such as CH stretches. Our *ab initio* calculations on CH_3NH_2 , CH_3OH_2^+ , and $\text{CH}_3\text{CH}_2\cdot$ have shown that the couplings connecting the torsion (α) and inversion (τ) are very similar across these systems despite the wide variation in the tunneling barriers. In all three cases, the dominant torsion-inversion coupling term is $V_{1,3}\tau \cos 3\alpha$ with $V_{1,3}$ in the range 280 to 450 cm^{-1} . For CH_3NH_2 and $\text{CH}_3\text{CH}_2\cdot$, we find that the torsion-inversion coupling to the CH stretch force constants has a very similar pattern, but that the pattern for the charged species CH_3OH_2^+ is very different [13]. The variation of the 2-D tunneling patterns in CH stretch excited states has been investigated across the series methanol, methylamine, 2-methylmalonaldehyde and 5-methyltropolone [5, 8]. In the latter two molecules, the second LAV is proton transfer rather than inversion.

V. Future Plans

The analysis and interpretation of the nitromethane work will continue, focusing on the torsionally excited states. Spectra of CH₃SH at CLS are planned to confirm the calculated vibrational CIs in that system. The quantum dynamics associated with vibrational CIs will be investigated.

VI. Publications from this Project, 2012-2015

- [1] D. S. Perry, J. Martens, B. Amyay, and M. Herman, Hierarchies of Intramolecular Vibration-Rotation Dynamical Processes in Acetylene up to 13,000 cm⁻¹, *Mol. Phys.* **110**, 2687-2705 (2012). <http://dx.doi.org/10.1080/00268976.2012.711493>.
- [2] R. S. Bhatta, Y. Yimer, M. Tsige, and D. S. Perry, Nonplanar Conformations and Torsional Potentials of Poly(3-hexylthiophene) Oligomers: Density Functional Calculations up to the Dodecamer, *Computational and Theoretical Chemistry* **995**, 36-42 (2012). <http://dx.doi.org/10.1016/j.comptc.2012.06.026>.
- [3] R. S. Bhatta and D. S. Perry, Correlated backbone torsional potentials in poly(3-methylthiophene), *Computational and Theoretical Chemistry* **1008**, 90-95 (2013). <http://dx.doi.org/10.1016/j.comptc.2013.01.003>.
- [4] K. Prozument, R. G. Shaver, M. Ciuba, J. S. Muentner, G. B. Park, J. F. Stanton, H. Guo, B. M. Wong, D. S. Perry, and R. W. Field, A New Approach toward Transition State Spectroscopy, *Faraday Discuss.* **163**, 33-57 (2013). <http://dx.doi.org/10.1039/C3FD20160K>.
- [5] M. B. Dawadi, C. M. Lindsay, A. Chirokolava, D. S. Perry and L.-H. Xu, Novel patterns of torsion-inversion-rotation energy levels in the ν_{11} asymmetric CH-stretch spectrum of methylamine, *J. Chem. Phys.* **138**, 104305 (2013). <http://dx.doi.org/10.1063/1.4794157>.
- [6] M. Herman and D. S. Perry, Molecular spectroscopy and dynamics: A polyad-based perspective, *Phys. Chem. Chem. Phys.* **15**, 9970-9993 (2013). <http://dx.doi.org/10.1039/C3CP50463H>.
- [7] M. B. Dawadi, R. S. Bhatta and D. S. Perry, Torsion-Inversion Tunneling Patterns in the CH-Stretch Vibrationally Excited States of the G₁₂ Family of Molecules Including Methylamine, *J. Phys. Chem. A.* (2013). <http://dx.doi.org/10.1021/jp406668w>.
- [8] R. S. Bhatta, Y. Yimer, D. S. Perry and M. Tsige, Improved force field for molecular modeling of poly(3-hexyl thiophene), *J. Phys. Chem. B.* **117**, 10035-10045 (2013). <http://dx.doi.org/10.1021/jp404629a>.
- [9] R. Bhatta, D. Perry and M. Tsige, Nanostructures and Electronic Properties of a High-Efficiency Electron-Donating Polymer, *J. Phys. Chem. A* (2013). <http://pubs.acs.org/doi/pdf/10.1021/jp409069d>.
- [10] R. Bhatta, M. Tsige, and D. Perry, Torsionally-induced blue-shift of the band gap in poly(3-hexylthiophene), *J. Compt. Theor. Nanosc.* **11**, 1-8 (2014). <http://dx.doi.org/10.1166/jctn.2014.3621>.
- [11] Mahesh B. Dawadi and David S. Perry, Conical Intersections between Vibrationally Adiabatic Surfaces in Methanol, *J. Chem. Phys.*, **140**, 161101 (2014). <http://dx.doi.org/10.1063/1.4871657>. (featured article)
- [12] Mahesh B. Dawadi, Sylvestre Twagirayezu, David S. Perry and Brant E. Billingham, High-resolution Fourier transform infrared synchrotron spectroscopy of the NO₂ in-plane rock band of nitromethane, *J. Mol. Spectrosc.* (2014), <http://dx.doi.org/10.1016/j.jms.2014.11.009>.
- [13] Mahesh B. Dawadi, Ram S. Bhatta, David S. Perry, *Chem. Phys. Lett.* **624**, 53-58 (2015). (editor's choice) <http://dx.doi.org/10.1016/j.cplett.2015.02.009>.

VII. Other References

- ¹ J. W. Zwanziger, and E. R. Grant, *J. Chem. Phys.* **87**, 2954 (1987).
- ² A. Viel and W. Einfeld, *J. Chem. Phys.* **120**, 4603 (2004).
- ³ L.-H. Xu, J. T. Hougen, and R. M. Lees, *J. Mol. Spectrosc.* **293-294**, 38 (2013).

New Single- and Multi-Reference Coupled-Cluster Methods for High Accuracy Calculations of Ground and Excited States

Piotr Piecuch

Department of Chemistry, Michigan State University, East Lansing, MI 48824
piecuch@chemistry.msu.edu

I. Program Scope

This research program focuses on new generations of *ab initio* electronic structure methods and computer codes exploiting the exponential wave function ansätze of single- and multi-reference coupled-cluster (CC) theories, which can provide an accurate description of chemical reaction pathways, especially those involving radicals, biradicals, and significant bond rearrangements, molecular electronic excitations, challenging cases of electronic near-degeneracies, and properties other than energy. The goal is to design and apply affordable approaches that enable precise modeling of molecular processes and properties relevant to combustion, catalysis, and photochemistry. The emphasis is on the development of methods that offer high accuracy, ease of use, and lower computational costs compared to other approaches that aim at similar precision, so that one can study complex molecular problems with dozens or hundreds of atoms, in addition to smaller systems, in a predictive and systematically improvable manner, supporting existing experiments or in the absence of experimental information. Methods pursued in this program can effectively utilize modern multi-node, multi-core computer architectures and are well suited for pursuing novel coding strategies, such as automated and parallel computer implementations. The most promising electronic structure approaches developed in this program are shared at no cost with the community through the GAMESS package. Some of the best methods discovered in this program are also available in NWChem.

II. Recent Progress (2012 – 2014 and January 1 – April 2, 2015)

We have generalized the previously developed biorthogonal moment expansions, which in the past resulted in the left-eigenstate completely renormalized (CR) CC and equation-of-motion (EOM) CC approaches [1,3,4,6,7,11,13,15,17,19], so that we can now correct the CC/EOMCC energies obtained with the conventional as well as unconventional truncations in the cluster operator T and the EOM excitation operator R_{μ} for essentially any category of electron correlation effects of interest [4,5,8]. The resulting CC($P;Q$) formalism [4,5,8] enables one to contemplate a wide variety of novel, computationally efficient *ab initio* schemes for high accuracy calculations of ground- and excited-state potential energy surfaces (PESs). Among them is the CC($t;3$), CC($t,q;3$), CC($t,q;3,4$), etc. hierarchy, in which energies obtained in the active-space CC/EOMCC calculations, such as CCSDt/EOMCCSDt or CCSDtq/EOMCCSDtq [4,19], which recover much of the non-dynamical and some dynamical electron correlation effects, are corrected for the higher-order, primarily dynamical, correlations, such as certain classes of triples ('3') or triples and quadruples ('3,4') missing in the active-space CC/EOMCC considerations [4,5,8]. Potential advantages of the CC($P;Q$) formalism were illustrated by the CC($t;3$) calculations for several multi-reference (MR) problems, including bond breaking in HF, F₂, and F₂⁺, automerization of cyclobutadiene, isomerization of bicyclo[1.1.0]butane to trans-but-1,3-diene, and singlet-triplet gaps in the methylene, trimethylenemethane (TMM), and (HFH)⁻ biradicals [4,5,8]. We showed that CC($t;3$) greatly improves the CCSD(T), CCSD(2)_T, Λ -CCSD(T), CR-CC(2,3), CCSDt, and CCSD(T)-h results, providing PESs and singlet-triplet gaps that agree with the parent CCSDT data to within small fractions of a millihartree for total energies and small fractions of kcal/mol for relative energies at the tiny fraction of the costs of the CCSDT computations, which are competitive with the MRCC and Quantum Monte Carlo calculations for the benchmarked systems.

We have extended the idea of the active-space EOMCC methods to the doubly electron-attached (DEA) and doubly ionized (DIP) formalisms, which are applicable to open-shell species with two electrons outside the closed-shell cores, particularly to the electronic spectra of biradicals and single bond breaking, without invoking complicated steps of genuine MRCC theories. In particular, we reported the development of the full and active-space DEA- and DIP-EOMCC methods with up to 4-particle–2-hole (4p2h) and 4-hole–2-particle (4h2p) excitations [10,16]. By examining bond break-

ing in F_2 and low-lying singlet and triplet states in CH_2 , $(HFH)^+$, and TMM, we demonstrated that the DEA- and DIP-EOMCC methods with an active-space treatment of 4p2h and 4h2p excitations reproduce the results of the analogous full calculations at the tiny fraction of the computer effort, allowing us to calculate the singlet-triplet and singlet-singlet gaps in biradicals to within fractions of kcal/mol [10,16]. We also showed that the DEA- and DIP-EOMCC approaches with the full and active-space treatments of 4p2h and 4h2p excitations provide results which are practically insensitive to the choice of the underlying molecular orbital (MO) basis, including orbitals of the target N -electron species and their $(N-/+2)$ -electron counterparts [16]. This should be contrasted with the DEA/DIP EOMCC methods truncated at 3p1h/3h1p excitations, which are less accurate and more sensitive to the choice of MO basis [16]. We have also continued working on the EA and IP EOMCC methodologies [2,18,19]. In particular, we reported the scalar relativistic IP- and EA-EOMCC calculations with up to 3h2p and 3p2h excitations, using the second-order Douglass-Kroll-Hess Hamiltonian, along with the corresponding SAC-CI calculations, for the electronic spectra of the $CuCl_4^{2-}$ and $CuBr_4^{2-}$ complexes [2], providing an accurate assignment of the observed strong bands and weaker shoulder transitions for the first time, and showing how special relativity affects excitation energies and nuclear geometries. We have also started exploring the utility of the IP-EOMCC methodology in applications involving transition metal nanoparticles. In particular, we used the scalar relativistic IP-EOMCC approaches, correlating valence and semi-core electrons and including up to 3h2p terms in the ionizing operator, to provide an accurate assignment of peaks and shoulders in the experimental photoelectron spectrum of Au_3^- for the first time [18]. We demonstrated that one has to correlate semi-core electrons, in addition to the valence ones, use larger basis sets, and include the higher-order 3h2p effects to obtain meaningful results. We showed that geometry relaxation during electron ejection from Au_3^- contributes to the peak widths, in addition to multiple electronic states behind a given spectral feature.

We implemented the rigorously size-intensive modification of the previously developed (see [4,19] for reviews) CR-EOMCC(2,3) approach, termed δ -CR-EOMCC(2,3) [1], which corrects the EOMCCSD energies for the effects of triple excitations using the non-iterative N^7 steps similar to CCSD(T), CR-CC(2,3), and CC(t,3), offering great improvements in the EOMCCSD results. The δ -CR-EOMCC(2,3) codes, along with the extension of the EOMCCSD routines to open shells [17], have been incorporated in GAMESS as additions to a variety of the CC and EOMCC options that we developed for GAMESS in the past. We used the δ -CR-EOMCC(2,3) approach to examine shifts in the $\pi \rightarrow \pi^*$ excitation energy in *cis*-7-hydroxyquinoline (*cis*-7HQ) induced by hydrogen bonding with environment, on the order of 500-2000 cm^{-1} , along with the corresponding excitation energies, on the order of 30,000 cm^{-1} , obtained in the frozen-density embedding theory (FDET) and supermolecular time-dependent density functional theory (TDDFT) calculations, and in experiment [1]. We demonstrated that the δ -CR-EOMCC(2,3) and FDET spectral shifts agree with one another and with experiment to within 100 cm^{-1} or 15 % on average, whereas the analogous shifts obtained in the supermolecular TDDFT calculations do not agree with the δ -CR-EOMCC(2,3) data, producing large errors (39% on average). We reported the unprecedented δ -CR-EOMCC(2,3) computations showing that the previously postulated doubly excited state of azulene below the ionization threshold and mediating the 1+2' multi-photon ionization that leads to a clear Rydberg fingerprint exists [11], proving a crucial role of doubly excited states in the Rydberg fingerprint spectroscopy. We also applied CR-EOMCC(2,3) and its ground-state CR-CC(2,3) counterpart to several singlet and triplet PESs corresponding to the dissociation of the water molecule into OH and H, showing that the black-box CR-CC(2,3) and CR-EOMCC(2,3) methods are as accurate as or more accurate than the expert MRCC approaches [17].

We have continued applying our CR-CC methods to important chemical problems relevant to combustion and catalysis, including accurate modeling of JP-10 (*exo*-tetrahydrodicyclopentadiene) high temperature oxidation, which has benefitted from the use of CR-CC(2,3) [3], and unprecedented scalar relativistic CR-CC(2,3) computations for the aerobic oxidation of methanol to formic acid on the Au_8^- nano-particles [13]. In the latter case, we did not only obtain a definitive description of the relevant catalytic reaction pathway, but we also used the CR-CC(2,3) results to benchmark representa-

tive DFT approaches, demonstrating that most of them fail. In the same spirit, we used parallel CCSD(T) codes in GAMESS based on our algorithms to evaluate performance of various DFT functionals in the examination of reaction mechanisms of Cu(I)-catalyzed indole synthesis and click chemistry of iodoalkynes and azides [14]. We also helped to incorporate our successful CR-CC(2,3) methodology, as a substitute for CCSD(T), into a correlation consistent composite approach (ccCA) for thermodynamic properties and reaction paths [6]. The new ccCA-CC(2,3) method, implemented in GAMESS, produces a mean absolute deviation of 1.7 kcal/mol for predicted heats of formation at 298 K, based on calibration with the G2/97 set of 148 molecules, while significantly improving performance of the CCSD(T)-based ccCA approaches in calculations for the more demanding radical and biradical species [6]. We also used our EOMCCSD codes, along with the MC-QDPT2 approach and TDDFT, to provide insights into the electronic structure of the low-lying excited states of methylcobalamin, showing that its S_1 state is a metal-to-ligand charge transfer (and not a $\pi \rightarrow \pi^*$) transition [9].

Some additional algorithmic advances in the reporting period include the development of efficient parallel numerical derivatives for fast geometry optimizations and vibrational frequency calculations at any level of CC/EOMCC theory through the utilization of modern multi-node, multi-core computer architectures. We used the resulting codes, combined with a parallel implementation of CCSD(T) in GAMESS, to optimize the geometries of the low-energy structures of the neutral Au_8 particle, answering one of the key questions in catalysis involving smaller gold nano-particles, which is their planar vs. non-planar shape [12]. We examined the effects of geometry relaxation at the high *ab initio* CCSD(T) level and of the combined effects of the basis set and core-valence correlations, comparing the results with MP2 and DFT. Our best CCSD(T) computations favor the planar configuration of Au_8 , with the next three non-planar structures separated by 4–6 kcal/mol [12]. We also demonstrated how our CR-CC ideas and algorithms, developed in the context of quantum chemistry, can be used to extend the CC theory with singles, doubles, and a non-iterative treatment of triples to the three-body interactions emerging in the nuclear structure considerations [15].

We have continued our work on the development and applications of the local correlation CCSD, CCSD(T), and CR-CC(2,3) approaches, and their multi-level extensions, which exist under the umbrella of ‘cluster-in-molecule’ (CIM) methods [7,19]. The resulting CIM-CCSD, CIM-CCSD(T), and CIM-CR-CC(2,3) methods, and their CIM- MP_n analogs enable high-accuracy calculations for systems with hundreds of correlated electrons. Our CIM-CC and CIM- MP_2 codes in GAMESS were released in May 2013. They are characterized by the linear scaling of the CPU time with the system size, when a single-level CIM-CC or CIM- MP_2 approach is used, memory requirements that do not grow with the size of the system, coarse-grain parallelism, which can be further enhanced by the fine-grain parallelism of each CIM subsystem calculation, and the purely non-iterative character of the local triples and other perturbative energy corrections. They enable one to fuse high- and low-level CC and MP_n calculations without splitting large molecular systems into *ad hoc* fragments and saturating dangling bonds. Among the most successful applications of the CIM methodology were the unprecedented CR-CC(2,3)-level calculations for the Co-methyl bond dissociation in methylcobalamin, which allowed us to produce the Co-methyl bond breaking curve and the dissociation energy of ~ 38 kcal/mol, where experiment gives 37 ± 3 or 36 ± 4 kcal/mol. DFT gave all kinds of values between -2 and 41 kcal/mol and the largest CASPT2 calculation we could afford yielded ~ 54 kcal/mol [7].

III. Immediate Future Plans (2015/2016)

- Further development of the active-space DEA and DIP EOMCC methods by examining various ways of selecting 3p1h/3h1p and 4p2h/4h2p excitations to obtain additional reductions in computer costs.
- Further development of the $CC(P;Q)$ formalism, especially, the $CC(t;3)$ approach for excited states and the $CC(t,q;3)$ and $CC(t,q;3,4)$ methods with connected triple and quadruple excitations.
- Initial steps toward implementing the triply electron-attached and triply ionized EOMCC methods aimed at triradicals and inorganic chromophores emerging out of a d^3 electronic configuration, especially those investigated in the context of solar energy conversion schemes.
- New studies of radical, biradical, and catalytic reactions and electronic and photo-detachment spectra, including systems relevant to combustion and nano-particles and complexes relevant to catalysis.

IV. Publications supported by DOE: 2012 – 2014 and January 1 – April 2, 2015)

- [1] G. Fradelos, J.J. Lutz, T.A. Wesolowski, P. Piecuch, M. Włoch, "Shifts in Excitation Energies Induced by Hydrogen Bonding: A Comparison of the Embedding and Supermolecular Time-Dependent Density Functional Theory Calculations with the Equation-of-Motion Coupled-Cluster Results," in: *Progress in Theoretical Chemistry and Physics*, Vol. 22, edited by P.E. Hoggan, E. Brändas, J. Maruani, P. Piecuch, and G. Delgado-Barrio (Springer, Dordrecht, 2012), pp. 219-248.
- [2] M. Ehara, P. Piecuch, J.J. Lutz, J.R. Gour, "Symmetry-Adapted-Cluster Configuration-Interaction and Equation-of-Motion Coupled-Cluster Studies of Electronically Excited States of Copper Tetrachloride and Copper Tetrabromide Dianions," *Chem. Phys.* **399**, 94-110 (2012).
- [3] G.R. Magoon, J. Aguilera-Iparraguirre, W.H. Green, J.J. Lutz, P. Piecuch, H.-W. Wong, O.O. Oluwole, "Detailed Chemical Modeling of JP-10 (*exo*-tetrahydrodicyclopentadiene) High Temperature Oxidation: Exploring the Role of Biradical Species in Initial Decomposition Steps," *Int. J. Chem. Kin.* **44**, 179-193 (2012).
- [4] J. Shen, P. Piecuch, "Biorthogonal Moment Expansions in Coupled-Cluster Theory: Review of Key Concepts and Merging the Renormalized and Active-Space Coupled-Cluster Methods," *Chem. Phys.* **401**, 180-202 (2012).
- [5] J. Shen, P. Piecuch, "Combining Active-Space Coupled-Cluster Methods with Moment Energy Corrections via the CC(*P;Q*) Methodology, with Benchmark Calculations for Biradical Transition States," *J. Chem. Phys.* **136**, 144104 (2012) (16 pp).
- [6] S.A. Nedd, N.J. De Yonker, A.K. Wilson, P. Piecuch, M.S. Gordon, "Incorporating a Completely Renormalized Coupled Cluster Approach into a Composite Method for Thermodynamic Properties and Reaction Paths," *J. Chem. Phys.* **136**, 144109 (2012) (13 pp).
- [7] P.M. Kozłowski, M. Kumar, P. Piecuch, W. Li, N.P. Bauman, J.A. Hansen, P. Lodowski, M. Jaworska, "The Cobalt-Methyl Bond Dissociation in Methylcobalamin: New Benchmark Analysis Based on Density Functional Theory and Completely Renormalized Coupled-Cluster Calculations," *J. Chem. Theory Comput.* **8**, 1870-1894 (2012).
- [8] J. Shen, P. Piecuch, "Merging Active-Space and Renormalized Coupled-Cluster Methods via the CC(*P;Q*) Formalism, with Benchmark Calculations for Singlet-Triplet Gaps in Biradical Systems," *J. Chem. Theory Comput.* **8**, 4968-4988 (2012).
- [9] K. Kornobis, N. Kumar, P. Lodowski, M. Jaworska, P. Piecuch, J.J. Lutz, B.M. Wong, P.M. Kozłowski, "Electronic Structure of the S_1 State in Methylcobalamin: Insight from CASSCF/MC-XQDPT2, EOM-CCSD, and TD-DFT Calculations," *J. Comp. Chem.* **34**, 987-1004 (2013).
- [10] J. Shen, P. Piecuch, "Doubly Electron-Attached and Doubly Ionized Equation of- Motion Coupled-Cluster Methods with 4-particle-2-hole and 4-hole-2-particle Excitations and their Active-Space Extensions," *J. Chem. Phys.* **138**, 194102 (2013) (16 pp).
- [11] P. Piecuch, J.A. Hansen, D. Staedter, S. Faure, V. Blanchet, "Communication: Existence of the Doubly Excited State that Mediates the Photoionization of Azulene," *J. Chem. Phys.* **138**, 201102 (2013) (4 pp).
- [12] J.A. Hansen, P. Piecuch, B.G. Levine, "Communication: Determining the Lowest-Energy Isomer of Au_8 : 2D, or not 2D," *J. Chem. Phys.* **139**, 091101 (2013) (4 pp).
- [13] J.A. Hansen, M. Ehara, P. Piecuch, "Aerobic Oxidation of Methanol to Formic Acid on Au_8^- : Benchmark Analysis Based on Completely Renormalized Coupled-Cluster and Density Functional Theory Calculations," *J. Phys. Chem. A* **117**, 10416-10427 (2013).
- [14] C.E.P. Bernardo, N.P. Bauman, P. Piecuch, P.J. Silva, "Evaluation of Density Functional Methods on the Geometric and Energetic Descriptions of Species Involved in Cu^+ -Promoted Catalysis," *J. Mol. Model.* **19**, 5457-5467 (2013).
- [15] S. Binder, P. Piecuch, A. Calci, J. Langhammer, P. Navrátil, R. Roth, "Extension of Coupled-Cluster Theory with a Non-iterative Treatment of Connected Triply Excited Clusters to Three-Body Hamiltonians," *Phys. Rev. C* **88**, 054319 (2013) (21 pp).
- [16] J. Shen, P. Piecuch, "Doubly Electron-Attached and Doubly Ionised Equation-of-Motion Coupled-Cluster Methods with Full and Active-Space Treatments of 4-particle-2-hole and 4-hole-2-particle Excitations: The Role of Orbital Choices," *Mol. Phys.* **112**, 868-885 (2014).
- [17] J.J.Lutz, P.Piecuch, "Performance of the Completely Renormalized Equation-of-Motion Coupled-Cluster Method in Calculations of Excited-State Potential Cuts of Water," *Comput. Theor. Chem.* **1040-41**, 20-34 (2014).
- [18] N.P. Bauman, J.A. Hansen, M. Ehara, P. Piecuch, "Communication: Coupled-Cluster Interpretation of the Photoelectron Spectrum of Au_3^- ," *J. Chem. Phys.* **141**, 101102 (2014) (5 pp).
- [19] P. Piecuch, M. Włoch, J.R. Gour, W. Li, J.J. Lutz, "Dealing with Chemical Reaction Pathways and Electronic Excitations in Molecular Systems via Renormalized and Active-Space Coupled-Cluster Methods," AIP Conf. Proc. **1642**, 172-175 (2015).

INVESTIGATION OF NON-PREMIXED TURBULENT COMBUSTION

Grant: DE-FG02-90ER14128

Stephen B. Pope & Perrine Pepiot
Sibley School of Mechanical & Aerospace Engineering
Cornell University, Ithaca, NY 14853
s.b.pope@cornell.edu, pp427@cornell.edu

1 Scope of the Research Program

The underlying theme of this work is the development of computational approaches which allow our detailed knowledge of the chemical kinetics of combustion to be applied to the modeling and simulation of combustion devices. The principal modeling approaches used are large-eddy simulation (LES) to describe the flow and turbulence, and particle-based probability density function (PDF) methods to treat the turbulence-chemistry interactions. Research is currently focused on 1) the development and validation of a pre-partitioned adaptive chemistry (PPAC) approach for use in LES-PDF simulations, in which individual particles evolve according to a reduced set of kinetic equations tailored for their specific compositions, thereby significantly reducing both the time and memory required for a computation with a given kinetic mechanism, and enabling affordable computations with significantly more detailed chemistry descriptions, and 2) the analysis of turbulent premixed counterflow flames using LES/PDF.

2 Recent Progress

The principal research results from this program are described in the publications listed in Section 4. The following subsections detail the progress made on the focused topics mentioned above. Further details are provided in Liang *et al.* (2015) and Pope and Tirunagari (2014).

2.1 An Adaptive Methodology to Implement Detailed Chemistry in LES/PDF

We have developed a pre-partitioned adaptive chemistry (PPAC) methodology tailored to LES/PDF simulation, in which each particle is assigned a specialized reduced representation and chemical model tailored to their individual composition. Instead of performing chemical reduction at runtime to determine the optimal set of equations to use for a given particle, an analysis of the composition space region likely accessed during the turbulent flow simulation is performed using simple Partially Stirred Reactor (PaSR) computations. The PPAC approach relies on an *a priori* partitioning of the composition space into a user-specified number of regions, over which suitable reduced chemical representations and chemical models are identified. This is done automatically using the Directed Relation Graph with Error Propagation (DRGEP) method, extended to simultaneously eliminate non-important species and reactions. A computational particle in the LES/PDF simulation evolves according to, and carries only the variables present in the reduced representation corresponding to the composition space region it belongs to, thereby simultaneously reducing both the CPU time and memory cost of the simulation. This region is identified using a low-dimensional binary tree search algorithm, thereby keeping the run-time overhead associated with the adaptive approach to a minimum. An overview of PPAC is provided in Fig. 1.

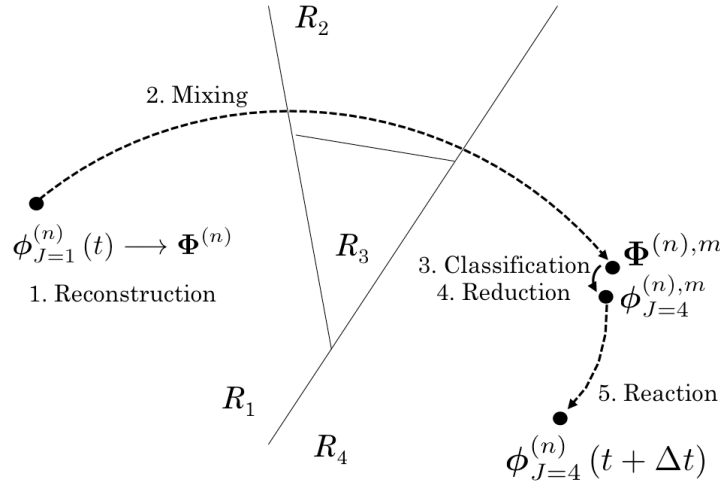


Figure 1: Overview of the adaptive strategy. The composition space is partitioned into N_R regions (R_1 to R_4 in the figure above), for which specific reduced kinetic models M_1 to M_4 are developed. At the beginning of the time step, particle n , represented by the black circle, has the reduced representation based on model M_1 . Its composition evolves through a mixing fractional step and a reaction fractional step. During mixing, the reduced representation $\phi_{J=1}^{(n)}$ is mixed according to the specified mixing model to obtain the composition after mixing $\Phi^{(n),m}$ (2). Because of the mixing process, the representation after mixing, $\Phi^{(n),m}$, has moved to region R_4 , which is determined from classification in the partition (3). $\Phi^{(n),m}$ is reduced to the appropriate representation, $\phi_{J=4}^{(n),m}$ (4), then integrated in time according to the reduced model M_4 (5) to yield the particle composition at the end of the time step: $\phi_{J=4}^{(n)}(t + \Delta t)$. In LES/PDF, only reduced representations ϕ_J are stored and transported.

The methodology has been tested in non-premixed PaSR configurations using a variety of fuels and kinetic mechanisms, including propane [1] and dodecane [2]. The results show that in each case, the observed errors in PaSR simulation using the adaptive framework are well controlled by a user-specified error tolerance, and can be reduced well below acceptable levels. While the methodology does not exactly conserve elements or enthalpy, the error in these conserved quantities is very small. Figure 2 illustrates the benefits of using the PPAC-DRGEP approach compared to DRGEP alone for a propane/air case, with a factor of two decrease observed in the number of species included in the reduced model to achieve a given simulation error (similar CPU gains are also obtained).

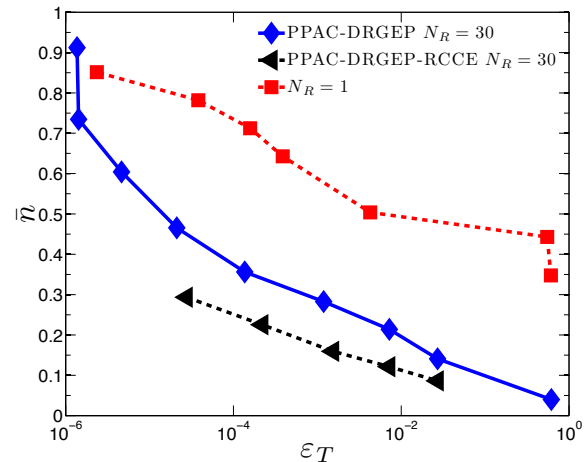


Figure 2: Relative number of species \bar{n} included in the reduced models as a function of the observed error on temperature ε_T in a non-premixed propane/air PaSR. Comparison between the non-adaptive case ($N_R = 1$, DRGEP only, red squares) and the adaptive cases ($N_R = 30$) without RCCE (blue diamonds) and with the addition of RCCE (black triangles).

To further decrease CPU and memory costs, PPAC-DRGEP has been combined with the rate-controlled constraint equilibrium methodology previously developed by Hiremath *et al.* [3], in which particle compositions are expressed in terms of a small number of represented species. While the procedure introduces an additional source of error due to the additional RCCE reconstruction step, the overall performance of the PPAC strategy is still significantly improved, with for example, an additional 30% reduction observed in the number of variables needed to achieve a given simulation error (Fig. 2.)

2.2 LES/PDF Calculations of Turbulent Premixed Counterflow Flames

LES/PDF simulations of the turbulent premixed counterflow flame experimentally studied by Coriton *et al.* [4] have been performed and analyzed. The counterflow burner consists of two opposed nozzles, one emitting fresh premixed reactants, $\text{CH}_4/\text{O}_2/\text{N}_2$, the other, hot stoichiometric combustion products. Four critical parameters are identified in this flame, which are the bulk strain rate, K_{bulk} , the turbulent Reynolds number of the reactant stream, Re_t , the equivalence ratio of the reactant stream, ϕ_u , and the temperature of the hot product stream, T_b . The instantaneous centerline profiles of OH mass fraction are used to identify the interface between the two counterflowing streams referred to as the Gas Mixing Layer interface (GMLI), and the turbulent flame region using a binary reaction progress variable, c . The results are then analyzed in the reference frame attached to the GMLI. In this analysis, the conditional mean progress variable, $\langle c|\Delta \rangle$, denotes the probability of detecting the combustion products from the turbulent flame at a distance Δ from the GMLI. The probability of localized extinction at the GMLI is therefore given by $1 - \langle c|\Delta = 0 \rangle$.

Figure 3 shows the profiles of conditional mean progress variable, $\langle c|\Delta \rangle$, as a function of distance from the GMLI, Δ , for the lean turbulent premixed flame for varying T_b but at fixed values of K_{bulk} and Re_t . The localized extinction increases as T_b decreases. The probabilities of localized extinction at the GMLI in the simulations for $T_b = 1950$ K, 1850 K, 1800 K, and 1700 K are approximately 16%, 24%, 80% and 100%, respectively. The corresponding experimental values are 20%, 40%, 80% and 96%, respectively. Clearly, T_b has a significant effect on the profiles of $\langle c|\Delta \rangle$ for the lean flame, and the simulations are able to predict the experimental trends well. In contrast to the behavior shown in Fig. 3, the stoichiometric turbulent premixed flame exhibits essentially no sensitivity to T_b . Both the experiments and simulations predict the probability of localized extinction at the GMLI to be approximately 10% for all values of T_b for this stoichiometric flame.

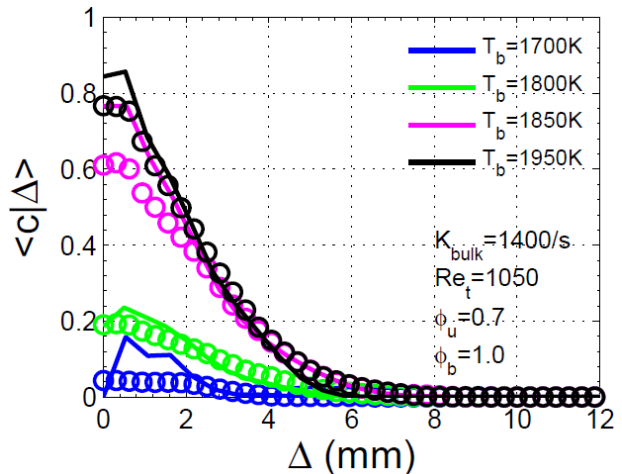


Figure 3: Effect of hot product stream temperature, T_b , on the lean turbulent premixed counterflow flame at bulk strain rate of 1400s^{-1} , turbulent Reynolds number of 1050, and reactant equivalence ratio of 0.7 – conditional mean progress variable as a function of distance from the GMLI, Δ . Lines: simulations, dots: experiments [4].

3 Future Plans

The work in the near future will focus on the efficient implementation and characterization of the PPAC adaptive strategy in LES/PDF code for turbulent flame simulation.

4 Publications from DOE Research 2012-2014

1. Y. Liang, S. B. Pope, and P. Pepiot (2015) “An adaptive methodology for the efficient implementation of combustion chemistry in particle PDF methods”, *Combust. Flame* (submitted).
2. M. Mehta, R. O. Fox, and P. Pepiot. (2015) “Reduced chemical kinetics for the modeling of TiO₂ nanoparticle synthesis in flame reactors”, *Ind. Eng. Chem. Res.* (submitted).
3. Pope, S. B. (2014) “The determination of turbulence-model statistics from the velocity-acceleration correlation”, *J. Fluid Mech.* 757, R1, DOI:10.1017/jfm.2014.563.
4. K. Narayanaswamy, P. Pitsch, and P. Pepiot (2014) “A chemical mechanism for low to high temperature oxidation of methylcyclohexane as a component of transportation fuel surrogates”, *Combust. Flame*, in press, DOI:10.1016/j.combustflame.2014.10.013.
5. Pope, S. B. and R. Tirunagari (2014) “Advances in probability density function methods for turbulent reactive flows”, In Proceedings of the Nineteenth Australasian Fluid Mechanics Conference. RMIT University, Melbourne.
6. Popov, P. and S. B. Pope (2014) “Large eddy simulation/probability density function simulations of bluff body stabilized flames”, *Combust. Flame* 161, 3100–3133.
7. K. Narayanaswamy, P. Pepiot, and P. Pitsch (2014) “A chemical mechanism for low to high temperature oxidation of *n*-dodecane as a component of transportation fuel surrogates”, *Combust. Flame*, 161:866–884.
8. Hiremath, V., S. R. Lantz, H. Wang, and S. B. Pope (2013) “Large-scale parallel simulations of turbulent combustion using combined dimension reduction and tabulation of chemistry”, *Proc. Combust. Inst.* 34, 205–215.
9. Hiremath, V. and S. B. Pope (2013) “A study of the rate-controlled constrained-equilibrium dimension reduction method and its different implementations”, *Combust. Theory Modelling* 17, 260–293.
10. Pope, S. B. (2013) “A model for turbulent mixing based on shadow-position conditioning”, *Phys. Fluids* 25, 110803.
11. Pope, S. B. (2013) “Small scales, many species and the manifold challenges of turbulent combustion”, *Proc. Combust. Inst.* 34, 1–31.
12. Ren, Z., G. M. Goldin, V. Hiremath, and S. B. Pope (2013) “Simulations of a turbulent non-premixed flame using combined dimension reduction and tabulation for combustion chemistry”, *Fuel* 105, 636–644.
13. Klimenko, A. Y. and S. B. Pope (2012) “Propagation speed of combustion and invasion waves in stochastic simulations with competitive mixing”, *Combust. Theory Modelling* 16, 679–714.
14. Hiremath, V., S. R. Lantz, H. Wang, and S. B. Pope (2012) “Computationally-efficient and scalable parallel implementation of chemistry in simulations of turbulent combustion”, *Combust. Flame* 159, 3096–3109.

References

- [1] H. Curran, T. Jayaweera, W. Pitz, WSSCI Proceedings, 2004.
- [2] K. Narayanaswamy, P. Pepiot, and P. Pitsch (2014), *Combustion and Flame*, 161 (2014) 866–884.
- [3] V. Hiremath, Z. Ren, and S. B. Pope. *Combustion and Flame*, 158 (2011) 2113–2127.
- [4] B. Coriton, J. H. Frank, A. Gomez, *Combustion and Flame*, 160 (2013), 2442-2456.

OPTICAL PROBES OF ATOMIC AND MOLECULAR DECAY PROCESSES

S.T. Pratt
Building 200, B-125
Argonne National Laboratory
9700 South Cass Avenue
Argonne, Illinois 60439
E-mail: spratt@anl.gov

PROGRAM SCOPE

The study of molecular photoabsorption, photoionization, and photodissociation dynamics can provide considerable insight into how energy and angular momentum flow among the electronic, vibrational, and rotational degrees of freedom in isolated, highly energized molecules. This project involves the study of these dynamics in small molecules, with an emphasis on understanding the mechanisms of intramolecular energy flow and determining how these mechanisms influence decay rates and product branching ratios. Such studies also shed light on related collision processes such as dissociative recombination, providing a connection between spectroscopy and dynamics. In recent years, one focus of the project has been trying to understand the factors that determine and influence photoabsorption and photoionization cross sections, as well as dissociative ionization processes. The experimental approach combines a variety of laser-based techniques, including nonlinear methods to generate tunable vacuum ultraviolet light, and double-resonance methods to prepare selected excited states of the species of interest. The detection methods include mass spectrometry, photoion- and photoelectron-imaging, and high-resolution photoelectron spectroscopy, which are used to characterize the decay processes of the selected excited states. In addition, synchrotron-based photoabsorption spectroscopy is now being used to provide high resolution spectra both above and below the ionization threshold, and synchrotron photoelectron-photoion coincidence experiments are being performed to characterize autoionization processes in small molecules and radicals.

RECENT PROGRESS

While much of the experimental work on this project is performed at Argonne, over the past year we have performed several experiments using synchrotron radiation, and we have spent a significant amount of time analyzing the resulting data.

High-Resolution Photoabsorption Studies of Alkynes

We have continued our project to study the photoabsorption spectra of a series of alkyne molecules using the Fourier-transform vacuum-ultraviolet spectrometer at the Soleil Synchrotron facility. The goal of this work is to study shape resonant features close to the ionization threshold, and to try to generalize the behavior to broader classes of molecules. In addition, we are interested in how the understanding of the continuum portion of the spectrum can inform the analysis of the bound state spectrum through the concept of continuity of oscillator strength through the ionization threshold. In our first beamtime at Soleil in 2013, we recorded room-temperature photoabsorption spectra between 6 and 12 eV for acetylene, propyne, 1-butyne, and 2-butyne, as well as jet-cooled spectra for acetylene and propyne. We completed and published our analysis of the propyne data this past year, presenting convincing evidence for previously unobserved/unassigned nf Rydberg series. The analysis was aided by calculations of the photoabsorption cross section just above the ionization threshold and a partial wave decomposition of the result performed by Robert Lucchese. As expected, absorption to ϵf continua is significant, suggesting that nf series should be observed below threshold as well. This past year, we have extended this approach and analysis to the spectra of 1- and 2-butyne. The HOMO of 1-butyne is very similar to that of propyne. Although the 1-butyne spectrum is not nearly as resolved as that of propyne, the two spectra show many similar features. In contrast, the HOMO of 2-butyne contains a significant fraction of $\ell = 3$ character, and thus transitions to Rydberg series with $\ell = 4$ character are expected. This expectation is supported by calculations showing the partial wave composition of the photoelectron wavefunction just above the ionization threshold. Our 2-butyne spectrum recorded at Soleil is better resolved than previous photoabsorption spectra, and we have reassigned a number of the features based on the new calculations.

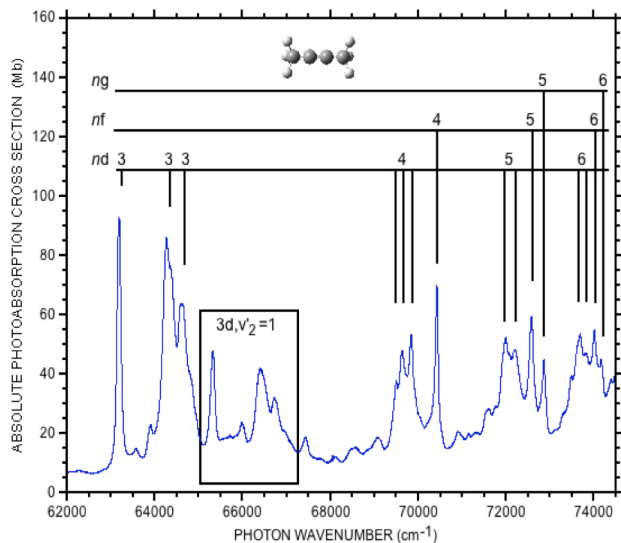


Figure 1. The photoabsorption spectrum of 2-butyne in the region of the lowest Rydberg bands. Our assignments show the presence of "new" Rydberg states at $n = 4$ and 5 , corresponding to the first members of the nf and ng Rydberg series, respectively. Calculations of the photoabsorption cross section just above threshold shows significant contributions from $\ell = 3$ and 4 partial waves, which is consistent with the presence of the corresponding states in the bound portion of the spectrum. The box corresponds to $n = 3$ levels with vibrational excitation in the $C\equiv C$ stretching mode.

Photoionization studies and photoionization cross sections

We were also granted beamtime at the Soleil Synchrotron to perform photoelectron-photoion coincidence experiments on the photoionization of N_2 just above the first ionization threshold in the region of the so-called "cathedral" bands. The DESIRS Beamline at Soleil provides extremely high photon-energy resolution that is not currently available in the US, allowing us to perform unique new experiments. The cathedral bands (they resemble a gothic cathedral) result from complex resonances of Rydberg series converging to vibrationally excited levels of the ground state of the cation, Rydberg series converging to two different electronically excited states of the cation, and high vibrational levels of valence levels. The interaction amongst these levels and the large autoionization widths of some of them makes the assignment quite difficult. Indeed, numerous studies over the last 40 years have failed to result in a definitive assignment. In our beamtime, we obtained very high resolution wavelength spectra of jet-cooled N_2 across these bands, recording photoelectron images at each energy. The wavelength resolution is sufficient to resolve or partially resolve rotational structure, which should simplify our analysis. We are currently analyzing the photoelectron angular distributions to see if they can help settle the assignment of these features that make up the cathedral. We hope to continue to receive beamtime at Soleil to use the combination of high-resolution excitation and photoelectron imaging to study the photoionization of the propargyl radical and other combustion species.

Photodissociation via the first Rydberg state of methyl iodide

In the past year, we performed a detailed study of the predissociation of CH_3I following excitation within the \tilde{B} state, which corresponds to the first Rydberg bands between 192 nm and 202 nm. This work built on our earlier study of the photodissociation of CH_3I at 193 nm, which used tunable vuv light to ionize the CH_3 and $I\ ^2P_{3/2}(I)$ and $I\ ^2P_{1/2}(I^*)$ fragments. That work revealed a non-zero branching fraction for $I\ ^2P_{3/2}$, and a surprising translational energy distribution in which the I fragments were slower than the I^* fragments. In our new study, we have used tunable ultraviolet light to excite individual vibronic bands of

In particular, we believe that there is significant evidence for both $\ell = 3$ and 4 Rydberg series. We have recently submitted a paper based on this analysis.

This past year we also recorded new high-resolution photoabsorption spectra at Soleil for 1- and 2-pentyne and 1-, 2-, and 3-hexyne to see how the findings in 1- and 2-butyne generalized to larger straight chain alkynes. Lucchese has also performed calculations of the photoabsorption spectrum and partial-wave composition of the ionization continua of these same species. As expected, there are considerable similarities among all of the 1-alkynes and propyne, as well as among all of the internal (2- and 3-) alkynes and 2-butyne. In particular, $\ell = 3$ partial waves are found to play a significant role in all of the 1-alkynes, and $\ell = 3$ and 4 partial waves are important in all of the internal alkynes. In addition, all of the internal alkynes appear to show an $\ell = 4$ shape resonance just above the first ionization limit. We are currently finishing the analysis of the new data and preparing a manuscript for publication.

the \tilde{B} state, and determined how the I and I* branching fractions depend on the nature of the vibronic intermediate level. We have found a small I branching fraction for all of the bands excited, although in most cases this branching fraction is quite small ($<0.04 \pm 0.02$). However, when the ν_3 mode of the \tilde{B} state was excited, the I branching fraction increased to 0.13 ± 0.02 . The latter observation is consistent with the measurements of Gonzalez et al. [J. Chem. Phys. **135**, 021102 (2011)], who first observed the production of I $^2P_{3/2}$ following excitation of this mode. The new results suggest that the predissociation of the \tilde{B} state does not necessarily follow the simple reaction coordinate for C - I bond fission, but instead involves geometries on the potential surface away from C_{3v} symmetry. More extensive calculations of the relevant potential surfaces would be helpful in understanding more details about the dissociation process.

Pump-probe experiments at the LCLS

This past May, I collaborated with the Atomic Physics Group at Argonne on a project that was carried out at the Linac Coherent Light Source this past May. These experiments used a two-color, time-resolved x-ray technique to study the dynamics and electron transfer processes occurring during the relaxation following inner-shell excitation. These experiments were performed on xenon difluoride, but substantial data was also obtained on N_2 and O_2 that were present as background gases. In principle, the multi-coincidence detector provided data that allows the correlation of different fragments (mass and charge states) with each other, allowing the reconstruction of the decay process. The goal of the work was to study the decay of a core hole generated on the Xe atom in XeF_2 , and the electronic relaxation that involves both the outer shells of the Xe atom and the electrons on the F atoms. The analysis of these data is quite complex, and is still underway.

FUTURE PLANS

I will complete the analysis of the photoabsorption data on the pentyne and hexynes, and will attempt to present a general picture of photoabsorption in the straight chain alkynes. At Argonne, I will also record photoelectron images for this series of alkynes at a photon energy of 10.48 eV to help aid the assignment of the Rydberg spectra. The angular distribution data obtained from the photoelectron images may also help identify contributions from high- ℓ partial waves. We will also attempt some new double-resonance experiments on selected alkynes using uv light to pump selected rotational levels of low-lying electronic states, followed by ionization with vuv light to access not only the electronic ground state of the cation, but electronically excited states as well. Photoelectron imaging will then be used to characterize these ionic states. Initial experiments will focus on acetylene, and progress to propyne and larger systems.

This past year we were distracted away from our studies of the absolute photoionization cross sections of radicals and other reactive species. In the coming year, we will return to these studies with a re-examination of some systems that we have attempted to study previously, including the benzyl and phenyl radicals. This past year we did examine a number of methods to generate cold molecular beams of radicals efficiently, and we will return to that project as well.

I will also work to complete the analysis of the new N_2 photoelectron images, and try to provide a more definitive assignment of the features of the cathedral bands. I have applied for additional beamtime at the DESIRS beamline to use the same photoelectron-photoion coincidence imaging approach to record high resolution photoionization spectra of the propargyl radical. This spectrum is known to show strong electronically autoionizing resonances [T. Zhang et al. J. Chem. Phys. **124**, 074302 (2006)], but these features have not been definitively assigned. The significantly higher resolution possible at Soleil may provide substantially better data on the important combustion radical. These data could also provide new information on the excited states of the propargyl cation.

I will continue to collaborate with Christian Jungen on theoretical models of vibrational autoionization and dissociative recombination in polyatomic molecules. While we have made only slight progress this past year, we are still working on possible approaches to explain remaining discrepancies between experiment and theory for the dissociative recombination of $H_3^+ + e$. On another front, we are also hoping to get information about the K matrix for photoabsorption in 2-butyne from Robert Lucchese. If the desired information can be extracted from his calculations, we should be able to analyze the K matrix and

see if there is evidence for the kinds of perturbations amongst higher- ℓ Rydberg states such as those we have assigned in the experimental spectrum. If successful, this effort would provide a new approach to connecting the continuum and bound-state portions of photoabsorption and photoionization spectra.

I will participate in some new experiments at Soleil with Katherine Reid (Nottingham) and David Holland (Daresbury) in which high-resolution vuv light from the synchrotron will pump high Rydberg states of NO and NH₃, and then laser light will ionize the states selected by the pump. Photoelectron-photoion imaging will be used to detect the products. While the initial experiments are mainly for proof-of-principle, the ability to record photoelectron spectra of selected rotational levels should provide new insight into the photoionization dynamics of these species.

ACKNOWLEDGEMENTS

This work was performed in collaboration with my postdoc Hong Xu. Work at Soleil was performed in collaboration with S. Boyé-Péronne and B. Gans (Institut des Sciences Moléculaires d'Orsay), D. M. P. Holland (STFC, Daresbury), U. Jacovella (ETH-Zürich), R. R. Lucchese (Texas A&M), E. F. McCormack (Bryn Mawr College) and N. de Oliveira (Soleil). Work on dissociative recombination was performed in collaboration with Ch. Jungen (Laboratoire Aime Cotton). This work was supported by the U.S. Department of Energy, Office of Science, Office of Basic Energy Sciences, Division of Chemical Sciences, Geosciences, and Biological Sciences under contract No. DE-AC02-06CH11357.

DOE-SPONSORED PUBLICATIONS SINCE 2013

1. H. Xu and S. T. Pratt
THE PHOTOIONIZATION CROSS SECTION OF PROPARGYL RADICAL AND SOME GENERAL IDEAS FOR ESTIMATING RADICAL CROSS SECTIONS
J. Phys. Chem. A **117**, 9331-9342 (2013).
2. H. Xu and S. T. Pratt
THE PHOTODISSOCIATION OF ANISOLE AND THE ABSOLUTE PHOTOIONIZATION CROSS SECTION OF THE PHENOXY RADICAL
J. Phys. Chem. A **117**, 12075-12081 (2013).
3. H. Xu and S. T. Pratt
A NEW LOOK AT THE PHOTODISSOCIATION OF METHYL IODIDE AT 193 NM
J. Chem. Phys. **139**, 214310 (2013).
4. S. T. Pratt
CHARGE TRANSFER GOES THE DISTANCE
Science **345**, 267-268 (2014).
5. U. Jacovella, D. M. P. Holland, S. Boyé-Péronne, D. Joyeux, L. E. Archer, N. de Oliveira, L. Nahon, R. R. Lucchese, Hong Xu, and S. T. Pratt
HIGH-RESOLUTION PHOTOABSORPTION SPECTRUM OF JET-COOLED PROPYNE
J. Chem. Phys. **141**, 114303 (14 pages) (2014).
6. H. Xu and S. T. Pratt
PHOTODISSOCIATION OF METHYL IODIDE VIA SELECTED VIBRATIONAL LEVELS OF THE \tilde{B} ($^2E_{3/2}$)6s RYDBERG STATE
Submitted to J. Phys. Chem. A.
7. U. Jacovella, D. M. P. Holland, S. Boyé-Péronne, B. Gans, N. de Oliveira, D. Joyeux, L. E. Archer, R. R. Lucchese, Hong Xu, and S. T. Pratt
HIGH-RESOLUTION VACUUM-ULTRAVIOLET PHOTOABSORPTION SPECTRA OF 1-BUTYNE AND 2-BUTYNE
Submitted to J. Chem. Phys.

Chirped-Pulse Fourier Transform Millimeter-Wave Spectroscopy for Dynamics and Kinetics Studies of Combustion-Related Reactions

Kirill Prozument
Chemical Sciences and Engineering Division
Argonne National Laboratory
Argonne, IL 60439
prozument@anl.gov

1. Scope of the Program

I am developing a new program to use microwave and millimeter-wave rotational spectroscopy to probe stable and reactive species relevant to combustion chemistry, and to use this capability to study reaction dynamics and kinetics. Rotational spectroscopy is known for its unsurpassed resolution and precision in determining molecular structure. The program will be based on chirped-pulse Fourier transform millimeter-wave (CP-FTmmW) spectroscopy¹⁻⁴, which is rapidly revolutionizing the field of molecular spectroscopy. The CP-FTmmW spectroscopy is capable acquiring ~10 GHz wide rotational spectra with sub-MHz resolution in several microseconds with meaningful relative intensities of the transitions of multiple reaction products. The technique is nearly universal (applicable to all polar species) chemical tool that is conformer- and state-specific, quantitative and non-destructive, and suitable for studies of stable and transient species.⁵⁻⁹ The versatility of the CP-FTmmW technique is sufficient to allow its application to a wide range of experiments in reaction dynamics and kinetics.

2. Previous work

While I am currently in the process of designing and setting up my laboratory at Argonne, I have previously been involved in a number of experiments that illustrate the capabilities of the technique. What follows are two examples of that past work.

2.1. Pyrolysis reaction dynamics^{6,7}

The thermal decomposition of ethyl nitrite, $\text{CH}_3\text{CH}_2\text{ONO}$, in a Chen-type flash pyrolysis reactor (Fig. 1) was studied using the CP-FTmmW spectroscopy. This decomposition is interesting because there are multiple fragmentation channels, and the branching fractions provide insight into the dissociation mechanism.

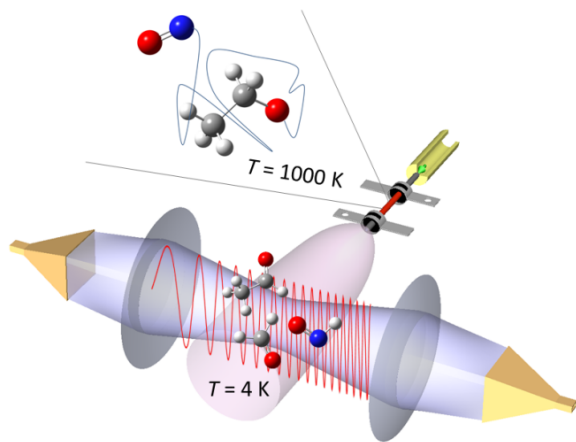


Fig. 1. The schematic of the experimental setup. The molecules exiting the heated flash pyrolysis reactor expand supersonically into the vacuum and are probed by the mm-wave beam of the CP-FTmmW spectrometer. The molecules are cooled in the expansion to ~4 K rotational temperature, which simplifies the spectral assignment and improves the signal-to-noise ratio of the CP-FTmmW spectra. The frequency of the mm-wave beam is swept linearly in time (chirped) to polarize the species in the broad spectral range. The free induction decay (FID) at the species' resonance frequencies is digitized by the spectrometer and Fourier-transformed to a frequency domain rotational spectrum.

In our experiment, the CH_2O , CH_3CHO and HNO products were detected and their branching ratios were measured at the reactor temperatures of 1000 – 1800 K.⁶ The experimentally determined branching ratios (Fig. 2) of the three products were compared to the results of the kinetic modeling (Fig. 3).⁷ In the model, the roaming reaction pathway $\text{CH}_3\text{CH}_2\text{ONO} \rightarrow \text{CH}_3\text{CHO} + \text{HNO}$ can be effectively “switched on” ($\alpha = 1$) and “off” ($\alpha = 0$). The rate of the roaming reaction is set to be proportional to that of the corresponding radical elimination reaction channel: $k(\text{CH}_3\text{CH}_2\text{ONO} \rightarrow \text{CH}_3\text{CHO} + \text{HNO}) = \alpha k(\text{CH}_3\text{CH}_2\text{ONO} \rightarrow \text{CH}_3\text{CH}_2\text{O} + \text{NO})$. The observed results are only in agreement with the model if the roaming reaction pathway is included in the model ($\alpha = 1$). The CP-FTmmW spectroscopy was shown to be a unique tool for gauging the relative importance of the i) simple bond fission $\text{CH}_3\text{CH}_2\text{ONO} \rightarrow \text{CH}_3\text{CH}_2\text{O} + \text{NO}$, ii) molecular elimination via a conventional tight transition state $\text{CH}_3\text{CH}_2\text{ONO} \rightarrow \text{CH}_3\text{CHO} + \text{HNO}$ and iii) the roaming pathway $\text{CH}_3\text{CH}_2\text{ONO} \rightarrow \text{CH}_3\text{CHO} + \text{HNO}$ in the thermal decomposition of ethyl nitrite.⁷ Future work will make use of this ability to characterize multiple reaction channels and to understand relative importance of each of them.

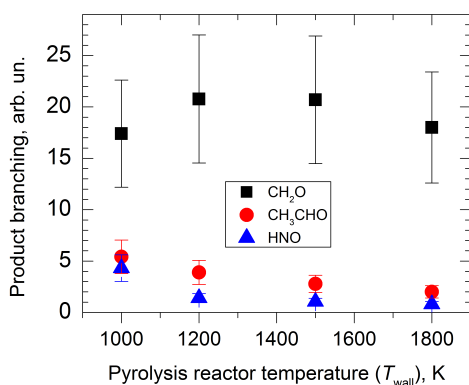


Fig. 2. Measured branching ratios of the CH_2O , CH_3CHO , and HNO products of the pyrolysis of $\text{CH}_3\text{CH}_2\text{ONO}$ at various reactor temperatures.⁷

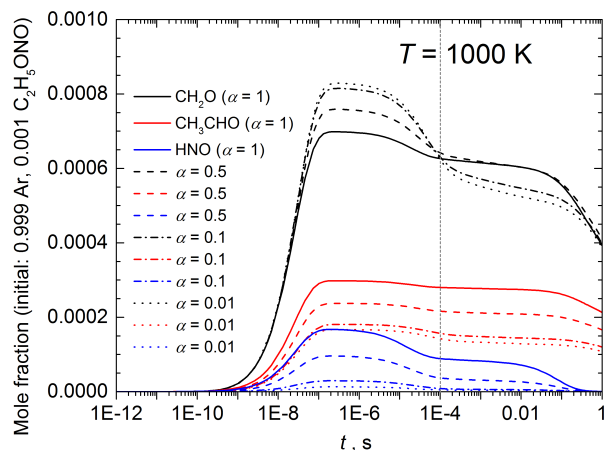


Fig. 3. Kinetic modeling of the CH_2O , CH_3CHO , and HNO products branching performed using the Python version of the Reaction Mechanism Generator.⁷

2.2. 193 nm photolysis of vinyl cyanide⁵

Transition state is an important characteristic of a potential energy surface. The information on the transition states is encoded in the nascent vibrational state population distribution (VPD) of the product molecules. We have used CP-FTmmW spectroscopy to characterize the nascent VPD of HCN and HNC produced in photodissociation of vinyl cyanide, CH_2CHCN , at 193 nm. In Fig. 4, well-resolved pure rotational transitions of HCN and HNC in many vibrational states, resulting from vinyl cyanide photolysis, are captured in a single broadband spectrum. More than 30 vibrational states are assigned. Several transition states are identified and their branching determined by comparing the measured VPDs to the results of *ab initio* calculations. The electric quadrupole constant $(eQq)_\text{N}$ is determined for each vibrational state. Because of the $I = 1$ nuclear spin of the ^{14}N atom and its electric quadrupole interaction with the electric field of the electrons in the molecule, the electric quadrupole constant $(eQq)_\text{N}$ is a valuable diagnostic for the $\text{HCN} \leftrightarrow \text{HNC}$ isomerization dynamics. The $(eQq)_\text{N}$ for the states with up to 14 quanta of bending in HCN and up to 6 in HNC , approaching the $\text{HCN} \leftrightarrow \text{HNC}$ isomerization barrier, are determined. Some irregularities in the near-the-barrier $(eQq)_\text{N}$ behavior are observed and attributed to the resonances between the HCN and HNC levels. The effect of the resonances on the $\text{HCN} \leftrightarrow \text{HNC}$ isomerization rate is being investigated. This example further illustrates the potential of the CP-FTmmW spectroscopy for reaction dynamics studies.

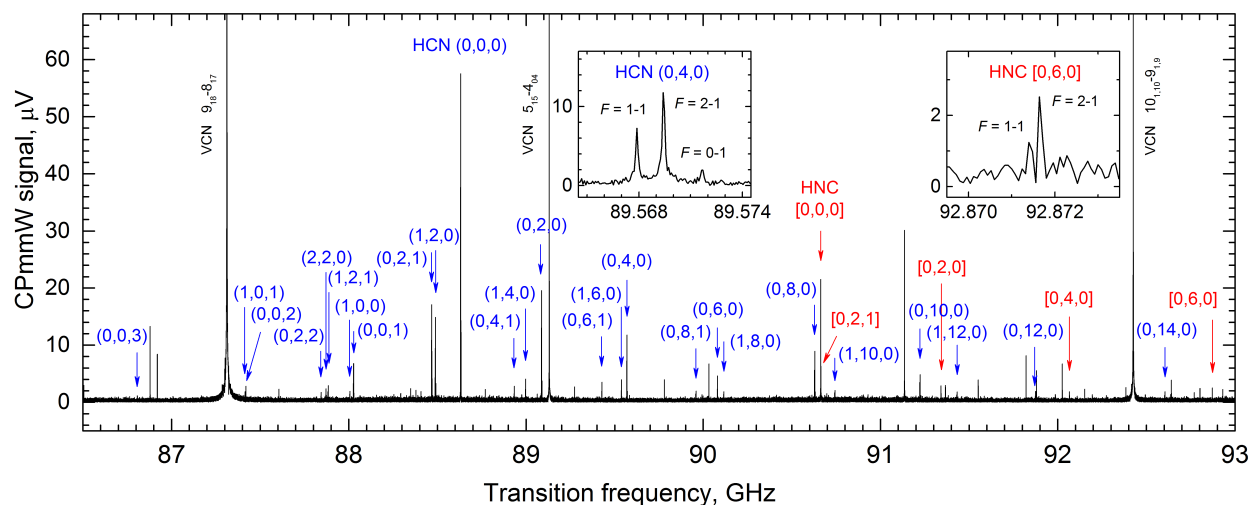


Fig. 4. CP-FTmmW spectrum of the vinyl cyanide (VCN) precursor molecules, and the HCN and HNC photolysis products. The VCN molecules entrained in Ar are expanded from a slit jet and photolyzed by the 193 nm laser. The vibrational states ($\nu_1 = \text{C-H stretch}$, $\nu_2 = \text{bend}$, $\nu_3 = \text{C-N stretch}$) of HCN and HNC molecules are shown in round and square brackets, respectively, near their rotational lines. Two inserts illustrate the electric quadrupole hyperfine (eQq)_N structure, with the corresponding assignment. The strongest transitions of the parent VCN molecule are labeled with $J_{K_a K_c}$ quantum numbers. Some VCN lines extend beyond the present plot and have the signal-to-noise ratio of more than 1000. The chirp covers the 84.5–97.0 GHz region, but only the region containing the HCN and HNC transitions is shown. The spectrum is a Fourier transform of the time domain trace, which is obtained by averaging 150,000 free induction decay traces. The data acquisition time is about 2 hours.

3. Future work

The CP-FTmmW spectroscopy will be used to experimentally determine the branching ratios of multiple reaction products and understanding the underlying reaction dynamics. The dynamics of both unimolecular and bimolecular reactions will be studied. Unimolecular photo- and thermal dissociation of acetaldehyde, acetone, esters, and carboxylic acids, which are important in combustion, will be investigated to gain understanding of the importance of the roaming dissociation channel in these reactions. Bimolecular reactions in a heated flash pyrolysis reactor or a flow tube reactor will also be studied. In particular, we are interested in the H-atom addition/elimination reactions with acetaldehyde, acetone, and other species that are important for combustion. In a carefully crafted experiment, the CP-FTmmW spectroscopy is capable of detecting and quantifying the reaction intermediates. Finding the complexes of molecules with H-atoms and determining the branching between the different addition sites will be an important direction. Identifying the isomers of the intermediate species will be aided by *ab initio* calculations. When the measured products result from a complex network of reactions, kinetic modeling will be essential in guiding our understanding of the reaction dynamics at hand. An additional focus will be on the experimental determination of vibrational state population distributions in the reaction products. Interpretation of the nascent vibrational populations will help uncovering the transition states that the system has passed through and the energy disposal into the products. The time-dependent versions of the above experimental approaches, in which the time-evolution of the product and vibrational state population distributions is experimentally determined, will also be pursued as a part of this program.

Acknowledgments

I am grateful to my postdoctoral advisors Robert W. Field and Arthur G. Suits for their guidance and the opportunity to perform the initial work in the area of chirped-pulse spectroscopy, molecular dynamics and kinetics. We are grateful to Brooks H. Pate for sharing his expertise and assisting in the development of the chirped-pulse millimeter-wave spectrometer. I thank my collaborators G. Barratt Park, John S. Muentner, G. Barney Ellison, John F. Stanton, AnGayle K. Vasiliou, Yury V. Suleimanov, William H. Green, Rachel G. Shaver, Joshua H. Baraban, Chamara Abeysekera and James M. Oldham. I gratefully acknowledge the personnel and equipment support by the U.S. Department of Energy, Office of Basic Energy Sciences under Award Number DEFG0287ER13671, the Donors of the American Chemical Society Petroleum Research Fund for support under the Grant Number 50650-ND6, the support of the National Science Foundation (Award CHE-0749821 and Award MRI-ID 1126380). This Program is supported by the U.S. Department of Energy, Office of Science, Office of Basic Energy Sciences, Division of Chemical Sciences, Geosciences, and Biological Sciences under contract No. DE-AC02-06CH11357.

References

1. Brown, G. G.; Dian, B. C.; Douglass, K. O.; Geyer, S. M.; Shipman, S. T.; Pate, B. H. A Broadband Fourier Transform Microwave Spectrometer Based on Chirped Pulse Excitation. *Rev. Sci. Instrum.* **2008**, *79* (5), 053103.
2. Dian, B. C.; Brown, G. G.; Douglass, K. O.; Pate, B. H. Measuring Picosecond Isomerization Kinetics via Broadband Microwave Spectroscopy. *Science* **2008**, *320* (5878), 924-928.
3. Park, G. B.; Steeves, A. H.; Kuyanov-Prozument, K.; Neill, J. L.; Field, R. W. Design and Evaluation of a Pulsed-Jet Chirped-Pulse millimeter-Wave Spectrometer for the 70-102 GHz Region. *J. Chem. Phys.* **2011**, *135* (2), 024202.
4. Prozument, K.; Colombo, A. P.; Zhou, Y.; Park, G. B.; Petrovic, V. S.; Coy, S. L.; Field, R. W. Chirped-Pulse Millimeter-Wave Spectroscopy of Rydberg-Rydberg Transitions. *Phys. Rev. Lett.* **2011**, *107* (14), 143001.
5. Prozument, K.; Shaver, R. G.; Ciuba, M. A.; Muentner, J. S.; Park, G. B.; Stanton, J. F.; Guo, H.; Wong, B. M.; Perry, D. S.; Field, R. W. A New Approach toward Transition State Spectroscopy. *Faraday Discuss.* **2013**, *163*, 33-57.
6. Prozument, K.; Park, G. B.; Shaver, G. R.; Vasiliou, A. K.; Oldham, J. M.; David, D. E.; Muentner, J. S.; Stanton, J. F.; Suits, A. G.; Ellison, G. B.; Field, R. W. Chirped-Pulse millimeter-Wave Spectroscopy for Dynamics and Kinetics Studies of Pyrolysis Reactions. *Phys. Chem. Chem. Phys.* **2014**, *16*, 15739-15751.
7. Prozument, K.; Suleimanov, Y. V.; Buesser, B.; Oldham, J. M.; Green, W. H.; Suits, A. G.; Field, R. W. A Signature of Roaming Dynamics in the Thermal Decomposition of Ethyl Nitrite: Chirped-Pulse Rotational Spectroscopy and Kinetic Modeling. *J. Phys. Chem. Lett.* **2014**, *5*, 3641-3648.
8. Oldham, J. M.; Abeysekera, C.; Joalland, B.; Zack, L. N.; Prozument, K.; Sims, I. R.; Park, G. B.; Field, R. W.; Suits, A. G. A chirped-pulse Fourier-transform microwave/pulsed uniform flow spectrometer. I. The low-temperature flow system. *J. Chem. Phys.* **2014**, *141* (15).
9. Abeysekera, C.; Zack, L. N.; Park, G. B.; Joalland, B.; Oldham, J. M.; Prozument, K.; Ariyasingha, N. M.; Sims, I. R.; Field, R. W.; Suits, A. G. A chirped-pulse Fourier-transform microwave/pulsed uniform flow spectrometer. II. Performance and applications for reaction dynamics. *J. Chem. Phys.* **2014**, *141* (21).

Photoinitiated Reactions of Radicals and Diradicals in Molecular Beams

Hanna Reisler

Department of Chemistry, University of Southern California

Los Angeles, CA 90089-0482

reisler@usc.edu

Program Scope

Open shell species such as radicals and diradicals are central to reactive processes in combustion and environmental chemistry. Our program is concerned with photoinitiated reactions of hydroxyalkyl radicals and carbenes. The goal is to investigate the detailed dynamics of dissociation of free radicals and diradicals in which multiple pathways participate, including molecular rearrangements, and compare them with high-level calculations. Studies include unimolecular reactions on the ground state as well as photodissociation dynamics on excited Rydberg and valence states that involve multiple potential energy surfaces.

Recent Progress

I. Excitation and dissociation of hydroxymethylene

Hydroxymethylene, the tautomer of formaldehyde, has been implicated in combustion and astrochemical processes, as well as an intermediate in the production of sugars, reactions of organometallic compounds, etc. While the photoinitiated unimolecular reaction of formaldehyde has been studied extensively, much less is known experimentally about hydroxymethylene, the prototype hydroxycarbene. Its lowest energy *trans* isomer was isolated in the matrix and characterized using IR and UV spectroscopy,¹ and very recently, its IR spectrum was measured also in He droplets.² The *trans*-HCOH isomer isomerizes via tunneling through a narrow barrier to formaldehyde in a cold Ar matrix with a half-life of ~ 2 hours, while HCOD remains stable.¹ We reported the formation of hydroxymethylene as a significant product in the photodissociation of CH₂OH in 2004,³ and later identified its *trans*- and *cis*-isomers.⁴ The *trans*-HCOH isomer lies $18,264 \pm 140$ cm⁻¹ above the zero point level of H₂CO, and the *cis-trans* separation is 1550 ± 40 cm⁻¹.⁴ Accurate potential energy surfaces (PESs) are now available for the S₀, S₁ and T₁ states that encompass the two tautomers, as well as the CO + H₂ and H + HCO product channels and the transition states for the relevant processes.

Our previous work has established that H₂CO and HCOH(D) can be prepared in the gas-phase by photodissociation of CH₂OH(D) following excitation to the 3s, 3p_x, and 3p_z Rydberg states. The product channels are reached via conical intersections along the O-H and C-H coordinates, resulting in breaking of the O-H and C-H bonds. Upon excitation to the origin band of 3p_x ($35,053$ cm⁻¹) and above, the *cis* isomer of HCOH is preferred over the lower energy *trans* isomer.

In the past year, H(D) photofragment sliced velocity map images were recorded at several excitation energies of the 3p_x and 3p_z Rydberg states of CH₂OH and CH₂OD ($E_{\text{exc}} = 35,000$ - $44,500$ cm⁻¹). We use CH₂OD to distinguish between the H₂CO and HCOD cofragments by monitoring D and H products, respectively. As the excitation energy of the CH₂OH(D) precursor increases, the internal energy of the molecular products increases as well. With excitation of CH₂OD to higher vibronic levels of 3p_z, new, low kinetic energy (KE) features appear in the H and D fragment KE distributions (KEDs), whose widths increase with increasing excitation energy. The appearance thresholds of these H/D fragments coincide with the dissociation energy of formaldehyde to H(D) + H(D)CO.

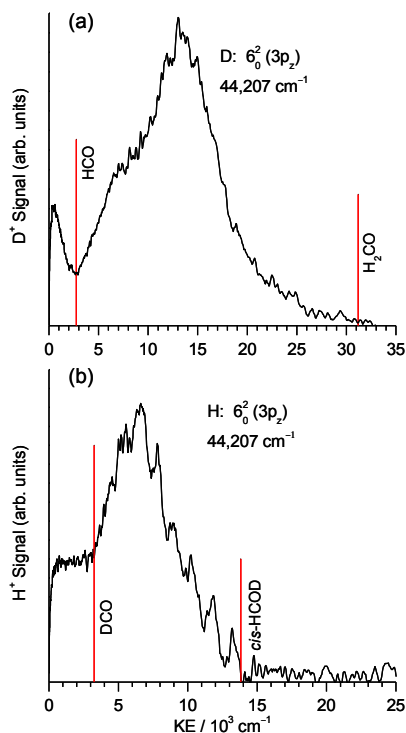


Figure 1 displays H and D KE release plots obtained by sliced velocity map imaging following excitation of CH₂OD to the 6₀² transition of 3p_z. The D-fragment KEDs are correlated with H₂CO cofragments, except for the small peak at low KE, which originates in secondary dissociation of HCOD. The H-photofragment KEDs, on the other hand, are correlated with HCOD cofragments, and their partially resolved peaks reflect vibrational excitation in HCOD. The increased signal at the lowest KEs corresponds to fragments generated by secondary dissociation of either “hot” HCOD or H₂CO products (or both). As the excitation energy increases, the secondary dissociation peak broadens and increases in integrated intensity, but its energy onset always corresponds to the H(D) + HCO channel threshold.

Figure 1: H and D-fragment KE release plots obtained by monitoring D (upper panel) and H (lower panel) following 3p_z excitation of CH₂OD to the 6₀² band ($E_{\text{exc}} = 44,207 \text{ cm}^{-1}$). Sticks in each panel indicate the KE onsets associated with H₂CO, *cis*-HCOD, and H and D from secondary dissociation.

D-fragment KEDs recorded at excitation energy below the threshold of secondary dissociation show that only a few of the H₂CO cofragments are born with the high internal energies required for secondary dissociation, and this fraction does not increase at higher excitation energies. Therefore H₂CO is not an important source of secondary H fragments. In contrast, the H-fragment KEDs show that a significant fraction of the HCOD cofragments possesses sufficient internal energies to dissociate to H(D) + D(H)CO. Therefore, HCOD is the only source of the observed secondary D atoms and the main source of secondary H fragments. Since the yields of the slow H and D secondary products are comparable, we conclude that they are generated predominantly by dissociation of vibrationally excited HCOD, and we propose that the major dissociation pathway involves isomerization to HDCO followed by dissociation.

High quality PESs now exist for the H₂CO/HCOH system, but in contrast to the wealth of information available on dissociation from the H₂CO global minimum, relatively little is known about the dissociation dynamics of HCOH. We hope that our new results would inspire additional theoretical work on the H₂CO/HCOH PES that includes trajectory calculations initiated from the global minima of *trans*- and *cis*-HCOH.

II. Effect of conical intersections in hydroxymethyl radicals on product state distributions

About a decade ago, Yarkony carried out conical intersection calculations on CH₂OH and identified conical intersection seams along the O-H and C-H coordinates following excitation to the 3s and 3p_x states.⁵ He predicted that in conical intersections from the 3s state, most of the formaldehyde products would have high translational energies and fairly low internal energies, but a small fraction would sample the global minimum and have a broad, statistical-like, internal energy distribution. He also predicted that *cis*- rather than *trans*-HCOH would be the predominant hydroxymethylene isomer. These predictions are confirmed by our recent work, except that we find that the situation regarding HCOH production is more complicated. In excitation to the 3s state, the yield of HCOH(D) is fairly small, and because of its high rotational excitation it is

impossible to distinguish between the *trans*- and *cis*-isomers. However, upon excitation to the $3p_x$ origin band, the rotational excitation in the HCOH(D) isomers is reduced considerably and vibrational structure is observed. This allowed us to show that the *cis*-isomer was preferentially produced and its relative population increased with increasing excitation energy. Nonetheless, the rotational excitation was still fairly high and obscured vibrational structure at high internal HCOH(D) energies.

Our most recent work shows that another abrupt reduction in the HCOH(D) rotational excitation occurs upon excitation to the higher-lying $3p_z$ state, allowing the observation of distinct vibrational structure in HCOD fragments with high internal energies. The vibrational excitation spans the full range of allowed internal energies, reaching up and above the dissociation limit of HCOH(D), as seen in Figures 1 and 2. The loss of structure observed at very high internal energies can signify either increasing IVR leading to a higher density of states and/or a greater contribution of triplet HCOH(D).

H/D photofragment yield spectra of CH₂OH(D) show that underlying the sharp $3p_z$ vibronic bands there is structureless absorption to $3s$ and $3p_x$. This gives us an opportunity to observe differences between the HCOD rovibrational state distributions at similar energies. Figure 2 presents a comparison of the H-fragment KEDs obtained at the 6_0^1 peak of $3p_z$ (after background subtraction) and the one recorded ~ 70 cm⁻¹ to the red, which corresponds to $3s/3p_x$ absorption. As expected, the latter displays a much greater rotational excitation that obscures much of the vibrational structure.

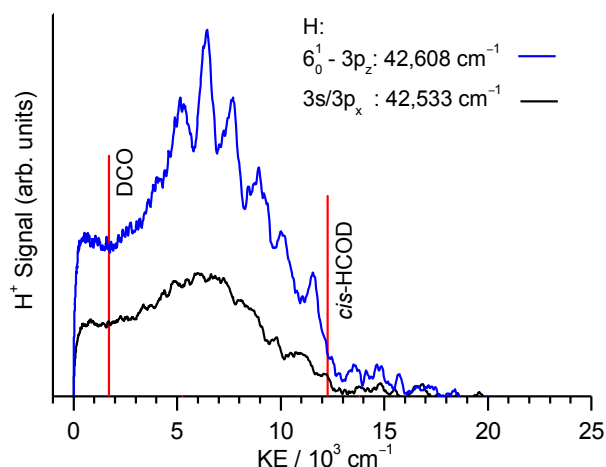


Figure 2: Comparison of *cis*-HCOD internal state distributions obtained via $3p_z$ excitation of CH₂OD to the 6_0^1 band ($E_{\text{exc}} = 42,608$ cm⁻¹), and by excitation to the $3s/3p_x$ underlying background ($E_{\text{exc}}=42,553$ cm⁻¹). Background contribution has been subtracted in the 6_0^1 plot. Sticks indicate the KE onsets associated with *cis*-HCOD and H from secondary dissociation.

These results indicate that the dissociation dynamics is not controlled solely by the $3s$ PES and its coupling to the ground state; rather, different dynamics ensues by passing through different conical intersections. In all cases the dissociation is fast; yet the resulting dynamics is different. It is not clear whether the $3p_z$ and $3p_x$ states couple directly to the ground state, or whether sequential conical intersections link the upper states to the ground state and guide the dissociating flux in ways that affect significantly the products' rovibrational state distributions. Yarkony and co-workers are carrying out new theoretical calculations on a three-state PES that includes the participating Rydberg states, and these calculations should shed further light on the dissociation dynamics.

III. Future work

We plan to expand our study of the importance of conical intersections in the hydroxymethyl radical to include vibrationally induced photodissociation. This will be achieved by first exciting OH-stretch vibrations in CH₂OH and its isotopologs followed by photodissociation.

We have initiated studies of the state-specific dissociation and isomerization of HCOH on the ground and electronic excited states. To this end, experiments are now in progress to generate HCOH by pyrolysis of glyoxylic acid.^{1,2} We have adapted published methods of preparing the dry acid, introduced it to our pyrolysis source, and identified CO (via REMPI at ~ 230 nm) as a combined pyrolysis/photolysis fragment. The CO product is rotationally and vibrationally excited, but it is not clear yet whether its source is the photolysis of glyoxylic acid or HCOH. This uncertainty has prompted us to examine more closely the pyrolysis and photolysis of glyoxylic acid by using sliced velocity map imaging. Following pyrolysis of the acid, we have obtained 3+1REMPI spectra of the CO₂ product by using several intermediate Rydberg states, and we are planning next to characterize CO₂ as product of UV photolysis.

References

1. Schreiner, P.R.; Reisenauer, H.P.; Pickard, F.C.; Simmonett, A.C.; Allen, W.D.; Matyus, E.; Csaszar, A.G.; *Nature* **2008**, *453*, 906.
2. Leavitt, C.M.; Moradi, C.P.; Stanton, J.F.; Doublerly, G.E. J.; *Chem. Phys.* **2014**, *140*, 171102.
3. Feng, L.; Demyanenko, A.V.; Reisler, H.; *J. Chem. Phys.* **2004**, *120*, 6524.
4. Rodrigo, C.; Zhou, C.; Reisler, H.; *J. Phys. Chem. A* **2013**, *117*, 12049.
5. Hoffman, B.C.; Yarkony, D.R.; *J. Chem. Phys.* **2002**, *116*, 8300; Yarkony, D.R.; *J. Chem. Phys.* **2005**, *122*, 084316.

Publications, 2012-2015

1. E. Kamarchik, C. Rodrigo, J.M. Bowman, H. Reisler, and A.I. Krylov, "Overtone-induced dissociation and isomerization dynamics of the hydroxymethyl radical (CH₂OH and CD₂OH). I. A theoretical study", *J. Chem. Phys.* *136*, 084304 (2012).
2. M. Ryazanov, C. Rodrigo and H. Reisler, "Overtone-induced dissociation and isomerization dynamics of the hydroxymethyl radical (CH₂OH and CD₂OH). II. Velocity map imaging studies", *J. Chem. Phys.* *136*, 084305 (2012).
3. M. Ryazanov and H. Reisler, "Improved sliced velocity map imaging apparatus optimized for H photofragments", *J. Chem. Phys.* *138*, 144201 (2013).
4. C. Rodrigo, C. Zhou, and H. Reisler, "Assessing multiple conical intersections in the 3s and 3p_x photodissociation of the hydroxymethyl radical", *J. Phys. Chem. A (Wittig Festschrift)* *117*, 12049-12059 (2013).
5. C.P. Rodrigo, S. Sutradhar, and H. Reisler, "Imaging studies of excited and dissociative states of hydroxymethylene produced in the photodissociation of the hydroxymethyl radical", *J. Phys. Chem. A (Yarkony Festschrift)*, *118*(51), 11916-11925 (2014).

Accurate Calculations and Analyses of Electronic Structure, Molecular Bonding and Potential Energy Surfaces

Klaus Ruedenberg

Ames Laboratory USDOE, Iowa State University, Ames, Iowa, 50011

ruedenberg@iastate.edu

Scope

Theoretical treatments of molecular reactions and their kinetics require accurate potential energy surfaces in non-equilibrium regions of coordinate space. A major challenge is the accurate calculation of the non-relativistic electron correlations when the dominant component of the electronic wave function is multi-configurational, which calls for a multi-configurational zeroth-order reference space, a requirement along many reaction paths. The recovery of this correlation energy is particularly challenging when it transpires that accurate contributions beyond second order perturbation theory and double excitations with respect to a many-dimensional active reference space are required for the attainment of chemical accuracy.

An advance towards this goal was made in this research group by the development of the method of correlation energy extrapolation by intrinsic scaling (CEEIS), which greatly reduces the number of excitations that have to be considered. This approach made it possible to recover contributions of up to eight-tuple excitations for quadruple-zeta basis sets in the diatomic molecules B_2 , C_2 , O_2 , F_2 and in water. In combination with the extrapolation to the complete basis limit, several diatomic potential energy curves were obtained with an accuracy of about 0.1 kcal/mol.

Recent Work

The CEEIS method has recently been generalized so that several states, notably the ground state and low excited states, can be calculated at the same time. In this approach, the extrapolation of the various states is based on state averaged excitations in terms of the natural orbitals of the virtual orbital space of a state averaged complete active reference space. This generalized CEEIS approach has been successful in diatomic molecules. It has now been used to obtain accurate knowledge about the ground state of the ozone molecule.

The potential energy surface of this state of O_3 is known to have three equivalent open minima and a theoretically predicted closed ring minimum, which has so far escaped all attempts at experimental creation. The ring isomer is surrounded by a substantial ridge in C_s symmetry on which three saddle points, each in C_{2v} symmetry, provide transition states to the open minima. The ridge is the result of an avoided crossing between the $^1A'$ ground state and an excited $^1A'$ state. Notably, the two states touch each other along a closed one-dimensional conical intersection seam, which crosses the three C_{2v} symmetry planes in intersection points close to the transition states. Very accurate quantitative information regarding the reaction path connecting the open minimum and the ring minimum and regarding the intersection is still outstanding.

Since the full valence space ("CAS") has about 25000 configurations, the dimension of the quadruple excitation space from this reference space is too large even for the CEEIS approach. Reduced subspaces must therefore be judiciously chosen as reference spaces for the generation of the correlating higher excitations. Since similar problems are to be expected for other systems where three atoms interact as closely with each other as in ozone, understanding the correlation in this molecule is of general interest.

Based on an analysis of the configurations that are dominant along the reaction path from the open to the closed equilibrium structure, various reduced subspaces of the full valence space were selected as reference spaces for generating the correlating excitations. In all cases, the linear relationships, which are the basis for the CEEIS method, were confirmed to be valid and allowed CEEIS extrapolations with error bars of less than about 0.5 kcal/mol at the quadruple excitation level. On the other hand, the critical energy differences on the potential energy surface were found to be very sensitive to the choice of the reference spaces. For instance, the widely used omission of excitations from the valence 2s orbitals entailed changes of 4 kcal/mole for correlated energy differences between different geometries. The ring minimum was found to lie about 29 to 34 kcal/mol above the open minimum. The barrier between the two minima was found to be about 55 to 60 kcal/mol above the open minimum.

A rigorous method was developed for determining molecule-modified atomic minimal basis orbitals in terms of which strongly correlated molecular electronic wave functions can be exactly expressed. These quasi-atomic orbitals were found to maintain their character along a reaction path even when their interactions with other atoms change. The analysis of the ab initio density in terms of these orbitals identifies the relevant bonding interactions in a molecule as well as the changes of these interactions along a reaction path.

Future Work

Accurate potential energy curves will be determined for the excited states of C₂ with higher multiplicities. Since the success of the CEEIS method appears to be based on the randomness of the small contributions from higher correlating excitations, the linear relations that have been found for correlation contributions from localized orbitals will be further explored with the aim of developing CEEIS-type extrapolations within the context of many-body expansions.

Publications in 2012, 2013, 2014

Accurate potential energy curve for B₂. Ab initio elucidation of the experimentally elusive ground state rotation-vibration spectrum. L. Bytautas, N.Matsunaga, G. Scuseria, K. Ruedenberg, *J. Phy. Chem. A.*, **116**, 1717-1729 (2012)

The dispersion interaction between quantum mechanics and effective fragment potential molecules. Q.A. Smith, K. Ruedenberg, M.S. Gordon, L.V. Slipchenko, *J. Chem. Phys.* **136**, 244107 (2012)

Three Millennia of Atoms and Molecules. K. Ruedenberg and W.H.E. Schwarz, Chapter 1, pages 1-45, in the book *Pioneers of Quantum Chemistry* (T. Strom and A. Wilson Editors, American Chemical Society, ACS Symposium Series **1122**, 2013)

Unusual Inorganic Biradicals: A Theoretical Analysis. E. Miliordos, K. Ruedenberg, S. S. Xantheas, *Angewandte Chemie, International Edition* **52**, (Issue 22) 5736–5739 (2013)

A comprehensive analysis of molecule-intrinsic quasi-atomic, bonding, and correlating orbitals. I. Hartree-Fock wave functions. A. C. West, M. W. Schmidt, M. S. Gordon, and K. Ruedenberg, *J. Chem. Phys.* **139**, 234107, 18 pages (2013)

Accurate ab initio potential energy curves and spectroscopic properties of the four lowest singlet states of C2. J. S. Boschen, D. Theis, K. Ruedenberg, T.L. Windus, *Theor Chem Acc* **33**, 1425, 12 pages (2014)

Weighted orthogonalization of atomic orbitals: A stable alternative to the Carlson–Keller method. Aaron C. West, *Comp. and Theor. Chem.* **1045**, 73–77 (2014) (under direction of K. Ruedenberg)

Covalent bonds are created by the drive of electron waves to lower their kinetic energy by expansion. M. W. Schmidt, J. Ivanic, K. Ruedenberg, *J. Chem. Phys.*, **140**, 204104, 14 pages (2014)

The Physical Origin of Covalent Binding. K. Ruedenberg, M. W. Schmidt, J. Ivanic, Chapter 1, pp. 1-67 of the book *The Chemical Bond. Fundamental Aspects.* (Edited by G. Frenking and S. Shaik, Wiley-VCH, 2014)

Active Thermochemical Tables

Branko Ruscic
Chemical Sciences and Engineering Division, Argonne National Laboratory,
9700 South Cass Avenue, Argonne, IL 60439
ruscic@anl.gov

Program Scope

The *spiritus movens* of this program is the need to provide the scientific community with accurate and reliable thermochemical information on chemical species that are relevant in combustion, or play prominent roles in related post-combustion environmental chemistry. Detailed knowledge of thermodynamic parameters for a broad array of stable and ephemeral chemical species is pivotal to chemistry and essential in many industries. In particular, the availability of accurate, reliable, and internally consistent thermochemical values is a *conditio sine qua non* in kinetics, reaction dynamics, formulation of plausible reaction mechanisms, and construction of predictive models of complex chemical environments. Furthermore, the availability of accurate thermochemical values has historically been the prime driver for steady advancement of increasingly sophisticated electronic structure theories.

The focus of this program is on bringing substantial innovations to the field of thermochemistry through the development of new methodologies, and utilizing them to systematically improve both the quality and quantity of available thermochemical data relevant to energy-producing processes. In order to achieve the stated goals, this program has developed a novel approach that is centered on analyzing and optimally utilizing the information content of *all available* thermochemically relevant determinations. The aim is not only to dynamically produce the best currently possible thermochemical parameters for the targeted chemical species, but also to allow efficient updates with new knowledge, properly propagating its consequences through all affected chemical species, as well as to provide critical tests of new experimental or theoretical data, and, when possible, to develop pointers to additional determinations that are most likely to efficiently improve the overall thermochemical knowledge base. In order to provide a broad perspective of this area of science, the effort of this program is synergistically coordinated with related experimental and theoretical efforts within the Gas-Phase Chemical Dynamics Group at Argonne.

Recent Progress

Over the past year we have continued the development of various aspects of Active Thermochemical Tables (ATcT). ATcT are a new paradigm of how to develop thermochemical values for stable, reactive, and transient chemical species by utilizing to the fullest all available experimental measurements as well as state-of-the-art theoretical data. Intertwined dependencies that underpin virtually all thermochemistry were historically considered to be an intractable complication, leading to the adoption of a simplified sequential approach to thermochemistry, which produces sets of values that are plagued by hidden progenitor-progeny relationships and thus are impossible to update with new knowledge without introducing serious inconsistencies. The success of ATcT is based on expressing the intertwined dependencies as a network of relationships that is amenable to mathematical and statistical manipulation. This effectively transforms the original problem into an asset that can be credited for the enhanced quality of the resulting thermochemistry. ATcT analyzes the Thermochemical Network (TN), attempts to bring it into self consistency by identifying determinations with ‘optimistic’ uncertainties, and then finds a solution that maximizes the number of the interdependencies that can be simultaneously satisfied.

One of the important recent results that we would like to highlight here are the values for the sequential bond dissociation enthalpies (at 298 K) and energies (at 0 K) of methane, ethane, and methanol, which were obtained by solving the latest ATcT TN (ver. 1.122, spanning over 1180 species and involving more than 19,000 determinations). The results accurately quantify all possible C-H, C-C, O-H, and C-O bond dissociations in the targeted systems. The 0 K values are indicated in Figure 1, and include, for the sake of completeness, the sequential bond energies of carbon dioxide and water. The accurate knowledge of all of these bond dissociation energies maps equivalently onto the accurate knowledge of enthalpies of formation of the related CH_n , $n = 4 - 0$ species (methane, methyl, methylene, methyldiyne, and carbon

atom), C_2H_n , $n = 6 - 0$ (ethane, ethyl, ethylene, ethylidene, vinyl, ethylidyne, acetylene, vinylidene, ethynyl, and ethynylene), COH_n , $n = 4 - 0$ (methanol, hydroxymethyl, methoxy, formaldehyde, hydroxymethylene, formyl, isoformyl, and carbon monoxide), as well as OH_n , $n = 2 - 0$ species (water, hydroxyl, oxygen atom) and carbon dioxide. These species appear as reactants, products, or intermediates in elementary chemical reactions in a variety of environments, ranging from anthropic industrial activities to astrochemistry, and are hence of substantial general interest. In particular, species from these groups play significant roles in combustion of even the simplest hydrocarbon fuels, and - due to the inherently hierarchical nature of C_n chemical reaction mechanisms - appear as important actors in virtually all combustion mechanisms. The provenances of these ATcT enthalpies of formation, which are quite distributed and involve a large number of relevant determinations, were analyzed by variance decomposition, allowing their understanding in terms of principal contributions. These ATcT results are the most accurate thermochemical values currently available for these species.

As seen in Figure 1, the sequential removals of hydrogen atoms often alternate between a ‘normal’ and a remarkably low bond dissociation energy. Due to the fact that the current results comprise a complete set of bond dissociation energies (and are significantly more accurate than prior values), the underlying reasons for alternations between high and low bond dissociation energies along the dissociation sequences can be rationalized both qualitatively and quantitatively. For example, the C-H bond dissociation energy of methoxy is quite low, $D_0(H-CH_2O) = 81.78 \pm 0.35$ kJ/mol, much lower (by 375.43 kJ/mol) than the C-H bond dissociation energy in CH_3 , 457.21 ± 0.13 kJ/mol, and may, *prima facie*, appear as an aberration. It can be easily shown that the reason for its weakness is that the removal of a hydrogen from methoxy is simultaneously accompanied by a significant strengthening of the C-O bond, from 367.73 ± 0.35 kJ/mol in methoxy to 743.15 ± 0.15 kJ/mol in formaldehyde. The ATcT results show that the strengthening of the C-O bond (by 375.42 kJ/mol) matches exactly (within the round-off error of 0.01 kJ/mol) the amount by which the C-H bond dissociation energy of methoxy is weaker than the C-H bond dissociation energy in methyl. Similar quantitative rationalizations can be made for all other C-H bond dissociation energies in all three systems studied here. With all these bond energies obtained in a consistent fashion, the study provides a number of interesting insights, including the relative strengths of the σ , first π , and second π C-C bond, and sheds some light on the peculiar bonding in C_2 , indicating that additional bonding (if any) beyond the two suspended π bonds adds negligibly to the C_2 bond strength, in contrast to recent proposals that this species has a quadruple C-C bond (two π , σ , and ‘inverted’ σ). These and other insights are discussed in the rather voluminous paper appearing in *J. Phys. Chem. A* (DOI: 10.1021/acs.jpca.5b01346).

Of the other activities here we will briefly mention the IUPAC Task Group on Radical Electrode Potentials, which adopted ATcT to optimize a set of standard electrode potentials involving radicals in aqueous solution and produce IUPAC-recommended values; this collaboration is an excellent example of the application of ATcT outside gas-phase combustion-related thermochemistry. Also, in collaboration with P. Glarborg, we have extended to chlorine our earlier study of flame inhibition by bromine.

Future Plans

Future plans of this program pivot around further development and expansion of the Active Thermochemical Tables approach, continuing to provide accurate thermochemistry, and driving targeted thermochemically-relevant theoretical and experimental investigations of radicals and transient species that are intimately related to combustion and post-combustion atmospheric processes. A significant part of the effort during the forthcoming period will be devoted to continued ‘finalization’ and dissemination of the resulting ATcT thermochemistry. A crucial component of the ‘finalization’ of results for groups of related chemical species consists of testing and analyzing their TN dependencies (in part by using the newly developed variance/covariance decomposition approach) as well as enhancing the accuracy of their partition functions (by gradually replacing them with new NRRAO partition functions), and, when suggested by ATcT analyses, adding new high-quality results (either virtual, i.e. computational, or actual, i.e. experimental) to coerce the resulting thermochemistry toward stable, ‘release quality’ values. This iterative process frequently results in an expansion of the number of species that are described by the current TN, which is an added benefit. Another important component in the future plans is the

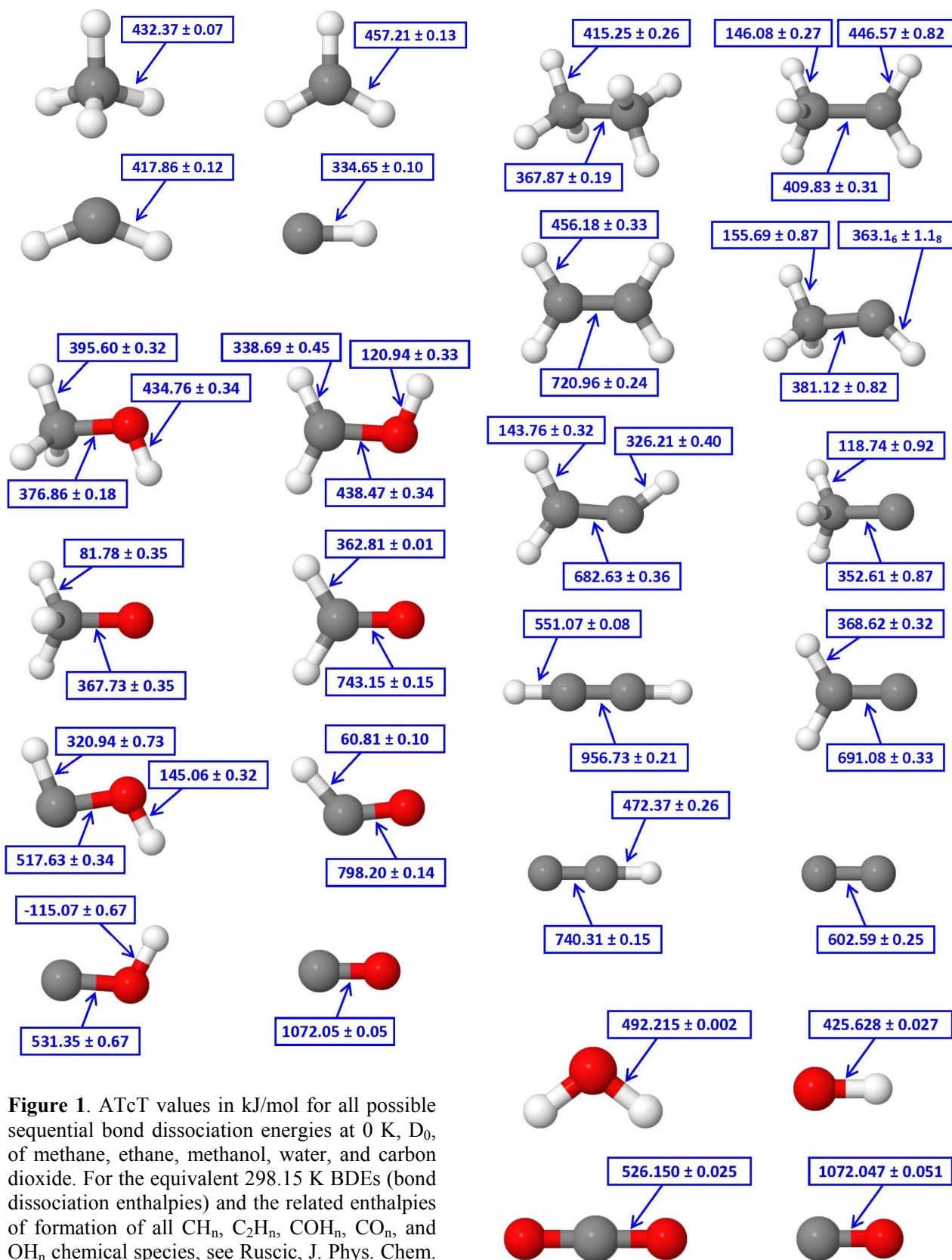


Figure 1. ATcT values in kJ/mol for all possible sequential bond dissociation energies at 0 K, D_0 , of methane, ethane, methanol, water, and carbon dioxide. For the equivalent 298.15 K BDEs (bond dissociation enthalpies) and the related enthalpies of formation of all CH_n , C_2H_n , COH_n , CO_n , and OH_n chemical species, see Ruscic, *J. Phys. Chem. A* **119** (2015) DOI: 10.1021/acs.jpca.5b01346

continuation of the current effort of designing and producing a computer-generated web site that will display the current ATcT thermochemistry, as well as all pertinent metadata, with rigorous archival capability. The pertinent metadata relates to documenting the provenance for every recommended thermochemical value. Finally, a significant long-term component of future progress consists in developing the next generation of ATcT software. This will be based on a thorough redesign of the current ATcT kernel, with the aim of making the software not only streamlined and more efficient, but also allowing sufficient flexibility that will enable the adoption and utilization of emerging computing technologies as they become available.

This work is supported by the U.S. Department of Energy, Office of Basic Energy Sciences, Division of Chemical Sciences, Geosciences, and Biosciences, under Contract No. DE-AC02-06CH11357.

Publications resulting from DOE sponsored research (2013 – present)

- *Extended Third Millennium Ideal Gas and Condensed Phase Thermochemical Database for Combustion with updates from Active Thermochemical Tables*, E. Goos, A. Burcat, and B. Ruscic (2013); (includes complete ATcT values ver. 1.112); progressive updates are currently available at <http://burcat.technion.ac.il/dir/> and mirrored at <http://garfield.chem.elte.hu/Burcat/burcat.html>
- *Prompt NO formation in flames: The influence of NCN thermochemistry*, E. Goos, C. Sickfeld, F. Mauss, L. Seidel, B. Ruscic, A. Burcat, and T. Zeuch, *Proc. Comb. Inst.* **34**, 657-666 (2013), DOI: 10.1016/j.proci.2012.06.128
- *Active Thermochemical Tables: Water and Water Dimer*, B. Ruscic, *J. Phys. Chem. A* **117**, 11940-11953 (2013), DOI: 10.1021/jp403197t
- *Active Thermochemical Tables enthalpies of formation based on ver. 1.110 of the Thermochemical Network*, B. Ruscic, <http://atct.anl.gov/Thermochemical%20Data/version%201.110/> (2013)
- *Improved Accuracy Benchmarks of Small Molecules Using Correlation Consistent Basis Sets*, D. Feller, K. A. Peterson, and B. Ruscic, *Theor. Chem. Acc.* **133**, 1407/1-16 (2014), DOI: 10.1007/s00214-013-1407-z
- *Active Thermochemical Tables: Dissociation Energies of Several Homonuclear First-Row Diatomics and Related Thermochemical Values*, B. Ruscic, D. Feller, and K. A. Peterson, *Theor. Chem. Acc.* **133**, 1415/1-12 (2014), DOI: 10.1007/s00214-013-1415-z
- *Uncertainty Quantification in Thermochemistry, Benchmarking Electronic Structure Computations, and Active Thermochemical Tables*, B. Ruscic, *Int. J. Quantum Chem.* **114**, 1097-1101 (2014), DOI: 10.1002/qua.24605
- *Electronic States of the Quasilinear Molecule Propargylene (HCCCH) from Negative Ion Photoelectron Spectroscopy*, D. L. Osborn, K. M. Vogelhuber, S. W. Wren, E. M. Miller, Y.-J. Lu, A. S. Case, L. Sheps, R. J. McMahon, J. F. Stanton, L. B. Harding, B. Ruscic, and W. C. Lineberger, *J. Am. Chem. Soc.* **136**, 10361-10372 (2014), DOI: 10.1021/ja5039984
- *High-Temperature Chemistry of HCl and Cl₂*, M. Pelucchi, A. Frassoldati, T. Faravelli, B. Ruscic, and P. Glarborg, *Combust. Flame* **162**, in press (2015)
- *Standard Electrode Potentials Involving Radicals in Aqueous Solution: Inorganic Radicals (IUPAC Technical Report)*, D. A. Armstrong, R. E. Huie, W. H. Koppenol, S. V. Lyman, G. Merényi, P. Neta, B. Ruscic, D. M. Stanbury, S. Steenken, and P. Wardman, *Pure Appl. Chem.* **87**, in press (2015)
- *Active Thermochemical Tables: Sequential Bond Dissociation Enthalpies of Methane, Ethane, and Methanol and the Related Thermochemistry*, B. Ruscic, *J. Phys. Chem. A* **119**, in press (2015), DOI: 10.1021/acs.jpca.5b01346
- *Thermal Dissociation and Roaming Isomerization of Nitromethane: Experiment and Theory*, C. J. Annesley, J. B. Randazzo, S. J. Klippenstein, L. B. Harding, A. W. Jasper, Y. Georgievski, B. Ruscic, and R. S. Tranter, *J. Phys. Chem. A* **119**, submitted (2015)

GAS-PHASE MOLECULAR DYNAMICS: HIGH RESOLUTION SPECTROSCOPY AND COLLISION DYNAMICS OF TRANSIENT SPECIES

Trevor J. Sears
Department of Chemistry, Brookhaven National Laboratory
Upton, NY 11973-5000
sears@bnl.gov

Program Scope

This research is carried out as part of the Gas-Phase Molecular Dynamics program in the Chemistry Department at Brookhaven National Laboratory. High-resolution spectroscopic methods, augmented by theoretical and computational work, are used to investigate the structure, collision dynamics and chemical behavior of intermediates in the elementary gas-phase reactions involved in combustion chemistry. There is an emphasis on new technique development with the aim of improving both the sensitivity and resolution of spectroscopic measurements.

I Recent Progress

A. Sub-Doppler frequency comb-stabilized spectroscopy

Doppler-free transition frequencies for ν_4 and ν_5 hot bands have been measured in the $\nu_1 + \nu_3$ band of acetylene using saturation dip spectroscopy with an extended cavity diode laser referenced to a frequency comb. Extensive modifications to the spectrometer during the past 12 months have improved the data quality, typically by an order of magnitude, enabling the measurement of weaker transitions. The frequency accuracy of the measured transitions, as judged from line shape model fits and the spectrometer stability, is better than 50 kHz, while the statistical precision of the measurements is 10-20 \times better than this.

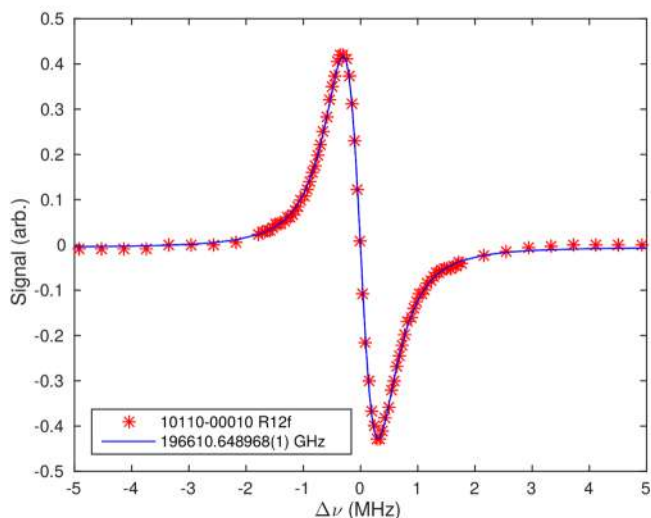


Figure 1: Sub-Doppler measurement of the R(12)f transition in the $\nu_4=1$ hot band. The asterisks are the experimental points and the line a result of line shape fit to determine the line center

This is some 2-3 orders of magnitude improvement on the accuracy and precision of previous line positions derived from the analysis of high-resolution Fourier transform infrared absorption spectra. An example of the recent data is shown in figure 1. The vibration-rotation levels of acetylene are probably the most extensively studied of any tetra-atomic molecule and recent work by Perry and Herman[1] used a polyad-based model to describe the levels to energies well above these accessed here ($\sim 7500 \text{ cm}^{-1}$) based on fitting to all spectroscopic data available at the time. Due to the extensive vibrational and vibration-rotation coupling in the upper states of the measured transitions, the upper energy levels cannot be well represented by a simple $J(J+1)$

polynomial expansion. To identify perturbations in these levels, the upper state energies were determined, using known[1] lower state level positions then were fit to a polynomial expansion in the rotational quantum numbers to identify outliers. Figure 2 illustrates the results; there are clear localized perturbations

in certain rotational levels that have not previously been identified, but which are brought out by the analysis. These perturbations derive from local avoided crossings of levels of the same J in the polyad eigenvalues and the Perry-Herman model gets the pattern of shifts qualitatively, but not quantitatively,

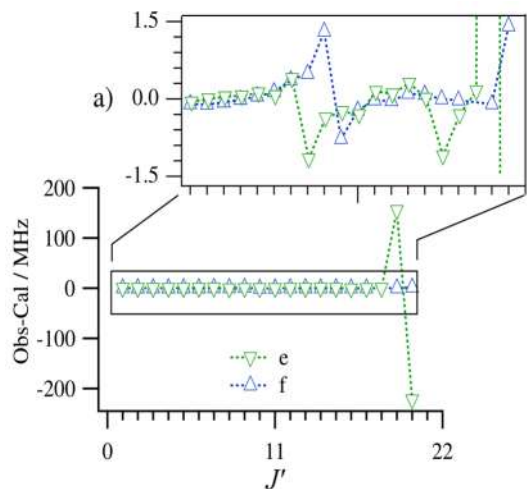


Figure 2: Residual plots (observed-calculated energy) for the upper levels in v_4 hot band transitions. Deviations from a smooth curve represent perturbed levels. The inset shows an expanded region illustrating the smaller shifts.

correct. The importance of the measurements is that they open up a way of accessing the positions of high bending vibration and angular momentum that are very difficult to access in other ways.

positions of a number of hot band lines underlying the main line of interest (P(11) of v_1+v_3), and developed a new multi-spectrum HTP fitting code in MATLAB. The results bring out some interesting aspects of multi-spectrum line shape fits to very precise data and quantify the errors associated with inaccurately accounting for weak underlying contaminating lines, such as those from hot band transitions. This work is currently being written up for publication.

C. Free Radical Spectroscopy

The laboratory at BNL was in temporary space for approximately three years and the move to permanent refurbished labs has just been completed. The transient absorption spectrometer has been reconstructed and we have obtained new spectra of C_2H radical near 7450 cm^{-1} . C_2H is an important combustion species and much work was carried out by the Curl group in the mid-IR more than a decade ago. The existence of spectroscopic transitions to mixed electronic character states in the near-IR has been known from theory and matrix spectroscopy, but the spectra were not previously observed in the gas phase until now. The band predicted at 7450 cm^{-1} is expected to be strong and the observed lines seem to bear this out. This may be a useful spectroscopic tool for monitoring C_2H in future kinetics and dynamics studies and in any case opens a window to the region of very strong vibronic mixing in the radical.

II. Future Work

A. Line shape and sub-Doppler measurements

Measurement of rest frequency line positions in hot band lines of C_2H_2 in the $1.55\mu\text{m}$ region are continuing to higher rotational levels. Limited by the current spectrometer sensitivity, we can reach levels with $J = 30$ in the bending hot bands. Initial results show Coriolis and anharmonic couplings combine to

B. Line Shape Studies

The Voigt profile has long been used as the standard line shape model for data bases since it is simple to implement and fairly accurate. However, with ever-increasing measurement accuracy, and demands from users for more accurate modeling, an IUPAC task force has recommended a new line shape model, the Hartmann-Tran Profile (HTP), be adopted [2]. We have recently recorded and analyzed an extensive set of frequency comb-referenced line shape data for acetylene using the alternative precision line profile models, SDV and QSDV [3, 4]. To compare these results to what may be achieved using the new HTP model, we have added to the original data, frequency measured the

result in much stronger perturbations than were observed for levels up to $J = 20$, shown above. The Herman-Perry polyad model predicts larger and more numerous perturbations for the higher rotational energies, but we have yet to compare the measurements with the calculations. In fact, the polyad model, which is based upon a harmonic oscillator, rigid-rotor basis may well be reaching the limit of usability; there are already nearly 370 parameters included. Together with Hua-Gen Yu in our group, we are investigating whether a model based on a combined *ab-initio* potential surface and dynamics calculation using TETRAVIB plus rotation might be implemented.

Preliminary measurements of pressure-induced broadening in the saturation dip measurements described above have also been made. The signal-to-noise currently attainable means that high quality line shapes can be recorded over more than an order of magnitude in pressure variation. Intriguingly, the apparent broadening coefficient seems larger than determined from measurements of Doppler-broadened lines. To some extent, differences might be expected as the sub-Doppler measurement just samples a velocity group with zero velocity along the laser propagation direction as compared to an average over an isotopic sample in the Doppler-limited case and collisional averaging will be different. However, this would be expected to reduce the pressure broadening because the speed-dependent term will be smallest at line center. Other differences might be imagined, for example a pressure dependent effect on the transit-time broadening as the diffusion constant decreases. But this would also be expected to reduce broadening compared to the Doppler background at higher pressures. We plan to investigate these observations more carefully in the near future.

B. Free radical spectroscopy and dynamics

Work will continue on the recently-observed C_2H spectrum described above. In addition, we have borrowed an infrared quantum cascade laser with coverage in the $5.4\mu m$ region. This laser provides more than 100mW with narrow line output over a tuning range of several hundred cm^{-1} . Previously, high resolution laser spectroscopy in this region was limited by the low power and tunability of Pb-salt diode lasers. With the QCL, we plan to return to a project started several years ago, but abandoned for technical reasons and related to work described in Greg. Hall's abstract. The collision-induced (CI) intersystem crossing (ISC) in CH_2 is of continuing interest. As is well known from work by ourselves and others, singlet-triplet ISC in CH_2 is mediated by a small set of rotational levels in the singlet that have appreciable triplet character. CI rotational energy transfer effects ISC since a singlet CH_2 molecule in one of the mixed levels has a finite chance that the next collision will result in a triplet radical.

To now, we have been able to follow loss of singlet state population but have not been able to monitor that population arriving in the triplet manifold because there has been no spectroscopic technique available to monitor the vibrationally excited triplet state molecules formed in the initial ISC step. The new QCL should permit direct detection of vibration-rotation transitions to and from the initially populated triplet levels and spectral searches for the transitions expected in the $5.4\mu m$ region are planned to begin very soon.

III. Publications supported by this project since 2013

Argon-induced pressure broadening, shifting and narrowing in the $CN A^2\Pi - X^2\Sigma^+$ (1-0) band, D. Forthomme, C. P. McRaven, T. J. Sears, and G. E. Hall. *J. Phys. Chem. A* **117**, 11837-46 (2013).
<http://dx.doi.org/10.1021/jp4030359>

The enhancement of triplet stability in benzene by substituents with triple bonds, P. M. Johnson, and T. J.

- Sears, *J. Phys. Chem. A* **117**, 7786-93 (2013). <http://dx.doi.org/10.1021/jp403727f>
- Temperature-dependent, nitrogen-perturbed line shape measurements in the $\nu_1+\nu_3$ band of acetylene using a diode laser referenced to a frequency comb, M. J. Cich, D. Forthomme, C. P. McRaven, G. V. Lopez, G. E. Hall, T. J. Sears, A. W. Mantz, *J. Phys. Chem. A* **117**, 13908-13918 (2013) <http://dx.doi.org/10.1021/jp408960e>
- An experimental and theoretical study of the electronic spectrum of HPS, a second row HNO analog, R. Grimminger, D. J. Clouthier, R. Tarroni, Z. Wang and T. J. Sears, *J. Chem. Phys.* **139**, 174306(12) (2013). <http://dx.doi.org/10.1063/1.4827099>
- Collinear two-color saturation spectroscopy in CN A-X (1-0) and (2-0) bands, D. Forthomme, C. P. McRaven, T. J. Sears, and G. E. Hall, *J. Molec. Spectrosc.* **296**, 36-42 (2014) <http://dx.doi.org/10.1016/j.jms.2013.12.006>
- Frequency Comb-Referenced Spectroscopy in the $\nu_1 + \nu_3$ Region of Acetylene, M.J. Cich, D. Forthomme, G.E. Hall, C.P. McRaven, T.J. Sears, S. Twagirayezu, *The 13th Biennial HITRAN Conference (HITRAN13), Harvard-Smithsonian Center for Astrophysics, Cambridge, MA, USA, 23-25 June, 2014.*, <http://dx.doi.org/10.5281/zenodo.11181>
- Doppler-Resolved Kinetics of Saturation Recovery, D. Forthomme, M. L. Hause, H-G. Yu, P. J. Dagdigian, T. J. Sears, and G. E. Hall, *J. Phys Chem A*, (in press, 2015).
- Frequency-comb referenced spectroscopy of ν_1 and ν_3 hot bands in the $\nu_1 + \nu_3$ combination band of C_2H_2 , S. Twagirayezu, M. J. Cich, T. J. Sears, C. P. McRaven, and G. E. Hall, *J. Molec. Spectrosc.* (submitted, 3/2015)

IV. Cited Literature

- [1] M. Herman, D.S. Perry, *Molecular spectroscopy and dynamics: A polyad-based perspective*, *PCCP* **15** (2013) 9970-9993.
- [2] J. Tennyson, P.E. Bernath, A. Campargue, A.G. Császár, L. Daumont, R.R. Gamache, J.T. Hodges, D. Lisak, O.V. Naumenko, L.S. Rothman, H. Tran, N.F. Zobov, J. Buldyreva, C.D. Boone, M.D.D. Vizia, L. Gianfrani, J.M. Hartmann, R. McPheat, D. Weidmann, J. Murray, N.H. Ngo, O.L. Polyansky, *Recommended isolated-line profile for representing high-resolution spectroscopic transitions*, *Pure Appl. Chem.* **86** (2014) 1931-1943.
- [3] M. Cich, C. McRaven, G. Lopez, T. Sears, D. Hurtmans, A. Mantz, *Temperature-dependent pressure broadened line shape measurements in the $\nu_1 + \nu_3$ band of acetylene using a diode laser referenced to a frequency comb*, *Applied Physics B: Lasers and Optics* **109** (2012) 373-384.
- [4] M.J. Cich, D. Forthomme, C.P. McRaven, G.V. Lopez, G.E. Hall, T.J. Sears, A.W. Mantz, *Temperature-Dependent, Nitrogen-Perturbed Line Shape Measurements in the $\nu_1 + \nu_3$ Band of Acetylene Using a Diode Laser Referenced to a Frequency Comb*, *The Journal of Physical Chemistry A* (2013).

Theoretical Studies of Potential Energy Surfaces and Computational Methods

Ron Shepard

Chemical Sciences and Engineering Division,
Argonne National Laboratory, Argonne, IL 60439
[email: shepard@tcg.anl.gov]

Program Scope: This project involves the development, implementation, and application of theoretical methods for the calculation and characterization of potential energy surfaces (PES) involving molecular species that occur in hydrocarbon combustion. These potential energy surfaces require an accurate and balanced treatment of reactants, intermediates, and products. This difficult challenge is met with general multiconfiguration self-consistent field (MCSCF) and multireference single- and double-excitation configuration interaction (MR-SDCI) methods. In contrast to the more common single-reference electronic structure methods, this approach is capable of describing accurately molecular systems that are highly distorted away from their equilibrium geometries, including reactant, fragment, and transition-state geometries, and of describing regions of the potential surface that are associated with electronic wave functions of widely varying nature. The MCSCF reference wave functions are designed to be sufficiently flexible to describe qualitatively the changes in the electronic structure over the broad range of molecular geometries of interest. The necessary mixing of ionic, covalent, and Rydberg contributions, along with the appropriate treatment of the different electron-spin components (e.g. closed shell, high-spin open-shell, low-spin open-shell, radical, diradical, etc.) of the wave functions are treated correctly at this level. Further treatment of electron correlation effects is included using large-scale multireference CI wave functions, particularly including the single and double excitations relative to the MCSCF reference space.

Recent Progress: ELECTRONIC STRUCTURE CODE MAINTENANCE, DEVELOPMENT, AND APPLICATIONS: A major component of this project is the development and maintenance of the COLUMBUS Program System. The COLUMBUS Program System computes MCSCF and MR-SDCI wave functions, MR-ACPF (averaged coupled-pair functional) energies, MR-AQCC (averaged quadratic coupled cluster) energies, spin-orbit CI energies, analytic energy gradients, and nonadiabatic coupling. Geometry optimizations to equilibrium and saddle-point structures can be done automatically for both ground and excited electronic states. The COLUMBUS Program System is maintained and developed collaboratively with several researchers including Russell M. Pitzer (Ohio State University), Thomas Mueller (Jülich Supercomputer Center, Germany), and Hans Lischka (University of Vienna, Austria, and Texas Tech University). The nonadiabatic coupling and geometry optimization for conical intersections is done in collaboration with David R. Yarkony (Johns Hopkins University). The distributed development effort and software coordination uses an svn repository of source code. The parallel sections of the code are based on the single-program multiple-data (SPMD) programming model with explicit message passing using the portable MPI library, and the portable Global Array Library (distributed from PNNL) is used for data distribution. The COLUMBUS codes incorporate several of the newer language features of F90 and later in order to facilitate future development and maintenance efforts.

<p>This work was performed under the auspices of the Office of Basic Energy Sciences, Division of Chemical Sciences, Geosciences, and Biosciences, U.S. Department of Energy, under contract number DE-AC02-06CH11357.</p>
--

GRAPHICALLY CONTRACTED FUNCTION METHOD: We have developed a novel expansion basis for electronic wave functions [see *J. Chem. Phys.* **141**, 064105 (2014) and references therein]. In this approach, the wave function is written as a linear combination of *graphically contracted functions* (GCF), and each GCF in turn is formally equivalent to a linear combination of configuration state functions (CSFs) that comprise an underlying full-CI linear expansion space of dimension N_{csf} . The CSF coefficients that define the GCFs are nonlinear functions of a smaller number of variables $N_{\varphi} \ll N_{\text{csf}}$. Relatively compact GCF expansions with $N_{\text{GCF}}=10$ to 20 basis functions can approach the full-CI PES to within chemical accuracy (1 kcal/mole or better). The method is formulated in terms of spin-eigenfunctions using the Graphical Unitary Group Approach (GUGA) of Shavitt, thereby eliminating artifacts that result from spin contamination or spin instability. No intrinsic restrictions are imposed on the orbital occupations, and in particular there are no artificial excitation-level or occupation restrictions with respect to a reference function or reference space; in this sense, the method is more correctly characterized as a multiconfigurational method rather than a multireference method. Because the wave function is a linear combinations of N_{GCF} basis functions rather than a single expansion term, the method is variational and may be applied to both ground and excited electronic states. Our recent focus has been on the development and implementation of a *multifacet* generalization of the GCF method in which each MFGCF has more flexibility than the previous single facet (SFGCF) expansion form. The individual CSF coefficients within an MFGCF are given by an ordered product of rectangular arc factor arrays; this means that it is formally a *matrix product state* (MPS), and the resulting wave function corresponds to a linear combination of such MPSs.

Because the underlying formalism is based on *Shavitt Graphs*, it is possible to analyze the resulting wave functions graphically using a generalization of this same representation called the *graph density*. The GCF expansion form allows the qualitative nature of the wave function to be extracted from potentially very large underlying linear expansions ($>10^{200}$ CSFs have been computed). In this representation, node (arc) density is defined as the sum of the square of all CSF coefficients that pass through that particular node (arc). The node density is displayed graphically as a circle whose area is proportional to the associated density. Several examples of this wave function analysis have been discussed in *Theor. Chem. Acc.* **133**, 1512 (2014). One interesting example is the set of dissociations, $C_2(X^1\Sigma_g^+, B^1\Delta_g, B'^1\Sigma_g^+) \rightarrow 2C(^3P)$, which are important to combustion, soot formation, and to interstellar chemistry. These states are the lowest 1A_1 states in the C_{2v} point group. State-averaged MFGCF calculations with equal weights with eight electrons in the eight valence orbitals were performed and the resulting graph densities were computed for all states along the dissociation curves. The dissociation curves are shown for reference in Fig. 1. The node density for the $B^1\Delta_g$ state at $R=2.25a_0$ is shown in Fig. 2. This is a multiconfigurational wave function that corresponds to the two configurations $2\sigma_g^2 2\sigma_u^2 1\pi_{u,x}^2 3\sigma_g^2$ and $2\sigma_g^2 2\sigma_u^2 1\pi_{u,y}^2 3\sigma_g^2$ with equal coefficient magnitudes and opposite signs. (The core= $[1\sigma_g^2 1\sigma_u^2]$ is not shown in the density graphs.) The node density plots for the $X^1\Sigma_g^+$ and $B'^1\Sigma_g^+$ states are shown for $R=2.25a_0$, $R=3.50a_0$, and $R=6.00a_0$ in Fig. 3. At the shorter distance, the $X^1\Sigma_g^+$ state is nominally the configuration $2\sigma_g^2 2\sigma_u^2 1\pi_{u,x}^2 1\pi_{u,y}^2$ with a coefficient of 0.84, although some significant multiconfigurational character is evident even near the equilibrium geometry due to the configuration $2\sigma_g^2 1\pi_{u,x}^2 1\pi_{u,y}^2 3\sigma_g^2$ with a coefficient of 0.39. The $B'^1\Sigma_g^+$ state at this short distance is a multiconfigurational state comprised predominantly of the same two CSFs as the $B^1\Delta_g$ state, but for which the coefficients have the same sign. At the intermediate bond distance $R=3.50a_0$, two things may be seen to occur. The first is an avoided crossing between the configurations comprising the $X^1\Sigma_g^+$ and $B'^1\Sigma_g^+$ states. This is seen in the

middle panels of Fig. 3 where the node densities are swapped relative to the $R=2.25a_0$ densities. The other important feature, seen in Fig. 1, is that the $B^1\Delta_g$ state, which is qualitatively unchanged from $R=2.25a_0$ in Fig. 2, crosses the $X^1\Sigma_g^+$ state. This is an allowed crossing. For the longer bond distances, the $X^1\Sigma_g^+$ node densities are similar to the $B^1\Sigma_g^+$ $R=2.25a_0$ densities, reflecting the nature of the avoided crossing along the dissociation curves, while the $B^1\Sigma_g^+$ node densities have begun to display open-shell character that is consistent with the atomic fragments.

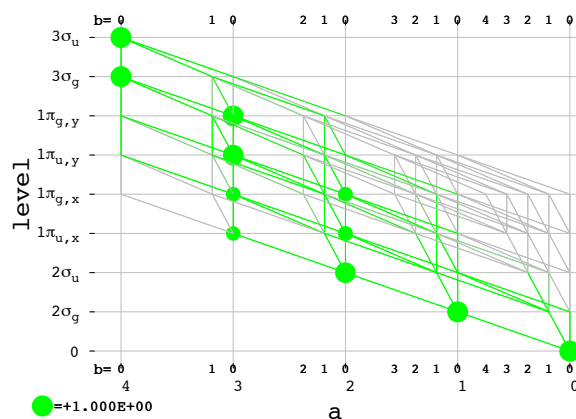
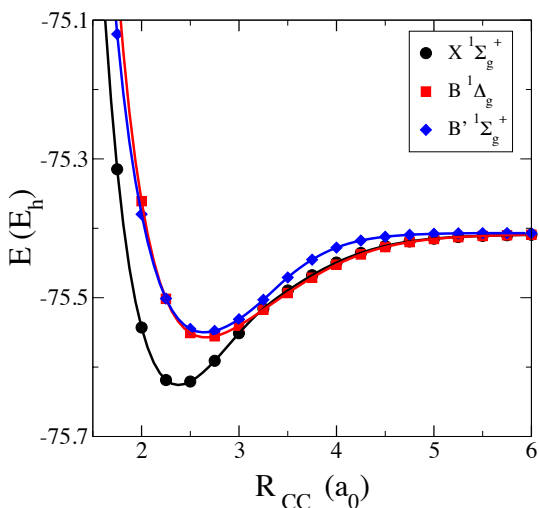


Fig. 1 Potential energy curves for the dissociation of the lowest three 1A_1 states of C_2 . **Fig. 2** Graph density plot for the $B^1\Delta_g$ state at $R=2.25a_0$.

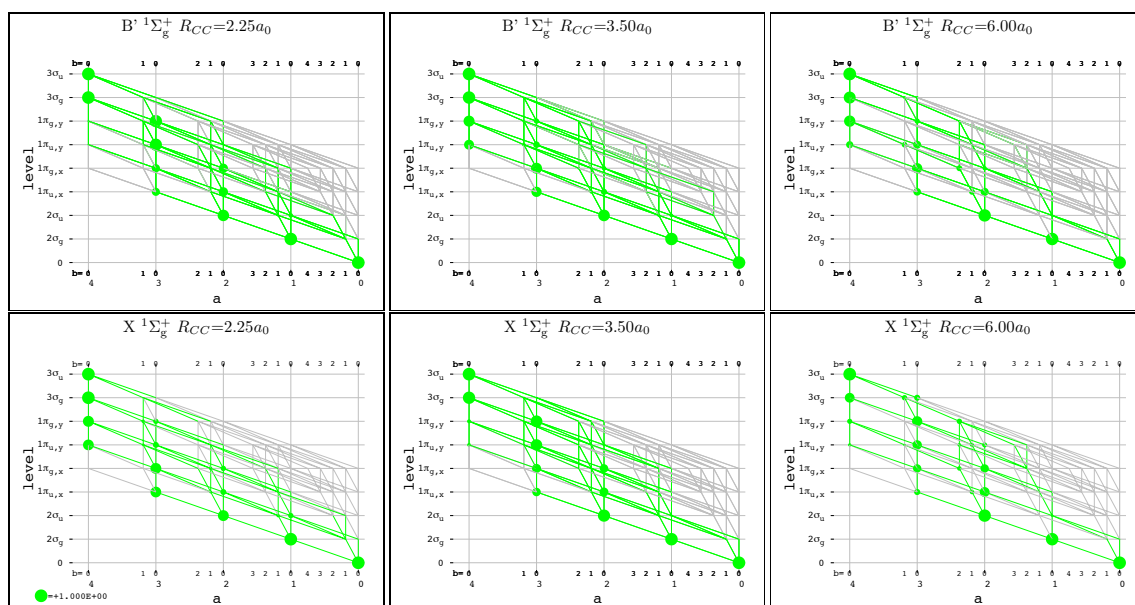


Fig. 3 Graph density plots for the $X^1\Sigma_g^+$ and $B^1\Sigma_g^+$ states at $R=2.25a_0$, $R=3.50a_0$, and $R=6.00a_0$.

Future Plans: Our MFGCF implementation has so far used single-headed Shavitt graphs appropriate for describing individual molecular states with a given number of electrons, with a particular spin state, and that belong to a particular point group irreducible representation (irrep). We will generalize this in several respects including the ability to average over multiple irreps, the ability to average states described with multiheaded Shavitt graphs, and the ability to allow multiple facets for the head nodes. These generalizations will allow the computation of Hamiltonian matrix elements corresponding to states with different numbers of electrons, different spin values, and different irreps simultaneously with only a relatively small increase in effort over the current single-state approach, allowing multistate calculations to approach the efficiency of the current single-state calculations. With these generalizations, the computation of transition properties is facilitated by the fact that all states are described with the same set of arc factors.

Publications:

- “Multiconfiguration Self-Consistent Field and Multireference Configuration Interaction Methods and Applications,” P. G. Szalay, T. Mueller, G. Gidofalvi, H. Lischka, R. Shepard, *Chem. Rev.* **112**, 108-181 (2012).
- “The Multiradical Character of One- and Two-Dimensional Graphene Nanoribbons,” F. Plasser, H. Pašalić, M. H. Gerzabek, F. Libisch, R. Reiter, J. Burgdörfer, T. Müller, R. Shepard, and H. Lischka, *Angewandte Chemie International Edition* **52**, 2581-2584 (2013).
- “Der Multiradikalcharakter ein- und zweidimensionaler Graphen-Nanobänder,” F. Plasser, H. Pašalić, M. H. Gerzabek, F. Libisch, R. Reiter, J. Burgdörfer, T. Müller, R. Shepard, and H. Lischka, *Angewandte Chemie* **125**, 2641-2644 (2013).
- “Graphically Contracted Function Electronic Structure Method,” R. L. Shepard, G. Gidofalvi, and S. R. Brozell, *Abstracts of Papers of the American Chemical Society* **246**, 159-PHYS (2013).
- “Comparison of Multireference Configuration Interaction Potential Energy Surfaces for $H+O_2 \rightarrow HO_2$: The Effect Of Internal Contraction,” L. B. Harding, S. J. Klippenstein, H. Lischka, and R. Shepard, *Theor. Chem. Acc.* **133**, 1429 (2014).
- “Wave Function Analysis with Shavitt Graph Density in the Graphically Contracted Function Method,” G. Gidofalvi, S. R. Brozell, and R. Shepard. *Theor. Chem. Acc.* **133**, 1512 (2014).
- “Wave function analysis with Shavitt graph density in the graphically contracted function method,” G. Gidofalvi, S. Brozell, R. Shepard, *Abstracts of Papers of the American Chemical Society* **248**, 450-COMP (2014).
- “The Multifacet Graphically Contracted Function Method. I. Formulation and Implementation,” R. Shepard , G. Gidofalvi, and S. R. Brozell. *J. Chem. Phys.* **141**, 064105 (2014).
- “The Multifacet Graphically Contracted Function Method. II. A General Procedure for the Parameterization of Orthogonal Matrices and its Application to Arc Factors,” R. Shepard , G. Gidofalvi, and S. R. Brozell. *J. Chem. Phys.* **141**, 064106 (2014).

In collaboration with N. J. Labbe and S. J. Klippenstein, we have used ab-initio based kinetics estimates for well-skipping radical-radical reactions of relevance to low-pressure flames for ethanol [4] and methyl formate [5]. These theoretical rate constants are then used in a kinetic model to assess their potential contributions to intermediate species formation in these low pressure flames [4,5]. Low pressure ethanol flame simulations indicate that addition-eliminations from $\text{H} + \text{CH}_3\text{CHOH}$ and $\text{CH}_3 + \text{CH}_3\text{CHOH}$ are a major source for C_2H_4 and C_3H_6 respectively. Simulations of low-pressure methyl formate flames indicate that addition-eliminations from $\text{H} + \text{CH}_2\text{OCHO}$ and $\text{CH}_3 + \text{CH}_2\text{OCHO}$ have a significant impact on CH_3OH and C_2H_4 predictions respectively. For acetaldehyde, rate constant estimates for $\text{H} + \text{CH}_2\text{CHO}$ and $\text{CH}_3 + \text{CH}_2\text{CHO}$ addition-elimination reactions were based on analogies from our ethanol and methyl formate theoretical studies. Inclusion of these reactions is shown to affect predictions of acetaldehyde flame speeds [6] by 2-3 cm/s. The present results suggest that addition-elimination reactions of relatively stable fuel radicals with ubiquitous flame radicals such as H, O, OH and CH_3 should be considered in combustion models.

In collaboration with J. V. Michael, L. B. Harding, and S. J. Klippenstein, we have conclusively [ref. 7 in section V] demonstrated the role of these bimolecular well-skipping reactions to explain product observations [2] from CH_3CHO pyrolysis using a micro-tubular reactor (see Fig. 1 above). Preliminary theoretical studies on $\text{H} + \text{CH}_3\text{CHO}$ and $\text{H} + \text{CH}_3\text{COCH}_3$ also indicate that addition-eliminations can occur in these reactions to form CH_2O and CH_3CHO respectively. While addition-elimination to form CH_2O is a minor process in $\text{H} + \text{CH}_3\text{CHO}$ [7], addition to form $\text{CH}_3\text{CH}(\text{O})\text{CH}_3$ radical is the lowest-energy pathway in $\text{H} + \text{CH}_3\text{COCH}_3$. We have initiated theoretical calculations to model micro-tubular experiments on these bimolecular reactions by Prozument and collaborators.

B. Thermal decompositions of iso-propanol, xylyl radicals

We continue our experiment/theory collaborations with J. V. Michael and S. J. Klippenstein. In the past year we have extended our thermal decomposition studies to higher alcohols such as iso-propanol. The formation of H-atoms was measured behind reflected shock waves by using atomic resonance absorption spectrometry (ARAS) over a temperature range of 1190–1450 K at different pressures ranging from 0.2 – 0.85 bar. Selectively deuterated iso-propanol decomposition experiments were also performed to characterize the contributions of the various dissociation channels and to gain mechanistic insights into the decomposition of the CH_3CHOH -radical formed by the dominant bond-dissociation, $i\text{-C}_3\text{H}_7\text{OH} \rightarrow \text{CH}_3\text{CHOH} + \text{CH}_3$. Theoretical predictions for this bond fission are found to be in good agreement with the present experimental data. Since the bimolecular reaction, $\text{H} + \text{iso-propanol}$, is an important fuel destruction process at high temperatures, the kinetics of this reaction was also experimentally characterized. Since H-atoms form from the thermal decomposition of iso-propanol, unambiguous measurements for this reaction rate required the use of a surrogate, $\text{D} + \text{iso-propanol}$, with the assumption that the kinetic isotope effect is close to unity. Measurements of D-atom profiles using D-ARAS allowed unambiguous rate constant measurements for the reaction $\text{D} + \text{iso-propanol} \rightarrow \text{HD} + \text{CH}_3\text{CH}(\text{OH})\text{CH}_2$ ($980 \text{ K} \leq T \leq 1250 \text{ K}$; $P \sim 0.4 \text{ bar}$). The bimolecular reaction of $\text{H/D} + \text{iso-propanol}$ was theoretically characterized to enable comparisons to experiment and extrapolation of the kinetics over a wide T-range.

In collaboration with J.V. Michael, S.J. Klippenstein, D. Polino and C. Cavallotti (Politecnico Milano), we have initiated a joint experiment-theory study of o-xylylbromide dissociation as a source for o-xylyl radicals and the subsequent dissociation kinetics of o-xylyl. o-xylyl radicals were produced via flash photolysis o-xylylbromide ($\text{o-CH}_3\text{C}_6\text{H}_4\text{CH}_2\text{Br}$) in a shock tube. Br-ARAS measurements confirm that at high-T ($>1200 \text{ K}$) o-xylyl radicals are generated instantaneously. The high sensitivity H-atom ARAS detection technique has been used to obtain quantitative measurements of the H-atom yields, and rate coefficients, for o-xylyl decomposition. These H-ARAS experiments span a temperature range of 1267-1597 K, and a pressure range of 0.3-1.0 atm. Computationally, the branching ratios for decomposition of o-xylylbromide to o-xylyl + H and o-xylylene + HBr were determined using VRC-TST and RRKM theories combined with master equation simulations on Potential Energy Surfaces (PES) determined at the CASPT2, M06-2X/6-311+G(d,p), and CBS-QB3 levels, finding that only 20-30% of o-

CH₃C₆H₄CH₂Br decomposes to o-xylyl in reasonable agreement with the present experiments. Theoretical predictions indicate that subsequent H-atom loss from o-xylyl is the major dissociation pathway in agreement with the present experimental observations.

C. Developing detailed and reduced chemical kinetics models for engine simulations

We continue our collaborations with M.J. Davis (Argonne), S. Som, D.E. Longman and S. Goldsborough (Engines & Emissions group at Argonne) on developing reduced and detailed kinetics models and their subsequent analyses for realistic engine modeling studies of diesel and biodiesel surrogates. Global sensitivity analysis (GSA) was used to identify reactions relevant to auto-ignition from practical engine simulations. We also propose to initiate kinetics modeling studies on dimethylether, DME, as a simple real fuel. Detailed kinetics without model reduction can be directly applied for DME in engine simulations and offers a test for the chemistry under practical conditions.

D. A detailed analysis of methanol and methylformate combustion kinetics

In collaboration with N.J. Labbe, S.J. Klippenstein, and the group of Y. Ju (Princeton University), an updated model for methanol combustion was developed. This joint effort was initiated to probe the kinetics of the simplest methylester, methylformate. Initial simulations indicated that methanol (as the dominant intermediate from methylformate) and its sub-set mechanisms required a substantial update. In particular, the methanol model includes new theoretical kinetics predictions for the decomposition of CH₂OH, CH₃O, with a re-analysis of the numerous H-atom abstractions from methanol by H, OH, CH₃, HO₂, and O₂. Simulations with the model indicate good agreement with literature data from shock-tubes, reactors, and flames (see Fig. 2). Recommendations for methanol combustion studies are also presented.

III. Future work

We have completed our small alcohol (C₁-C₂) combustion modeling/theoretical studies and plan to use this kinetics experiment/theory based methodology to develop kinetics models for selected C₃-C₄ alcohols. We also propose to initiate joint experiment/theory studies on C₃-C₄ aldehydes. Our current efforts on modeling methylformate combustion are expected to lead into systematic modeling studies of larger C₂-C₄ methylesters. The effects of stable fuel-radical + H/CH₃/OH reactions will be systematically explored for larger oxygenated molecules.

IV. References

1. C.A. Taatjes, N. Hansen, J.A. Miller, T.A. Cool, J. Wang, P.R. Westmoreland, M.E. Law, T. Kasper, K. Kohse-Höinghaus, *J. Phys. Chem. A* **2006**, 110, 3254-3260.
2. A. Vasiliou, K.M. Piech, B. Reed, X. Zhang, M. R. Nimlos, M. Ahmed, A. Golan, O. Kostko, D.L. Osborn, D. E. David, K. N. Urness, J.W. Daily, J.F. Stanton, G.B.; Ellison, *J Chem. Phys.* **2012**, 137, 164308.
3. Prozument, K.; Suleimanov, Y. V.; Buesser, B.; Oldham, J. M.; Green, W. H.; Suits, A. G.; Field, R. W. *J. Phys. Chem. Lett.* **2014**, 5, 3641-3648.
4. H. Xu, C. Yao, T. Yuan, K. Zhang, H. Guo, *Combust. Flame* **2011**, 158, 1673-1681.
5. S. Dooley, F.L. Dryer, B. Yang, J. Wang, T.A. Cool, T. Kasper, N. Hansen, *Combust. Flame* **2011**, 158, 732-741.
6. M.T. Abebe, *Laminar Burning Velocity of Ethanol, Acetaldehyde, and Ethanol-Acetaldehyde Flames*, Master's Thesis, Lund University, June 2013.
7. R. Sivaramakrishnan, J. V. Michael, S. J. Klippenstein, *J. Phys. Chem. A* **2010**, 114, 755-764.

V. Journal articles supported by this project 2013-2015

1. S. L. Peukert, R. Sivaramakrishnan, M.-C. Su, and J. V. Michael, "High temperature rate constants for H/D + methylformate and methylacetate", *Proc. Combust. Inst.* **34**, 463-471 (2013).
2. R. Sivaramakrishnan, W. Liu, M. J. Davis, S. Som, D. E. Longman, and T. F. Lu, "Development of a reduced biodiesel surrogate model for compression ignition engine modeling", *Proc. Combust. Inst.* **34**, 401-409 (2013).
3. S. L. Peukert, R. Sivaramakrishnan, and J. V. Michael, "High temperature shock tube and theoretical studies on the thermal decomposition of dimethylcarbonate and its bimolecular reactions with H and D-Atoms", *J. Phys. Chem. A* **117**, 3718-3728 (2013).
4. S. L. Peukert, R. Sivaramakrishnan, and J. V. Michael, "High temperature shock tube studies on the thermal dissociation of O₃ and the reaction of dimethyl carbonate with O-atoms", *J. Phys. Chem. A* **117**, 3729-3738 (2013).
5. S. Som, W. Liu, D. D. Y. Zhou, G. M. Magnotti, R. Sivaramakrishnan, D. E. Longman, R. T. Skodje, and M. J. Davis "Quantum Tunneling Affects Engine Performance", *J. Phys. Chem. Lett.* **4**, 2021-2025 (2013).
6. N. J. Labbe, R. Sivaramakrishnan, S. J. Klippenstein, "The Role of Radical + Fuel-Radical Well-Skipping Reactions in Ethanol and Methylformate Low-pressure Flames", *Proc. Combust. Inst.* **35** (2014) 447-455.
7. R. Sivaramakrishnan, J. V. Michael, L. B. Harding and S. J. Klippenstein, "Resolving some paradoxes in the thermal decomposition mechanism of CH₃CHO", In Press, 100 Years of Combustion Kinetics at Argonne: A Festschrift for Lawrence B. Harding, Joe V. Michael, and Albert F. Wagner, *J. Phys. Chem. A* **119**, (2015) doi: 10.1021/acs.jpca.5b01032
8. N. J. Labbe, P. Dievart, X. L. Yang, R. Sivaramakrishnan, S. J. Klippenstein, Y. Ju, "A detail analysis of the kinetics of methanol combustion", In Preparation, *Comb. And Flame* (2015).
9. D. Polino, R. Sivaramakrishnan, S. J. Klippenstein, J. V. Michael, C. Cavallotti "Experimental and theoretical studies on the thermal decomposition of xylyl radicals", In Preparation, *J. Phys. Chem. A* (2015).
10. S. L. Peukert, R. Sivaramakrishnan, S. J. Klippenstein, J. V. Michael, "Shock tube and theoretical kinetics studies on the thermal decomposition of iso-propanol and it's reaction with D-atoms", In Preparation, *J. Phys. Chem. A* (2015).

Other Publications and Presentations supported by this project 2013-2015

1. S. L. Peukert, R. Sivaramakrishnan, J. V. Michael, "Shock tube and modeling study on the pyrolysis of dimethyl carbonate and its reaction with D- and O-atoms", 8th US National Combustion Meeting, Park City, UT, May 19-22, 2013.
2. R. Sivaramakrishnan, N. J. Labbe, W Liu, M. J. Davis, "A high temperature mechanism for methylformate combustion", 8th US National Combustion Meeting, Park City, UT, May 19-22, 2013.
3. W. Liu, S. Som, D. D. Y. Zhou, R. Sivaramakrishnan, D. E. Longman, R. T. Skodje, M. J. Davis, "The role of individual rate coefficients in the performance of compression ignition engine models", 8th US National Combustion Meeting, Park City, UT, May 19-22, 2013.
4. D. Polino, C. Cavallotti, R. Sivaramakrishnan, S. J. Klippenstein, J. V. Michael, "The decomposition kinetics of xylyl radicals", 8th International Conference on Chemical Kinetics, Seville, Spain, July 8-12, 2013.
5. S. L. Peukert, R. Sivaramakrishnan, S. J. Klippenstein, J. V. Michael, "A shock tube and modeling study on the thermal decomposition of iso-propanol and its reaction with D-atoms", 8th International Conference on Chemical Kinetics, Seville, Spain, July 8-12, 2013.
6. N. J. Labbe, R. Sivaramakrishnan, S. J. Klippenstein, "The role of addition-elimination reactions in small oxygenate flames" Central States Section of the Combustion Institute, Tulsa, OK, Mar 16-18, 2014.

Quantum Chemistry of Radicals and Reactive Intermediates

John F. Stanton
Institute for Theoretical Chemistry
University of Texas
Austin, TX 78712
jfstanton@mail.utexas.edu

Scope of Research

My research group works in the area of theoretical chemical physics, especially on the thermodynamic properties, spectra, and reactions of organic radicals and other transient intermediates. In addition, we are active developers of software for computational electronic structure (quantum chemistry), computational and theoretical spectroscopy, and more recently, chemical kinetics. Our quantum chemistry research follows a number of paths, including first-principles calculations of bond energies and other thermochemical information (as well as development of methodology for such calculations), methods tailored for the analysis of molecular spectroscopy, especially for situations in which the Born-Oppenheimer approximation breaks down, and the development of *ab initio* methods suitable for the accurate treatment of transient organic molecules and radicals.

Summary of Recent Accomplishments

We have made a number of investigations in the area of chemical kinetics, work that is accomplished by a combination of very high-level *ab initio* methods (the “HEAT” protocol¹), master equation simulations, and the use of semiclassical transition state theory (SCTST)² to calculate the microcanonical rate constants that are needed for the master equation models. In addition, we have also developed a new computer code for chemical kinetics that is now available to the community. This code, named 2DME-SSS (an acronym for two-dimensional master equation, steady-state solution) solves an approximate two-dimensional master equation (energy and angular momentum) subject to a steady state approximation and an assumption that *J* does not change in collisions between the activated species and the bath gas. This program has been documented already in the literature, and is currently being applied to the ozonolysis reaction. Preliminary results suggest that the observed distribution of products (including the stabilized Criegee intermediate) is predicted quite accurately by the model and, significantly, that the angular momentum effects in this reaction are important.

In other work on chemical kinetics, we have investigated the quite remarkable finding regarding the Criegee intermediate that was made in the McCarthy laboratory at the Smithsonian Center for Astrophysics. Specifically, this celebrated molecule - first observed in the laboratory by Taatjes *et al.*³ after synthesis from halogenated precursors - was produced abundantly and with high selectivity in a simple electric discharge comprising just methane and oxygen in a carrier gas. This discovery would appear to have important atmospheric implications, as both CH₄ and O₂ are clearly atmospheric species, and an electric discharge is a proxy for atmospheric lightning.

¹A. Tajti *et al.* *J. Chem. Phys.* 121, 11599 (2004).

²W.H. Miller *Faraday Transactions* 62, 40 (1977).

³O. Welz, J.D. Savee, D.L. Osborn, S.S. Vasu, C.J. Percival, D.E. Shallcross, C.A. Taatjes *Science* 335, 204 (2012).

We have investigated the mechanism of this reaction and find the most plausible pathway to be one in which an O_2 molecule abstracts a hydrogen atom from CH_3O_2 , to produce the “cold” Criegee species, which is observed. In addition, a combined experimental-theoretical effort with the McCarthy laboratory yielded the precise equilibrium structure of the Criegee species, as well as a considerable amount of detailed information regarding its molecular properties. Finally, the reaction between ground-state oxygen atoms and the H_2 molecule – a vital reaction in the field of hydrogen combustion – has been investigated with high-level theory, and it is believed that we have determined the most accurate activated complex properties yet. Chemical kinetics calculations, which are of course quite sensitive to these parameters, give rate constants within 5 to 15% experiment over a temperature range of 300-3000 K, over which the rate constant varies by eight orders of magnitude. The results are excellent, both at the low temperatures where quantum tunneling is important and at the higher temperatures where anharmonicity (which is included via VPT2 in the SCTST theory) is the dominant complicating effect.

Like kinetics, our work in spectroscopy has involved both applications and new code development. The latter is a new code developed for massively parallel computing environments that significantly extends the range of applications that can be done with the vibronic coupling model of Köppel, Domcke and Cederbaum, which has been a workhorse in our research program for many years. Extending the first efforts in this area by Schuurman and Yarkony, this new code uses modern concepts from parallel programming, and is capable of doing calculations with direct product basis sets of dimension 10^{10-11} , meaning that molecules with 10-20 “important” vibrational coordinates can be treated accurately and comprehensively. This work is already being used to do a 13-mode, three electronic state simulation of butadiene and will soon also be applied to the tert-butoxy radical $(CH_3)_3O$. This latter molecule has a daunting number (13) of atoms which has an interesting Jahn-Teller spectrum and is being studied jointly by our group, the Miller group at Ohio State, and the Liu group at Louisville.

Our work on fourth-order vibrational perturbation theory (VPT4) based on the Watson Hamiltonian also progresses. We now have fully checked algebraic expressions for the linear, quadratic and cubic anharmonicity coefficients, and have carried out a number of calculations for the vibrational levels of small molecules. More interesting, however, is the use of VPT4 within the context of semi-classical transition state theory, where the extremely complicated algebraic expressions for the anharmonicity constants are essential. This work is ongoing and will be summarized in the next section.

In terms of quantum chemistry, the NCC program module that includes an extremely efficient treatment of quadruple excitation effects within coupled-cluster theory (the CCSDTQ and CCSDT(Q)) models, has undergone additional development. In addition to the energy calculation capabilities that are now part of the public release of the CFOUR program system – which have been documented recently in the literature – analytic derivatives and equation-of-motion methods have also been implemented for CCSD and CCSDT. The implementation of these extensions, which are vital for chemical applications, for the CCSDTQ method will be accomplished within a year.

Ongoing Research and Future Plans

Work is currently underway in a number of areas. As mentioned above, the VPT4 treatment of anharmonicity is being studied in the context of semiclassical transition state theory. Because of the high complexity of the equations, the first set of systems being studied are two-dimensional reactive systems, as exemplified by the collinear $H+H_2$ reaction. Using a well-known surface for this reaction, VPT4-based SCTST calculation have been done, and the results are neither spectacular nor are they tremendously disappointing. VPT2-based SCTST, which does so well for normal reactive systems, also fails here in the below-threshold region. This is an extremely anharmonic system, and it may well be that the energy level structure (these are the Siegert eigenvalues in

the context of a reactive system) are so poorly represented by a quantum number scheme that the semiclassical approximation fails, to say nothing of a perturbation treatment of it. As a result, we are developing a model system, which will transform from a purely harmonic barrier with harmonic bath (for which harmonic SCTST is exact) to a pathological system like collinear H + H₂ by variation of a parameter. A comparison of the VPT2- and VPT4-based approximations should be quite interesting.

Other work involves a grid-based (DVR) scheme for vibronic coupling calculations. This work, which is currently underway will extend the model to rovibronic coupling and various spin-orbit effects, and the grid-based picture should extend the range of problems treatable by these models significantly.

We also continue development of the NCC code and the study of chemical applications, although space prevents further details from being provided.

Students and Postdoctoral Supported:

T.L. Nguyen (postdoc) B. Xue (undergrad) H. Lee (undergrad)

References acknowledging DE-FG02-07ER15884 (mid-2014 through mid-2015)

M.C. McCarthy, L. Cheng, K.N. Crabtree, O. Martinez, T.L. Nguyen, C.C. Womack and J.F. Stanton The Simplest Criegee Intermediate (H₂C=OO): Isotopic Spectroscopy Equilibrium Structure and Possible Formation from Atmospheric Lightning, *J. Phys. Chem. Lett.* 4, 4133 (2013).

S.M. Rabidoux, V. Eijkhout and J.F. Stanton A Parallelization Strategy for Large-Scale Vibronic Coupling Calculations *J. Phys. Chem. A.* 118, 12059 (2014).

N.M. Kidwell, V. Vaquero-Vara, T.K. Ormond, G.T. Buckingham, D. Zhang, M.R. Nimlos, J.W. Daily, G.B. Ellison, J.F. Stanton and T.S. Zwier Chirped-Pulse Fourier Transform Microwave Spectroscopy Coupled with a Flash Vacuum Pyrolysis Micro-Reactor: Structural Determination of the Anti-Aromatic Molecule Cyclopentadienone, *J. Phys. Chem. Lett.* 5, 2201 (2014).

C.C. Womack, K.N. Crabtree, L. McCaslin, O. Martinez, R.W. Field, J.F. Stanton and M.C. McCarthy Gas-phase structure determination of dihydroxycarbene, one of the smallest stable singlet carbenes, *Angew. Chem.* 53, 4089 (2014).

L.T. Nguyen and J.F. Stanton Accurate Ab Initio Thermal Rate Constants for Reaction of the Ground-State Oxygen Atom with Molecular Hydrogen, and Isotopic Variants, *J. Phys. Chem. A* 118, 4918 (2014).

D.A. Matthews and J.F. Stanton Nonorthogonal Spin-Adaptation of High-Order Coupled-Cluster Methods. A New Implementation of Methods Involving Quadruple Excitations *J. Chem. Phys.* 142, 064108 (2015).

O. Martinez, K.N. Crabtree, C.A. Gottlieb, J.F. Stanton and M.C. McCarthy A Precise Molecular Structure of Phenyl, the Simplest Aryl Radical, *Angew. Chemie* 54, 1808 (2015).

Universal and State-Resolved Imaging Studies of Chemical Dynamics

Arthur G. Suits

Department of Chemistry, Wayne State University
5101 Cass Ave, Detroit, MI 48202
asuits@chem.wayne.edu

I. Program Scope

The focus of this program is on combining universal ion imaging probes providing global insight, with high-resolution state-resolved probes providing quantum mechanical detail, to develop a molecular-level understanding of chemical phenomena. Particular emphasis is placed upon elementary reactions important in understanding and predicting combustion chemistry. This research is conducted using state-of-the-art molecular beam machines, photodissociation, reactive scattering, and vacuum ultraviolet lasers in conjunction with ion imaging techniques. An ongoing parallel effort is made to develop new tools and experimental methods directed to these goals.

II. Recent Progress

Despite a gap in funding of this program associated with the forward-funding requirement, we have continued our studies along three directions. In the first, we have continued and extended our investigations of polyatomic reaction dynamics using crossed-beams with DC slice imaging. Secondly, we have continued to pursue the use of strong-field ionization as a universal but selective probe of reaction products. Thirdly, we have now begun to apply the chirped-pulse microwave technique in uniform supersonic flows (“CPUF”) to obtain detailed product branching in combustion-relevant reactions.

Systematic studies of polyatomic reaction dynamics. In the last abstract we described our study of Cl + alkene reactions. In these crossed-beam studies of Cl with a range of butene isomers we showed both the importance of the addition/elimination pathway and demonstrated, through theory in collaboration with Alex Mebel, that the latter reaction occurs exclusively by way of a roaming-type excursion of the Cl atom. Analogous results along with supporting direct dynamics calculations were subsequently reported by Orr-Ewing and coworkers.

In a new but related direction, we have begun a systematic investigation of F atom reactions with saturated hydrocarbons. Although F atoms are not important reactants in combustion, as a probe of fundamental reaction dynamics they offer a very informative contrast to the Cl atom reactions we have extensively studied in recent years. F atom reactions are similar to Cl atom reactions in many ways except with greatly increased exoergicity. In addition, the reactions are amenable to very accurate theoretical treatment. In our initial studies, we examined the reaction dynamics of F atom with selected alkanes using crossed beam scattering with DC slice ion imaging. The target alkanes were propane, n-butane and n-pentane. The product alkyl radicals are probed by 157 nm single photon ionization following reaction at a collision energy of 10 kcal.mol⁻¹. Reduced translational energy distributions for each system show similar trends with little of the reaction exoergicity appearing in translation. However, the pentane reaction shows a somewhat smaller fraction of available energy in translation than the other two, suggesting greater energy channeled into pentyl internal degrees of freedom. The center-of-angular distributions all show sharp forward scattering as well as backward scattering that increases with the size of the molecule.

Isomer-specific detection and imaging via “semi-soft” ionization. We have continued to explore the use of non-resonant strong-field ionization as a universal but selective probe of reaction products. In our most recent investigations, we have coupled this probe to a flash pyrolysis beam source. In this work we have

shown that we can use both the characteristic fragmentation patterns and the saturation intensities to

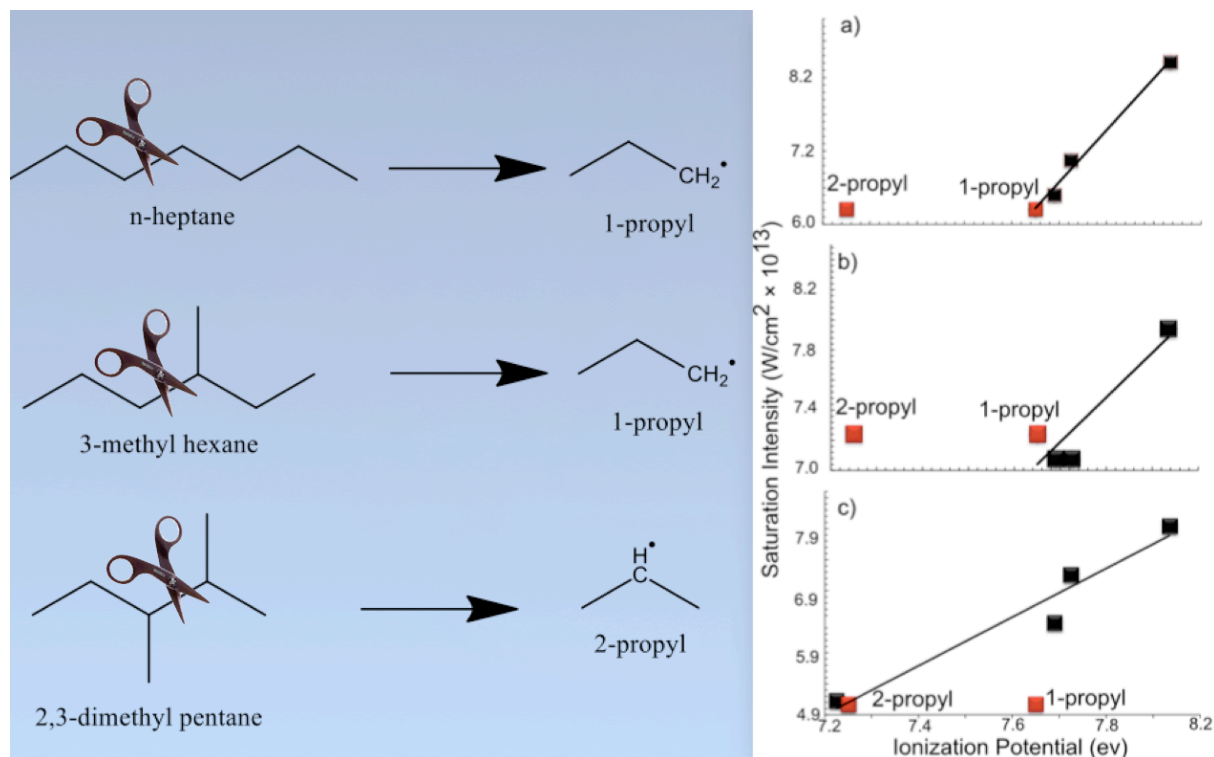


Fig. 1. Pyrolysis of heptane isomers yields distinct propyl radicals which are readily identified on the basis of their saturation intensities. Correlation of the saturation intensities of the various products with their vertical ionization energies is seen to match only for the anticipated propyl radicals.

achieve isomer selective product detection. Saturation intensities for non-resonant ionization are obtained by plotting the ion yield vs. the logarithm of the laser intensity, and finding the intercept of the linear region with the intensity axis. Saturation intensities reflect the ease of ionization, and show a strong correlation with the vertical ionization energy. An illustration of this approach is shown in Fig. 1 for propyl radicals from pyrolysis of heptane isomers. It is seen that the saturation intensities for the products do show a strong correlation with the ionization energies, and the 1- and 2-propyl radicals can be readily distinguished on the basis of their saturation intensities.

CPUF probe of product branching in bimolecular reactions. Nearly all kinetics studies report the observed rate of *reactant disappearance*, with product identity and branching largely unknown. This limitation arises from considerable experimental challenges inherent in the quantitative detection of the full range of products of a given reaction, particularly for large polyatomic systems. Recent advances have relied on the use of synchrotron photoionization or low-energy electron impact ionization to achieve selective product detection in dynamics, kinetics, and flame studies. Challenges remain, however, as these studies require fitting of composite, often incompletely resolved spectra to infer branching, and clear product signatures are often lacking. In collaboration with the Field group, we have developed an alternative approach to address this challenge, which incorporates chirped-pulse microwave spectroscopy in low-temperature uniform supersonic flows (“Chirped-pulse/uniform flow”, CUPF). This technique provides clear quantifiable spectroscopic signatures of polyatomic products in bimolecular or unimolecular reactions for virtually any species with a modest electric dipole moment. With this technique, bimolecular reactions can be initiated in a cold, thermalized, high-density molecular flow and a broadband microwave spectrum acquired for all products with rotational transitions within a chosen frequency window. In our first detailed bimolecular reaction we studied the CN + CH₃CCH system. All

four product channels are readily accessible and quantifiable with the CPUF technique; the spectra are

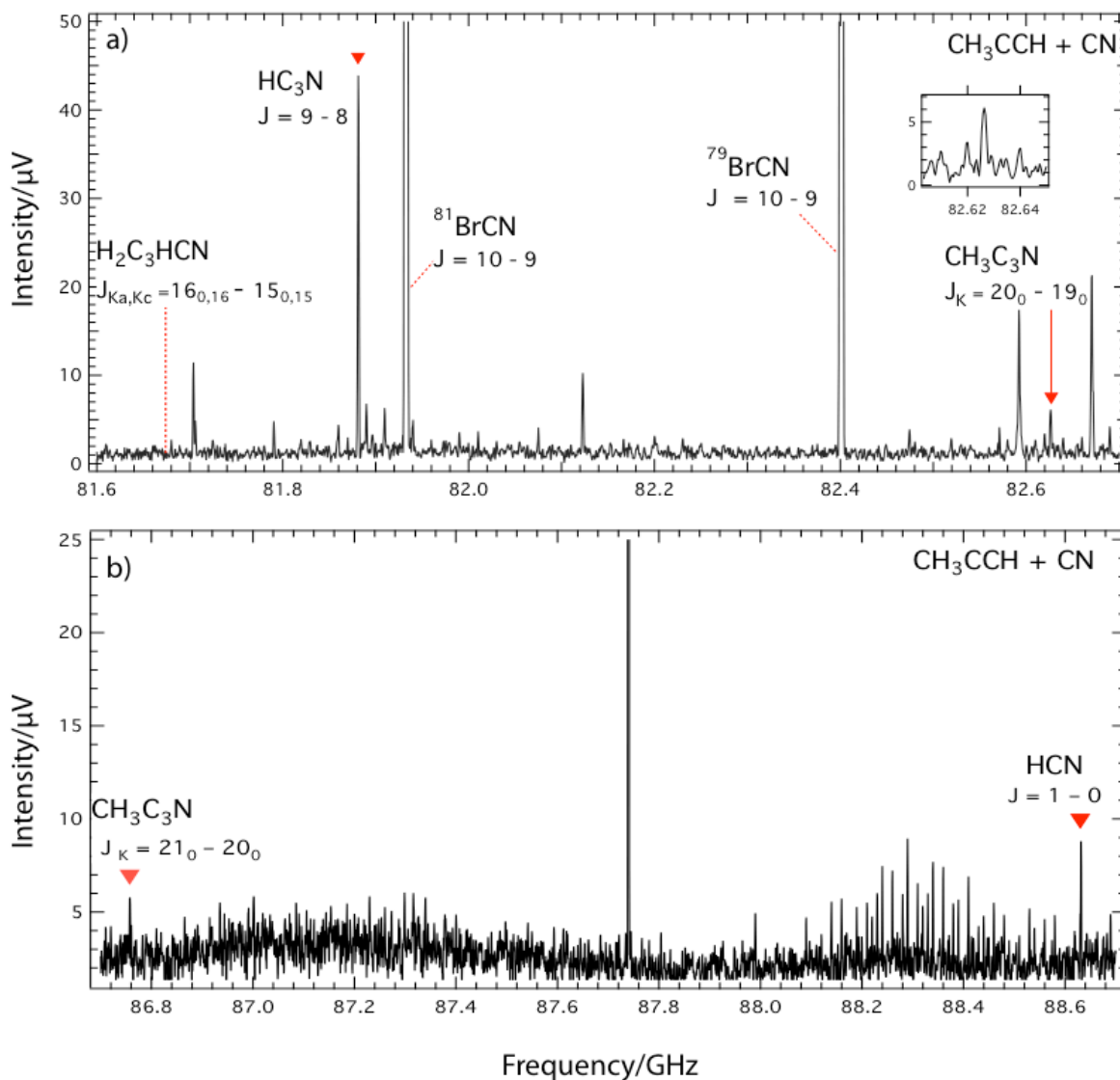


Fig. 2. Chirped-pulse Fourier transform microwave spectra for reaction products of the CN + propyne reaction. A) a segmented multichirp scan that targets transitions of HC_3N , CH_2CCHCN and CH_3CCCN ; $J=9-8$ transition at 81.881 GHz, $J_{K_a, K_c}=16_{0,16}-15_{0,15}$ at 81.674 GHz and $J_K=20_0 - 19_0$ at 82.627 GHz. The inset shows the $K=0,1,2,3$ transitions of CH_3CCCN . B) A broad scan from 86.63-88.73 GHz that targets the $J_{K_a, K_c}=17_{0,17}-16_{0,16}$ transition of CH_2CCHCN at 86.668 GHz, the $J_K=21_0-20_0$ transition of CH_3CCCN at 86.750 GHz, and the $J=1-0$ transition of HCN at 88.631 GHz. Each spectrum is averaged for 125000 acquisitions.

shown in Fig. 2. The reaction was found to yield HCN via a direct H-abstraction reaction, while indirect addition/elimination pathways to HC_3N , $\text{CH}_3\text{C}_3\text{N}$, and CH_2CCHCN were also probed. From these observations, quantitative branching ratios were established for all products as 12(5)%, 66(4)%, 22(6)% and 0(8)% into HCN , HC_3N , $\text{CH}_3\text{C}_3\text{N}$, and $\text{H}_2\text{C}_3\text{HCN}$, respectively. The values are consistent with statistical calculations based on new ab initio results at the CBS-QB3 level of theory. This work is a demonstration of CPUF as a powerful technique for quantitatively determining the branching into polyatomic products from a bimolecular reaction.

III. Selected Future Plans

State-resolved and universal crossed-beam DC slice imaging. We will continue our crossed-beam imaging studies with VUV probe. We have incorporated a new stacked-piezo valve that delivers intense short pulses, and we are interested in extending the range of radical species as reactants. We are also planning to extend our VUV probe to shorter wavelengths taking advantage of the techniques developed by the Davis group at Cornell. We are interested in complementary studies using the crossed-beam imaging here as well as the CPUF technique to obtain detailed dynamics and accurate product branching at the same time.

Chirped-pulse mm-wave detection in uniform supersonic flows. We will build on our recent successes with the CPUF technique focusing next on the CN + propene reaction which has been studied in some detail at the ALS. As mentioned above, we plan a range of joint studies using CPUF to complement the DC slice crossed-beam imaging investigations. Among these will be O(¹D) and S(¹D) reactions in addition to further studies of CN reaction with unsaturated hydrocarbons.

V. DOE Publications 2012-present

A. M. Estillore, L. M. Visger-Kiefer and A. G. Suits, "Reaction dynamics of Cl + butanol isomers by crossed-beam sliced ion imaging," *Faraday Discussion* **157** 181 (2012).

B. Joalland, Van Camp, R. D., Shi, Y., Patel, N., & Suits, A. G., "Crossed-Beam Slice Imaging of Cl Reaction Dynamics with Butene Isomers." *J. Phys. Chem. A.* (2013) DOI: 10.1021/jp403030s.

L. Yan, F. Cudry, W. Li, and A. G. Suits, "Isomer-Specific Mass Spectrometric Detection Via Semi-Soft Strong-Field Ionization," *J. Phys. Chem. A* (2013) DOI: 10.1021/jp403118c.

B. Joalland, Shi, Y., Patel, N., Van Camp, R., & Suits, A., "Dynamics of Cl+ Propane, Butanes Revisited: A Crossed Beam Slice Imaging Study." *Phys. Chem. Chem. Phys.* (2014) DOI: 10.1039/C3CP51785C.

B. Joalland, Y. Shi, A. G. Suits and A. M. Mebel, "Roaming dynamics in radical addition/elimination reactions," *Nature Comm.* (2014) DOI: 10.1038/ncomms5064

B. Joalland, Y. Shi, A. D. Estillore, A. Kamasah, A. M. Mebel, A. G. Suits, "Dynamics of chlorine atom reactions with hydrocarbons: Insights from imaging the radical product in crossed beams," *The Journal of Physical Chemistry A.* (2014) doi:10.1021/jp504804n (Feature Article).

F. Cudry, J. M. Oldham, S. Lingenfelter, and A. G. Suits. "Strong-Field Ionization of Flash Pyrolysis Reaction Products." *J. Phys. Chem. A* (2015) **119**, 460-467. DOI: 10.1021/jp510552a.

Y. Shi, A. Kamasah, B. Joalland, and A. G. Suits. "Crossed-Beam DC Slice Imaging of Fluorine Atom Reactions with Linear Alkanes." *J. Chem. Phys.* (accepted 2015).

An Update on the Implementation of a Novel Multiscale Simulation Strategy for Reacting Flows

PI: James C. Sutherland
Department of Chemical Engineering, The University of Utah
Salt Lake City, UT 84112-9203
James.Sutherland@utah.edu
Project start date: October, 2012

I. Lattice Based Multiscale Simulation

A. Introduction

Direct Numerical Simulation (DNS) of turbulent flows, particularly at high Reynold numbers, is prohibitively expensive due to the range of length scales present. The One-Dimensional Turbulence (ODT) model is a cost effective alternative that fully resolves length scales down to the Kolmogorov length scales in a single dimension while using a stochastic model to account for turbulence. Although ODT has been shown to capture buoyant flows, stratified flows and, of most interest to us, combusting flows [1, 3, 5] accurately, it fails to capture some large scale phenomena such as vortex pairing, recirculation or three dimensional flows that cannot easily be reduced to lower dimensions such as asymmetric geometries.

We have previously proposed a new methodology to bridge the gap between Large Eddy Simulation (LES) and DNS. This methodology, termed Lattice-Based Multiscale Simulation (LBMS), creates a system of ODT models that overcomes the shortcomings of ODT at a cost significantly cheaper than DNS. Furthermore, by fully solving all governing equations at the smallest scales, all phenomena associated with turbulent combustion can be accurately captured.

B. Basic Formulation

The LBMS model is a lattice like structure of ODT models, as depicted in Figure 1. The governing equations take the form

$$\int_{V(t)} \frac{\partial \rho \psi}{\partial t} dV = - \int_{S(t)} \Theta_{\psi} \cdot \mathbf{n} dS + \int_{V(t)} R_{\psi} dV, \quad (1)$$

where ψ is the transported variable, Θ_{ψ} is the flux through surface S and R_{ψ} are source terms. We solve equations for mass, momentum, internal energy, and species with an ideal gas equation of state and appropriate constitutive models for diffusive fluxes.

The fine spacing, δx_i , where i denotes a cartesian direction, is the resolution required for the smallest spatial structures in the flow field. The coarse spacing, Δx_i , is the spacing between each individual line (on the order of the integral length scale), and all lines in a given direction form a *bundle*.

Fluxes between ODT lines (*i.e.*, perpendicular to the bundle direction they are calculated on) are under-resolved due to the coarse spacing Δx_i . This issue is resolved in one of two ways, both of which interpolate a fully resolved flux from the bundle parallel to said flux direction to the other bundles. In the first method, flux interpolation is completed by imposing the fluxes that live on other bundles. In the second, the flux is reconstructed by setting the high wave number but underresolved flux information from the bundle that is receiving the fully resolved flux to the integral of the fully resolved flux to ensure conservation across control volumes. This is shown for a two dimensional case in Figure 2, where Θ represents the total flux, the subscript represents the flux direction and the superscript represents the bundle in which the flux lives on.

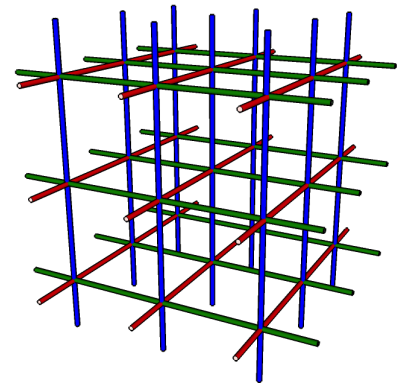


Figure 1: Representation of a 3D LBMS mesh. Each color denotes a different directional bundle. Lines are fully resolved.

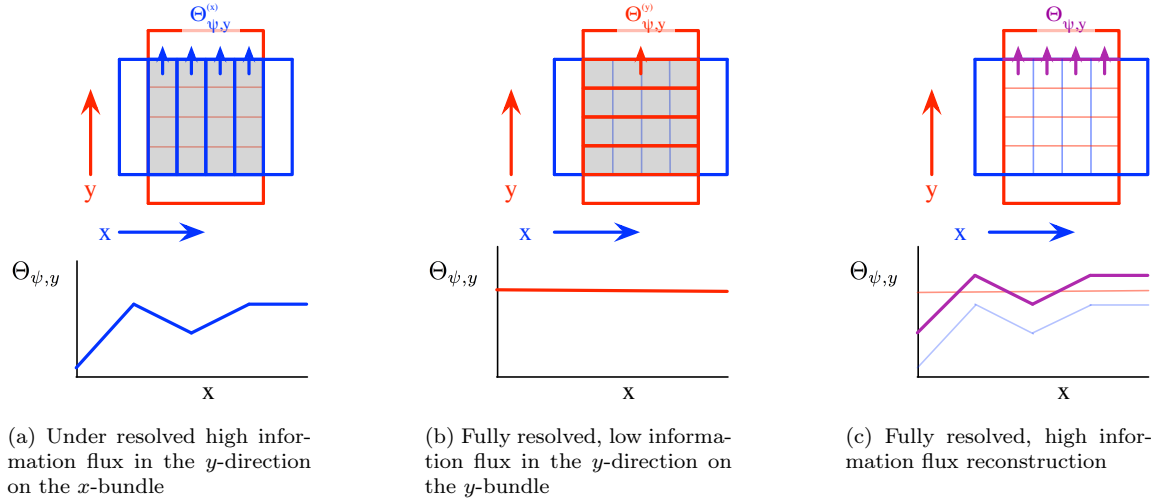


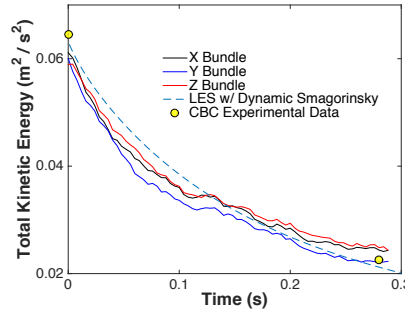
Figure 2: Two dimensional flux reconstruction

II. Progress Summary

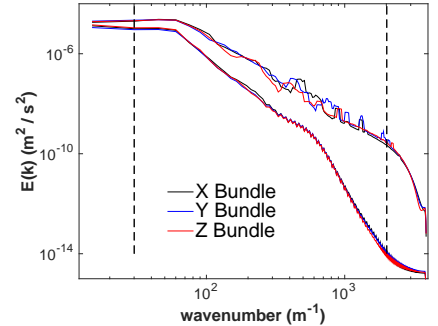
A. Isotropic Turbulence Decay

Controlling the Size of Triplet Mapping Initially, LBMS struggled to obtain reasonable results. This was because the formulation resolved large scale features of turbulence while also modeling the same features through the One-Dimensional Turbulence (ODT) triplet mapping transformations. The solution to this issue was to tune the maximum length of the eddy size. This was done by setting the integral length scale, L , to the coarse spacing, Δ , between lines as opposed to the width of the domain. In order to ensure correct physics, the Kolmogorov length scale, $\eta = Re^{-3/4}L$, at which viscous forces dissipate the kinetic energy associated with turbulence, was kept constant. To ensure that the Kolmogorov length is kept constant, LBMS utilizes the cell Reynolds number, termed Re_λ , associated with the spacing between each ODT line, instead of the overall Re .

Verification of the Turbulence Modeling We have seen that LBMS can accurately capture the turbulent kinetic energy spectra across a range of scales as well as the appropriate decay of the total kinetic energy for isotropic turbulence. Initial conditions are created using a synthetic turbulence generator, matching the kinetic energy of experimental grid generated turbulence data [2]. Additional verification is done by comparing intermediate time steps to a traditional Large Eddy Simulation (LES) run with a dynamic Smagorinsky model. Figure 3a compares the decay of the total kinetic energy in time for LBMS, LES and the experimental data. For this case, $N_x = N_y = N_z = 4$ coarse grid points were used with $n_x = n_y = n_z = 512$ fine grid points ($\Delta/\delta = 128$). That is, the simulation has a total of 16 ODT lines for each bundle direction, where each line has 512 points. The reference LES simulation utilized $(\Delta_{LES}/L)^3 = 32^3$ grid points. Thus, the LBMS lattice spacing was 8 times coarser than the reference LES simulation.



(a) Total kinetic energy decay in time for each bundle with $\Delta/\delta = 128$.



(b) Kinetic energy spectra in wave space for each bundle with $\Delta/\delta = 128$.

Looking at the kinetic energy spectra in wave space, as shown in Figure 3b, LBMS exhibits the $-5/3$ scaling law across the inertial range scales. Furthermore, the kinetic energy decay in time occurs across all scales, as expected. There is additional dissipation at the higher frequencies due to the effects of filtering. We have found

that this high wavenumber filter is particularly necessary for LBMS. In a compressible ODT code, the triplet map transformations, which simulate eddies, occur instantaneously and create artificially strong pressure fluctuations. By utilizing a high wavenumber filter (implemented via sixth order finite difference filters), the structure of the spectra remains intact through much of the inertial range. Only the smallest scale (highest frequency) features of turbulence are lost. These results show that we can capture isotropic turbulence with a drastically large coarse spacing that extends into the production range scales.

This represents a significant milestone in our efforts. With a functioning isotropic turbulence decay demonstration, we have increased confidence that the formulation can adequately handle turbulent flow. As will be discussed below, we have also added species transport with detailed reaction mechanism support and are now positioned to begin examining LBMS on reacting flows.

B. Species Transport

Full species transport with the appropriate source terms have been implemented into the LBMS framework and coupled to the Cantera package for detailed treatment of thermochemistry. Ignition and premixed flame propagation studies have been run to ensure proper treatment of species transport and source terms.

C. Boundary Conditions

We are currently implementing the Navier-Stokes Characteristic Boundary Conditions (NSCBC) treatment [6] into the LBMS framework. The NSCBC boundary condition treatment is a necessary condition for consistency when simulating highly turbulent and highly reactive flows in LBMS for inflow and outflow conditions.

We also have implemented the ability to specify arbitrary boundary condition geometries, which will facilitate the reacting jet configurations that we will be moving to during the upcoming year.

D. Scalability

The LBMS solver uses a task graph approach [4] that facilitates asynchronous communication to allow some overlap of communication with computation. A unique feature of LBMS is the ability to change the coarse grid (lattice) spacing independently of the fine grid spacing. To determine the effect of scalability on the coarse-fine ratio, Δ/δ , a number of scaling studies were conducted. Figure 3 shows the results for $\Delta/\delta = 16, 32$ and 64 and a range of fine grid spacings from $n_x = n_y = n_z = 512$ up to 4096 . The solid lines indicate strong scaling while the dashed lines are weak scaling. These results are encouraging and suggest that the LBMS code scales well on a range of problem sizes. These results were obtained for the Taylor-Greene vortex problem, a laminar flow problem that involves momentum, continuity and energy transport.

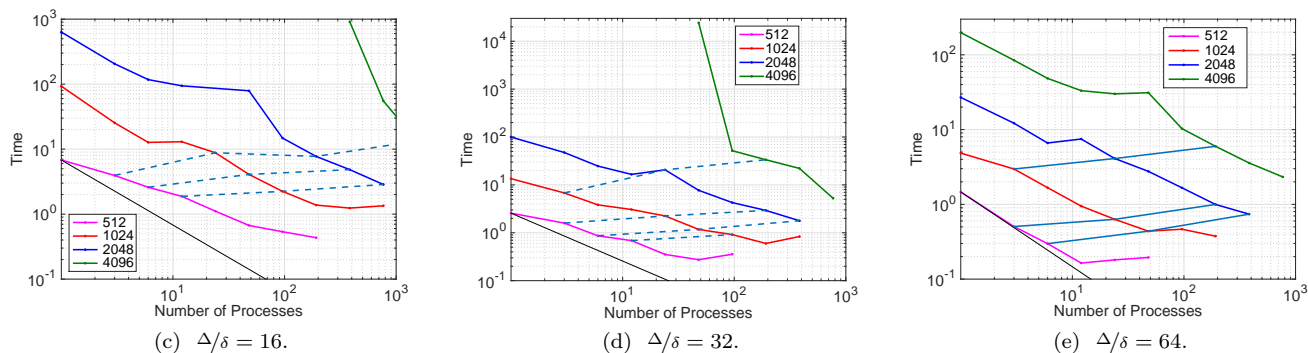


Figure 3: Scaling results for various coarse-fine ratios (Δ/δ), showing both strong and weak scalability of the LBMS code.

Figure 4 shows scaling for a fixed $N_x = N_y = N_z = 64$ with $n_x = n_y = n_z = 1024, 2048$ and 4096 so that Δ/δ is changing. In the absence of flux reconstruction, only coarse-level information must be exchanged. For this reason, Figure 4 indicates that the strong scaling is relatively insensitive to the number of fine grid points.

III. Future Work

A. Parameter Studies

Two parameters of particular importance are the eddy rate constant and the ratio of coarse to fine scales, Δ/δ . The eddy rate constant affects the number of eddies and thus, the transfer of momentum to thermal energy through viscous dissipation. The eddy rate constant must be tuned appropriately to ensure that the kinetic energy decay in time matches DNS, experimental or model data sets. The coarse to fine ratio, Δ/δ , directly affects the scale at which three-dimensional effects are directly resolved (Δ). Scales between Δ and δ are resolved along individual lines in each direction, but turbulent mixing in this range of length scales is modeled through ODT. We expect that, for isotropic turbulence, large Δ/δ will be feasible, but other flows involving strong recirculation such as confined jets may require somewhat smaller Δ/δ . This must be quantified through validation studies.

B. Turbulent Reacting Flow Calculations

With geometry, NSCBC, species transport and turbulence all implemented, the next step is to begin turbulent combustion calculations. We will be investigating source term closure approaches as well. As $\Delta \gg \delta$, there will be a wealth of information on the fine mesh that will need to be interpolated from each bundle to the coarse mesh to integrate the source terms over the control volumes. This will be particularly important for species source terms during combustion as flame fronts tend to be highly reactive but at small length scales. Various interpolation/reconstruction methods have been tested on the unique LBMS mesh with simple configurations to explore their efficacy, and this work will continue through the next year as we begin simulating reactive flows.

IV. Publications & Presentations

1. D. Cline, J. C. Sutherland, and T. Saad. Lattice based multiscale simulation. In SIAM Computational Science and Engineering Conference (poster) www.siam.org/meetings/cse15, March 2015.
2. J. Hutchins, D. Cline, and J. C. Sutherland. A task-parallel approach for solving PDEs on a lattice. In SIAM Computational Science and Engineering Conference (poster) www.siam.org/meetings/cse15, March 2015.

References

- [1] Wm. T. Ashurst and Alan R. Kerstein. *Physics of Fluids*, 17(2):025107, 2005.
- [2] Stanley Corrsin and Geneviève Comte-Bellot. *Journal of Fluid Mechanics*, 48(2):273–337, 1971.
- [3] J C Hewson and A R Kerstein. *Combust. Theory Modelling*, 5:669–697, 2001.
- [4] Patrick K. Notz, Roger P. Pawlowski, and James C. Sutherland. *ACM Transactions on Mathematical Software*, 39(1):1–21, November 2012.
- [5] Naveen Punati, James C. Sutherland, Alan R. Kerstein, Evatt R. Hawkes, and Jacqueline H. Chen. *Proceedings of the Combustion Institute*, 33(1):1515–1522, 2011.
- [6] James C. Sutherland and Christopher a. Kennedy. *Journal of Computational Physics*, 191(2):502–524, November 2003.

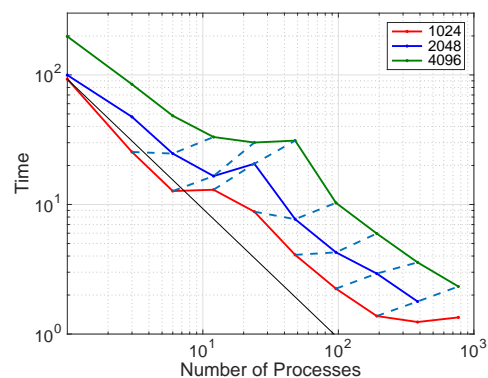


Figure 4: Cross ratio weak and strong scaling comparison

as confined jets may require somewhat

Elementary Reaction Kinetics of Combustion Species

Craig A. Taatjes

*Combustion Research Facility, Mail Stop 9055, Sandia National Laboratories,
Livermore, CA 94551-0969
cataatj@sandia.gov*

SCOPE OF THE PROGRAM

This program aims to develop new methods for studying chemical kinetics and to apply these methods to the investigation of fundamental chemistry relevant to combustion science. One central goal is to perform accurate measurements of the rates at which important free radicals react with each other and with stable molecules. Another goal is to characterize complex reactions that occur via multiple potential wells by investigating the formation of products. These investigations employ simultaneous time-resolved detection of multiple species in well-characterized photolytically-initiated reaction systems where multiple consecutive and competing reactions may occur. Understanding the reactions in as much detail as possible under accessible experimental conditions increases the confidence with which modelers can extrapolate to the conditions of real-world devices. This research often requires the development and application of new detection methods for precise and accurate kinetics measurements. Absorption-based techniques and mass-spectrometric methods have been emphasized, because many radicals critical to combustion are not amenable to fluorescence detection.

An important part of our strategy, especially for complex reaction systems, is using experimental data to test and refine detailed calculations (working in close cooperation with Stephen Klippenstein at Argonne and Ahren Jasper and Judit Zádor at Sandia), where the theory enables rigorous interpretation of experimental results and guides new measurements that will probe key aspects of potential energy surfaces. This methodology has been applied in our investigations of the reactions of fuel radicals with O₂. The combination of rigorous theory and validation by detailed experiments has made great strides toward a general quantitative model for alkyl oxidation, and now extends to reactions of oxygenated molecules relevant to biofuel combustion and to the effects of unsaturation on the chemistry leading to autoignition. Moreover, we have increasingly aimed at producing species that are intermediates in oxidation systems (e.g., Criegee intermediates, hydroperoxyalkyl radicals) and directly probing their reaction kinetics.

RECENT PROGRESS

We continue to apply frequency-modulation and direct absorption spectroscopy to measurements of product formation in reactions of alkyl radicals with O₂ and kinetics of unsaturated hydrocarbon radicals. In addition, the multiplexed photoionization mass spectrometric reactor at the Advanced Light Source (ALS), an experimental effort led by David Osborn (see his abstract), has become a major part of our investigations of low-temperature hydrocarbon oxidation chemistry. In the past year we have been largely occupied with expanding our understanding of the fundamental chemistry of carbonyl oxides (Criegee intermediates), but our attention is returning to details of reactions that are important in the ignition chemistry of biofuels, such as the reactions of molecular oxygen with fuel radicals

Effects of resonance stabilization on ROO and QOOH chemistry. As detailed in David Osborn's abstract, we have directly measured the kinetics of a resonance-stabilized QOOH radical,^b the first time that a QOOH radical has ever been directly detected. The resonance stabilization of the 2-hydroperoxy-4,6-cycloheptadienyl QOOH radical makes it relatively unreactive with molecular oxygen, increasing its concentration in the experiments, and likely leading to larger steady-state concentrations in combustion environments. The effects of resonance stabilization on oxidation chemistry have been the subject of broader investigation in our group over the past few years. For example, the vinoxylic stabilization of QOOH or ROO that occurs in ketone oxidation can steer the oxidation reaction via the resonance-stabilized intermediates.¹

The chlorine atom-initiated oxidation of two unsaturated primary C5 alcohols, prenil (3-methyl-2-buten-1-ol, $(\text{CH}_3)_2\text{CCHCH}_2\text{OH}$) and isoprenol (3-methyl-3-buten-1-ol, $\text{CH}_2\text{C}(\text{CH}_3)\text{CH}_2\text{CH}_2\text{OH}$), has been studied at 550 K and low pressure (8 Torr).^d The time- and isomer-resolved formation of products was probed with multiplexed photoionization mass spectrometry (MPIMS) using tunable vacuum ultraviolet ionizing synchrotron radiation. The peroxy radical chemistry of the unsaturated alcohols appears much less rich than that of saturated C4 and C5 alcohols. The main products observed are the corresponding unsaturated aldehydes – prenal (3-methyl-2-butenal) from prenil oxidation and isoprenal (3-methyl-3-butenal) from isoprenol oxidation. No significant products arising from QOOH chemistry are observed. These results can be qualitatively explained by the formation of resonance stabilized allylic radicals via H-abstraction in the $\text{Cl} + \text{prenil}$ and $\text{Cl} + \text{isoprenol}$ initiation reactions. The loss of resonance stabilization upon O_2 addition causes the energies of the intermediate wells, saddle points, and products to increase relative to the energy of the initial radicals and O_2 . These energetic shifts make most product channels observed in the peroxy radical chemistry of saturated alcohols inaccessible for these unsaturated alcohols. The experimental findings are underpinned by quantum-chemical calculations for stationary points on the potential energy surfaces for the reactions of the initial radicals with O_2 . Under our conditions, the dominant channels in prenil and isoprenol oxidation are the chain-terminating HO_2 -forming channels arising from radicals, in which the unpaired electron and the $-\text{OH}$ group are on the same carbon atom, with stable prenal and isoprenal co-products, respectively. These findings suggest that the presence of $\text{C}=\text{C}$ double bonds in alcohols will reduce low-temperature reactivity during autoignition.

Ketohydroperoxide formation and decomposition. The chain branching reaction sequence that is initiated by the reaction of a QOOH radical with O_2 continues via isomerization of OOQOOH to a dihydroperoxyalkyl radical HOOPOOH that loses OH to form a ketohydroperoxide, and is completed by the dissociation of this ketohydroperoxide to OH and an oxy radical. Ketohydroperoxides have been observed in alkane oxidation by several groups, and in work supported under another program, we have identified the main ketohydroperoxide observed in butane oxidation as 3-hydroperoxybutanal, a γ -ketohydroperoxide.² We have now begun to characterize the decomposition of this ketohydroperoxide. The γ -ketohydroperoxides can also undergo a Korcek decomposition to form an organic acid and a carbonyl compound; this dissociation forms two closed-shell species and therefore impedes chain branching. In new Cl -initiated butane oxidation experiments, and in jet-stirred reactor measurements

carried out in collaboration with Nils Hansen, Denisia Popolan-Vaida (LBNL) and Steve Leone (LBNL) we have observed the formic acid product from the Korcek decomposition of 3-hydroperoxybutanal, as well as the distinct acetone- d_3 Korcek product in $\text{CH}_3\text{CD}_2\text{CD}_2\text{CH}_3$ oxidation. By modeling the time dependence of the ketohydroperoxide concentration and the yield of formic acid we have been able to constrain the possible contribution of this channel to the ketohydroperoxide removal. Although the Korcek reaction is potentially a major part of the production of organic acids, it appears to be a very minor part of the overall ketohydroperoxide removal.

In another jet-stirred reactor experiment, described in Nils Hansen's abstract,^a a ketohydroperoxide intermediate was observed in the oxidation of dimethyl ether. Also in these measurements a small amount of the product of Korcek decomposition, carbonic acid in this case, was observed. This oxidation also forms hydroperoxymethyl formate and hydroperoxymethanol, species that have been observed in the reactions of the Criegee intermediate formaldehyde oxide (CH_2OO) with formic acid^f and with water.

FUTURE DIRECTIONS

We will continue to expand our exceptionally productive collaboration with David Osborn, using the photoionization mass spectrometry machine at the Advanced Light Source. The effects of unsaturation and oxygenation on low-temperature oxidation chemistry will be further explored. Measurements of elementary oxidation reactions of representative biofuel molecules in the temperature region 500 K – 800 K will continue, with a continuing goal of developing a more general understanding of the ignition chemistry of alternative fuels.

References

1. A. M. Scheer, O. Welz, J. Zador, D. L. Osborn and C. A. Taatjes, *Phys. Chem. Chem. Phys.*, 2014, 16, 13027-13040.
2. A. J. Eskola, O. Welz, J. Zádor, I. O. Antonov, L. Sheps, J. D. Savee, D. L. Osborn and C. A. Taatjes, *Proc. Combust. Inst.*, DOI: 10.1016/j.proci.2014.05.011.

Publications acknowledging BES support for CAT, 2013 –

- a. Kai Moshhammer, Ahren W. Jasper, Denisia M. Popolan-Vaida, Arnas Lucassen, Pascal Diévert, Hatem Selim, Arkke J. Eskola, Craig A. Taatjes, Stephen R. Leone, S. Mani Sarathy, Yiguang Ju, Philippe Dagaut, Katharina Kohse-Höinghaus, and Nils Hansen, "Detection and Identification of the Keto-Hydroperoxide ($\text{HOOCH}_2\text{OCHO}$) and Other Intermediates during Low-Temperature Oxidation of Dimethyl Ether," *J. Phys. Chem. A* **in press** DOI: 10.1021/acs.jpca.5b00101 (2015).
- b. Savee, John D., Ewa Papajak, Brandon Rotavera, Haifeng Huang, Arkke J. Eskola, Oliver Welz, Leonid Sheps, Craig A. Taatjes, Judit Zador and David L. Osborn. "Direct Observation and Kinetics of a Hydroperoxyalkyl Radical (QOOH)," *Science* **347**, 643-646 (2015).
- c. L. G. Dodson, L. Shen, J. D. Savee, N. C. Eddingsaas, O. Welz, C. A. Taatjes, D. L. Osborn, S. P. Sander and M. Okumura, "VUV Photoionization Cross Sections of HO_2 , H_2O_2 , and H_2CO ," *J. Phys. Chem. A*, 119, 1279-1291 (2015).
- d. O. Welz, J. D. Savee, D. L. Osborn, C. A. Taatjes, "Chlorine Atom-Initiated Low-Temperature Oxidation of Prenol and Isoprenol: The Effect of C=C Double Bonds on the Peroxy Radical Chemistry in Alcohol Oxidation," *Proc. Combust. Inst.* doi:10.1016/j.proci.2014.05.004
- e. Martin Ng, Jordan Nelson, Craig A. Taatjes, David L. Osborn, and Giovanni Meloni, "Synchrotron Photoionization Study of Mesitylene Oxidation Initiated by Reaction with $\text{Cl} (^2\text{P})$ or $\text{O} (^3\text{P})$ Radicals," *J. Phys. Chem. A* **118**, 3735–3748 doi:10.1021/jp500260f (2014).

- f. Oliver Welz, Arkke J. Eskola, Leonid Sheps, Brandon Rotavera, John D. Savee, Adam M. Scheer, David L. Osborn, Douglas Lowe, A. Murray Booth, Ping Xiao, M. Anwar H. Khan, Carl J. Percival, Dudley E. Shallcross, and Craig A. Taatjes, "Rate Coefficients of C1 and C2 Criegee Intermediate Reactions with Formic and Acetic Acid Near the Collision Limit: Direct Kinetics Measurements and Atmospheric Implications," *Angew. Chem.* **53**, 4547–4550 doi:10.1002/anie.201400964 (2014).
- g. D. E. Shallcross, C. A. Taatjes, C. J. Percival, "Criegee intermediates in the indoor environment: new insights," *Indoor Air* **24**, 495–502 doi:10.1111/ina.12102 (2014).
- h. W. G. Roeterdink, J. Bulthuis, E. P. F. Lee, D. Ding, and C. A. Taatjes, "Hexapole transmission spectrum of formaldehyde oxide," *Chem. Phys. Lett.* **598**, 96–101 doi: 10.1016/j.cplett.2014.03.009 (2014).
- i. Craig A. Taatjes, Dudley E. Shallcross, and Carl J. Percival, "Research frontiers in the chemistry of Criegee intermediates and tropospheric ozonolysis," *Phys. Chem. Chem. Phys.* **16**, 1704–1718 (2014).
- j. John D. Savee, Jessica F. Lockyear, Sampada Borkar, Arkke J. Eskola, Oliver Welz, Craig A. Taatjes and David L. Osborn, "Absolute photoionization cross-section of the vinyl radical," *J. Chem. Phys.* **139**, 056101 (2013).
- k. Oliver Welz, Judit Zádor, John D. Savee, Leonid Sheps, David L. Osborn, and Craig A. Taatjes, "Low-Temperature Combustion Chemistry of Biofuels: Principal Oxidation Pathways for Hydroxybutyl Radicals Derived from n-Butanol," *J. Phys. Chem. A* **117**, 11983–12001 (2013).
- l. Jessica F Lockyear, Oliver Welz, John D. Savee, Fabien Goulay, Adam J. Trevitt, Craig A. Taatjes, David L. Osborn, and Stephen R Leone, "Isomer Specific Product Detection in the Reaction of CH with Acrolein," *J. Phys. Chem. A* **117**, 11013–11026 (2013).
- m. Carl Percival, Oliver Welz, Arkke J. Eskola, John D. Savee, David L. Osborn, David O. Topping, Doug Lowe, Steve Utembe, Asan Bacak, Gordon McFiggans, Mike Cooke, Alexander T. Archibald, Michael Jenkin, R. G. Derwent, Ilona Riipinen, Daniel Mok, Edmond P. F. Lee, John Dyke, Craig A. Taatjes and Dudley E. Shallcross, "Regional and Global Impacts of Criegee Intermediates on Atmospheric Sulphuric Acid Concentrations and First Steps of Aerosol Formation," *Faraday Discuss.* **165**, 45–73 (2013).
- n. Adam J. Trevitt, Matthew B. Prendergast, Fabien Goulay, John D. Savee, David L. Osborn, Craig A. Taatjes, and Stephen R. Leone, "Product Branching Fractions of the CH + Propene Reaction from Synchrotron Photoionization Mass Spectrometry," *J. Phys. Chem. A* **117**, 6450–6457 (2013).
- o. Joseph Czekner, Craig A. Taatjes, David L. Osborn, and Giovanni Meloni, "Absolute Photoionization Cross-Sections of Selected Furanic and Lactonic Potential Biofuels," *Int. J. Mass Spectrom.* **348**, 39–46 (2013).
- p. Judit Zádor, Haifeng Huang, Oliver Welz, Johan Zetterberg, David L Osborn and Craig A Taatjes, "Directly Measuring Reaction Kinetics of QOOH – a Crucial but Elusive Intermediate in Hydrocarbon Autoignition," *Phys. Chem. Chem. Phys.* **15**, 10753-10760 (2013).
- q. Craig A. Taatjes, Oliver Welz, Arkke J. Eskola, John D. Savee, Dudley E. Shallcross, Adam M. Scheer, Brandon Rotavera, Edmond P. F. Lee, John M. Dyke, Daniel K. W. Mok, David L. Osborn, and Carl J. Percival, "Direct Measurements of Conformer-Dependent Reactivity of the Criegee intermediate CH₃CHOO," *Science* **340**, 177-180 (2013).
- r. Xia Zhang, Chris J. Eyles, Craig A. Taatjes, Dajun Ding and Steven Stolte, "A general scaling rule for the collision energy dependence of a rotationally inelastic differential cross-section and its application to NO(X) + He," *Phys. Chem. Chem. Phys.* **15**, 5620-5635 (2013).
- s. Fabien Goulay, Adeeb Derakhshan, Eamonn Maher, Adam J. Trevitt, John D. Savee, Adam M. Scheer, David L. Osborn, and Craig A. Taatjes, "Formation of dimethylketene and methacrolein by reaction of the CH radical with acetone," *Phys. Chem. Chem. Phys.* **15**, 4049–4058 (2013).
- t. Oliver Welz, Stephen J. Klippenstein, Lawrence B. Harding, Craig A. Taatjes and Judit Zádor "Unconventional Peroxy Chemistry in Alcohol Oxidation – The Water Elimination Pathway," *J. Phys. Chem. Lett.* **4**, 350–354 (2013).
- u. Oliver Welz, John D. Savee, Arkke J. Eskola, Leonid Sheps, David L. Osborn, and Craig A. Taatjes, "Low-Temperature Combustion Chemistry of Biofuels: Pathways in the Low-Temperature (550–700 K) Oxidation Chemistry of Isobutanol and tert-Butanol," *Proc. Combust. Inst.* **34**, 493-500 (2013).
- v. Haifeng Huang, Brandon Rotavera, Arkke J. Eskola and Craig A. Taatjes, "Correction to Pressure-dependent I atom yield in the reaction of CH₂I with O₂ shows a remarkable apparent third-body efficiency for O₂," *J. Phys. Chem. Lett.* **4**, 3824–3824 (2013).

Elementary Reactions of PAH Formation

Robert S. Tranter

Chemical Sciences and Engineering Division, Argonne National Laboratory

Argonne, IL-60439

tranter@anl.gov

I. Program Scope

This program is focused on the experimental determination of kinetic and mechanistic parameters of elementary reactions, in particular those involved in the formation and destruction of the building blocks for aromatic species. The program also encompasses dissociation of novel fuels such as ethers and cyclic species and their dissociation products that are representative of oxygenated intermediates in combustion mechanisms. Thermal sources of radicals are also investigated and characterized for use in more complex reaction systems where secondary chemistry can be significant. Recently, the scope has been increased to include thermally initiated roaming reactions. The approach involves a diaphragmless shock tube (DFST) equipped with laser schlieren (LS) and a time-of-flight mass spectrometer (TOF-MS) and low pressure, fast flow, reactor equipped with a quadrupole MS. The combination of these techniques accesses a wide range of reaction temperatures and pressures.

II. Recent Progress

A. Very Reproducible Shock Tube Experiments

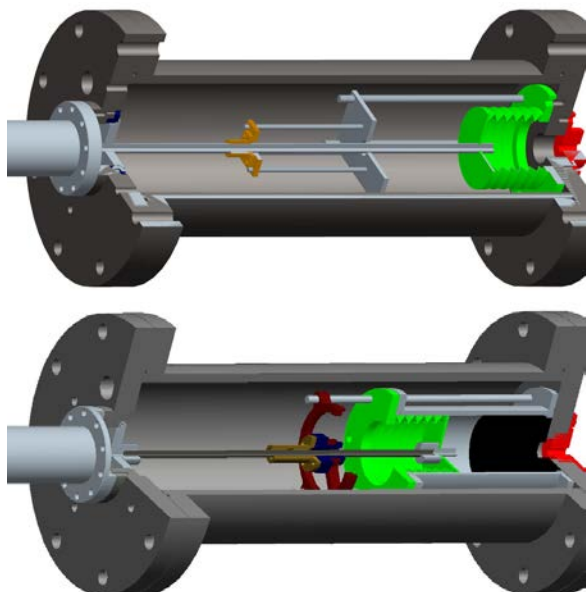


Figure 1: Top: Original configuration of the DFST; Bottom: New configuration with bellows reversed. The bellows is shown in green. The black block in the bottom figure is a neoprene block to prevent overexpansion of the bellows and reduce vibration.

The diaphragmless shock tube is based around a bellows actuated valve built inside the driver section of the shock tube. Compared to conventional shock tubes it creates reproducible reaction conditions behind the shock wave which have allowed for limited signal averaging. The principle benefit of the DFST to date, however, has been for studying unimolecular reactions in the high temperature fall off region as reaction pressures can be kept effectively constant while the reaction temperature is varied independently by making small adjustments to the loading pressures. In its original form the bellows that is the heart of the DFST was extended to seal the driver from the driven section of the shock tube, Fig.1, prior to filling the tube. The stresses this action induced in the bellows resulted in changes in its the behavior and hence a slow change in shock properties from experiment to experiment. On a practical basis this limited the utility of the apparatus for signal averaging and repeating experiments at a later date. Furthermore, the stress caused the bellows to rupture after an average 550 shocks with a maximum of ~800. Recently, the DFST has been reconfigured by rotating the bellows 180 degrees to the configuration in the

lower part of Fig. 1.¹ Consequently, the bellows is now compressed rather than extended to seal the shock tube sections from each other. This simple change has had a remarkable effect on the performance of the apparatus. As shown in Fig. 2 the shock conditions are entirely reproducible over at least a month and

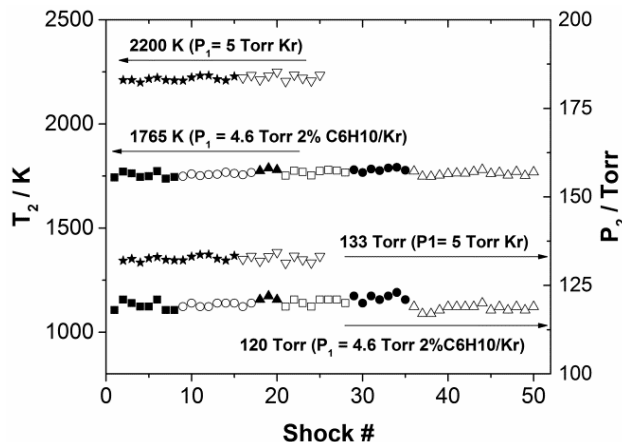


Figure 2: Repeatability of T_2 and P_2 from helium driven shocks in non-reactive and reactive mixtures with fixed initial pressures in the driver (P_4) and driven (P_1) sections of the diaphragmless shock tube. a) $P_4 = 30.0$ psi and $P_1 = 5.00$ Torr (Kr). Mean $T_2 = 2200$ K and $\sigma = 12.5$ K (0.56%). Mean $P_2 = 133$ Torr and $\sigma = 0.8$ Torr (0.6%) Closed stars represent experiments performed in one day. Open down triangles represent experiments performed 11 days later after ~ 200 additional experiments over a range of T_2 and P_2 . b) $P_4 = 28$ psi and $P_1 = 4.6$ Torr (2% cyclohexene/Kr). Mean $T_2 = 1765$ K and $\sigma = 12.9$ K (0.73%). Mean $P_2 = 120$ Torr and $\sigma = 1.4$ Torr (1.1%). The alternating open and closed symbols show experiments performed on different days over the course of a month. Solid squares represent day 0. The remaining symbols from left to right are days 1, 15, 16, 17 and 35.

considerably. Dissociation of nitromethane is of interest for a number of reasons including its practical application as an energetic fuel and a monopropellant. However, it is also of interest due to the possibility of roaming mediated isomerization (RMI) competing with scission of the C-N bond in thermally activated systems. RMI in CH_3NO_2 leads to methylnitrite rather than $\text{CH}_3 + \text{NO}_2$ the products of reaction (1). These channels have been recently examined theoretically^{ii,iii} and as part of the current work a comprehensive theoretical analysis of the dynamics and kinetics of CH_3NO_2 dissociation and RMI have been performed by Jasper, Harding and Klippenstein as a complement to the LS experiments. Additionally, thermochemical properties of key species have been refined by Ruscic.

Under the conditions of the LS experiments methyl nitrite formed by RMI will not be stabilized but rather dissociate immediately to $\text{CH}_3\text{O} + \text{NO}$, reaction (2). The experimental profiles and modeling of these are consistent with reaction (1) being the dominant channel. This results in relatively high concentrations of CH_3 and NO_2 and thus the reaction of CH_3 with NO_2 has to be accounted for. The most significant channel is reaction (3) yielding methoxy radical and NO rather than recombination by (-1). A theoretical estimate was made of k_3 as part of this study however a full analysis of the reaction was beyond the scope of the work and for modeling the LS density gradient profiles the value of Glarborg^{iv} et al. is preferred. This value is about a factor of 2.5 lower than the theoretical predictions of k_3 from the current work. The high temperature literature on k_3 is very sparse with uncertainties of at least a factor of 3 and the Glarborg and present theoretical k_3 fall within the limits of the only shock tube study.^v Clearly, further experimental and theoretical work on this reaction is highly desirable.

Shown in Fig. 3a are the k_1 obtained from the LS experiments and theoretical predictions from a master equation analysis based on the current theory. The agreement is very good with both the magnitude and pressure dependence being captured. Fig. 3b shows a similar comparison between the LS results and

several hundred experiments. For example, the experiments on dissociation of cyclohexene shown in Fig. 2 have a mean $T_2 = 1765$ K with one standard deviation of 12.9 K (0.73%). In fact periodic tests with a standard experiment show excellent reproducibility over several months. Additionally the lifetime of the bellows is significantly improved and since the new configuration was adopted over 1600 shocks have been performed with no sign of degradation in the bellows. As a consequence of the stability of the apparatus signal averaging is possible as a routine part of LS and TOF-MS experiments and is likely to be very beneficial in future investigations where weak signals are encountered. In particular, it is anticipated that more dilute mixtures can be used to reduce effects of secondary reactions without sacrificing S/N.

B. Dissociation of Nitromethane

In a previous abstract, results from initial DFST\LS studies on the dissociation of nitromethane were presented. Subsequently, the experimental range has been expanded to cover $1200 < T_2 < 1860$ K and nominal P_2 of 30, 60 and 120 Torr with reagent mixtures of 0.5%, 1%, 2% and 4% nitromethane dilute in krypton. Furthermore, the model used to simulate the density gradients from the DFST\LS experiments has been refined



theory for the branching ratio (BR=0.13, $\sigma=0.02$), $k_2/(k_1+k_2)$, the main focus of this work. The agreement is good although the experimental results do not appear to show the small pressure dependence predicted by the current theory which is also less pronounced than that of Zhu et al.ⁱⁱⁱ It should be noted that while the experimental BR are consistent with the theoretical predictions the LS profiles can also be simulated by assuming BR=0. This apparent contradiction arises from the effective ΔH_r for reaction (2) being only 16.2 kcal/mol lower than reaction (1) and (2) being a minor channel. However, differences in secondary chemistry resulting from reactions (1) and (2) allow an upper limit of BR to be established and this is essentially that shown in Fig. 3b. Values of BR much larger generate simulations inconsistent with the LS profiles and the simulations cannot be corrected with reasonable changes to rates or mechanism.

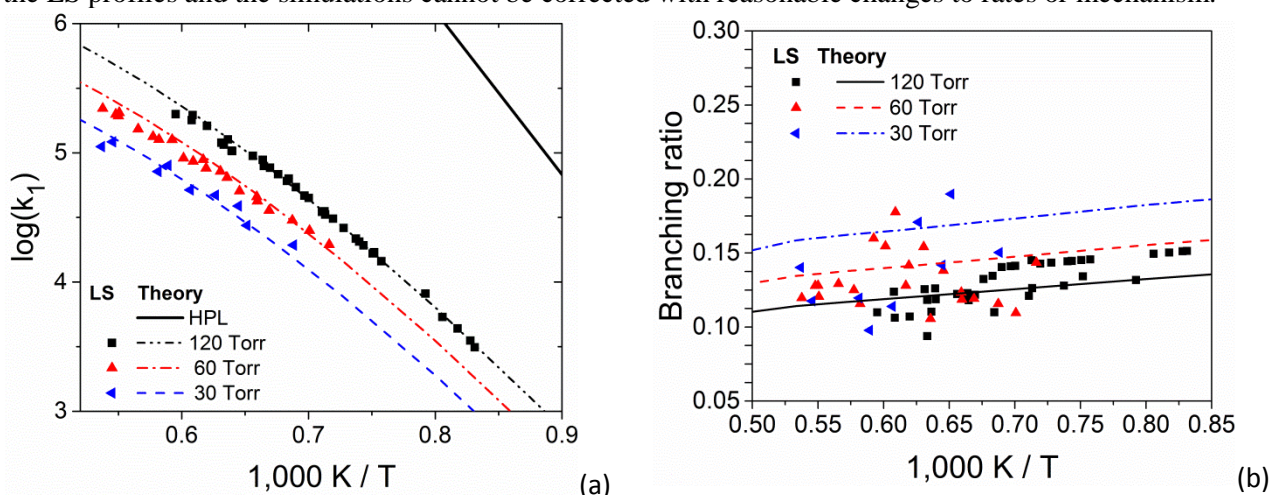
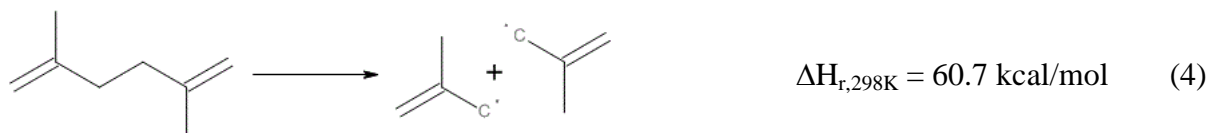


Figure 3: Comparison of experimental and theoretical predictions of kinetic parameters for CH_3NO_2 pyrolysis. a) k_1 for dissociation by C-N scission. b) Branching ratios $k_2/(k_1+k_2)$

C. Methylallyl Radical

A significant aspect of this program is the study of reactions of resonantly stabilized and aromatic radicals. Previously, studies on the decomposition and self-reaction of a number of these species have been reported and recently this has been extended to include resonantly stabilized methyl allyl radicals. This work complements prior work on allyl radicals^{vi,vii} and the recombination of methyl allyl radicals is a key reaction in the low temperature combustion of isobutene.

DFST\LS experiments were performed over the range $1100 < T_2 < 1400 \text{ K}$ at nominal P_2 of 70 and 135 Torr with dilute mixtures of 2,5-dimethylhexa-1,5-diene (25DM15HD) which dissociates via scission of the weak central C-C bond, reaction (4).



As usual in LS experiments k_4 is recovered from the density gradient at t_0 , the start of reaction, and the desired recombination rate coefficient is obtained through the equilibrium constant. The measured k_4 are shown in Fig. 4 and show a small pressure dependence. At the lower temperatures of these

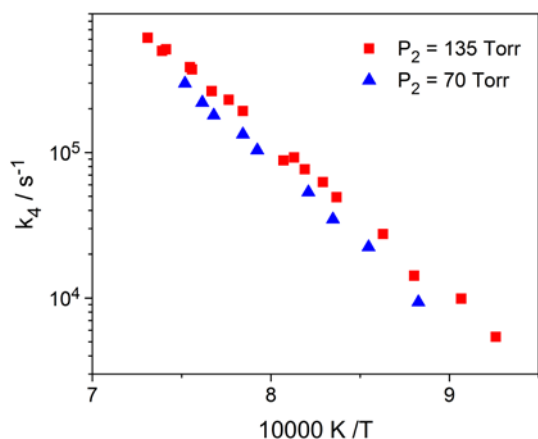


Figure 4: $k_{(15DM25HD \rightarrow 2i-C4H7)}$ from DFST\LS experiments.

+ O₂. Further investigations of PAH formation are planned with studies of the H-atom catalyzed conversion of fulvene to benzene and dimethyl fulvenes to xylenes. A study of the dissociation and isomerization of C₄H₆ species is ongoing and should result in a single reaction mechanism that describes the complex behavior of these molecules.

IV. References

- i. Randazzo J. B., Annesley C. J. and Tranter R. S., *Rev. Sci. Instrum.* **2015**, 86, 0161170
- ii. Homayoon Z. and Bowman J. M., *J. Phys. Chem. A*, **2013**, 10.1021/jp312076z
- iii. Zhu R. S.; Raghunath P.; Lin M. C., *J. Phys. Chem. A*, **2013**, 117, 7308
- iv. Glarborg, P.; Bendtsen, A. B.; Miller, J. A., *Int. J. Chem. Kin.* **1999**, 31, 591.
- v. Srinivasan N. K., Su M. C., Sutherland J. W. and Michael J. V., *J. Phys. Chem. A*, **2005**, 109, 1857.
- vi. Lynch P. T., Annesley C. J., Aul C. J., Yang X. and Tranter R. S., *J. Phys. Chem. A*, **2013**, 117, 4750
- vii. Fridlyand A., Lynch P. T., Tranter R. S. and Brezinsky K., *J. Phys. Chem. A*, **2013**, 117, 4762

V. Publications and submitted journal articles supported by this project 2013-2015

- 1 Randazzo J. B., Annesley C. J. and Tranter R. S., 'Note: an improved driver section for a diaphragmless shock tube' *Rev. Sci. Instrum.* **2015**, 86, 016117
- 2 Lynch P. T., Annesley C. J. and Tranter R. S. 'Dissociation of *ortho*-Benzyne Radicals in the High Temperature Fall-off Regime' *Proc. Combust. Inst.* **2015**, 35, 145-152.
- 3 Annesley C. J., Goldsmith C. F. and Tranter R. S. 'A shock tube laser schlieren study of methyl acetate dissociation in the fall-off regime' *Phys. Chem. Chem. Phys.* **2014**, 16, 7241-7250
- 4 Tranter R. S. and Brezinsky K., 'Shock tube studies of combustion relevant elementary chemical reactions and sub-mechanisms' in *Cleaner Combustion: Developing Detailed Chemical Kinetic Models* ISBN - 978-1-4471-5306-1 **2013**
- 5 Yasunaga K. and Tranter R. S., 'Speciation in shock tubes' in *Cleaner Combustion: Developing Detailed Chemical Kinetic Models* ISBN - 978-1-4471-5306-1 **2013**
- 6 Tranter R. S. and Lynch P. T., 'A miniature high repetition rate shock tube' *Rev. Sci. Instrum.* DOI:10.1063/1.4820917 **2013**
- 7 Lynch P. T., Annesley C. J., Aul C. J., Yang X. and Tranter R. S., 'Recombination of allyl radicals in the high temperature fall-off regime' *J. Phys. Chem. A*: **2013**, 117, 4750-4761
- 8 Fridlyand A., Lynch P. T., Tranter R. S. and Brezinsky K., 'Single pulse shock tube study of allyl radical recombination' *J. Phys. Chem. A*, **2013**, 117, 4762-4776
- 9 Tranter R. S., Lynch P. T., Yang X., 'Dissociation of dimethyl ether at high temperatures' *Proc. Combust. Inst.* **2013**, 34, 591-598

experiments, the very stable methylallyl radicals predominantly recombine to the parent molecule. As T₂ increases the dissociation of methylallyl to methyl radicals and allene becomes increasingly important which initiates a mild chain reaction through reaction between CH₃ and 25DM25HD. The simulations are reasonably sensitive to the rate of dissociation of methylallyl and thus from modeling the profiles an estimate of this rate coefficient has also been obtained.

III. Future Work

The DFST/TOF-MS/LS studies of aromatics and resonantly stabilized radicals are being expanded to include reactions between radicals and oxygen molecules. These represent a new application of the LS technique and initial efforts are focusing on phenyl

Variational Transition State Theory

Donald G. Truhlar

Department of Chemistry, University of Minnesota
207 Pleasant Street SE, Minneapolis, Minnesota 55455
truhlar@umn.edu

Program scope

This project involves the development of variational transition state theory (VTST) for gas-phase reactions, including optimized multidimensional tunneling (OMT) contributions and the application of this theory to gas-phase reactions with a special emphasis on developing reaction rate theory in directions that are important for applications to combustion. The development of VTST/OMT as a useful computational tool for combustion kinetics involves six objectives:

- (i) developing and applying new methods of electronic structure calculations for the input potential energy surface, which is an implicit surface defined by an electronic structure model chemistry;
- (ii) methods to interface reaction-path and reaction-swath dynamics calculations with electronic structure theory, either by straight direct dynamics or by an interpolation of electronic structure calculations;
- (iii) methods to treat vibrational anharmonicity and vibration-rotation coupling;
- (iv) efficient methods to calculate accurate rate constants from the results of the electronic structure calculations and statistical mechanical treatments of vibrational anharmonicity;
- (v) development and implementation of practical techniques, algorithms, and software for applying the theory to various classes of reactions and transition states; and
- (vi) applications to specific reactions, with special emphasis on combustion reactions and reactions that provide good test cases for methods needed to study combustion reactions.

The direct dynamics approach to gas-phase reactions in this project involves electronic structure calculations of potential energy surfaces and the use of these surfaces to calculate generalized free energies of activation and multidimensional tunneling probabilities. A key emphasis is the interface of electronic structure calculations with dynamics algorithms as achieved in the POLYRATE computer program and its various RATE interfaces to electronic structure packages.

Recent progress

The atomistic simulation of reactions of complex molecules, such as those involved in combustion, requires one to treat anharmonic, coupled torsions in both reactants and transition states, along with the accompanying torsional anharmonicity, and to consider reaction along more than one reaction path. Our major recent theoretical accomplishment is the development of an internal coordinate method for including multiple structures and torsional anharmonicity of torsions coupled to each other and to overall rotation and for including multiple reaction paths in reaction rate calculations that include both variationally optimized transition states and multi-dimensional tunneling. Our original version used an uncoupled torsional potential, and we have recently extended that to a coupled torsional potential as required to treat anharmonicity all along

the reaction path of a low-barrier bimolecular reaction. These methods have been incorporated in a computer code called *MSTor* that is now available to the community at no charge in an international program library and on our Web site. We have applied the method to calculate thermochemical quantities for many molecules, radicals, and transition states, and to calculate reaction rates of combustion reactions. Examples are given in the references below.

An example application is our work on sorting out the mechanism of the combustion of isobutanol (a prototype biofuel) where we provided information that is unavailable and not easily obtained by experiment. The rate constants and branching ratios for the hydrogen abstraction reactions from isobutanol were calculated using multi-path variational transition-state theory with small-curvature tunneling. We used hybrid degeneracy-corrected vibrational perturbation theory to show that it is critical to consider the anharmonicity difference of high-frequency modes between reactants and transition states. The factors determining the reaction rate constants were analyzed in detail, including variational effects, tunneling contributions, the effect of multiple reaction paths on transmission coefficients, and anharmonicities of low- as well as high-frequency vibrational modes. The analysis quantifies the uncertainties in the rate calculations. A key result was the prediction of the site dependence of hydrogen abstraction from isobutanol by hydroxyl radical.

We also made progress on calculating thermochemical quantities by Feynman path integral (FPI) methods. In particular we presented an improved version of our “path-by-path” enhanced same path extrapolation scheme for FPI calculations of free energies that permits rapid convergence with discretization errors ranging from $O(P^{-6})$ to $O(P^{-12})$, where P is the number of path discretization points. We also presented two extensions of our importance sampling and stratified sampling schemes for calculating vibrational–rotational partition functions by the FPI method. The first is the use of importance functions for dihedral angles between sets of generalized Jacobi coordinate vectors. The second is an extension of our stratification scheme to allow some strata to be defined based only on coordinate information while other strata are defined based on both the geometry and the energy of the centroid of the Feynman path. These enhanced methods were applied to calculate converged partition functions by FPI methods, and these results were compared to ones obtained earlier by vibrational configuration interaction (VCI) calculations on the same potential energy surface. The earlier VCI calculations are found to agree well within $\sim 1.5\%$ with the new FPI benchmarks, which were converged to within a 2σ statistical uncertainty of 0.07% or better for temperatures in the range 300–3000 K and are the most completely converged partition functions for a given potential energy surface for any molecule with five or more atoms. We also tabulated free energies, enthalpies, entropies, and heat capacities.

Software distribution

We have developed several software packages for applying variational transition state theory with optimized multidimensional tunneling coefficients to chemical reactions. These packages are well documented and distributed with manuals, installation scripts, and test suites. The license requests that we fulfilled during the period Jan. 1, 2012–March 17, 2015, for RATE packages developed under DOE support is as follows:

	<i>Total</i>	<i>academic</i>	<i>government//DoD/non-profit/industry</i>
POLYRATE	456	418	38
GAUSSRATE	254	238	16
7 other RATE programs	79	66	13

The total number of requests fulfilled for all RATE programs since we began keeping statistics in 1995 is 3040. Beginning with version 2011, we have distributed *MSTor* through both the *Computer Physics Communications* web site (<http://www.cpc.cs.qub.ac.uk>) and own web site (t1.chem.umn.edu/truhlar/index.htm#software). So far about 130 requests have been fulfilled by the former and 55 by the latter.

Future plans

The general objective of this project is to develop and employ improved methods for calculating the rate constants of gas-phase chemical reactions. Our work in the coming period will be focused on improved methods for calculating thermodynamics properties (enthalpies, energies, and free energies) for reactants and transition states of combustion calculations and for rate constants of such reactants. We will concentrate mainly on reactions with intrinsic barriers where the variational transition state can reasonably be expected to be well approximated by a search for dividing surfaces orthogonal to the minimum energy path. We will carry out applications to reactions of small molecular radicals (H, O, OH, and HO₂) with alkanes, alcohols, and *n*-alkyl benzenes, and we will develop integrated methods for including pressure dependence on rate constants of association reactions. We are presently working on extended versions of POLYRATE and GAUSSRATE with new capabilities for microcanonical rate constants and pressure dependence.

Publications supported by this grant, 2012-present

1. "Multipath Variational Transition State Theory. Rate Constant of the 1,4-Hydrogen Shift Isomerization of the 2-Cyclohexylethyl Radical," T. Yu, J. Zheng, and D. G. Truhlar, *Journal of Physical Chemistry A* **116**, 297-308 (2012). [dx.doi.org/10.1021/jp209146b](https://doi.org/10.1021/jp209146b)
2. "Multi-Structural Variational Transition State Theory: Kinetics of the 1,5-Hydrogen Shift Isomerization of 1-Butoxyl Radical Including All Structures and Torsional Anharmonicity," X. Xu, E. Papajak, J. Zheng, and D. G. Truhlar, *Physical Chemistry Chemical Physics* **14**, 4204-4216 (2012). [dx.doi.org/10.1039/c2cp23692c](https://doi.org/10.1039/c2cp23692c).
3. "Multi-path Variational Transition State Theory for Chemical Reaction Rates of Complex Polyatomic Species: Ethanol + OH Reactions," J. Zheng and D. G. Truhlar, *Faraday Discussions* **157**, 59-88 (2012). [dx.doi.org/10.1039/C2FD20012K](https://doi.org/10.1039/C2FD20012K).
4. "MSTor: A program for calculating partition functions, free energies, enthalpies, entropies, and heat capacities of complex molecules including torsional anharmonicity," J. Zheng, S. L. Mielke, K. L. Clarkson, and D. G. Truhlar, *Computer Physics Communications* **183**, 1803-1812 (2012). [dx.doi.org/10.1016/j.cpc.2012.03.007](https://doi.org/10.1016/j.cpc.2012.03.007)
5. "A Product Branching Ratio Controlled by Vibrational Adiabaticity and Variational Effects: Kinetics of the H + trans-N₂H₂ Reactions," J. Zheng, R. J. Rocha, M. Pelegrini, L. F. A. Ferrão, E. F. V. Carvalho, O. Roberto-Neto, F. B. C. Machado, and D. G. Truhlar, *Journal of Chemical Physics* **136**, 184310/1-10 (2012). [dx.doi.org/10.1063/1.4707734](https://doi.org/10.1063/1.4707734)
6. "What are the Most Efficient Basis Set Strategies for Correlated Wave Function Calculations of Reaction Energies and Barrier Heights?" E. Papajak and D. G. Truhlar, *Journal of Chemical Physics* **137**, 064110/1-8 (2012). [dx.doi.org/10.1063/1.4738980](https://doi.org/10.1063/1.4738980)
7. "Thermochemistry of Radicals Formed by Hydrogen Abstraction from 1-Butanol, 2-Methyl-1-propanol, and Butanal," E. Papajak, P. Seal, X. Xu, and D. G. Truhlar, *Journal of Chemical Physics* **137**, 104314/1-13 (2012). [dx.doi.org/10.1063/1.4742968](https://doi.org/10.1063/1.4742968)

8. "Role of Conformational Structures and Torsional Anharmonicity in Controlling Chemical Reaction Rates and Relative Yields: Butanal + HO₂ Reactions," J. Zheng, P. Seal, and D. G. Truhlar, *Chemical Science* **4**, 200-212 (2013). [dx.doi.org/10.1039/c2sc21090h](https://doi.org/10.1039/c2sc21090h)
9. "Multi-Structural Variational Transition State Theory: Kinetics of the Hydrogen Abstraction from Carbon-2 of 2-Methyl-1-propanol by Hydroperoxyl Radical Including All Structures and Torsional Anharmonicity," X. Xu, T. Yu, E. Papajak, and D. G. Truhlar, *Journal of Physical Chemistry A* **116**, 10480-10487 (2012). [dx.doi.org/10.1021/jp307504](https://doi.org/10.1021/jp307504)
10. "Biofuel Combustion. Energetics and Kinetics of Hydrogen Abstraction from Carbon-1 in *n*-Butanol by the Hydroperoxyl Radical Calculated by Coupled Cluster and Density Functional Theories and Multi-Structural Variational Transition State Theory with Multidimensional Tunneling," I. M. Alecu, J. Zheng, E. Papajak, T. Yu, and D. G. Truhlar, *Journal of Physical Chemistry A* **116**, 12206-12213 (2012). [dx.doi.org/10.1021/jp308460y](https://doi.org/10.1021/jp308460y)
11. "Quantum Thermochemistry: Multi-Structural Method with Torsional Anharmonicity Based on a Coupled Torsional Potential," J. Zheng and D. G. Truhlar, *Journal of Chemical Theory and Computation* **9**, 1356-1367 (2013). [dx.doi.org/10.1021/ct3010722](https://doi.org/10.1021/ct3010722)
12. "Including Torsional Anharmonicity in Canonical and Microcanonical Reaction Path Calculations," J. Zheng and D. G. Truhlar, *Journal of Chemical Theory and Computation* **9**, 2875-2881(2013). [dx.doi.org/10.1021/ct400231q](https://doi.org/10.1021/ct400231q)
13. "Chemical Kinetics and Mechanisms of Complex Systems: A Perspective on Recent Theoretical Advances," S. J. Klippenstein, V. Pande, and D. G. Truhlar, *Journal of the American Chemical Society* **136**, 528-546 (2014). (Perspective Article)
[dx.doi.org/10.1021/ja408723a](https://doi.org/10.1021/ja408723a)
14. "Army Ants Tunneling for Classical Simulations," J. Zheng, X. Xu, R. Meana-Pañeda, and D. G. Truhlar, *Chemical Science* **5**, 2091-2099 (2014). [dx.doi.org/10.1039/C3SC53290a](https://doi.org/10.1039/C3SC53290a)
15. "Anchor Points Reactive Potential for Bond-Breaking Reactions," K. R. Yang, X. Xu, and D. G. Truhlar, *Journal of Chemical Theory and Computation* **10**, 924-933 (2014).
[dx.doi.org/10.1021/ct401074s](https://doi.org/10.1021/ct401074s)
16. "Prediction of Experimentally Unavailable Product Branching Ratios for Biofuel Combustion: The Role of Anharmonicity," by J. Zheng, R. Meana-Pañeda, and D. G. Truhlar, *Journal of the American Chemical Society* **136**, 5150-5160 (2014).
[dx.doi.org/10.1021/ja5011288](https://doi.org/10.1021/ja5011288). Spotlight: see [dx.doi.org/10.1021/ja503143p](https://doi.org/10.1021/ja503143p)
17. "Quantum Mechanical Fragment Methods Based on Partitioning Atoms or Partitioning Coordinates," B. Wang, K. R. Yang, X. Xu, M. Isegawa, H. R. Leverentz, and D. G. Truhlar, *Accounts of Chemical Research* **47**, 2731-2738 (2014). (Special Issue: Beyond QM/MM: Fragment Quantum Mechanical Methods) [dx.doi.org/10.1021/ar500068a](https://doi.org/10.1021/ar500068a)
18. "Zero-Point Energy, Tunneling, and Vibrational Adiabaticity in the Mu + H₂ Reaction," S. L. Mielke, B. C. Garrett, D. G. Fleming, and D. G. Truhlar, *Molecular Physics* **113**, 160-175 (2014). [dx.doi.org/10.1080/00268976.2014.951416](https://doi.org/10.1080/00268976.2014.951416)
19. "Improved Methods for Feynman Path Integral Calculations and Their Application to Calculate Converged Vibrational–Rotational Partition Functions, Free Energies, Enthalpies, Entropies, and Heat Capacities for Methane," S. L. Mielke and D. G. Truhlar, *Journal of Chemical Physics* **142**, 044105/1-18 (2015). [dx.doi.org/10.1063/1.4905526](https://doi.org/10.1063/1.4905526)

Developing a predictive model for the chemical composition of soot nanoparticles: Integrating Model and Experiment

Lead PI: Prof. Angela Violi, University of Michigan, Ann Arbor avioli@umich.edu

Collaborating Institutions:

Combustion Research Facility - Sandia National Laboratories Livermore: PIs: Dr. N. Hansen and Dr. H. Michelsen

Program Scope / Definition

The goal of this proposal is to develop a validated predictive model to describe the chemical composition of soot nanoparticles in premixed and diffusion flames. The collaborative nature of the proposed study combines expertise in computational (Violi) and experimental (Hansen, Michelsen, and Wilson) areas to tackle the complex problem of soot nucleation and growth at the molecular level. The computational effort is tightly coupled to experimental data produced by the research groups of Michelsen and Hansen at Sandia National Laboratories and Wilson at Lawrence Berkeley National Laboratory. We have addressed several key questions concerning the formation and growth of soot nanoparticles and their precursor species with an array of state-of-the-art computational and experimental approaches. Our research provides critical insights for the development of the next generation of soot models, including those that model chemical and/or physical growth, with the capability to predict the nucleation process, and hence the number and size of nanoparticles, together with the evolution of their chemical composition. In particular, we can predict the morphologies of measured structures given their masses.

Recent Progress

Recent progress has involved both experimental and theoretical investigations as well as the integration of these respective studies to create insight as to the composition of nascent polycyclic aromatic hydrocarbons (PAHs) in premixed and counterflow flames. This project closely couples experimental investigations of soot precursors and incipient particle characteristics with the development of a predictive model for the chemical composition of soot nanoparticles.

Our collaborators studied premixed and counterflow argon-ethylene-oxygen and nitrogen-ethylene-oxygen atmospheric flames in laboratory scale reactors. They are able to analyze the mass spectra of the species in the flames as well as identify isomers based on photoionization efficiency curves. We use the measurements from these experiments to inform, constrain, and validate the methodology of our newly developed code for Stochastic Nanoparticle Simulation (SNAPS).

We developed new software for simulating gas-phase nanoparticle growth named SNAPS (Stochastic Nanoparticle Simulator). We have implemented our software to simulate the formation and growth of nanoparticles and their precursor species, polycyclic aromatic

hydrocarbons (PAHs), in high temperature flame environments. Recently, we have used SNAPS to model PAH growth in premixed flames, in order to elucidate the chemical composition of species associated with peaks in experimentally measured mass spectra provided by Michelsen and coworkers. SNAPS employs a probabilistic kinetic Monte Carlo approach to generating stochastic trajectories of the growth of small gas-phase molecules in a flame environment. The governing kinetic reactions are gathered from literature and when necessary calculated from first principles. The kinetic mechanism as originally constructed relied heavily on traditional PAH growth pathways, including Hydrogen-abstraction-C₂H₂-addition (HACA), addition of ethylene and benzene, and addition of vinyl, methyl, propargyl, cyclopentadienyl, and phenyl radicals. Because of the probabilistic nature of each growth trajectory, we rely on generating an ensemble of thousands of trajectories to generate statistically significant predictions about the likely growth pathways and final morphologies of nanoparticles. The ensemble of trajectories represents the macroscopic number of particles in a flame measured in a flame. We can compare our computed number of particles at each mass with mass spectra generated from experiments. For example, Figure 1 shows a comparison between experimentally measured and computed mass spectra for a counterflow acetylene/oxygen flame at a distance of 5.75 mm from the fuel outlet, showing good reproduction of the experimental data. This comparison corroborates the validity of SNAPS simulations and the credibility of further detailed analysis of the simulation trajectories.

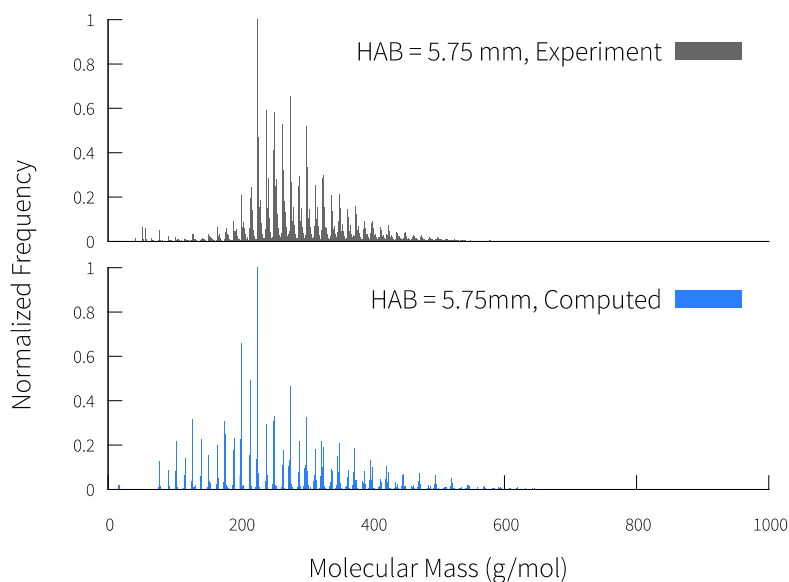


Figure 1: Comparison of ensemble-averaged mass distributions computed by SNAPS (2000 trajectories) compared with experimentally measured values in the counterflow acetylene/oxygen flame at a height of 5.75 mm above burner.

More recent work has focused on expanding and refining the SNAPS growth mechanism and incorporating oxygen interaction. Traditional PAH growth models do not consider oxygen involvement in the chemistry of PAH growth or oxygen incorporation into the particles. Recently, however, researchers have begun to suspect that measured PAH-like species in flames may in fact be oxygenated because they see peaks in mass spectra that cannot be explained by the existing growth pathways. We have updated our growth mechanism to account for the role oxygen plays in the growth of these species as well as predict the extent of oxygen absorption in

the structures of PAHs. A manuscript is in preparation regarding oxygen involvement in the growth mechanism of PAHs.

Building on the continued development of SNAPS and maintaining the methodology of the approach, we have assembled a mechanism that describes oxygenated species interactions with nanoparticles and how oxygen atoms may become embedded in the particles. We have worked in parallel with our collaborators at Sandia National Laboratories who are measuring oxygenated species in premixed and counterflow flames. We have observed that oxygen incorporation is integral to the overall growth of nanoparticles. The traditional HACA growth patterns are still prevalent, but new pathways involving oxygen are proving to be important. In fact, the oxygen pathways are necessary in order to reproduce experimental observations of mass spectra in recently studied flames by Michelsen et al. Accounting for possible oxygen addition onto the particles yields computed mass spectra in much closer alignment with the mass spectra generated in experimental flames than the computed spectra produced with only carbon chemistry. We have observed that oxygen atoms are often absorbed by the particle; subsequent acetylene additions and ring closure reactions – i.e. traditional HACA reactions – yield oxygen-containing rings. These oxygenated rings still produce active sites, thus subsequent chemical and physical growth is possible. Typical oxygenated molecular structures that represent many of those observed during nanoparticles growth simulations are shown in Figure 2. The most commonly predicted oxygenated molecular groups on nanoparticles are ether groups and carbonyl groups. The former is most often formed when an oxygen addition to a ring carbon is followed by a subsequent aliphatic addition to the oxygen, the latter most often occurs when a hydroxyl addition to an aliphatic chain is succeeded by hydrogen abstractions from the oxygen and carbon leading to a carbonyl formation. Both ether and carbonyl groups maintain reactivity and neither stunt the kinetic growth of that section of the particle.

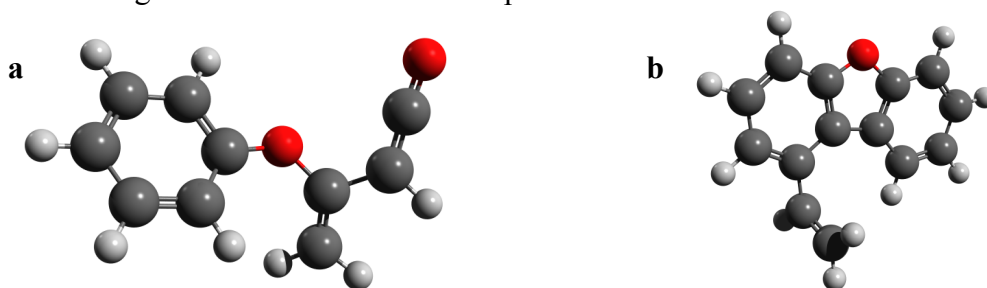


Figure 2: Mid-simulation morphology of a structure of mass a) 160 amu and b) 194 amu using SNAPS to model particle growth in a Argon-diluted premixed flame studied by Michelsen et al. Figure 2a demonstrates the ether group and carbonyl group. Figure 2b demonstrates the continued ring closure reactions embedding an oxygen atom into a 5 membered ring and allowing subsequent HACA growth yielding another 6 carbon-membered ring.

Experimental analysis compares photoionization efficiency (PIE) curves of known species to those measured on sampled PAH mass to conjecture about the types of PAH species associated with a given peak. Aiding this approach, the SNAPS simulations allow the evaluation of the plausibility of such conjecture and elucidate molecular detail about peaks in mass spectra. In this way, we can achieve synergy between experimental and theory to further drive our collective efforts and create deeper insight into the PAH growth process, particularly providing information about the role oxygen incorporation plays in the growth of PAHs.

Future Work

Future work will involve close coupling experimental and modeling efforts, towards further characterizing PAH growth in a variety of flame environments. These efforts will involve further experimental probing of soot precursors, searching in particular for oxygenated species predicted by simulations. The success or failure of these predictions will further enable refinement of the simulation methodology and oxygen chemistry, thus building a strong description of the beginnings of the soot formation process.

References DOE sponsored research appeared since 2012

1. S.H. Chung, A. Violi “Pericondensed aromatics with aliphatic chains as key intermediates for the nucleation of aromatic hydrocarbons” *Proc. Combust. Inst.* 33(1), 693-700, (2011).
2. S. A. Skeen, H. A. Michelsen, K. R. Wilson, D. M. Popolan, A. Violi, and N. Hansen, “Near-threshold photoionization mass spectra of combustion-generated high-molecular-weight soot precursors,” *J. Aerosol Sci.*, vol. 58, pp. 86–102, Apr. 2013.
3. S.A. Skeen, B. Yang, H.A. Michelsen, J.A. Miller, A. Violi, N. Hansen “Studies of laminar opposed-flow diffusion flames of acetylene at low-pressures with photoionization mass spectrometry”, *Proceedings of the Combustion Institute* 34 (2013), pp. 1067-1075.
4. P. Elvati, A. Violi “Thermodynamics of poly-aromatic hydrocarbon clustering and the effects of substituted aliphatic chains” *Proceedings of the Combustion Institute* 34 (2013), pp. 1837-1843.
5. K.O. Johansson, J. Lai, S.A. Skeen, K.R. Wilson, N. Hansen, A. Violi and H.A. Michelsen “Soot precursor formation and the breakdown of the stabilomer concept” *Proc. Combust. Inst.*: 35, submitted, accepted for oral presentation.
6. J.Y. Lai, P. Elvati, A. Violi, “Stochastic Atomistic Simulation of Polycyclic Aromatic Hydrocarbon Growth in Combustion”, *Phys. Chem. Chem. Phys.*, 16 (17), 7969 – 7979 (2014).
7. J.S. Lowe, J.Y.W. Lai, P. Elvati and A. Violi. “Towards a predictive model for polycyclic aromatic hydrocarbon dimerization propensity”, *Proceedings of the Combustion Institute* 35 (2015), pp. 1827-1832.

PRESSURE DEPENDENCE OF COMBUSTION REACTIONS: QUANTUM INELASTIC DYNAMICS ON AUTOMATICALLY GENERATED POTENTIAL ENERGY SURFACES

Albert Wagner
Chemical Sciences and Engineering Division
Argonne National Laboratory
9700 South Cass Avenue
Argonne, IL 60439
Email: wagner@anl.gov

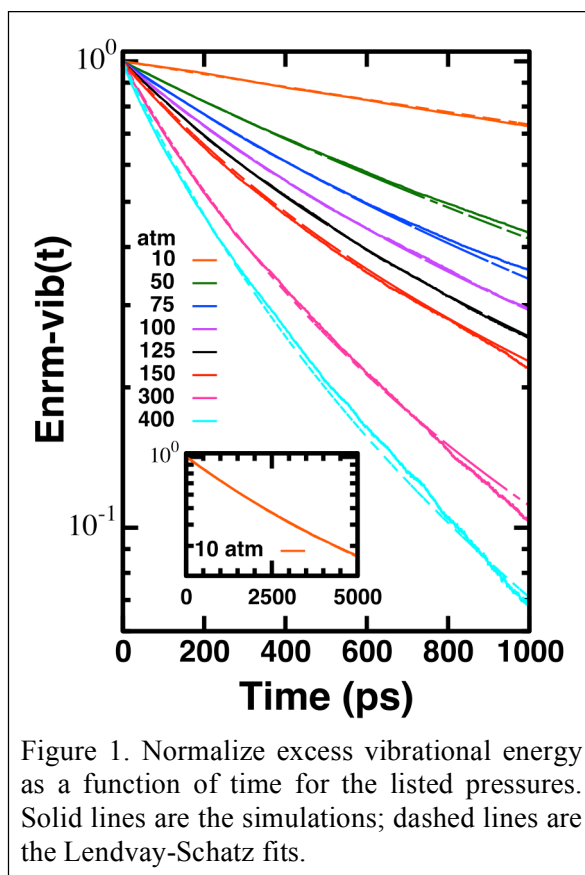
PROJECT SCOPE

This program is aimed both at developing improved ways to automatically construct a reliable potential energy surface (PES) and at using such surfaces to understand pressure effects on relaxation and reaction processes. In this last year, opportunities in studying both inelastic relaxation at high pressures and tunneling processes in bimolecular reactions were pursued.

RECENT PROGRES

High Pressure Relaxation: We are using molecular dynamics simulations to study the transition in relaxation and reaction rates from low-pressure behavior where bath-gas/molecule collisions are binary to high-pressure behavior where most collisions involve multiple bath gas atoms. In collaboration with the Thompson group (U. Missouri), we are examining the vibrational and rotational relaxation of initially excited molecules in a thermal Ar bath gas at pressures that range over two orders of magnitude from ~10 atm to ~1000 atm. With periodic boundary conditions both molecule and bath gas motion is explicitly followed. At low pressures, the relaxation rate to thermal equilibrium is directly proportional to pressure because pressure controls the frequency at which isolated binary collisions happen. At much higher pressures, relaxation rate changes increasingly lag behind pressure changes because most collisions involve multiple partners. These studies seek to determine the nature and mechanisms behind the change in pressure dependence.

In Fig. 1, the color-coded solid lines are the computed decay of the vibrational component of 50 kcal/mol of initial excitation in CH_3NO_2 in a room temperature Ar bath

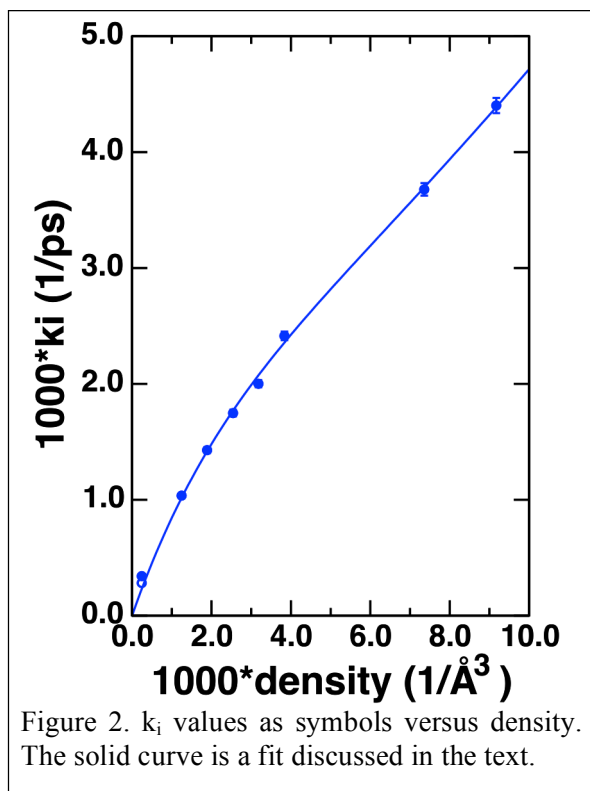


gas. (See publication 1.) The decay curves are ensemble averages over 1000 trajectories each one of which explicitly follows 1000 Ar atoms and one CH₃NO₂ molecule for up to 5 ns. In the figure En_{rm-vib} is the ensemble average of *excess* initial vibrational energy over the thermal vibrational energy normalized to unity at zero time. The figure shows that vibrational relaxation has ns time constants. The computed decay of excess rotational energy (not shown) is 100x slower.

The figure clearly shows, even for the lowest pressure of 10 atm, that the relaxation is not a single exponential decay. The computed decays are well fit (see dashed lines) by the Lendvay-Schatz form of $En_{rm}(t) = [1 - (1-m)k_i t]^{1/(1-m)}$ where m and k_i are two adjustable constants. With this form, the rate of decay at $t = 0$ is k_i while the increase of m above 1 measures the global curvature of the decay from a straight line, single exponential decay on a semi-log plot. The Lendvay-Schatz form arises out of single collision studies in which the average energy lost per collision is assumed to be proportional to the energy of the molecule raised to the power m .

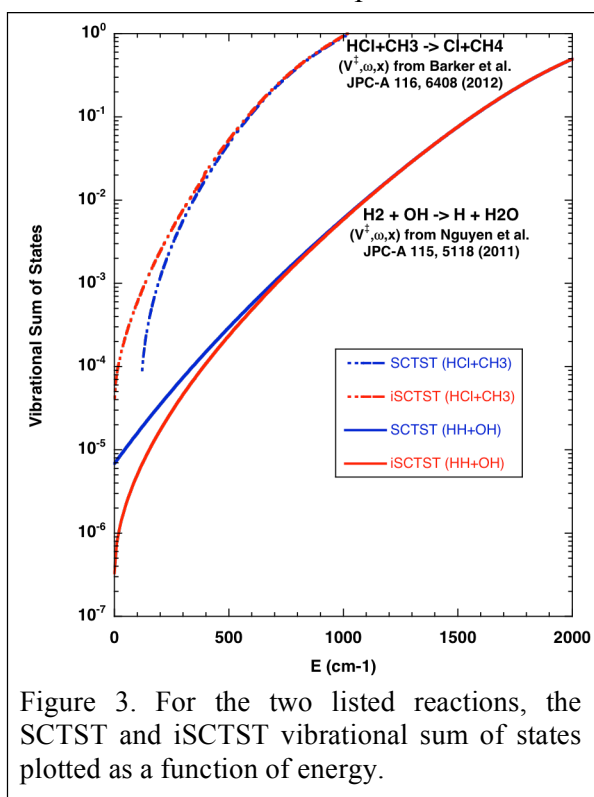
Figure 2 plots as symbols the value of k_i as a function of the computed bath gas density (which of course is controlled by the pressure). The results in the figure show that the initial rate is curving over with increased density. Where this curvature first occurs is ~ 100 atm. To give some notion of scale, given the radius of Ar used in the simulation (1.675 Å), Ar will become a solid at a $\sim 4x$ larger density than the maximum density in the figure. The solid line in the figure is an adjustable model based on multiple collisions. This model is a 3D combinatorial model based on discretizing all space not taken up by CH₃NO₂ in to cubes that can hold only one Ar atom. The bath gas density at a given pressure sets the number of Ar atoms in a finite region of this discretized volume. Analytic combinatorial formulas then determine the probability that an Ar atom is in a discretized volume adjacent to the CH₃NO₂ volume. This becomes the probability at a given density of a molecular collision event with L Ar atoms. Associating cross sections with each collision event adjusted to fit k_i in Fig. 2 leads to the curve in that figure. The end results is that while a collision event involving $L > 1$ Ar atoms is more efficient in relaxing the molecule than a single collision, it is not L times more efficient. This leads to k_i curving over with density as density increases.

Tunneling in Bimolecular Reactions: Most tunneling methods are based on reaction paths whose calculation is typically not readily parallelized. Miller et al.¹ developed an alternative approach based on readily parallelized, higher order vibrational perturbation



theory (VPT) at the saddle point. This approach recognizes that the saddle point energy when expanded in various powers of the quantum numbers will have imaginary expansion coefficients connected to the quantum number for motion along the reaction path. The replacement of this quantum number by an imaginary semiclassical action leads to a polynomial expansion of the energy in the action whose order depends on the VPT order. For up to fourth order in the action, the energy as a function of action can be analytically inverted to the action as a function of energy. From this an analytic, multi-dimensional, semiclassical tunneling probability can be readily obtained. Applications to date have used only second order (VPT2) theory and this tunneling approach is labeled SCTST in the Multiwell² suite of codes for thermal kinetics. For deep tunneling substantially below the top of the barrier, the VPT2 analytic formula is not qualitatively correct. In this case, the energy expansion is a quadratic function of action with a maximum that sets a limit to the smallest energy that the expansion can represent. That limit is only indirectly related to the true forward and reverse barriers at the saddle point. To incorporate the actual computed barrier, we developed a composite three-segment Eckart potential continuous everywhere in value and derivative that correctly represents in the middle segment the VPT2 properties of the saddle point and in the first and third segments the correct forward and reverse barriers. When incorporated into a semiclassical barrier penetration integral, this composite potential analytically extends the original VPT2 formula all the way to the base of the true barrier. This improved iSCTST option will be in the next release of Multiwell.

In publication 2, this approach was applied to unimolecular tunneling of H(D)OCO to H(D)+CO₂ and the results on high quality PESs are consistent with both experiment and tunneling computed by the reaction-path based small curvature tunneling method of Polyrate. We are now testing this approach to bimolecular abstraction reactions. In Fig. 3 the sum of states is displayed for the two listed reactions whose VPT2 characterization of the saddle point has been published in kinetics papers by the Barker (U. Michigan) and Stanton/Nguyen (U. Texas) team associated with Multiwell. For HCl+CH₃ the limiting energy for SCTST is smaller than the true barrier, resulting in the deepest tunneling not being described. For H₂+OH, the limiting energy is larger than the true barrier, producing a tunneling probability at the base of the barrier that does not go to zero. The iSCTST results based on composite potentials have the qualitatively correct deep tunneling properties and properly merge with SCTST at higher energies.



FUTURE PLANS

The pressure dependent studies of relaxation are continuing on multiple fronts. For CH_3NO_2 , the molecular mechanisms involved in the rate constant curvature are unknown. We are converting trajectory information into time-dependent normal mode populations to see if bottlenecks in internal vibrational energy flow are part of the explanation. A trajectory simulation of HO_2 in an Ar bath gas has just completed and is now being analyzed. In collaboration with the Hase group (Texas Tech U.), we plan to further analyze the pressure dependence of published³ trajectory simulations on C_6F_6 in N_2 . Finally in collaboration with the Dawes group (Missouri Institute for Science and Technology) and Thompson group, we are planning a study of C_2H_5 in an Ar. The C_2H_5 PES is based on direct dynamics unimolecular dissociation simulations using M05 DFT calculations and exploits permutation invariances.

The bimolecular tunneling studies are continuing in multiple directions in collaboration with the Stanton, Nguyen, and Barker team. First, SCTST/iSCTST methods have been tested against reaction-path based methods (in Polyrate) only twice: the HOCO tunneling (publication 2) and a H_2+OH study⁴ early in the development of Multiwell. In both cases, the two approaches produced comparable results. We intend to expand upon this small sample with further studies on a greater variety of reactions. Second, typically iSCTST is only significantly different from SCTST in the deep tunneling regime that translates into low temperature kinetics. How low a temperature will be investigated for a variety of published SCTST kinetics calculations. Finally, we are exploring the implications of VPT4 and higher orders on semiclassical tunneling.

References

- ¹ W. H. Miller, R. Hernandez, N. C. Handy, D. Jayatilaka, and A. Willets, *Chem. Phys. Lett.* **1990**, 172, 62.
- ² As developed by T. L. Nguyen, J. F. Stanton, and J. R. Barker and contained in Multiwell at <http://aoss-research.engin.umich.edu/multiwell/>
- ³ A. K. Paul, S. C. Kohale, S. Pratihar, R. Sun, S. W. North, and W. L. Hase, *J. Chem. Phys.* **140**, 194103 (2014).
- ⁴ T. L. Nguyen, J. F. Stanton, and J. R. Barker, *Chem. Phys. Lett.* **499**, 9 (2010).

DOE-SPONSORED PUBLICATIONS SINCE 2012

1. L. A. Rivera-Rivera, A. F. Wagner, T. D. Sewell, and D. L. Thompson PRESSURE EFFECTS ON THE RELAXATION OF AN EXCITED NITROMETHANE MOLECULE IN AN ARGON BATH, *J. Chem. Phys.* **142**, 014303 (2015).
2. A. F. Wagner, R. Dawes, R. E. Continetti, and H. Guo, THEORETICAL/EXPERIMENTAL COMPARISON OF DEEP TUNNELING DECAY OF QUASI-BOUND H(D)OCO TO H(D)+CO₂, *J. Chem. Phys.* **141**, 054304 (2014)
3. A. F. Wagner, IMPROVED MULTIDIMENSIONAL SEMICLASSICAL TUNNELING THEORY, *J. Phys. Chem. A* **117**, 13089-13100 (2013).
4. J. W. Perry, R. Dawes, A. F. Wagner, and D. L. Thompson, CLASSICAL TRAJECTORY STUDY OF THE INTRAMOLECULAR DYNAMICS, ISOMERIZATION, AND UNIMOLECULAR DISSOCIATION OF HO₂, *J. Chem. Phys.* **139**, 084319 (2013)
5. A. F. Wagner, L. A. Rivera, D. Bachelierie, J. W. Perry, and D. L. Thompson, A CLASSICAL TRAJECTORY STUDY OF THE DISSOCIATION AND ISOMERIZATION OF C₂H₅, *J. Phys. Chem. A* **117**, 11624-11639 (2013)

Chemical Kinetic Modeling of Combustion Chemistry

William J. Pitz, Charles K. Westbrook
Lawrence Livermore National Laboratory, Livermore, CA 94550
pitz1@llnl.gov

1. Program Scope

We develop chemical kinetic reaction mechanisms to describe the combustion of hydrocarbons and other related fuels, including fuels derived from biomass. These mechanisms are validated through comparisons between computations and experimental results in carefully controlled laboratory-scale facilities including shock tubes, laminar flames, stirred reactors, and rapid compression machines. After validation, these mechanisms are then used to understand more complex combustion phenomena in practical engines and other combustion systems. We determine particularly sensitive parts of these mechanisms and provide that information to other DOE/BES researchers who can use theory and new experiments to refine the kinetic models. We try to anticipate kinetic modeling needs of the DOE combustion community, so other researchers can have accurate models to assist in their own research projects. Our kinetic mechanisms are freely available at https://www-pls.llnl.gov/?url=science_and_technology-chemistry-combustion and provide a valuable service to the combustion community.

2. Recent Progress

Since kinetic reaction mechanisms can be large and complex, we try to identify specific reaction classes that can apply to many different types of fuel molecules. Some examples of reaction classes include H atom abstraction, radical decomposition, addition of O₂ to hydrocarbon radicals, alkyl and alkylperoxy radical isomerization; current models consider nearly 30 reaction classes. When this project began in about 1980, very few of the reaction classes, especially those dealing with complex radical isomerization and addition reactions of O₂ to alkyl and related radical species, had been studied using either chemical theory or direct laboratory experiments, so most of these important reaction classes had to use estimated rates, usually based on similar but sometimes not very close chemical analogies. In the past few years, new theory, new experiments, and new kinetic modeling approaches have greatly improved the accuracy of these kinetic models. In many cases, our publications of kinetic models and modeling results stimulated new attention for others to contribute new theoretical and experimental studies that were extremely useful, and this type of exchange accelerates the development of more accurate and powerful kinetic models.

A. Reaction rate rules for alkane fuels

Reaction rates in the alkylperoxy radical isomerization pathways have received an enormous amount of excellent kinetic theory attention in the past 3-5 years, requiring us to revise thoroughly all of the low temperature reaction rates and reaction pathways. In particular, in the past year we have done a complete renovation of the low temperature kinetics of saturated hydrocarbons (specifically for *n*-heptane) and produced much improved agreement between computed and experimental observations. This work will be continued into the next year to complete the renovation of our *n*-alkane (*n*-heptane to *n*-eicosane), branched alkanes (2-methyl hexane to 2-methyl nonadecane), and primary reference fuels (PRF) (iso-octane, iso-cetane) that are an important part of the legislated quality controls of engine fuels. At first, we had assumed

that the reaction rate rules governing low temperature alkylperoxy radical isomerization and cool flame pathways, depended only on the transition state ring size and the C-H bonds being broken and formed, but the new theory studies, combined with inaccurate model predictions, led to a conclusion that the overall structure of the fuel molecule plays a stronger role in determining the reaction rate rules than previously believed, and the new rules are now being implemented into our new kinetic models for multiply-branched alkane fuels including 2,5-Dimethylhexane [1] and 2,7-dimethyloctane [2].

B. Reaction rate rules for olefinic fuels, allylic C-H bonds, and Octane Sensitivity

We used the small olefin fuel 2-methyl 2-butene (2M2B) to study the kinetics of allylic C-H bonds in hydrocarbon fuel oxidation, and our recently published paper [3] has shown that such bonds encourage rapid H atom abstraction but that the resulting allyl radicals are too stable to react at the same low temperature conditions where saturated hydrocarbon fuels are reacting very rapidly via cool flame kinetics and radical isomerization reactions. Octane Sensitivity is a phenomenon where a fuel has a high Research Octane Number but a surprisingly low Motored Octane Number, resulting in a high Octane Sensitivity S , which is defined as $RON - MON = S$. A high Octane Sensitivity has unusual advantages for use of such fuels under “boosted” operating conditions, where fuel is injected into a Spark-Ignition (SI) engine using elevated intake pressures to increase power production in that engine. Fuels with zero or low Sensitivity will respond to boosted fuel injection by knocking, but fuels with considerable Octane Sensitivity can withstand such elevated intake pressures without knocking, and our kinetic model for 2M2B traces these effects to details in the kinetic reaction mechanism and the thermochemistry of olefinic fuels. We are currently extending our kinetic model development and analysis to deal with additional classes of fuels, butyl and pentyl alcohols [4-6], several ketones, and methyl and ethyl esters including biodiesel fuels, where each of these classes of fuels has C-H bonds in the fuel that are unusually weak due to the thermochemistry of an adjacent O atom in the fuel, that leads to significant levels of Octane Sensitivity. This work will also be continued in the coming year, with a goal of providing valuable fuel formulation insights to engine designers who would like to design fuels and engines together to enhance performance and limit emissions.

C. Reaction rate rules for alkyl cyclohexanes and cyclo-benzenes

An important class of hydrocarbon fuels for which little kinetic modeling has been done are the alkyl benzenes. The chemical kinetic field has taken more than 20 years to develop a reasonably accurate mechanism for toluene (methyl benzene)[7, 8], and using that toluene mechanism as a reference, we have extended the kinetic models for alkyl benzenes to n-propyl benzene [9] and n-butyl benzene [10]. In this process, we found again that the presence of the aromatic ring produces a sufficiently different electronic environment that most or all of the low temperature radical isomerization and many other kinetic classes required new reaction rate rules. In similar studies in the past year on alkyl cycloalkanes, specifically methyl cyclohexane, new reaction class rules were required to be able to produce the observed degree of low temperature kinetic behavior that is observed in experiments.

3. Future Plans

We plan to continue developing kinetic mechanisms for fuels important for energy production in modern engines, including conventional reciprocating engines as well as promising

next-generation engine and gas turbines, and using these models to address practical combustion problem. We welcome the contributions of more fundamental scientists and engineers who can help us refine the current and upcoming kinetic models to improve their functionality.

References

1. Paper 5 below.
2. Paper 18 below.
3. Paper 17 below.
4. Paper 3 below.
5. K. A. Heufer, S. M. Sarathy, H. J. Curran, A. C. Davis, C. K. Westbrook, W. J. Pitz, *Energy & Fuels* 26 (11) (2012) 6678-6685.
6. S. M. Sarathy, S. Vranckx, K. Yasunaga, M. Mehl, P. Oßwald, W. K. Metcalfe, C. K. Westbrook, W. J. Pitz, K. Kohse-Höinghaus, R. X. Fernandes, H. J. Curran, *Combust. Flame* 159 (6) (2012) 2028–2055.
7. M. Mehl, W. J. Pitz, C. K. Westbrook, H. J. Curran, *Proc. Combust. Inst.* 33 (1) (2011) 193-200.
8. W. K. Metcalfe, S. Dooley, F. L. Dryer, *Energy & Fuels* 25 (11) (2011) 4915–4936.
9. Paper 2 below.
10. Paper 1 below.

Published papers in 2013 to 2015

1. Nakamura, H., Darcy, D., Mehl, M., Tobin, C. J., Metcalfe, W. K., Pitz, W. J., Westbrook, C. K. and Curran, H. J., "An Experimental and Modeling Study of Shock Tube and Rapid Compression Machine Ignition of n-Butylbenzene/Air Mixtures," **Combust. Flame** 161 (1) (2014) 49-64.
2. Darcy, D., Nakamura, H., Tobin, C. J., Mehl, M., Metcalfe, W. K., Pitz, W. J., Westbrook, C. K. and Curran, H. J., "A High-Pressure Rapid Compression Machine Study of n-Propylbenzene Ignition," **Combust. Flame** 161 (1) (2014) 65-74.
3. Sarathy, S.M., Park, S., Weber, B.W., Wang, W., Veloo, P.S., Davis, A.C., Togbe, C., Westbrook, C.K., Park, O., Dayma, G., Luo, Z., Oehlschlaeger, M.A., Egolfopoulos, F.N., Lu, T., Pitz, W.J., Sung, C.-J., and Dagaut, P., "A comprehensive experimental and modeling study of iso-pentanol combustion", **Combust. Flame** 160, 2712-2728 (2013).
4. Darcy, D., Nakamura, H., Tobin, C. J., Mehl, M., Metcalfe, W. K., Pitz, W. J., Westbrook, C. K. and Curran, H. J., (2013). "An Experimental and Modeling Study of a Surrogate Mixtures of n-Propyl- and n-Butylbenzene in n-Heptane to Simulate n-Decylbenzene Ignition," **Combust. Flame** 161 (6) (2014) 1460-1473.
5. Sarathy, S. M., Javed, T., Karsenty, F., Heufer, A., Wang, W., Park, S., Elwardany, A., Farooq, A., Westbrook, C. K., Pitz, W. J., Oehlschlaeger, M. A., Dayma, G., Curran, H. J. and Dagaut, P., "A Comprehensive Combustion Chemistry Study of 2,5-Dimethylhexane," **Combust. Flame** 161 (6) (2014) 1444–1459.
6. Weber, B. W., W. J. Pitz, M. Mehl, E. J. Silke, A. C. Davis and C.-J. Sung (2014). "Experiments and Modeling of the Autoignition of Methylcyclohexane at High Pressure." **Combust. Flame** 161 (8) (2014).

7. Sarathy, S. M., Kukkadapu, G., Mehl, M., Wang, W., Javed, T., Park, S., Oehlschlaeger, M. A., Farooq, A., Pitz, W. J. and Sung, C.-J., "Ignition of Alkane-Rich Face Gasoline Fuels and Their Surrogate Mixtures," **Proc. Combust. Inst.** **35** (1) (2015) 249–257. 11.
8. C. K. Westbrook and W. J. Pitz, "Fundamental Chemical Kinetics," in Encyclopedia of Automotive Engineering (David Crolla; David E. Foster; Toshio Kobayashi; Nicholas Vaughan, Eds.), Wiley Online Library (2014).
9. Mehl, M., Herbinet, O., Dirrenberger, P., Bounaceur, R., Glaude, P.-A., Battin-Leclerc, F. and Pitz, W. J., "Experimental and Modeling Study of Burning Velocities for Alkyl Aromatic Components Relevant to Diesel Fuels," **Proc. Combust. Inst.** **35** (2015) 341-348.
10. Goldsborough, S. S., Johnson, M. V., Banyon, C., Pitz, W. J. and McNenly, M. J., "Experimental and Modeling Study of Fuel Interactions with an Alkyl Nitrate Cetane Enhancer, 2-Ethyl-Hexyl Nitrate," **Proc. Combust. Inst.** **35** (1) (2015) 571–579.
11. Nakamura, H., Curran, H., Córdoba, A. D. P., Pitz, W. J., Dagaut, P., Togbé, C., Sarathy, S. M., Mehl, M., Agudelo, J. and Bustamante, F., "An Experimental and Modeling Study of Diethyl Carbonate Oxidation," **Combust. Flame** **162** (4) (2015) 1395–1405.
12. Kukkadapu, G., Kumar, K., Sung, C.-J., Mehl, M. and Pitz, W. J., "Autoignition of Gasoline Surrogates at Low Temperature Combustion Conditions," *Combustion and Flame* (2015) <http://dx.doi.org/10.1016/j.combustflame.2015.01.025>
13. Farooq, A., Davidson, D.F., Hanson, R.K., and Westbrook, C.K., "A comparative study of the chemical kinetics of methyl and ethyl propanoate", **Fuel** **134**, 26-38 (2014).
14. Korobeinichev, O. P., Yakimov, S.W., Knyazkov, D.A., Shmakov, A.G., Bolshova, T.A., Gerisomov, I.E., Hansen, N., Westbrook, C.K., and Dayma, G., "Study of Premixed Methyl Pentanoate Flame Using MBMS Mass Spectrometry with Synchrotron Photoionization and Soft Electron Impact Ionization, as well as Computer Simulation"
15. Wagon, S.W., Karwat, D.M.A., Wooldridge, M.S., and Westbrook, C.K., "Experimental and Modeling Study of Methyl trans-Hexenoate Autoignition", **Ener. Fuels** **28**, 7227-7234 (2014).
16. Korobeinichev, O.P., Gerasimov, I.E., Knyazkov, D.A., Shmakov, A.G., Bolshova, T.A., Hansen, N., Westbrook, C.K., Dayma, G., and Yang, B., "An Experimental and Kinetic Modeling Study of Premixed Laminar Flames of Methyl Pentanoate and Methyl Hexanoate", **Z. Phys. Chem.** accepted for publication (2015). DOI 10.1515/zpch-2014-0596.
17. Westbrook, C.K., Pitz, W.J., Mehl, M., Glaude, P.-A., Herbinet, O., Bax, S., Battin-Leclerc, F., Mathieu, O., Petersen, E.L., Bugler, J., Curran, H.J., "An Experimental and Kinetic Modeling Study of 2-Methyl-2-Butene: Allylic Hydrocarbon Kinetics", **J. Phys. Chem. A** in press (2015). DOI: 10.1021/acs.jpca.5b0068
18. Li, S., Sarathy, S.M., Davidson, D.F., Hanson, R.K., and Westbrook, C.K., "Shock tube and modeling study of 2,7-dimethyloctane pyrolysis and oxidation", **Combust. Flame** in press (2015). <http://dx.doi.org/10.1016/j.combustflame.2015.01.027>.
19. Wang, Y.L, Lee, D.J., Westbrook, C.K., Egolfopoulos, F.N., Tsotsis, T.T., "Oxidation of small alkyl esters in flames", **Combust. Flame** **161**(3), 810-817 (2014).
20. Cai, L., Sudholt, A., Lee, D.J., Egolfopoulos, F.N., Pitsch, H., Westbrook, C.K., Sarathy, S. M., "Chemical kinetic study of a novel lignocellulosic biofuel: Di-n-butyl ether oxidation in a laminar flow reactor and flames", **Combust. Flame** **161**, 798-809 (2014).

Low Temperature Combustion Chemistry and Fuel Component Interactions

Margaret S. Wooldridge

Departments of Mechanical and Aerospace Engineering, University of Michigan

2350 Hayward Street, Ann Arbor, MI 48109-2121

mswool@umich.edu

I. Program Scope

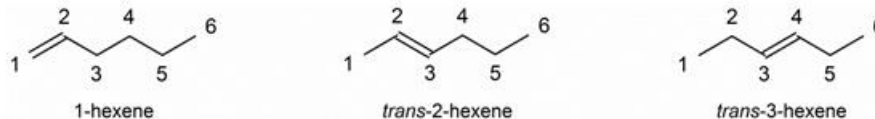
Recent research into combustion chemistry has shown that reactions at “low temperatures” (700 – 1100 K) have a dramatic influence on ignition and combustion of fuels in virtually every practical combustion system. A powerful class of laboratory-scale experimental facilities that can focus on fuel chemistry in this temperature range is the rapid compression facility (RCF), which has proven to be a powerful tool to examine the details of fuel chemistry in this important regime. Our past studies have advanced our understanding of low temperature chemistry of important fuel compounds and has identified areas of high uncertainty for further research. In particular, we have shown how factors including fuel molecular structure, the presence of unsaturated C=C bonds, and the presence of alkyl ester groups influence fuel auto-ignition and produce variable amounts of negative temperature coefficient behavior of fuel ignition. We have also reported new discoveries of synergistic ignition interactions between alkane and alcohol fuels, with both experimental and kinetic modeling studies of these complex interactions. This project focuses on further clarifying the effects of molecular structure on combustion chemistry including carbon bond saturation, through low temperature experimental studies of esters, alkanes, alkenes, and alcohols.

II. Recent Progress

During the past year, we completed ignition and speciation studies of the three linear isomers of hexene [1], and we completed an ignition study of ethanol [2]. Ignition delay time data were acquired using the University of Michigan (UM) RCF over a range of state and mixture conditions for each of these fuels. Mass sampling and gas chromatography were applied to quantify the stable intermediates present during ignition of the 3 hexene isomers. Additionally, in collaboration with Dr. Darshan Karwat (a doctoral graduate of this project, currently an AAAS fellow at the DOE) and Drs. Stephen Klippenstein and Michael Davis of Argonne National Laboratory [3], we completed a computational study that revisited n-butanol ignition and speciation data previously acquired as part of this project [4]. Details of the studies of ethanol and n-butanol study are not presented here, but can be found in Barraza-Botet *et al.* [2] and Karwat *et al.* [3,4].

The UM RCF is an innovative and robust experimental apparatus that can be used to isolate reaction kinetics by creating uniform conditions over a broad range of temperatures ($T = 500\text{-}3000\text{ K}$) and pressures ($P = 0.5\text{-}60\text{ atm}$). The long test times of the UM RCF allow application of rapid gas sampling methods to simultaneously measure a large number of stable species during ignition experiments. Details on the dimensions, components and performance characterization of the UM RCF can be found in Donovan *et al.* [5]. Previous UM RCF studies have considered ignition chemistry of numerous important reference fuel compounds including iso-octane [6], n-heptane [7], n-butanol [4], H_2/CO mixtures [8], and C_5 esters [9,10]. UM RCF studies include continuous absolute measurements of OH radicals during iso-octane ignition [11], as well as discrete measurements of intermediate species formed during ignition for several different fuel compounds [7,4,10,12].

This report presents a brief summary of the results of the recent UM RCF study of the three linear hexene isomers [1]:



Experiments were conducted using the UM RCF to determine ignition delay times from pressure time histories. Stoichiometric ($\phi = 1.0$) mixtures at dilution levels of buffer gas: $\text{O}_2 = 7.5$ (mole basis) were investigated at an average pressure of 11 atm and temperatures from 837-1086 K. The measured ignition delay times are presented in **Fig. 1**. The UM RCF data are highlighted in the inset of **Fig. 1** and show the three hexene isomers exhibited virtually identical reactivity (within the uncertainty of the measurements) at the conditions studied. Arrhenius behavior was observed for 2-hexene and 3-hexene throughout the range of temperatures studied and for temperatures above 875 K for 1-hexene. The lowest temperature data ($<875\text{ K}$) show a slight increase in reactivity and decrease in activation energy for 1-hexene, consistent with theory and previous studies indicating the possible onset of non-Arrhenius behavior at these conditions. The results show the new data from the current work bridge the void between previous hexene ignition studies, and the new data are in good agreement with the previous low

and high temperature studies by Vanhove *et al.* [13] and Mehl *et al.* [14], respectively.

Fast gas sampling and gas chromatography were used to quantitatively measure 13 stable intermediate species formed during the ignition delay period of each isomer at a temperature of ~ 900 K. **Figures 2-4** present some of the species data, specifically the time histories of the hexenes, propene, and propanal. The data show consistent rates of fuel consumption for the three isomers at this experimental condition and highlight differences (both expected and unexpected) in the reaction pathways of the three hexene isomers.

The results were modeled using a gasoline surrogate reaction mechanism from Lawrence Livermore National Laboratory (LLNL) [15], which contains a sub-mechanism for the trans-hexene isomers. The model predictions are shown in **Figs. 2-4** as the solid lines. The initial conditions and compositions for the 0-D, isometric, adiabatic CHEMKIN simulations were the average conditions of the fast gas sampling experiments: 1-hexene ($P = 11.1$ atm, $T = 896$ K, $\phi = 1.0$, $O_2 = 11.63\%$, buffer gas: $O_2 = 7.5$), trans-2-hexene ($P = 11.3$ atm, $T = 905$ K, $\phi = 1.0$, $O_2 = 11.62\%$, buffer gas: $O_2 = 7.5$), and trans-3-hexene ($P = 11.2$ atm, $T = 899$ K, $\phi = 1.0$, $O_2 = 11.63\%$, buffer gas: $O_2 = 7.5$). The reactivity of the hexene isomers is well captured by the model results and supports the current

understanding that at high temperatures ($>$ approximately 850 K) the ignition delay times of the isomers are virtually identical and exhibit Arrhenius dependence on temperature. As seen in **Fig. 2**, agreement between the experimental data and the model is excellent, and within 20% for the majority of the time history of the hexenes. At later times (t/τ_{ign} greater than ~ 0.9) during the ignition delay period, the model over-predicts the rate of consumption of trans-3-hexene. For the majority of the ignition delay period (t/τ_{ign} less than ~ 0.9), the hexene concentrations and the measured stable intermediate account for greater than 80% of the carbon initially in the test mixtures, indicating good capture of the carbon balance and representation of the overall reaction pathways.

The experimental data for propene shown in **Fig. 3** indicate a longer alkyl chain promotes significantly increased propene production (a factor of ~ 5 increase in propene comparing trans-3-hexene and 1-hexene at $t/\tau_{ign} \sim 0.93$), and this trend is well predicted by the mechanism simulations. For 1-hexene and trans-2-hexene, the experimental data and the simulations for propanal (C_2H_5CHO) presented in **Fig. 4** are in excellent agreement, within a factor of two. Unlike propene, the experimental measurements indicate propanal production decreases for

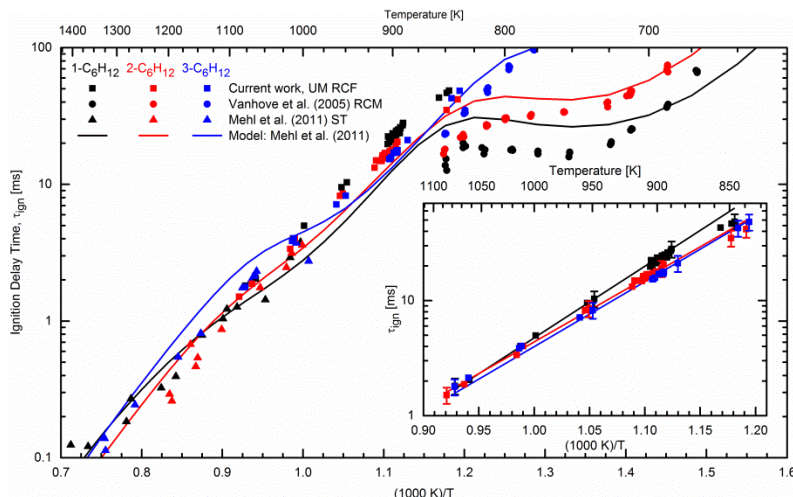


Fig. 1. Comparison of results from the current work with previous ignition studies of the linear hexene isomers. Predicted results for ignition delay time using the LLNL mechanism by Mehl *et al.* [15] are shown as the solid lines in the main figure and linear regression to only the UM RCF data are shown in the inset. All experimental data have been normalized to $\phi = 1$, buffer gas: $O_2 = 7.5$, and $P = 11$ atm.

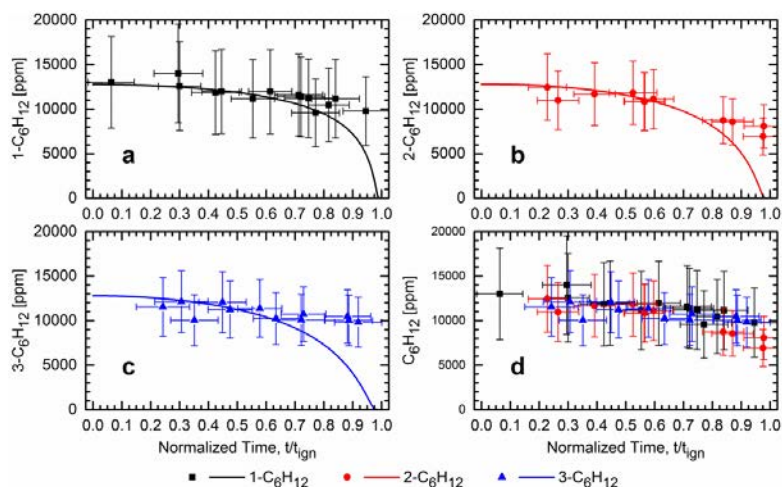


Fig 2. Fuel time histories during autoignition of the three hexene isomers. Measured (symbols) and predicted (lines) concentrations of a) 1-hexene, b) trans-2-hexene, c) trans-3-hexene, and d) all three hexene isomers. Simulations used the LLNL Mehl *et al.* [15] mechanism at the average compositions and conditions of the experiments.

the longer alkyl chain isomers and exhibits less sensitivity to the double bond position (a factor of ~ 2 decrease in propanal comparing trans-3-hexene and 1-hexene at $t/t_{\text{ign}} \sim 0.93$). However, the simulations over-predict the experimental measurements for propanal during 3-hexene ignition by more than an order of magnitude.

The trends for the intermediate species measurements indicate the small alkene and small alkane chemistry is generally well represented in the LLNL reaction mechanism for 1-hexene and 2-hexene; however, some reaction pathways for 3-hexene differ significantly with the experimental measurements, e.g. ethanal (acetaldehyde), propanal, and 1,3-butadiene. As described in Vanhove et al. [13] and Mehl et al. [14], alkene chemistry undergoes a transition from low temperatures where allyl radical reactions dominate to higher temperatures (>900 K) where β -decomposition of alkenyl radicals dominate. The over-prediction of the LLNL reaction mechanism for propanal indicates the OH addition to the double bond of 3-hexene may be too fast, and would be a good candidate reaction for further experimental and computational studies.

The results of the hexene isomer study emphasize the value of bulk reactivity data (e.g. ignition delay time) and species measurements as important methods to identify similarities and differences in reactivity and reaction pathways, which are particularly vital towards developing reaction rate rules for classes of fuel compounds. In particular, the results of the current work are the first species measurements in the high/transition temperature regime for this important alkene.

III. Future Work

Our future work includes ignition and speciation studies to understand the effect of cis- versus trans-isomerization on combustion reactions. This work will leverage the hexene ignition study presented here. We will also continue to explore fuel component interactions through studies of ethanol and iso-octane blends. We continue to work with Dr. Charles Westbrook to develop a more accurate understanding of the intermediates formed during ignition of hydrocarbons and oxygenated hydrocarbons. We are also continuing our collaboration with Dr. Robert Tranter of Argonne National Laboratories to develop a high-pressure sampling valve system that will enable speciation at significantly higher pressures than we can study currently.

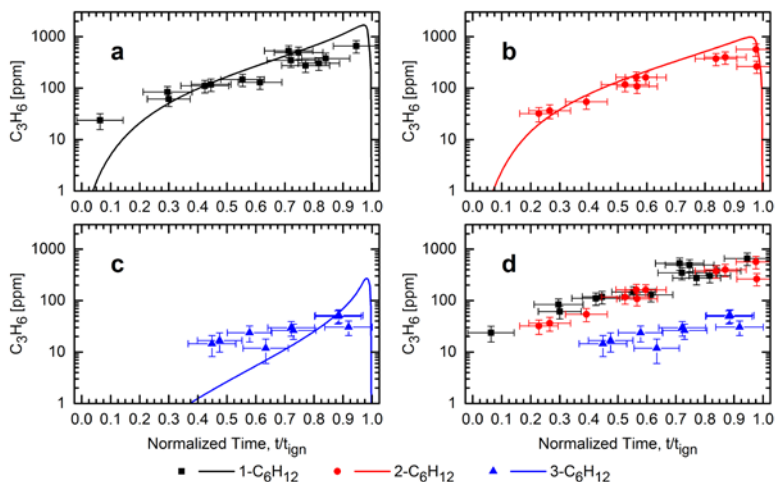


Fig. 3. Propene (C_3H_6) time histories during autoignition of the three hexene isomers. Measured (symbols) and predicted (lines) concentrations of propene from a) 1-hexene, b) trans-2-hexene, c) trans-3-hexene, and d) all three hexene isomers. Simulations used the LLNL Mehl *et al.* [15] mechanism at the average compositions and conditions of the experiments.

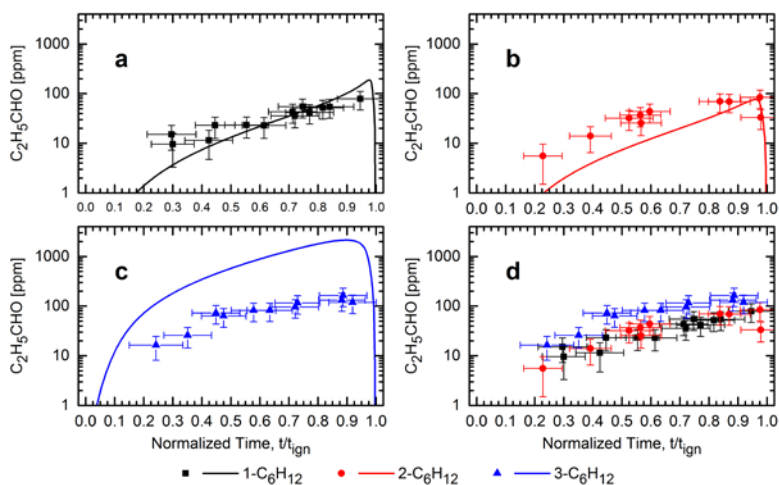


Fig. 4. Propanal (C_2H_5CHO) time histories during autoignition of the three hexene isomers. Measured (symbols) and predicted (lines) concentrations of propanal from a) 1-hexene, b) trans-2-hexene, c) trans-3-hexene, and d) all three hexene isomers. Simulations used the LLNL Mehl *et al.* [15] mechanism at the average compositions and conditions of the experiments.

IV. References

1. Wagnon, S. W., Botet, C.B., Wooldridge, M. S., "The Effects of Bond Location on the Ignition and Reaction Pathways of trans-Hexene Isomers," accepted to *J. Phys. Chem. A*, March 2015.
2. Barraza-Botet, C., Wagnon, S., Wooldridge M. S., (2014) "Ignition Delay Time Measurements and High-speed Imaging Analysis for Ethanol-Air Mixtures in a Rapid Compression Facility," Spring Meeting of the Canadian Section of the Combustion Institute, May 2014.
3. Karwat, D. M. A., Wooldridge, M. S., Klippenstein, S. J., Davis, M. J., (2015) "Effects of New Ab Initio Rate Coefficients on Predictions of Species Formed During n-Butanol Ignition," accepted to *J. Phys. Chem. A*, January 2015, in press.
4. Karwat, D. M. A., Wagnon, S., Teini, P. D., Wooldridge, M. S. (2011) *J. Phys. Chem. A* **115** 4909.
5. Donovan, M.T., He, X., Zigler, B.T., Palmer, T.R., Wooldridge, M.S., Atreya, A. (2004) *Combust. Flame* **137** 351.
6. He, X., Donovan, M.T., Zigler, B.T., Palmer, T.R., Walton, S.M., Wooldridge, M.S., Atreya, A. (2005) *Combust. Flame* **142** 266.
7. Karwat, D. M. A., Wagnon, S., Wooldridge, M. S., Westbrook, C. K. (2013) *Combust. Flame* **160** 2693.
8. Walton, S.M., He, X., Zigler, B.T., Wooldridge, M.S. (2007) *Proc. Combust. Inst.* **31** 3147.
9. Walton, S. M., Wooldridge, M. S., and Westbrook, C. K. (2009) *Proc. Combust. Inst.* **32** 255.
10. Walton, S.M., Karwat, D.M., Teini, P.D., Gorny, A., Wooldridge, M.S. (2011) *Fuel* **90** 1796.
11. He, X., Zigler, B.T., Walton, S.M., Wooldridge, M.S., Atreya, A. (2006) *Combust. Flame* **145** 552.
12. He, X., Walton, S.M., Zigler, B.T., Wooldridge, M.S., Atreya, A. (2007) *Int. J. Chem. Kinet.* **39** 498.
13. Vanhove, G., Ribaucour, M., Minetti, R. (2005) *Proc. Combust. Inst.* **30** 1065.
14. Mehl, M., Pitz, W. J., Westbrook, C. K., Yasunaga, K., Conroy, C., Curran, H. J. (2011) *Proc. Combust. Inst.* **33** 201.
15. Mehl, M., Pitz, W. J., Westbrook, C. K., Curran, H. J. (2011) *Proc. Combust. Inst.* **33**, 193.

V. Publications and submitted journal articles supported by this project 2011-present

1. Wagnon, S. W., Botet, C.B., Wooldridge, M. S., "The Effects of Bond Location on the Ignition and Reaction Pathways of trans-Hexene Isomers," accepted to the *Journal of Physical Chemistry A*, March 2015.
2. Karwat, D. M. A., Wooldridge, M. S., Klippenstein, S. J., Davis, M. J., (2015) "Effects of New Ab Initio Rate Coefficients on Predictions of Species Formed During n-Butanol Ignition," accepted to the *Journal of Physical Chemistry A*, January 2015, in press.
3. Barraza-Botet, C., Wagnon, S., Wooldridge M. S., (2014) "Ignition Delay Time Measurements and High-speed Imaging Analysis for Ethanol-Air Mixtures in a Rapid Compression Facility," Spring Meeting of the Canadian Section of the Combustion Institute, May 2014.
4. Wagnon, S. W., Karwat, D. M. A., Wooldridge, M. S., and Westbrook, C. K. (2014) "On the Ignition Chemistry of Methyl Trans-3-Hexenoate," accepted to *Fuel*, September 2014, in press
5. Wagnon, S. W., Wooldridge, M. S., (2014) "Effects of Diluent Gas Composition on Autoignition," *Combustion and Flame*, **161**, pp. 898-907, <http://dx.doi.org/10.1016/j.combustflame.2013.09.022>.
6. Karwat, D. M. A., Wagnon, S., Wooldridge, M. S., Westbrook, C. K. (2013) "Low Temperature Speciation and Chemical Kinetic Studies of n-Heptane," *Combustion and Flame* **160**, pp. 2693-2706.
7. Karwat, D. M. A., Wagnon, S., Wooldridge, M. S., Westbrook, C. K., (2012) "On the Combustion Chemistry of n-Heptane and n-Butanol Blends," *Journal of Physical Chemistry A*, DOI 10.1021/jp3093 58h, **116**, pp. 12406-12421.
8. Karwat, D. M. A., Wagnon, S., Teini, P. D., Wooldridge, M. S. (2011) "On the Chemical Kinetics of n-Butanol: Ignition and Speciation Studies," *Journal of Physical Chemistry A*, **115**, pp. 4909-4921.
9. Walton, S. M., Karwat, D. M., Teini, P. D., Gorny, A., and Wooldridge, M. S. (2011) "Speciation Studies of Methyl Butanoate Ignition," *Fuel*, **90**, pp. 1796-1804.

THEORETICAL STUDIES OF THE REACTIONS AND SPECTROSCOPY OF RADICAL SPECIES RELEVANT TO
COMBUSTION REACTIONS AND DIAGNOSTICS

DAVID R. YARKONY, DEPARTMENT OF CHEMISTRY, JOHNS HOPKINS UNIVERSITY, BALTIMORE, MD 21218
yarkony@jhu.edu

Overview

The construction of quasi-diabatic representations of adiabatic potential energy surfaces coupled by conical intersections, for both bound (used in our treatments of nonadiabatic photoelectron spectroscopy) and dissociative systems (used to treat nonadiabatic photodissociation and nonadiabatic chemical reactions) is a key aspect of our research effort.

A. Photoionization Spectra

We have begun a study of the negative ion electron photodetachment spectra of cycloalkoxide molecules that reveal the spectrum of cycloalkoxy radicals, molecules whose states are strongly coupled by conical intersections. Alkoxy radicals are important participants in atmospheric^{1, 2} and combustion processes.³ In combustion processes alkoxy radicals are produced from the reaction of alkyl radicals with O or O₂.² The prevalence of cyclic hydrocarbons in nontraditional fuel sources such as oil shales and oil sands has stimulated interest in cyclic alkoxy.

We have completed our initial study of the electronic structure of cyclopentoxy, a system studied experimentally by Continetti⁴ and will subsequently study cyclohexoxy complementing experimental work in the group of Miller (OSU).⁵

B. Nonadiabatic Dynamics

While electronic structure is essential to explain chemical mechanisms, quantification of those results requires nuclear dynamics. As part of other funded research, we developed algorithms to construct coupled diabatic states representations, \mathbf{H}^d , of adiabatic potential energy surfaces (PESs) coupled by conical intersections.⁶ The method, a generalization of the approach we use to treat the coupled bound states encountered in photoelectron spectroscopy, is based on electronic structure data, energies, energy gradients and derivative couplings obtained from multireference configuration interaction single and double excitation (MRCISD) wave functions. The method treats all internal degrees of freedom (so far 33 is our

largest) and can treat large amplitude nuclear motions including dissociation. The electronic structure data are calculated at points determined by quasi classical surface hopping trajectories (QCT) obtained using Truhlar's ANT program. The representation can smooth the irregularities in the electronic energies attributable to the orbital changes in the active space that are inherent to nonadiabatic processes and can describe seams of conical intersections of two or three states. The resulting quasi diabatic representations of coupled adiabatic potential energy surfaces (PESs) will enable accurate dynamics studies, avoiding the accuracy limitations inherent in the dynamics on the fly approach usually used.

We have completed, and submitted for publication,⁷ an initial representation of the D₀ and D₁ coupled adiabatic PESs that describe photodissociation of CH₂OH through the D₁ state and have used those results to analyze photodissociation studied in the group of Reisler⁸(USC). We are currently finishing a more complete/accurate representation of three states D₀, D₁ and D₂ for CH₂OH. We will shortly report a four coupled state representation of C₆H₅OH photodissociation involving S₀, S₁ and S₂, in the full 33 internal coordinates, based on MRCISD wave functions comprised of over 100 million configuration state functions (CSFs). These projects were made possible by a generous grant of computer time from NERSC.

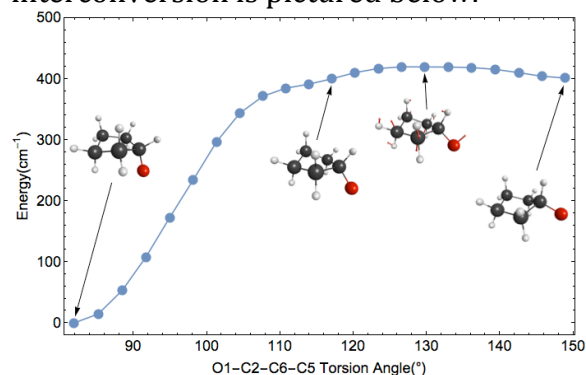
WORK COMPLETED.

A. Electronic Structure of cyclopentoxy: The case for a two state approximation

Cycloalkoxy radicals have been the subject of both experimental and computational studies.^{1, 2, 4, 9-12} Previous studies of cyclopentoxy have assumed that the ground electronic state can be treated as a single isolated state. Our recent study of the electronic structure of cyclopentoxy showed this not to be the

case.¹³ The two lowest states of cyclopentoxy were described using MRCISD wave functions. It is found that these states are coupled by a conical intersection seam beginning only 550 cm⁻¹ above the ground state minimum. Conical intersections were found with the oxygen located both axial and equatorial with respect to the ring. The conical intersection seam is attributed to the fact that cyclopentoxy can be viewed as a substitutional isomer of the methoxy radical which has a symmetry required and Jahn-Teller distorted ²E ground state. The spin-orbit coupling computed for points on this seam is found to be 60 cm⁻¹ in good accord with the 67 cm⁻¹ reported for methoxy.

For computing the cyclopentoxide photoelectron spectrum, the interconversion of the axial and equatorial structures is an important issue. The computed barrier to axial-equatorial interconversion is pictured below.



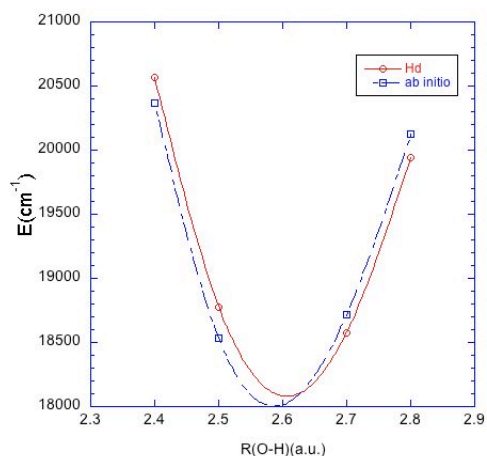
These calculations advise our determination of the cyclopentoxide photoelectron spectrum which is in progress.

B. Multichannel PESs coupled by conical intersections: The photodissociation $\text{CH}_2\text{OH}(\text{X}) + h\nu \rightarrow \text{CH}_2\text{OH}^* \rightarrow \text{CH}_2\text{O}(\text{X}) + \text{H}$, $\text{CHOH}(\text{X})$ [cis/trans] + H

For the photodissociation of CH₂OH studied in Reisler's (USC) laboratory,⁸ we have developed an MRCISD expansion of ~67 million CSFs which is capable of describing all channels in the above captioned reaction.

We have completed the determination of a three quasi-diabatic state representation of D₀ and D₁ the 1,2²A adiabatic states⁷ of CH₂OH and are in the process of constructing a three quasi-diabatic state representation of the 1,2,3²A adiabatic states using a more elaborate functional form.

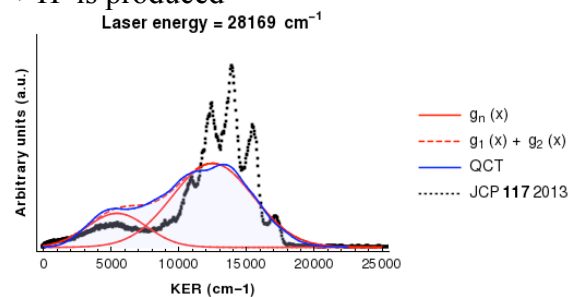
When representing nonadiabatic processes it is important to get an accurate representation of the seam of conical intersections and its local topography. The figure below addresses this issue



reporting four points on the 1²A- 2²A seam of conical intersection in the CH₂O-H dissociation channel. For each point R(O-H) was fixed at the indicated value and the remainder of the internal coordinates were optimized to minimize the crossing energy. The optimization is performed separately for the *ab initio* and H^d representations. None of these *ab initio* points were included in the data used to build H^d. Only the minimum energy crossing (at R(O-H) ~ 2.6 a₀) was so included in this region. The agreement between the H^d and *ab initio* determined energies is seen to be excellent. Similarly good agreement is found for the **g** and **h** vectors. These results strongly support the ability of our representation to accurately describe the vicinity and locus of a conical intersection seam.

The representation of D₀ and D₁ was used to simulate kinetic energy release (KER)

spectra reported by Reisler,⁸ in which $\text{CH}_2\text{O} + \text{H}$ is produced



The above figure reports a simulation of the KER spectrum obtained using trajectory surface hopping techniques. Note that this figure is based on 10,000 trajectories which would not be possible using direct dynamics. The issue here is the origin of bimodal character clearly evident in the experimental spectrum (dotted black line). The simulated spectrum, solid blue line, is bimodal, being well described as the sum (dashed red line) of two gaussians g_1 and g_2 , the solid red lines. An analysis of the trajectories shows that the slow hydrogens are produced in an indirect or quasi-statistical manner, with a hop to D_0 preceding a significant residence time on D_0 prior to H dissociation. On the other hand, the fast hydrogens are produced by trajectories that, while they may oscillate on D_1 prior to a surface hop, following transfer to D_0 the H dissociates promptly.

Work in Progress/Future Work

As was noted above we intend to finish the simulation of the anion photoelectron spectrum of cyclopentoxy. The photoelectron spectrum of cyclohexoxide will also be considered.

A. Hydroxymethyl Photodissociation

We are continuing our work on the multichannel, multistate photodissociation of hydroxymethyl. It is known from experiments and confirmed by our simulations that even at energies well above the threshold for producing $\text{HCOH}[cis, trans]$ when only D_1 is excited essentially no HCOH is produced. The situation changes dramatically when D_2 is excited, with significant amounts of hydroxymethylene produced. In this case both $D_2 - D_1$ and $D_1 - D_0$ seams of conical intersections are expected to be accessed. The completion of the enhanced three state global quasi diabatic

representation of the $1,2,3^2A$ states of hydroxymethyl noted above will enable both KER simulations and mechanistic inferences. In particular the determination of contributions of the energetically accessible conical intersection seams will provide valuable sights into the mechanisms of nonadiabatic processes.

B. Representing PESs coupled by conical intersections for significantly larger molecules: $\text{C}_6\text{H}_5\text{OH}(\tilde{X}) + h\nu \rightarrow \text{C}_6\text{H}_5\text{OH}(\tilde{A}) \rightarrow \text{C}_6\text{H}_5\text{O}(\tilde{X}, \tilde{A}) + \text{H}$

The photodissociation of phenol, $\text{C}_6\text{H}_5\text{OH}(\tilde{X}^1A') + h\nu \rightarrow \text{C}_6\text{H}_5\text{OH}^* \rightarrow \text{C}_6\text{H}_5\text{O}(\tilde{X}^2B_1, \tilde{A}^2B_2) + \text{H}$ is a problem of considerable current interest. At the time of preparing this report a four coupled diabatic state representation of the S_0, S_1, S_2 , states of phenol capable of describing the above noted photodissociation processes is (almost) complete! *Ab initio* electronic structure data for the $1,2,3,4^1A$ states were obtained exclusively from an MRCISD expansion comprised of over 100 million CSFs! Electronic structure data at ~ 4700 nuclear configurations were required to construct the H^d .

This representation of a three electronic state photodissociation process in a molecule with 33 degrees of freedom based on accurate MRCISD wave functions is unique and will provide unprecedented opportunities for studying nonadiabatic photodissociation.

References

- [1] J. J. Orlando, L. T. Iraci, and G. S. Tyndall, *J. Phys. Chem. A* **104**, 5072(2000).
- [2] K. Hoyermann, Jorg Nothdurft, M. Olzmann, J. Wehmeyer, and T. Zeuch, *J. Phys. Chem. A* **110**, 3165(2006).
- [3] C. A. Taatjes, N. Hansen, J. A. Miller, T. A. Cool, J. Wang, P. R. Westmoreland, M. E. Law, T. Kasper, and K. Kohse-Höinghaus, *J. Phys. Chem. A* **110**, 3254(2006).
- [4] L. S. Alconcel, H. J. Deyerl, M. DeClue, and R. E. Continetti, *J. Am. Chem. Soc.* **123**, 3125(2001).
- [5] J. Liu, and T. A. Miller, *J. Phys. Chem. A* **118**, 11871(2014).

- [6] X. Zhu, and D. R. Yarkony, J. Chem. Phys. **140**, 024112 (2014).
- [7] C. L. Malbon, and D. R. Yarkony, J. Phys. Chem. A submitted(2015).
- [8] C. P. Rodrigo, C. Zhou, and H. Reisler, J. Phys. Chem. A **117**, 12049(2013).
- [9] L. S. Alconcel, H. J. Deyerl, and R. E. Continetti, J. Am. Chem. Soc. **123**, 12675(2001).
- [10] S. Wilsey, P. Dowd, and K. N. Houk, J. Org. Chem. **64**, 8801(1999).
- [11] H.-G. Yu, Chem. Phys. Lett. **441**, 20(2007).
- [12] L. Zu, J. Liu, G. Tarczay, P. Dupré, and T. A. Miller, J. Chem. Phys. **120**, 10579(2004).
- [13] C. L. Malbon, D. R. Yarkony, and X. Zhu, J. Mol. Spec. 2015). (available on line)

PUBLICATIONS ACKNOWLEDGING (EXCLUSIVELY) CURRENT DOE SUPPORT (2012-2015)

1. *A Lippmann – Schwinger Approach for the Determination of Photoionization and Photodetachment Cross Sections Based on a Partial Wave Green’s Function Expansion and Configuration Interaction Wave Functions.*
Seunguk Han and David R. Yarkony, Mol. Phys. 110, 845-859 (2012).
2. *Nonadiabatic Effects in Substitutional Isomers of Jahn-Teller Molecules. The Strange Case of Hydroxymethoxy*
Joseph Dillon and David R. Yarkony, J. Chem. Phys. **137**, 154315 (2012)
3. *Reactive quenching of OH(A²Σ⁺) by O₂ and CO: Experimental and nonadiabatic theoretical studies of H- and O-atom product channels*
Julia H. Lehman, Marsha I. Lester, and David R. Yarkony, J. Chem. Phys. 137, 094312 (2012)
4. *Seams of Conical Intersections Relevant to the Quenching of OH(A²Σ⁺) by Collisions with H₂.*
Joseph Dillon and David R. Yarkony, J. Phys. Chem. A, 117, 7344-7355 (2013)
5. *On the Mechanism for the Nonadiabatic Reactive Quenching of OH(A²Σ⁺) by H₂(¹Σ⁺_g). The Role of the 2²A State*
Joseph Dillon and David R. Yarkony, J. Chem. Phys. **139**, 064314 (2013).
6. *On the Photoionization Spectrum of Propyne. A fully ab initio Simulation of the Low-Energy Spectrum including the Jahn-Teller Effect and the Spin-Orbit Interaction*
Sara Marquez, Joseph Dillon and David R. Yarkony, J. Phys. Chem A. 117, 12002-12010 (2013)
7. *Full-dimensional quantum state-to-state non-adiabatic dynamics for photodissociation of ammonia in its A-band* Changjian Xie, Jianyi Ma, Xiaolei Zhu, Dong Hui Zhang, David R. Yarkony Daiqian Xie and Hua Guo, J. Phys. Chem. Lett. 5,1055-1060 (2014).
8. *On the Electronic Structure of the Ground State of Cyclopentoxy. The Case for a Two Coupled State Description*
Christopher L. Malbon, David R. Yarkony and Xiaolei Zhu, J. Mol. Spec. (2015)
9. *On the Nonadiabatic Photodissociation of the Hydroxymethyl Radical from the 2²A State. Surface Hopping Simulations Based on a Full Nine Dimensional Representation of the 1,2,3²A Potential Energy Surfaces Coupled by Conical Intersections*
Christopher L. Malbon and David R. Yarkony, J. Phys. Chem. A submitted.

GAS-PHASE MOLECULAR DYNAMICS: THEORETICAL STUDIES IN SPECTROSCOPY AND CHEMICAL DYNAMICS

Hua-Gen Yu (hgy@bnl.gov)

Chemistry Department, Brookhaven National Laboratory, Upton, NY 11973-5000

Program Scope

The main goal of this program is the development and application of computational methods for studying chemical reaction dynamics and molecular spectroscopy in the gas phase. We are interested in developing rigorous quantum dynamics algorithms for small polyatomic systems and in implementing approximate approaches for complex ones. Our particular focus is on the dynamics and kinetics of chemical reactions and on the rovibrational spectra of species involved in combustion processes. This research also explores the potential energy surfaces of these systems of interest using state-of-the-art quantum chemistry methods, and extends them to understand some important properties of materials in condensed phases and interstellar medium as well as in combustion environments.

Recent Progress

Quantum dynamics calculations of resonance states

Resonance states are important in chemical dynamics of reactions. They can be studied by using an extended Hamiltonian including a negative imaginary potential. The extended Hamiltonian matrix is no longer Hermitian but is instead complex symmetric. Its complex eigenvalues give resonance energies and widths. Currently, it is very

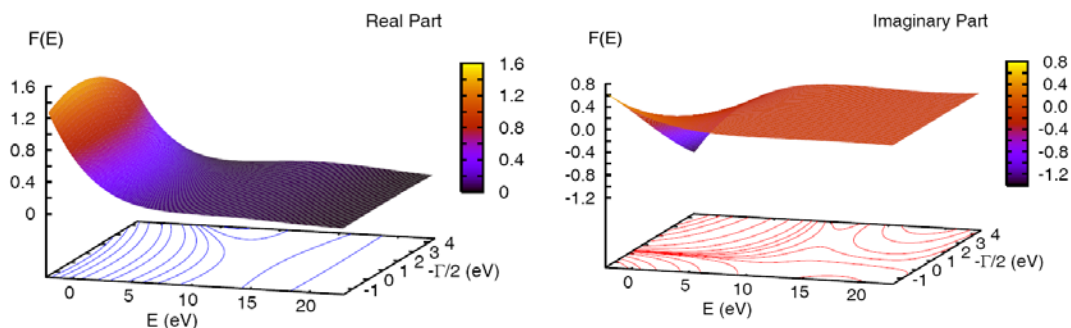


Figure 1: A plot for a Green function-guided spectral transform surface as a function of energy and resonance width in eV, where its real and imaginary part is shown in the left and right panels, respectively.

challenging to efficiently diagonalize the large matrix that occurs for molecules with deep potential wells. In this research, we proposed a complex guided spectral transform Lanczos (cGSTL) algorithm to compute both bound and resonance states including energies, widths and wavefunctions. The algorithm comprises of two layers of complex-

symmetric Lanczos iterations. A short inner layer iteration produces a set of complex formally orthogonal Lanczos (cFOL) polynomials. The polynomials are used to span the guided spectral transform function determined by a retarded Green operator (e.g., see Fig.1). An outer layer iteration is then carried out with the transform function to compute the eigen-pairs of the system. The guided spectral transform function is designed to have the same wavefunctions as the eigenstates of the original Hamiltonian in the spectral range of interest. Therefore the energies and/or widths of bound or resonance states can be easily computed with their wavefunctions or by using a root-searching method from the guided spectral transform surface. The new cGSTL algorithm has been applied to bound and resonance states of HO₂.

Exact full dimensional diagonalization method for molecular vibrational spectra

We have developed a multi-layer Lanczos algorithm (see Fig.2 for its flow chart) for computing vibrational energies and IR/Raman transition intensities of polyatomic molecules with the help of the elegant recursive residue generation method (RRGM), the guided spectral transform Lanczos technique, the reduced dimension strategy of the two-layer Lanczos method, and the DVR basis contraction. The two latter techniques allow us to construct (dipole-) eigenstate wavefunctions without explicitly accessing the huge primitive basis set, which makes it possible to calculate the vibrational spectra of large molecules. The algorithm uses only an initial state wavefunction in a reduced dimension basis set to give its transition spectrum to all final states with a single Lanczos propagation. No product wavefunction is needed. Furthermore, it is a rigorous full dimensional quantum dynamics algorithm without any dynamics approximation. In particular, the algorithm is general and problem-independent for polyatomic molecules. The large amplitude motions of vibrations are naturally described in terms of the use of scattering coordinates, i.e., the orthogonal polyspherical coordinates.

An application is presented by calculating the infrared vibrational dipole transition spectrum of CH₄ based on the *ab initio* T8 potential energy surface of Schwenke and Partridge and the low-order truncated *ab initio* dipole moment surfaces of Yurchenko and co-workers. Results show that the multi-layer Lanczos method is very efficient and accurate. Now the multi-layer Lanczos algorithm has been implemented with the PetroVib program. Therefore, once a global potential energy surface and dipole moment (or polarizability tensor) surfaces are provided, it becomes just a routine to

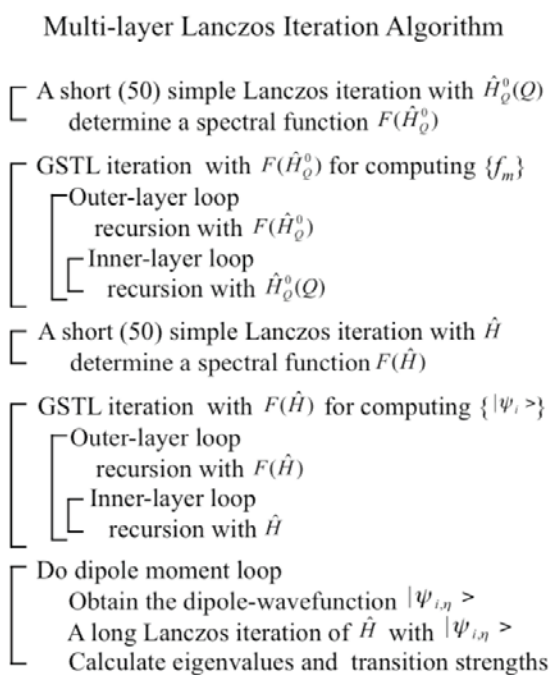


Figure 2: A schematic flow chart of the multi-layer Lanczos iteration algorithm for computing vibrational IR and/or Raman spectra of polyatomic molecules.

calculate both the vibrational energies and IR/Raman transition intensities of a general five-atomic molecule in a rigorous full dimension approach.

Electronic circular dichroism spectrum and molecular inelastic collisions

We (in collaboration with experimentalists) have carried out electronic structure and molecular dynamics studies to help understand experimental results. Based on TDDFT calculations, we suggested a new mechanism for the origin of anomalous electronic circular dichroism (ECD) spectra of the $\text{RuPt}_2(\text{tpz})_2\text{Cl}_2(\text{PF}_6)_4$ complex in acetonitrile. In addition, we also provided theoretical assistance to explore energy transfer rates in molecular collisions such as $\text{CN} + \text{He}/\text{Ar}$ which were measured in the GPMD group.

Future Plans

Neural network iterative diagonalization method to solve eigenvalues

Recently, the neural network functional has been found to be a powerful technique to represent electronic densities, potential energy surfaces, and vibrational wavefunctions in chemical physics. In this research, we are going to apply the neural network method for developing a new neural network-based eigen-solver of complex symmetric or Hermitian matrices. The main goal is to minimize the usage of core-memory in matrix diagonalization calculations while keeping the high efficiency of iterative diagonalization algorithms. As a result, the algorithm would be used to study the molecular spectra of large polyatomic molecules. Initially, the algorithm will be tested by calculating the bound and resonance states of HO_2 , N_2H_2 , CH_4 , and/or C_2H_2 etc. The N_2H_2 application will be done in collaboration with Varandas at Coimbra.

Development of a general program for calculating vibrational spectra of polyatomic systems

In this proposal, we aim to develop computational algorithms to accurately calculate the vibrational spectra of polyatomic molecules, and to assist experimentalists in understanding their observed spectra. For polyatomic systems beyond six-atom, the challenge in rigorous quantum dynamics calculations comes from the huge basis size arising out of high-dimensional problems. The Lanczos method is an iterative eigensolver capable of solving the eigenvalue problem of a large sparse matrix with a size up to $N \sim 10^7$, a typical size for a chemical system with six degrees of freedom. In order to overcome this difficulty, we may try to reduce the basis size by using a compact basis set. The reduction of the basis size is the crucial idea of the sequential truncation approach widely used in direct diagonalization methods. This approach however requires too much CPU time and fast memory to be tractable for polyatomic molecules beyond five-atom molecules. During the past decade, several methods to obtain a compact basis set have been developed, e.g., the pruned basis functions.

Instead, in this proposal, we will use our recently developed ZDVR (coherent DVR) method to build a compact basis set. The ZDVR is a multi-dimensional PO-DVR method so that the ZDVR basis is very compact, which can substantially reduce the basis size. Numerical tests also demonstrated that it has the Gauss convergence speed with the basis size. Importantly, the ZDVR is a grid basis representation. As a result, the matrix representation of system Hamiltonian in ZDVR is often very sparse, which guarantees the efficiency of an iterative diagonalization method as well as the low memory requirement. The new algorithm will be called ZDVRMode.

We will apply the ZDVRMode program to study the vibrational spectra of combustion-related radicals such as vinyl (C_2H_3) and propargyl (C_3H_3) radicals, in collaboration with Sears and Hall in the GPMD group of BNL. They will measure the overtones of both radicals using high-resolution near infrared spectroscopy. Currently, the Hamiltonian in normal mode coordinates has been numerically tested with propargyl radical in full dimension. The full coupled potential energy surface is used. The results obtained are very promising.

Kinetics and dynamics study of combustion-related reactions

Electronically excited species such as 1CH_2 also play an important role in combustion chemistry. However, the studies of their reactivity are rather limited because their reactions often occur on multiple potential energy surfaces and non-adiabatic effects are important. In this research, we will extend the surface hopping direct *ab initio* molecular dynamics algorithm, developed for the SECH MD studies, to simulate the bimolecular reactions and photodissociation chemistry. The first application would be the photodissociation dynamics of acetone at 193-230 nm. This system has been investigated by Suits et al. using a universal ion imaging technique. Excited acetone dissociates via two major channels: $CH_3CO + CH_3$ and $CO + 2CH_3$. The latter products result from a poorly understood dissociation mechanism. Here, we will attempt to explore the dissociation pathways of acetone on its three low-lying electronic states we propose to develop a zero-point energies-constrained NA-AIMD algorithm.

Publications since 2013

- G. Nyman and H.-G. Yu, *Quantum approaches to polyatomic reaction dynamics*, Int. Rev. Phys. Chem., **32**, 39 (2013).
- P.P Dholabhai and H.-G. Yu, *Electronic structure and quantum dynamics of photoinitiated dissociation of O_2 on rutile TiO_2 nanocluster*, J. Chem. Phys., **138**, 194705 (2013).
- H.-G. Yu, *Origin of anomalous electronic circular dichroism spectra of $[RuPt_2(tppz)_2Cl_2]^{4+}$ in acetonitrile*, J. Phys. Chem. A **118**, 5400 (2014).
- H.-G. Yu, *A complex guided spectral transform Lanczos method for studying quantum resonance states*, J. Chem. Phys. **141**, 244114 (2014).
- H.-G. Yu, *Multi-layer Lanczos iteration approach to calculations of vibrational energies and dipole transition intensities for polyatomic molecules*, J. Chem. Phys. **142**, 044106 (2015).
- D. Forthomme, M.L. Hause, H.-G. Yu, P. J. Dagdigian, T. J. Sears, and G. E. Hall, *Doppler-resolved kinetics of saturation recovery*, J. Phys. Chem. A (in press, 2015).

Chemical Kinetics of Elementary Reactions

Judit Zádor

Combustion Research Facility, Mail Stop 9055, Sandia National Laboratories

Livermore, CA 94551-0969

jzador@sandia.gov

I. PROGRAM SCOPE

My program focuses on the theoretical determination of rate coefficients and branching fractions of reactions relevant to combustion chemistry, such as the formation and dissociation of radicals derived from various fuel molecules and the bimolecular reactions associated with low-temperature autoignition. I use accurate quantum chemical methods and transition-state theory (TST) in combination with time-dependent master equations (ME) to calculate the pressure and temperature dependence of the chemical processes. I develop methods to automatically explore reactive potential energy surfaces (PES) to systematize and significantly accelerate research in elementary chemical kinetics, and study how theoretical predictions can be made more accurate. I also collaborate closely with experimentalists in order to achieve goals that neither theory nor experiments could alone.

II. RECENT PROGRESS

A. Reactions with the OH radical

OH radicals are the single most important chain carriers at low combustion temperatures and in the atmosphere, and alkenes are also pervasive in both environments. Between ~500 and ~800 K pressure-dependent adduct formation, backdissociation, isomerization, and simple H atom abstraction compete in OH + alkene reactions, with important implications for instance for alcohol combustion.

As a continuation of my work on the reaction of OH radicals with unsaturated molecules, in collaboration with Leonid Sheps, we studied the OH + cis/trans-2-butene reactions. We used our KinBot code to explore the relevant stationary points on the PES automatically at the CCSD(T)-F12//M06-2X level, and calculated pressure-dependent rate coefficients in a ME framework using the PAPER code.ⁱ The calculations were supplemented with a two-transition-state model for the dynamically complex entrance channel. We also refined our previously developed methodology to analyze experimental [OH]-time profiles with two time scalesⁱⁱ and achieved an overall good agreement between theory and experiments after tuning some barriers slightly. We observed, however, larger discrepancies for the abstraction channels, pointing to remaining, and probably significant uncertainties in our approach. Our overall analysis methodology is generally applicable to other OH + alkene reactions, or even more broadly, to reactions with competing timescales.

Related to OH + alkene reactions, and using our previously validated PES for propene + OH,ⁱⁱⁱ in collaboration with Jim Miller, I calculated the unimolecular dissociation and isomerization rate coefficients of seven C₃H₇O isomers corresponding to radicals obtained from propanols by H-abstraction, inherently important in setting the stage for propanol combustion. Several interesting pathways were uncovered, such as catalytic dehydration, well-skipping reactions, and reactions forming enols.

Increasing the unsaturation significantly increases the number of reaction pathways. Allene and propyne, small, doubly unsaturated molecules, play an important role in the reaction sequence contributing to molecular weight growth processes. Also in collaboration with Jim Miller I mapped out the stationary points and the corresponding conformational space on the C₃H₅O potential energy surface relevant for the OH + allene and OH + propyne reactions systematically and automatically using our KinBot software at the UCCSD(T)-F12b//M06-2X level of theory. Using RRKM-based 1-D master equations we calculated pressure- and temperature-dependent, channel-specific phenomenological rate coefficients for the bimolecular reactions OH + allene and OH + propyne, and for the unimolecular decomposition of the CH₃CCHOH, CH₃C(OH)CH, CH₂CCH₂OH, CH₂C(OH)CH₂ primary adducts, and also for the related acetyl, propionyl, 2-methylvinoxy, and 3-oxo-1-propyl radicals. The major channel

of the bimolecular reactions at high temperatures is the formation propargyl + H₂O, which makes the reactions important players in soot formation at high temperatures. However, below ~1000 K the chemistry is more complex, involving the competition of stabilization, isomerization and dissociation processes. We found that the OH addition to the central carbon of allene has a particularly interesting and complex pressure dependence, caused by the low-lying exit channel to form ketene + CH₃ bimolecular products. We compared our results to a wide range of experimental data and assessed possible uncertainties arising from certain aspects of the theoretical framework.

Theoretical methods to obtain rate coefficients are essential to fundamental combustion chemistry research, yet the associated uncertainties are largely unexplored in a systematic manner. In an exploratory work, in collaboration with Habib Najm, we focused on the parametric uncertainties for the hydrogen-atom-abstraction reaction, CH₃CH(OH)CH₃ + OH → CH₃C(OH)CH₃ + H₂O. Bayesian inference was employed to determine the joint probability distribution function of key parameters. We found that although most of the commonly used high-level ab initio calculations result in not more than a factor of two difference in the rate coefficient for this specific reaction in the 293 – 745 K temperature range, significant uncertainties remain in these types of calculations. We have clearly demonstrated that it is not necessarily true that the lion's share of the uncertainty in the calculated rate coefficient arises solely due to the uncertainties in the barrier height, and the presented methodology provided a transparent way of assessing the various quantum chemical methods.

B. Low-temperature autoignition chemistry

The single largest experimental obstacle when studying ephemeral species such as QOOH radicals is their generation in sufficient quantities and purity. QOOH radicals are very short-lived transients in the R + O₂ → ROO → QOOH → Products sequence, and, therefore, are usually present in low concentrations when starting with an alkyl radical. Previously, in collaboration with Craig Taatjes and David Osborn, we devised an experimental strategy to make QOOH radicals in an alternative way: we reacted tert-butyl hydroperoxide molecules with photolytically generated Cl atoms at room temperature.

The formed QOOH radical dissociates exclusively to the corresponding cyclic ether (2,2-dimethyl oxirane) + OH, which we monitored by multiplexed photoionization mass spectrometry and absorption spectroscopy. We could not detect the QOOH radical itself because of poor Frank-Condon overlap at threshold and likely photodissociation coinciding with strong background at higher energies. In the presence of oxygen, however, we were able to detect the related OOQOOH radical and record its photoionization spectrum. This is the first such spectrum in the literature. The ionization mechanism of this substituted alkylperoxy radical was found to be fundamentally different from that of small unsubstituted alkylperoxy radicals. We also calculated, using variable reaction coordinate TST, capture rate coefficients for QOOH + O₂. The long-range interaction potential was sampled using CASPT2 supplemented with several 1-D correction potentials. This work is the first where QOOH dissociation and QOOH + O₂ rate coefficients were directly measured providing crucial validation for theory.

In our more recent work, we studied low-temperature oxidation using cycloheptadiene precursor in photolytically initiated oxidation experiments in collaboration with David Osborn and Craig Taatjes. One of the several possible QOOH radicals have two advantageous properties: due to double resonance stabilization it is very stable (in fact, more stable than the related ROO radical), and can be detected using photoionization mass spectrometry. Our investigation yielded kinetic traces of this QOOH radical containing both its formation and decay time scales. Theory played a crucial role, as it enabled the systematic investigation and simplification of the fundamentally complex PES, provided strong support for the observed rate coefficients, and most importantly, enabled the interpretation of the measured quantities. Our calculations showed the importance of tunneling and chemical activation pathways under low-temperature combustion conditions. The results establish that resonance stabilization dramatically changes QOOH reactivity, and, hence, oxidation of unsaturated organics can produce exceptionally long-lived QOOH intermediates, which likely contribute to secondary aerosol formation in the atmosphere as well. Also, re-examination of assumed equivalences between rate coefficients for R + O₂ and QOOH + O₂ reactions used in many organic oxidation models might be necessary. Our work breaks fresh ground for

further studies on QOOH radicals, and helps build more accurate autoignition models, which critically depend on the chemistry of these short-lived species.

For the detailed modeling of combustion chemistry the possibility of unknown pathways is of continual concern, especially for biofuels, where the presence of oxygen atoms can significantly alter the chemical pathways. We found and characterized a new low-lying water elimination pathway from key QOOH radicals derived from alcohols. The corresponding saddle-point structure involves the interaction of radical and zwitterionic electronic states. This interaction presents extreme difficulties for electronic structure characterizations, as most standard methods produce two completely different potential curves depending on whether one starts with the corresponding orbital guesses from the reactant side or the product side. On the reactant side, the ROHF HOMO has the character of a carbon-centered radical orbital, while on the product side the HOMO has the character of an OO σ^* orbital associated with the breaking OO bond. The latter is a zwitterionic state and has a large dipole moment. In collaboration with Stephen Klippenstein and Larry Harding we demonstrated that the properties of this saddle point can be well captured by M06-2X and CCSD(T) methods, which produce comparable and low barrier heights. In the HF, MP2, CCSD and CCSD(T) progression the character of the calculated radical and zwitterionic states converge to each other, indicating the importance of excited states.

Experimental evidence for the existence and relevance of this pathway was shown using recently reported multiplex photoionization mass spectrometry (MPIMS) data from our group on the low-temperature oxidation of isopentanol and isobutanol. In these systems, water elimination is a major pathway, and is likely ubiquitous in low-temperature alcohol oxidation. These findings will substantially alter current alcohol oxidation mechanisms. Moreover, the methods described will be useful for the more general phenomenon of interacting radical and zwitterionic states. More recently, in collaboration with Craig Taatjes, we have investigated the importance of water elimination pathways in QOOH radicals derived from diethyl ketone. However, we found that these QOOHs display a large barrier to eliminate water, and, therefore, it is not an important pathway in this case.

We investigated several other low-temperature oxidation systems (*n*-butane, propane, *n*-butanol, 2,5-dimethyl hexane), with varying degree of contribution from theory. For instance, we determined the pathways for all four *n*-butanol radical + O₂ reactions and compared them to experimentally determined branching ratios. Also, we automatically generated rate coefficients for the isomerization of radicals derived from 2,5-dimethyl hexane, which were key to interpret some of the experimental results.

Alkylperoxy chemistry plays also an important role in the degradation of organic polymers in the condensed phase. In collaboration with Kevin Leung (Sandia, NM), we investigated the degradation mechanisms of poly(3-hexylthiophene) (P3HT) theoretically and explored reaction pathways that may lead to the oxidation of the thiophene backbone as a critical step toward disrupting the polymer conjugation. We calculated barrier heights for reactions of the P3HT backbone with oxidizing agents including the hydroxyl radical (OH), hydroperoxide (ROOH), and the peroxy radical (ROO). We found that an attack of a peroxy radical on the side chain on the P3HT backbone may provide low barrier reaction pathways to photodegradation of P3HT and other similar polymers with side chains.

III. NEW DIRECTIONS AND FUTURE WORK

In collaboration with David Osborn, Balint Sztaray (University of the Pacific) and PIs from the Paul Scherrer Institut (Switzerland) we studied the photoelectron spectrum of the benzyl radical. I used the CASPT2 electronic structure method to characterize its ground and excited cationic states, both triplet and singlet, from which several contribute to the measured spectrum in the 7.0–10.5 eV range. The Franck-Condon simulations are in almost perfect agreement for the lowest singlet ($\tilde{X}^+{}^1A_1$) and triplet ($\tilde{a}^+{}^3B_2$) states, and we were able to identify most of the sharp higher energy features as well associated with state $\tilde{A}^+{}^1B_2$ and with possible contributions from $\tilde{b}^+{}^3A_1$. I will continue the collaboration, and contribute to the spectroscopic investigation of other species.

My primary research goal for the near-term is the further development of our automated kinetics code, KinBot. There are several reaction systems where it is applied either at Sandia or in collaboration with others, exploring reactions of tetrahydrofuran, pentanol, ketohydroperoxides, and

methylcyclopentane. KinBot is an expert system relying mostly on chemical rules translated into the 3-D space of molecular structures. This approach, while very efficient and quite reliable for many problems, clearly has limitations. We are exploring molecular dynamics toolsets to extend the abilities of this automated framework and also exploring the option to couple KinBot to automated reaction generators. KinBot potentially can discover pathways which were either not known or simply not thought of in the context of combustion. It already surprised us and provided, for instance, the basis for discovering the water elimination channel.

IV. REFERENCES

- i. Zádor, J.; Jasper, A. W.; Miller, J. A., *Phys. Chem. Chem. Phys.* **2009**, *11*, 11040-11053.
- ii. Georgievskii, Y.; Miller, J. A.; Burke, M. P.; Klippenstein, S. J., Reformulation and solution of the master equation for multiple-well chemical reactions. *J. Phys. Chem. A* **2013**, *117*, 12146-12154.
- iii. Kappler, C.; Zádor, J.; Welz, O.; Fernandes, R. X.; Olzmann, M.; Taatjes, C. A., *Z. Phys. Chem.* **2011**, *225*, 1271-1293.

V. DOE SUPPORTED PUBLICATIONS, 2013-PRESENT

In review

1. Burke, M. P.; Goldsmith, C. F.; Klippenstein, S. J.; Welz, O.; Huang, H.; Antonov, I. O.; Savee, J. D.; Osborn, D. L.; Zádor, J.; Taatjes, C. A.; Sheps, L., Multi-scale informatics for low-temperature propane oxidation: Further complexities in studies of complex reactions. *J. Phys. Chem. A* **2015**, *in review*.
2. Antonov, I. O.; Kwok, J.; Zádor, J.; Sheps, L., OH + 2-butene: S combined experimental and theoretical study in the 300-800 K temperature range. *J. Phys. Chem. A* **2015**, *in review*.

Published

1. Savee, J. D.; Zádor, J.; Hemberger, P.; Sztaray, B.; Bodi, A.; Osborn, D. L., Threshold photoelectron spectrum of the benzyl radical. *Mol. Phys.* **2015**, DOI:10.1080/00268976.2015.1021398.
2. Savee, J. D.; Papajak, E.; Rotavera, B.; Huang, H.; Eskola, A. J.; Welz, O.; Sheps, L.; Taatjes, C. A.; Zádor, J.; Osborn, D. L., Direct observation and kinetics of a critical reactive intermediate in hydrocarbon oxidation. *Science* **2015**, *347*, 643-646.
3. Eskola, A. J.; Welz, O.; Zádor, J.; Antonov, I. O.; Sheps, L.; Savee, J. D.; Osborn, D. L.; Taatjes, C. A., Probing the low-temperature chain-branching mechanism for *n*-butane autoignition chemistry via time-resolved measurements of ketohydroperoxide formation in photolytically initiated *n*-C₄H₁₀ oxidation. *Proc. Combust. Inst.* **2015**, *35*, 291-298.
4. Zádor, J.; Miller, J. A., Adventures on the C₃H₅O potential energy surface: OH + propyne, OH + allene and related reactions. *Proc. Combust. Inst.* **2015**, *35*, 181-188.
5. Scheer, A. M.; Welz, O.; Zádor, J.; Osborn, D. L.; Taatjes, C. A., Low-temperature combustion chemistry of novel biofuels: Resonance-stabilized QOOH in the oxidation of diethyl ketone. *Phys. Chem. Chem. Phys.* **2014**, *16*, 13027-13040.
6. Sai, N.; Leung, K.; Zádor, J.; Graeme, H., First principles study of photo-oxidation degradation mechanisms in P3HT for organic solar cells. *Phys. Chem. Chem. Phys.* **2014**, *16*, 8092-8099
7. Rotavera, B.; Zádor, J.; Welz, O.; Sheps, L.; Scheer, A. M.; Savee, J. D.; Ali, M. A.; Lee, T. S.; Simmons, B. A.; Osborn, D. L.; Violi, A.; Taatjes, C. A., Photoionization mass spectrometric measurements of initial reaction pathways in low-temperature oxidation of 2,5-dimethylhexane. *J. Phys. Chem. A* **2014**, *118*, 10188-10200.
8. Zádor, J.; Miller, J. A., Unimolecular dissociation of hydroxypropyl and propoxy radicals. *Proc. Combust. Inst.* **2013**, *34*, 519-526.
9. Zádor, J.; Huang, H.; Welz, O.; Zetterberg, J.; Osborn, D. L.; Taatjes, C. A., Directly measuring reaction kinetics of QOOH – a crucial but elusive intermediate in hydrocarbon autoignition. *Phys. Chem. Chem. Phys.* **2013**, *15*, 10753-10760.
10. Welz, O.; Zádor, J.; Savee, J. D.; Sheps, L.; Osborn, D. L.; Taatjes, C. A., Low-temperature combustion chemistry of *n*-butanol: Principal oxidation pathways of hydroxybutyl radicals. *J. Phys. Chem. A* **2013**, *117*, 11983-12001.
11. Welz, O.; Klippenstein, S. J.; Harding, L. B.; Taatjes, C. A.; Zádor, J., Unconventional peroxy chemistry in alcohol oxidation: The water elimination pathway. *J. Phys. Chem. Lett.* **2013**, *4*, 350-354.
12. Prager, J.; Najm, N. H.; Zádor, J., Uncertainty quantification in the ab initio rate-coefficient calculation for the CH₃CH(OH)CH₃ + OH → CH₃C(OH)CH₃ + H₂O reaction. *Proc. Combust. Inst.* **2013**, *34*, 583-590.

Isomer-specific Spectroscopy and Pyrolysis of Model Aromatic Fuels

Timothy S. Zwier

Department of Chemistry, Purdue University, West Lafayette, IN 47907-2084
zwier@purdue.edu

Program Definition and Scope

The chemical complexity of hydrocarbon fuels and the fast-expanding list of potential plant-derived biofuels offer a challenge to the scientific community seeking to provide a molecular-scale understanding of their combustion. The development of accurate combustion models stands on a foundation of experimental data on the kinetics and product branching ratios of individual reaction steps. Spectroscopic tools need to continue to be developed to selectively detect and characterize the widening array of fuel components and the reactive intermediates they generate upon pyrolysis and combustion. There is growing recognition that a key component of future progress in the field is the development of detection schemes that are isomer-specific and even conformation-specific. This project uses an array of laser-based and broadband microwave methods to carry out isomer-specific and conformation-specific spectroscopy on key fuel components and the reactive intermediates formed during their pyrolysis and combustion.

Recent Progress

A. Toward a first principles model of the alkyl CH stretch region

(ref. 1, 2, 6, 8, 13)

The alkyl CH stretch region of the infrared is a region rich in information content, but a challenge to assign, due to the ubiquitous presence of strong Fermi resonance mixing between the alkyl CH stretch and CH bend overtone levels. Conformational assignments based on a comparison of the observed alkyl CH stretch spectra with *ab initio* predictions of harmonic frequencies

often fail in spectacular fashion due to these Fermi resonances, which shift and split bands to the point that comparison with harmonic calculations is fruitless. Working in collaboration with Ned Sibert (UW-Madison), we are developing a first-principles model of the alkyl CH stretch region built around a reduced dimension Hamiltonian in which anharmonic CH stretches and scissor modes are Fermi coupled. Earlier studies had concentrated on the CH₂ groups present in conformationally flexible chains (e.g., 1,2-diphenylethane (C₆H₂-CH₂-CH₂-C₆H₅, DPE, ref. 1) and 1,2-diphenoxyethane (C₆H₅-O-CH₂-CH₂-O-C₆H₅, DPOE, ref. 2), hydrogenated naphthalenes (tetralin, 1,2-dihydronaphthalene, 1,4-dihydronaphthalene, indene, and indane, ref. 6) and hydronaphthyl radicals (trihydronaphthyl and inden-2-ylmethyl radicals), where the model was able to account for the complicated stretch-bend Fermi resonances in quantitative detail (8). During the past year, we have extended our collaborative work to include molecules containing methyl and methoxy groups, taking on the more complicated spectroscopy that accompanies these groups. We recorded conformation-specific alkyl CH stretch spectra of jet-cooled 1,1-

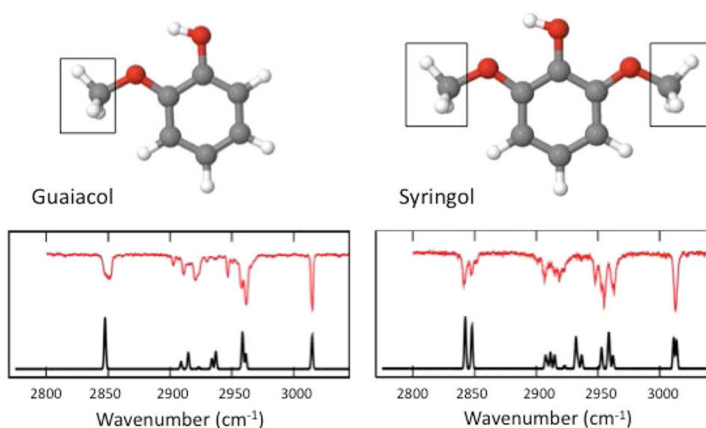


Figure 1: Experimental fluorescence-dip infrared spectra (red) compared to the results of the model Hamiltonian for methyl CH stretch including stretch-bend Fermi resonance.

diphenylethane (DPE, -CHCH₃ chain), 1,1-diphenylpropane (DPP, -CHCH₂CH₃ chain), 2-methoxyphenol (guaiacol), and 1,3-dimethoxy-2-hydroxybenzene (syringol).(13) Transforming the bending normal mode vibrations of CH₃ groups to local scissor vibrations leads to model Hamiltonians which share many features with the model Hamiltonian developed for CH₂ groups. The central difference arises from the greater scissor–scissor coupling present in the CH₃ case. Comparing anharmonic couplings between these modes and the stretch–bend Fermi coupling for a variety of systems, we observed that the anharmonic couplings of the methyl group are robust to chemical environment and level of theory. This robustness suggests a new parameterization of the model Hamiltonian that reduces the number of fitting parameters. In contrast, the harmonic contributions to the Hamiltonian vary substantially between the molecules, leading to important changes in the spectra. The resulting Hamiltonian predict the major spectral features observed in these molecules' CH stretch spectra, and provides insights into mode mixing and the consequences of the mixing on dynamical processes that follow ultrafast CH stretch excitation.

B. Vibronic coupling in near-degenerate excited states (ref. 3, 9)

Working in collaboration with David Plusquellic (NIST) and Lyudmila Slipchenko (Purdue), we experimentally characterized and theoretically modeled the vibrationally and rotationally resolved electronic spectra of diphenylmethane-*d*₅ (DPM-*d*₅). While small, the asymmetry induced by deuteration of one of the aromatic rings is sufficient to cause several important effects that change the principle mechanism of vibronic coupling between the close-lying S₁ and S₂ states, and spectroscopic signatures such coupling produces. The splitting between S₁ and S₂ origins is sufficiently larger than in DPM-*d*₀ (123 cm⁻¹), that the S₂ zero-point level is brought into near-resonance with the *v*=1 level in the S₁ state of a low-frequency phenyl flapping mode, *v*_R=191 cm⁻¹. Dispersed fluorescence spectra bear clear evidence that Δ*v*(R)=1 Herzberg-Teller coupling dominates the near-resonant internal mixing between the S₁ and S₂ manifolds. The experimental data on DPM-*d*₅ is serving as an important foundation for a multi-mode vibronic coupling model developed by the Slipchenko group, that is capable of being applied to asymmetric bichromophores much more generally.

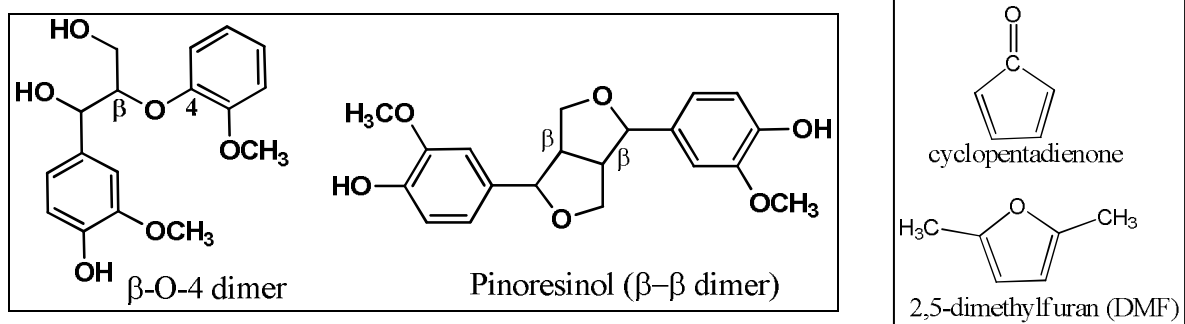
C. Resonance-stabilized radicals (ref. 9, 12)

We also continue to pursue isomer-specific and conformation-specific spectroscopy of resonance-stabilized radicals. Building off recently published studies of α-methylbenzyl radical C₆H₅-CH-CH₃ (ref. 9), trihydronaphthyl radical, and inden-2-ylmethyl radical, we are pursuing a series of phenylalkyl radicals, both conjugated to the phenyl ring and with radical sites remote to the phenyl ring. Our current focus is primarily on the series of alkyl-substituted benzyl radicals PhĊH(CH₂)_nCH₃, where conformation-specific spectroscopy is needed. Two-color resonant two-photon ionization (2C-R2PI) spectra and resonant ion-dip infrared (RIDIR) spectroscopy is being used to study the spectra of these radicals.

D. Model lignin compounds and biofuels (ref. 5, 7, 12, 14)

In a project that is the vestige of a theme developed in a previous funding cycle, we have studied the IR and UV spectroscopy of sinapoyl malate and a series of similar sinapoyl derivatives(12), with the goal of understanding the molecule's role as a UV-B sunscreens for plants. The spectrum of sinapoyl malate in the UV-B region was quite unique, showing inherent spectral broadening even under jet-cooled conditions in the gas phase. As a result, the inherent quantum mechanical properties of sinapoyl malate are ideal for its role as a sunscreen, giving complete coverage of the UV-B even under jet-cooled, isolated conditions.

We have also studied the single-conformation IR and UV photofragment spectroscopy of cryo-cooled, metalated cations of the prototypical β -O-4 and β - β linked dilignols shown below.(14) The spectroscopy is used to determine the sites of binding for the Li^+ and Na^+ in oxygen-rich pockets associated with the β -O-4 and β - β linkages. Photofragment mass spectra demonstrate that UV fragmentation occurs by a combination of backbone fragmentation and side-chain loss that is unique to each linkage/cation combination. This bodes well for future studies on longer lignin oligomers, designed to test whether UV photofragmentation can be used to selectively fragment a lignin oligomer chain at the site of electronic excitation.



E. Broadband microwave spectroscopy of intermediates formed in flash pyrolysis (ref. 10)

We continue to develop the hyperthermal nozzle (or Chen nozzle) as a source of reactive pyrolysis or combustion intermediates for spectroscopic interrogation via chirped-pulse Fourier transform microwave (CP-FTMW) spectroscopy. In collaboration with G. Barney Ellison and John Stanton, we completed and published our study of the prototypical anti-aromatic molecule cyclopentadienone. Using isotopic data available from ^{13}C isotopomers present in natural abundance, we obtained r_0 and r_e structures for cyclopentadienone with accuracies on atomic positions approaching 0.001 Å.

Over the summer, we acquired a new 40 GHz digitizer (Guzik ADC6131) based on a successful Purdue internal equipment grant program, which has accelerated our signal averaging rates by more than a factor of 100. Studies of the pyrolysis of prototypical biofuels (e.g., methylfuran, dimethylfuran) is currently underway.

Future Work

In collaboration with Ned Sibert, we are extending our CH stretch model to a series of phenyl alkanes with $n=2-10$. We are recording both ground and excited state IR spectra in the alkyl CH stretch region. We also will study the R2PI and IR spectroscopy of phenylalkyl radicals with radical sites along the alkyl chain. R2PI, IR, and CP-FTMW spectra of key pyrolysis intermediates from methylfuran and 2,5-dimethylfuran will also be subjects of future work. Finally, we are beginning to explore whether two-dimensional CP-FTMW spectra, with its off-diagonal couplings connecting microwave transitions due to a single species, can be used to characterize complex gas phase mixtures such as flash pyrolysis effluent. We hope that such 2D spectra can provide a powerful means of deciphering which microwave transitions are shared by a single species, aiding in their assignment, much as is done in NMR spectroscopy.

Publications acknowledging DOE support, 2012-present

1. Evan G. Buchanan, Jacob C. Dean, Timothy S. Zwier, and Edwin L. Sibert III, "Towards a first-principles model of Fermi resonances in the alkyl CH stretch region: Application to 1,2-diphenylethane and 2,2,2-paracyclophane", *J. Chem. Phys.* **134**, 064308 (2013).

2. Evan G. Buchanan, Edwin L. Sibert III, and Timothy S. Zwier, Ground state Conformational Preferences and CH stretch-bend coupling in a model alkoxy chain: 1,2-diphenoxyethane”, *J. Phys. Chem. A* **117**, 2800-2811 (2013).
3. Evan G. Buchanan, David F. Plusquellic, and Timothy S. Zwier, “Excitonic splitting and vibronic coupling in 1,2-diphenoxyethane: Conformation-specific effects in the weak coupling limit”, *J. Chem. Phys.* **138** 204313 (2013).
4. Nathanael M. Kidwell, Neil J. Reilly, Ben Nebgen, Deepali N. Mehta-Hurt, Ross D. Hoehn, Damian L. Kokkin, Michael C. McCarthy, Lyudmila V. Slipchenko, and Timothy S. Zwier, “Jet-cooled Spectroscopy of the α -Methylbenzyl Radical: Probing the State-Dependent Effects of Methyl Rocking against a Radical Site”, *J. Phys. Chem. A*, **117**, 13465-80 (2013).
5. Jacob C. Dean, Polina Navotnaya, Alexander P. Parobek, Rachel M. Clayton, and Timothy S. Zwier, “Ultraviolet spectroscopy of fundamental Lignin sub-units: Guaiacol, 4-methylguaiacol, syringol, and 4-methylsyringol”, **139**, 144313 (2013). (16 pages)
6. Nathanael M. Kidwell, Deepali N. Mehta-Hurt, Joseph A. Korn, Edwin L. Sibert III, and Timothy S. Zwier, “Ground and Excited State Infrared Spectroscopy of Jet-Cooled Radicals: Exploring the Photophysics of Trihydronaphthyl and Inden-2-ylmethyl”, *J. Phys. Chem. A*. **117**, 13465–13480 (2013).
7. Jacob C. Dean, Patrick S. Walsh, Bidyut Biswas, P. V. Ramachandran, and Timothy S. Zwier, “Single-conformation UV and IR spectroscopy of model G-type lignin dilignols: the β -O-4 and β - β linkages”, *Chem. Sci.*, **5**, 1940 – 1955 (2014).
8. Edwin L. Sibert III, Nathanael M. Kidwell, and Timothy S. Zwier, “A First-Principles Model of Fermi Resonance in the Alkyl CH Stretch Region: Application to Hydronaphthalenes, Indanes, and Cyclohexane”, *J. Phys. Chem. B* **118**, 8236-8245 (2014).
9. Nathan R. Pillsbury, Nathanael M. Kidwell, Benjamin Nebgen, Lyudmila V. Slipchenko, John R. Cable, David F. Plusquellic, and Timothy S. Zwier, “Vibronic Coupling in Asymmetric Bichromophores: I. Experimental Investigation of Diphenylmethane- d_5 ”, *J. Chem. Phys.* **141**, 064316 (2014).
10. Nathanael M. Kidwell, Vanesa Vaquero-Vara, Thomas K. Ormond, Grant T. Buckingham, Di Zhang, Deepali N. Mehta-Hurt, Laura McCaslin, Mark R. Nimlos, John W. Daily, Brian C. Dian, John F. Stanton, G. Barney Ellison, and Timothy S. Zwier, “Chirped-Pulse Fourier Transform Microwave Spectroscopy coupled with a Flash Pyrolysis Microreactor: Structural Determination of the Reactive Intermediate Cyclopentadienone”, *J. Phys. Chem. Lett.* **5**, 2201-07 (2014).
11. Jamie D. Young, Michael Staniforth, Jacob C. Dean, Gareth M. Roberts, Federico Mazzoni, Tolga N.V. Karsili, Michael N.R. Ashfold, Timothy S. Zwier, and Vasilios G. Stavros, “Towards Understanding Photodegradation Pathways in Lignins: The Role of Intramolecular Hydrogen Bonding in Excited States”, *J. Phys. Chem. Lett.* **5**, 2138-43 (2014).
12. Jacob C. Dean, Ryoji Kusaka, Patrick C. Walsh, Florent Allais, and Timothy S. Zwier, “Plant Sunscreens in the UV-B: Ultraviolet Spectroscopy of Jet-Cooled Sinapoyl Malate, Sinapic Acid, and Sinapate Ester Derivatives”, *J. Am. Chem. Soc.* **136**, 14780-95 (2014).
13. Edwin L. Sibert III, Daniel P. Tabor, Nathanael M. Kidwell, Jacob C. Dean, and Timothy S. Zwier, “Fermi Resonance Effects in the Vibrational Spectroscopy of Methyl and Methoxy Groups”, *J. Phys. Chem. A* **118**, 11272-81 (2014).
14. Jacob C. Dean, Nicole L. Burke, John R. Hopkins, James G. Redwine, P.V. Ramachandran, Scott A. McLuckey, and Timothy S. Zwier, “UV Photofragmentation and IR Spectroscopy of Cold, G-type β -O-4 and β - β Dilignol-Alkali Metal Complexes: Structure and Linkage-Dependent Photofragmentation”, *J. Phys. Chem. A* (accepted).

Critical Issues



Critical Issues for the DOE Gas Phase Chemical Physics Program – P. Dagdigian (Johns Hopkins Univ.)

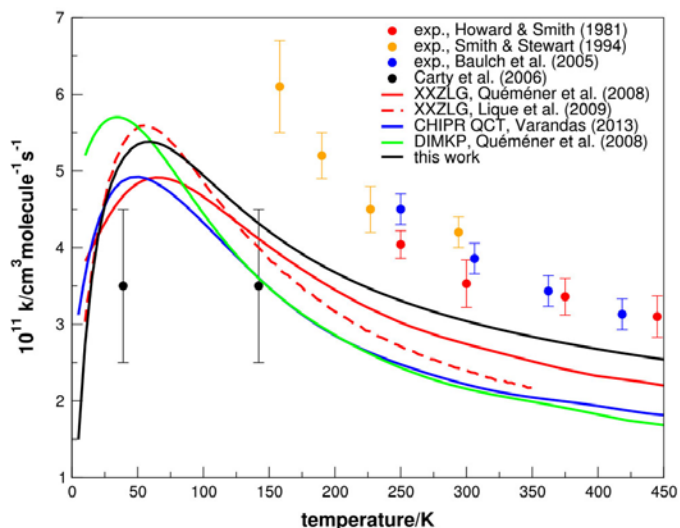
Radical-Radical Reactions

- More difficult to measure rate constants than for radical-stable molecule reactions
- Branching ratios for reactions with several product channels harder to measure
- Radical-radical recombination an important pressure-dependent process
- Issues in the theoretical description:

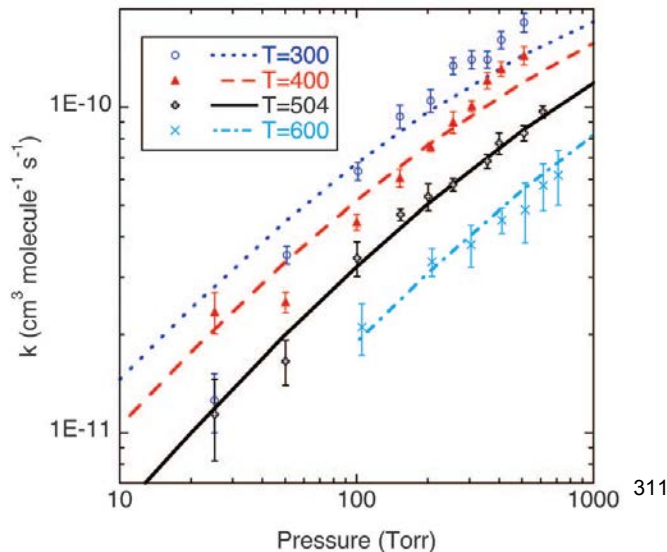
Usually focus only on PES's leading to products

Statistical vs. dynamical branching in the entrance channel.

Rate constant for O+OH Reaction



P-dep. rate constant for CH₃+H Recomb.



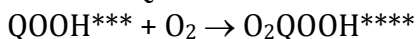
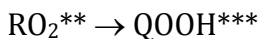
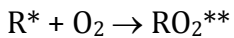
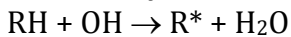
Experimental Studies of the Effect of Non-Thermal Initial Distributions on the Kinetics of Radicals

Radicals are generally produced with non-thermal energy distributions. How does this affect their subsequent kinetics?

Possible Effects:

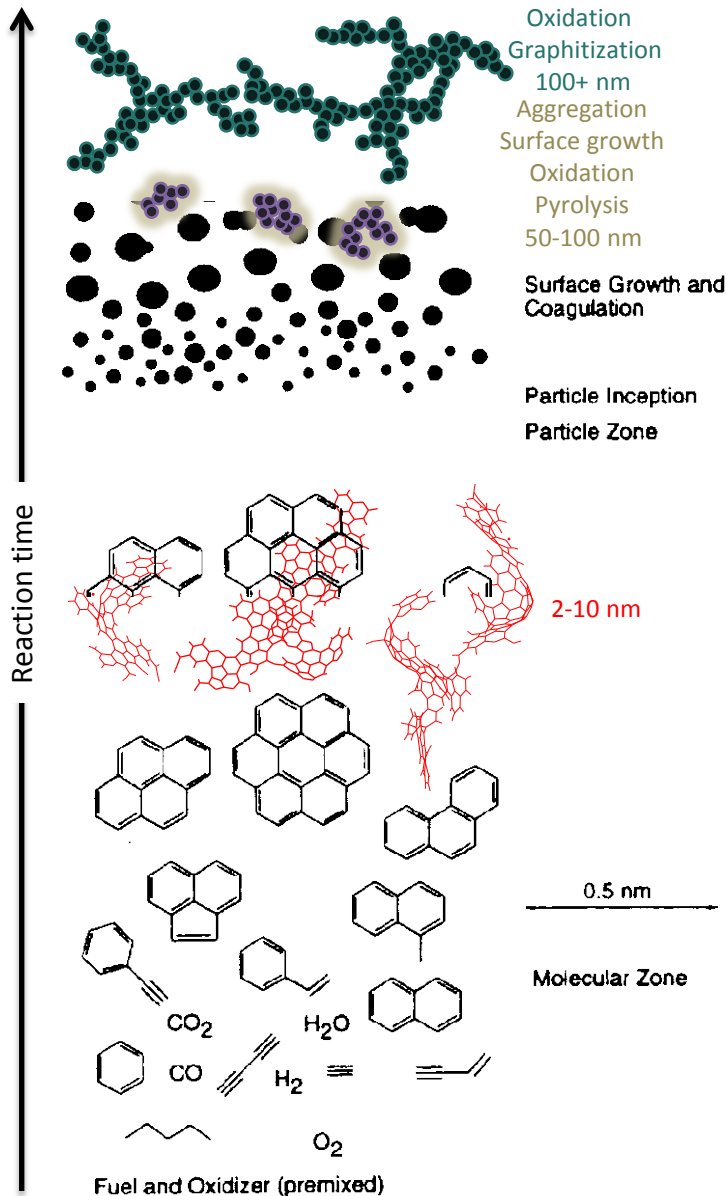
- (i) Direct dissociation – dissociation prior to complete thermalization
- (ii) Enhanced rate of reaction with other species
- (iii) Transformed product distributions for reactions with other species

Effects may be cumulative for a sequence of radical reactions, e. g., for



Need experiments probing how the kinetics changes for species that are in the process of thermalization. For example, laser photolysis induced experiments could be performed under situations where the subsequent reaction occurs during the thermalization of the radical. Varying conditions such as pressure, dilution, and/or bath gas would provide a probe of the coupling of energy transfer and dynamics on the overall kinetics. Such an understanding is central to continued progress in modeling the chemistry of combustion.

Multiphase Chemistry in Combustion



Heterogeneous Oxidation of Soot Particles – Gas-Surface Chemistry in Combustion and Atmosphere

- Soot particles – size, morphology, composition, coating, hydrophobic-to-hydrophilic conversion, temperature, ...
- Oxidants – OH, O₂, O₃, ...
- Novel detection schemes for optical, physical, and chemical properties of soot – laser-induced incandescence, laser scattering, aerosol mass spectrometry (IR vaporization, VUV ionization), ...
- Kinetics of gaseous uptake, product formation

Mitigating Climate Change by Reducing Soot from Fossil and Biofuel Combustion

- Radiative forcing from Black Carbon is ~40% (with larger uncertainty) that of CO₂
- Climate heating effect – soot absorbs light, lowers snow reflectivity, increases glacial melt

[IPCC, 2013]

Critical Issues in Flame Extinction Experiments

- Background
 - Extinction is important for many combustion problems: minimum ignition energy, flame stabilization, strongly turbulent flame propagation etc.
 - Pathways controlling ignition and extinction phenomena are very different; current experiments are heavily focused on ignition and flame speed problems
 - Current fuel chemistry are overall under-validated for extinction problems
- Challenges in flame extinction diagnostics: extremely small time and length scales
- To resolve local extinction in turbulent flames
 - Timescale: $O(1\sim 0.01)$ ms; length scale: $O(100)$ microns
 - Critical diagnostic tools: $O(10)$ micron spatial resolution; $O(10-10^3)$ KHz frequency
- To resolve a steady state 1-D near-extinction flame
 - Length scale: $O(100)$ microns
 - Critical diagnostic tools: $O(10)$ micron spatial resolution
- An ideal reactor for extinction kinetics study: perfectly stirred reactor
 - Current diagnostic tools are adequate
 - How to make the flow uniform (i.e. to be 0-D) at a residence time of $O(1\sim 0.01)$ ms?

Effects of combustion on atmospheric chemistry (Neumark)

- Current combustion program focuses on what happens during combustion, not so much on what happens to combustion products once they are exhausted into the atmosphere
- Programatically relevant given the DOE/BES investment in carbon sequestration (two EFRC's, for example)
- Many scientific questions in atmospheric chemistry mirror those studied in this program, although under different T,P
 - Internal H-abstractions; peroxy radical isomerizations, QOOH. A more general understanding of the energetics, dynamics, and kinetics and working through some specific examples over a range of T and P and concentration would be interesting and important.
 - Polymerization, condensation and aerosol formation--soot and organic aerosol in the flame, in the exhaust, and after catalytic treatment.
 - Low temperature flames--e.g forest fires, wood/coal burning stoves and agricultural burns. Nitrogen chemistry in these systems is especially important because the C:N ratio of the fuel is so much higher than in fossil fuels. Aerosol from stoves is probably the single largest public health problem on the planet.



Isomer and state specific photoproduct branching ratio measurements of prototype aromatic molecules

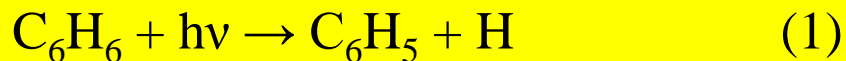
Goal: (i) To determine isomer and state specific photoproduct branching ratios of aromatic molecules for benchmarking theoretical predictions. (ii) Reverse of soot formation and complementary to pyrolytic and chemical studies.

Experiment approach:

- (i) VUV-photodissociation pump and VUV-photoionization probe.
- (ii) Two-color photoexcitation, photoionization and photoelectron method.
- (iii) time-sliced velocity-map-imaging-photoion method.

Example:

Photodissociation of benzene:



DOE/BES Critical Issues in Gas Phase Chemical Physics/Combustion

- **FLAME INITIATION:** Flame initiation currently occurs in spark plug engines with a localized electrical spark. Are there practical advantages for flames to be initiated in a more delocalized manner? Mechanisms for this might include intense electric fields that generate temporary plasmas or intense laser pulses that generate molecular ions. The research focus for this would include a wide range of topics from the basic science of hydrocarbon molecules within intense fields, to the hydrodynamics of flowing charged particles, to the applied aspects of designing lasers that can withstand combustion conditions and that have up to 10K Hz repetition rates.
- **METHANE FUEL MIXTURES:** Methane has become widely available due to fracking technology. A practical problem with methane fuel for mobile situations such as automobiles is that it does not liquefy at reasonably low pressures at room temperature. This results in safety concerns associated with high-pressure tanks, and it presents driving-range challenges due to the relatively low energy density of the compressed gas fuel. However, other low molecular weight hydrocarbons do liquefy at low pressures (propane and butane) or are already liquid at room temperature (pentane, hexane, and higher). Is it practical to dissolve large volumes of methane in these heavier nonpolar liquids under low pressure and to use that pressurized mixture as a fuel? Upon injection into a combustion cylinder, the increased temperatures and reduced pressures would cause the volatile methane to evaporate from the fuel droplets, presenting challenges to the engine design to eliminate knocking and preignition. Research would be directed toward modeling of ignition and combustion of various fuel-air mixtures and on the design of engines that are capable of adjusting to a wide range of combustion conditions resulting from these mixture changes.

Droplet Combustion

Albert Wagner, Argonne National Laboratory

Problem: How do droplets of fuel blends burn? Does species-specific evaporation rates and surface segregation rates influence combustion? Do transport properties and turbulence within the droplet from on-going combustion influence subsequent combustion? Can trace inorganic metals in the fuel influence sooting or ash formation?

Motivation: In ICEs, the standard rule of thumb is that injected liquid fuel fully atomizes before combustion. If that is true, does this lead to spatial distributions for fuel blends where the more volatile fuel is nearest the injector and the least volatile fuel is farthest away? Does the heat of the atomization process “cook” the fuel so that the last fraction to atomize contains species not originally in the droplet at the point of injection? If atomization is *not* complete before combustion, can the least volatile fuel fraction have soot formation mechanisms different from the most volatile fuel fraction? Spray fidelity is important in ICE CFD modeling and has been identified in the PreSICE report as a major industrial concern. An investment in this topic can provide fundamental information that would be necessary to achieve high fidelity.

Solution:

Experimental: There are very reliable droplet generators. Sprays can also be tuned to produce a distribution of droplets. However generally these have not been used in an environment where pressure and temperature can be controlled over the ranges experienced in ICEs. Shock tubes are designed to create relatively cleanly and “instantaneously” temperature and pressure ranges relevant to combustion. Chemical processes in the shock tube can be interrogated by laser-based spectroscopies, mass spectroscopy, and X-ray scattering. Marrying shock tubes and droplet generation can open a new window on the evaporation and combustion of droplets.

Theoretical: With high performance computing, atomistic MD simulations have progressed well beyond one million atom sizes. Coarse graining is routinely used to simulate bulk properties of liquids, including hydrocarbons. Methods exist to handle rare event by combining multiple realizations of a trajectory run in parallel. While a challenge, for small droplets atomistic or coarse-grained simulations on massively parallel computers could be done with pairwise intermolecular forces that could follow species-specific surface segregation, evaporation, transport, and turbulence. Adding chemical reaction would be still more challenging but in the context of multiscale modeling could probably be done. Such simulations could make contact with measurements and begin a theory/experiment dialogue.

Implications:

In a general sense, this would strengthen the multi-phase component in the Chemical Sciences combustion portfolio and bring fuel injection into the chemical realm. From the computing and X-ray perspective, such a program could exploit DOE user-facilities. From the theory side, it could be a bridge between Chemical Sciences supported CFD efforts and kinetics/dynamics efforts. From the spray side, it would be a step into the world of splashing sprays and stochastic phenomena highlighted in several BES reports.

Problem statements

The effects of ultra high pressure on combustion physics and kinetics are highly uncertain. There are few researchers and facilities focusing on fundamental combustion reaction chemistry and flow physics at 300+ bar. Some efforts include Tranter, Brezinsky and co-workers.

Fuel +HO₂ reactions are increasingly important for low temperature combustion strategies, yet there are few fundamental experimental or computational studies of this important class of reactions and the branching fractions. Several research groups are working in this area, but more is needed.

Tools necessary

From an experimental standpoint, more ultra high pressure facilities are required and the development of associated high fidelity diagnostics.

Ab initio studies of fuel +HO₂ involve complex transitions states; are we limited by theory or computational power?

Impact

Ultra high pressure combustion has potential for significantly higher efficiencies in stationary power generation and the reaction chemistry at ultra high pressures plays a role in super-knock phenomena that limit boosted reciprocating engines.

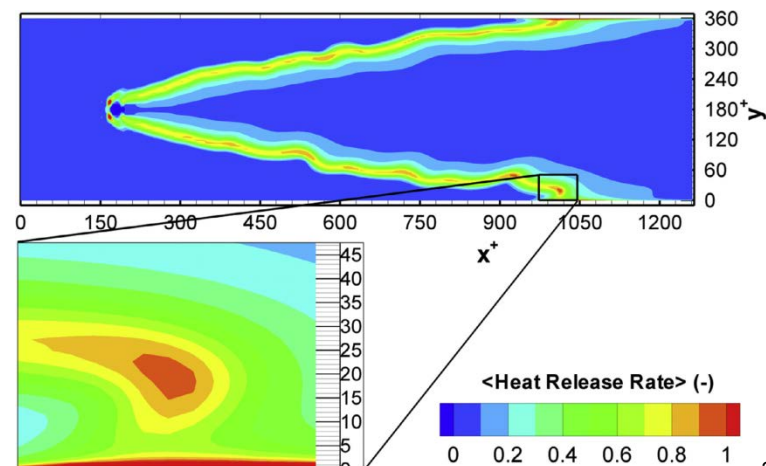
Low temperature chemistry limits reactivity, particularly lean dilute limits of many combustion strategies in turbines and reciprocating engines.

Next-Generation Multiplexed Probes of Flames

- Ultimate understanding of flames would involve comprehensive knowledge of the molecular composition of flames with high spatial and temporal resolution.
- Current state-of-the-art:
 - Steady state spatial resolution + tunable VUV for molecular specificity
 - Time + laser sheet + species specificity (e.g., CARS), T-measurements
- Are new imaging schemes possible that combine broadband, high-resolution spectral data with good spatial and temporal resolution?



CRF/ALS



A. Gruber, R. Sankaran, E.R. Hawkes, J.H. Chen,
J. Fluid Mech. 658 (2010) 5–32.

Participant List

35th Annual Combustion Research Meeting Participation List

Last Name	First Name	Organization	Email
Ahmed	Musahid	Lawrence Berkeley National Laboratory	MAhmed@lbl.gov
alexander	millard	University of Maryland	mha@umd.edu
Allen	Wesley	University of Georgia	wdallen@uga.edu
Barlow	Robert	Sandia National Laboratories	barlow@sandia.gov
Bellan	Josette	California Institute of Technology	Josette.Bellan@jpl.nasa.gov
Blanquart	Guillaume	California Institute of Technology	g.blanquart@caltech.edu
Bunel	Emilio	Argonne National Laboratory	ebunel@anl.gov
Butler	Laurie	The University of Chicago	L-Butler@uchicago.edu
Chandler	David	Sandia National Laboratories	chand@sandia.gov
Chen	Jacqueline	Sandia National Laboratories	jhchen@sandia.gov
Continetti	Robert	University of California	rcontinetti@ucsd.edu
Dagdigian	Paul	Johns Hopkins University	pjdagdigian@jhu.edu
Dahms	Rainer	Sandia National Laboratories	Rndahms@sandia.gov
Daily	John	University of Colorado at Boulder	john.daily@colorado.edu
Davis	Michael	Argonne National Laboratory	davis@tcg.anl.gov
Davis	Floyd	Cornell University	hfd1@cornell.edu
Dawes	Richard	Missouri University	dawesr@mst.edu
Dibble	Theodore	SUNY-ESF	tsdibble@esf.edu
Douberly	Gary	University of Georgia	douberly@uga.edu
Ellison	Barney	University of Colorado	barney@jila.colorado.edu
Frank	Jonathan	Sandia National Laboratories	jhfrank@sandia.gov
Goldsborough	Scott	Argonne National Laboratory	scott.goldsborough@anl.gov
Gord	James	Air Force Research Laboratory	james.gord@us.af.mil
Green	William	Massachusetts Institute of Technology	whgreen@mit.edu
Guo	Hua	University of New Mexico	hguo@unm.edu

Hansen	Nils	Sandia National Laboratories	nhansen@sandia.gov
Hanson	Ronald	Stanford University	rkhanson@stanford.edu
Harding	Lawrence	Argonne National Laboratory	harding@anl.gov
Harris	Alexander	Brookhaven National Laboratory	alexh@bnl.gov
Head-Gordon	Martin	Univ of California/LBNL	mhg@cchem.berkeley.edu
Hershberger	John	North Dakota State University	john.hershberger@ndsu.edu
Hirata	So	University of Illinois, Urbana-Champaign	sohirata@illinois.edu
Hwang	Robert	Sandia National Laboratories	gdecast@sandia.gov
Jasper	Ahren	Sandia National Laboratories	ajasper@sandia.gov
Kaiser	Ralf	University of Hawaii	ralfk@hawaii.edu
Kellman	Michael	University of Oregon	kellman@uoregon.edu
Kliewer	Christopher	Sandia National Laboratories	cjkliew@sandia.gov
Klippenstein	Stephen	Argonne National Laboratory	sjk@anl.gov
Krause	Jeffrey	U.S. Department of Energy/BES	Jeff.Krause@science.doe.gov
Krylov	Anna	University of Southern California	krylov@usc.edu
Leone	Stephen	University of California/LBNL	srl@berkeley.edu
Lester	Marsha	University of Pennsylvania	milester@sas.upenn.edu
Lester Jr.	William	Lawrence Berkeley National Laboratory	walester@lbl.gov
Lucht	Robert	Purdue University	lucht@purdue.edu
Lu	Tianfeng	University of Connecticut	tlu@engr.uconn.edu
Manley	Dawn	Sandia National Laboratories	dmanley@sandia.gov
Marceau	Diane	U.S. Department of Energy/BES	diane.marceau@science.doe.gov
Mebel	Alexander	Florida International University	mebela@fiu.edu
Michael	Joe	Argonne National Laboratory	jmichael@anl.gov
Michelsen	Hope	Sandia National Laboratories	hamiche@sandia.gov
Miller	John	U.S. Department of Energy/BES	John.Miller@science.doe.gov
Miller	William	University of California/LBNL	millerwh@berkeley.edu
Mullin	Amy	University of Maryland	mullin@umd.edu
Najm	Habib	Sandia National Laboratories	hnnajm@sandia.gov
Nesbitt	David	JILA/University of Colorado	djn@jila.colorado.edu
Neumark	Daniel	University of California, Berkeley	dneumark@berkeley.edu
Ng	Cheuk-Yiu	University of California, Davis	cyng@ucdavis.edu

Oefelein	Joseph	Sandia National Laboratories	oefelei@sandia.gov
Osborn	David	Sandia National Laboratories	dlosbor@sandia.gov
Parish	Carol	University of Richmond	cparish@richmond.edu
Pepiot	Perrine	Cornell University	pp427@cornell.edu
Perry	David	University of Akron	dperry@uakron.edu
Piecuch	Piotr	Michigan State University	piecuch@chemistry.msu.edu
Pietraß	Tanja	U.S. Department of Energy/BES	tanja.pietrass@science.doe.gov
Pitz	William	Lawrence Livermore National Laboratory	pitz1@llnl.gov
Pope	Stephen	Cornell University	s.b.pope@cornell.edu
Pratt	Stephen	Argonne National Laboratory	stpratt@anl.gov
Prozument	Kirill	Argonne National Laboratory	prozument@anl.gov
Reisler	Hanna	University of Southern California	reisler@usc.edu
Ruscic	Branko	Argonne National Laboratory	ruscic@anl.gov
Schaefer	Henry	University of Georgia	ccq@uga.edu
Sears	Trevor	Brookhaven National Laboratory	sears@bnl.gov
Shaddix	Christopher	Sandia National Laboratories	crshadd@sandia.gov
Shepard	Ron	Argonne National Laboratory	shepard@tcg.anl.gov
Sheps	Leonid	Sandia National Laboratories	lsheps@sandia.gov
Sisk	Wade	U.S. Department of Energy/BES	sisk007@msn.com
Sivaramakrishnan	Raghu	Argonne National Laboratory	raghu@anl.gov
Stanton	John	University of Texas	jfstanton@mail.utexas.edu
Suits	Arthur	Wayne State University	asuits@wayne.edu
Sutherland	James	University of Utah	james.sutherland@chemeng.utah.edu
Taatjes	Craig	Sandia National Laboratories	cataatj@sandia.gov
Tranter	Robert	Argonne National Laboratory	tranter@anl.gov
Violi	Angela	University of Michigan	avioli@umich.edu
Wagner	Albert	Argonne National Laboratory	wagner@anl.gov
Westbrook	Charles	Lawrence Livermore National Laboratory	westbrookck@earthlink.net
Wilson	Kevin	Lawrence Berkeley National Laboratory	krwilson@lbl.gov
Wittig	Curt	University of Southern California	wittig@usc.edu
Wooldridge	Margaret	University of Michigan	mswool@umich.edu
Yarkony	David	Johns Hopkins University	yarkony@jhu.edu

Yu
Zador
Zwier

HuaGen
Judit
Timothy

Brookhaven National Laboratory
Sandia National Laboratories
Purdue University

hgy@bnl.gov
jzador@sandia.gov
zwier@purdue.edu